IntechOpen

Adaptive Control

Edited by Kwanho You

Adaptive Control

Edited by
Kwanho You

Adaptive Control
http://dx.doi.org/10.5772/99
Edited by Kwanho You

Notice

Statements and opinions expressed in the chapters are these of the individual contributors and not necessarily those of the editors or publisher. No responsibility is accepted for the accuracy of information contained in the published chapters. The publisher assumes no responsibility for any damage or injury to persons or property arising out of the use of any materials, instructions, methods or ideas contained in the book.

First published in Croatia, 2009 by INTECH d.o.o.
eBook (PDF) Published by IN TECH d.o.o.
Place and year of publication of eBook (PDF): Rijeka, 2019.
IntechOpen is the global imprint of IN TECH d.o.o.
Printed in Croatia

Legal deposit, Croatia: National and University Library in Zagreb

Additional hard and PDF copies can be obtained from orders@intechopen.com

Adaptive Control
Edited by Kwanho You

p. cm.

ISBN 978-953-7619-47-3

eBook (PDF) ISBN 978-953-51-6405-0

Preface

Adaptive control has been a remarkable field for industrial and academic research since 1950s. Since more and more adaptive algorithms are applied in various control applications, it is considered as important for practical implementation. As it can be confirmed from the increasing number of conferences and journals on adaptive control topics, it is certain that the adaptive control is a significant guidance for technology development.

Also adaptive control has been believed as a breakthrough for realization of intelligent control systems. Even with the parametric and model uncertainties, adaptive control enables the control system to monitor the time varying changes and manipulate the controller for desired performance. Therefore adaptive control has been considered to be essential for time varying multivariable systems. Moreover, now with the advent of high-speed microprocessors, it is possible to implement the innovative adaptive algorithms even in real time situation.

With the efforts of many control researchers, the adaptive control field is abundant in mathematical analysis, programming tools, and implementational algorithms. The authors of each chapter in this book are the professionals in their areas. The results in the book introduce their recent research results and provide new idea for improved performance in various control application problems.

The book is organized in the following way. There are 16 chapters discussing the issues of adaptive control application to model generation, adaptive estimation, output regulation and feedback, electrical drives, optical communication, neural estimator, simulation and implementation:

Chapter One: Automatic 3D Model Generation based on a Matching of Adaptive Control Points, by N. Lee, J. Lee, G. Kim, and H. Choi

Chapter Two: Adaptive Estimation and Control for Systems with Parametric and Nonparametric Uncertainties, by H. Ma and K. Lum

Chapter Three: Adaptive Output Regulation of Unknown Linear Systems with Unknown Exosystems, by I. Mizumoto and Z. Iwai

Chapter Four: Output Feedback Direct Adaptive Control for a Two-Link Flexible Robot Subject to Parameter Changes, by S. Ozcelik and E. Miranda

Chapter Five: Discrete Model Matching Adaptive Control for Potentially Inversely Non-Stable Continuous-Time Plants by Using Multirate Sampling, by S. Alonso-Quesada and M. De la Sen

Chapter Six: Hybrid Schemes for Adaptive Control Strategies, by R. Ribeiro and K. Queiroz

Chapter Seven: Adaptive Control for Systems with Randomly Missing Measurements in a Network Environment, by Y. Shi and H. Fang

Chapter Eight: Adaptive Control based on Neural Network, by S. Wei, Z. Lujin, Z. Jinhai, and M. Siyi

Chapter Nine: Adaptive Control of the Electrical Drives with the Elastic Coupling using Kalman Filter, by K. Szabat and T. Orlowska-Kowalska

Chapter Ten: Adaptive Control of Dynamic Systems with Sandwiched Hysteresis based on Neural Estimator, by Y. Tan, R. Dong, and X. Zhao

Chapter Eleven: High-Speed Adaptive Control Technique based on Steepest Descent Method for Adaptive Chromatic Dispersion Compensation in Optical Communications, by K. Tanizawa and A. Hirose

Chapter Twelve: Adaptive Control of Piezoelectric Actuators with Unknown Hysteresis, by W. Xie, J. Fu, H. Yao, and C. Su

Chapter Thirteen: On the Adaptive Tracking Control of 3-D Overhead Crane Systems

Chapter Fourteen: Adaptive Inverse Optimal Control of a Magnetic Levitation System, by Y. Satoh, H. Nakamura, H. Katayama, and H. Nishitani

Chapter Fifteen: Adaptive Precision Geolocation Algorithm with Multiple Model Uncertainties, by W. Sung and K. You

Chapter Sixteen: Adaptive Control for a Class of Non-affine Nonlinear Systems via Neural Networks, by Z. Tong

We expect that the readers have taken a basic course in automatic control, linear systems, and sampled data systems. This book is tried to be written in a self-contained way for better understanding. Since this book introduces the development and recent progress of the theory and application of adaptive control research, it is useful as a reference especially for industrial engineers, graduate students in advanced study, and the researchers who are related in adaptive control field such as electrical, aeronautical, and mechanical engineering.

Kwanho You
Sungkyunkwan University, Korea

Contents

1

Automatic 3D Model Generation based on a Matching of Adaptive Control Points

Na-Young Lee[1], Joong-Jae Lee[2], Gye-Young Kim[3] and Hyung-Il Choi[4]
[1]*Radioisotope Research Division, Korea Atomic Energy Research Institute*
[2]*Center for Cognitive Robotics Research, Korea Institute of Sciene and Technology*
[3]*School of Computing, Soongsil University*
[4]*School of Media, Soongsil University*
Republic of Korea

Abstract

The use of a 3D model helps to diagnosis and accurately locate a disease where it is neither available, nor can be exactly measured in a 2D image. Therefore, highly accurate software for a 3D model of vessel is required for an accurate diagnosis of patients. We have generated standard vessel because the shape of the arterial is different for each individual vessel, where the standard vessel can be adjusted to suit individual vessel. In this paper, we propose a new approach for an automatic 3D model generation based on a matching of adaptive control points. The proposed method is carried out in three steps. First, standard and individual vessels are acquired. The standard vessel is acquired by a 3D model projection, while the individual vessel of the first segmented vessel bifurcation is obtained. Second is matching the corresponding control points between the standard and individual vessels, where a set of control and corner points are automatically extracted using the Harris corner detector. If control points exist between corner points in an individual vessel, it is adaptively interpolated in the corresponding standard vessel which is proportional to the distance ratio. And then, the control points of corresponding individual vessel match with those control points of standard vessel. Finally, we apply warping on the standard vessel to suit the individual vessel using the TPS (Thin Plate Spline) interpolation function. For experiments, we used angiograms of various patients from a coronary angiography in Sanggye Paik Hospital.
Keywords: Coronary angiography, adaptive control point, standard vessel, individual vessel, vessel warping.

1. Introduction

X-ray angiography is the most frequently used imaging modality to diagnose coronary artery diseases and to assess their severity. Traditionally, this assessment is performed directly from the angiograms, and thus, can suffer from viewpoint orientation dependence and lack of precision of quantitative measures due to magnification factor uncertainty

(Messenger et al., 2000), (Lee et al., 2006) and (Lee et al., 2007). 3D model is provided to display the morphology of vessel malformations such as stenoses, arteriovenous malformations and aneurysms (Holger et al., 2005). Consequently, accurate software for a 3D model of a coronary tree is required for an accurate diagnosis of patients. It could lead to a fast diagnosis and make it more accurate in an ambiguous condition.

In this paper, we present an automatic 3D model generation based on a matching of adaptive control points. Fig. 1 shows the overall flow of the proposed method for the 3D modelling of the individual vessel. The proposed method is composed as the following three steps: image acquisition, matching of the adaptive control points and the vessel warping. In Section 2, the acquisitions of the input image in standard and individual vessels are described. Section 3 presents the matching of the corresponding control points between the standard and individual vessels. Section 4 describes the 3D modelling of the individual vessel which is performed through a vessel warping with the corresponding control points. Experimental results of the vessel transformation are given in Section 5. Finally, we present the conclusion in Section 6.

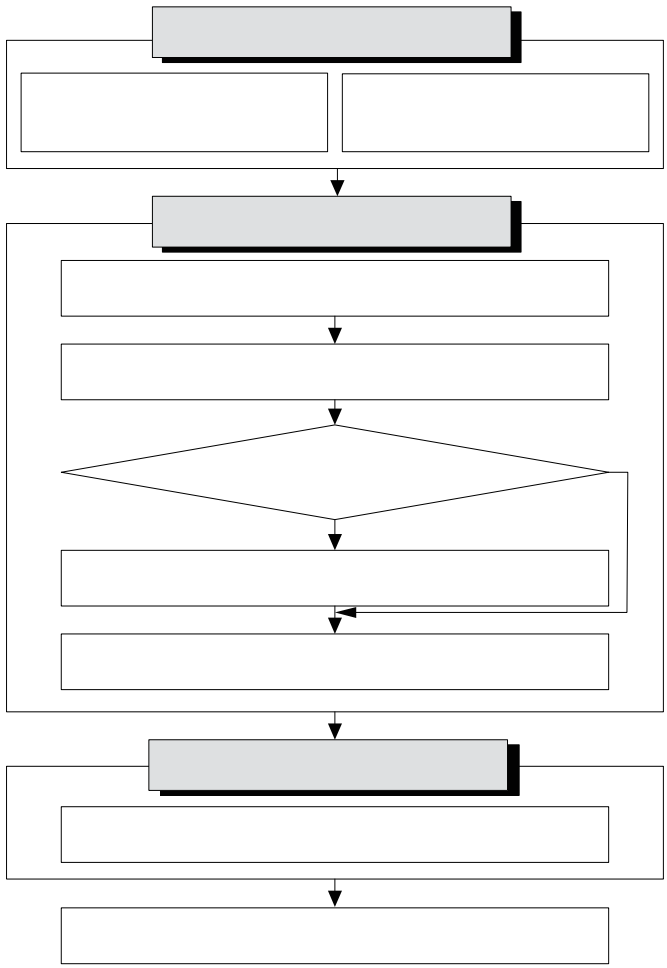

Fig. 1. Overall flow of the system configuration

2. Image Acquisition

We have generated a standard vessel because the shape of the arterial is different for each individual vessel, where the standard vessel can be adjusted to suit the individual vessel (Chalopin et al., 2001), (Lee et al., 2006) and (Lee et al., 2007). The proposed approach is based on a 3D model of standard vessel which is built from a database that implemented a Korean vascular system (Lee et al., 2006).
We have limited the scope of the main arteries for the 3D model of the standard vessel as depicted in Fig. 2.

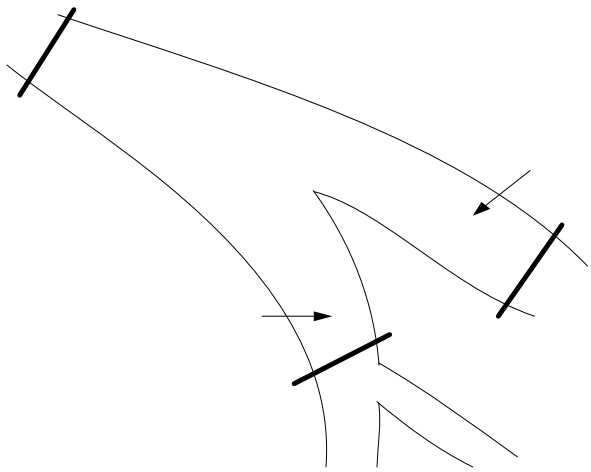

Fig. 2. Vessel scope of the database for the 3D model of the standard vessel

Table 1 shows the database of the coronary artery of Lt. main (Left Main Coronary Artery), LAD (Left Anterior Descending) and LCX (Left Circumflex artery) information. This database consists of 40 people with mixed gender information.

	age	Lt. main			LAD			LCX		
		Os	distal	length	Os	distal	length	Os	distal	length
below 60 years of old (male)	48.4±5.9	4.3±0.4	4.1±0.5	9.9±4.2	3.8±0.4	3.6±0.4	17.0±5.2	3.5±0.4	3.3±0.3	19.2±6.1
above 60 years of old (male)	67.5±5.4	4.5±0.5	4.4±0.4	8.4±3.8	3.9±0.3	3.6±0.3	17.2±5.8	3.6±0.4	3.4±0.4	24.6±8.9
below 60 years of old (female)	44.9±19.9	3.7±1.8	3.4±1.6	10.6±6.2	3.3±1.5	3.1±1.4	14.1±5.5	2.9±1.3	2.8±1.2	21.3±9.2
above 60 years of old (female)	70.7± 4.4	4.3±0.7	4.1±0.6	12.5±7.9	3.5±0.6	3.4±0.5	22.3±7.3	3.3±0.4	3.1±0.3	27.5±3.7

Table 1. Database of the coronary artery

To quantify the 3D model of the coronary artery, the angles of the vessel bifurcation are measured with references to LCX, Lt. main and LAD, as in Table 2. Ten individuals regardless of their gender and age were selected randomly for measuring the angles of the vessel bifurcation from six angiograms. The measurement results, and the average and standard deviations of each individual measurement are shown in Table 2.

	RAO30° CAUD30°	RAO30° CRA30°	AP0° CRA30°	LAO60° CRA30°	LAO60° CAUD30°	AP0° CAUD30°
1	69.17	123.31	38.64	61.32	84.01	50.98
2	53.58	72.02	23.80	51.75	99.73	73.92
3	77.28	97.70	21.20	57.72	100.71	71.33
4	94.12	24.67	22.38	81.99	75.6	69.57
5	64.12	33.25	31.24	40.97	135.00	61.87
6	55.34	51.27	41.8	80.89	119.84	57.14
7	71.93	79.32	50.92	87.72	114.71	58.22
8	67.70	59.14	31.84	58.93	92.36	70.16
9	85.98	60.85	35.77	54.45	118.80	78.93
10	47.39	60.26	34.50	47.39	67.52	34.79
Average	68.67	66.18	33.21	62.31	100.83	62.69
Standard deviation	14.56	29.07	9.32	15.86	21.46	13.06

Table 2. Measured angles of the vessel bifurcation from six angiographies

Fig. 3 illustrates the results of the 3D model generation of the standard vessel from six angiographies: RAO (Right Anterior Oblique)30° CAUD (Caudal)30°, RAO30° CRA (Cranial Anterior)30°, AP (Anterior Posterior)0° CRA (Cranial Anterior)30°, LAO (Left Anterior Oblique)60° CRA30°, LAO60° CAUD30°, AP0° CAUD30°.

View	RAO30° CAUD30°	RAO30° CRA30°	AP0° CRA30°
Angiogram			
3D Model	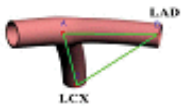	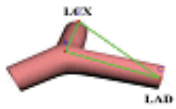	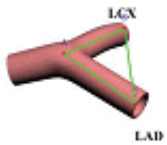
View	**LAO60° CRA30°**	**LAO60° CAUD30°**	**AP0° CAUD30°**
Angiogram	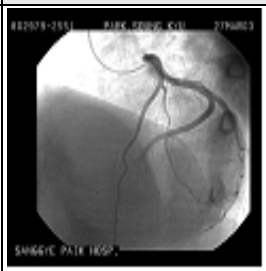		
3D Model	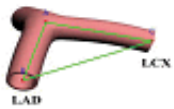	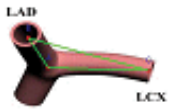	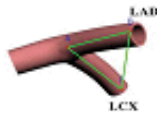

Fig. 3. 3D model generation of the standard vessel from six angiographies

Evaluating the angles of the vessel bifurcation from six angiographies can reduce the possible measurement error which occurs when the angle from a single view is measured.

It is difficult to transform the standard vessel into individual vessel in a 3D space (Lee et al., 2006) and (Lee et al., 2007). Therefore, we projected the 3D model of the standard vessel into 2D projection. Fig. 4 shows the projected images of the standard vessel on a 2D plane through the projection. The projection result can be view as vertices or polygons based.

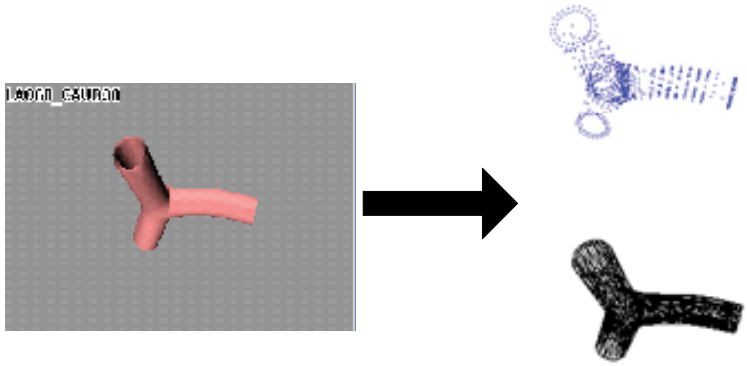

Fig. 4. Projection result for 2D image of standard vessel

3. Matching of the Adaptive Control Points

To transform a standard vessel into an individual vessel, it is important to match corresponding control points (Lee et al., 2006) and (Lee et al., 2007). In this paper, we extracted feature points of the vessel automatically and defined as control points (Lee et al., 2006) and (Lee et al., 2007). Feature points mean is referred to the corner points of an object or points with higher variance brightness compared to the surrounding pixels in an image, which are differentiated from other points in an image. Such feature points can be defined in many different ways in (Parker, 1996) and (Pitas, 2000). They are sometimes defined as points that have a high gradient in different directions, or as points that have properties that do not change in spite of specific transformations. Generally feature points can be divided into three categories (Cizek et al., 2004). The first one uses a non-linear filter, such as the SUSAN corner detector proposed by Smith (Woods et al., 1993) which relates each pixel to an area centered by a pixel. In this area, it is called the SUSAN area; all the pixels have similar intensities as the center pixel. If the center pixel is a feature point (some times a feature point is also referred to as a "corner"), SUSAN area is the smallest one among the pixels around it. A SUSAN corner detector can suppress a noise effectively without derivating an image. The second one is based on a curvature, such as the Kitchen and Rosenfeld's method (Maes et al., 1997). This kind of method needs to extract edges in advance, and then elucidate the feature points using the information on the curvature of the edges. The disadvantage of this method is required more needs a complicated computation, e.g. curve on fitting, thus its processing speed is relatively slow. The third method is exploits a change of the pixel intensity. A typical one is the Harris and Stephens' method (Pluim et al., 2003). It produces a corner response through an eigenvalues analysis. Since it does not need to use a slide window explicitly, its processing speed is very fast. Accordingly, this

paper used the Harris corner detector to find the control points of standard and individual vessels (Lee et al., 2006) and (Lee, 2007).

3.1 Extraction of the Control Points

The Harris corner detector is a popular interest point detector due to its strong invariance such as rotation, scale, illumination variation and image noise (Schmid et al., 2000) and (Derpanis, 2004). It is based on the local auto-correlation function of a signal. The local auto-correlation function measures the local changes of the signal with patches shifted by a small amount in different directions (Derpanis, 2004). However, the Harris corner detector has a problem where it can mistake those non-corner points.

Fig. 5 shows extracted 9 control points in individual vessel by using the Harris corner detector. We noticed that some of the extracted control points are non-corner points. To solve this problem of the Harris corner detector, we extracted more control points of individual vessel than standard vessel. Fig. 6 shows the extraction of control points from individual and standard vessels.

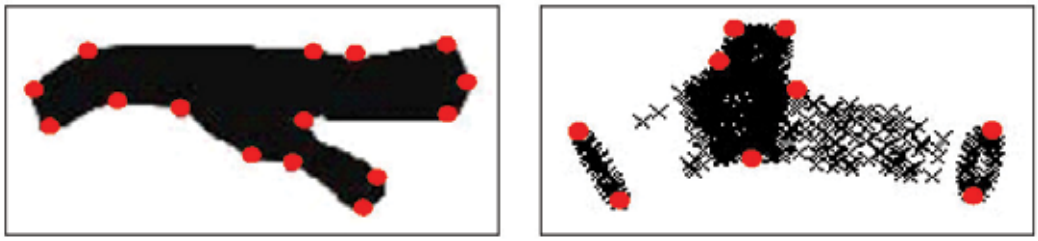

Fig. 5. Extracted 9 control points in individual vessel

3.2 Extraction of Corner Points

We performed thinning by using the structural characteristics of vessel to find the corner points among the control points of individual vessel which is extracted with the Harris corner detector (Lee, 2007). Fig. 7 shows the thinning process for detection of corner points in individual vessel.

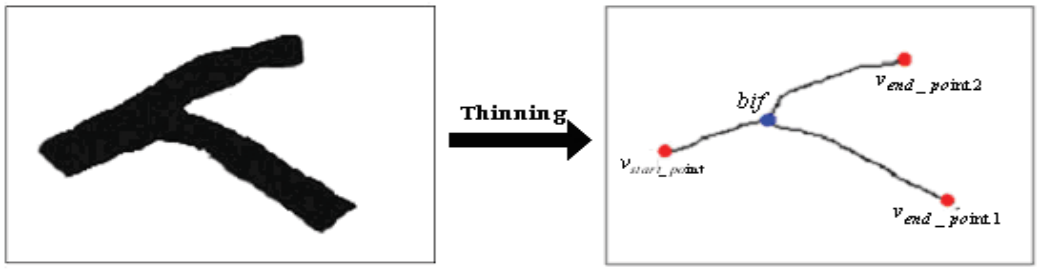

(a) Segmented vessel (b) Thinned vessel

Fig. 6. Thinning process for detection of corner points in individual vessel

A vascular tree can be divided into a set of elementary components, or primitives, which are the vascular segments, and bifurcation (Wahle et al., 1994). Using this intuitive

representation, it is natural to describe the coronary tree by a graph structure (Chalopin et al., 2001) and (Lee, 2007).
A vascular tree of thinned vessel consists of three vertices (v_{point}) and one bifurcation (bif) as the following equation (1). Here, vertices (v_{point}) are comprised a start point (v_{start_point}) and two end points ($v_{end\_point1}, v_{end\_point2}$).

$$I_{thin} = \{ v_{point}, bif \}$$
$$v_{point} = \{ v_{start\_point}, v_{end\_point1}, v_{end\_point2} \} \quad (1)$$

If the reference point is a vertex, the closest two control points to the vertex are defined as the corner points. If the reference point is a bifurcation, the three control points that are closest to it after comparing the distances between the bifurcation and all control points are defined as the corner points. As shown in Fig. 7, if the reference point is the vertex (v_{start_point}), v_1 and v_2 become the corner points; if the reference point is the bifurcation (bif), v_6, v_{11} and v_{15} become the corner points (Lee, 2007).

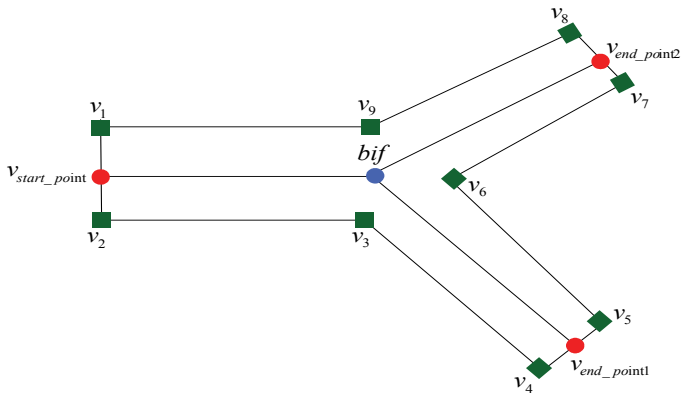

Fig. 7. Primitives of a vascular net

3.3 Adaptive Interpolation of the Control Points between Corner Points

Once the control points and corner points are extracted from an individual vessel, an interpolation for a standard vessel is applied. For an accurate matching, the control points are adaptively interpolated into the corresponding standard vessel in proportion to the distance ratio if there are control points between the corner points in an individual vessel (Lee, 2007).
Fig. 8 shows the process of an interpolation of the control points. Control points of a standard vessel are adaptively interpolated by the distance rate between control point (v_3) and two corner points (v_2, v_4) of an individual vessel. Fig. 8 (a) shows the extracted control

points from an individual vessel, and (b) shows an example of control point interpolated between a standard vessel and the corresponding corner points from (a) image.

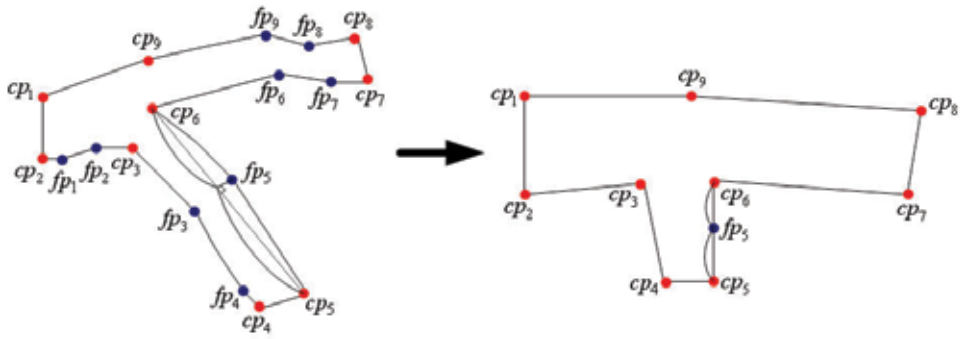

(a) Individual vessel (b) Standard vessel

Fig. 8. Interpolation of the control points for a standard vessel

Fig. 9 shows the result of extracting the control points by using the Harris corner detector to the segmented vessel in the individual vessel and an adaptive interpolation of the corresponding the control points in the standard vessel.

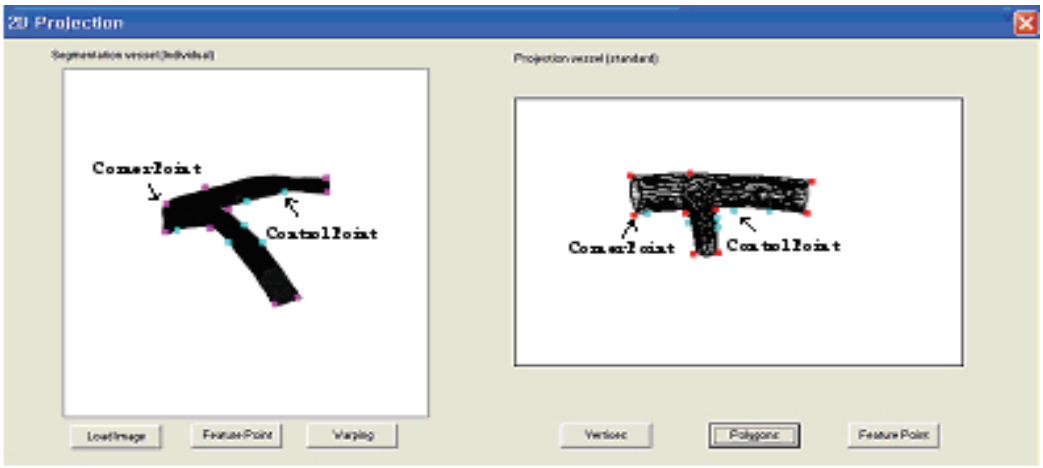

Fig. 9. Result of an adaptive interpolation of the corresponding control points

4. Vessel Warping

We have warped the standard vessel with respect to the individual vessel. Given the two sets of corresponding control points, $S = \{s_1, s_2, \ldots s_m\}$ and $I = \{i_1, i_2, \ldots i_m\}$, the warping is applied the standard vessel to suit the individual vessel. Here, S is a set of control points in the standard vessel and I is a set of one in the individual vessel (Lee et al., 2006) and (Lee et al., 2007).

Standard vessel warping was performed using the TPS (Thin-Plate-Spline) algorithm (Bentoutou et al., 2002) from the two sets of control points.
The TPS is the interpolation functions that exactly represent a distortion at each feature point, and for defining a minimum curvature surface between control points. A TPS function is a flexible transformation that allows for a rotation, translation, scaling, and skewing. It also allows for lines to bend according by the TPS model (Bentoutou et al., 2002). Therefore, a large number of deformations can be characterized by the TPS model.
The TPS interpolation function can be written as equation (2).

$$h(x) = Ax + t + \sum_{i=1}^{m} W_i K(\| x - x_i \|) \tag{2}$$

The variables A and t are the affine transformation parameters matrices, W_i are the weights of the non-linear radial interpolation function K , and x_i are the control points. The function $K(r)$ is the solution of the biharmonic equation $(\Delta^2 K = 0)$ that satisfies the condition of a bending energy minimization, namely $K(r) = r^2 \log(r^2)$.
The complete set of parameters, the interpolating registration transformation is defined, and then it is used to transform the standard vessel. It should be noted that in order to be able to carry out the warping of the standard vessel with respect to the individual vessel, it is required to have a complete description of the TPS interpolation function (Lee et al., 2006) and (Lee et al., 2007).
Fig. 10 shows the results of modifying the standard vessel to suit the individual vessel.

(a) Individual vessel (b) Standard vessel (c) Warped vessel
Fig. 10. Results of the warped vessel in standard vessel

5. Results of the Vessel Transformation

We simulated the system environment that is Microsoft Windows XP on a Pentium 3GHz, Intel Corp. and the compiler VC++ 6.0 is used. The image of 512× 512 is used for the experimentation. Each image has a gray-value resolution of 8 bits, i.e., 256 gray levels.
Fig. 11 shows the 3D model of the standard vessel from six different angiographic views. The results of the standard vessel warping using TPS algorithm to suit the individual vessel is shown in Fig. 13.

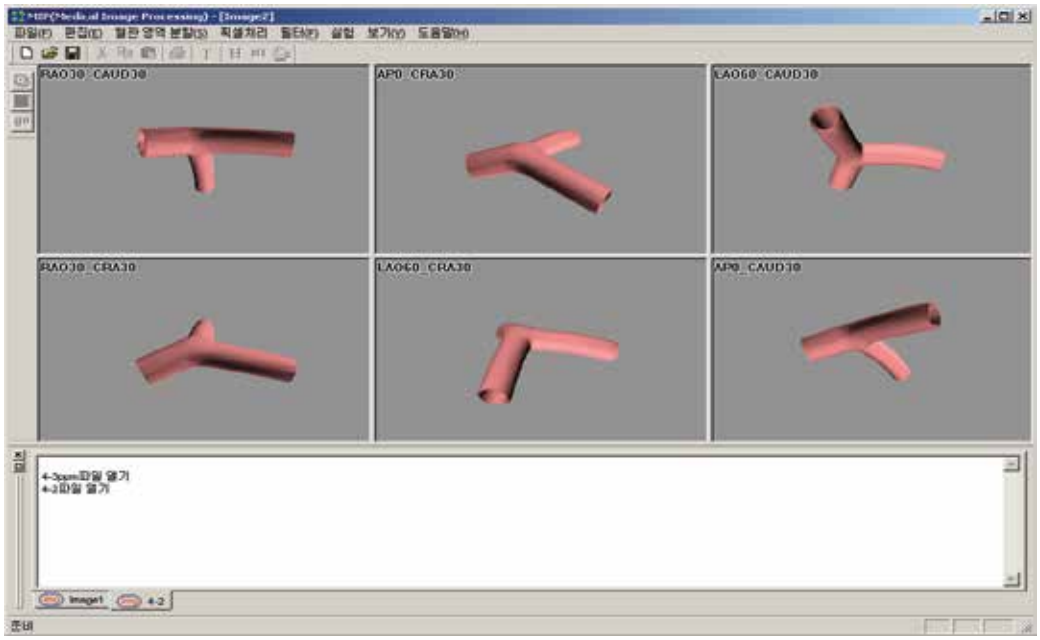

Fig. 11. 3D model of the standard vessel in angiographic of six different views

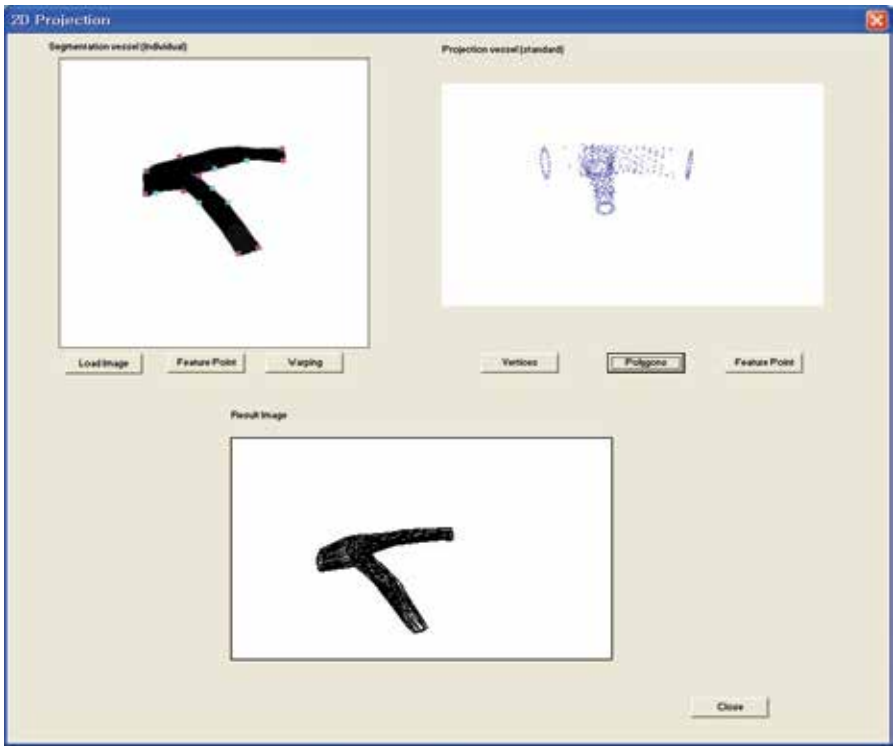

Fig. 12. Result of standard vessel warping

Fig. 13 shows the result for an automatically 3D model generation of individual vessel.

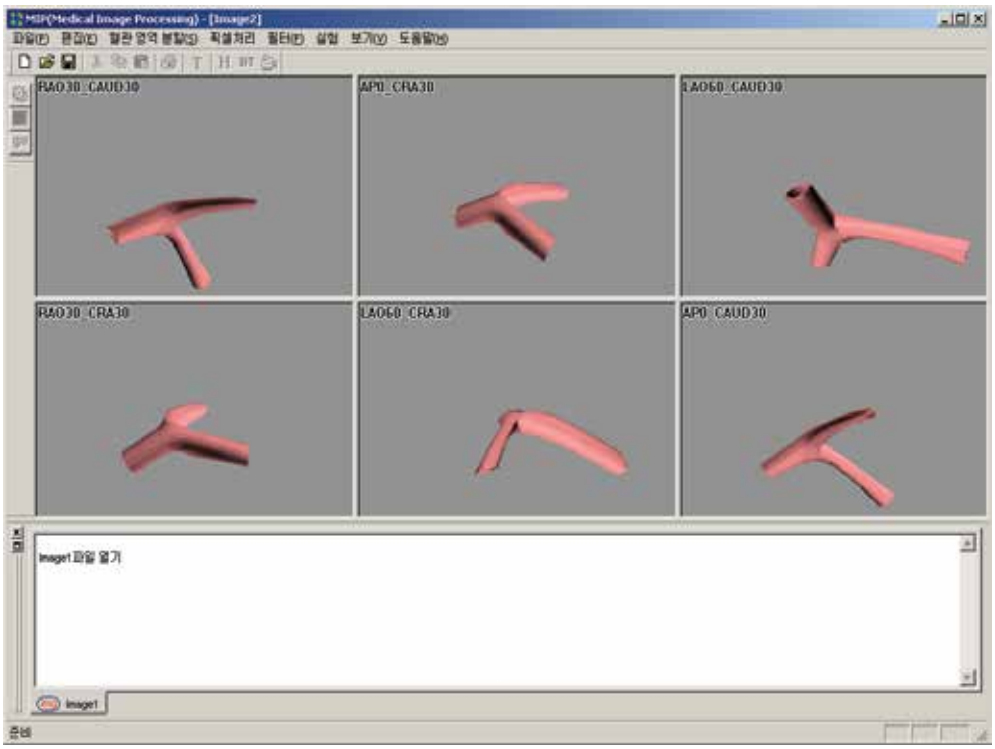

Fig. 13. Result of 3D model generation for the individual vessel in six views

6. Conclusion

We proposed a fully automatic and effective algorithm to perform a 3D modelling of individual vessel from angiograms in six views. This approach can be used to recover the geometry of the main arteries. The 3D model of the vessel enables patients to visualize their progress and improvement for a disease. Such a model should not only enhance the level of reliability but also provide a fast and accurate identification. In order words, this method can be expected to reduce the number of misdiagnosed cases (Lee et al., 2006) and (Lee et al., 2007).

7. Acknowledgement

"This Work was supported by Soongsil University and Korea Research Foundation Grant (KRF-2006-005-J03801) Funded by Korean Government."

8. References

A, Venot.; J.F, Lebruchec. & J.C, Roucayrol. (1984). A new class of similarity measures for robust image registration, *Comput. Vision Graph. Image Process,* pp. 176-184.

A, Wahle.; E, Wellnhofer.; I, Mugaragu.;H.U, Sauer.; H, Oswald. & E, Fleck. (1994). Accurate 3-D reconstruction and statistics for assessment of diffuse coronary artery disease, *Computers in Cardiology*, IEEE Computer Society, Los Alamitos, CA, pp.669-672

B.G, Brown.; E, Bolson.; M, Frimer. & H, Dodge. (1977). Quantitative coronary arteriography estimation of dimensions, hemodynamic resistance, and atheroma mass of coronary artery lesions using the arteriogram and digital computation, *Circulation*, vol. 55, pp. 329-337

C, Blondel.; R, Vaillant.; F, Devernary. ; G, Malandain. & N, Ayache. (2002). Automatic trinocular 3D reconstruction of coronary artery centerlines from rotational X-ray angiography, *Computer Assisted Radiology and Surgery 2002 Proceedings*, Paris, June 2002, Springer Publishers, Heidelberg

Claire, Chalopin.; Gerard, Finet. & Isabelle E, Magnin. (2001). Modeling the 3D coronary tree for labeling purposes. *Medical Image Analysis*, pp.301-315

Chris, Harris. & Mike, Stephens. (1988). A combined corner and edge detector, *Proceedings of the Fourth Alvey Vision Conference*, pp.147-151, Manchester

C, Lorenz.; S, Renisch.; S, Schlatholter. & T, Bulow. (2003). Simultaneous Segmentation and Tree Reconstruction of the Coronary Arteries in MSCT Images*, Int. Symposium Medical Imaging, San Diego, Proc. SPIE* Vol. 5032, pp. 167-177

C, Schmid.; R, Mohr. & C, Bauckhage. (2000). Evaluation of interest point detectors. *International Journal of Computer Vision*, pp. 151-172

F.L, Bookstein. (1989). Principal warps: thin-plate splines and the decomposition of deformations, *IEEE-PAMI* 11, pp. 567-585

F, Maes.; A, Collignon.; G, Marchal. & P, Suetens. (1997). Multimodality image registration by maximization of mutual information, IEEE Transaction on Medical Imaging, Vol. 16, No. 2, pp.187-198

Holger, Schmitt.; Michael, Grass.; Rolf, Suurmond.; Thomas Kohler.; Volker, Rasche.; Stefan, Hahnel. & Sabine, Heiland. (2005). Reconstruction of blood propagation in three-dimensional rotational X-ray angiography. *Computerized Medical Imaging and Graphics*, 29, pp. 507-520

I, Pitas. (2000). *Digital image processing algorithms and applications, 1st Ed.*, John Wiley & Sons, Inc., ISBN 0471377392, New York

J.C, Messenger.; S.Y,Chen.; J.D, Carroll.; J.E, Burchenal.; K, Kioussopoulos. & B.M, Groves. (2000). 3D coronary reconstruction from routine single-place coronary angiograms: clinical validation and quantitative analysis of the right coronary artery in 100 patients, *The International Journal of Cardiac Imaging* 16(6), pp.413-427

J, Cizek.; K, Herholz.; S, Vollmar.; R, Schrader.; J, Klein. & W.D, Heiss. (2004). Fast and robust registration of PET and MR image of human brin, Neuroimage, Vol. 22, Iss. 1, pp.434-442

J, Flusser. & T,Suk. (1998). Degraded image analysis: an invariant approach*, IEEE Trans. Pattern Anal. Mach. Intell*, pp. 590-603

Jianbo, Shi. & Carlo, Tomasi. (1994). Good features to track, *IEEE Conference on CVPR Seattle*, pp. 593-600

J.P.W, Pluim.; J.B.A, Maintz. & M.A, Viergever. (2003). Mutual information based registration of medical images: a survey, IEEE Transactions on Medical Imaging, Vol. 22, No. 8, pp. 986-1004

J.R, Parker. (1996). *Algorithms for image processing and computer vision, 1st Ed.*, John Wiley & Sons, Inc., IBSN 0471140562, USA

J, Ross. et al. (1987). Guidelines for coronary angiography, *Circulation*, vol.76

K, Derpanis. (2004). The Harris corner detector

M, Grass.; R, Koppe.; E, Klotz.; R, Proksa.; MH, Kuhn.; H, Aerts. & etc (1999). 3D reconstruction of high contrast objects using C-arm image intensifier projection data, *Computer Med Imaging Graphics*, 23(6):311-321

M, Grass.; R, Koppe.; E, Klotz.; Op de Beek J. & R, Kemkers. (1999). 3D reconstruction and imaging based on C-arm systems, *Med Biol Eng Comput*, 37(2):1520-1

M, Grass.; R, Guillemaud.; R, Koppe.; E, Klotz.; V, Rasche. & Op de Beek J. (2002). *La radiologie tridimensionelle, La tomography medicale-imagerie morphologique et imagerie fonctionelle*, Hermes Science Publications, Paris

Na-Young, Lee.; Gye-Young, Kim. & Hyung-Il, Choi. (2006). Automatic generation technique of three-dimensional model corresponding to individual vessels, *Computational Science and Its Applications-ICCSA 2006*, LNCS 3984, PP.441-449, Glasgow, UK, May 2006, Springer-Verlag Berlin Heidelberg

Na-Young, Lee. (2006). An automatic generating technique of individual vessels based on general vessels, *The 7th International Workshop on Image Analysis for Multimedia Interactive Services*, pp.241-244, Korea, April, 2006, Incheon

NaYoung, Lee.; JeongHee, Cha.; JinWook, On.; GyeYoung, Kim. & HyungIl, Choi. (2006). An automatic generation technique of 3D vessels model form angiograms, *Proceedings of The 2006 International Conference on Image Processing, Computer Vision, & Pattern Recognition*, pp.371-376, USA, June, 2006, CSREA Press, Las Vegas

Na-Young, Lee. (2007). Automatic generation of 3D vessels model using vessels image matching based on adaptive control points, *Sixth International Conference on Advanced Language Processing and Web Information Technology*, pp.265-270, ISBN 0-7695-2930-5, China, August 2007, IEEE Computer Society, Luoyang, Henan

Na-Young, Lee.; Gye-Young, Kim. & Hyung-Il, Choi. (2007). 3D modelling of the vessels from X-ray angiography, *Digital Human Modeling, HCII 2007*, LNCS 4561, pp.646-654, IBSN 978-3-540-73318-8 , Springer Berlin Heidelberg

Na-Young, Lee.; Gye-Young, Kim. & Hyung-Il, Choi. (2007). 3D model of vessels from angiograms, *Proceedings of the 13th Japan-Korea join workshop on frontiers of computer vision*, pp.235-240, Korea, January 2007, Busan

Na-Young, Lee. (2007). Three Dimensional Modeling of Individual Vessels Based on Matching of Adaptive Control Points, *MICAI 2007: Advances in Artificial Intelligence*, LNAI 4827, pp. 1143–1150, Springer-Verlag Berlin Heidelberg

P, de Feyter.; J, Vos.; J, Reiber. & P, Serruys. (1993). Value and limitations of quantitative coronary angiography to assess progression and regression of coronary atherosclerosis. *In Advances in Quantitative Coronary Arteriography*, pp. 255-271

R.P, Woods.; J.C, Mazziotta. & S.R, Cherry. (1993). MRI-PET registration with automated algorithm, *Journal of computer assisted tomography.* Vol. 17:44, pp.536-546

Y, Bentoutou.; N, Taleb.; M, Chikr El Mezouar, M, Taleb. & L, Jetto. (2002). An invariant approach for image registration in digital subtraction angiography. *Pattern Recognition*, Vol. 35, Iss. 12, December 2002, pp. 2853-2865

2

Adaptive Estimation and Control for Systems with Parametric and Nonparametric Uncertainties

Hongbin Ma* and Kai-Yew Lum†
Temasek Laboratories, National University of Singapore
*tslmh@nus.edu.sg**
tsllumky@nus.edu.sg†

Abstract

Adaptive control has been developed for decades, and now it has become a rigorous and mature discipline which mainly focuses on dealing parametric uncertainties in control systems, especially linear parametric systems. Nonparametric uncertainties were seldom studied or addressed in the literature of adaptive control until new areas on exploring limitations and capability of feedback control emerged in recent years. Comparing with the approach of robust control to deal with parametric or nonparametric uncertainties, the approach of adaptive control can deal with relatively larger uncertainties and gain more flexibility to fit the unknown plant because adaptive control usually involves adaptive estimation algorithms which play role of "learning" in some sense.

This chapter will introduce a new challenging topic on dealing with both parametric and nonparametric internal uncertainties in the same system. The existence of both two kinds of uncertainties makes it very difficult or even impossible to apply the traditional recursive identification algorithms which are designed for parametric systems. We will discuss by examples why conventional adaptive estimation and hence conventional adaptive control cannot be applied directly to deal with combination of parametric and nonparametric uncertainties. And we will also introduce basic ideas to handle the difficulties involved in the adaptive estimation problem for the system with combination of parametric and nonparametric uncertainties. Especially, we will propose and discuss a novel class of adaptive estimators, i.e. *information-concentration (IC) estimators*. This area is still in its infant stage, and more efforts are expected in the future for gainning comprehensive understanding to resolve challenging difficulties.

Furthermore, we will give two concrete examples of semi-parametric adaptive control to demonstrate the ideas and the principles to deal with both parametric and nonparametric uncertainties in the plant. (1) In the first example, a simple first-order discrete-time nonlinear system with both kinds of internal uncertainties is investigated, where the uncertainty of non-parametric part is characterized by a Lipschitz constant L, and the nonlinearity of parametric part is characterized by an exponent index b. In this example, based on the idea of the IC estimator, we construct a unified adaptive controller in both cases of $b = 1$ and

$b > 1$, and its closed-loop stability is established under some conditions. When the parametric part is bilinear ($b = 1$), the conditions given reveal the magic number $\frac{3}{2}+\sqrt{2}$ which appeared in previous study on capability and limitations of the feedback mechanism. (2) In the second example with both parametric uncertainties and non-parametric uncertainties, the controller gain is also supposed to be unknown besides the unknown parameter in the parametric part, and we only consider the noise-free case. For this model, according to some *a priori* knowledge on the non-parametric part and the unknown controller gain, we design another type of adaptive controller based on a gradient-like adaptation law with time-varying deadzone so as to deal with both kinds of uncertainties. And in this example we can establish the asymptotic convergence of tracking error under some mild conditions, althouth these conditions required are not as perfect as in the first example in sense that $L < 0.5$ is far away from the best possible bound $\frac{3}{2}+\sqrt{2}$.

These two examples illustrate different methods of designing adaptive estimation and control algorithms. However, their essential ideas and principles are all based on the *a priori* knowledge on the system model, especially on the parametric part and the non-parametric part. From these examples, we can see that the closed-loop stability analysis is rather nontrivial. These examples demonstrate new adaptive control ideas to deal with two kinds of internal uncertainties simultaneously and illustrates our elementary theoretical attempts in establishing closed-loop stability.

1. Introduction

This chapter will focus on a special topic on adaptive estimation and control for systems with parametric and nonparametric uncertainties. Our discussion on this topic starts with a very brief introduction to adaptive control.

1.1 Adaptive Control

As stated in [SB89], "Research in adaptive control has a long and vigorous history" since the initial study in 1950s on adaptive control which was motivated by the problem of designing autopilots for air-craft operating at a wide range of speeds and altitudes. With decades of efforts, adaptive control has become a rigorous and mature discipline which mainly focuses on dealing parametric uncertainties in control systems, especially linear parametric systems.

From the initial stage of adaptive control, this area has been aiming at study how to deal with *large uncertainties* in control systems. This goal of adaptive control essentially means that one adaptive control law cannot be a *fixed* controller with fixed structure and fixed parameters because any fixed controller usually can only deal with *small uncertainties* in control systems. The fact that most fixed controllers with certain structure (e.g. linear feedback control) designed for an exact system model (called *nominal model*) can also work for a small range of changes in the system parameter is often referred to as *robustness*, which is the kernel concept of another area, *robust control*. While robust control focuses on studying the stability margin of fixed controllers (mainly linear feedback controller), whose

design essentially relies on priori knowledge on exact nominal system model and bounds of uncertain parameters, adaptive control generally does not need a priori information about the bounds on the uncertain or (slow) time-varying parameters. Briefly speaking, comparing with the approach of robust control to deal with parametric or nonparametric uncertainties, the approach of adaptive control can deal with relatively larger uncertainties and gain more flexibility to fit the unknown plant because adaptive control usually involves adaptive estimation algorithms which play role of "learning" in some sense.
The advantages of adaptive control come from the fact that adaptive controllers can adapt themselves to modify the control law based on estimation of unknown parameters by recursive identification algorithms. Hence the area of adaptive control has close connections with system identification, which is an area aiming at providing and investigating mathematical tools and algorithms that build dynamical models from measured data. Typically, in system identification, a certain model structure is chosen by the user which contains unknown parameters and then some recursive algorithms are put forward based on the structural features of the model and statistical properties of the data or noise. The methods or algorithms developed in system identification are borrowed in adaptive control in order to estimate the unknown parameters in the closed loop. For convenience, the parameter estimation methods or algorithms adopted in adaptive control are often referred to as *adaptive estimation* methods. Adaptive estimation and system identification share many similar characteristics, for example, both of them originate and benefit from the development of statistics. One typical example is the frequently used least-squares (LS) algorithm, which gives parameter estimation by minimizing the sum of squared errors (or residuals), and we know that LS algorithm plays important role in many areas including statistics, system identification and adaptive control. We shall also remark that, in spite of the significant similarities and the same origin, adaptive estimation is different from system identification in sense that adaptive estimation serves for adaptive control and deals with dynamic data generated in the closed loop of adaptive controller, which means that statistical properties generally cannot be guaranteed or verified in the analysis of adaptive estimation. This unique feature of adaptive estimation and control brings many difficulties in mathematical analysis, and we will show such difficulties in later examples given in this paper.

1.2 Linear Regression Model and Least Square Algorithm

Major parts in existing study on regression analysis (a branch of statistics) [DS98, Ber04, Wik08j], time series analysis [BJR08, Tsa05], system identification [Lju98, VV07] and adaptive control [GS84, AW89, SB89, CG91, FL99] center on the following linear regression model

$$z_k = \theta^\tau \phi_k + v_k \tag{1}$$

where $\{z_k\}$, ϕ_k, v_k represent observation data, regression vector and noise disturbance (or external uncertainties), respectively. Here θ is the unknown parameter to be estimated. Linear regression models have many applications in many disciplines of science and engineering [Wik08g, web08, DS98, Hel63, Wei05, MPV07, Fox97, BDB95]. For example, as

stated in [web08], *Linear regression is probably the most widely used, and useful, statistical technique for solving environmental problems. Linear regression models are extremely powerful, and have the power to empirically tease out very complicated relationships between variables.* Due to the importance of model (1.1), we list several simple examples for illustration:

• Assume that a series of (stationary) data (x_k, y_k) $(k = 1, 2, \cdots, N)$ are generated from the following model

$$Y = \beta_0 + \beta_1 X + \varepsilon$$

where β_0 , β_1 are unknown parameters, $\{x_k\}$ are i. i. d. taken from a certain probability distribution, and $\varepsilon_k \approx N(0, \sigma^2)$ is random noise independent of X . For this model, let $\theta = [\beta_0, \beta_1]^\tau$, $\varphi_k = [1, x_k]^\tau$, then we have $y_k = \theta^\tau \phi_k + \varepsilon_k$. This example is a classic topic in statistics to study the statistical properties of parameter estimates $\hat{\theta}_N$ as the data size N grows to infinity. The statistical properties of interests may include $\mathrm{E}(\hat{\theta} - \theta), \mathrm{Var}(\hat{\theta})$, and so on.

• Unlike the above example, in this example we assume that x_k and x_{k+1} have close relationship modeled by

$$x_{k+1} = \beta_0 + \beta_1 x_k + \varepsilon_k$$

where β_0, β_1 are unknown parameters, and $\varepsilon_k \approx N(0, \sigma^2)$ are i. i. d. random noise independent of $\{x_1, x_2, \cdots, x_k\}$.

This model is an example of linear time series analysis, which aims to study asymptotic statistical properties of parameter estimates $\hat{\theta}_N$ under certain assumptions on statistical properties of ε_k . Note that for this example, it is possible to deduce an explicit expression of x_k in terms of ε_j $(j = 0,1,\cdots,k-1)$.

• In this example, we consider a simple control system

$$x_{k+1} = \beta_0 + \beta_1 x_k + b u_k + \varepsilon_k$$

where $b \neq 0$ is the controller gain, ε_k is the noise disturbance at time step k. For this model, in case where b is known *a priori*, we can take; $\theta = [\beta_0, \beta_1]^\tau$, $\phi_k = [1, x_{k-1}]^\tau$, $z_k = x_k - b u_{k-1}$;otherwise, we can take $\theta = [\beta_0, \beta_1, b]^\tau$, $\phi_k = [1, x_{k-1}]^\tau$, $z_k = x_k - b u_{k-1}$. In both cases, the system can be rewritten as

$$z_k = \theta^\tau \phi_k + \varepsilon_k$$

which implies that intuitively, θ can be estimated by using the identification algorithm since both data z_k and ϕ_k are available at time step k. Let $\hat{\theta}_k$ denote the parameter estimates at time step $\hat{\theta}_k$, then we can design the control signal u_k by regarding as the real parameter θ:

$$u_k = \frac{1}{\hat{b}}[r_{k+1} - \hat{\beta}_0 - \hat{\beta}_1 x_k]$$

where $\{r_k\}$ is the known reference signal to be tracked, and $\hat{b}$, $\hat{\beta}_0$, $\hat{\beta}_1$ are estimates of b, β_0, β_1, respectively. Note that for this example, the closed-loop system will be very complex because the data generated in the closed loop essentially depend on all history signals. In the closed-loop system of an adaptive controller, generally it is difficult to analyze or verify statistical properties of signals, and this fact makes that adaptive estimation and control cannot directly employ techniques or results from system identification. Now we briefly introduce the frequently-used LS algorithm for model (1.1) due to its importance and wide applications [LH74, Gio85, Wik08e, Wik08f, Wik08d]. The idea of LS algorithm is simply to minimize the sum of squared errors, that is to say,

$$\hat{\theta}_n^{LS} \triangleq \arg\min_{\zeta} \sum_{k=1}^{n} [z_k - \zeta^\tau \phi_k]^\tau [z_k - \zeta^\tau \phi_k] \tag{1.2}$$

This idea has a long history rooted from great mathematician Carl Friedrich Gauss in 1795 and published first by Legendre in 1805. In 1809, Gauss published this method in volume two of his classical work on celestial mechanics, *heoria Motus Corporum Coelestium in sectionibus conicis solem ambientium*[Gau09], and later in 1829, Gauss was able to state that the LS estimator is optimal in the sense that in a linear model where the errors have a mean of zero, are uncorrelated, and have equal variances, the best linear unbiased estimators of the coefficients is the least-squares estimators. This result is known as the Gauss-Markov theorem [Wik08a].

By Eq. (1.2), at every time step, we need to minimize the sum of squared errors, which requires much computation cost. To improve the computational efficiency, in practice we often use the recursive form of LS algorithm, often referred to as *recursive LS algorithm*, which will be derived in the following. First, introducing the following notations

$$Z_n = \begin{bmatrix} z_1^\tau \\ \vdots \\ z_n^\tau \end{bmatrix}, \quad \Phi_n = \begin{bmatrix} \phi_1^\tau \\ \vdots \\ \phi_n^\tau \end{bmatrix}, \quad V_n = \begin{bmatrix} v_1^\tau \\ \vdots \\ v_n^\tau \end{bmatrix}, \tag{1.3}$$

and using Eq. (1.1), we obtain that

$$Z_n = \Phi_n \theta + V_n.$$

Noting that

$$\begin{aligned}
& \sum_{k=1}^{n}[z_k-\zeta^\tau\phi_k]^\tau[z_k-\zeta^\tau\phi_k] \\
= \; & [Z_n-\Phi_n\zeta]^\tau[Z_n-\Phi_n\zeta] \\
= \; & Z_n\tau Z_n-2\Phi_n\zeta+\zeta^\tau\Phi_n^\tau\Phi_n\zeta \\
= \; & [\zeta-(\Phi_n^\tau\Phi_n)^+\Phi_n^\tau Z_n]^\tau\Phi_n^\tau\Phi_n[\zeta-(\Phi_n^\tau\Phi_n)^+\Phi_n^\tau Z_n] \\
& +Z_n^\tau[I-\Phi_n(\Phi_n^\tau\Phi_n)^+\Phi_n^\tau]Z_n
\end{aligned}$$

where the last equation is derived from properties of Moore-Penrose pseudoinverse [Wik08h]

$$\Phi_n^\tau=\Phi_n^\tau\Phi_n\Phi_n^+=\Phi_n^\tau\Phi_n(\Phi_n^\tau\Phi_n)^+\Phi_n^\tau$$

we know that the minimum of $[Z_n-\Phi_n\zeta]^\tau[Z_n-\Phi_n\zeta]$ can be achieved at

$$\hat{\theta}_n^{LS}=(\Phi_n^\tau\Phi_n)^+\Phi_n^\tau Z_n \tag{1.4}$$

which is the LS estimate of θ. Let

$$P_n \triangleq (\Phi_n^\tau\Phi_n)^+$$

and then, by Eq. (1.3), with the help of matrix inverse identity

$$[A^{-1}+A^{-1}B^\tau C^{-1}BA^{-1}]^{-1}=A-B^\tau(C+BA^{-1}B^\tau)^{-1}B$$

we can obtain that

$$\begin{aligned}
P_n &= (P_{n-1}{}^{-1}+\phi_n\phi_n^\tau)^{-1} \\
&= [A^{-1}+A^{-1}B^\tau C^{-1}BA^{-1}]^{-1} \\
&= P_{n-1}-(P_{n-1}\phi_n)[1+(\phi_n^\tau P_{n-1})P_{n-1}^{-1}(P_{n-1}\phi_n)]^{-1}(\phi_n^\tau P_{n-1}) \\
&= P_{n-1}-a_nP_{n-1}\phi_n\phi_n^\tau P_{n-1}
\end{aligned}$$

where

$$a_n=(1+\phi_n^\tau P_{n-1}\phi_n)^{-1}$$

Further,

$$
\begin{aligned}
\hat{\theta}_n &= P_n \sum_{k=1}^{n} \phi_k z_k^\tau \\
&= [P_{n-1} - a_n P_{n-1}\phi_n\phi_n^\tau P_{n-1}][\sum_{k=1}^{n-1} \phi_k z_k^\tau + \phi_n z_n^\tau] \\
&= \hat{\theta}_{n-1} - a_n P_{n-1}\phi_n\phi_n^\tau P_{n-1}\hat{\theta}_{n-1} + P_{n-1}\phi_n z_n^\tau - a_n P_{n-1}\phi_n\phi_n^\tau P_{n-1}\phi_n z_n^\tau \\
&= \hat{\theta}_{n-1} - a_n P_{n-1}\phi_n\phi_n^\tau P_{n-1}\hat{\theta}_{n-1} + P_{n-1}\phi_n[1 - a_n\phi_n^\tau P_{n-1}\phi_n] z_n^\tau \\
&= \hat{\theta}_{n-1} - a_n P_{n-1}\phi_n\phi_n^\tau P_{n-1}\hat{\theta}_{n-1} + a_n P_{n-1}\phi_n z_n^\tau \\
&= \hat{\theta}_{n-1} + a_n P_{n-1}\phi_n(z_n^\tau - \phi_n^\tau\theta_{n-1})
\end{aligned}
$$

Thus, we can obtain the following recursive LS algorithm

$$\hat{\theta}_n = \hat{\theta}_{n-1} + a_n P_{n-1}\phi_n(z_n^\tau - \phi_n^\tau\theta_{n-1})$$

where P_{n-1} and θ_{n-1} reflect only information up to step $n-1$, while a_n, ϕ_n and $z_n^\tau - \phi_n^\tau\theta_{n-1}$ reflect information up to step n.

In statistics, besides linear parametric regression, there also exist generalized linear models [Wik08b] and non-parametric regression methods [Wik08i], such as kernel regression [Wik08c]. Interested readers can refer to the wiki pages mentioned above and the references therein.

1.3 Uncertainties and Feedback Mechanism

By the discussions above, we shall emphasize that, in a certain sense, linear regression models are kernel of classical (discrete-time) adaptive control theory, which focuses to cope with the parametric uncertainties in linear plants. In recent years, parametric uncertainties in nonlinear plants have also gained much attention in the literature[MT95, Bos95, Guo97, ASL98, GHZ99, LQF03]. Reviewing the development of adaptive control, we find that parametric uncertainties were of primary interests in the study of adaptive control, no matter whether the considered plants are linear or nonlinear. Nonparametric uncertainties were seldom studied or addressed in the literature of adaptive control until some new areas on understanding limitations and capability of feedback control emerged in recent years. Here we mainly introduce the work initiated by Guo, who also motivated the authors' exploration in the direction which will be discussed in later parts.

Guo's work started from trying to understand fundamental relationship between the uncertainties and the feedback control. Unlike traditional adaptive theory, which focuses on investigating closed-loop stability of certain types of adaptive controllers, Guo began to think over a general set of adaptive controllers, called *feedback mechanism*, i.e., all possible feedback control laws. Here the feedback control laws need not be restricted in a certain class of controllers, and any series of mappings from the space of history data to the space of control signals is regarded as a feedback control law. With this concept in mind, since the most fundamental concept in automatic control, *feedback*, aims to reduce the effects of the

plant uncertainty on the desired control performance, by introducing the set *F* of internal uncertainties in the plant and the whole feedback mechanism *U*, we wonder the following basic problems:

1. Given an uncertainty set *F*, does there exist any feedback control law in *U* which can stabilize the plant? This question leads to the problem of how to characterize the maximum capability of feedback mechanism.
2. If the uncertainty set *F* is too large, is it possible that any feedback control law in *U* cannot stabilize the plant? This question leads to the problem of how to characterize the limitations of feedback mechanism.

The philosophical thoughts to these problems result in fruitful study [Guo97, XG00, ZG02, XG01, LX06, Ma08a, Ma08b].

The first step towards this direction was made in [Guo97], where Guo attempted to answer the following question for a nontrivial example of discrete-time nonlinear polynomial plant model with parametric uncertainty: What is the largest nonlinearity that can be dealt with by feedback? More specifically, in [Guo97], for the following nonlinear uncertain system

$$y_{t+1} = \theta\phi_t + u_t + w_{t+1}, \quad \phi_t = O(y_t^b), \qquad b > 0 \tag{1.5}$$

where θ is the unknown parameter, b characterizes the nonlinear growth rate of the system, and $\{w_t\}$ is the Gaussian noise sequence, a critical stability result is found — system (1.5) is not a.s. globally stabilizable if and only if $b \geq 4$. This result indicates that there exist limitations of the feedback mechanism in controlling the discrete-time nonlinear adaptive systems, which is not seen in the corresponding continuous-time nonlinear systems (see [Guo97, Kan94]). The "impossibility" result has been extended to some classes of uncertain nonlinear systems with unknown vector parameters in [XG99, Ma08a] and a similar result for system (1.5) with bounded noise is obtained in [LX06].

Stimulated by the pioneering work in [Guo97], a series of efforts ([XG00, ZG02, XG01, MG05]) have been made to explore the maximum capability and limitations of feedback mechanism. Among these work, a breakthrough for non-parametric uncertain systems was made by Xie and Guo in [XG00], where a class of first-order discrete-time dynamical control systems

$$y_{t+1} = f(y_t) + u_t + w_{t+1}, \quad f(\cdot) \in \mathcal{F}(L) \tag{1.6}$$

is studied and another interesting critical stability phenomenon is proved by using new techniques which are totally different from those in [Guo97]. More specifically, in [XG00], $F(L)$ is a class of nonlinear functions satisfying Lipschitz condition, hence the Lipschitz constant L can characterize the size of the uncertainty set $F(L)$. Xie and Guo obtained the following results: if $L \geq \frac{3}{2} + \sqrt{2}$, then there exists a feedback control law such that for any $f \in F(L)$, the corresponding closed-loop control system is globally stable; and if $L < \frac{3}{2} + \sqrt{2}$, then for any feedback control law and any $y_0 \in R^1$, there always exists

some $f \in F(L)$ such that the corresponding closed-loop system is unstable. So for system (1.6), the "magic" number $\frac{3}{2}+\sqrt{2}$ characterizes the capability and limits of the whole feedback mechanism. The impossibility part of the above results has been generalized to similar high-order discrete-time nonlinear systems with single Lipschitz constant [ZG02] and multiple Lipschitz constants [Ma08a]. From the work mentioned above, we can see two different threads: one is focused on parametric nonlinear systems and the other one is focused on non-parametric nonlinear systems. By examining the techniques in these threads, we find that different difficulties exist in the two threads, different controllers are designed to deal with the uncertainties and completely different methods are used to explore the capability and limitations of the feedback mechanism.

1.4 Motivation of Our Work

From the above introduction, we know that only parametric uncertainties were considered in traditional adaptive control and non-parametric uncertainties were only addressed in recent study on the whole feedback mechanism. This motivates us to explore the following problems: When both parametric and non-parametric uncertainties are present in the system, what is the maximum capability of feedback mechanism in dealing with these uncertainties? And how to design feedback control laws to deal with both kinds of internal uncertainties? Obviously, in most practical systems, there exist parametric uncertainties (unknown model parameters) as well as non-parametric uncertainties (e.g. unmodeled dynamics). Hence, it is valuable to explore answers to these fundamental yet novel problems. Noting that parametric uncertainties and non-parametric uncertainties essentially have different nature and require completely different techniques to deal with, generally it is difficult to deal with them in the same loop. Therefore, adaptive estimation and control in systems with parametric and non-parametric uncertainties is a new challenging direction. In this chapter, as a preliminary study, we shall discuss some basic ideas and principles of adaptive estimation in systems with both parametric and non-parametric uncertainties; as to the most difficult adaptive control problem in systems with both parametric and non-parametric uncertainties, we shall discuss two concrete examples involving both kinds of uncertainties, which will illustrate some proposed ideas of adaptive estimation and special techniques to overcome the difficulties in the analysis closed-loop system. Because of significant difficulties in this new direction, it is not possible to give systematic and comprehensive discussions here for this topic, however, our study may shed light on the aforementioned problems, which deserve further investigation.

The remainder of this chapter is organized as follows. In Section 2, a simple semi-parametric model with parametric part and non-parametric part will be introduced first and then we will discuss some basic ideas and principles of adaptive estimation for this model. Later in Section 3 and Section 4, we will apply the proposed ideas of adaptive estimation and investigate two concrete examples of discrete-time adaptive control: in the first example, a discrete-time first-order nonlinear semi-parametric model with bounded external noise disturbance is discussed with an adaptive controller based on information-contraction estimator, and we give rigorous proof of closed-loop stability in case where the uncertain parametric part is of linear growth rate, and our results reveal again the magic number

$\frac{3}{2}+\sqrt{2}$; in the second example, another noise-free semi-parametric model with parametric uncertainties and non-parametric uncertainties is discussed, where a new adaptive controller based on a novel type of update law with deadzone will be adopted to stabilize the system, which provides yet another view point for the adaptive estimation and control problem for the semi-parametric model. Finally, we give some concluding remarks in Section 5.

2. Semi-parametric Adaptive Estimation: Principles and Examples

2.1 One Semi-parametric System Model

Consider the following semi-parametric model

$$z_k = \theta^\tau \phi_k + f(\phi_k) + \varepsilon_k \tag{2.1}$$

where $\theta \in \Theta$ denotes unknown parameter vector, $f(\cdot) \in F$ denotes unknown function and $\varepsilon_k \in \Delta_k$ denote external noise disturbance. Here Θ, F and Δk represent *a priori* knowledge on possible θ, $f(\phi_k)$ and ε_k, respectively. In this model, let

$$v_k = f(\phi_k) + \epsilon_k$$

then Eq. (2.1) becomes Eq. (1.1). Because each term of right hand side of Eq. (2.1) involves uncertainty, it is difficult to estimate θ, $f(\phi_k)$ and ε_k simultaneously.

Adaptive estimation problem can be formulated as follows: Given *a priori* knowledge on θ, $f(\cdot)$ and ε_k, how to estimate θ and $f(\cdot)$ according to a series of data $\{\phi_k, z_k; k = 1,2,\cdots,n\}$

Or in other words, given *a priori* knowledge on θ and v_k, how to estimate θ and v_k according to a series of data $\{\phi_k, z_k; k = 1,2,\cdots,n\}$.

Now we list some examples of *a priori* knowledge to show various forms of adaptive estimation problem.

Example 2.1 *As to the unknown parameter θ, here are some commonly-seen examples of* a priori *knowledge:*

• *There is no any a priori knowledge on* θ *except for its dimension. This means that θ can be arbitrary and we do not know its upper bound or lower bound.*

• *The upper and lower bounds of θ are known, i.e.* $\underline{\theta} \le \theta \le \overline{\theta}$, *where* $\underline{\theta}$ *and* $\overline{\theta}$ *are constant vector and the relationship "≤" means element-wise "less or equal".*

• *The distance between θ and a nominal* θ_0 *is bounded by a known constant, i.e.* $||\theta - \theta_0|| \le r_\theta$, *where* $r_\theta \ge 0$ *is a known constant and* θ_0 *is the center of set* Θ.

• *The unknown parameter lies in a known countable or finite set of values, that is to say,* $\theta \in \{\theta_1, \theta_2, \theta_3, \cdots\}$.

Example 2.2 *As to the unknown function f(·), here are some possible examples of* a priori *knowledge:*

• $f(x) = 0$ *for all x. This case means that there is no unmodeled dynamics.*

• *Function f is bounded by other known functions, that is to say,* $\underline{f}(x) \le f(x) \le \overline{f}(x)$ *for any x.*

• *The distance between f and a nominal* f_0 *is bounded by a known constant, i.e.* $||f - f_0|| \le r_f$, *where* $r_f \ge 0$ *is a known constant and* f_0 *can be regarded as the center of a ball F in a metric functional space with norm* $||\cdot||$.

• *The unknown function lies in a known countable or finite set of functions, that is to say,* $f \in \{f_1, f_2, f_3, \cdots\}$.

• *Function f is Lipschitz, i.e.* $|f(x_1) - f(x_2)| \le L|x_1 - x_2|$ *for some constant* $L > 0$.

• *Function f is monotone (increasing or decreasing) with respect to its arguments.*

• *Function f is convex (or concave).*

• *Function f is even (or odd).*

Example 2.3 *As to the unknown noise term* ε_k, *here are some possible examples of* a priori *knowledge:*

• *Sequence* $\varepsilon_k = 0$. *This case means that no noise/disturbance exists.*

• *Sequence* ε_k *is bounded in a known range, that is to say,* $\underline{\varepsilon} \le \varepsilon_k \le \overline{\varepsilon}$ *for any k. One special case is* $\underline{\varepsilon} = -\overline{\varepsilon}$.

• *Sequence* ε_k *is bounded by a diminishing sequence, e.g,* $|\varepsilon_k| \le \frac{1}{k}$ *for any* k. *This case means that the noise disturbance converges to zero with a certain rate. Other typical rate sequences include* $\{\frac{1}{k^2}\}$, $\{\delta^k\}$ $(0 < \delta < 1)$, *and so on.*

• *Sequence* ε_k *is bounded by other known sequences, that is to say,* $\underline{\epsilon}_k \le \epsilon_k \le \bar{\epsilon}_k$ *for any k. This case generalizes the above cases.*

• *Sequence* ε_k *is in a known finite set of values, that is to say,* $\varepsilon_k \in \{e_1, e_2, \cdots, e_N\}$. *This case may happen in digital systems where all signals can only take values in a finite set.*

• *Sequence* ε_k *is oscillatory with specific patterns, e.g.* $\varepsilon_k > 0$ *if k is even and* $\varepsilon_k < 0$ *if k is odd.*

• *Sequence* ε_k *has some statistical properties, for example,* $Ee_k = 0$, $Ee_k^2 = \sigma^2$ *;; for another example, sequence* $\{\varepsilon_k\}$ *is i.i.d. taken from a probability distribution e.g.* $\varepsilon_k \approx U(0,1)$.

Parameter estimation problems (without non-parametric part) involving statistical properties of noise disturbance are studied extensively in statistics, system identification and traditional adaptive control. However, we shall remark that other non-statistic descriptions on *a priori* knowledge is more useful in practice yet seldom addressed in existing literature. In fact, in practical problems, usually the probability distribution of the noise/disturbance (if any) is not known and many cases cannot be described by any probability distribution since noise/disturbance in practical systems may come from many different types of sources. Without any *a priori* knowledge in mind, one frequently-used way to handle the noise is to simply assume the noise is Gaussian white noise, which is

reasonable in a certain sense. But in practice, from the point of view of engineering, we can usually conclude the noise/disturbance is bounded in a certain range. This chapter will focus on uncertainties with non-statistical *a priori* knowledge. Without loss of generality, in this section we often regard $v_k = f(\phi_k) + \varepsilon_k$ as a whole part, and correspondingly, *a priori* knowledge on v_k, (e.g. $\underline{v}_k \le v_k \le \bar{v}_k$), should be provided for the study.

2.2 An Example Problem

Now we take a simple example to show that it may not be appropriate to apply traditional identification algorithms blindly so as to get the estimate of unknown parameter.
Consider the following system

$$z_k = \theta\phi_k + f(\phi_k, k) + \varepsilon_k \tag{2.2}$$

where θ, $f(\cdot)$ and ε_k are unknown parameter, unknown function and unmeasurable noise, respectively. For this model, suppose that we have the following *a priori* knowledge on the system:

- No *a priori* knowledge on θ is known.
- At any step k, the term $f(\phi_k, k)$ is of form $f(\phi_k, k) = \exp(\xi_k \phi_k)$. Here $\{\xi_k\}$ is an unknown sequence satisfying $0 \le \xi_k \le 1$.
- Noise ε_k is diminishing with $|\epsilon_k| \le \frac{1}{k}$.

And in this example, our problem is how to use the data generated from model (2.2) so as to get a good estimate of true value of parameter θ. In our experiment, the data is generated by the following settings (k = 1, 2, $\cdots$, 50):

$$\theta = 5,\ \phi_k = \frac{k}{10},\ f(\phi_k, k) = \exp(|\sin k\,|\,\phi_k),\ \varepsilon_k = \frac{1}{k}(\alpha_k - 0.5)$$

where $\{\alpha_k\}$ are i.i.d. taken from uniform distribution $U(0, 1)$. Here we have N = 50 groups of data (ϕ_k, z_k).
Since model (2.2) involves various uncertainties, we rewrite it into the following form of linear regression

$$z_k = \theta\phi_k + v_k \tag{2.3}$$

by letting

$$v_k = f(\phi_k, k) + \varepsilon_k .$$

From the *a priori* knowledge for model (2.2), we can obtain the following *a priori* knowledge for the term v_k

$$\underline{v}_k \le v_k \le \bar{v}_k$$

where

$$\bar{v}_k = \begin{cases} \exp(\phi_k) + \frac{1}{k} & \text{if } \phi_k \ge 0 \\ 1 + \frac{1}{k} & \text{if } \phi_k < 0 \end{cases}$$

$$\underline{v}_k = \begin{cases} 1 + \frac{1}{k} & \text{if } \phi_k \ge 0 \\ \exp(\phi_k) + \frac{1}{k} & \text{if } \phi_k < 0 \end{cases}$$

Since model (2.3) has the form of linear regression, we can use try traditional identification algorithms to estimate θ. Fig. 1 illustrates the parameter estimates for this problem by using standard LS algorithm, which clearly show that LS algorithm cannot give good parameter estimate in this example because the final parameter estimation error $\tilde{\theta}_k = \hat{\theta} - \theta \approx 5.68284$ is very large.

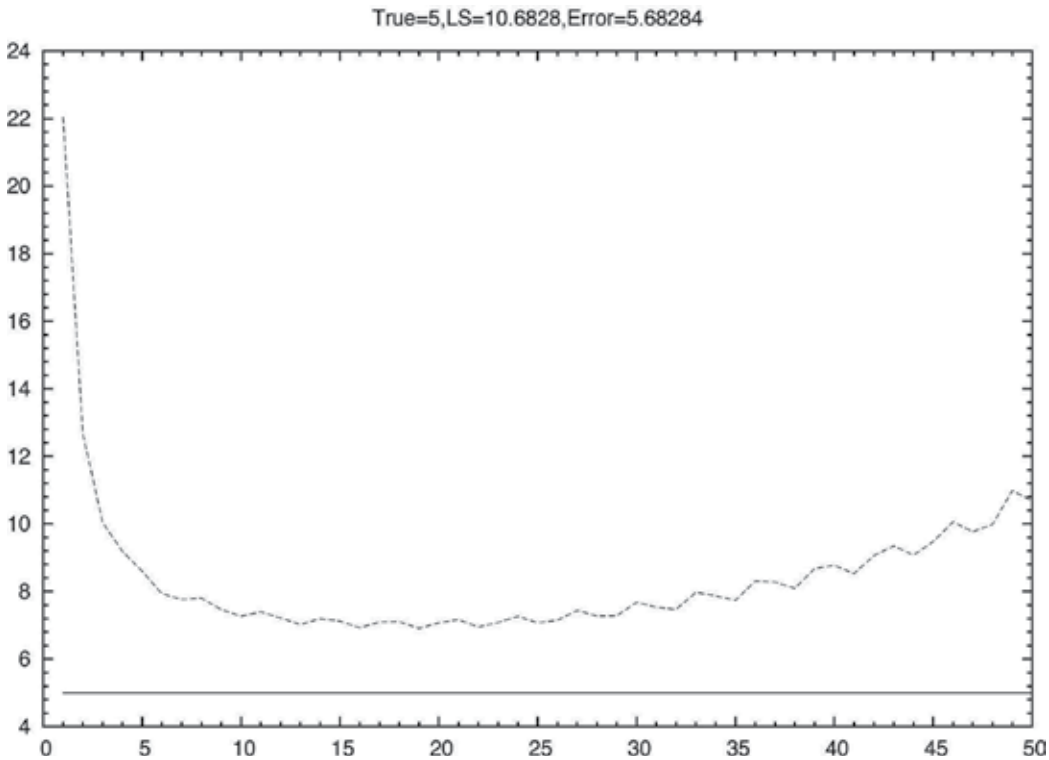

Fig. 1. The dotted line illustrates the parameter estimates obtained by standard least-squares algorithm. The straight line denotes the true parameter.

One may then argue that why LS algorithm fails here is just because the term v_k is in fact biased and we indeed do not utilize the *a priori* knowledge on v_k. Therefore, we may try a modified LS algorithm for this problem: let

$$
\begin{aligned}
c_k &= \frac{1}{2}(\underline{v}_k + \bar{v}_k) \\
d_k &= \frac{1}{2}(\bar{v}_k - \underline{v}_k) \\
w_k &= v_k - c_k \\
y_k &= z_k - c_k
\end{aligned}
$$

then we can conclude that $y_k = \theta^\tau \phi_k + w_k$ and $w_k \in [-d_k, d_k]$, where $[-d_k, d_k]$ is a symmetric interval for every *k*. Then, intuitively, we can apply LS algorithm to data $\{(\phi_k, z_k)$, *k* = 1, 2, $\cdots$,*N*}. The curve of parameter estimates obtained by this modified LS algorithm is plotted in Fig. 2. Since the modified LS algorithm has removed the bias in the *a priori* knowledge, one may expect the modified LS algorithm may give better parameter estimates, which can be verified from Fig. 2 since the final parameter estimation error $\tilde{\theta}_N = \hat{\theta}_N - \theta \approx -1.83314$. In this example, although the modified LS algorithm can work better than the standard LS algorithm, the modified LS algorithm in fact does not help much in solving our problem since the estimation error is still very large comparing with the true value of the unknown parameter.

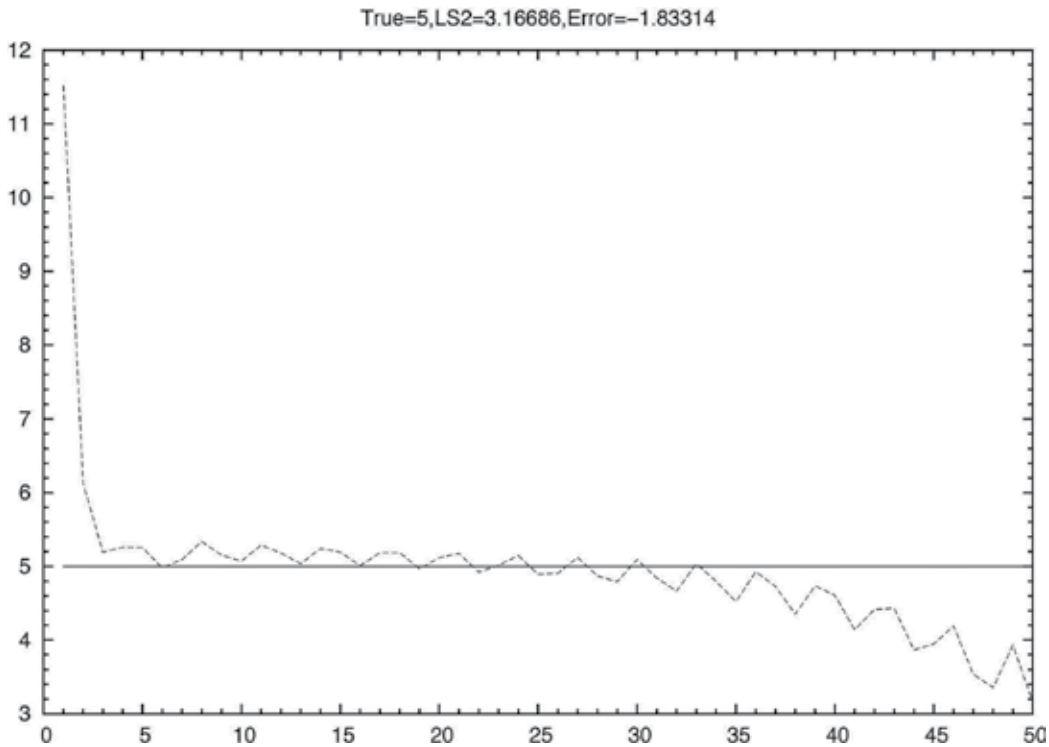

Fig. 2. The dotted line illustrates the parameter estimates obtained by modified least-squares algorithm. The straight line denotes the true parameter.

From this example, we do not aim to conclude that traditional identification algorithms developed in linear regression are not good, however, we want to emphasize the following particular point: *Although traditional identification algorithms (such as LS algorithm) are very powerful and useful in practice, generally it is not wise to apply them blindly when the matching conditions, which guarantee the convergence of those algorithms, cannot be verified or asserted a priori.* This particular point is in fact one main reason why the so-called *minimum-variance self tuning regulator*, developed in the area of adaptive control based on the LS algorithm, attracted several leading scholars to analyze its closed-loop stability throughout past decades from the early stage of adaptive control.
To solve this example and many similar examples with *a priori* knowledge, we will propose new ideas to estimate the parametric uncertainties and the non-parametric uncertainties.

2.3 Information-Concentration Estimator

We have seen that there exist various forms of *a priori* knowledge on system model. With the *a priori* knowledge, how can we estimate the parametric part and the non-parametric part? Now we introduce the so-called information-concentration estimator. The basic idea of this estimator is, the *a priori* knowledge at each time step can be regarded as some constraints of the unknown parameter or function, hence the growing data can provide more and more information (constraints) on the true parameter or function, which enable us to reduce the uncertainties step by step. We explain this general idea by the simple model

$$z_k = \theta^\tau \phi_k + v_k \tag{2.4}$$

with *a priori* knowledge that $\theta \in \Theta \subseteq R^d, v_k \in V_k$. Then, at k-th step ($k \geq 1$), with the current data k, ϕ_k, z_k we can define the so-called *information set* I_k at step k:

$$I_k \triangleq \{\theta \in \Theta : z_k - \theta^\tau \phi_k \in V_k\}. \tag{2.5}$$

For convenience, let $I_0 = \Theta$. Then we can define the so-called *concentrated information set* C_k at step k as follows

$$C_k = \bigcap_{j=0}^{k} I_k \tag{2.6}$$

which can be recursively written as

$$C_k = C_{k-1} \cap I_k \tag{2.7}$$

with initial set $C_0 = \Theta$. Eq. (2.7) with Eq. (2.5) is called *information-concentration estimator* (short for *IC estimator*) throughout this chapter, and any value in the set C_k can be taken as one possible estimate of unknown parameter θ at time step k. The IC estimator differs from existing parameter identification in the sense that the IC estimator is in fact a set-

valued estimator rather than a real-valued estimator. In practical applications, generally C_k is a domain in R^d, and naturally we can take the center point of C_k as $\hat{\theta}_k$.

Remark 2.1 *The definition of* information set *varies with system model. In general cases, it can be extended to the set of possible instances* of θ (and/or f) *which do not contradict with the data at step k. We will see an example involving unknown f in next section.*

From the definition of the IC estimator, the following proposition can be obtained without difficulty:

Proposition 2.1 *Information-concentration estimator has the following properties:*

(i) Monotonicity: $C_0 \supseteq C_1 \supseteq C_2 \supseteq \cdots$

(ii) Convergence: Sequence {Ck} has a limit set $C_\infty = \bigcap_{k=1}^{\infty} C_k$;

(iii) If the system model and the a priori *knowledge are correct, then* C_∞ *must be a non-empty set with property* $\theta \in C_\infty$ *and any element of* C_∞ *can match the data and the model;*

(iv) If $C_\infty = \varnothing$, *then the data* $\{\phi_k, z_k\}$ *cannot be generated by the system model used by the IC estimator under the specified* a priori *knowledge.*

Proposition 2.1 tells us the following particular points of the IC estimator: property (i) implies that the IC estimator will provide more and more exact estimation; property (ii) means that the there exists a limitation in the accuracy of estimation; property (iii) means that true parameter lies in every C_k if the system model and *a priori* knowledge are correct; and property (iv) means that the IC estimator provides also a method to validate the system model and the *a priori* knowledge. Now we discuss the IC estimator for model (2.4) in more details. In the following discussions, we only consider a typical *a priori* knowledge on $\underline{v}_k \le v_k \le \bar{v}_k$ are two known sequences of vectors (or scalars).

2.3.1 Scalar case: *d* = 1

By Eq. (2.5), we have

$$I_k = \{\theta \in \Theta : \underline{v}_k \le z_k - \theta\phi_k \le \bar{v}_k\}$$

Solving the inequality in I_k, we obtain that

$$\theta\phi_k \in [z_k - \underline{v}_k, z_k - \bar{v}_k]$$

and consequently, if $\phi_k \neq 0$, then we have

$$\theta \in [\underline{b}_k, \bar{b}_k]$$

where

$$\begin{aligned} \underline{b}_k &= \frac{\min(\text{sign}(\phi_k)(z_k - \underline{v}_k), \text{sign}(\phi_k)(z_k - \bar{v}_k))}{|\phi_k|}, \\ \bar{b}_k &= \frac{\max(\text{sign}(\phi_k)(z_k - \underline{v}_k), \text{sign}(\phi_k)(z_k - \bar{v}_k))}{|\phi_k|}, \end{aligned}$$

Here sign(x) denotes the sign of x: sign(x) = 1, 0,−1 for positive number, zero, and negative number, respectively. Then, by Eq. (2.7), we can explicitly obtain that

$$C_k = [\underline{\beta}_k, \bar{\beta}_k]$$

where $\underline{\beta}_k$ and $\bar{\beta}_k$ can be recursively obtained by

$$\begin{aligned} \underline{\beta}_k &= \max(\underline{\beta}_{k-1}, \underline{b}_k) \\ \bar{\beta}_k &= \min(\bar{\beta}_{k-1}, \bar{b}_k) \end{aligned}$$

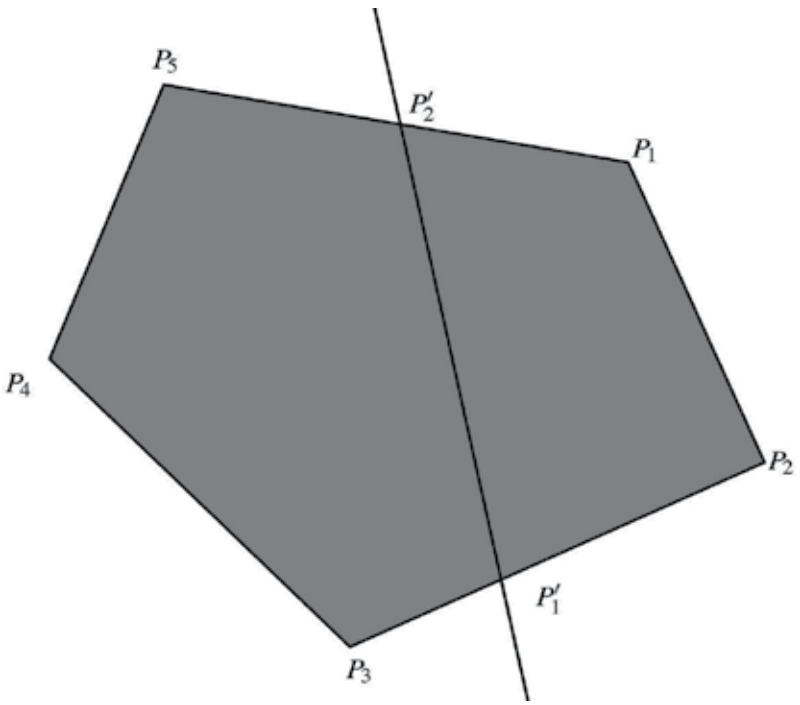

Fig. 3. The straight line may intersect the polygon V and split it into two sub-polygons, one of which will become new polygon V'. The polygon V' can be efficiently calculated from the polygon V.

2.3.2 Vector case: *d* > 1

In case of $d > 1$, since θ and ϕ_k are vectors, we cannot directly obtain explicit solution of inequality

$$\theta^\tau \phi_k \in [z_k - \underline{v}_k, z_k - \bar{v}_k] \tag{2.8}$$

Notice that Eq. (2.8) can be rewritten into two separate inequalities:

$$\phi_k^\tau \cdot \theta \le z_k - \bar{v}_k, \quad (-\phi_k)^\tau \cdot \theta \le -(z_k - \underline{v}_k)$$

we need only study linear equalities of the form $\phi^T \theta \le c$. Generally speaking, the solution to a system of inequalities represents a polyhedral (or polygonal) domain in R^d, hence we need only determine the vertices of the polyhedral (or polygonal) domain. In case of $d = 2$, it is easy to graph linear equalities since every inequality $\phi^T \theta \le c$ represents a half-plane. In general case, let $v_k = \{\psi_i, i = 1,2,\cdots, p_k\}$ denote the distinct vertices of the domain C_k and p_k denote the number of vertices of domain C_k, then we discuss how to deduce V_k from V_{k-1}. The domain C_k has two more linear constraints than the domain C_{k-1}

$$\phi_{k,j}^\tau \cdot \theta \le c_{k,j}, j = 1,2$$

with

$$\begin{aligned} \phi_{k,1} &= \phi_k, & c_{k,1} &= z_k - \bar{v}_k \\ \phi_{k,2} &= -\phi_k, & c_{k,2} &= -(z_k - \bar{v}_k) \end{aligned}$$

We need only add these two constraints one by one, that is to say,

$$\begin{aligned} \mathcal{V}'_{k-1} &= \textbf{AddLinearContraint}(\mathcal{V}_{k-1}, \phi_{k,1}, c_{k,1}) \\ \mathcal{V}_k &= \textbf{AddLinearContraint}(\mathcal{V}'_{k-1}, \phi_{k,2}, c_{k,2}) \end{aligned}$$

where $\textbf{AddLinearConstraint}(\mathcal{V}, \phi, c)$ is an algorithm whose function is to add linear constraint $\phi^T \theta \le c$ to the polygon represented by vertex set V and to return the vertex set of the new polygon with added constraint.

Now we discuss how to implement the algorithm **AddLinearConstraint**.

2D Case: In case of $d = 2$, $\phi^T \theta \le c$ represents a straight line which splits the plane into two half-planes (see Fig. 3). In this case, we can use an efficient algorithm **AddLinearConstraint2D** which is listed in Algorithm 1. Its basic idea is to simply test each vertex of V to see whether to keep original vertex or generate new vertex. The time

complexity of Algorithm 1 is $O(s)$, where s is the number of vertices of domain V. Note that it is possible that $V' = \varnothing$ if the straight line $L: \phi^T\theta \le c$ does not intersect with the polygon V and any vertex P_i of polygon V does not satisfy $\phi^T P_i > c$. And the vertex number of polygon V' can in fact vary within the range from 0 to s according to the geometric relationship between the straight line L and the polygon V.

Algorithm 1 AddLinearConstraint2D($\mathcal{V}, \phi, c$): Add linear constraint $\phi^T\theta \le c\ (\phi \in \mathcal{R}^2)$ to a polygon $\mathcal{V}$

Input: $\mathcal{V}$: represented by clock-wise arranged vertices $P_1, P_2, \cdots, P_s$
Output: $\mathcal{V}'$: clock-wise arranged vertices

Let $P_0 \leftarrow P_s$
Let $\mathcal{Q}$ be an empty queue
for $i = 1$ to s **do**
  Let $\delta_i \leftarrow \phi^T P_i - c$
end for
Let $\delta_0 \leftarrow \delta_s$
for $i = 1$ to s **do**
  if $(\delta_i = 0)$ or $(\delta_i < 0$ and $\delta_{i-1} \le 0)$ **then**
    Append vertex P_i to queue $\mathcal{Q}$
  else if $(\delta_i > 0$ and $\delta_{i-1} < 0)$ or $(\delta_i < 0$ and $\delta_{i-1} > 0)$ **then**
    Let $w \leftarrow \frac{\delta_{i-1}}{\delta_{i-1} - \delta_i}$
    Generate new vertex $P' \leftarrow w \cdot P_i + (1 - w) \cdot P_{i-1}$
    Append vertex P' to queue $\mathcal{Q}$
  end if
end for
Return vertices in queue $\mathcal{Q}$ as the vertices of new domain $\mathcal{V}'$

High-dimensional Case: In case of $d > 2$, $\phi^T\theta \le c$ represents a hyperplane which splits the whole space into two half-hyperplanes.
Unlike in case of $d = 2$, the vertices in this case generally cannot be arranged in a certain natural order (such as clock-wise order). In this case, we can use an algorithm AddLinearConstraintND which is listed in Algorithm 2. The idea of this algorithm is to classify the vertices of V first according to their relationship with the hyperplane determined by hyperplane $\phi^T\theta \le c$.

Algorithm 2 AddLinearConstraintND(V, '', c): Add linear constraint $\phi^T\theta \le c$ ('' % Rd) to a polyhedron V

2.3.3 Implementation issues

In the IC estimator, the key problem is to calculate the information set I_k or the concentrated information set C_k at every step. From the discussions above, we can see that it is easy to solve this basic problem in case of $d = 1$. However, in case of $d > 1$, generally the vertex

number of domain C_k may grow as $k \to \infty$. Therefore, it may be impractical to implement the IC estimator in case of $d > 1$ since it may require growing memory as $k \to \infty$ To overcome this problem, noticing the fact that the domain C_k will shrink gradually as $k \to \infty$ in order to get a feasible IC estimate of the unknown parameter vector, generally we need not use too many vertices to represent the exact concentrated information set C_k. That is to say, in practical implementation of IC estimator in high-dimensional case, we can use a domain $\hat{C}_k$ with only a small number (say up to M) of vertices to approximate the exact concentrated information set C_k. With such an idea of *approximate IC estimator*, the issue of computational complexity will not hinder the applications of IC estimator.

We consider two typical cases of *approximate IC estimator*. One typical case is that $\hat{C}_k \supseteq C_k$ for any k, and the other case is that $\hat{C}_k \supseteq C_k$ for any k. Let $\hat{C}_\infty = \bigcap_{k=1}^{\infty} \hat{C}_k$, then in the former case (called *loose IC estimator*, see Fig. 4), we must have

$$C_\infty = \bigcap_{k=1}^{\infty} C_k \subseteq \hat{C}_\infty$$

which means that we will never mistakenly exclude the true parameter from the concentrated approximate information sets; while in the latter case (called *tight IC estimator*, see Fig. 5), we must have

$$C_\infty = \bigcap_{k=1}^{\infty} C_k \supseteq \hat{C}_\infty$$

which means that the true parameter may be outside of $\hat{C}_\infty$ however any value in $\hat{C}_\infty$ can be served as good estimate of true parameter.

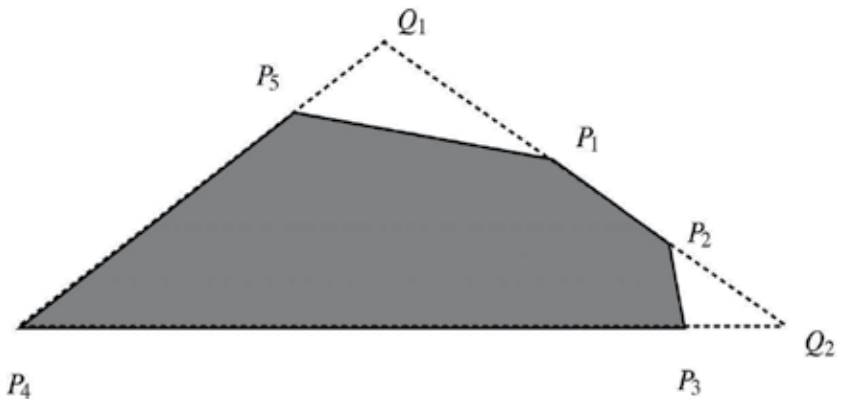

Fig. 4. Idea of loose IC estimator: The polygon $P_1P_2P_3P_4P_5$ can be approximated by a triangle $Q_1P_4Q_2$. Here $M = 3$.

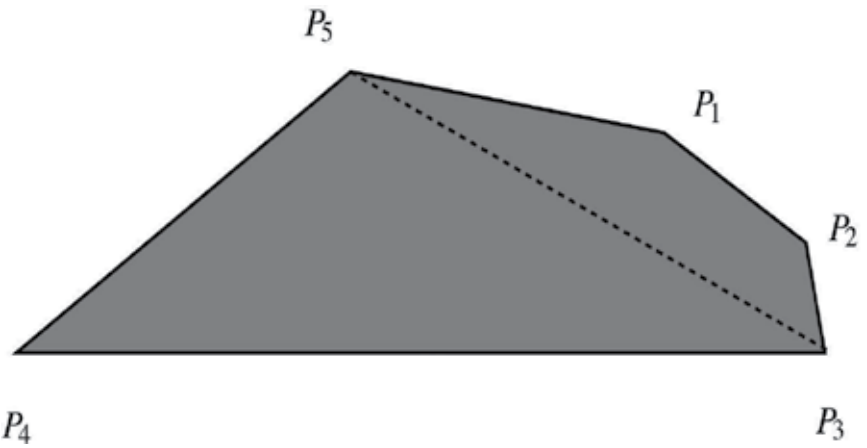

Fig. 5. Idea of tight IC estimator: The polygon $P_1P_2P_3P_4P_5$ can be approximated by a triangle $P_3P_4P_5$. Here $M = 3$.

Now we discuss implementation details of *tight IC estimator* and *loose IC estimator*. Without loss of generality, we only explain the ideas in case of $d = 2$. Similar ideas can be applied in cases of $d > 2$ without difficulty.

Tight IC estimator: To implement a tight IC estimator, one simple approach is to modify Algorithm 1 so as it just keeps up to M vertices in the queue Q. To get good approximation, in the loop of Algorithm 1, it is suggested to abandon the generated vertex P' (in Line 12 of Algorithm 1) which is very close to existing vertex P_j (let $j = i$ if $\delta_i < 0$ and $\delta_{i-1} > 0$ or $j = i - 1$ if $\delta_i > 0$ and $\delta_{i-1} < 0$). The closeness between P' and existing vertex P_j can be measured by checking the corresponding weight w.

Loose IC estimator: To implement a loose IC estimator, one simple approach is to modify Algorithm 1 so as it can generate M vertices which surround all vertices in the queue Q. To this end, in the loop of Algorithm 1, if the generated vertex P' (in Line 12 of Algorithm 1) is very close to existing vertex P_j (let $j = i$ if $\delta_i < 0$ and $\delta_{i-1} > 0$ or $j = i - 1$ if $\delta_i > 0$ and $\delta_{i-1} < 0$), we can simply append vertex P_j instead of P' to queue Q. In this way, we can avoid increasing the vertex number by generating new vertices. The closeness between P' and existing vertex P_j can be measured by checking the corresponding weight w.

Besides the ideas of tight or loose IC estimator, to reduce the complexity of IC estimator, we can also use other flexible approaches. For example, to avoid growth in the vertex number of V_k as $k \to \infty$, we can approximate V_k by using a simple outline rectangle (see Fig. 6) every certain steps. For a polygon V_k with vertices $P_1, P_2, \cdots, P_s$, we can easily obtain its outline rectangle by algorithm FindPolygonBounds listed in Algorithm 3. Here for convenience, the operators max and min for vectors are defined element-wisely, i.e.

$$\max(A, B) \triangleq [\max(A_1, B_1), \max(A_2, B_2), \cdots, \max(A_d, B_d)]^\tau$$
$$\min(A, B) \triangleq [\min(A_1, B_1), \min(A_2, B_2), \cdots, \min(A_d, B_d)]^\tau$$

where $A = [A_1, A_2, \cdots, A_d]^\tau, B = [B_1, B_2, \cdots, B_d]^\tau$ are two vectors in R_n.

Algorithm 3 FindPolygonBounds($\mathcal{V}$): Find the outline rectangle of polygon $\mathcal{V}$

Input: $\mathcal{V}$: represented by vertices $P_1, P_2, \cdots, P_s$

Output: $\mathcal{V}'$: the outline rectangle represented by upper and lower bounds of each component of vertices

1: Let $\bar{B} \leftarrow P_1$
2: Let $\underline{B} \leftarrow P_1$
3: **for** $i = 2$ to s **do**
4: Let $\bar{B} \leftarrow \max(\bar{B}, P_i)$
5: Let $\underline{B} \leftarrow \min(\underline{B}, P_i)$
6: **end for**
7: Return vertices of rectangle represented by coordinate bounds $\bar{B}$ and $\underline{B}$ as the vertices of new domain $\mathcal{V}'$

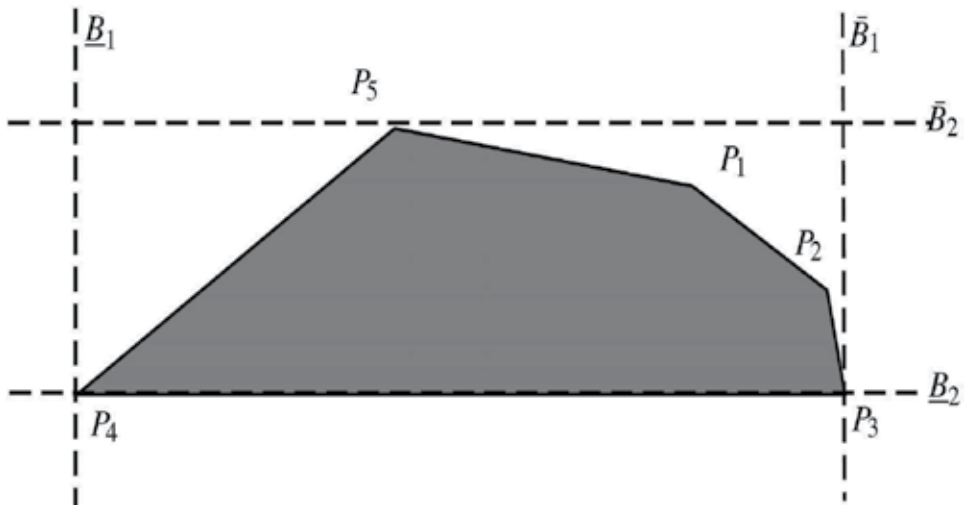

Fig. 6. Idea of outline rectangle: The polygon $P_1P_2P_3P_4P_5$ can be approximated by an outline rectangle. In this case, $\underline{B}_1, \overline{B}_1$ denote the lower bound and upper bound in the x-axis (1st component of each vertex), and $\underline{B}_2, \overline{B}_2$ denote the lower bound and upper bound in the y-axis (2nd component of each vertex)

2.4 IC Estimator vs. LS Estimator

2.4.1 Illustration of IC Estimator

Now we go back to the example problem discussed before. For this example, ϕ_k and z_k are scalars, hence we need only apply the IC estimator introduced in Section 2.3.1. Since IC estimator yields concentrated information set C_k at every step, we can take any value in

C_k as parameter estimate of true parameter. In this example, C_k is an interval at every step step. For comparison with other parameter estimation methods, we simply take $\hat{\theta}_k = \frac{1}{2}(\bar{b}_k + \underline{b}_k)$, i.e. the center of interval C_k, as the parameter estimate at step *k*.

In Fig. 7, we plot three curves $\bar{b}_k$, $\underline{b}_k$ and $\hat{\theta}_k$. From this figure, we can see that, for this particular example, with the help of *a priori* knowledge, the upper estimates $\bar{b}_k$ and lower estimates $\underline{b}_k$ given by the IC estimator converge to true parameter θ = 5 quickly, and consequently $\hat{\theta}_k$ also converges to true parameter.

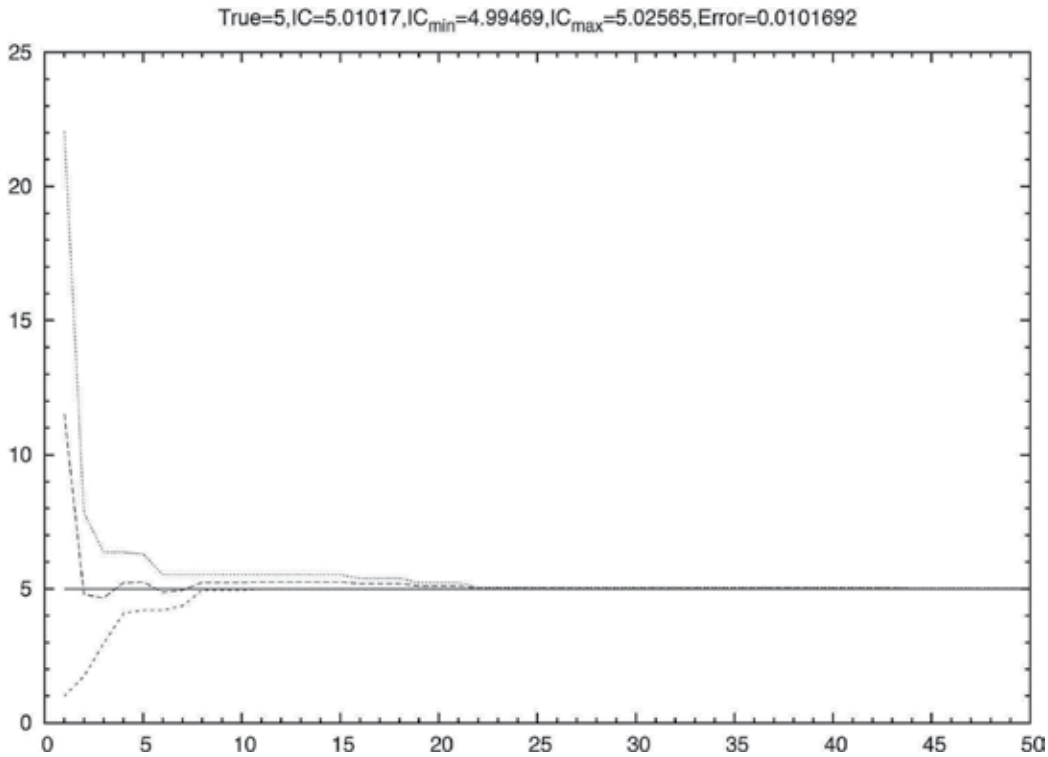

Fig. 7. This figure illustrates the parameter estimates obtained by the proposed information-concentration estimator. The upper curve and lower curve represent the upper bounds $\bar{b}_k$ and lower bounds $\underline{b}_k$ for the parameter estimates. We use the center curve $\hat{\theta}_k = \frac{1}{2}\left(\bar{b}_k + \underline{b}_k\right)$ to yield the parameter estimates.

We should also remark that the parameter estimates given by the IC estimator are not necessarily convergent as in this example. Whether the IC parameter estimates converge

largely depend on the accuracy of *a priori* knowledge and the richness of the practical data. Note that the IC estimator generally does not require classical richness concepts (like *persistent excitation*) which are useful in the analysis of traditional recursive identification algorithms.

2.4.2 Advantages of IC Estimator

We have seen practical effects of IC estimator for the simple example given above. Why can it perform better than the LS estimator? Roughly speaking, comparing with traditional identification algorithm like LS algorithm, the proposed IC estimator has the following advantages:

1. It can make full use of *a priori* information and posterior information. And in the ideal case, no information is wasted in the iteration process of the IC estimator. This property is not seen in traditional identification algorithms since only partial information and certain stochastic *a priori* knowledge can be utilized in those algorithms.
2. It does not give single parameter estimate at every step; instead, it gives a (finite or infinite) set of parameter estimates at every step. This property is also unique since traditional identification algorithms always give parameter estimates directly.
3. It can gradually find out all (or most) possible values of true parameters; and this property can even help people to check the consistence between the practical data and the system model with *a priori* knowledge. This property distinguishes traditional identification algorithms in sense that traditional identification algorithms generally have no mechanism to validate the correctness of the system model.
4. The *a priori* knowledge can vary from case to case, not necessarily described in the language of probability theory or statistics. This property enables the IC estimator to handle various kinds of non-statistic *a priori* knowledge, which cannot be dealt with by traditional identification algorithms.
5. It has great flexibilities in its implementation, and its design is largely determined by the characteristics of *a priori* knowledge. *The IC estimator has only one basic principle – information concentration*! Any practical implementation approach using such a principle can be regarded as an IC estimator. We have discussed some implementation details for a certain type of IC estimator in last subsection, which have shown by examples how to design the IC estimator according the known *a priori* knowledge and how to reduce computational complexity in practical implementation.
6. Its accuracy will never degrade as time goes by. Generally speaking, the more steps calculated, the more data involved, and the more accurate the estimates are. Generally speaking, traditional identification algorithms can only have similar property (called *strong consistency*) under certain matching conditions.
7. The IC estimator can not only provide reasonably good parameter estimates but also tell people how accurate these estimates are. In our previous example, when we use $\hat{\theta}_k = \frac{1}{2}\left(\overline{b}_k + \underline{b}_k\right)$ as the parameter estimate, we know also that the absolute parameter estimation error $\left|\tilde{\theta}\right| = \left|\hat{\theta} - \theta\right|$ will not exceed $\frac{1}{2}\left(\overline{b}_k + \underline{b}_k\right)$. In some sense, such a property may be conceptually similar to the so-called *confidence level* in statistics.

2.4.3 Disadvantages of IC Estimator

Although the IC estimator has many advantages over traditional identification algorithms, it may have the following disadvantages:

1. The proposed IC estimator is relatively difficult to incorporate stochastic *a priori* knowledge on noise term, especially unbounded random noise. In fact, in such cases without non-parametric uncertainties, traditional identification algorithms like LS algorithm may be more suitable and efficient to estimate the unknown parameter.
2. The efficiency of IC estimator largely depends on its implementation via the characteristics of the *a priori* knowledge. Generally speaking, the IC estimator may involve a little more computation operations than recursive identification algorithms like LS algorithm. We shall remark also that this point is not always true since the numerical operations involved in the IC estimator are relatively simple (see algorithms listed before), while many traditional identification algorithms may involve costly numerical operations like matrix product, matrix inversion, etc.
3. Although the IC estimator has simple and elegant properties such as monotonicity and convergence, *due to its nature of set-valued estimator*, no explicit and recursive expressions can be given directly for the IC parameter estimates, which may bring mathematical difficulties in the applications of the IC estimator. However, generally speaking, we also know that closed-loop analysis for adaptive control using traditional identification algorithms is not easy, too.

Summarizing the above, we can conclude that the IC estimator provides a new approach or principle to estimate parametric and even non-parametric uncertainties, and we have shown that it is possible to design efficient IC estimator according to characteristics of *a priori* knowledge.

3. Semi-parametric Adaptive Control: Example 1

In this section, we will give a first example of semi-parametric adaptive control, whose design is essentially based on the IC estimator introduced in last section.

3.1 Problem Formulation

Consider the following system

$$y_{t+1} = \theta\phi_t + f(y_t) + u_t + w_{t+1} \tag{3.1}$$

where y_t, u_t and w_t are the output, input and noise, respectively; $f(\cdot) \in F(L)$ is an unknown function (the set $F(L)$ will be defined later) and θ is an unknown parameter. To make further study, the following assumptions are used throughout this section:

Assumption 3.1 *The unknown function* $f : R \to R$ *belongs to the following uncertainty set*

$$\mathcal{F}(L) = \{f : |f(x) - f(y)| \le L|x - y| + c\} \tag{3.2}$$

where c is an arbitrary non-negative constant.

Assumption 3.2 *The noise sequence* $\{w_t\}$ *is bounded, i.e.*

$$|w_t| \leq w$$

where w is an arbitrary positive constant.

Assumption 3.3 *The tracking signal* $\{y_t^*\}$ *is bounded, i.e.*

$$|y_t^*| \leq S, \forall t \geq 0 \tag{3.3}$$

where S is a positive constant.

Assumption 3.4 *In the parametric part* $\theta\phi_t$ *, we have no any a priori information of the unknown parameter θ, but* $\phi_t = g(y_t)$ *is measurable and satisfies*

$$M' \leq |\frac{g(x_1)-g(x_2)}{x_1^b - x_2^b}| \leq M \tag{3.4}$$

for any $x_1 \neq x_2$ *, where M' ≤ M are two positive constants and* $b \geq 1$ *is a constant.*

Remark 3.1 *Assumption 3.4 implies that function g(·) has linear growth rate when b = 1. Especially when g(x) = x, we can take M = M' = 1. Condition (3.4) need only hold for sufficiently large* x_1 *and* x_2*, however we require it holds for all* $x1 \neq x2$ *to simplify the proof. We shall also remark that Sokolov [Sok03] has ever studied the adaptive estimation and control problem for a special case of model (3.1), where* ϕ_t *is simply taken as* ay_t *.*

Remark 3.2 *Assumption 3.4 excludes the case where g(·) is a bounded function, which can be handled easily by previous research. In fact, in that case* $w'_{t+1} = \theta\phi_t + w_{t+1}$ *must be bounded, hence by the result of [XG00], system (3.1) is stabilizable if and only if* $L < \frac{3}{2} + \sqrt{2}$ *.*

3.2 Adaptive Controller Design

In the sequel, we shall construct a unified adaptive controller for both cases of b =1 and b >1. For convenience, we introduce some notations which are used in later parts. Let I = [a, b] be an interval, then $m(I) \overset{\Delta}{=} \frac{1}{2}(a+b)$ (a+ b) denotes the center point of interval I, and $r(I) \overset{\Delta}{=} \frac{1}{2}|b-a|$ denotes the radius of interval I. And correspondingly, we let $I(x,\delta) = [x-\delta, x+\delta]$ denote a closed interval centered at $x \in R$ with radius $\delta \geq 0$.

Estimate of Parametric Part: At time t, we can use the following information: y_0, y_1, $\cdots$, y_t, u_0, u_1, $\cdots$, u_{t-1} and $\phi_1, \phi_2, \cdots, \phi_t$. Define

$$z_j \triangleq y_{j+1} - u_j \tag{3.5}$$

and

$$I_t \triangleq \bigcap_{(i,j)\in J_t} I\left(\frac{z_j - z_i}{\phi_j - \phi_i}, \frac{L|y_j - y_i|}{|\phi_j - \phi_i|} + \frac{2w+c}{|\phi_j - \phi_i|}\right) \tag{3.6}$$

where

$$J_t \triangleq \{(i,j) \in \mathcal{N} : i < j < t, \phi_i \neq \phi_j\} \tag{3.7}$$

then, we can take

$$\hat{\theta}_t = m(I_t), \quad \delta_t = r(I_t) \tag{3.8}$$

as the estimate of parameter θ at time t and corresponding estimate error bound, respectively. With $\hat{\theta}_t$ and δ_t defined above, $\overline{\theta}_t = \hat{\theta}_t + \delta_t$ and $\underline{\theta}_t = \hat{\theta}_t - \delta_t$ are the estimates of the upper and lower bounds of the unknown parameter θ, respectively.

According to Eq. (3.6), obviously we can see that $\{\overline{\theta}_t\}$ is a non-increasing sequence and $\{\underline{\theta}_t\}$ is non-decreasing.

Remark 3.3 *Note that Eq. (3.6) makes use of* a priori *information on nonlinear function f*($\cdot$). *This estimator is another example of the IC estimator which demonstrates how to design the IC estimator according to the Lipschitz property of function f*($\cdot$). *With similar ideas, the IC estimator can be designed based on other forms of* a priori *information of function f*($\cdot$).

Estimate of Non-parametric Part: Since the non-parametric part $f(y_t)$ may be unbounded and the parametric part is also unknown, generally speaking it is not easy to estimate the non-parametric part directly. To resolve this problem, we choose to estimate

$$g_t \triangleq \theta\phi_t + f(y_t)$$

as a whole part rather than to estimate $f(y_t)$ directly. In this way, consequently, we can obtain the estimate of $f(y_t)$ by removing the estimate of parametric part from the estimate of g_t.

Define

$$i_t = \arg\min_{i<t} |y_t - y_i| \tag{3.9}$$

then, we get

$$\begin{aligned} g_t &= g_t - z_{i_t} + z_{i_t} \\ &= [\theta\phi_t + f(y_t)] - [\theta\phi_{i_t} + f(y_{i_t}) + w_{i_t+1}] + z_{i_t} \\ &= [\theta(\phi_t - \phi_{i_t}) + z_{i_t}] + [f(y_t) - f(y_{i_t}) - w_{i_t+1}] \end{aligned} \tag{3.10}$$

Thus, intuitively, we can take

$$\hat{g}_t \triangleq \hat{\theta}_t(\phi_t - \phi_{i_t}) + z_{i_t} = \hat{\theta}_t(\phi_t - \phi_{i_t}) + (y_{i_t+1} - u_{i_t}) \tag{3.11}$$

as the estimate of g_t at time t.

Design of Control u_t: Let

$$\begin{aligned} \bar{b}_t &\triangleq \max_{i \le t} y_i = \max(\bar{b}_{t-1}, y_t) \\ \underline{b}_t &= \min_{i \le t} y_i = \min(\underline{b}_{t-1}, y_t). \end{aligned} \tag{3.12}$$

Under Assumptions 3.1-3.4, we can design the following control law

$$u_t = \begin{cases} -\hat{g}_t + y^*_{t+1} & \text{if } |y_t - y_{i_t}| \le D \\ -\hat{g}_t + \frac{1}{2}(\bar{b}_t + \underline{b}_t) & \text{if } |y_t - y_{i_t}| > D \end{cases} \tag{3.13}$$

where D is an appropriately large constant, which will be addressed in the proof later.

Remark 3.4 *The controller designed above is different from most traditional adaptive controllers in its special form, information utilization and computational complexity. To reduce its computational complexity, the interval I_t given by Eq. (3.6) can be calculated recursively based on the idea in Eq. (3.12).*

3.3 Stability of Closed-loop System

In this section, we shall investigate the closed-loop stability of system (3.1) using the adaptive controller given above. We only discuss the case that the parametric part is of linear growth rate, i.e. $b = 1$. For the case where the parametric part is of nonlinear growth rate, i.e. $b > 1$, though simulations show that the constructed adaptive controller can stabilize the system under some conditions, we have not rigorously established corresponding theoretical results; further investigation is needed in the future to yield deeper understanding.

3.3.1 Main Results

The adaptive controller constructed in last section has the following property:

Theorem 3.1 *When* $b = 1, \dfrac{ML}{M'} < \dfrac{3}{2} + \sqrt{2}$, *the controller defined by Eqs. (3.5) – (3.13) can guarantee that the output $\{y_t\}$ of the closed-loop system is bounded. More precisely, we have*

$$\limsup_{t\to\infty} |y_t - y_t^*| \le 2w + c. \tag{3.14}$$

Based on Theorem 3.1, we can classify the capability and limitations of feedback mechanism for the system (3.1) in case of $b = 1$ as follows:

Corollary 3.1 *For the system (3.1) with both parametric and non-parametric uncertainties, the following results can be obtained in case of* $b = 1$*:*

(i) If $b = 1, \dfrac{ML}{M'} < \dfrac{3}{2} + \sqrt{2}$ *, then there exists a feedback control law guaranteeing that the closed-loop system is stabilized.*

(ii) When $\phi_t = y_t$ (i.e. $g(x) = x$)*, the presence of uncertain parametric part* $\theta\phi_t$ *does not reduce the critical value* $\dfrac{3}{2} + \sqrt{2}$ *of the feedback mechanism which is determined by the uncertainties of non-parametric part.*

Proof of Corollary 3.1: (i) This result follows from Theorem 3.1 directly. (ii) When $g(x) = x$, we can take $M = M' = 1$. In this case, the sufficiency can be immediately obtained via Theorem 3.1; on the other hand, the necessity can be obtained by the "impossibility" part of Theorem 1 in [XG00]. In fact, if $L \ge \dfrac{3}{2} + \sqrt{2}$, for any given control law $\{u_t\}$, we need only take the parameter $\theta = 0$, then by [XG00, Theorem 2.1], there exists a function f such that system (3.1) cannot be stabilized by the given control law.

Remark 3.5 *As we have mentioned in the introduction part, system (1.6), a special case of system (3.1), has been studied in [XG00]. Comparing system (3.1) and system (1.6), we can see that system (3.1) has also parametric uncertainty besides nonparametric uncertainty and noise disturbance. Hence intuitively speaking, it will be more difficult for the feedback mechanism to deal with uncertainties in system (3.1) than those in system (1.6). Noting that* $M' \le M$*, we know this fact has been partially verified by Theorem 3.1. And Corollary 3.1 (ii) indicates that in the special case of* $\phi_t = y_t$ *, since the structure of parametric part is completely determined, the uncertainty in non-parametric part becomes the main difficulty in designing controller, and the parametric uncertainty has no influence on the capability of the feedback mechanism, that is to say, the feedback mechanism can still deal with the non-parametric uncertainty characterized by the set* $F(L)$ *with* $L < \dfrac{3}{2} + \sqrt{2}$ *.*

Remark 3.6 *Theorem 3.1 is also consistent with classic results on adaptive control for linear systems. In fact, when* $L = 0$*, the non-parametric part* $f(y_t)$ *vanishes, consequently system (3.1) becomes a linear-in-parameter system*

$$y_{t+1} = \theta\phi_t + u_t + w_{t+1} \tag{3.15}$$

where θ *is the unknown parameter, and* $\phi_t = g(y_t)$ *can have arbitrary linear growth rate because by Theorem 3.1, we can see that no restrictions are imposed on the values of* M *and* M' *when L = 0. Based on the knowledge from existing adaptive control theory [CG91], system (3.15) can be always stabilized by algorithms such as minimum-variance adaptive controller no matter how large the* θ *is. Thus the special case of Theorem 3.1 reveals again the well-known result in a new way, where the adaptive controller is defined by Eq. (3.13) together with Eqs. (3.5) – (3.12).*

Corollary 3.2 *If b = 1,* $\frac{ML}{M'} < \frac{3}{2} + \sqrt{2}, c = w = 0$ *, then the adaptive controller defined by Eqs. (3.5) – (3.13) can asymptotically stabilize the corresponding noise-free system, i.e.*

$$\lim_{t\to\infty} |y_t - y_t^*| = 0. \tag{3.16}$$

3.3.2 Preliminary Lemmas

To prove Theorem 3.1, we need the following Lemmas:

Lemma 3.1 *Assume* $\{x_n\}$ *is a bounded sequence of real numbers, then we must have*

$$\lim_{n\to\infty} \min_{i<n} |x_n - x_i| = 0. \tag{3.17}$$

Proof: It is a direct conclusion of [XG00, Lemma 3.4]. It can be proved by argument of contradiction.

Lemma 3.2 *Assume that* $L \in (0, \frac{3}{2} + \sqrt{2}), d \geq 0, n_0 \geq 0$ *. If non-negative sequence* $\{h_n,\ n \geq 0\}$ *satisfies*

$$h_{n+1} \leq \left(L \max_{i\leq n} h_i - \frac{1}{2} \sum_{i=0}^{n} h_i + d \right)^+, \forall n \geq n_0 \tag{3.18}$$

where $x^+ \overset{\Delta}{=} \max(x, 0), \forall x \in R$ *, then we must have*

$$\lim_{n\to\infty} \sum_{i=0}^{n} h_i < \infty. \tag{3.19}$$

Proof: See [XG00, Lemma 3.3].

3.3.3 Proof of Theorem 3.1

Proof of Theorem 3.1: We divide the proof into four steps. In Step 1, we deduce the basic relation between y_{t+1} and $\tilde{\theta}_t$, and then a key inequality describing the upper bound of $| y_t - y_{i_t} |$ is established in Step 2. Consequently, in Step 3, we prove that $| y_t - y_{i_t} | \to 0$

as $t \to \infty$ if y_t is not bounded, and hence the boundedness of output sequence $\{y_t\}$ can be guaranteed. Finally, in the last step, the bound of tracking error can be further estimated based on the stability result obtained in Step 3.

Step 1: Let

$$\begin{aligned} \tilde{\theta}_t &\triangleq \theta - \hat{\theta}_t \\ y_{t+1}^{\#} &\triangleq \theta\phi_t + f(y_t) + w_{t+1} - \hat{g}_t \end{aligned} \tag{3.20}$$

then, by definition of ut and Eq. (3.13), obviously we get

$$y_{t+1} = \begin{cases} y_{t+1}^{\#} + y_{t+1}^{*} & \text{if } |y_t - y_{i_t}| \le D \\ y_{t+1}^{\#} + \frac{1}{2}(\bar{b}_t + \underline{b}_t) & \text{if } |y_t - y_{i_t}| > D \end{cases} \tag{3.21}$$

Now we discuss $y_{t+1}^{\#}$. By Eq. (3.11) and Eq. (3.1), we get

$$\begin{aligned} y_{t+1}^{\#} &= \theta\phi_t + f(y_t) + w_{t+1} - \hat{g}_t \\ &= \theta\phi_t + f(y_t) + w_{t+1} - \hat{\theta}_t(\phi_t - \phi_{i_t}) \\ &\quad -(\theta\phi_{i_t} + f(y_{i_t}) + w_{i_t+1}) \\ &= (\theta - \hat{\theta}_t)(\phi_t - \phi_{i_t}) \\ &\quad +[f(y_t) - f(y_{i_t})] + (w_{t+1} - w_{i_t+1}) \\ &= \tilde{\theta}_t(\phi_t - \phi_{i_t}) + [f(y_t) - f(y_{i_t})] + (w_{t+1} - w_{i_t+1}) \end{aligned} \tag{3.22}$$

In case of $\phi_t = \phi_{i_t}$, i.e. $y_t = y_{it}$, obviously we get

$$|y_{t+1}^{\#}| = |w_{t+1} - w_{i_t+1}| \le 2w; \tag{3.23}$$

otherwise, we get

$$y_{t+1}^{\#} = (\tilde{\theta}_t + D_{t,i_t})(\phi_t - \phi_{i_t}) + (w_{t+1} - w_{i_t+1}) \tag{3.24}$$

where

$$D_{i,j} \triangleq \frac{f(y_i) - f(y_j)}{\phi_i - \phi_j}.$$

Obviously $D_{ij} = D_{ji}$. In the latter case, i.e. when $\phi_t \neq \phi_{i_t}$, for any $(i, j) \in J_t$, noting that

$$\begin{aligned} z_j - z_i &= (y_{j+1} - u_j) - (y_{i+1} - u_i) \\ &= \theta(\phi_j - \phi_i) + [f(y_j) - f(y_i)] \\ &\quad + [w_{j+1} - w_{i+1}] \end{aligned} \tag{3.25}$$

we obtain that

$$\theta - \frac{z_j - z_i}{\phi_j - \phi_i} = -D_{i,j} - \frac{w_{j+1} - w_{i+1}}{\phi_j - \phi_i}. \tag{3.26}$$

Therefore

$$\begin{aligned} \tilde{\theta}_t + D_{t,i_t} &= (\theta - \tfrac{z_j - z_i}{\phi_j - \phi_i}) - (\hat{\theta}_t - \tfrac{z_j - z_i}{\phi_j - \phi_i}) + D_{t,i_t} \\ &= D_{t,i_t} - D_{i,j} - \tfrac{w_{j+1} - w_{i+1}}{\phi_j - \phi_i} + \Delta_{i,j}(t) \end{aligned} \tag{3.27}$$

where

$$\Delta_{i,j}(t) = \frac{z_j - z_i}{\phi_j - \phi_i} - \hat{\theta}_t. \tag{3.28}$$

Step 2: Since $\frac{ML}{M'} < \frac{3}{2} + \sqrt{2}$, there exists a constant $\varepsilon > 0$ such that $\frac{ML}{M'} + \varepsilon < \frac{3}{2} + \sqrt{2}$.

Let

$$B_t \triangleq [\underline{b}_t, \bar{b}_t], \Delta B_t = B_t - B_{t-1} \tag{3.29}$$

and consequently

$$|B_t| = \bar{b}_t - \underline{b}_t, |\Delta B_t| = |B_t| - |B_{t-1}| \tag{3.30}$$

By the definitions of $\underline{b}_t$, $\overline{b_t}$ and B_t, we obtain that

$$|B_{t+1}| = \begin{cases} |B_t| & \text{if } y_{t+1} \in B_t \\ \frac{1}{2}|B_t| + |y_{t+1} - \frac{1}{2}(\underline{b}_t + \bar{b}_t)| & \text{if } y_{t+1} \notin B_t \end{cases} \tag{3.31}$$

By the definition of i_t, obviously we get

$$|y_t - y_{i_t}| \begin{cases} = |\Delta B_t| & \text{if } y_t \notin B_{t-1} \\ \le |\Delta B_i| & \text{if } y_t \in \Delta B_i \subset B_{t-1} \end{cases} \tag{3.32}$$

Step 3: Based on Assumption 3.4, for any fixed $\varepsilon > 0$, we can take constants D and D' such that $|\phi_i - \phi_j| > D' > \frac{4M(2w+c)}{\varepsilon}$ when $|y_t - y_{i_t}| > D$. Now we are ready to show that *for any $s > 0$, there always exists $t > s$ such that* $|y_t - y_{i_t}| > D$.

In fact, suppose that it is not true, then there must exist $s > 0$ such that $|y_t - y_{i_t}| > D$ for any $t > s$, correspondingly $|\phi_t - \phi_{it}| > D'$. Consequently, by the definition of D, for sufficiently large t and $j < t$, we obtain that

$$|\frac{w_{j+1} - w_{i_j+1}}{\phi_j - \phi_{i_j}}| \le |\frac{2w}{D'}| < \frac{1}{4M}\epsilon \tag{3.33}$$

together with the definition of $\hat{\theta}_t$, we know that for any $s < i < j < t$,

$$|\Delta_{i,j}(t)| = |\frac{z_j - z_i}{\phi_j - \phi_i} - \hat{\theta}_t| \le \frac{L}{M'} + \frac{2w+c}{|\phi_j - \phi_i|}. \tag{3.34}$$

hence for $s < j < t, i = i_j$, we get

$$|\Delta_{j,i_j}(t)| = |\Delta_{i_j,j}(t)| \le \frac{L}{M'} + \frac{2w+c}{D'} \le \frac{L}{M'} + \frac{1}{4M}\epsilon. \tag{3.35}$$

Now we consider $D_{t,i_t} - D_{j,i_j}$.

Let $d_n = D_{n,i_n}$, then, by the definition of $D_{i,j}$, noting that $|y_j - y_i| \ge |y_j - y_{i_j}| > D$ for any $j > s$, we obtain that

$$|D_{i,j}| = |\frac{f(y_i) - f(y_j)}{y_i - y_j}| \cdot |\frac{y_i - y_j}{\phi_i - \phi_j}| \le \frac{L}{M'}, \tag{3.36}$$

so we can conclude that $\{d_n, n > s\}$ is bounded. Then, by Lemma 3.1, we conclude that

$$\lim_{t\to\infty} \min_{s<j<t} |d_t - d_j| = 0. \tag{3.37}$$

Consequently there exists $s' > s$ such that for any $t > s'$, we can always find a corresponding $j=j(t)$ satisfying

$$|D_{t,i_t} - D_{j,i_j}| = |d_t - d_j| < \frac{1}{4M}\epsilon. \tag{3.38}$$

Summarizing the above, for any $t > s'$, by taking $j = j(t)$, we get

$$\begin{aligned} |\tilde{\theta}_t + D_{t,i_t}| &= |D_{t,i_t} - D_{i_j,j} - \tfrac{w_{j+1}-w_{i+1}}{\phi_j - \phi_{i_j}} + \Delta_{i_j,j}(t)| \\ &\le |D_{t,i_t} - D_{i_j,j}| + |\tfrac{w_{j+1}-w_{i+1}}{\phi_j - \phi_{i_j}}| + |\Delta_{i_j,j}(t)| \\ &\le \tfrac{1}{4M}\epsilon + \tfrac{1}{4M}\epsilon + (\tfrac{L}{M'} + \tfrac{1}{4M}\epsilon) \\ &= \tfrac{L}{M'} + \tfrac{3}{4M}\epsilon \\ &\triangleq L_\epsilon. \end{aligned} \tag{3.39}$$

Therefore

$$\begin{aligned} |y^{\#}_{t+1}| &= |(\tilde{\theta}_t + D_{t,i_t})\tfrac{\phi_t - \phi_{i_t}}{y_t - y_{i_t}}(y_t - y_{i_t}) + (w_{t+1} - w_{i_t+1})| \\ &\le L_\epsilon M |y_t - y_{i_t}| + 2w. \end{aligned} \tag{3.40}$$

Since $|y_t - y_{it}| > D$, we know that

$$y_{t+1} = y^{\#}_{t+1} + \frac{1}{2}(\bar{b}_t + \underline{b}_t). \tag{3.41}$$

From Eq. (3.39) together with the result in Step 2, we obtain that

$$\begin{aligned} |B_t| \le |B_{t+1}| &\le \max\{|B_t|, \tfrac{1}{2}|B_t| + |y_{t+1} - \tfrac{1}{2}(\underline{b}_t + \bar{b}_t)|\} \\ &= \max\{|B_t|, \tfrac{1}{2}|B_t| + |y^{\#}_{t+1}|\} \end{aligned} \tag{3.42}$$

Thus noting (3.40), we obtain the following key inequality:

$$|\Delta B_t| \le (L_\epsilon M |y_t - y_{i_t}| + 2w - \tfrac{1}{2}|B_t|)^+ \tag{3.43}$$

where

$$L_\epsilon M = (\tfrac{L}{M'} + \tfrac{3}{4M}\epsilon)M = \tfrac{ML}{M'} + \tfrac{3}{4}\epsilon < \tfrac{3}{2} + \sqrt{2}. \tag{3.44}$$

Considering the arbitrariness of $t > s'$, together with Lemma 3.2, we obtain that

$$\sum_{j>s'} |\Delta B_j| < \infty, \tag{3.45}$$

and consequently $\{|B_t|\}$ must be bounded. By applying Lemma 3.1 again, we conclude that

$$|y_t - y_{i_t}| \le \min_{i<t} |y_t - y_i| \to 0 \tag{3.46}$$

which contradicts the former assumption!
Step 4: According to the results in Step 3, for any $s > 0$, there always exists $t > s$ such that $|y_t - y_{i_t}| \le D$. Then, we can easily obtain that $\{|\widetilde{\theta}_t|\}$ is bounded, say $|\widetilde{\theta}_t| \le L'$. Considering that

$$y_{t+1}^{\#} = \tilde{\theta}_t(\phi_t - \phi_{i_t}) + [f(y_t) - f(y_{i_t})] + (w_{t+1} - w_{i_t+1}) \tag{3.47}$$

we can conclude that

$$\begin{aligned} |y_{t+1}| &\le |y_{t+1}^{\#} + y_{t+1}^{*}| \\ &\le L'|\phi_t - \phi_{i_t}| + (L|y_t - y_{i_t}| + c) + 2w \\ &\le Y \end{aligned} \tag{3.48}$$

where $Y = L'MD + LD + c + 2w + S$.
The proof below is similar to that in [XG00]. Let

$$t_0 = \inf_{t>0}\{t : |y_t| \le Y\},\ t_n = \inf_{t>t_{n-1}}\{t : |y_t| \le Y\}. \tag{3.49}$$

Because of the result obtained above, we conclude that for any $n \ge 1$, t_n is well-defined and $t_n < \infty$. Let $v_n = y_{t_n}$, then obviously $\{v_n\}$ is bounded. Then, by applying Lemma 3.1, we get

$$\min_{i<n} |v_n - v_i| \to 0 \tag{3.50}$$

as $n \to \infty$. Thus for any $\varepsilon > 0$, there exists an integer n_0 such that for any $n > n_0$,

$$\min_{i<n} |v_n - v_i| < \varepsilon. \tag{3.51}$$

So

$$|y_{t_n} - y_{i_{t_n}}| = \min_{i<t_n} |y_{t_n} - y_i| \le \min_{i<n} |y_{t_n} - y_{t_i}| < \varepsilon. \tag{3.52}$$

By taking ε sufficiently small, we obtain that

$$|y_{t_n+1}| \le L'M\varepsilon + L\varepsilon + c + 2w + S \le Y \tag{3.53}$$

for any $n > n_0$.
Thus based on definition of t_n, we conclude that $t_{n+1} = t_n + 1$! Therefore for any $t \ge t_{n_0}$,

$$|y_t| \le Y \tag{3.54}$$

which means that the sequence $\{y_t\}$ is bounded.
Finally, by applying Lemma 3.1 again, for sufficiently large t, $| y_t - y_{i_t} | \le \varepsilon$ consequently

$$|y_{t+1} - y^*_{t+1}| = |y^{\#}_{t+1}| \le L'M\varepsilon + L\varepsilon + c + 2w. \tag{3.55}$$

Because of arbitrariness of ε, Theorem 3.1 is true.

3.4 Simulation Study

In this section, two simulation examples will be given to illustrate the effects of the adaptive controller designed above. In both simulations, the tracking signal is taken as $y^*_t = 10 \sin \frac{t}{10}$ and the noise sequence is i.i.d. randomly taken from uniform distribution $U(0, 1)$. The simulation results for two examples are depicted in Figure 8 and Figure 9, respectively. In each figure, the output sequence y_t and the reference sequence y^*_t are plotted in the top-left subfigure; the tracking error sequence $e_t \overset{\Delta}{=} y_t - y^*_t$ is plotted in the bottom-left subfigure; the control sequence u_t is plotted in the top-right subfigure; and the parameter θ together with its upper and lower estimated bounds is plotted in the bottom-right subfigure.
Simulation Example 1: This example is for case of $b = 1$, and the unknown plant is

$$y_{t+1} = f(y_t) + \theta g(y_t) + w_{t+1}, \quad f(\cdot) \in \mathcal{F}(L) \tag{3.56}$$

with $L = 2.9 < \frac{3}{2} + \sqrt{2}, g(x) = x$ (i.e. $b = 1, M = M' = 1$)

and

$$f(x) = 1.4x \sin \log(|x| + 1). \tag{3.57}$$

For this example, we can verify that

$$|f'(x)| = 1.4|\sin\log(|x|+1) \pm \frac{x\cos\log(|x|+1)}{|x|+1}| \le 2.8 < L \tag{3.58}$$

consequently $|f(x)-f(y)| < L|x-y|$, i.e. $f(\cdot) \in F(L)$..

Simulation Example 2: This example is for case of $b > 1$, and the unknown plant is

$$y_{t+1} = f(y_t) + \theta g(y_t) + w_{t+1}, \quad f(\cdot) \in \mathcal{F}(L) \tag{3.59}$$

with $L = 2.9$, $g(x) = x^2$ (i.e. $b = 2$, $M = M' = 1$), and

$$f(x) = 2x + \sin x^2. \tag{3.60}$$

For this example, we can verify that $|f(x)-f(y)| < L|x-y| + 2$, i.e. $f(\cdot) \in F(L)$.

From the simulation results, we can see that in both examples, the adaptive controller can track the reference signal successfully. The simulation study verified our theoretical result and indicate that under some conditions, the adaptive control law constructed in this paper can deal with both parametric and non-parametric uncertainties, even in some cases when the parametric part is of nonlinear growth rate. In case of $b = 1$, the stabilizability criteria have been completely characterized by a simple algebraic condition; however, in case of $b > 1$, it is very difficult to give complete theoretical characterization. Note that usually more accurate estimate of parameter can be obtained in case of $b > 1$ than in case of $b = 1$, however, worse transient performance may be encountered.

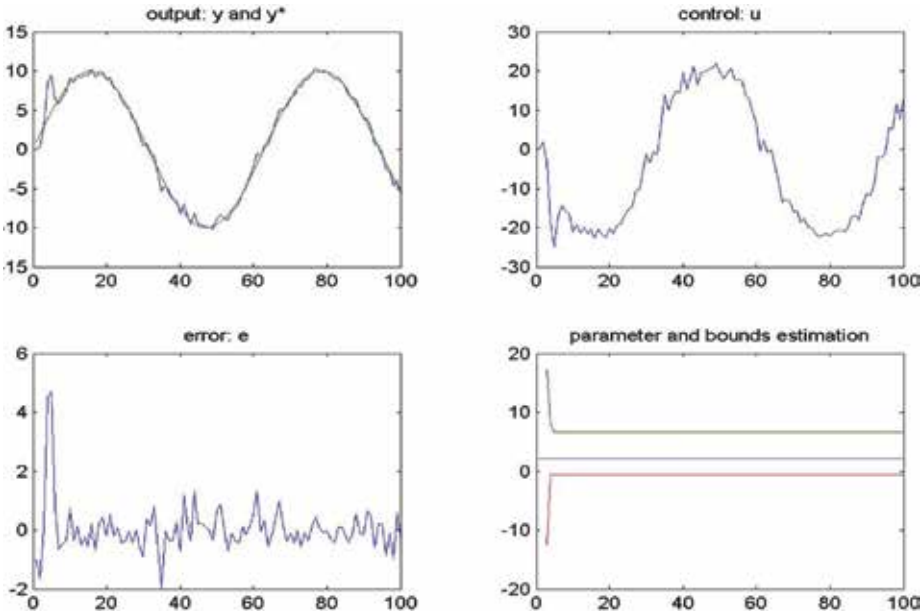

Fig. 8. Simulation example 1: ($g(x) = x$, $b = 1$,$M = M' = 1$)

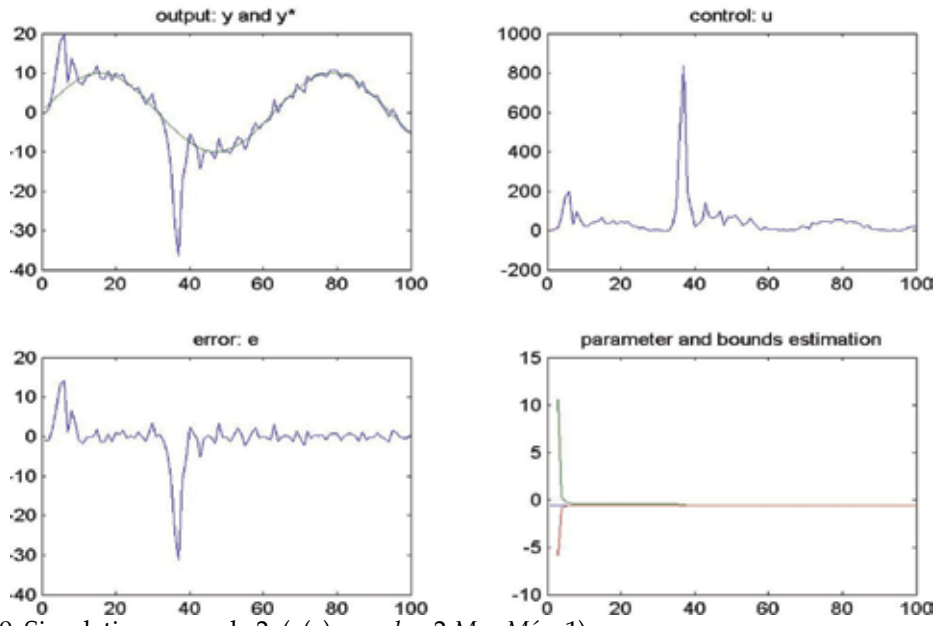

Fig. 9. Simulation example 2: ($g(x) = x_2$, $b = 2$,$M = M' = 1$)

4. Semi-parametric Adaptive Control: Example 2

In this section, we shall give another example of adaptive estimation and control for a semi-parametric model. Although the system considered in this section is similar to the model considered in last section, there are several particular points in this example:

• The controller gain in this model is also unknown with *a priori* knowledge on its sign and its lower bound.

• The system is noise-free, and correspondingly the asymptotic tracking is rigorously established in this example.

• The algorithm in this example has a form of gradient algorithm, however, it partially makes use of *a priori* knowledge on the non-parametric part.

• Due to the limitation of this algorithm and technical difficulties, unlike the algorithm in last section, we can only establish stability of the closed-loop system under condition $0 < L < 0.5$ for the parametric part, which is much stronger than the condition $0 \le L < \frac{3}{2} + \sqrt{2}$.

This example is given here only for the purpose of demonstrating that there exist other possible ways to make use of *a priori* knowledge on the parametric uncertainties and non-parametric uncertainties. By comparing the examples in this section and last section, the readers may get a deeper understanding to adaptive estimation and control problems for semi-parametric models.

4.1 Problem Formulation

We consider the following system model

$$y_{k+1} = \theta\Phi(y(k)) + f(y_k) + bu_k \tag{4.1}$$

where $y_k \in R^1$ and $u_k \in R^1$ are output and control signals, respectively. Here $\theta \in R^1$ is the unknown parameter, $b \in R^1$ is the unknown controller gain, $\Phi(\cdot)$ is a known function, and $f(\cdot)$ is the unknown function. We have the following *a priori* knowledge on the real system:

Assumption 4.1 *The nonparametric uncertain function $f(\cdot)$ is Lipschitz, i.e., $\| f(x_1) - f(x_2) \| \leq L \| x_1 - x_2 \|, \forall x_1, x_2 \in R$, where L < 0.5. The known function $\Phi(\cdot)$ is also a Lipschitz function with Lipschitz constant L.*

Assumption 4.2 *The sign of unknown controller gain b is known. Without loss of generality, we assume that $b \geq \underline{b} > 0$ where $\underline{b}$ is a known constant.*

Assumption 4.3 *The reference signal y_k^* is a known bounded deterministic signal.*

The control objective is to design the control law u_k such that the output signal y_k asymptotically tracks a bounded reference trajectory y_k^* and all the closed-loop signals are guaranteed to be bounded.

4.2 Adaptive Control Design

To design the adaptive controller, the following notations will be used throughtout this section:

$$\begin{aligned} l_k &= \arg\min_{l \leq k-1} |y_k - y_l| \\ e_k &= y_k - y_k^* \end{aligned} \tag{4.2}$$

Obviously, at time step k, with the history information $\{y_j, j \leq k\}$ and the *a priori* knowledge, the index l_k and the tracking error e_k are available. Later we will see important roles of l_k and e_k in the controller design.

Estimation of parametric part: The estimates of the parameter θ and the controller gain b at time step k are denoted by $\hat{\theta}_k$ and $\hat{b}_k$, respectively. We design the following adaptive update law to update the parameter estimates recursively:

$$\begin{aligned}
\hat{\theta}_k &= \hat{\theta}_{k-1} + \gamma \frac{a_k e_k [\Phi(y_{k-1}) - \Phi(y_{l_{k-1}})]}{D_{k-1}} \\
\hat{b}_k &= \begin{cases} \hat{b}'_k & \text{if } \hat{b}'_k > \underline{b} \\ \underline{b} & \text{otherwise} \end{cases} \\
\hat{b}'_k &= \hat{b}_{k-1} + \text{Proj}_{\hat{b}}\{\frac{\gamma a_k e_k}{D_{k-1}}[u_{k-1} - u_{l_{k-1}}]\} \\
D_{k-1} &= \frac{1}{2}\|\Phi(y_{k-1}) - \Phi(y_{l_{k-1}})\|^2 + \frac{1}{2}[u_{k-1} - u_{l_{k-1}}]^2
\end{aligned}$$

where $0 < \gamma < 1$ and the coefficient a_k is defined by a time-varying deadzone:

$$a_k = \begin{cases} 1 - \frac{\lambda|y_{k-1} - y_{l_{k-1}}|}{|e_k|} & \text{if } |e_k| > \lambda|y_{k-1} - y_{l_{k-1}}| \\ 0 & \text{otherwise} \end{cases} \tag{4.4}$$

Estimation of non-parametric part: As in last section, we do not estimate the non-parametric part directly. Instead, we try to estimate the parametric part and non-parametric part as a whole part

$$y_k^{\#} \triangleq \theta\Phi(y_k) + f(y_k) \tag{4.5}$$

Noticing of the system model (4.1), we know that

$$y_{k+1} = y_k^{\#} + bu_k \tag{4.6}$$

consequently, from Eqs. (4.5) and (4.6), it is easy to derive

$$\begin{aligned}
y_k^{\#} &= y_k^{\#} - y_{l_k}^{\#} + y_{l_k}^{\#} \\
&= \theta[\Phi(y_k) - \Phi(y_{l_k})] + f(y_k) - f(y_{l_k}) \\
&\quad + y_{l_k+1} - bu_{l_k}
\end{aligned} \tag{4.7}$$

Since function $f(\cdot)$ is unknown and parameters θ and b are unknown, we simply estimate $y_k^{\#}$ by the following eqution

$$\hat{y}_k^{\#} = \hat{\theta}_k[\Phi(y_k) - \Phi(y_{l_k})] + y_{l_k+1} - \hat{b}_k u_{l_k} \tag{4.8}$$

where $\hat{\theta}_k$ and $\hat{b}_k$ are regarded as true parameters, and the unknown term $f(y_k) - f(y_{l_k})$ in Eq. (4.7) is simply dropped off.

Adaptive control law: By Eq. (4.6), according to the certainty equivallence principle, we can design the following adaptive control law

$$u_k = -\frac{1}{\hat{b}_k}(\hat{y}_k^{\#} - y_{k+1}^*) \tag{4.9}$$

Where $\hat{b}_k$ and $\hat{y}_k^{\#}$ are given by Eqs. (4.3) and (4.7). The closed-loop stability will be given later.

4.3 Asymptotic Tracking Performance

4.3.1 Main Results

Theorem 4.1 *In the closed-loop system (4.1) with control law (4.9) and parameters adaptation law (4.3), under Assumptions 4.1 – 4.3, all the signals in the closed-loop system are bounded and further the tracking error* e_k *will converge to zero.*

4.3.2 Preliminaries

Definition 4.1 *Let* x_k *and* y_k *(*$k \geq 0$*) be two discrete-time scalar or vector signals.*

• *We denote* $x_k = O[y_k]$*, if there exist positive constants* m_1 *and* m_2 *such that* $\| x_k \| \leq m_1 \max_{j \leq k} \| y_j \| + m_2$*,* $\forall k > k_0$ *and* k_0 *is the initial time step.*

• *We denote* $x_k = o[y_k]$*, if there exists* a sequence α_k *satisfying* $\lim_{k \to \infty} \alpha_k \to 0$ *such that* $\| x_k \| \leq m_1 \max_{j \leq k} \| y_j \| + m_2$*,* $\forall k > k_0$*.*

• *We denote* $x_k \sim y_k$ if they satisfy $x_k = O[y_k]$ and $y_k = O[x_k]$.

Lemma 4.1 *Consider the following parameter update law*

$$\hat{\theta}_k = \begin{cases} \hat{\theta}'_k & \text{if } \hat{\theta}'_k > \mu \\ \mu & \text{otherwise} \end{cases} \tag{4.10}$$

$$\hat{\theta}'_k = \hat{\theta}_{k-1} + Proj_{\hat{\theta}}(\eta_k) \tag{4.11}$$

$$Proj_{\hat{\theta}}(\eta_k) = \begin{cases} -\eta_k, & \text{if } \hat{\theta}_{k-1} = \mu \text{ and } \eta_k < 0 \\ \eta_k, & \text{otherwise} \end{cases} \tag{4.12}$$

where $\theta \in R$ *is an unknown scalar,* $\hat{\theta}_k$ is its estimate at time step k, μ *is the lower bound of* θ, *and* $\eta_k \in R$ *is any sequence. Then,* $\hat{\theta}_k \geq \mu$ *is guaranteed and the following properties hold:*

$$\tilde{\theta}_k'^2 \geq \tilde{\theta}_k^2,\ \mathit{Proj}_{\hat{\theta}}^2(\eta_k) = \eta_k^2,\ \tilde{\theta}_k^T(\mathit{Proj}_{\hat{\theta}}(\eta_k) - \eta_k) \quad \leq \quad 0$$

where $\tilde{\theta}_k' = \hat{\theta}_k' - \theta$ *and* $\tilde{\theta}_k = \hat{\theta}_k - \theta$.

Proof: According to Eqs. (4.10) and (4.11), it is obvious that $\hat{\theta}_k \geq \mu$ always hold. From Eq. (4.12), we see that $|\,\mathrm{Proj}_{\hat{\theta}}(\eta_k)\,| = |\,\eta_k\,|$, hence $\mathrm{Proj}_{\hat{\theta}}^2(\eta_k) = \eta_k^2$. Further, we have

$$\begin{aligned} & \tilde{\theta}_{k-1}(\mathrm{Proj}_{\hat{\theta}}(\eta_k) - \eta_k) \\ = & \begin{cases} (\hat{\theta}_{k-1} - \theta)(-\eta_k - \eta_k) \leq 0, & \text{if } \hat{\theta}_{k-1} = \mu \text{ means } (\hat{\theta}_{k-1} - \theta) \leq 0 \text{ and } \eta_k < 0 \\ (\hat{\theta}_{k-1} - \theta)(\eta_k - \eta) = 0 & \text{otherwise} \end{cases} \end{aligned}$$

From (4.10), we see that $\hat{\theta}_k' = \hat{\theta}_k$ if $\hat{\theta}_k' > \mu$ such that $\tilde{\theta}_k'^2 = \tilde{\theta}_k^2$ when $\hat{\theta}_k' > \mu$. Noticing that when $\hat{\theta}_k' \leq \mu$, we have $\mu \leq \theta$, so that

$$\begin{aligned} \tilde{\theta}_k'^2 &= (\hat{\theta}_k' - \theta)^2 = [(\hat{\theta}_k' - \mu) + (\mu - \theta)]^2 \\ &= (\hat{\theta}_k' - \mu)^2 + (\mu - \theta)^2 + 2(\hat{\theta}_k' - \mu)(\mu - \theta) \\ &\geq (\mu - \theta)^2 = (\hat{\theta}_k - \theta)^2 = \tilde{\theta}_k^2 \end{aligned} \tag{4.13}$$

Therefore, we always have $\tilde{\theta}_k'^2 \geq \tilde{\theta}_k^2$. This completes the proof.

Lemma 4.2 *Given a bounded sequence* $X_k \in R^m$. *Define*

$$l_k = \arg \min_{l \leq k-1} \|X_k - X_l\|$$

Then, we have

$$\lim_{k \to \infty} \|X_k - X_{l_k}\| = 0$$

Proof: This lemma is an extension of Lemma 3.1. Its proof can be found in [Ma06].

Lemma 4.3 *(Key Technical Lemma)Let* $\{s_t\}$ *be a sequence of real numbers and* $\{\sigma_t\}$ *be a sequence of vectors such that*

$$\|\sigma_t\| \leq c_1 + c_2 \max_{0 \leq k \leq t} |s_k|$$

Assume that

$$z_t = \frac{s_t^2}{\alpha_1 + \alpha_2 \sigma_t^\tau \sigma_t} \to 0 \; as \; t \to \infty$$

where $\alpha_1 > 0, \alpha_2 > 0$. *Then* $\| \sigma_t \|$ *is bounded.*

Proof: This lemma can be found in [AW89, GS84].

4.3.3 Proof of Theorem 4.1

Define parameter estimate errors $\tilde{b}_k = \hat{b}_k - b$ and $\tilde{\theta}_k = \hat{\theta}_k - \theta$. From Eqs. (4.7) and (4.8), we have

$$\begin{aligned} \tilde{y}_k^{\#} &\triangleq \hat{y}_k^{\#} - y_k^{\#} \\ &= \tilde{\theta}_k[\Phi(y_k) - \Phi(y_{l_k})] - f(y_k) + f(y_{l_k}) - \tilde{b}_k u_{l_k} \end{aligned} \tag{4.14}$$

Then, we can derive the following error dynamics:

$$\begin{aligned} e_{k+1} &\triangleq y_{k+1} - y_{k+1}^* \\ &= y_k^{\#} + \hat{b}_k u_k - \tilde{b}_k u_k - y_{k+1}^* \\ &= -\tilde{y}_k^{\#} - \tilde{b}_k u_k \\ &= -\tilde{\theta}_k[\Phi(y_k) - \Phi(y_{l_k})] + f(y_k) - f(y_{l_k}) - \tilde{b}_k[u_k - u_{l_k}] \end{aligned} \tag{4.15}$$

According to Assumption 4.1, we have

$$|f(y_k) - f(y_{l_k})| \leq \lambda |y_k - y_{l_k}| \tag{4.16}$$

where λ can be any constant satisfying $L \leq \lambda < 0.5$.

From the error dynamics Eq. (4.15), we have

$$\begin{aligned} e_k &= -\tilde{\theta}_{k-1}[\Phi(y_{k-1}) - \Phi(y_{l_{k-1}})] + f(y_{k-1}) - f(y_{l_{k-1}}) \\ &\quad -\tilde{b}_{k-1}[u_{k-1} - u_{l_{k-1}}] \end{aligned} \tag{4.17}$$

Choose Lyapunov function candidate as

$$V_k = \tilde{\theta}_k^2 + \tilde{b}_k^2 \tag{4.18}$$

From the adaptation laws (4.3), we obtain that

$$\tilde{\theta}_k^2 - \tilde{\theta}_{k-1}^2 = \gamma^2 \frac{a_k^2 e_k^2}{D_{k-1}^2}[\Phi(y_{k-1}) - \Phi(y_{l_{k-1}})]^2 + 2\gamma \frac{a_k e_k}{D_{k-1}}[\Phi(y_{k-1}) - \Phi(y_{l_{k-1}})] \tag{4.19}$$

$$\tilde{g}_k^2 - \tilde{g}_{k-1}^2 \leq \tilde{g}_k'^2 - \tilde{g}_{k-1}^2 \tag{4.20}$$

$$= \gamma^2 \frac{a_k^2 e_k^2}{D_{k-1}^2}[u_{k-1} - u_{l_{k-1}}]^2 + 2\gamma \frac{a_k e_k}{D_{k-1}}[u_{k-1} - u_{l_{k-1}}] \tag{4.21}$$

Together with the error dynamics Eq. (4.17), we can derive that the difference of V_k

$$\Delta V_k = V_k - V_{k-1} \leq -\frac{2\gamma(1-\gamma)a_k^2 e_k^2}{D_{k-1}} \tag{4.22}$$

Noting that 0 < (< 1 and taking summation on both hand sides of Eq. (4.22), we obtain

$$\sum_{k=0}^{\infty} 2\gamma(1-\gamma)\frac{a_k^2 e_k^2}{D_{k-1}} \leq V(0) - V(\infty)$$

Which implies

$$\lim_{k\to\infty} \frac{a_k^2 e_k^2}{D_{k-1}} = 0 \tag{4.23}$$

and the boundedness of $\hat{\theta}_k$ and $\hat{b}_k$. Considering $y_k \sim e_k$, we have

$$|y_{k-1}| \leq \max_{j\leq k}\{|e_j|\} + C_2,\ k > k_0$$

where and C_2 are some constants. From the definition of deadzone in Eq. (4.4), we have $|e_k| - \lambda|y_{k-1} - y_{l_{k-1}}| \leq a_k|e_k|$.

Therefore, we have

$$\begin{aligned} |y_{k-1}| &\leq \max_{j\leq k}\{|e_j|\} + C_2 \\ &= \max_{j\leq k}\{|e_j| - \lambda|y_{j-1} - y_{l_{j-1}}| + \lambda|y_{j-1} - y_{l_{j-1}}|\} + C_2 \\ &\leq \max_{j\leq k}\{a_j|e_j|\} + \lambda \max_{j\leq k-1}\{|y_j - y_{l_j}|\} + C_2,\ k > k_0 \end{aligned} \tag{4.24}$$

Therefore, we have

$$\max_{j\leq k-1}\{|y_j|\} \leq \max_{j\leq k}\{a_j|e_j|\} + 2\lambda \max_{j\leq k-1}\{|y_j|\} + C_3,\ k > k_0 \tag{4.25}$$

Note that $\lambda < 0.5$, we have

$$\max_{j\leq k-1}\{|y_j|\} \leq \frac{1}{1-2\lambda}\max_{j\leq k}\{a_j|e_j|\} + \frac{C_3}{1-2\lambda},\ k > k_0 \tag{4.26}$$

holds for all $\lambda < \lambda^*$, where C_3 is some finite number. Note that inequality Eq. (4.26) means that $y_{k-1} = O[a_k e_k]$. Further we have

$$D_{k-1}^{\frac{1}{2}} \leq |\Phi(y_{k-1}) - \Phi(y_{l_{k-1}})| + |u_{k-1} - u_{l_{k-1}}| = O[y_{k-1}] = O[a_k e_k]$$

Therefore, we can apply the Key Technical Lemma (Lemma 4.3) to Eq. (4.23) and obtain that

$$\lim_{k\to\infty} a_k e_k = 0 \tag{4.27}$$

which guarantees the boundedness of y_k from Eq. (4.26) and thus, the boundedness of output y_k, tracking error e_k. Therefore, applying Lemma 4.2 yields

$$\lim_{k\to\infty} |y_k - y_{l_k}| = 0 \tag{4.28}$$

Next, we will show that $\lim_{k\to\infty} \alpha_k e_k \to 0$ leads to $\lim_{k\to\infty} e_k \to 0$. From the definition of deadzone in Eq. (4.4), we have $a_k \in [0,1)$. Let us define the following sets:

$$\begin{aligned} Z_1^+ &= \{k | a_k = 0, k \in Z^+\} \\ Z_2^+ &= \{k | a_k \neq 0, k \in Z^+\} \end{aligned} \tag{4.29}$$

which results in $Z_1^+ \cap Z_2^+ = \varnothing$ and $Z_1^+ \cup Z_2^+ = Z^+$. The following three cases need to be considered. In every case, we only need to discuss the case where k belongs to an infinite set.

Case i). Z_1^+ is an infinite set and Z_2^+ is a finite set. Let us discuss $k \in Z_1^+$. From the definition in Eq. (4.29), it follows that $a_k = 0$. Hence it is clear from the definition of deadzone (4.4) that $0 \le |e_k| \le \lambda |y_{k-1} - y_{l_{k-1}}|$ which means $\lim_{k\to\infty} e_k \to 0$ according to Eq. (4.28).

Case ii). Z_1^+ is a finite set and Z_2^+ is an infinite set. Let us discuss $k \in Z_2^+$. From the definition in (4.29), it follows that $a_k \neq 0$. Hence it is clear from deadzone (4.4) that $|e_k| = a_k |e_k| + \lambda |y_{k-1} - y_{l_k-1}|$ which means $\lim_{k\to\infty} e_k = 0$ due to Eqs. (4.27) and (4.28).

Case iii). Z_1^+ and Z_2^+ are infinite sets. If $k \in Z_1^+$ then $a_k = 0$. Following Case i) gives $\lim_{k\to\infty} e_k = 0$. Otherwise, $a_k \neq 0$, it follows from Case ii) that $\lim_{k\to\infty} e_k = 0$.

Based on the discussions for the above three cases, we can conclude that $\lim_{k\to\infty} a_k e_k = 0$ implies that $\lim_{k\to\infty} e_k = 0$. This completes the proof.

5. Conclusion

In this chapter, we have formulated and discussed the adaptive estimation and control problems for a class of semi-parametric models with both parametric uncertainty and non-parametric uncertainty. For a typical semi-parametric system model, we have discussed new ideas and principles in how to estimate the unknown parameters and non-parametric part by making full use of *a priori* knowledge, and for a typical type of *a priori* knowledge on the non-parametric part, we have proposed novel information-concentration estimator so as to deal with both kinds of uncertainties in the system, and some implementation issues in various cases have been discussed with applicable algorithm descriptions. Furthermore, we have applied the ideas of adaptive estimation for semi-parametric model into two examples of adaptive control problem for two typical semi-parametric control systems, and discussed in details how to establish the closed-loop stability of the whole system with semi-parametric adaptive estimator and controller. Our discussions have demonstrated that the topic in this chapter is very challenging yet important due to its wide
background. Especially, for the closed-loop analysis problem of semi-parametric adaptive control, the examples given in this chapter illustrate different methods to overcome the difficulties.

In the first example of semi-parametric adaptive control, we have investigated a simple first-order nonlinear system with both non-parametric uncertainties and parametric uncertainties, which is largely motivated by the recent-year exploration of the capability and limitations of the feedback mechanism. For this model, based on the principle of the proposed IC estimator, we have constructed a unified adaptive controller which can be used in both cases of $b = 1$ and $b > 1$. When the parametric part is of linear growth rate ($b = 1$), we have proved the closed-loop stability under some assumptions and a simple algebraic condition $\frac{ML}{M'} < \frac{3}{2} + \sqrt{2}$, which reveals essential connections with the known magic

number $L = \frac{3}{2} + \sqrt{2}$ discovered in recent work [XG00] on the study of feedback mechanism capability.

In the second example of semi-parametric adaptive control, we further assume that the control gain is also unknown, yet the system is noise-free, and we have designed an adaptive controller based on gradient-like estimation algorithm with time-varying deadzone according to the *a priori* knowledge on the non-parametric part and the unknown controller gain. In this example, although we cannot establish perfect results revealing the magic number $\frac{3}{2} + \sqrt{2}$ as in the first example, we can still establish good results of asymptotic tracking performance under some mild conditions. This example has demonstrated yet another method to deal with uncertainties in semi-parametric model.

Finally, we shall remark that the discussed topic in this chapter is still in its infant stage, and many more chanlenging problems can be investigated in the future. These problems may root in wide practical background where the system model is only partially known *a priori*, that is to say, the major part of the system can be parameterized and the other part is unknown and non-parameterized with only limited *a priori* knowledge. Solving such problems can definitely improve our understanding to the whole feedback mechanism and help us gain more insights on the capability of adaptive control, especially non-traditional adaptive control methods which were not extensively addresed and studied in previous study. Therefore, we expect more theoretical study in this new topic, i.e. semi-parametric adaptive estimation and control.

6. Acknowledgement

The authors would like to thank Chenguang Yang for his helpful discussion and valuable comments.

7. References

[ASL98] A. M. Annaswamy, F. P. Skantzes, and A.-P. Loh, "Adaptive control of continuous time systems with convex/concave parametrization," *Automatica*, vol. 34, no. 1, pp. 33–49, 1998.

[AW89] K. Aström and B. Wittenmark, *Adaptive Control*. Addison-Wesley Pupl. Comp., 1989.

[BDB95] R. M. Bethea, B. S. Duran, and T. L. Boullion, *Statistical Methods for Engineers and Scientists*. CRC Press, 1995.

[Ber04] R. A. Berk, *Regression Analysis: A Constructive Critique*. SAGE, 2004.

[BJR08] G. E. P. Box, G. M. Jenkins, and G. C. Reinsel, *Time Series Analysis: Forecasting and Control*, 4th ed. Wiley, Jun 2008.

[Bos95] J. D. Boskovic, "Stable adaptive control of a class of first-order nonlinearly parameterized plants," *IEEE Transactions on Automatic Control*, vol. 40, pp. 347–350, 1995.

[CG91] H. F. Chen and L. Guo, *Identification and Stochastic Adaptive Control*. Boston, MA: Birkhäuser, 1991.

[DS98] N. R. Draper and H. Smith, *Applied Regression Analysis*, 3rd ed. Wiley-Interscience, Apr 1998.

[FL99] G. Feng and R. Lozano, *Adaptive Control Systems*. Butterworth Heinemann, 1999.

[Fox97] J. Fox, *Applied Regression Analysis, Linear Models, and Related Methods*. SAGE, 1997.

[Gau09] C. F. Gauss, *Theoria motus corporum coelestium in sectionibus conicis solem ambientium: in sectionibus conicis solem ambientium* (Theorie der Bewegung der Himmelskörper, die die Sonne in Kegelschnitten umkreisen). Dover, New York, 1809, english translation by C. H. Davis, reprinted 1963.

[GHZ99] S. S. Ge, C. C. Hang, and T. Zhang, "A direct adaptive controller for dynamic systems with a class of nonlinear parameterizations," *Automatica*, vol. 35, pp. 741–747, (1999.

[Gio85] A. A. Giordano, *Least Square Estimation With Applications to Digital Signal Processing*. Wiley-Interscience, Mar 1985.

[GS84] G. Goodwin and K. Sin, *Adaptive Filtering, Prediction and Control*. Englewood Cliffs, NJ: Prentice-Hall, 1984.

[Guo97] L. Guo, "On critical stability of discrete-time adaptive nonlinear control," *IEEE Transactions on Automatic Control*, vol. 42, no. 11, pp. 1488–1499, 1997.

[Hel63] Z. Hellwig, *Linear regression and its application to economics*. Pergamon Press, 1963.

[Kan94] I. Kanellakopoulos, "A discrete-time adaptive nonlinear system," *IEEE Transactions on Automatic Control*, vol. 39, Nov. 1994.

[LH74] C. Lawson and R. Hanson, *Solving Least Squares Problems*. Prentice-Hall, 1974.

[Lju98] L. Ljung, *System Identification – Theory for the User*, 2nd ed. Upper Saddle River, NJ 07458: Prentice Hall, 1998.

[LQF03] A. P. Loh, C. Y. Qu, and K. F. Fong, "Adaptive control of discrete time systems with concave/convex parametrizations," *IEEE Transactions on Automatic Control*, vol. 48, no. 6, 2003.

[LX06] C. Y. Li and L. L. Xie, "On robust stability of discrete-time adaptive nonlinear control," *Systems and Control Letters*, vol. 55, no. 6, pp. 452–458, June 2006.

[Ma06] H. B. Ma, "Capability and limitation of feedback mechanism in dealing with uncertainties of some discrete-time control systems," Phd Thesis, Graduate School of Chinese Academy of Sciences, Beijing, China, June 2006.

[Ma08a] ——, "Further results on limitations to the capability of feedback," *International Journal of Control*, vol. 81, no. 1, pp. 21 – 42, 2008. [Online]. Available: http://www.informaworld.com/10.1080/00207170701218333

[Ma08b] ——, "An "impossibility" theorem on a class of high-order discrete-time nonlinear control systems," *Systems & Control Letters*, vol. 57, no. 6, pp. 497–504, 2008. [Online]. Available: http://dx.doi.org/10.1016/j.sysconle.2007. 11.008

[MG05] H. B. Ma and L. Guo, "An "impossibility" theorem on second-order discrete-time nonlinear control systems," in *Proceedings of the 24th Chinese Control Conference*. South China University of Technology Press: Guangzhou, July. 2005, pp. 57–61.

[MPV07] D. C. Montgomery, E. A. Peck, and G. G. Vining, *Introduction to Linear Regression Analysis, Solutions Manual*, 4th ed., ser. Wiley Series in Probability and Statistics. Wiley, John Sons, Incorporated, Feb 2007.

[MT95] R. Marino and P. Tomei, *Nonlinear adaptive design: Geometric,adaptive, and robust*. London: Printice-Hall, 1995.

[SB89] S. Sastry and M. Bodson, *Adaptive Control: Stability, Convergence, and Robustness*. Englewood, New Jersey: Prentice-Hall, 1989.

[Sok03] V. F. Sokolov, "Adaptive suboptimal tracking for the first-order plant with lipschitz uncertainty," *IEEE Transactions on Automatic Control*, vol. 48, no. 4, Apr 2003.

[Tsa05] R. S. Tsay, *Analysis of Financial Time Series*, 2nd ed., ser. Wiley Series in Probability and Statistics. Wiley, John Sons, Incorporated, Aug 2005, no. 543.

[VV07] M. Verhaegen and V. Verdult, *Filtering and System Identification: A Least Squares Approach*, 1st ed. Cambridge University Press, May 2007.

[web08] "Statistics & data analysis for environmental science and management," 2008, available online from http://www.esm.ucsb.edu/academics/courses/206/Readings/re ader Ch8.pdf.

[Wei05] S. Weisberg, *Applied Linear Regression*, 3rd ed. Wiley-Interscience, Jan 2005.

[Wik08a] Wikipedia, "Gauss-Markov theorem — wikipedia, the free encyclopedia," 2008. [Online]. Available: http://en.wikipedia.org/w/index.php?title=Gauss%E2%80%93Markov theorem&oldid=232973932

[Wik08b] ——, "Generalized linear model — wikipedia, the free encyclopedia," 2008. [Online]. Available: http://en.wikipedia.org/w/index.php?title=Generalized linear model&oldid=237425065

[Wik08c] ——, "Kernel regression — wikipedia, the free encyclopedia," 2008. [Online]. Available: http://en.wikipedia.org/w/index.php?title=Kernel regression&oldid=234955359

[Wik08d] ——, "Kriging — wikipedia, the free encyclopedia," 2008. [Online]. Available: http://en.wikipedia.org/w/index.php?title=Kriging&oldid=234876679

[Wik08e] ——, "Least squares — wikipedia, the free encyclopedia," 2008. [Online]. Available: http://en.wikipedia.org/w/index.php?title=Least squares&oldid=233230305

[Wik08f] ——, "Linear least squares — wikipedia, the free encyclopedia," 2008. [Online]. Available:http://en.wikipedia.org/w/index.php?title=Linearleastsquares&oldid= 23323034 42

[Wik08g] ——, "Linear regression — wikipedia, the free encyclopedia," 2008. [Online]. Available: http://en.wikipedia.org/w/index.php?title=Linear regression&oldid=237064808

[Wik08h] ——, "Moore-Penrose pseudoinverse — wikipedia, the free encyclopedia," 2008. [Online].Available:http://en.wikipedia.org/w/index.php?title=Moore-Penrosepseudoinver se&oldid=237863190

[Wik08i] ——, "Nonparametric regression — wikipedia, the free encyclopedia," 2008. [Online].Available:http://en.wikipedia.org/w/index.php?title=Nonparametricreg ression& oldid=235577025

[Wik08j] ——, "Regression analysis — wikipedia, the free encyclopedia," 2008. [Online]. Available:http://en.wikipedia.org/w/index.php?title=Regressionanalysis&oldid =2322210 82

[XG99] L. L. Xie and L. Guo, "Fundamental limitations of discrete-time adaptive nonlinear control," *IEEE Transactions on Automatic Control*, vol. 44, no. 9, pp. 1777–1782, 1999.

[XG00] ——, "How much uncertainty can be dealt with by feedback?" *IEEE Transactions on Automatic Control*, vol. 45, no. 12, pp. 2203–2217, 2000.

[XG01] F. Xue and L. Guo, "Necessary and sufficient conditions for adaptive stabilizability of jump linear systems," *Communications in Information and Systems*, vol. 1, no. 2, pp. 205–224, Apr. 2001.

[YDG+08] C. G. Yang, S. L. Dai, S. S. Ge, Z. X. Jiao, and T. H. Lee, "Adaptive asymptotic tracking control of a class of strict-feedback discrete-time nonlinear systems," *IEEE Transactions on Automatic Control*, 2008, to be submitted.

[ZG02] Y. X. Zhang and L. Guo, "A limit to the capability of feedback," *IEEE Transactions on Automatic Control*, vol. 47, no. 4, pp. 687–692, 2002.

3

Adaptive output regulation of unknown linear systems with unknown exosystems

Ikuro Mizumoto and Zenta Iwai
Department of Intelligent Mechanical Systems, Kumamoto University,
2-39-1 Kurokami, Kumamoto, 860-8555, Japan

1. Introduction

The problems of the output regulations and/or disturbance reductions have attracted a lot of interest and have been actively researched in the consideration of the control problem for systems which are required to have servomechanism and for vibration attenuation in mechanical systems. It is well known that such problems are solvable using the Internal Model Principle in cases where the system to be controlled and the exosystem which generates the output reference signal and external disturbances are known. In the case where the controlled system is unknown and/or the exosystem is unknown, adaptive control strategies have played active roles in solving such problems for systems with uncertainties. For known systems with unknown exosystems, solutions with adaptive internal models have been provided in (Feg & Palaniswami, 1991), (Nikiforov, 1996) and (Marino & Tomei, 2001). In (Marino & Tomei, 2001), an output regulation system with an adaptive internal model is proposed for known non-minimum phase systems with unknown exosystems. Adaptive regulation problems have also been presented for time varying systems and nonlinear systems (Marino & Tomei, 2000; Ding, 2001; Serrani et al., 2001). Most of these methods, however, assumed that either the controlled system or the exosystem was known. Only few adaptive regulation methods for unknown systems with unknown exosystems have been provided (Nikiforov, 1997a; Nikiforov, 1997b). The method in (Nikiforov, 1997a) is an adaptive servo controller design based on the MRAC strategy, so that it was essentially assumed that the order of the controlled system was known. The method in (Nikiforov, 1997b) is one based on an adaptive backstepping strategy. In this method, it was necessary to design an adaptive observer that had to estimate all of the unknown system parameters depending on the order of the controlled system. Further, the controller design based on the backstepping strategy essentially depends on the order of the relative degree of the controlled system. As a result, the controller's structure was quite complex in both methods for higher order systems with higher order relative degrees.

In this paper, the adaptive regulation problem for unknown controlled systems is dealt with and an adaptive output feedback controller with an adaptive internal model is proposed for single input/single output linear minimum phase unknown systems with unknown exosystems. The proposed method is based on the adaptive output feedback control

utilizing the almost strictly positive real-ness (ASPR-ness) of the controlled system and the controller is designed based on an expanded backstepping strategy with a parallel feedforward compensator (PFC) (Mizumoto et al., 2005). It is shown that, under certain assumptions, without a priori knowledge of the order of the controlled system and without state variables, one can design an adaptive controller with a single step backstepping strategy even when the system to be controlled has an unknown order and a higher order relative degree. Using the proposed method, one can not attain perfect output regulation, however, the obtained controller structure is relatively simple even if the system has a higher order and a higher order relative degree.

2. Problem Statement

Consider the following single input/single output LTI system.

$$\begin{aligned} \dot{\mathbf{x}}(t) &= A\mathbf{x}(t) + \mathbf{b}u(t) + C_d\mathbf{w}(t) \\ y(t) &= \mathbf{c}^T\mathbf{x}(t) + \mathbf{d}^T\mathbf{w}(t), \end{aligned} \tag{1}$$

where $\mathbf{x} = [x_1, \cdots, x_n]^T \in R^n$ is the state vector and $u, y \in R$ are the input and the output, respectively. Further $\mathbf{w}(t) \in R^m$ is an unknown vector disturbance.

We assume that the disturbances and the reference signal which the output y is required to track are generated by the following unknown exosystem:

$$\begin{aligned} \dot{\mathbf{w}}(t) &= A_d\mathbf{w}(t) \\ y_m(t) &= \mathbf{c}_m^T\mathbf{w}(t), \end{aligned} \tag{2}$$

where $A_d \in R^{m\times m}$ is a stable matrix with all its eigenvalues on the imaginary axis. It is also assumed that the characteristic polynomial of A_d is expressed by

$$\det(\lambda\mathbf{I} - A_d) = \lambda^m + \alpha_{m-1}\lambda^{m-1} + \cdots + \alpha_1\lambda + \alpha_0. \tag{3}$$

The objective is to design an adaptive controller that has the output y(t) track the reference signal $y_m(t)$ generated by an unknown exosystem given in (2) for unknown systems with unknown disturbances generated by the unknown exosystem in (2) using only the output signal under the following assumptions.

Assumption 1 The system (1) is minimum-phase.

Assumption 2 The system (1) has a relative degree of r.

Assumption 3 $\mathbf{c}^T A^{r-1}\mathbf{b} > 0$, i.e. the high frequency gain of the system (1) is positive.

Assumption 4 The output y(t) and the reference signal $y_m(t)$ are available for measurement.

3. System Representation

From Assumption 2, since the system (1) has a relative degree of r, there exists a smooth nonsingular variable transformation: $\left[\mathbf{z}^{\mathrm{T}},\boldsymbol{\eta}^{\mathrm{T}}\right]^{\mathrm{T}}=\Phi\mathbf{x}$ such that the system (1) can be transformed into the form (Isidori, 1995):

$$\begin{aligned}\dot{\mathbf{z}}(t)&=A_z\mathbf{z}(t)+\mathbf{b}_z u(t)+\begin{bmatrix}\mathbf{0}\\ \mathbf{c}_z^{\mathrm{T}}\end{bmatrix}\boldsymbol{\eta}(t)+D_d\mathbf{w}(t)\\ \dot{\boldsymbol{\eta}}(t)&=Q_\eta\boldsymbol{\eta}(t)+\begin{bmatrix}\mathbf{0}\\ 1\end{bmatrix}z_1(t)+F_d\mathbf{w}(t)\\ y&=[1,0,\cdots,0]z_1(t)+\mathbf{d}^{\mathrm{T}}\mathbf{w}(t),\end{aligned}\tag{4}$$

where

$$\begin{aligned}A_z&=\begin{bmatrix}\mathbf{0} & \mathbf{I}_{r-1\times r-1}\\ -a_0\cdots-a_{r-1}\end{bmatrix},\\ \mathbf{b}_z&=[0,\cdots,b_z],\ b_z=\mathbf{c}^{\mathrm{T}}A^{r-1}\mathbf{b},\end{aligned}$$

and $\mathbf{c}_z\in R^{n-r}$ is an appropriate constant vector. From assumption 1, Q_η is a stable matrix because $\dot{\boldsymbol{\eta}}(t)=Q_\eta\boldsymbol{\eta}(t)$ denotes the zero dynamics of system (1).

3.1 Virtual controlled system

We shall introduce the following (r-1)th order stable virtual filter $1/f(s)$ with a state space representation:

$$\begin{aligned}\dot{\mathbf{z}}_f(t)&=A_{u_f}\mathbf{z}_f(t)+\mathbf{b}_{u_f}u(t)\\ u_{f_1}(t)&=\mathbf{c}_{u_f}^{\mathrm{T}}\mathbf{z}_f(t),\end{aligned}\tag{5}$$

where $\mathbf{z}_f=\left[z_{f_1},\cdots,z_{f_{r-1}}\right]^{\mathrm{T}}$ and

$$\begin{aligned}A_{u_f}&=\begin{bmatrix}\mathbf{0} & \mathbf{I}_{r-2\times r-2}\\ -\beta_0\cdots-\beta_{r-2}\end{bmatrix},\\ \mathbf{b}_{u_f}^{\mathrm{T}}&=[0,\cdots,1],\ \mathbf{c}_{u_f}^{\mathrm{T}}=[1,0,\cdots,0].\end{aligned}$$

With the following variable transformation using the filtered signal z_{f_i} given in (5):

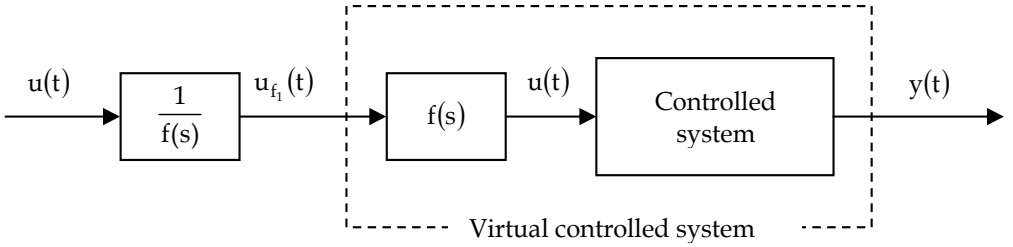

Fig. 1. Virtual controlled system with a virtual filter

$$\begin{aligned}\xi_1(t) &= z_1(t)\\ \xi_i(t) &= -b_z u_{f_{i-1}}(t) + z_i(t) + \sum_{j=1}^{i-1} c_{\xi_j} z_{i-j}(t),\end{aligned} \tag{6}$$

where

$$\begin{aligned}c_{\xi_i} &= \theta_i - a_{r-i}, \quad (1 \le i \le r-1)\\ c_{\xi_r} &= -a_0 + \sum_{j=1}^{r-1} \beta_{j-1} c_{\xi_j}\\ \theta_1 &= \beta_{r-2}\\ \theta_i &= \beta_{r-i-1} + \sum_{j=1}^{i-1} \beta_{r-i+j-1} c_{\xi_j},\end{aligned}$$

the system (1) can be transformed into the following virtual system which has u_{f_1} given from a virtual input filter as the control input (Michino et al., 2004) (see Fig.1):

$$\begin{aligned}\dot{\xi}_1(t) &= \alpha_z \xi(t) + \mathbf{c}_1^T \boldsymbol{\eta}_y(t) + b_z u_{f_1}(t) + \bar{\mathbf{c}}_{d_1}^T \mathbf{w}(t)\\ \dot{\boldsymbol{\eta}}_y(t) &= A_\eta \boldsymbol{\eta}_y(t) + \mathbf{c}_\eta \xi_1(t) + \bar{C}_{d_\eta} \mathbf{w}(t)\\ y(t) &= \xi_1(t) + \mathbf{d}^T \mathbf{w}(t),\end{aligned} \tag{7}$$

where $\boldsymbol{\eta}_y = \left[\boldsymbol{\xi}^T, \boldsymbol{\eta}^T\right]^T$, $\boldsymbol{\xi} = [\xi_2, \xi_3, \cdots, \xi_r]^T$ and $\mathbf{c}_1^T = [1,0,\cdots,0]$, $\mathbf{c}_\eta = \left[\mathbf{c}_\xi^T, 0, \cdots, 0, 1\right]^T$. $\bar{\mathbf{c}}_{d_1}$ and $\bar{C}_{d_\eta}$ are a vector and a matrix with appropriate dimensions, respectively. Further, A_η is given by the form of

$$A_\eta = \left[\begin{array}{c|c} A_{u_f} & \begin{matrix}\mathbf{0}\\ \mathbf{c}_z^T\end{matrix} \\ \hline \mathbf{0} & Q_\eta \end{array}\right].$$

Since A_{u_f} and Q_η are stable matrices, A_η is a stable matrix.

3.2 Virtual error system

Now, consider a stable filter of the form:

$$\begin{aligned}\dot{\mathbf{z}}_{c_f}(t) &= A_{c_f}\mathbf{z}_{c_f}(t) + \mathbf{c}_{c_f}u_{f_1}(t)\\ u_f(t) &= \boldsymbol{\theta}^T\mathbf{z}_{c_f}(t) + u_{f_1}(t),\end{aligned} \tag{8}$$

where $\mathbf{c}_{c_f} = [0,\cdots,0,1]^T$ and

$$\begin{aligned}A_{c_f} &= \begin{bmatrix}\mathbf{0} & \mathbf{I}_{m-1\times m-1}\\ -\beta_{c_0},\cdots,-\beta_{c_{m-1}}\end{bmatrix}\\ \boldsymbol{\theta}^T &= \left[\alpha_0-\beta_{c_0},\cdots,\alpha_{m-1}-\beta_{c_{m-1}}\right].\end{aligned}$$

$\beta_{c_0},\beta_{c_1},\cdots,\beta_{c_{m-1}}$ are chosen such that A_{c_f} is stable.

Let's consider transforming the system (7) into a one with u_f given in (8) as the input. Define new variables X_1 and $\mathbf{X}_2$ as follows:

$$\begin{aligned}X_1 &= \xi_1^{(m)} + \alpha_{m-1}\xi_1^{(m-1)} + \cdots + \alpha_1\dot{\xi}_1 + \alpha_0\xi_1\\ \mathbf{X}_2 &= \boldsymbol{\eta}_y^{(m)} + \alpha_{m-1}\boldsymbol{\eta}_y^{(m-1)} + \cdots + \alpha_1\dot{\boldsymbol{\eta}}_y + \alpha_0\boldsymbol{\eta}_y.\end{aligned} \tag{9}$$

Since it follows from the Cayley-Hamilton theorem that

$$A_m^m + \alpha_{m-1}A_m^{m-1} + \cdots + \alpha_1A_m + \alpha_0 I = 0, \tag{10}$$

we have from (2) and (7) that

$$\begin{aligned}\dot{X}_1(t) &= \alpha_z X_1(t) + \mathbf{c}_1^T\mathbf{X}_2(t) + b_z\overline{u}_f(t)\\ \dot{\mathbf{X}}_2(t) &= A_\eta\mathbf{X}_2(t) + \mathbf{c}_\eta X_1(t),\end{aligned} \tag{11}$$

where

$$\overline{u}_f = u_{f_1}^{(m)} + \alpha_{m-1}u_{f_1}^{(m-1)} + \cdots + \alpha_1\dot{u}_{f_1} + \alpha_0 u_{f_1} \tag{12}$$

Further we have from (10) that

$$e^{(m)} + \alpha_{m-1}e^{(m-1)} + \cdots + \alpha_1\dot{e} + \alpha_0 e = X_1. \tag{13}$$

Therefore defining $\mathbf{E} = \left[e, \dot{e}, \cdots, e^{(m-1)}\right]^T$, the following error system is obtained:

$$\begin{aligned}
\dot{\mathbf{E}}(t) &= A_E \mathbf{E}(t) + X_1(t) \\
\dot{X}_1(t) &= \alpha_z X_1(t) + \mathbf{c}_1^T \mathbf{X}_2(t) + b_z \bar{u}_f(t) \\
\dot{\mathbf{X}}_2(t) &= A_\eta \mathbf{X}_2(t) + \mathbf{c}_\eta X_1(t) \\
e(t) &= [1, 0, \cdots, 0]\mathbf{E}(t).
\end{aligned} \tag{14}$$

Obviously this error system with the input $\bar{u}_f$ and the output e has a relative degree of m+1 and a stable zero dynamics (because A_η is stable).

Furthermore, there exists an appropriate variable transformation such that the error system (14) can be represented by the following form (Isidori, 1995):

$$\begin{aligned}
\dot{\mathbf{z}}_e(t) &= A_{z_e} \mathbf{z}_e(t) + \begin{bmatrix} \mathbf{0} \\ b_{z_e} \end{bmatrix} \bar{u}_f(t) + \begin{bmatrix} \mathbf{0} \\ \mathbf{c}_{z_e}^T \end{bmatrix} \boldsymbol{\eta}_{z_e}(t) \\
\dot{\boldsymbol{\eta}}_{z_e}(t) &= \mathbf{Q}_{z_e} \boldsymbol{\eta}_{z_e}(t) + \begin{bmatrix} \mathbf{0} \\ 1 \end{bmatrix} z_{e_1}(t) \\
e(t) &= z_{e_1}(t),
\end{aligned} \tag{15}$$

where $\mathbf{z}_e = \left[z_{e_1}, \cdots, z_{e_{m+1}}\right]^T$ and $\boldsymbol{\eta}_{z_e} \in R^{n-1}$. Since the error system (14) has stable zero dynamics, $\mathbf{Q}_{z_e}$ is a stable matrix.

Recall the stable filter given in (8). Since we have from (8) that

$$\begin{aligned}
&u_f^{(m)} + \beta_{c_{m-1}} u_f^{(m-1)} + \cdots + \beta_{c_1} \dot{u}_f + \beta_{c_0} u_f \\
&= u_{f_1}^{(m)} + \alpha_{m-1} u_{f_1}^{(m-1)} + \cdots + \alpha_1 \dot{u}_{f_1} + \alpha_0 u_{f_1} = \bar{u}_f,
\end{aligned} \tag{16}$$

the filter's output signal u_f can also be obtained from

$$\begin{aligned}
\dot{\bar{\mathbf{z}}}_{c_f}(t) &= A_{c_f} \bar{\mathbf{z}}_{c_f}(t) + \begin{bmatrix} \mathbf{0} \\ 1 \end{bmatrix} \bar{u}_f(t) \\
u_f(t) &= [1, 0, \cdots, 0] \bar{\mathbf{z}}_{c_f}(t)
\end{aligned}$$

by defining $\bar{\mathbf{z}}_{c_f} = \left[u_f, \dot{u}_f, \cdots, u_f^{(m-1)}\right]^T$. Using this virtual filter signal in the variable transformation given in (6), the error system (15) can be transformed into the following form, the same way as the virtual system (7) was derived, with u_f as the input.

$$\begin{aligned}
\dot{e}(t) &= \alpha_e e(t) + b_e u_f(t) + \mathbf{c}_e^T \boldsymbol{\eta}_e(t) \\
\dot{\boldsymbol{\eta}}_e(t) &= Q_e \boldsymbol{\eta}_e(t) + \mathbf{b}_\eta e(t),
\end{aligned} \tag{17}$$

where

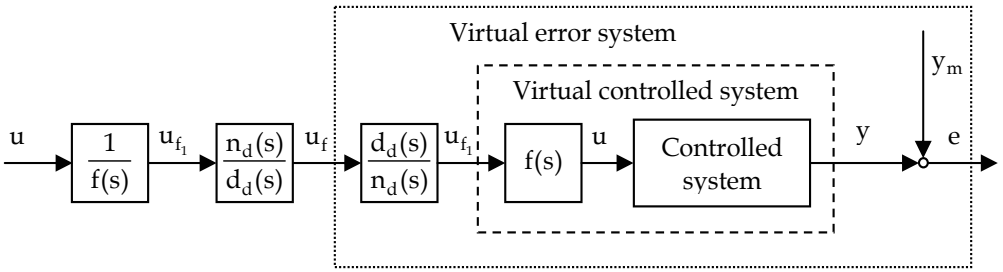

Fig. 2. Virtual error system with an virtual internal model

$$Q_e = \left[\begin{array}{c|c} A_{c_f} & \begin{matrix}\mathbf{0}\\ \mathbf{c}_{z_e}^T\end{matrix} \\ \hline \mathbf{0} & Q_{z_e} \end{array}\right].$$

Since A_{c_f} and Q_{z_e} are stable matrices, Q_e is a stable matrix. Thus the obtained virtual error system (17) is ASPR from the input u_f to the output e.

The overall configuration of the virtual error system is shown in Fig.2.

4. Adaptive Controller Design

Since the virtual error system (17) is ASPR, there exists an ideal feedback gain k^* such that the control objective is achieved with the control input: $u_f(t) = -k^* e(t)$ (Kaufman et al., 1998; Iwai & Mizumoto, 1994). That is, from (8), if the filter signal u_{f_1} can be obtained by

$$u_{f_1}(t) = -k^* e(t) - \boldsymbol{\theta}^T \mathbf{z}_{c_f}(t), \tag{18}$$

one can attain the goal. Unfortunately one can not design u_{f_1} directly by (18), because u_{f_1} is a filter signal given in (8) and the controlled system is assumed to be unknown. In such cases, the use of the backstepping strategy on the filter (5) can be considered as a countermeasure. However, since the controller structure depends on the relative degree of the system, i.e. the order of the filter (5), it will become very complex in cases where the controlled system has higher order relative degrees. Here we adopt a novel design strategy using a parallel feedforward compensator (PFC) that allows us to design the controller through a backstepping of only one step (Mizumoto et al., 2005; Michino et al., 2004).

4.1 Augmented virtual filter

For the virtual input filter (5), consider the following stable and minimum-phase PFC with an appropriate order n_f:

$$\begin{aligned}\dot{y}_f(t) &= -a_{f_1} y_f(t) + \mathbf{a}_{f_2}^T \boldsymbol{\eta}_f(t) + b_a u(t) \\ \dot{\boldsymbol{\eta}}_f(t) &= A_f \boldsymbol{\eta}_f(t) + \mathbf{b}_f y_f(t),\end{aligned} \tag{19}$$

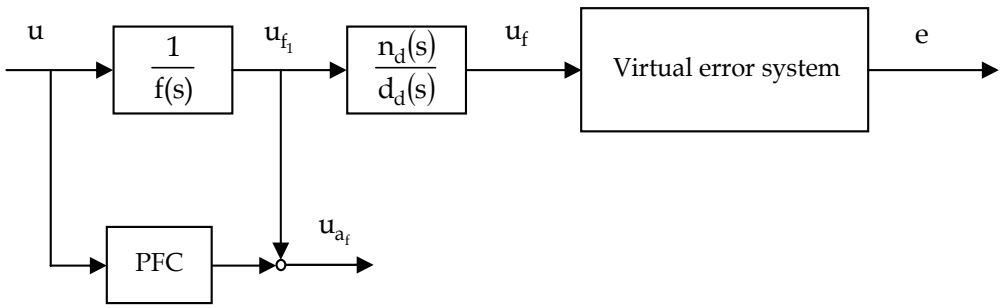

Fig. 3. Virtual error system with an augmented filter

where $y_f \in R$ is the output of the PFC. Since the PFC is minimum-phase A_f is a stable matrix.

The augmented filter obtained from the filter (5) by introducing the PFC (19) can then be represented by

$$\begin{aligned}\dot{\mathbf{z}}_{u_f}(t) &= A_{z_f} \mathbf{z}_{u_f}(t) + \mathbf{b}_{z_f} u(t) \\ u_{a_f}(t) &= \mathbf{c}_{z_f}^T \mathbf{z}_{u_f}(t) = u_{f_1}(t) + y_f(t),\end{aligned} \tag{20}$$

where $\mathbf{z}_{u_f} = \left[\mathbf{z}_f^T, y_f, \boldsymbol{\eta}_f^T\right]^T$ and

$$A_{z_f} = \begin{bmatrix} A_{u_f} & 0 & \mathbf{0} \\ \mathbf{0} & -a_{f_1} & \mathbf{a}_{f_2}^T \\ \mathbf{0} & \mathbf{b}_f & A_f \end{bmatrix}, \mathbf{b}_{z_f} = \begin{bmatrix} \mathbf{b}_{u_f} \\ b_a \\ \mathbf{0} \end{bmatrix},$$
$$\mathbf{c}_{z_f}^T = \left[\mathbf{c}_{u_f}, 1, 0, \cdots, 0\right]$$

Here we assume that the PFC (19) is designed so that the augmented filter is ASPR, i.e. minimum-phase and a relative degree of one. In this case, there exists an appropriate variable transformation such that the augmented filter can be transformed into the following form (Isidori, 1995):

$$\begin{aligned}\dot{u}_{a_f}(t) &= a_{a_1} u_{a_f}(t) + \mathbf{a}_{a_2}^T \boldsymbol{\eta}_a(t) + b_a u(t) \\ \dot{\boldsymbol{\eta}}_a(t) &= A_a \boldsymbol{\eta}_a(t) + \begin{bmatrix} \mathbf{0} \\ 1 \end{bmatrix} u_{a_f}(t),\end{aligned}$$

where A_a is a stable matrix because the augmented filter is minimum-phase.

Using the augmented filter's output u_{a_f}, the virtual error system is rewritten as follows (see Fig.3):

$$\begin{aligned}\dot{e}(t) &= \alpha_e e(t) + b_e\left(u_{a_f}(t) + \boldsymbol{\theta}^T \mathbf{z}_{c_f}(t) - y_f(t)\right) + \mathbf{c}_e^T \boldsymbol{\eta}_e(t)\\ \dot{\boldsymbol{\eta}}_e(t) &= Q_e \boldsymbol{\eta}_e(t) + \mathbf{b}_\eta e(t).\end{aligned} \tag{21}$$

4.2 Controller design by single step backstepping

[Pre-step] We first design the virtual input α_1 for the augmented filter output u_{a_f} in (21) as follows:

$$\alpha_1(t) = -k(t)e(t) - \hat{\boldsymbol{\theta}}(t)^T \mathbf{z}_{c_f}(t) + \Psi_0(t), \tag{22}$$

where $k(t)$ is an adaptive feedback gain and $\hat{\boldsymbol{\theta}}(t)$ is an estimated value of $\boldsymbol{\theta}$, these are adaptively adjusted by

$$\begin{aligned}\dot{k}(t) &= \gamma_k e^2(t) - \sigma_k k(t), \quad \gamma_k > 0, \sigma_k > 0\\ \dot{\hat{\boldsymbol{\theta}}}(t) &= \Gamma_\theta \mathbf{z}_{c_f}(t) e(t) - \sigma_\theta \hat{\boldsymbol{\theta}}(t), \quad \Gamma_\theta^T = \Gamma_\theta > 0, \sigma_\theta > 0.\end{aligned} \tag{23}$$

Further, $\Psi_0(t)$ is given as follows:

$$\begin{aligned}\dot{\Psi}_0(t) &= D(y_f)\left(-a_{f_1}\Psi_0(t) + b_a u(t)\right)\\ D(y_f) &= \begin{cases}0, & \text{if} \quad |y_f| \le \delta_{y_f}\\ 1, & \text{if} \quad |y_f| > \delta_{y_f}\end{cases}\end{aligned} \tag{24}$$

where δ_{y_f} is any positive constant.

Now consider the following positive definite function:

$$V_0 = \frac{1}{2b_e}e^2 + \frac{1}{2\gamma_k}\Delta k^2 + \frac{1}{2}\Delta\boldsymbol{\theta}^T\Gamma_\theta^{-1}\Delta\boldsymbol{\theta} + \boldsymbol{\eta}_e^T P_e \boldsymbol{\eta}_e, \tag{25}$$

where

$$\Delta k = k(t) - k^*, \quad \Delta\boldsymbol{\theta} = \hat{\boldsymbol{\theta}}(t) - \boldsymbol{\theta},$$

k^* is an ideal feedback gain to be determined later and P_e is a positive definite matrix that satisfies the following Lyapunov equation for any positive definite matrix R_e.

$$P_e Q_e + Q_e^T P_e = -R_e < 0.$$

Since Q_e is a stable matrix, there exists such P_e.
The time derivative of V_0 can be evaluated by

$$\begin{aligned}\dot{V}_0 \le & -\left(k^* - v_0\right)e^2 - \left(\lambda_{\min}\left[R_e\right] - \rho_1\right)\left\|\boldsymbol{\eta}_e\right\|^2 + \omega_1 e \\ & - \left\{y_f - \Psi_0\right\}e - \left(\frac{\sigma_k}{\gamma_k} - \rho_2\right)\Delta k^2 \\ & - \left(\sigma_\theta \lambda_{\min}\left[\Gamma_\theta^{-1}\right] - \rho_3\right)\Delta\boldsymbol{\theta}^2 + R_0\end{aligned} \tag{26}$$

with any positive constant ρ_1 to ρ_3. Where $\omega_1 = u_{a_f} - \alpha_1$ and

$$\begin{aligned}v_0 &= \frac{\alpha_e}{b_e} + \frac{\left(\left\|\mathbf{c}_e\right\| + 2\left\|P_e\right\|\left\|\mathbf{b}_\eta\right\|b_e\right)^2}{4b_e^2\rho_1} \\ R_0 &= \frac{\sigma_k^2 k^{*2}}{4\rho_2\gamma_k^2} + \frac{\sigma_\theta^2\left(\lambda_{\min}\left[\Gamma_\theta^{-1}\right]\right)^2}{4\rho_3}\left\|\boldsymbol{\theta}\right\|^2.\end{aligned} \tag{27}$$

[Step 1] Consider the error system, ω_1-system, between u_{a_f} and α_1. The ω_1-system is given from (21) by

$$\begin{aligned}\dot{\omega}_1 &= \dot{u}_{a_f} - \dot{\alpha}_1 \\ &= a_{a_1} u_{a_f} + \boldsymbol{a}_{a_2}^T \boldsymbol{\eta}_a + b_a u - \dot{\alpha}_1.\end{aligned} \tag{28}$$

The time derivative of α_1 is obtained as follows:

$$\begin{aligned}\dot{\alpha}_1 = & \frac{\partial\alpha_1}{\partial e}\alpha_e e + \frac{\partial\alpha_1}{\partial e}\boldsymbol{\theta}_1^T\mathbf{z}_{c_f} + \frac{\partial\alpha_1}{\partial e}b_e u_{f_1} + \frac{\partial\alpha_1}{\partial e}\mathbf{c}_e^T\boldsymbol{\eta}_e \\ & + \frac{\partial\alpha_1}{\partial k(t)}\dot{k} + \frac{\partial\alpha_1}{\partial \mathbf{z}_{c_f}}\dot{\mathbf{z}}_{c_f} + \frac{\partial\alpha_1}{\partial\hat{\boldsymbol{\theta}}}\dot{\hat{\boldsymbol{\theta}}} \\ & + D(y_f)\left(-a_{f_1}\Psi_0 + b_a u\right),\end{aligned} \tag{29}$$

where $\boldsymbol{\theta}_1^T = b_e\boldsymbol{\theta}^T$. Taking (28) and (29) into consideration, the actual control input is designed as follows:

$$u = \begin{cases} -\dfrac{1}{b_a}\left[c_1\omega_1 + \varepsilon_0\left(\left|u_{a_f}\right|^2 + \left\|\boldsymbol{\eta}_a\right\|^2\right)\omega_1 + \varepsilon_1\Psi_1\omega_1 - \Psi_2\right], \\ \qquad\qquad\qquad\qquad\qquad\qquad \text{if} \quad \left|y_f\right| \le \delta_{y_f} \\ -\dfrac{\omega_1}{b_a y_f}\left[c_1\omega_1 + \varepsilon_0\left(\left|u_{a_f}\right|^2 + \left\|\boldsymbol{\eta}_a\right\|^2\right)\omega_1 + \varepsilon_1\Psi_1\omega_1 - \Psi_2\right] \\ \quad -\dfrac{1}{b_a}\left[\gamma_f y_f + \varepsilon_2\left\|\boldsymbol{\eta}_f\right\|^2 y_f\right] - \dfrac{\varepsilon_3}{b_a y_f}\Psi_0^2 \quad , \quad \text{if} \quad \left|y_f\right| > \delta_{y_f} \end{cases} \tag{30}$$

where ε_0 to ε_3 and γ_f are any positive constants, and Ψ_1 and Ψ_2 are given by

$$\Psi_1 = \left|\frac{\partial \alpha_1}{\partial k}\right|^2 |\dot{k}|^2 + \left\|\frac{\partial \alpha_1}{\partial \hat{\boldsymbol{\theta}}}\right\|^2 \left\|\dot{\hat{\boldsymbol{\theta}}}\right\|^2 + \left\|\frac{\partial \alpha_1}{\partial \mathbf{z}_{c_f}}\right\|^2 \|\dot{\mathbf{z}}_{c_f}\|^2 + l$$

$$\Psi_2 = -\frac{\partial \alpha_1}{\partial e}\hat{a}_e e - \frac{\partial \alpha_1}{\partial e}\hat{\boldsymbol{\theta}}_1^T \mathbf{z}_{c_f} - \frac{\partial \alpha_1}{\partial e}\hat{b}_e u_{f_1} + \hat{\beta}_1 \left(\frac{\partial \alpha_1}{\partial e}\right)^2 \omega_1,$$

where l is any positive constant and $\hat{a}_e, \hat{b}_e, \hat{\boldsymbol{\theta}}_1, \hat{\beta}_1$ are estimated values of $a_e, b_e, \boldsymbol{\theta}_1, \beta_1$, respectively, and adaptively adjusted by the following parameter adjusting laws.

$$\begin{aligned}
\dot{\hat{a}}_e(t) &= -\gamma_a \omega_1(t) \frac{\partial \alpha_1}{\partial e} e(t) - \sigma_a \hat{a}_e(t) \\
\dot{\hat{b}}_e(t) &= -\gamma_b \omega_1(t) \frac{\partial \alpha_1}{\partial e} u_{f_1}(t) - \sigma_b \hat{b}_e(t) \\
\dot{\hat{\boldsymbol{\theta}}}_1(t) &= -\Gamma_{\theta_1} \mathbf{z}_{c_f}(t) \frac{\partial \alpha_1}{\partial e} \omega_1(t) - \sigma_{\theta_1} \hat{\boldsymbol{\theta}}_1(t) \\
\dot{\hat{\beta}}_1(t) &= \gamma_{\beta_1} \omega_1(t)^2 \left(\frac{\partial \alpha_1}{\partial e}\right)^2 - \sigma_{\beta_1} \hat{\beta}_1(t)
\end{aligned} \tag{31}$$

where $\gamma_a, \gamma_b, \gamma_{\beta_1}, \sigma_a, \sigma_b, \sigma_{\theta_1}, \sigma_{\beta_1}$ are any positive constants and $\Gamma_{\theta_1} = \Gamma_{\theta_1}^T > 0$.

4.3 Boundedness analysis

For the designed control system with control input (30), we have the following theorem concerning the boundedness of all the signals in the control system.

Theorem 1 Under assumptions 1 to 3 on the controlled system (1), all the signals in the resulting closed loop system with the controller (30) are uniformly bounded.

Proof: Consider the following positive and continuous function V_1.

$$V_1 = \begin{cases} V_0 + \frac{1}{2}\omega_1^2 + \frac{1}{2}\Delta\boldsymbol{\theta}_1^T \Gamma_{\theta_1}^{-1} \Delta\boldsymbol{\theta}_1 + \frac{1}{2\gamma_a}\Delta a_e^2 \\ \quad + \frac{1}{2\gamma_b}\Delta b_e^2 + \frac{1}{2\gamma_{\beta_1}}\Delta\beta_1^2 + \frac{1}{2}\delta_{y_f}^2, \quad \text{if} \quad |y_f| \le \delta_{y_f} \\ V_0 + \frac{1}{2}\omega_1^2 + \frac{1}{2}\Delta\boldsymbol{\theta}_1^T \Gamma_{\theta_1}^{-1} \Delta\boldsymbol{\theta}_1 + \frac{1}{2\gamma_a}\Delta a_e^2 \\ \quad + \frac{1}{2\gamma_b}\Delta b_e^2 + \frac{1}{2\gamma_{\beta_1}}\Delta\beta_1^2 + \frac{1}{2}y_f^2, \quad \text{if} \quad |y_f| > \delta_{y_f}, \end{cases} \tag{32}$$

where

$$\Delta\alpha_e = \hat{\alpha}_e(t) - \alpha_e, \quad \Delta b_e = \hat{b}_e(t) - b_e$$
$$\Delta\boldsymbol{\theta}_1 = \hat{\boldsymbol{\theta}}_1(t) - \boldsymbol{\theta}_1, \quad \Delta\beta_1 = \hat{\beta}_1(t) - \beta_1,$$

and δ_{y_f} is any positive constant.

From (26) and (32), the time derivative of V_1 for $|y_f| \le \delta_{y_f}$ can be evaluated by

$$\begin{aligned}\dot{V}_1 \le & -\left(k^* - v_0 - \frac{1}{4\varepsilon l}\right)e^2 - \left(\lambda_{\min}[R_e] - \rho_1 - \mu_0\right)\|\boldsymbol{\eta}_e\|^2 \\ & -\left(\frac{\sigma_k}{\gamma_k} - \rho_2\right)\Delta k^2 - \left(\sigma_\theta \lambda_{\min}\left[\Gamma_\theta^{-1}\right] - \rho_3\right)\Delta\boldsymbol{\theta}^2 \\ & - c_1\omega_1^2 - \left(\sigma_{\theta_1}\lambda_{\min}\left[\Gamma_{\theta_1}^{-1}\right] - \mu_1\right)\Delta\boldsymbol{\theta}_1^2 \\ & -\left(\frac{\sigma_\alpha}{\gamma_\alpha} - \mu_2\right)\Delta\alpha_e^2 - \left(\frac{\sigma_b}{\gamma_b} - \mu_3\right)\Delta b_e^2 \\ & -\left(\frac{\sigma_{\beta_1}}{\gamma_{\beta_1}} - \mu_4\right)\Delta\beta_1^2 - \left(y_f - \Psi_0(y_f)\right)e + R_1\end{aligned} \tag{33}$$

with any positive constants μ_0 to μ_4. Where

$$R_1 = R_0 + \frac{3}{4\varepsilon_1} + \frac{\sigma_{\theta_1}^2\left(\lambda_{\min}\left[\Gamma_{\theta_1}^{-1}\right]\right)^2}{4\mu_1}\|\boldsymbol{\theta}_1\|^2 + \frac{\sigma_\alpha^2\alpha_e^2}{4\mu_2\gamma_\alpha} + \frac{\sigma_b^2 b_e^2}{4\mu_3\gamma_b} + \frac{\sigma_\beta^2\beta^2}{4\mu_4\gamma_\beta}.$$

Here we have

$$-\left(y_f - \Psi_0\right)e = -\mu_5\left\{e - \frac{\left(y_f + \Psi_0\right)}{2\mu_5}\right\}^2 + \frac{\left(y_f - \Psi_0\right)^2}{4\mu_5} + \mu_5 e^2 \tag{34}$$

with any positive constant μ_5. Furthermore, for $|y_f| \le \delta_{y_f}$, since $\dot{\Psi}_0(t) = 0$ is held, there exists a positive constant Ψ_M such that $|y_f(t) - \Psi_0(t)| \le \Psi_M$.

Therefore the time derivative of V_1 can be evaluated by

$$\dot{V}_1 \le -\alpha_a V_1 + \overline{R}_1 \tag{35}$$

for $|y_f| \le \delta_{y_f}$, where

$$\alpha_a = \min\left[2b_e\left(k^* - v_0 - \frac{1}{4\varepsilon l} - \mu_5\right), s_a, 2\right]$$

$$s_a = \min\left[\frac{\lambda_{\min}[R_e] - \rho_1 - \mu_0}{\lambda_{\max}[P_e]}, 2\gamma_k\left(\frac{\sigma_k}{\gamma_k} - \rho_2\right), 2\frac{\left(\sigma_\theta \lambda_{\min}\left[\Gamma_\theta^{-1}\right] - \rho_3\right)}{\lambda_{mac}\left[\Gamma_\theta^{-1}\right]}, 2c_1, 2\frac{\left(\sigma_{\theta_1}\lambda_{\min}\left[\Gamma_{\theta_1}^{-1}\right] - \mu_1\right)}{\lambda_{\max}\left[\Gamma_{\theta_1}^{-1}\right]}, 2\gamma_\alpha\left(\frac{\sigma_\alpha}{\gamma_\alpha} - \mu_2\right), 2\gamma_b\left(\frac{\sigma_b}{\gamma_b} - \mu_3\right), 2\gamma_\beta\left(\frac{\sigma_{\beta_1}}{\gamma_{\beta_1}} - \mu_4\right)\right]$$

$$\overline{R}_1 = R_1 + \frac{\Psi_M^2}{4\mu_5} + \delta_{y_f}^2.$$

For $|y_f| > \delta_{y_f}$, the time derivative of V_1 is evaluated as

$$\begin{aligned}\dot{V}_1 \le & -\left(k^* - v_0 - \frac{1}{4\varepsilon l}\right)e^2 - \left(\lambda_{\min}[R_e] - \rho_1 - \mu_0\right)\|\boldsymbol{\eta}_e\|^2 \\ & - \left(\frac{\sigma_k}{\gamma_k} - \rho_2\right)\Delta k^2 - \left(\sigma_\theta \lambda_{\min}\left[\Gamma_\theta^{-1}\right] - \rho_3\right)\Delta\boldsymbol{\theta}^2 - c_1\omega_1^2 \\ & - \left(\sigma_{\theta_1}\lambda_{\min}\left[\Gamma_{\theta_1}^{-1}\right] - \mu_1\right)\Delta\boldsymbol{\theta}_1^2 - \left(\frac{\sigma_\alpha}{\gamma_\alpha} - \mu_2\right)\Delta\alpha_e^2 \\ & - \left(\frac{\sigma_b}{\gamma_b} - \mu_3\right)\Delta b_e^2 - \left(\frac{\sigma_{\beta_1}}{\gamma_{\beta_1}} - \mu_4\right)\Delta\beta_1^2 + R_1 \\ & - a_{f_1}y_f^2 + \mathbf{a}_{f_2}\boldsymbol{\eta}_f y_f - \gamma_f y_f^2 - \varepsilon_2\|\boldsymbol{\eta}_f\|^2 y_f^2 - \varepsilon_3\Psi_0^2 \\ & + \Psi_0 e - y_f e,\end{aligned} \tag{36}$$

and thus we have for $|y_f| > \delta_{y_f}$ that

$$\dot{V}_1 \le -\alpha_b V_1 + R_2, \tag{37}$$

where

$$\begin{aligned}\alpha_b &= \min\left[2b_e\left(k^* - v_0 - \frac{1}{4\varepsilon l} - \frac{1}{a_{f_1}} - \frac{1}{4\varepsilon_3}\right), s_a, 2\gamma_f\right] \\ R_2 &= R_1 + \frac{\|\mathbf{a}_{f_2}\|^2}{4\varepsilon_2}.\end{aligned} \tag{38}$$

Finally, for an ideal feedback gain k^* which satisfies

$$k^* > v_0 + \frac{1}{4\varepsilon l} + v_1, \quad v_1 = \max\left[\mu_5, \frac{1}{a_{f_1}} - \frac{1}{4\varepsilon_3}\right],$$

the time derivative of V_1 can be evaluated by

$$\dot{V}_1 \le -\alpha V_1 + R, \tag{39}$$

where $\alpha = \min[\alpha_a, \alpha_b] > 0$, $R = \max[\overline{R}_1, R_2]$. Consequently it follows that V_1 is uniformly bounded and thus the signals $e(t), \omega_1(t), \boldsymbol{\eta}_e(t), y_f(t), \boldsymbol{\eta}_f(t)$ and adjusted parameters $k(t), \hat{\boldsymbol{\theta}}(t)$, $\hat{\alpha}_e(t), \hat{\boldsymbol{\theta}}_1(t), \hat{b}_e(t), \hat{\beta}_1(t)$ are also uniformly bounded.

Next, we show that the filter signal $\mathbf{z}_{c_f}$ and the control input u are uniformly bounded. Define new variable z_{ξ_1} as follows:

$$z_{\xi_1}^{(m)} + \beta_{c_{m-1}} z_{\xi_1}^{(m-1)} + \cdots + \beta_{c_0} z_{\xi_1} = \xi_1 \tag{40}$$

$$\dot{\xi}_1 = \alpha_z \xi_1 + \mathbf{c}_\xi^T \boldsymbol{\eta}_y + b_z u_{f_1} + \bar{\mathbf{c}}_{d_1}^T \mathbf{w} \tag{41}$$

$$\dot{\boldsymbol{\eta}}_y = A_\eta \boldsymbol{\eta}_y + \mathbf{b}_\eta \xi_1 + \overline{C}_{d_\eta} \mathbf{w}, \tag{42}$$

where ξ_1 and $\boldsymbol{\eta}_y$ have been given in (7). Further define z_{β_1} by

$$\dot{z}_{\beta_1} = \alpha_z z_{\beta_1} + b_z z_{c_f} + \eta_{\beta_1} \tag{43}$$

$$\eta_{\beta_1}^{(m)} + \beta_{c_{m-1}} \eta_{\beta_1}^{(m-1)} + \cdots + \beta_{c_0} \eta_{\beta_1} = \mathbf{c}_\xi^T \boldsymbol{\eta}_y + \bar{\mathbf{c}}_{d_1}^T \mathbf{w}, \tag{44}$$

where $z_{c_{f1}} = [1, 0, \cdots, 0]\mathbf{z}_{c_f}$ and we set $z_{\beta_1}^{(k)}(0) = z_{\xi_1}^{(k)}(0), k = 0, \cdots, m$ .We have from (40) and (41) that

$$\begin{aligned} \dot{\xi}_1 - \alpha_z \xi_1 &= z_{\xi_1}^{(m+1)} + \left(\beta_{c_{m-1}} - \alpha_z\right) z_{\xi_1}^{(m)} \\ &\quad + \left(\beta_{c_{m-2}} - \alpha_z \beta_{c_{m-1}}\right) z_{\xi_1}^{(m-1)} + \cdots \\ &\quad + \left(\beta_{c_0} - \alpha_z \beta_{c_1}\right) \dot{z}_{\xi_1} - \alpha_z z_{\xi_1} \\ &= b_z u_{f_1} + \mathbf{c}_\xi^T \boldsymbol{\eta}_y + \bar{\mathbf{c}}_{d_1}^T \mathbf{w}. \end{aligned} \tag{45}$$

Further, we have from (43), (44) and (8) that

$$\begin{aligned} & z_{\beta_1}^{(m+1)} + \left(\beta_{c_{m-1}} - \alpha_z\right) z_{\beta_1}^{(m)} + \left(\beta_{c_{m-2}} - \alpha_z \beta_{c_{m-1}}\right) z_{\beta_1}^{(m-1)} \\ & \quad + \cdots + \left(\beta_{c_0} - \alpha_z \beta_{c_1}\right) \dot{z}_{\beta_1} - \alpha_z z_{\beta_1} \\ & \quad = b_z u_{f_1} + \mathbf{c}_\xi^T \boldsymbol{\eta}_y + \bar{\mathbf{c}}_{d_1}^T \mathbf{w}. \end{aligned} \tag{46}$$

It follows from (45) and (46) that $z_{\xi_1}^{(k)} = z_{\beta_1}^{(k)}$, $k = 0, \cdots, m$.

Define $\mathbf{z}_\xi = \left[z_{\xi_1}, \dot{z}_{\xi_1}, \cdots, z_{\xi_1}^{(m-1)}\right]^T$ and $\mathbf{z}_\beta = \left[z_{\beta_1}, \dot{z}_{\beta_1}, \cdots, z_{\beta_1}^{(m-1)}\right]^T$. Since $s^m + \beta_{c_{m-1}} s^{m-1} + \cdots + \beta_{c_0}$ is a stable polynomial, we obtain from (40) that

$$\left\|\mathbf{z}_\beta\right\| = \left\|\mathbf{z}_\xi\right\| \le l_1 \left|\xi_1\right| + l_2, \tag{47}$$

with appropriate positive constants l_1, l_2. From the boundedness of $\mathbf{w}(t)$ and e(t), we have $\xi_1(t)$ is bounded and thus $\mathbf{z}_\beta$ is also bounded.

Furthermore defining $\boldsymbol{\eta}_\beta = \left[\eta_{\beta_1}, \dot{\eta}_{\beta_1}, \cdots, \eta_{\beta_1}^{(m-1)}\right]^T$, we have from (44) that

$$\dot{\boldsymbol{\eta}}_\beta(t) = A_{c_f} \boldsymbol{\eta}_\beta(t) + \begin{bmatrix} \mathbf{0} \\ 1 \end{bmatrix} \left(\mathbf{c}_\xi^T \boldsymbol{\eta}_y(t) + \bar{\mathbf{c}}_{d_1}^T \mathbf{w}(t)\right). \tag{48}$$

From (8) and (48), we obtain

$$\begin{aligned} & b_z \dot{\mathbf{z}}_{c_f}(t) + \dot{\boldsymbol{\eta}}_\beta(t) \\ & = A_{c_f} \left(b_z \mathbf{z}_{c_f}(t) + \boldsymbol{\eta}_\beta(t)\right) + b_z \begin{bmatrix} \mathbf{0} \\ 1 \end{bmatrix} u_{f_1}(t) + \begin{bmatrix} \mathbf{0} \\ 1 \end{bmatrix} \left(\mathbf{c}_\xi^T \boldsymbol{\eta}_y(t) + \bar{\mathbf{c}}_{d_1}^T \mathbf{w}(t)\right). \end{aligned} \tag{49}$$

Therefore $b_z \dot{\mathbf{z}}_{c_f}(t) + \dot{\boldsymbol{\eta}}_\beta(t)$ can be evaluated from (48) and the fact that $u_{f_1} = \omega_1 + \alpha_1 - y_f$ by

$$\begin{aligned} \left\|b_z \dot{\mathbf{z}}_{c_f}(t) + \dot{\boldsymbol{\eta}}_\beta(t)\right\| \le & \left\|A_{c_f}\right\| \left\|b_z \mathbf{z}_{c_f}(t) + \boldsymbol{\eta}_\beta(t)\right\| \\ & + b_z \left|\alpha_1(t) - y_f(t)\right| + b_z \left|\omega_1(t)\right| \\ & + \left\|\mathbf{c}_\xi\right\| \left\|\boldsymbol{\eta}_y(t)\right\| + \left\|\bar{\mathbf{c}}_{d_1}\right\| \left\|\mathbf{w}(t)\right\|. \end{aligned} \tag{50}$$

Here, we have from (22) that

$$\alpha_1(t) - y_f(t) = -k(t) e(t) - \frac{\hat{\boldsymbol{\theta}}^T(t)}{b_z} \left\{b_z \mathbf{z}_{c_f}(t) + \boldsymbol{\eta}_\beta(t)\right\} + \frac{\hat{\boldsymbol{\theta}}^T(t)}{b_z} \boldsymbol{\eta}_\beta(t) + \Psi_0(y_f) - y_f(t). \tag{51}$$

Since it follows from (19) and (24) that

$$\dot{y}_f(t) - \dot{\Psi}_0(t) = -a_{f_1}\left(y_f(t) - \Psi_0(t)\right) + \mathbf{a}_{f_2}^T \boldsymbol{\eta}_f(t) \tag{52}$$

for $|y_f| > \delta_{y_f}$ and from the boundedness of $\boldsymbol{\eta}_f(t)$, there exists a positive constant such that $|y_f - \Psi_0(t)| \le \overline{\Psi}_M$. Further, from the boundedness of $\mathbf{w}(t)$ and e(t) i.e. $\xi_1(t)$, we can confirm that $\boldsymbol{\eta}_y(t)$ and $\boldsymbol{\eta}_\beta(t)$ are also bounded from (7) and (48). Finally, taking the boundedness of the signals e(t), $\omega_1(t), k(t), \hat{\boldsymbol{\theta}}(t)$ and $\boldsymbol{\eta}_y(t), \boldsymbol{\eta}_\beta(t)$ into consideration, from (50) $b_z \dot{\mathbf{z}}_{c_f}(t) + \dot{\boldsymbol{\eta}}_\beta(t)$ can be evaluated by

$$\left\| b_z \dot{\mathbf{z}}_{c_f}(t) + \dot{\boldsymbol{\eta}}_\beta(t) \right\| \le l_{z_1} \left\| b_z \mathbf{z}_{c_f}(t) + \boldsymbol{\eta}_\beta(t) \right\| + l_{z_2} \tag{53}$$

with appropriate positive constants l_{z_1} and l_{z_2}. Consequently, considering the system:

$$\dot{\mathbf{z}}_\beta(t) = \alpha_z \mathbf{z}_\beta + b_z \mathbf{z}_{c_f} + \boldsymbol{\eta}_\beta(t) \tag{54}$$

from (44) with $b_z \mathbf{z}_{c_f} + \boldsymbol{\eta}_\beta(t)$ as the input and $\mathbf{z}_\beta$ as the output, since this system is minimum-phase and the inequality (53) is held, we have from the Output/Input L_p Stability Lemma (Sastry & Bodson, 1989) that the input $b_z \mathbf{z}_{c_f} + \boldsymbol{\eta}_\beta(t)$ in the system (54) can be evaluated by

$$\left\| b_z \mathbf{z}_{c_f}(t) + \boldsymbol{\eta}_\beta(t) \right\| \le \bar{l}_{z_1} \left\| \mathbf{z}_\beta(t) \right\| + \bar{l}_{z_2} \tag{55}$$

with appropriate positive constants $\bar{l}_{z_1}$ and $\bar{l}_{z_2}$. From the boundedness of $\mathbf{z}_\beta(t)$ and $\boldsymbol{\eta}_\beta(t)$, we can conclude that $\mathbf{z}_{c_f}(t)$ is uniformly bounded and then the control input u(t) is also uniformly bounded. Thus all the signals in the resulting closed loop system with the controller (30) are uniformly bounded.

5. Simulation Results

The effectiveness of the proposed method is confirmed through numerical simulation for a 3rd order SISO system with a relative degree of 3, which is given by

$$\begin{aligned} \dot{\mathbf{z}} &= \begin{bmatrix} -1 & -0.5 & 0.5 \\ 1.5 & -2.5 & -0.5 \\ -2.5 & 0.5 & 1 \end{bmatrix} \mathbf{z} + \begin{bmatrix} 0 \\ 0 \\ 1 \end{bmatrix} u + \begin{bmatrix} 1 & 0.1 & 0.1 & 0.1 \\ 0.1 & 0.1 & 1 & 0.1 \\ 0.1 & 0.1 & 0.1 & 1 \end{bmatrix} \mathbf{w} \\ y &= z_1 + \begin{bmatrix} 0.1 & 0.1 & 1 & 0.1 \end{bmatrix} \mathbf{w}, \end{aligned} \tag{56}$$

where $\mathbf{w}$ is an unknown disturbance which has the following form:

$$\mathbf{w} = \begin{bmatrix} \sin(2t) \\ 2\cos(2t) \\ 0.5\sin(5t) \\ 2.5\cos(5t) \end{bmatrix} \tag{57}$$

Before designing a controller, we first introduce the following pre-filter:

$$\frac{b}{s+a} \tag{58}$$

in order to reduce the chattering phenomenon to be expected by switching the controller given in (30). Therefore, the considered controlled system has a relative degree of 4.

Since the relative degree of the controlled system is 4, we consider a 3rd order input virtual filter in (5). Further we consider a stable internal model filter (8) of the order of 4.

For the input virtual filter, in this simulation, we consider a first order PFC:

$$\dot{y}_f = -a_{f_1} y_f + b_a u$$

in order to make an ASPR augmented filter.

The design parameters for the pre-filter (58), the input virtual filter (5) and the internal model filter (8) are set as follows:

$$a = b = 1000$$
$$\beta_0 = 15, \beta_1 = 75, \beta_2 = 125$$
$$\beta_{c_0} = 20, \beta_{c_1} = 150, \beta_{c_2} = 500, \beta_{c_3} = 625$$

and the PFC parameters are set by

$$a_{f_1} = 10, b_a = 0.01.$$

Further design parameters in the controller given in (23), (24), (30) and (31) are designed by

$$\gamma_k = 500, \sigma_k = 0.01, \delta_{y_f} = 10$$
$$l = 0.5, \sigma_\theta = 0.05, \sigma_{\theta_1} = \sigma_a = \sigma_b = \sigma_{\beta_1} = 0.1$$
$$\Gamma_\theta = \Gamma_{\theta_1} = 5000 I_4, \gamma_a = \gamma_b = \gamma_\beta = 100$$
$$c_1 = 1000, \varepsilon_0 = \varepsilon_1 = \varepsilon_2 = 0.01, \varepsilon_3 = \gamma_f = 100.$$

Figure 4 shows the simulation results with the proposed controller. In this simulation, the disturbance **w** is changed at 50 [sec]:

$$\mathbf{w} = \begin{bmatrix} \sin(2t) \\ 2\cos(2t) \\ 0.5\sin(5t) \\ 2.5\cos(5t) \end{bmatrix} \Rightarrow \mathbf{w} = \begin{bmatrix} 2\sin(4t) \\ 4\cos(4t) \\ 0.5\sin(20t) \\ 2.5\cos(20t) \end{bmatrix}.$$

Figure 5 is the tracking error and Fig.6 shows the adaptively adjusted parameters in the controller.

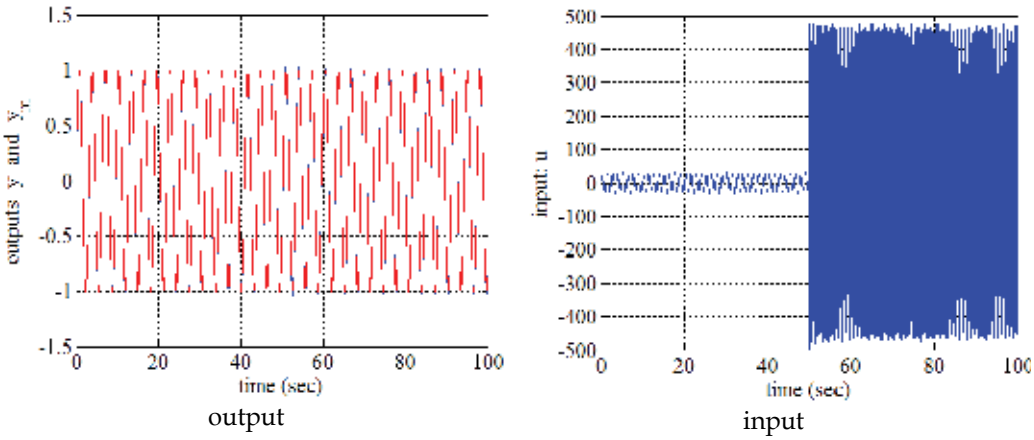

Fig. 4. Simulation results with the proposed controller

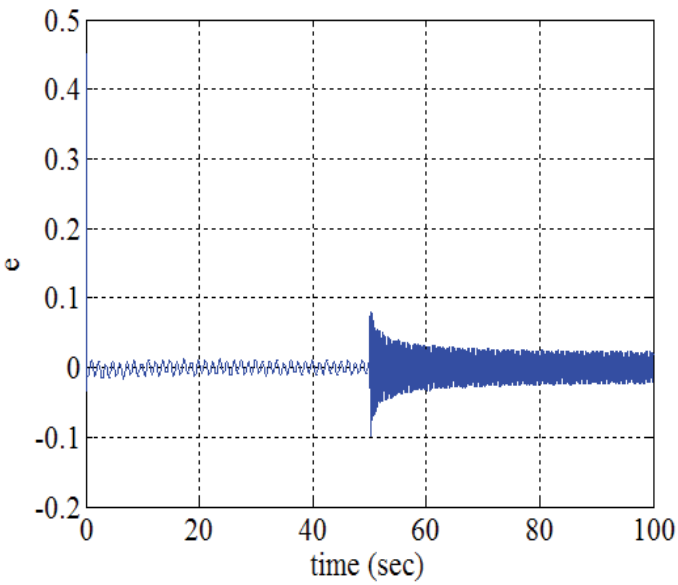

Fig. 5. Tracking error with the proposed controller

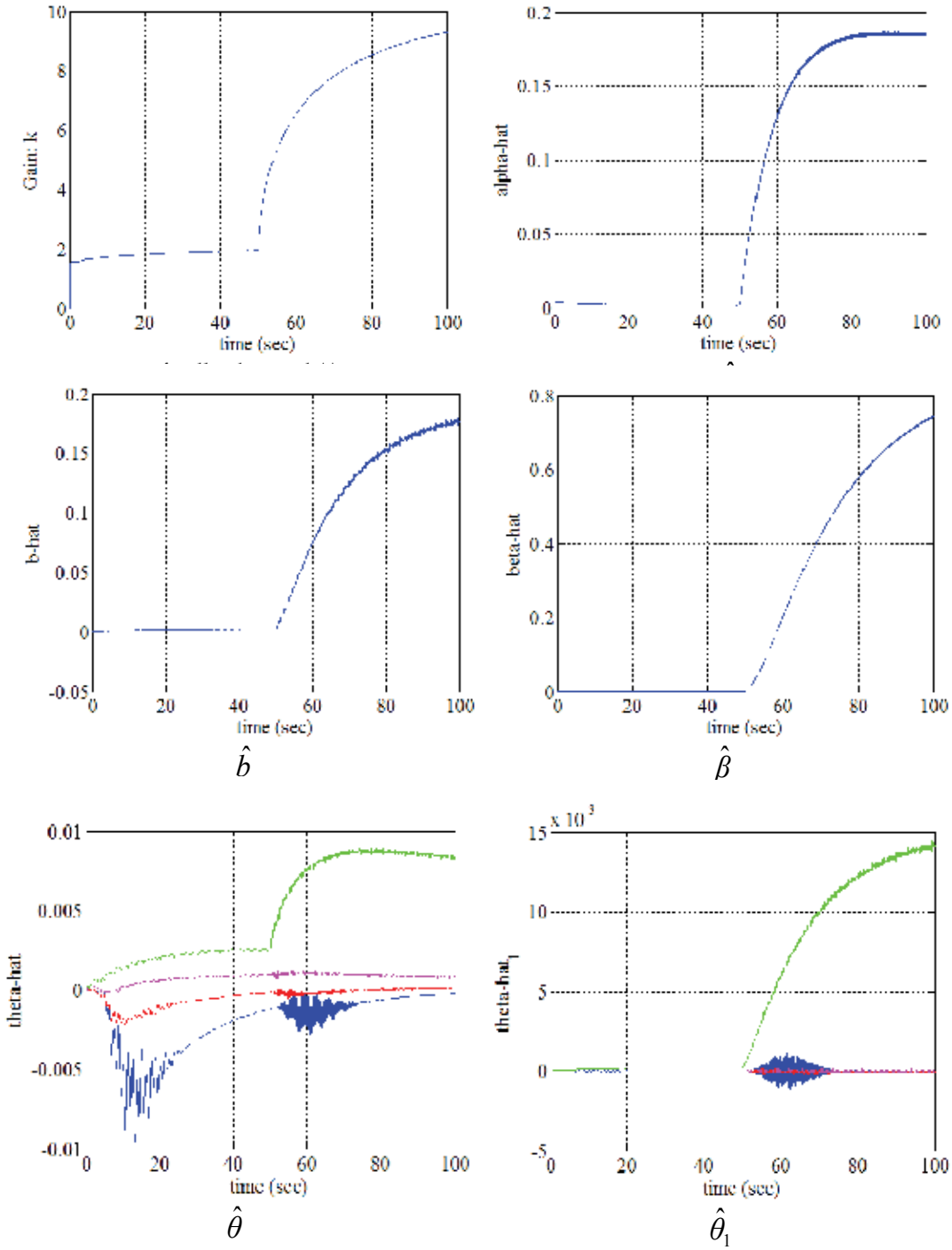

Fig. 6. Adaptively adjusted parameters

A very good control result was obtained and we can see that a good control performance is maintained even as the frequencies of the disturbances were changed at 50 [sec].

Figures 7 and 8 show the simulation results in which the adaptively adjusted parameters in the controller were kept constant after 40 [sec]. After the disturbances were changed, the control performance deteriorated.

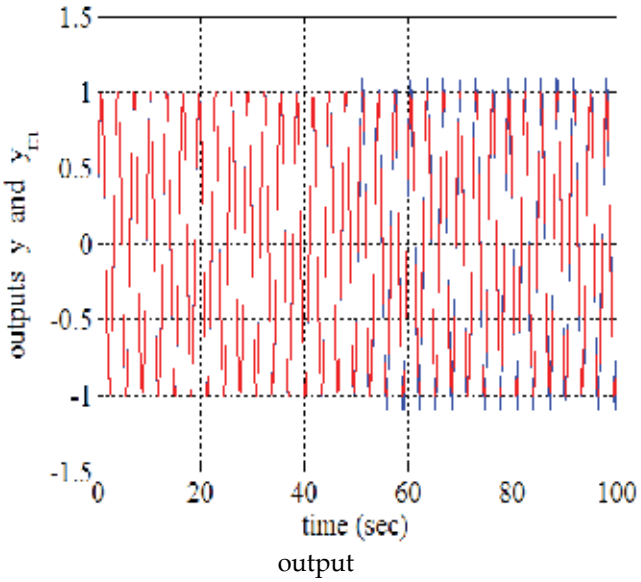

output

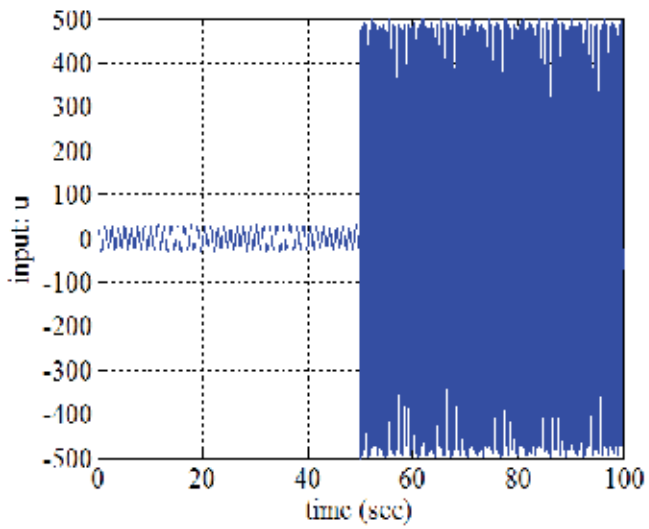

input

Fig. 7. Simulation results without adaptation after 40 [sec].

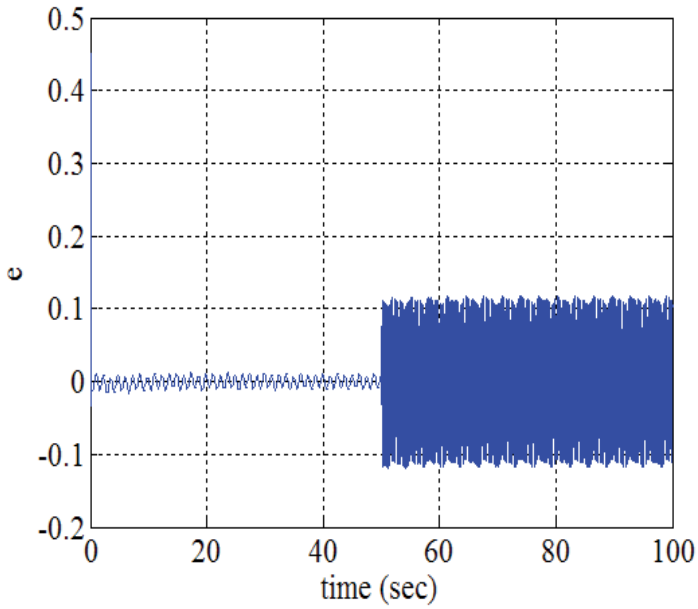

Fig. 8. Tracking error without adaptation

6. Conclusions

In this paper, the adaptive regulation problem for unknown controlled systems with unknown exosystems was considered. An adaptive output feedback controller with an adaptive internal model was proposed for single input/single output linear minimum phase systems. In the proposed method, a controller with an adaptive internal model was designed through an expanded backstepping strategy of only one step with a parallel feedforward compensator (PFC).

7. References

A, Isidori. (1995). *Nonlinear Control Systems-3rd ed.*, Springer-Verlag, 3-540-19916-0, London

A, Serrani.; A, Isidori. & L, Marconi. (2001). Semiglobal Nonlinear Output Regulation With Adaptive Internal Model. *IEEE Trans. on Automatic Control*, Vol.46, No.8, pp. 1178—1194, 0018-9286

G, Feg. & M, Palaniswami. (1991). Unified treatment of internal model principle based adaptive control algorithms. *Int. J. Control*, Vol.54, No.4, pp. 883—901, 0020-7179

H, Kaufman.; I, Bar-Kana. & K, Sobel. (1998). *Direct Adaptive Control Algorithms-2nd ed.*, Springer-Verlag, 0-387-94884-8, New York

I, Mizumoto.; R, Michino.; M, Kumon. & Z, Iwai. (2005). One-Step Backstepping Design for Adaptive Output Feedback Control of Uncertain Nonlinear systems, *Proc. of 16th IFAC World Congress*, DVD, Prague, July

R, Marino. & P, Tomei. (2000). Robust Adaptive Regulation of Linear Time-Varying Systems. *IEEE Trans. on Automatic Control*, Vol.45, No.7, pp. 1301—1311, 0018-9286

R, Marino. & P, Tomei. (2001). Output Regulation of Linear Systems with Adaptive Internal Model, *Proc. of the 40th IEEE CDC*, pp. 745—749, 0-7803-7061-9, USA, December, Orlando, Florida

R, Michino.; I, Mizumoto.; M, Kumon. & Z, Iwai. (2004). One-Step Backstepping Design of Adaptive Output Feedback Controller for Linear Systems, *Proc. of ALCOSP 04*, pp. 705-710, Yokohama, Japan, August

S, Sastry. & M, Bodson. (1989). *Adaptive Control Stability, Convergence, and Robustness*, Prentice Hall, 0-13-004326-5

V, O, Nikiforov. (1996). Adaptive servocompensation of input disturbances, *Proc. of the 13th IFAC World Congress*, Vol.K, pp. 175—180, San-Francisco

V, O, Nikiforov. (1997a). Adaptive servomechanism controller with implicit reference model. *Int J. Control*, Vol.68, No.2, pp. 277—286, 0020-7179

V, O, Nikiforov. (1997b). Adaptive controller rejecting uncertain deterministic disturbances in SISO systems, *Proc. of European Control Conference*, Brussels, Belgium

Z, Ding. (2001). Global Output Regulation of A Class of Nonlinear Systems with Unknown Exosystems, *Proc. of the 40th IEEE CDC*, pp. 65—70, 0-7803-7061-9, USA, December, Orlando, Florida

Z, Iwai. & I, Mizumoto. (1994). Realization of Simple Adaptive Control by Using Parallel Feedforward Compensator. *Int. J. Control*, Vol.59, No.6, pp. 1543—1565, 0020-7179

4

Output Feedback Direct Adaptive Control for a Two-Link Flexible Robot Subject to Parameter Changes

Selahattin Ozcelik and Elroy Miranda
Texas A&M University-Kingsville, Texas
USA

1. Introduction

Robots today have an ever growing niche. Many of today's robots are required to perform tasks which demand high level of accuracy in end effector positioning. The links of the robot connecting the joints are large, rigid, and heavy. These manipulators are designed with links, which are sufficiently stiff for structural deflection to be negligible during normal operation. Also, heavy links utilize much of the joint motor's power moving the link and holding them against gravity. Moreover the payloads have to be kept small compared to the mass of the robot itself, since large payloads induce sagging and vibration in the links, eventually bringing about uncertainty in the end effector position. In an attempt to solve these problems lightweight and flexible robots have been developed. These lightweight mechanical structures are expected to improve performance of the robot manipulators with typically low payload to arm weight ratio. The ultimate goal of such robotic designs is to accurate tip position control in spite of the flexibility in a reasonable amount of time. Unlike industrial robots, these robot links will be utilized for specific purposes like in a space shuttle arm. These flexible robots have an increased payload capacity, lesser energy consumption, cheaper construction, faster movements, and longer reach. However, link flexibility causes significant technical problems. The weight reduction leads the manipulator to become more flexible and more difficult to control accurately. The manipulator being a distributed parameter system, it is highly non-linear in nature. Control algorithms will be required to compensate for both the vibrations and static deflections that result from the flexibility. This provides a challenge to design control techniques that:

a) gives precise control of desired parameters of the system in desired time,
b) cope up with sudden changes in the bounded system parameters,
c) gives control on unmodeled dynamics in the form of perturbations, and
d) robust performance.

Conventional control system design is generally a trial and error process which is often not capable of controlling a process, which varies significantly during operation. Thus, the quest for robust and precise control led researchers to derive various control theories. Adaptive control is one of these research fields that is emerging as timely and important class of controller design. Area much argued about adaptive control is its simplicity and ease of

physical implementation on actual real-life systems. In this work, an attempt has been made to show the simplicity, ease and effectiveness of implementation of direct model reference adaptive control (DMRAC) on a multi input multi output (MIMO) flexible two-link system. The plant comprises of a planar two-link flexible arm with rotary joints subject only to bending deformations in the plane of motion. A payload is added at the tip of the outer link, while hub inertias are included at actuated joints. The goal is to design a controller that can control the distal end of the flexible links.

Probably the first work done pertaining to the control of flexible links was presented by (Cannon & Schmitz, 1984). Considering a flexible link, which was only flexible in one dimension (perpendicular to gravity), a Linear Quadratic Gaussian controller was designed for the position control. Direct end point sensing was used and the goal was to execute a robot motion as fast as possible without residual vibrations in the beam. Also, experiments were carried out on end point control of a flexible one link robot. These experiments demonstrated control strategies for position of one end to be sensed and precisely positioned by applying torque at the other end. These experiments were performed to uncover and solve problems related to the control of very flexible manipulators, where sensors are collocated with the actuators.

(Geniele et al., 1995) worked on tip-position control of a single flexible link, which rotates on a horizontal plane. The dynamic model was derived using assumed-modes method based on the Euler-Bernoulli beam theory. The model is then linearized about an operating point. The control strategy for this non-minimum phase linear time varying system consisted of two parts. The first part had an inner stabilizing control loop that incorporates a feedforward term to assign the system's transmission zeros at desired locations in the complex plane, and a feedback term to move the system's poles to the desire positions in the left half plane. In the second part, the other loop had a feedback servo loop that allowed tracking of the desired trajectory. The controller was implemented on an experimental test bed. The performance was then compared with that of a pole placement state feedback controller.

(Park & Asada, 1992) worked on an integrated structure and control design of a two-link non-rigid robot arm for the purpose of high speed positioning. A PD control system was designed for the simple dynamic model minimizing the settling time. Optimal feedback gains were obtained as functions of structural parameters involved in the dynamic model. These parameters were then optimized using an optimization technique for an overall optimal performance.

(Lee et al., 2001) worked on the adaptive robust control design for multi-link flexible robots. Adaptive energy-based robust control was presented for both close loop stability and automatic tuning of the gains for desired performance. A two-link finite element model was simulated, in which each link was divided into four elements of same length. The controller designed was independent of system parameters and hence possessed stability robustness to parameter variations.

Variations in flexible links have also been researched. Control of a two-link flexible arm in contact with a compliant surface was shown in (Scicliano & Villani, 2001). Here, for a given tip position and surface stiffness, the joint and deflection variables are computed using closed loop inverse kinematics algorithm. The computed variables are then used as the set points for a simple joint PD control, thus achieving regulation of the tip position and contact force via a joint-space controller.

(Ider et al., 2002) proposed a new method for the end effector trajectory tracking control of robots with flexible links. In order to cope with the non-minimum phase property of the system, they proposed to place the closed-loop poles at desire locations using full state feedback. A composite control law was designed to track the desired trajectory, while at the same time the internal dynamics were stabilized. A two-link planar robot was simulated to illustrate the performance of the proposed algorithm. Moreover the method is valid for all types of manipulators with any degree of freedom.
(Green, A. & Sasiadek, J., 2004) presented control methods for endpoint tracking of a two-link robot. Initially, a manipulator with rigid links is modeled using inverse dynamics, a linear quadratic regulator and fuzzy logic schemes actuated by a Jacobian transpose control law computed using dominant cantilever and pinned-pinned assumed mode frequencies. The inverse dynamics model is pursued further to study a manipulator with flexible links where nonlinear rigid-link dynamics are coupled with dominant assumed modes for cantilever and pinned-pinned beams. A time delay in the feedback control loop represents elastic wave travel time along the links to generate non-minimum phase response.
An energy-based nonlinear control for a two-link flexible manipulator wasstudied in (Xu et al., 2005). It was claimed that their method can provide more physical insights in nonlinear control as well as provide a direct candidate for the Lyapunov function. Both simulation and experimental results were provided to demonstrate the effectiveness of the controllers
A robust control method of a two-link flexible manipulator with neural networks based quasi-static distortion compensation was proposed in (Li et al., 2005). The dynamics equation of the flexible manipulator was divided into a slow subsystem and a fast subsystem based on the assumed mode method and singular perturbation theory. A decomposition based robust controller is proposed with respect to the slow subsystem, and H_∞ control is applied to the fast subsystem. The proposed control method has been implemented on a two-link flexible manipulator for precise end-tip tracking control.
In this work a direct adaptive controller is designed and the effectiveness of this adaptive control algorithm is shown by considering the parametric variations in the form of additive perturbations. This work emphasizes the robust stability and performance of adaptive control, in the presence of parametric variations. This approach is an output feedback method, which requires neither full state feedback nor adaptive observers. Other important properties of this class of algorithms include:

a) Their applicability to non-minimum phase systems,
b) The fact that the plant (physical system) order may be much higher than the order of the reference model, and
c) The applicability of this approach to MIMO systems.

Its ease of implementation and inherent robustness properties make this adaptive control approach attractive.

2. Mathematical Modeling of the System

In this section mathematical model of the system is derived using Lagrange equations with the assumed-modes method. The links are assumed to obey Euler-Bernoulli beam model with proper boundary conditions. A payload has been added to the tip of the second link, while hub inertias are included at the actuator joints.

2.1 Kinematic Modeling

A planar two-link flexible arm with rotary joints subject to only bending deformations in the plane of motion is considered. The following coordinate frames, as seen in Fig. 1, are established: the inertial frame (X_0, Y_0), the rigid body moving frame associated to link *i* (X_i, Y_i), and the flexible body moving frame associated with link *i* $(\hat{X}_i, \hat{Y}_i)$ (Brook, 1984).

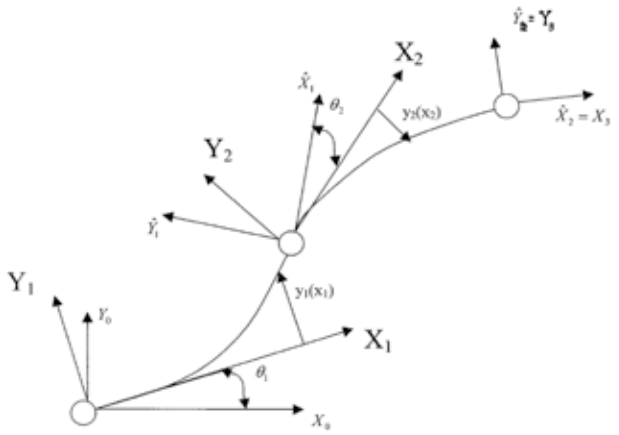

Fig. 1. Planar Flexible Two-Link Arm

The rigid body motion is described by the joint angle, θ_i, while $y_i(x_i)$ denoted the transversal deflection of link *i* at abscissa, $0 \le x_i \le l_i$, l_i being the link length. Let $p_i^i(x_i) = (x_i, y_i(x_i))^T$ be the position of a point along the deflected link *i* with respect to frame (X_i, Y_i) and p_i be the absolute position of the same point on frame (X_0, Y_0). Also, $r_{i+1}^i = p_i^i(l_i)$ indicates the position of the origin of frame (X_{i+1}, Y_{i+1}) with respect to frame (X_i, Y_i), and r_i gives absolute positioning of the origin of frame (X_i, Y_i) with respect to frame (X_0, Y_0). The rotation matrix A_i for rigid body motion and the rotation matrix E_i for the flexible mode are, respectively,

$$A_i = \begin{bmatrix} \cos\theta_i & -\sin\theta_i \\ \sin\theta_i & \cos\theta_i \end{bmatrix} \qquad \mathrm{E}_i = \begin{bmatrix} 1 & -y'_{ie} \\ y'_{ie} & 1 \end{bmatrix} \tag{1}$$

where $y'_{ie} = (\delta_{yi} / \delta_{xi})|_{x_i = l_i}$ and for small deflections $\arctan(y'_{ie}) \approx y'_{ie}$. Therefore, the previous absolute position vectors can be expressed as,

$$\mathrm{p}_i = \mathrm{r}_1 + \mathrm{W}_i{}^i \mathrm{p}_i \qquad \mathrm{E}_i = \mathrm{r}_{i+1} = \mathrm{r}_1 + \mathrm{W}_i{}^i \mathrm{r}_{i+1} \tag{2}$$

where, W_i is the global transformation matrix from (X_0, Y_0) to (X_i, Y_i), which obeys the recursive equation $W_i = W_{i-1} E_{i-1} A_i = \hat{W}_{i-1} A_i$ and $\hat{W}_0 = I$

2.2. Lagrangian Modeling

The equations of motion for a planar n-link flexible arm are derived by using the Lagrange equations. The total kinetic energy is given by the sum of the following contributions:

$$T = \sum_{i-1}^{n} T_{hi} + \sum_{i-1}^{n} T_{li} + T_p \tag{3}$$

where the kinetic energy of the rigid body located at the hub *i* of mass m_{hi} and the moment of inertia J_{hi} is

$$T_{hi} = \frac{1}{2} m_{hi} \dot{r}_i + \frac{1}{2} J_{hi} \alpha_i^2 \tag{4}$$

where $\dot{\alpha}_i$ is the (scalar) absolute angular velocity of frame (X_i, Y_i) given by

$$\dot{\alpha}_i = \sum_{j=1}^{1} \dot{\theta}_j + \sum_{k=1}^{i-1} \dot{y}'_{ke} \tag{5}$$

Moreover, the absolute linear velocity of an arm is

$$\dot{p} = \dot{r}_i + \dot{W}_i p_i^i + W_i^i \dot{p}_i \tag{6}$$

and $\dot{r}_{i+1}^i = \dot{p}_i^i(l_i)$. Since the links are assumed inextensible ($\dot{x}_i = 0$), then $\dot{p}_i^i(x_i) = (0, \dot{y}_i(x_i))^T$. The kinetic energy pertaining to link *i* of linear density ρ_i is

$$T_{li} = \frac{1}{2} \int_0^{li} \rho_i(x_i) \dot{p}_i^T(x_i) dx_i \tag{7}$$

and the kinetic energy associated to a payload of mass m_p and moment of inertia J_p located at the end of link *n* is

$$T_p = \frac{1}{2} m_p \dot{r}_{n+1}^T \dot{r}_{n+1} + \frac{1}{2} J_p (\dot{\alpha}_n + \dot{y}'_{ne})^2 \tag{8}$$

Now, in the absence of gravity (horizontal plane motion), the potential energy is given by

$$U = \sum_{i=1}^{n} U_i = \sum_{i=1}^{n} \frac{1}{2} \int_0^{li} (EI)_i(x_i) \left[\frac{d^2 y_i(x_i)}{dx_i^2} \right]^2 dx_i \tag{9}$$

Where U_i is the elastic energy stored in link *i*, and $(EI)_i$ being its flexural rigidity. No

discretization of structural link flexibility has been made so far, so the Lagrangian will be a functional.

2.3. Assumed Mode Shapes

Links are modeled as Euler Bernoulli beams of uniform density ρ_i and constant flexural rigidity $(EI)_i$ with the deformation $y_i(x_i,t)$ satisfying the partial differential equation

$$(EI)_i \frac{\partial^4 y_i(x_i,t)}{\partial x_i^4} + \rho_i \frac{\partial^2 y_i(x_i,t)}{\partial t^2} = 0, i = 1,...,n. \tag{10}$$

Boundary conditions are imposed at the base of and the end of each link to solve this equation. The inertia of a light weight link is small compared to the hub inertia, and then constrained mode shapes can be used. We assume each slewing link to be *clamped* at the base

$$y_i(0,t) = 0, y_i'(0,t) = 0, i = 1,...,n \tag{11}$$

For the remaining boundary conditions it is assumed that the link end is free of dynamic constraints, due to the difficulty in accounting for time-varying or unknown masses and inertias. However, we consider mass boundary conditions representing balance of moment and shearing force, i.e.

$$\begin{aligned}
(EI)_i \left[\frac{\partial^2 y_i(x_{i,t})}{\partial x_i^2}\right]_{x_i=l_i} &= -J_{Li}\frac{d^2}{dt^2}\left[\left(\frac{\partial y_i(x_i,t)}{\partial x_i}\right)_{x_i=l_i}\right] - (MD)_i \frac{d^2}{dt^2}(y_i(x_{i,t})_{x_i=l_i}) \\
(EI)_i \left[\frac{\partial^3 y_i(x_{i,t})}{\partial x_i^3}\right]_{x_i=l_i} &= -M_{Li}\frac{d^2}{dt^2}(y_i(x_{i,t})_{x_i=l_i}) - (MD)_i \frac{d^2}{dt^2}\left[\left(\frac{\partial y_i(x_i,t)}{\partial x_i}\right)_{x_i=l_i}\right] \\
i &= 1,....,n
\end{aligned} \tag{12}$$

where, M_{Li} and J_{Li} are the actual mass and moment of inertia at the end of link *i*. $(MD)_i$ accounts for the contribution of masses of distal links, i.e. non-collocated at the end of link *i*. A finite-dimensional model of link flexibility can be obtained by assumed modes technique. Using this technique the link deflections can be expressed as

$$y_i(x_i,t) = \sum_{j=1}^{m_i} \phi_{ij}(x_i)\delta_{ij}(t) \tag{13}$$

where $\delta_{ij}(t)$ are the time varying variables associated with the assumed spatial mode shapes $\varphi_{ij}(x_i)$ of link *i*. Therefore each term in the general solution of (10) is the product of a time harmonic function of the form

$$\delta_{ij(t)} = \exp(j\omega_{ij}t) \tag{14}$$

and of a space eigenfunction of the form

$$\phi_{ij}(x_i) = C_{1,ij}\sin(\beta_{ij}x_i) + C_{2,ij}\cos(\beta_{ij}x_i) + C_{3,ij}\sinh(\beta_{ij}x_i) + C_{3,ij}\cosh(\beta_{ij}x_i) \tag{15}$$

In (14) ω_{ij} is the *j*th natural angular frequency of the eigenvalue problem for link *i*, and in (15) $\beta_{ij} = \omega_{ij}^2\rho_i/(EI)_i$.

Application of the aforementioned boundary conditions allows the determination of the constant coefficients in (15). The clamped link conditions at the link base yield

$$C_{3,ij} = -C_{1,ij}, C_{4,ij} = -C_{2,ij} \tag{16}$$

while, the mass conditions at the link end lead to homogeneous system of the form

$$\left[F\left(\beta_{ij}\right)\right]\begin{bmatrix} C_{1,ij} \\ C_{2,ij} \end{bmatrix} \tag{17}$$

The so-called frequency equation is obtained by setting to zero the determinant of the (2×2) matrix $F(\beta_{ij})$ that depends on explicitly on the values of M_{Li}, J_{Li}, and $(MD)_i$. The first m_i roots of this equation give the positive values of β_{ij} to be plugged in (15). Using this the coefficients $C_{1,ij}$ and $C_{2,ij}$ are determined up to a scale factor that is chosen via a suitable normalization. Further the resulting eigenfunctions φ_{ij} satisfy a modified orthogonality condition that includes the actual M_{Li}, J_{Li}, and $(MD)_i$. In an open kinematic chain arrangement, M_{Li} is the constant sum of all masses beyond link *i*, but J_{Li} and $(MD)_i$ depend on the position of successive links. This will considerably increase the complexity of model derivation and overload the computational burden of on-line execution. Thus, some practical approximation leading to constant although nonzero boundary conditions at the link end is done. Thus, a convenient position is set to $(MD)_i = 0$ and compute J_{Li} for a fixed arm configuration. In this case, it can be shown that det(*F*) = 0 results in the following transcendental equation (De Luca & Scicliano, 1989)

$$\begin{aligned} &\left(1+\cos\left(\beta_{ij}l_i\right)\cosh\left(\beta_{ij}l_i\right)\right) - \frac{M_{Li}\beta_{ij}}{\rho_i}\left(\sin\left(\beta_{ij}l_i\right)\cosh\left(\beta_{ij}l_i\right) - \cos\left(\beta_{ij}l_i\right)\sinh\left(\beta_{ij}l_i\right)\right) \\ &- \frac{J_{Li}\beta_{ij}^3}{\rho_i}\left(\sin\left(\beta_{ij}l_i\right)\cosh\left(\beta_{ij}l_i\right) + \cos\left(\beta_{ij}l_i\right)\sinh\left(\beta_{ij}l_i\right)\right) \\ &+ \frac{M_{Li}J_{Li}\beta_{ij}^4}{\rho_i^2}\left(1-\cos\left(\beta_{ij}l_i\right)\cosh\left(\beta_{ij}l_i\right)\right) = 0 \end{aligned} \tag{18}$$

2.4. Closed-Form Equations of Motion

On the basis of the discretization introduced in the previous section, the Lagrangian L becomes a function of set of N generalized coordinates $q_i(t)$ the dynamic model is obtained satisfying the Lagrange-Euler equations

$$\frac{d}{dt}\left(\frac{\partial L}{\partial \dot{q}_i}\right)-\frac{\partial L}{\partial q_i}=f_{i,} \qquad i=1\cdots N \tag{19}$$

where, f_i are the generalized forces performing work on $q_i(t)$. Under the assumption of constant mode shapes, it can be shown that spatial dependence present in the kinetic energy term (7) can be resolved by the introduction of a number of constant parameters, characterizing the mechanical properties of the (uniform density) links (De Luca, et. al. 1988, Cetinkunt, et. al., 1986)

$$m_i=\int_0^{li}\rho_i dx_i=\rho_i l_i \tag{20}$$

$$d_i=\frac{1}{m_i}\int_0^{li}\rho_i x_i x_i=\frac{1}{2}l_i \tag{21}$$

$$J_{0i}=\int_0^{li}\rho_i x_i^2 dx_i=\frac{1}{3}m_i l_i^2 \tag{22}$$

$$v_{ij}=\int_0^{li}\rho_i\varphi_{ij}\left(x_i\right)dx_i \tag{23}$$

$$w_{ij}=\int_0^{li}\rho_i\varphi_{ij}\left(x_i\right)x_i dx_i \tag{24}$$

$$z_{ijk}=\int_0^{li}\rho_i\varphi_{ij}\left(x_i\right)\varphi_{ik}\left(x_i\right)dx_i \tag{25}$$

$$k_{ijk}=\int_0^{li}(EI)_i\varphi_{ij}\left(x_i\right)\varphi_{ik}\left(x_i\right)dx_i \tag{26}$$

where, m_i is the mass of the link i, d is the distance of center of mass of link i from joint i axis, J_{0i} is the inertia of link i about joint i axis, v_{ij} and ω_{ij} are the deformation moments of order zero and one of mode j of the link i. Also, k_{ijk} is the cross elasticity coefficient of modes j and k of link i. The actual numerical values of the previous parameters are calculated off-line. As a result of this procedure, the equations of motion for a planar n-link arm can be written in a familiar closed form

$$B(q)\ddot{q}+h(q,\dot{q})+Kq=Qu \tag{27}$$

where $q = \left(\theta_1\ \theta_n\ \delta_{11}\ \delta_{1,m_1}\ \delta_{n,1}\ \delta_{n,m_n}\right)^T$ is the N-vector of generalized coordinates ($N = n + \sum_i m_i$), and u is the n-vector of joint actuator torques. B is the positive definite symmetric inertia matrix, h is the vector of Corriolis and centrifugal forces, K is the stiffness matrix and Q is the input weighting matrix that is of the form $\left[I_{nxn}\ O_{nx(N-n)}\right]^T$ due to the clamped link assumptions. Joint viscous friction and link structural damping can be added as $D\dot{q}$, where D is a diagonal matrix. It is noted that orthonormalization of mode shapes implies convenient simplification in the diagonal blocks of the inertia matrix relative to the deflections of each link, due to the particular values attained by z_{ijk} in (25). Also the stiffness matrix becomes diagonal $\left(K_1 = \cdots = K_n = 0; K_{n+1}, \ldots, K_N > 0\right)$ being $k_{ijk} = 0$ for $j \neq k$ in (27). The components of h can be evaluated through the Christoffel symbols given by

$$h_i = \sum_{j=1}^{N}\sum_{k=1}^{N}\left(\frac{\partial B_{ij}}{\partial q_k} - \frac{1}{2}\frac{\partial B_{jk}}{\partial q_j}\right)\dot{q}_j\dot{q}_k \tag{28}$$

2.5. Explicit Dynamic Model of Two-Link Flexible Arm

Two assumed mode shapes are considered for each link ($m_1 = m_2 = 2$). Thus, the vector of Lagrangian coordinates reduces to $q = \left(\theta_1\ \theta_2\ \delta_{11}\ \delta_{12}\ \delta_{21}\ \delta_{22}\right)^T$, i.e. N = 6. It can be shown (Brook, 1984, De Luca et. al. 1988) that the contributions of kinetic energy due to deflection variables are

$$\left\{factor\ of\ \dot{\delta}_{i1}^2\right\} = z_{i11} \tag{29}$$

$$\left\{factor\ of\ 2\dot{\delta}_{i1}\dot{\delta}_{i2}\right\} = \left[\varphi_{i1,e}\quad \varphi'_{i1,e}\right]\begin{bmatrix} M_{Li} & \frac{1}{2}(MD)_i \\ \frac{1}{2}(MD)_i & J_{Li}\end{bmatrix}\begin{bmatrix}\varphi_{i2,e} \\ \varphi'_{i2,e}\end{bmatrix} + z_{i12} \tag{30}$$

$$\left\{factor\ of\ \dot{\delta}_{i2}^2\right\} = z_{i22} \tag{31}$$

where, $\varphi_{ij,e} = \varphi_{ij}(x_i)|_{x_i=l_i}$ and $\varphi'_{ij,e} = \varphi'_{ij}(x_i)|_{x_i=l_i}$, $i, j = 1, 2$. The above equations are obtained expanding terms (7) and (8) by using (5) and (6). Accounting for separability (13) then leads to expressions for the factors of the quadratic deflection rate terms, in which parameters defined in (25) and the mass coefficients on the right hand side of (12) can be identified. It is found for link-1:

$$M_{L1} = m_2 + m_{h2} + m_p \tag{32}$$

$$J_{L1} = J_{02} + J_{h2} + J_p + m_P l_2^2 \tag{33}$$

$$(MD)_1 = \left(m_2 d_2 + m_p l_2\right)\cos\theta_2 - \left[\left(v_{21} + m_p\varphi_{21,e}\right)\delta_{21} + \left(v_{22} + m_p\varphi_{22,e}\right)\delta_{22}\right]\sin\theta_2 \tag{34}$$

Note that in the case of only two links, J_{L1} is a constant. On the other hand for link-2:

$$M_{L2} = m_p, \quad J_{L2} = J_p, \quad (MD)_2 = 0 \tag{35}$$

A convenient normalization of mode shapes is accomplished by setting:

$$z_{iii} = m_i, \quad i, j = 1, 2 \tag{36}$$

This also implies that the nonzero coefficients in the stiffness matrix *K* take on values $w_{ij}^2 m_i$. It is stressed that, if the exact values for the boundary conditions in (12) were used the natural orthogonality of the computed mode shapes would imply that $\{ factor\ of\ 2\dot{\delta}_{11}\dot{\delta}_{12} \}$ is zero for both links. For link-2 the use of (35) automatically ensures the "correct" orthogonality of mode shapes. On the other hand, however for link-1, the off-diagonal term $(MD)_1$ varies with arm configuration. This implies that the mode shapes– which are *spatial* quantities–would become implicit functions of time, thus conflicting with the original separability assumption. It is seen that for different positions of second link, $(MD)_1$ results in variations of (34), so the actual mode shapes of the first link become themselves functions of time-varying variables describing the deflection of the second link. A common approximation in computing the elements of the inertia matrix for flexible structures is to evaluate kinetic energy in correspondence to the undeformed configuration. In our case, it is equivalent to neglecting the second term $(MD)_1$ in (34), which is an order of magnitude smaller than the first term. Accordingly, $(MD)_1$ is constant for a fixed arm configuration. Taking $\theta_2 = \pm\pi/2$ leads to $(MD)_1 = 0$ and thus the eigen-frequencies can be computed through (19). This is equivalent to having zeroed only that portion of the $\{ factor\ of\ 2\dot{\delta}_{11}\dot{\delta}_{12} \}$ generated by constant diagonal terms, i.e.

$$\begin{bmatrix} \varphi_{11,e} & \varphi'_{11,e} \end{bmatrix} \begin{bmatrix} M_{Li} & 0 \\ 0 & J_{Li} \end{bmatrix} \begin{bmatrix} \varphi_{12,e} \\ \varphi'_{12,e} \end{bmatrix} + z_{112} = 0 \tag{37}$$

This will produce nonzero off-diagonal terms in the relative block of the inertia matrix. The resulting model is cast in a computational advantageous form, where a set of constant coefficients appear that depend on the mechanical properties of the arm. The inertia matrix as well as other derivations can be found in (Miranda, 2004). Once having obtained the expressions of the inertia matrix, the components of *h* can be evaluated using (28). Viscous friction and passive structural damping are included in matrix *D* for improvement in arm movement, and finally, the stiffness matrix *K* is of the form,

$$K = diag \left\{ 0,\ 0,\ w_{11}^2 m_1,\ w_{12}^2 m_1,\ w_{21}^2 m_2,\ w_{22}^2 m_2 \right\} \tag{38}$$

Then the equations of motion is given in its standard form as

$$B(q)\ddot{q} + h(q, \dot{q}) + D\dot{q} + Kq = Qu \tag{39}$$

After tremendous of algebra and neglecting friction, (39) can be written as,

$$\begin{aligned}
B_{11}\,\ddot{\theta}_1 + B_{12}\,\ddot{\theta}_2 + B_{13}\,\ddot{\delta}_{11} + B_{14}\,\ddot{\delta}_{12} + B_{15}\,\ddot{\delta}_{21} + B_{16}\,\ddot{\delta}_{22} + h_1 &= u_{p1}\\
B_{21}\,\ddot{\theta}_1 + B_{22}\,\ddot{\theta}_2 + B_{23}\,\ddot{\delta}_{11} + B_{24}\,\ddot{\delta}_{12} + B_{25}\,\ddot{\delta}_{21} + B_{26}\,\ddot{\delta}_{22} + h_2 &= u_{p2}\\
B_{31}\,\ddot{\theta}_1 + B_{32}\,\ddot{\theta}_2 + B_{33}\,\ddot{\delta}_{11} + B_{34}\,\ddot{\delta}_{12} + B_{35}\,\ddot{\delta}_{21} + B_{36}\,\ddot{\delta}_{22} + h_3 + K_3\,\delta_{11} &= 0\\
B_{41}\,\ddot{\theta}_1 + B_{42}\,\ddot{\theta}_2 + B_{43}\,\ddot{\delta}_{11} + B_{44}\,\ddot{\delta}_{12} + B_{45}\,\ddot{\delta}_{21} + B_{46}\,\ddot{\delta}_{22} + h_4 + K_4\,\delta_{12} &= 0\\
B_{15}\,\ddot{\theta}_1 + B_{52}\,\ddot{\theta}_2 + B_{53}\,\ddot{\delta}_{11} + B_{54}\,\ddot{\delta}_{12} + B_{55}\,\ddot{\delta}_{21} + B_{56}\,\ddot{\delta}_{22} + h_2 + K_5\,\delta_{21} &= 0\\
B_{61}\,\ddot{\theta}_1 + B_{62}\,\ddot{\theta}_2 + B_{63}\,\ddot{\delta}_{11} + B_{64}\,\ddot{\delta}_{12} + B_{65}\,\ddot{\delta}_{21} + B_{66}\,\ddot{\delta}_{22} + h_2 + K_6\,\delta_{22} &= 0
\end{aligned} \tag{40}$$

where, u_{p1} and u_{p2} are input torques to joints 1 and 2, respectively. Plant outputs are considered to be link tip displacements y_1 and y_2. As seen from above equations, the system is highly nonlinear and of 12th order. For the flexible robot, the following physical parameters were considered

$$\begin{gathered}
\rho_1 = \rho_2 = 0.2\ kg/m\\
l_1 = l_2 = 0.5\ m,\ d_2 = 0.25\ m\\
m_1 = m_2 = m_p = 0.1\ kg,\ m_{h2} = 1\ kg\\
J_{01} = J_{02} = 0.0083\ kgm^2\\
J_{h1} = J_{h2} = 0.1\ kgm^2,\ J_p = 0.0005\ kgm^2\\
(EI)_1 = (EI)_2 = 1\ Nm^2
\end{gathered} \tag{41}$$

The natural frequencies $f_{ij} = w_{ij}/2\pi$ and the remaining parameters in the model coefficients are computed as (Miranda, 2004):

$$\begin{gathered}
f_{11} = 0.48\ Hz,\ f_{12} = 1.80\ Hz,\\
f_{21} = 2.18\ Hz,\ f_{22} = 15.91\ Hz,\\
\varphi_{11,e} = 0.186,\ \varphi_{12,e} = 0.215,\ \varphi'_{11,e} = 0.657,\ \varphi'_{12,e} = -0.560,\\
\varphi_{21,e} = 0.883,\ \varphi_{22,e} = -0.069,\ \varphi'_{21,e} = 2.641,\ \varphi'_{22,e} = -10.853,\\
v_{11} = 0.007,\ v_{12} = 0.013,\ v_{21} = 0.033,\ v_{22} = 0.054,\\
w_{11} = 0.002,\ w_{12} = 0.004,\ w_{21} = 0.012,\ w_{22} = 0.016
\end{gathered} \tag{42}$$

In order to design the proposed adaptive controller, the plant needs to be linearized and the transfer function matrix be obtained. After linearization, neglecting higher order terms, and tremendous amount of algebra, it can be shown (Miranda, 2004) that the plant $G_{po}(s) = y_p(s)/u_p(s)$ with nominal parameters can be obtained as,

$$G_{p0}(s) = \begin{bmatrix} y_{p1}(s) \\ y_{p2}(s) \end{bmatrix} \begin{bmatrix} \dfrac{0.01641s^{10} + 7.061*10^{-5}\ s^8}{s^{12} + 3.68*10^{-3}\ s^{10}} & \dfrac{-2.259s^{10} - 1.362*10^{-3}\ s^8}{s^{12} + 3.68*10^{-3}\ s^{10}} \\ \dfrac{-7.357s^{10} - 9.636*10^{-3}\ s^8}{s^{12} + 3.68*10^{-3}\ s^{10}} & \dfrac{1317\ s^{10} + 0.674s^8}{s^{12} + 3.68*10^{-3}\ s^{10}} \end{bmatrix} \begin{bmatrix} u_{p1}(s) \\ u_{p2}(s) \end{bmatrix} \tag{43}$$

where, $G_{po}(s)$ is the nominal plant transfer function matrix. Now, performing minimal realization, $G_{po}(s)$ can be reduced to

$$G_{po}(s)=\begin{bmatrix} \dfrac{0.01641s^2+7.061*10^{-5}}{s^4+3.68*10^{-3}\,s^2} & \dfrac{-2.259s^2-1.362*10^{-3}}{s^4+3.68*10^{-3}\,s^2} \\ \dfrac{-7.357s^2-9.636*10^{-3}}{s^4+3.68*10^{-3}\,s^2} & \dfrac{1317s^2+0.674}{s^4+3.68*10^{-3}\,s^2} \end{bmatrix} \tag{44}$$

From (44), it is straight forward to obtain the actual plant in general form as

$$G_p(s)=\frac{y_p(s)}{u_p(s)}=\begin{bmatrix} \dfrac{C_1^{11}\,s^2+C_0^{11}}{s^4+B_2^{11}\,s^2} & \dfrac{C_1^{12}\,s^2+C_0^{12}}{s^4+B_2^{12}\,s^2} \\ \dfrac{C_1^{21}\,s^2+C_0^{21}}{s^4+B_2^{21}\,s^2} & \dfrac{C_1^{22}\,s^2+C_0^{22}}{s^4+B_2^{22}\,s^2} \end{bmatrix} \tag{45}$$

where, above coefficients of $G_p(s)$ are functions of plant parameters and can vary with the range as defined below:

$$\begin{cases} \underline{C}_{p-j}^{ij} \le C_{p-j}^{ij} \le \overline{C}_{p-j}^{ij} & i=1,2, \quad j=1,2 \\ \underline{B}_{r-j}^{ij} \le B_{r-j}^{ij} \le \overline{B}_{r-j}^{ij} & i=1,2, \quad j=1,2 \end{cases} \tag{46}$$

The values of the nominal plant parameters are defined in the following table. The range considered for each parameter is ±30%.

Parameter	Nominal	Range
C_1^{11}	0.01641	0.011487 *to* 0.02133
C_0^{11}	$7.061*10^{-5}$	$4.9427*10^{-5}$ *to* $9.1793*10^{-5}$
$B_2^{11}=B_2^{12}=B_2^{21}=B_2^{22}$	$3.68*10^{-3}$	$2.576*10^{-3}$ *to* $4.784*10^{-3}$
C_1^{12}	2.259	1.5813 *to* 2.9367
C_0^{12}	$1.362*10^{-3}$	$9.583*10^{-4}$ *to* $1.7797*10^{-3}$
C_1^{21}	7.357	5.1499 *to* 9.5641
C_0^{21}	$9.636*10^{-3}$	$6.7452*10^{-1}$ *to* $12.5268*10^{-3}$
C_1^{22}	1317	921.9 *to* 1712.1
C_0^{22}	0.674	0.4718 *to* 0.8762

Table 1. Plant parameters, nominal values, and variation range.

For comparison reasons, uncompensated response of the nominal plant is given below

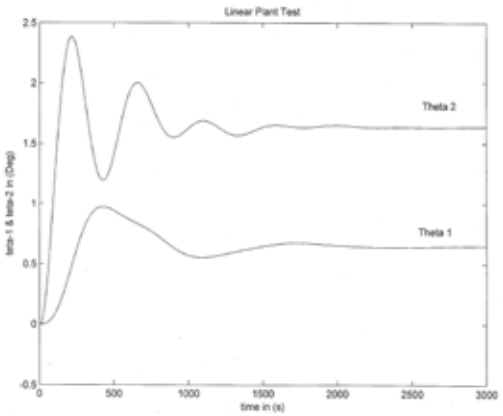

Fig. 2. Uncompensated response of the nominal plant

3. Controller Design

Consider now that the plant given by (45) is represented by the following state-space equations:

$$\begin{aligned} \dot{x}_p(t) &= A_p x_p(t) + B_p u_p(t) \\ y_p(t) &= C_p x_p(t) \end{aligned} \tag{47}$$

where $x_p(t)$ is the (n ×1) state vector, $u_p(t)$ is the (m×1) control vector, $y_p(t)$ is the (q × 1) plant output vector, and A_p, B_p and C_p are matrices with appropriate dimensions. The range of the plant parameters given by (46) is now given by

$$\begin{aligned} \underline{a}_{ij} \le a_p(i,j) \le \bar{a}_{ij}, i, j = 1, \ldots, n \\ \underline{b}_{ij} \le b_p(i,j) \le \bar{b}_{ij}, i, j = 1, \ldots, n \end{aligned} \tag{48}$$

where $a_p(i, j)$ is the $(i, j)^{th}$ element of A_p and $b_p(i, j)$ is the $(i, j)^{th}$ element of B_p. Consider also the following reference model, for which plant output is expected to follow the model output without explicit knowledge of A_p and B_p.

$$\begin{aligned} \dot{x}_m(t) &= A_m x_m(t) + B_m u_m(t) \\ y_m(t) &= C_m x_m(t) \end{aligned} \tag{49}$$

In light of this objective, consider now the following output feedback adaptive control law,

$$u_p(t) = K_e(t) e_y(t) + K_x(t) x_m(t) + K_u(t) u_m(t) \tag{50}$$

where $e_y(t) = y_m(t) - y_p(t)$ and $K_e(t)$, $K_x(t)$, and $K_u(t)$ are adaptive gains defined below. The control law consists of a feedback term from output error and a feedforward terms from model states and inputs. The adaptive gains $K_e(t)$, $K_x(t)$, and $K_u(t)$ are combination of proportional and integral gains as given below,

$$K_j(t) = K_{pj}(t) + K_{ij}(t) \quad j = e, x, u \tag{51}$$

and they are updated according to the following adaptation law (Kaufman, et. al. 1998, Ozcelik & Kaufman, 1999)

$$K_{pj}(t) = e_y(t)[e_y(t) + x_m(t) + u_m(t)]T_p \quad j = e, x, u, T_p \geq 0 \tag{52}$$

$$K_{ij}(t) = e_y(t)[e_y(t) + x_m(t) + u_m(t)]T_i \quad j = e, x, u, \ T_i > 0 \tag{53}$$

where T_i and T_p are constant proportional and integral weighting matrices, respectively. It is seen from (53) that the term $K_{ij}(t)$ is a perfect integrator and may steadily increase whenever *perfect* following ($e_y(t) = 0$) is not possible. The gain may reach unnecessarily large values, or may even diverge. Thus, a σ-term is introduced in order to avoid the divergence of integral gains (Ionnou & Kokotovic, 1983). With the σ -term, $K_i(t)$ is now from a first-order filtering of $e_y(t)r^T(t)T_i$ and therefore cannot diverge, unless $e_y(t)$ diverges. However, in this context, the σ -term does more for the concept of '*adaptive control*'. The gains increase only if high gains are needed and decrease if they are not needed any more. They are also allowed to change at any rate without affecting stability, such that the designer can adjust this rate to fit the specific needs of the particular plant. Thus, using σ -term we rewrite the equation (53) as follows,

$$K_{ij}(t) = e_y(t)[e_y(t) + x_m(t) + u_m(t)]T_i - \sigma K_{ij}(t) \quad j = e, x, u \tag{54}$$

For this adaptive control to work and for asymptotic tracking to be achieved, the plant is required to be almost strictly positive real (ASPR) (Bar-Kana, 1994); that is, there exists a gain matrix K_e, not needed for implementation, such that the closed-loop transfer function

$$G_c(s) = [I + G_p(s)K_e]^{-1}G_p(s) \tag{55}$$

is strictly positive real (SPR). And that it can be shown that (Kaufman, et. al., 1998) a MIMO system represented by a transfer function $G_p(s)$ is ASPR if it:

a) is minimum phase (zeros of the transfer function are on the left-half plane),
b) has relative degree of m or zero (i.e., the difference in the degree of denominator and numerator, (n-m=m) or (n-m=0)), and
c) has minimal realization with high frequency gain $C_pB_p > 0$ (positive definite).

Obviously, the plant given by (45) does not satisfy the so-called ASPR conditions and that can not be applied. However, it has been shown in (Kaufman, et. al., 1998) and (Ozcelik,

2004) that there exist a feedforward compensator $H(s)$ such that the augmented plant $G_a(s) = G_p(s) + H(s)$ is ASPR and the proposed adaptive algorithm can be implemented confidently.

3.1. Design of a Feedforward Compensator (FFC) for the Flexible Robot

From the above restrictions it is obvious that the plant given by (45) is not ASPR and that an FFC has to be designed. Now consider the actual plant $G_p(s)$ again,

$$G_p(s) = \begin{bmatrix} \dfrac{C_1^{11}s^2 + C_0^{11}}{s^4 + B_2^{11}s^2} & \dfrac{C_1^{12}s^2 + C_0^{12}}{s^4 + B_2^{12}s^2} \\ \dfrac{C_1^{21}s^2 + C_0^{21}}{s^4 + B_2^{21}s^2} & \dfrac{C_1^{22}s^2 + C_0^{22}}{s^4 + B_2^{22}s^2} \end{bmatrix} \tag{56}$$

Assuming that the nominal plant parameters are known, the parametric uncertainty of the plant can be transformed into a frequency dependent additive perturbation of the plant by representing of the actual plant $G_p(s)$ as $G_p(s) = G_{p0}(s) + \Delta_a(s)$, with $G_{p0}(s)$ being a nominal plant and $\Delta_a(s)$ being a frequency dependent additive perturbation. Then, one can write

$$\Delta_a(s) = G_p(s) - G_{p0}(s) \tag{57}$$

From (57), the additive uncertainty transfer function can be obtained as

$$\Delta_a(s) = \begin{bmatrix} \lambda_{11}(s) & \lambda_{12}(s) \\ \lambda_{21}(s) & \lambda_{22}(s) \end{bmatrix} \tag{58}$$

where,

$$\begin{aligned}
\lambda_{11}(s) &= \frac{(C_1^{11} - 0.016411)s^6 + \left(3.68*10^{-3}C_1^{11} + C_0^{11} - 7*10^{-5} - 0.01641B_2^{11}\right)s^4 + \left(3.68*10^{-3}C_0^{11} - 7*10^{-5}B_2^{11}\right)s^2}{s^8 + \left(3.68*10^{-3} + B_2^{11}\right)s^6 + B_2^{11}3.68*10^{-3}s^4} \\
\lambda_{12}(s) &= \frac{(2.25 + C_1^{12})s^6 + \left(3.68*10^{-3}C_1^{12} + C_0^{12} + 1.36*10^{-3} + 2.25B_2^{12}\right)s^4 + \left(3.68*10^{-3}C_0^{12} + 1.36*10^{-3}B_2^{12}\right)s^2}{s^8 + \left(3.68*10^{-3} + B_2^{12}\right)s^6 + b_1 3.68*10^{-3}s^4} \\
\lambda_{21}(s) &= \frac{(7.32 + C_1^{21})s^6 + \left(3.68*10^{-3}C_1^{21} + C_0^{21} + 9.63*10^{-3} + 7.35B_2^{21}\right)s^4 + \left(3.68*10^{-3}C_0^{21} + 9.63*10^{-3}B_2^{21}\right)s^2}{s^8 + \left(3.68*10^{-3} + B_2^{21}\right)s^6 + b_1 3.68*10^{-3}s^4} \\
\lambda_{22}(s) &= \frac{(C_1^{22} - 1317)s^6 + \left(3.68*10^{-3}C_1^{22} + C_0^{22} - 0.674 - 1317B_2^{21}\right)s^4 + \left(3.68*10^{-3}C_0^{22} - 0.674B_2^{21}\right)s^2}{s^8 + \left(3.68*10^{-3} + B_2^{21}\right)s^6 + B_2^{21}3.68*10^{-3}s^4}
\end{aligned} \tag{59}$$

It is seen that the uncertainty is a function of plant parameters, which vary in a given range. Thus, in the design of a feedforward compensator, the worst case uncertainty should be taken into account. To this effect, the following optimization procedure is considered for determining the worst case uncertainty at each frequency (suitable number of discrete values). Define a vector whose elements are plant parameters, i.e.

$$v = \begin{bmatrix} C_p^{ij} & C_{p-1}^{ij} & \cdots & C_0^{ij} & B_r^{ij} & B_{r-1}^{ij} & \cdots & B_0^{ij} \end{bmatrix} \tag{60}$$

Then

$$\begin{aligned} &\underbrace{\text{maximize}}_{v} \left|\lambda_{ij}(jw)\right| \quad \textit{at each } w \\ &\textit{subject to}: \begin{cases} \underline{C}_{p-j}^{ij} \le C_{p-j}^{ij} \le \overline{C}_{p-j}^{ij} \\ \underline{B}_{r-j}^{ij} \le B_{r-j}^{ij} \le \overline{B}_{r-j}^{ij} \end{cases} \end{aligned} \tag{61}$$

where λ_{ij} is the ij^{th} element of $\Delta(jw)$. In other words, this optimization is performed for each element of $\Delta(jw)$. After having obtained the worst case (maximum) perturbation, we will assume that the perturbation is not exactly known but its upper bound is known. In other words, there exists a known rational function as an upper bound of the worst case uncertainty. Now the upper bound is characterized by an element by element interpretation, where the upper bound means that each entry of $\lambda(jw)$ is replaced by its corresponding bound. In other words, given the worst case uncertainty for each $\lambda(jw)$, it is assumed that there exists a known rational function $w_{ij}(s) \in RH_\infty$ such that

$$\left|w_{ij}(jw)\right| \ge \max\left|\lambda_{ij}(jw)\right| \forall w \tag{62}$$

Knowing that the plant parameters can vary within their lower and upper bounds, this parametric uncertainty is formulated as an additive perturbation in the transfer function matrix. It is important to note that the controller be designed with respect to worst case uncertainty for each λ_{ij}. This can be achieved by performing an optimization procedure given by (61) for 200 frequencies. Here an element by element uncertainty bound model is used for the characterization of upper bound of the uncertainty matrix. Then w_{ij} , which satisfies (62) for each λ_{ij} is given in matrix form as,

$$W(s) = \begin{bmatrix} \dfrac{7*10^2}{800s^2 + 22s + 0.05} & \dfrac{9*10^4}{80s^2 + 4s + 0.05} \\ \dfrac{425*10^3}{150s^2 5.75s + 0.05} & \dfrac{2*10^9}{25s^2 + 3.75s + 0.125} \end{bmatrix} \tag{63}$$

The magnitude responses for each $max(|\lambda_{ij}|)$ and the corresponding $(|w_{ij}|)$ are given in Figures 3-6. Having obtained the nominal plant and formulated unmodeled dynamics, let's have the following assumptions on the plant,

Assumption 1:

a) The nominal plant parameters are known.

b) The off-diagonal elements of $G_{po}(s)$ and $\Delta_a(s)$ are strictly proper.

c) $\Delta_a(s) \in RH_\infty^{mxm}$ and satisfies (62)

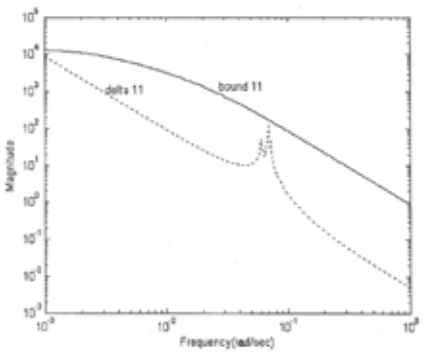

Fig. 3. $|\lambda_{11}(jw)|$ and $|w_{11}(jw)|$

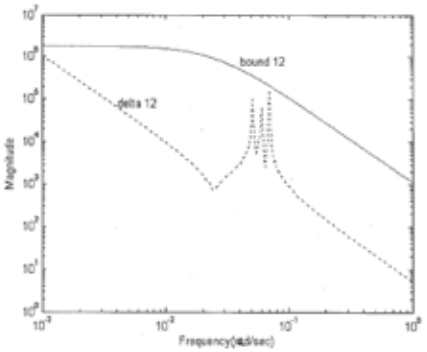

Fig. 4. $|\lambda_{12}(jw)|$ and $|w_{12}(jw)|$

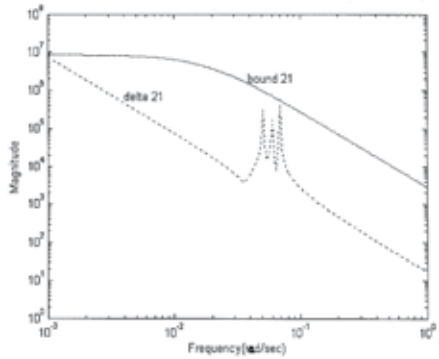

Fig. 5. $|\lambda_{21}(jw)|$ and $|w_{21}(jw)|$

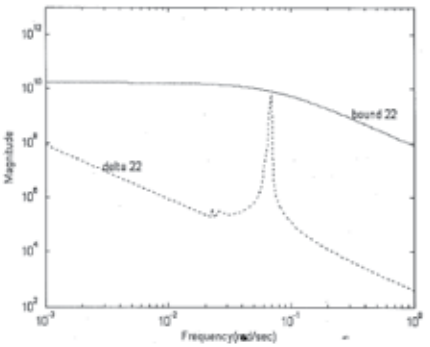

Fig. 6. $|\lambda_{22}(jw)|$ and $|w_{22}(jw)|$

Now, consider the augmented nominal plant with the parallel feedforward compensator

$$G_{ao}(s) = G_{po}(s) + H(s) \tag{64}$$

and the following lemma

Lemma 1:
Let the feedforward compensator H(s) be of the form,

$$H(s) = \begin{bmatrix} h_{11} & 0 & \dots & 0 \\ 0 & h_{22} & \cdots & 0 \\ \vdots & \vdots & \ddots & \vdots \\ 0 & 0 & \dots & h_{mm} \end{bmatrix} \tag{65}$$

with each element $h_{ii}(s)$ of a feedforward compensator being relative degree zero, then the augmented nominal plant $G_{ao}(s) = G_{po}(s)+H(s)$ will have positive definite high frequency gain and relative McMillan degree zero (Ozcelik & Kaufman, 1999).

In other words, the new plant $G_{ao}(s)$ including $H(s)$ becomes ASPR. Now that the ASPR conditions are satisfied for the nominal plant case, we next need to guarantee that the ASPR conditions are also satisfied in the presence of plant perturbations. To this effect, consider the following theorem

Theorem 1: *If $H(s)$ is designed according to the following conditions, then the augmented plant $G_a(s) = G_p(s)+H(s)$ with the plant perturbations will be ASPR.*

a) $H(s)$ is stable with each h_{ij} (s) being relative degree zero

b) H^{-1} (s) stabilizes the nominal closed loop system

c) $\tilde{\Delta}(s) \in RH_\infty$ *and* $\left\|\tilde{\Delta}(s)\right\|_\infty < 1$

where $\tilde{\Delta}(s)$ *is the uncertainty of the augmented plant and given in the following* (Ozcelik & Kaufman, 1999)

$$\tilde{\Delta}(s) = \left(G_{p0}(s) + H(s)\right)^{-1} W(s) \tag{66}$$

In light of the Theorem 1, we can readily determine the FFC as follows:

a) The order of each element $h_{ii}(s)$ of a feedforward compensator is chosen to be equal to the order of the corresponding diagonal element of the nominal plant $G_{p0}(s)$.

$$H(s) = \begin{bmatrix} \dfrac{h_1 s^4 + h_2 s^3 + h_3 s^2 + h_4 s + h_5}{s^4 + 4s^3 + 6s^2 + 4s + 1} & 0 \\ 0 & \dfrac{h_6 s^4 + h_7 s^3 + h_8 s^2 + h_9 s + h_{10}}{s^4 + 4s^3 + 6s^2 + 4s + 1} \end{bmatrix} \tag{67}$$

Denominator of the compensator $H(s)$ appears in the numerator of the closed-loop transfer function and therefore, can be pre-determined such that its time constant is fast enough that its dynamics is negligible.

b) Compensator parameters are determined from the following optimization procedure:

$$\begin{aligned} &\underbrace{\text{minimize}}_{X} \left\|\tilde{\Delta}(jw)\right\|_\infty \\ &\textit{subject to}: \ \text{Re}\,al\left[roots(Z(s))\right] < 0 \end{aligned} \tag{68}$$

where $Z(s)$ is the characteristic polynomial of the nominal closed-loop system matrix and X is a vector composed of the parameters of each $H_{ij}(s)$.

$$\begin{aligned} &\textit{numerator of } h_{11} = 3.7444e^{-4}s^4 + 4.6805e^{-4}s^3 + 9.5966e^{-3}s^2 + 1.1650e^{-3}s + 4.0310e^{-4} \\ &\textit{numerator of } h_{22} = 9.2748e^{-5}s^4 + 5.7746e^{-4}s^3 + 2.3495e^{-4}s^2 + 2.9786e^{-5}s + 5.6472e^{-4} \end{aligned} \tag{69}$$

With this FFC, all the conditions of Theorem 1 are satisfied. Thus, the augmented plant satisfies the almost strictly positive real conditions over a wide range of plant parameter variations. It is expected that the DMRAC augmented with this feedforward compensator will be robust for the maximum deviations from the nominal plant. The block diagram of the overall control system is depicted in Figure 7.

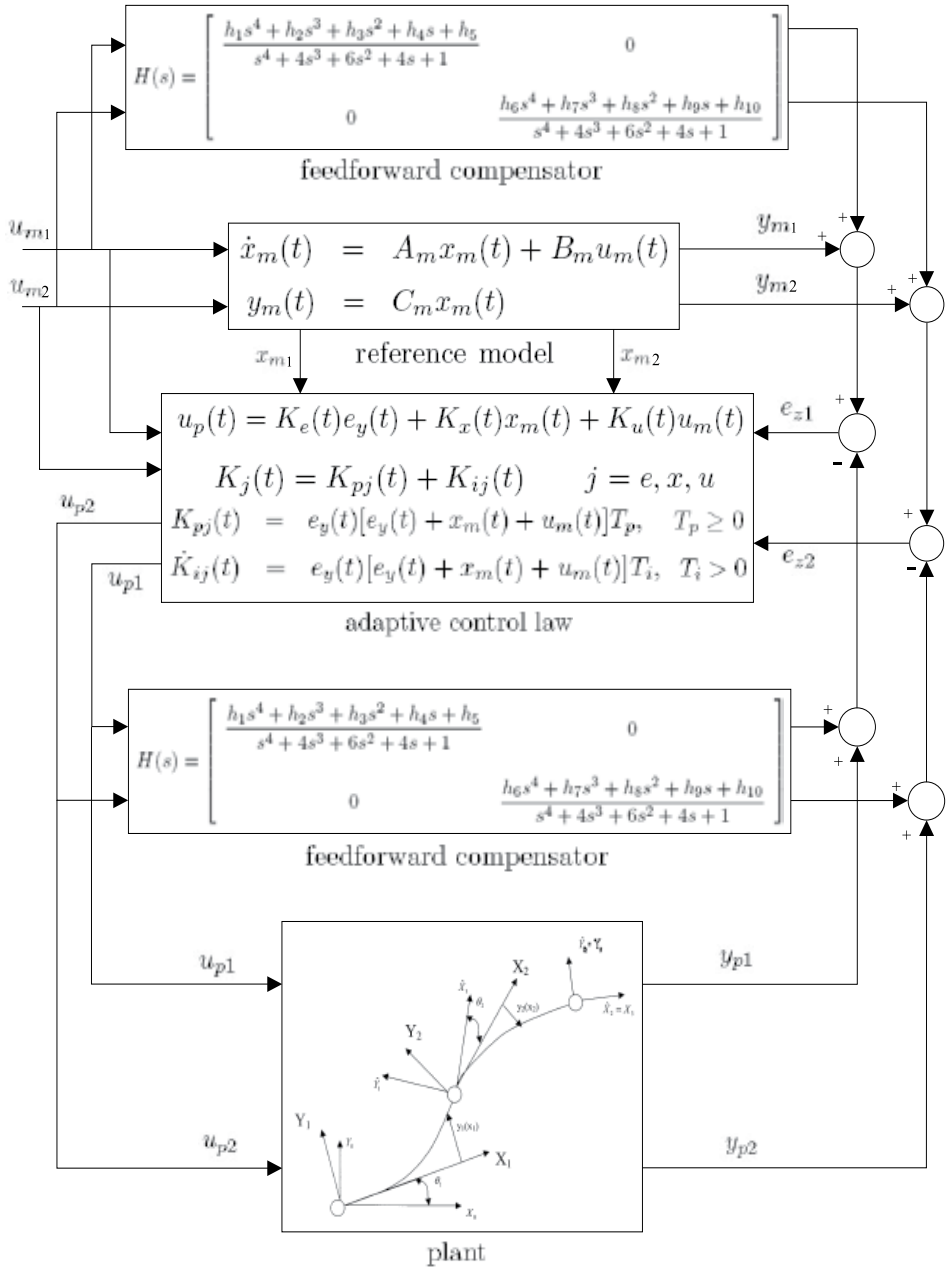

Fig. 7. DMRAC with Two-Link Arm

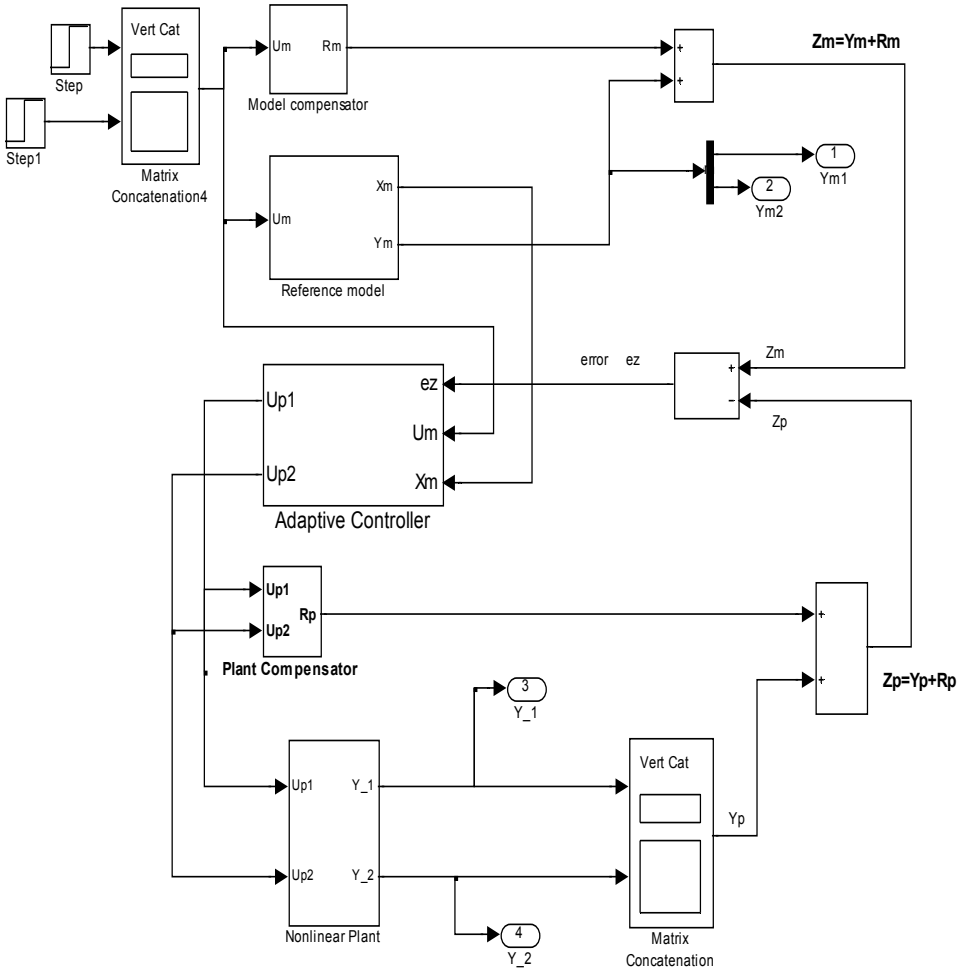

Fig. 8. Simulink Block Diagram of the overall control system with nonlinear plant.

4. Simulation Results

The nonlinear equations were used in building the plant in Simulink/MATLAB (Figure 8) and with the above described DMRAC algorithm, the following cases were simulated.

4.1 Case 1

- All initial conditions were set to zero.
- For both links the reference models were set to $G_{m1}(s) = G_{m2}(s) = 1/(30s+1)$
- For both links tip displacements were set to=0.05m
- Upper bound of plant parameters was used.

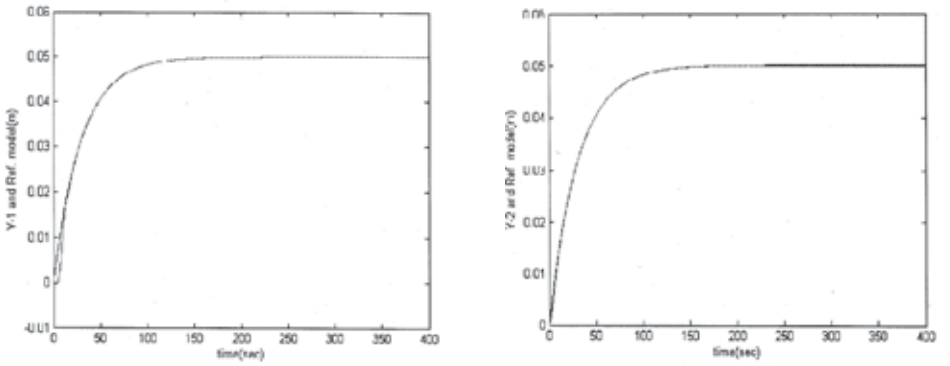

Fig. 9. Case 1: y_1 and reference model (left), y_2 and reference model (right)

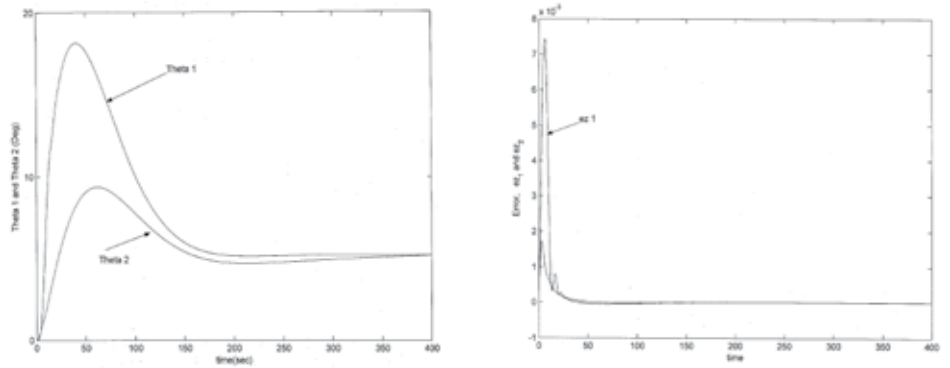

Fig. 10. Case 1: θ_1 and θ_2 (left), errors e_{z1} and e_{z2} (right)

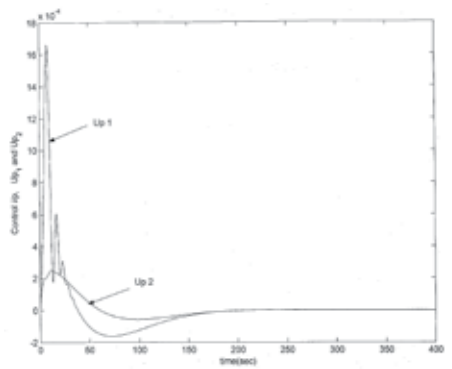

Fig. 11. Case 1: Control inputs, u_{p1} and u_{p2}

4.2. Case 2

- All initial conditions were set to zero.
- For both links the reference models were set to $G_{m1}(s) = G_{m2}(s) = 1/(15s+1)$
- For both links tip displacements were set to=0.05m
- Lower bound of plant parameters was used.

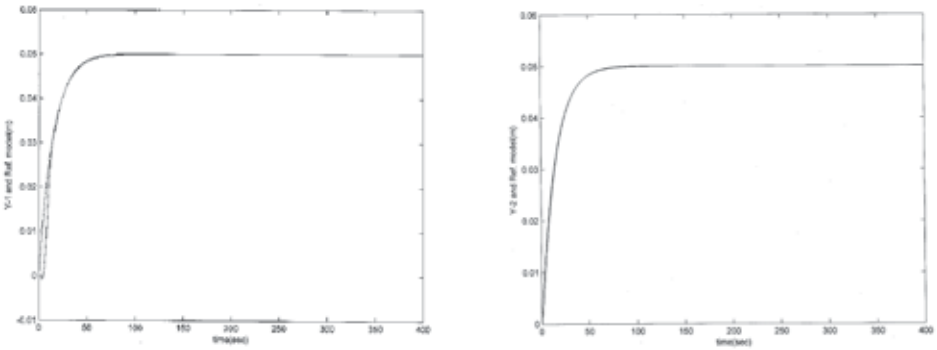

Fig. 12. Case 2: y_1 and reference model (left), y_2 and reference model (right)

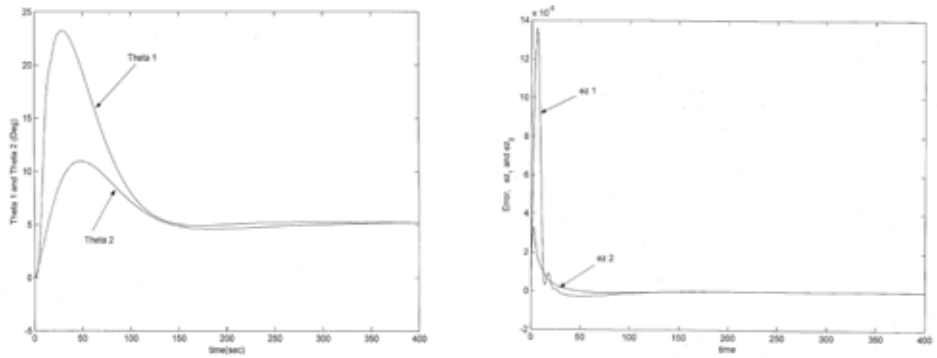

Fig. 13. Case 2: θ_1 and θ_2 (left), errors e_{z1} and e_{z2} (right)

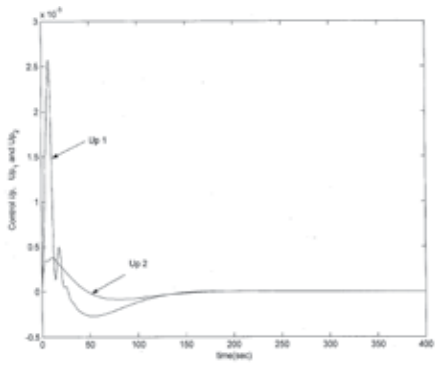

Fig. 14. Case 2: Control inputs, u_{p1} and u_{p2}

From the Figures 9-11 of Case 1 and the Figures 12-14 of Case 2, we can see that the tips of both links in each case follow the reference input. In Case 2 we have used a faster reference model to show the effectiveness of the DMRAC.

4.3. Case 3

- $\theta_1(0) = 5^\circ, \quad \theta_2(0) = 0^\circ$

- For both links the reference models were set to $G_{m1}(s) = G_{m2}(s) = 1/(30s+1)$
- For both links tip displacements were set to=0.01m
- Nominal set of plant parameters were used.

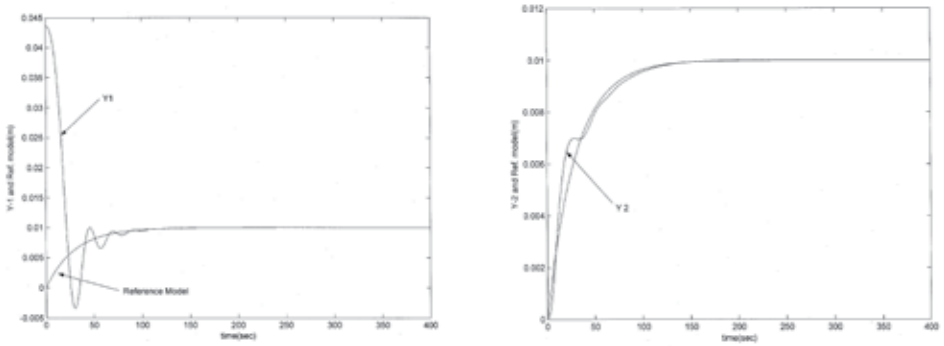

Fig. 15. Case 3: y_1 and reference model (left), y_2 and reference model (right)

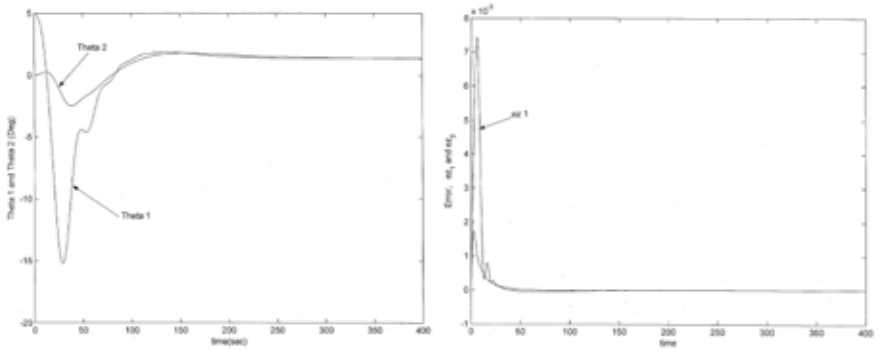

Fig. 16. Case 3: θ_1 and θ_2 (left), errors e_{z1} and e_{z2} (right)

From Figure 15 we see that at t=0, the tip position of link 2, y_2 begins at zero, however due to the initial condition for θ_1 tip position of first link, y_1 is displaced with respect to the desired reference model at t=0. From Figure 16 it is seen that θ_1 and θ_2 come to steady-state, while errors approach to zero.

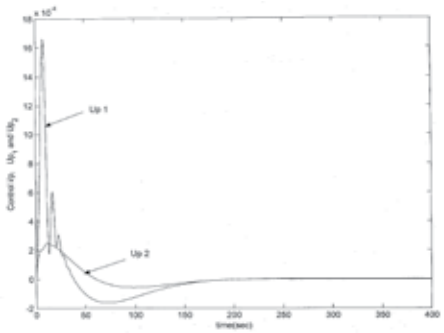

Fig. 17. Case 3: Control inputs, u_{p1} and u_{p2}

4.5. Case 4

- $\theta_1(0) = 0^\circ, \quad \theta_2(0) = 0^\circ$
- For both links the reference models were set to $G_{m1}(s) = G_{m2}(s) = 1/(50s+1)$
- For both links tip displacements were set to=± 0.01m
- Nominal plant parameters were used

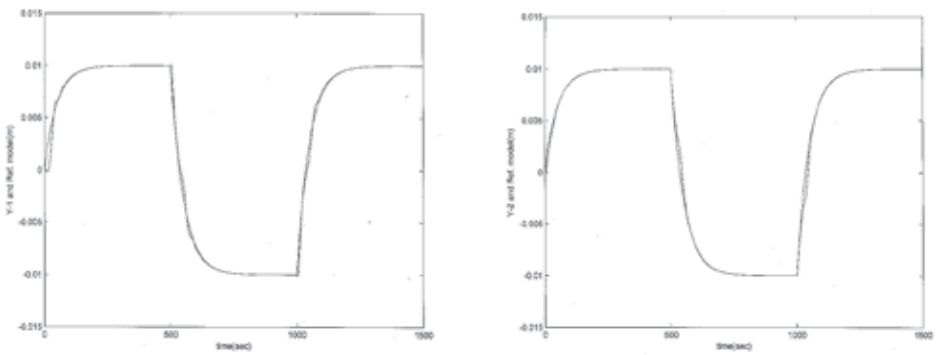

Fig. 18. Case 4: y_1 and reference model (left), y_2 and reference model (right)

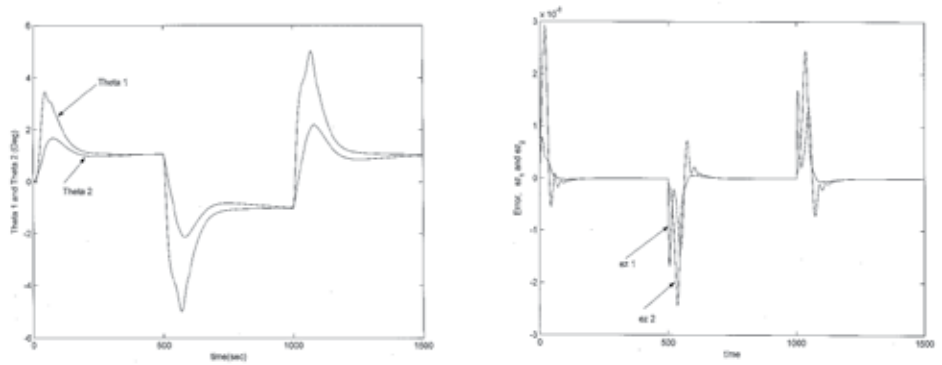

Fig. 19. Case 4: θ_1 and θ_2 (left), error e_z (right)

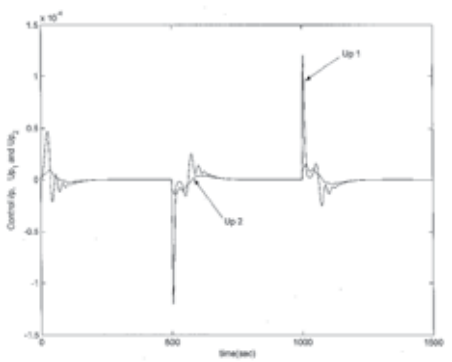

Fig. 20. Case 4: Control inputs, u_{p1} and u_{p2}.

5. Conclusions

Direct Model Reference Adaptive Control is utilized to control two-link flexible robot, whose parameters vary. The feedforward compensator was designed for the system and it was showed that the augmented plant satisfies the ASPR conditions over the range of parameter variations. As seen from the results of the tip position response, the system closely follows the reference model. During the simulations it was observed that DMRAC was capable of controlling the plant despite the changes in the plant parameters. The ease of its implementation and its robustness were demonstrated.

6. References

Cannon, R. H. & Schmitz, E. (1984). Initial Experiments on the End-Point Control of a Flexible One-Link Robot. *Int. J. Robotics Research*, Vol 3, No. 3, pages 325-338.

Geniele, H, Patel, R.V. & Khorasani, K. (1995). Control of a Flexible Link Manipulator. *IEEE Int. Conf. Robotics and Automation,* Vol. 1, pp 1217-1222, May 1995.

Ge, S. S., Lee, T.H. & Wang, Z. P. (2001). Adaptive Robust Controller Design for Multi-Link Flexible Robots. *Proceedings of the American Control Conference*, Vol. 2, pp 947-952, June, 2001.

Park, J. H. & Asada, H. (1992). Integrated Structure/Control Design of a Two-Link Nonrigid Robot Arm for High Speed Positioning, *IEEE Int. Conf. Robotics and Automation,* pp 735-741, Nice, France, May 1992.

Green, A. & Sasiadek, J. (2004). Dynamics and Trajectory Tracking Control of a Two-Link Robot Manipulator, *Journal of Vibration and Control*, Vol. 10, No. 10, 1415-1440.

Ider , K., S., Ozgoren, M., K. & Ay, O. (2002) Trajectory Tracking Control of Robots with Flexible Links, *Mechanism and Machine Theory,* Vol 37, pp 1377-1394.

Siciliano, B. & Villani, L. (2001). An Inverse Kinematics Algorithm for Interaction Control of a Flexible Arm with a Compliant Surface, *Control Engineering Practice,* Vol 9, pp 191-198.

De Luca, A. & Scicliano, B. (1989). Trajectory Control of a Nonlinear One-Link Flexible Arm *International Journal of Control,* Vol 50, pp 1699-1716.

Xu, B., Kenji, F. & Yoshikazun, H. (2005). An Energy-Based Nonlinear Control for a Two-Link Flexible Manipulator, *Trans Japan Soc Aeronautical Space Sc.*, Vol 48, No 160, pp. 92-101.

De Luca, A, Lucibello, P. & Nicolo, F. (1988). Automatic Symbolic Modeling and Non Linear Control of Robots with Flexible Links. *Proc. IEE Work On Robot Control,* pp. 62-70, Oxford, UK, April 1988.

Li, Y., Liu, G, Hong, T. & Liu, K. (2005). Robust Control of a Two-Link Flexible Manipulator with Quasi-Static Deflection Compensation Using Neural Networks, *Journal of Intelligent and Robotic Systems* Vol 44 , No 3 pp. 263-276. Kluwer Academic Publishers, MA, USA

Cetinkunt, S., Scicliano, B. & Book, J. W. (1984). Symbolic Modeling and Dynamic Analysis of Flexible Manipulators *Proc. IEEE Int. Conf. Syst., Man and Cyber.,*pp. 798-803, Georgia, USA.

Book, W., J. (1984). Recursive Lagrangian Dynamics of Flexible Manipulator Arms. *Int. Journal of Robotics Research,* Vol. 3, No. 3, pp. 87-101.

Miranda, E. (2004). Direct Adaptive Control of a Flexible Manipulator, *Thesis,* Texas A&M University, Kingsville, TX, USA.

Kaufman, H., Bar-Kana, I., & Sobel, K. (1998). *Direct Adaptive Control Algorithms: Theory and Applications,* Springer Communication and Control Eng., 2nd Edition, Springer-Verlag.

Ozcelik, S. & Kaufman, H. (1999). Design of robust direct adaptive controllers for SISO: time and frequency domain design conditions. *Intl. Journal of Control*, Vol.72, No. 6, pp. 517-530.

Ionnou, P. & Kokotovic, P. (1983). *Adaptive Systems with reduced models,* Springer-Verlag, New York, USA.

Bar-Kana, I. (1994). *Positive realness in multivariable stationary linear systems, Journal of Franklin Institute* ,No. 328, pp. 403-417.

Ozcelik, S. (2004). *Robust direct adaptive control for MIMO Systems Using Q-Parameterization*, *IFAC ALCOSP,* pp 93-98, Yokohama, Japan.

5

Discrete Model Matching Adaptive Control for Potentially Inversely Non-Stable Continuous-Time Plants by Using Multirate Sampling

S. Alonso-Quesada & M. De La Sen
Electricity and Electronics Department, Faculty of Science and Technology
Basque Country University, Spain

1. Introduction

Adaptive control theory has been widely applied for stabilizing linear time invariant plants of unknown parameters (Goodwin & Sin, 1984). One of the more used methods for such a purpose is based on the model reference adaptive control (MRAC) problem (Aström & Wittenmark, 1997). Such a method requires some assumptions relative to the plant to be controlled in order to carry out the synthesis of a stable controller (Narendra & Annaswamy, 1989). One of them is that the plant has to be inversely stable, what means that its zeros have to be located within the stability domain. However, this information is not always available to the designer when the system under control contains unknown parameters. There are several alternatives to circumvent this drawback and carry out the stable adaptive control design. Some of them consist on relaxing the control performance from the model matching to that achievable from the closed-loop pole placement (Alonso-Quesada & De la Sen, 2004 and Arvanitis, 1999). In this way, the stabilization of the closed-loop system can be ensured although its transient behaviour cannot be fixed to a predefined one.

On one hand, the work (Alonso-Quesada & De la Sen, 2004) includes an estimates modification in the estimation algorithm to ensure the controllability of the estimated plant model without assuming any knowledge about the parameters of the plant to be controlled. This controllability property is crucial to avoid pole-zero cancellations between the estimated plant and the controller, which are both time-varying. In this context, a projection of the estimated plant parameters into a region in the parameter space where the closed-loop system is free of pole-zero cancellations for all time can be alternatively used provided that the true plant is controllable and the knowledge of a region where the true plant parameters belong to (Goodwin & Mayne, 1987).

On the other hand, the research (Arvanitis, 1999) proposes an adaptive pole-placement control for linear systems using generalized sampled-data hold functions. Following such a technique, gain controllers essentially need to be designed. Concretely, a periodic piecewise constant gain controller is added in the feedback chain. In the non-adaptive case, such constant gain values are those required so that the discretized closed-loop model under a fundamental sampling period and a zero-order hold (ZOH) be stabilized. For such a

purpose, each sampling period is divided in a certain finite number of uniform subintervals and the controller gain takes a different value within each of them in order to locate the discretized poles at the stable desired locations. In other words, the controller consists of a constant vector of gains. In this sense, the controller works with a sampling rate faster than that used to discretize the plant to be controlled. In the adaptive case, an estimated model of the discretized plant is on-line updated by means of an estimation algorithm. Such a model is used to parameterize the controller gains vector which becomes time-varying and converges asymptotically to a constant one.

Another alternative, which does not relax the MRAC objective, to overcome the drawback of the unstable zeros in a continuous-time plant is the design of discrete-time controllers which are synthesized from the discretization of the continuous-time plant by means of a holder device combined with a multirate with fast input sampling rate (De la Sen & Alonso-Quesada, 2007 and Liang & Ishitobi, 2004). The main motivation of this method is that an inversely stable discretized model of the plant can be obtained with an appropriate choice of the multirate gains. In this way, an adaptive controller can be designed to match a discrete-time reference model since all the discretized plant zeros may be cancelled if suited.

In this context, *a fractional-order hold (FROH) with a multirate input is used in this paper to obtain an inversely stable discretized plant model from a possible non-inversely stable and unstable time invariant continuous-time plant. Then, a control design for matching a discrete-time reference model is developed for both non-adaptive and adaptive cases.* Note that a FROH includes as particular cases the ZOH and the FOH (first-order hold). In this way, the stabilization of the continuous-time plant is guaranteed without any assumption about the stability of its zeros and without requiring estimates modification in contrast with previous works on the subject. In this sense, this paper is an extension of the work (De La Sen & Alonso-Quesada, 2007) where the same problem is addressed. *The main contribution is related to the method used to built the continuous-time plant input from the discrete-time controller output.* In the present paper, the FROH acts on the fundamental sampling period used to discretize the plant (plant output sampling) while in the aforementioned paper the FROH acted on the sampling period used to define the multirate device at the plant input. This later sampling period is an integer fraction of the plant output one, i.e. an integer number of input samples takes place within each output sampling period. Such an integer has to be suitably chosen for disposing of the enough freedom degrees being necessary to place the discretized plant zeros at desired locations, namely within the unity circle in order to guarantee the inverse stability of the discretized plant model.

The assumptions about the plant to guarantee the closed-loop stability of the adaptive control system are the following: (1) the stabilizability of the plant and (2) the knowledge of the continuous-time plant order. The motivation for using a multirate sampling input instead of the most conventional single rate one resides in the fact that the former, with the appropriate multirate gains, provides an inversely stable discretized plant model without requirements on either the stability of the continuous-time plant zeros or the size of the sampling period. In this sense, a single rate input can only provide an inversely stable discretized plant from an inversely stable continuous-time plant and, moreover, the fundamental sampling period to discretized the plant has to be sufficiently small (Blachuta, 1999). Finally, the use of a FROH, instead of the most conventional ZOH, allows to accommodate better some discrete adaptive techniques to the transient response of discrete-time controlled continuous-time plants (Bárcena et al., 2000 and Liang et al., 2003).

The paper is organized as follows. Section 2 formulates a discrete state-space description under fast input sampling to then obtain an input-output discrete transfer function for the running slow sampling rate, namely, that acting on the output signal. The selection of the scalar gains that generate the fast sampled input so that the discrete plant zeros are stable is focused on depending on the continuous-time plant parametrization. Section 3 discusses the synthesis of a model-matching based controller with a possible potential free design of all the zeros of the reference model. The case of known plant parameters and the adaptive case for not fully known plant parameters are both considered. Two alternatives are proposed to update on-line the time-varying multirate gains in the adaptive case. The first one updates the multirate gains for all sampling instants in order to maintain the zeros of the estimated discretized plant fixed within the stability domain. On the contrary, the other one updates the multirate gains only when the change of gains is crucial to guarantee the stability of the estimated discretized plant zeros. In this way, the multirate gains are not updated for all sampling instants and then they became piecewise constant. As a result, the zeros of the estimated discretized plant become time-varying within the stability domain. Section 4 deals with the stability analysis of the adaptive control system. Simulated examples which highlight the proposed design philosophy are provided in Section 5. A comparison of the results obtained with the two different methods for updating the multirate gains is presented. Finally, conclusions end the paper in Section 6.

2. Discretized Plant Representation

Consider a linear time-invariant, single-input single-output and strictly proper continuous-time plant described by the following state space equations:

$$\dot{x}(t) = Ax(t) + Bu(t) \quad ; \quad y(t) = Cx(t) \tag{1}$$

where $u(t)$ and $y(t)$ are, respectively, the input and output signals, $x(t) \in \Re^n$ denotes the state vector and A, B and C are constant matrices of suitable dimensions. A FROH and a multirate sampling on the fast input sampling will be used in order to obtain an inversely stable discretized plant model. The signal generated by such a device is given by,

$$u(t) = \alpha_j \left\{ u(k) + \beta \frac{u(k) - u(k-1)}{T} (t - kT) \right\} \tag{2}$$

for $t \in \left[kT + (j-1)T', kT + jT' \right)$, $j \in \{1, 2, \ldots, N\}$ and FROH correcting gain $\beta \in [-1, 0) \cup (0, 1]$, where T is the sampling period (slow sampling) which is divided in N equal subperiods of length $T' = T/N$ (fast sampling) to generate the multirate plant input, $u(k)$ denotes the value of a discrete-time controller output signal at the instant kT, for all non-negative integer k, and α_j's are real constants. Note that the FROH device operates on the sequence $\{u(k)\}$ defined at the slow sampling instants kT and then the input $u(t)$ is generated over each subperiod with the corresponding gain α_j, for $j \in \{1, 2, \ldots, N\}$, via (2). By substituting (2) into (1) and sampling the plant output $y(t)$ over the sampling period T, the following

state space representation is obtained which corresponds to the discrete-time plant model that relates the sequences $\{u(k)\}$ and $\{y(k)\}$:

$$x(k+1) = F\,x(k) + G_1\,u(k) + G_2\,u(k-1) \quad ; \quad y(k) = C\,x(k) \tag{3}$$

where $F = \psi^N = \phi(T) = e^{AT}$ is the continuous-time state transition matrix computed for a slow sampling period and,

$$G_1 = \left(\sum_{\ell=1}^{N} \alpha_\ell \psi^{N-\ell}\right)\left(\Gamma + \frac{\beta}{T}\Gamma'\right) \in \Re^{n\times 1} \quad ; \quad G_2 = -\frac{\beta}{T}\left(\sum_{\ell=1}^{N} \alpha_\ell \psi^{N-\ell}\right)\Gamma' \in \Re^{n\times 1} \tag{4}$$

with,

$$\Gamma = \int_0^{T'} \phi(T'-s)\,B\,ds \in \Re^{n\times 1} \quad ; \quad \Gamma' = \int_0^{T'} \phi(T'-s)\,B\,s\,ds \in \Re^{n\times 1} \tag{5}$$

The transfer function of this discrete-time plant model is,

$$H(z) = C(zI_n - \psi^N)^{-1}\left(G_1 + \frac{1}{z}G_2\right) = \frac{B(z)}{A(z)} \tag{6}$$

where,

$$\begin{aligned} B(z) &= C\ \mathrm{Adj}(zI_n - \psi^N)C_\Delta(z)g = \mathrm{Det}\begin{bmatrix} zI_n - \psi^N & C_\Delta(z)g \\ -C & 0 \end{bmatrix} = \sum_{i=1}^{n+1} b_i z^{n-i+1} \\ A(z) &= z\ \mathrm{Det}(zI_n - \psi^N) = z^{n+1} + \sum_{i=1}^{n} a_i z^{n-i+1} \end{aligned} \tag{7}$$

with $\mathrm{Adj}(\cdot)$ and $\mathrm{Det}(\cdot)$ denoting, respectively, the adjoint matrix and the determinant of the square matrix (.), I_n denoting the n-th order identity matrix, and

$$\begin{aligned} g &= \begin{bmatrix}\alpha_1 \cdots \alpha_N\end{bmatrix}^T \in \Re^{N+1}; C_\Delta(z) \cdots \begin{bmatrix}\psi^{N-1}\Delta(z) & \cdots & \psi\Delta(z) & \Delta(z)\end{bmatrix} \in \Re^{nxN} \\ \Delta(z) &= z\left(\Gamma + \frac{\beta}{T}\Gamma'\right) - \frac{\beta}{T}\Gamma' \end{aligned} \tag{8}$$

Note that the coefficients b_i, for $i \in \{1, 2, \ldots, n+1\}$, of the polynomial $B(z)$ in (7) depend on the values α_j, for $j \in \{1, 2, \ldots, N\}$, which define the multirate device. This fact lets to allocate the zeros of the discretized plant model at desired locations if a suitable number of multirate gains is provided. In this sense, the multirate gains α_j, being the components of the vector g, are calculated to guarantee that such zeros are maintained within the stability domain, i.e., the unity circle. In particular, the coefficients b_i can be

expressed as:

$$b_i = \sum_{j=1}^{N} b_{i,j}\alpha_j \Leftrightarrow v = M\ g \tag{9}$$

where $M = \left[b_{i,j} \right] \in \Re^{(n+1)\times N}$ and $v = \left[b_1 \quad b_2 \quad \dots \quad b_{n+1} \right]^T$. The coefficients $b_{i,j}$ depend on the parameters of the continuous-time plant, the sampling period T and the correcting gain β of the FROH considered in the discretization process.

Assumptions 1.
(i) The plant is stabilizable, i.e. its transfer function does not possess unstable pole-zero cancellations,
(ii) the plant order n is known, and
(iii) the correcting gain β of the FROH device and the sampling period T are chosen such that M is a full rank matrix. ***

Remark 1. The multirate gains vector g required to place the zeros of the discretized plant transfer function (6) at desired locations may be calculated from (9) provided Assumptions 1 and that $N \geq n+1$. In this sense, such locations are prefixed via a suitable choice of the vector v composed by the coefficients of the desired polynomial for the transfer function numerator. If $N > n+1$, different solutions can be obtained for g. Otherwise, i.e. if $N = n+1$, there is a unique solution for the multirate gains vector from the linear algebraic system (9) which places the discretized zeros at desired locations. ***

The discretized model (6) can be described by the following difference equation:

$$\begin{aligned} y(k) &= -\sum_{i=1}^{n} a_i\ y(k-i) + \sum_{i=1}^{n+1} b_i\ u(k-i) = -\sum_{i=1}^{n} a_i\ y(k-i) + \sum_{i=1}^{n+1}\sum_{j=1}^{N} b_{i,j}\ \alpha_j\ u(k-i) \\ &= -\sum_{i=1}^{n} a_i\ y(k-i) + \sum_{i=1}^{n+1}\sum_{j=1}^{N} b_{i,j}\ \bar{u}_j(k-i) = \theta^T\ \varphi(k-1) \end{aligned} \tag{10}$$

where,

$$\begin{aligned} &\theta = \left[\theta_a^T \quad \theta_{b,1}^T \quad \theta_{b,2}^T \quad \dots \quad \theta_{b,n+1}^T \right]^T \ ;\ \varphi(k-1) = \left[\varphi_y^T(k-1) \quad \varphi_u^T(k-1) \quad \varphi_u^T(k-2) \quad \dots \quad \varphi_u^T(k-n-1) \right]^T \\ &\theta_a = \left[-a_1 \quad -a_2 \quad \dots \quad -a_n \right]^T \ ;\ \varphi_y(k-1) = \left[y(k-1) \quad y(k-2) \quad \dots \quad y(k-n) \right]^T \\ &\theta_{b,i} = \left[b_{i,1} \quad b_{i,2} \quad \dots \quad b_{i,N} \right]^T \ ;\ \varphi_u(k-i) = \left[\bar{u}_1(k-i) \quad \bar{u}_2(k-i) \quad \dots \quad \bar{u}_N(k-i) \right]^T \\ &\bar{u}_j(k-i) = \alpha_j u(k-i) \end{aligned} \tag{11}$$

for all $i \in \{1, 2, \dots, n+1\}$ and all $j \in \{1, 2, \dots, N\}$. In the rest of the paper, the case $N = n+1$ will be considered for simplicity purposes.

3. Control Design

The control objective in the case of known plant parameters is that the discretized plant model matches a stable discrete-time reference model $H_m(z) = \frac{B_m(z)}{A_m(z)}$ whose zeros can be freely chosen, where z is the Z-transform argument. Such an objective is achievable if the discretization process uses the multirate sampling input with the appropriate multirate gains, what guarantees the inverse stability of the discretized plant. Then, all the discretized plant zeros may be cancelled by controller poles. In this way, the continuous-time plant output tracks the reference model output at the sampling instants. The tracking-error between such signals is zero at all sampling instants in the case of known plant parameters while it is maintained bounded for all time while it converges asymptotically to zero as time tends to infinity in the adaptive case considered when the plant parameters are fully or partially unknown. A self-tuning regulator scheme is used to meet the control objective in both non-adaptive and adaptive cases.

3.1 Known Plant

The proposed control law is obtained from the difference equation:

$$R(q)\, u(k) = T(q)\, c(k) - S(q)\, y(k) \tag{12}$$

for all non-negative integer k, where $\{c(k)\}$ is the input reference sequence and q is the running sample rate advance operator being formally equivalent to the Z-argument used in discrete transfer functions. The reconstruction of the continuous-time plant input u(t) is made by using (2), with the control sequence $\{u(k)\}$ obtained from (12), with the appropriate multirate gains α_j, for $j \in \{1, 2, \ldots, N\}$, to guarantee the stability of the discretized plant zeros.

The discrete-time transfer function of the closed-loop system obtained from the application of the control law (12) to the discretized plant (6) is given by:

$$\frac{Y(z)}{C(z)} = \frac{B(z)T(z)}{A(z)R(z) + B(z)S(z)} = \frac{T(z)}{A(z) + S(z)} \tag{13}$$

where the second equality is fulfilled if the control polynomial $R(z) = B(z)$. In this way, the polynomial $B(z)$, which is stable, is cancelled. Then, the polynomials $T(z)$, $R(z)$ and $S(z)$ of the controller (12) so that $\frac{Y(z)}{C(z)} = \frac{B_m(z)}{A_m(z)}$ are obtained from:

$$T(z) = B_m(z)A_s(z) \;\; ; \;\; R(z) = B(z) \;\; ; \;\; S(z) = A_m(z)A_s(z) - A(z) \tag{14}$$

where $A_s(z)$ is a stable monic polynomial of zero-pole cancellations of the closed-loop system. The following degree constraints are satisfied in the synthesis of the controller:

$$\begin{cases} \mathrm{Deg}[A_m(z)] + \mathrm{Deg}[A_s(z)] = \mathrm{Deg}[A(z)] = n+1 \\ \mathrm{Deg}[S(z)] = \mathrm{Deg}[A(z)] - 1 = n \;\Rightarrow\; S(z) = \sum_{i=0}^{n} s_{i+1}\, z^{n-i} \\ \mathrm{Deg}[T(z)] = \mathrm{Deg}[B_m(z)] + \mathrm{Deg}[A_s(z)] \le n \end{cases} \tag{15}$$

3.2 Unknown Plant

If the continuous-time plant parameters are unknown then the vector θ in (11) composed of the discretized plant model parameters is also unknown. However, all the above control design in the previous subsection remains valid if such a parameter vector is estimated by an estimation algorithm. In this way, the controller parameterization can be obtained from $R(z,k) = \hat{B}(z,k)$, with $\hat{B}(z,k)$ denoting the estimated of $B(z)$ at the current slow sampling instant kT, and equations similar to (14) by replacing the discretized plant polynomial $A(z)$ by its corresponding estimated one $\hat{A}(z,k)$ (Alonso-Quesada & De la Sen, 2004). Note that $T(z)$ in (14) has to be calculated once for all since $B_m(z)$ and $A_s(z)$ are time-invariant while $S(z)$ is updated at each running sampling time since the polynomial $\hat{A}(z,k)$ is time-varying. The coefficients of the unknown polynomial $B(z)$ depend, via (9), on the multirate input gains α_j, for $j \in \{1, 2, \ldots, N\}$, being applicable to calculate the input within the inter-sample slow period. However, the estimation algorithm provides an adaptation of each parameter $b_{i,j}$, namely $\hat{b}_{i,j}(k)$, for $i, j \in \{1, 2, \ldots, N\}$ and all non negative integer k. Then, the α_j -gains have to be also updated in order to ensure the stability of the zeros of the estimated discretized plant, i.e. the roots of $\hat{B}(z,k)$ be stable. Then, the gains α_j become time-varying, namely $\hat{\alpha}_j(k)$. The estimation algorithm for updating the parameters vector $\hat{\theta}(k)$, which denotes the estimated of θ, and two different design alternatives for the adaptation of the multirate gains are presented below. Also, the main boundedness and convergence properties derived from the use of such algorithms are established.

3.2.1. Estimation algorithm

An 'a priori' estimated parameters vector is obtained at each slow sampling instant by using a recursive least-squares algorithm (Goodwin & Sin, 1984) defined by:

$$\begin{aligned} P(k) &= P(k-1) - \frac{P(k-1)\,\varphi(k-1)\,\varphi^T(k-1)\,P(k-1)}{1+\varphi^T(k-1)\,P(k-1)\,\varphi(k-1)} \\ \hat{\theta}^0(k) &= \hat{\theta}^0(k-1) + \frac{P(k-1)\,\varphi(k-1)\,e^0(k)}{1+\varphi^T(k-1)\,P(k-1)\,\varphi(k-1)} \end{aligned} \tag{16}$$

for all integer $k > 0$ where $e^0(k) = \left(\theta - \hat{\theta}^0(k-1)\right)^T \varphi(k-1) = \tilde{\theta}^{0T}(k-1)\varphi(k-1)$ denotes the 'a priori' estimation error and $P(k)$ is the covariance matrix initialized as $P(0) = P^T(0) > 0$.

Such an algorithm provides an estimation $\hat{\theta}^0(k)$ of the parameters vector by using the regressor $\varphi(k-1)$, defined in (11), built with the output and input measurements with the multirate gains $\hat{\alpha}_j(k-1)$ obtained at the previous slow sampling instant, i.e. $\bar{u}_j(k-i) = \hat{\alpha}_j(k-1)\, u(k-i)$ for all $i \in \{1,\ 2,\ \ldots,\ n+1\}$. Then, an 'a posteriori' estimates vector is obtained in the following way:

Modification algorithm.
This algorithm consists of three steps:

Step 1: Built the matrix $\hat{M}^0(k) = \left[\hat{b}^0_{i,j}(k)\right] \in \Re^{N\times N}$, for $i, j \in \{1,\ 2,\ \ldots,\ N\}$, from the 'a priori' estimates $\hat{\theta}^0_{b,i}(k)$, included in $\hat{\theta}^0(k)$, of the corresponding $\theta_{b,i}$ defined in (11).

Step 2: $\hat{M}(k) = \hat{M}^0(k)$

If $\mathrm{Det}\left[\hat{M}(k)\right] \geq \delta_0$ *then* $\hat{\theta}_{b,i}(k) = \hat{\theta}^0_{b,i}(k)$

else while $\mathrm{Det}\left[\hat{M}(k)\right] < \delta_0$

$\hat{M}(k) = \hat{M}(k) + \delta I_N$

end;

for $i = 1$ *to* N

$\hat{\theta}_{b,i}(k) = \hat{M}_i(k)$

end

end.

Step 3: $\hat{\theta}(k) = \left[\hat{\theta}^{0T}_a(k) \quad \hat{\theta}^T_{b,1}(k) \quad \hat{\theta}^T_{b,2}(k) \quad \ldots \quad \hat{\theta}^T_{b,N}(k)\right]^T$,

for some real positive constants $\delta << 1$ and $\delta_0 << 1$, and where $\hat{M}_i(k)$ denotes the *i*-th row of $\hat{M}(k)$. ***

Remark 2. Note that the estimate $\hat{\theta}^0_a(k)$ corresponding to the parameters of θ_a is not affected by the modification algorithm. Also, note that the *while* instruction part of the second step is doing a finite number of times since there exists a finite integer number ℓ such that $\mathrm{Det}\left[\hat{M}(k)\right] = \mathrm{Det}\left[\hat{M}^0(k) + \ell\delta I_N\right] = (\ell\delta)^N + f\left(\delta,\ \hat{\theta}^0_{b,1}(k),\ \hat{\theta}^0_{b,2}(k),\ \ldots,\ \hat{\theta}^0_{b,N}(k)\right) \geq \delta_0$. ***

3.2.2. Updating of the time-varying multirate gains

Once the estimated parameters vector is obtained at each slow sampling instant the multirate input gains have to be updated. Two alternative algorithms are considered to carry out such an operation.

Algorithm 1.
A vector of multirate gains is updated at all slow sampling instants in order to maintain the zeros of the estimated discretized plant fixed at desired locations within the stability domain $|z| < 1$. Such desired zeros are the roots of a predefined polynomial $B'(z)$. For such a

purpose, the required vector $\hat{g}(k)$ is obtained from the resolution of the following matrix equation:

$$\hat{M}(k)\,\hat{g}(k) = v \tag{17}$$

at each slow sampling instant, where $v = \left[b'_1 \quad b'_2 \quad \dots \quad b'_N\right]^T$ is composed by the coefficients of $B'(z)$, $\hat{M}(k) = \left[\hat{b}_{i,j}(k)\right] \in \Re^{N\times N}$, with $\hat{b}_{i,j}(k)$ denoting each of the 'a posteriori' estimated parameters corresponding to the components of the vectors $\theta_{b,i}$ defined in (11), and $\hat{g}(k) = \left[\hat{\alpha}_1(k) \quad \hat{\alpha}_2(k) \quad \dots \quad \hat{\alpha}_N(k)\right]^T$. In this way, $\hat{g}(k)$ is composed by the multirate gains which make the numerator of the estimated discretized plant model be equal to the desired polynomial $B'(z)$. Note that the matrix equation (17) can be solved at all slow sampling instants since the parameters modification added to the estimation algorithm ensures the non-singularity of the matrix $\hat{M}(k)$.

Algorithm 2.
It consists of solving the equation (17) only when it is necessary to modify the previous values of the multirate gains in order to guarantee the stability of the zeros of the estimated discretized plant model. i.e., the multirate gains remain equal to those of the preceding slow sampling instant if the zeros of the estimated discretized plant obtained with the current estimated parameters vector, $\hat{\theta}(k)$, and the previous multirate gains, $\hat{\alpha}_j(k-1)$, are within the discrete-time stability domain. Otherwise, the multirate gains are updated by the resolution of the equation (17), which can be solved whenever it is necessary since the matrix $\hat{M}(k)$ is invertible at all slow sampling instant due to the modification included in the estimation algorithm. In this way, the multirate gains are piecewise constant, the estimated discretized plant zeros are time-varying and the computational burden associated with the updating of the multirate gains is reduced with respect to that of Algorithm 1.

3.2.3. Properties of the estimated models

The parameter estimation algorithm, together with any of the considered adaptation algorithms for the multirate gains, possesses the properties given in the following lemma, whose proof is presented in Appendix A.

Lemma 1. ***Main properties of the estimation and multirate gains adaptation algorithms***

(i) $P(k)$ is uniformly bounded for all non-negative integer k, and it asymptotically converges to a finite, at least semidefinite positive, limit as $k \to \infty$.

(ii) $\hat{\theta}^0(k)$ and $\hat{\theta}(k)$ are uniformly bounded and they asymptotically converge to a finite limit as $k \to \infty$.

(iii) The vector $\hat{g}(k)$ of multirate gains is bounded and converges to a finite limit as $k \to \infty$.

(iv) $\dfrac{\left(e^0(k)\right)^2}{1+\varphi^T(k-1)\,P(k-1)\,\varphi(k-1)}$ is uniformly bounded and it asymptotically converges to

zero as $k \to \infty$.

(v) $e^0(k)$ asymptotically converges to zero as $k \to \infty$.

(vi) Assuming that the external input $c(k)$ is sufficiently rich such that $\varphi(k-1)$ in (11) is persistently exciting, $\hat{\theta}^0(k)$ tends to the true parameters vector θ as $k \to \infty$. Then, $\hat{\theta}(k)$ tends to $\hat{\theta}^0(k)$ and $e(k) = \left(\theta - \hat{\theta}(k-1)\right)^T \varphi(k-1)$ tends to zero as $k \to \infty$. ***

Remark 3. The convergence of the estimated parameters to their true values in θ requires that $\varphi(k-1)$ is persistently exciting. In this context, $\varphi(k-1)$ is persistently exciting if there exists an integer ℓ such that $\rho_1 I_m > \sum_{k=k_0}^{k_0+\ell} \varphi(k-1)\varphi^T(k-1) > \rho_2 I_m$ where $\rho_1 > 0$, $\rho_2 > 0$ and $m = n + N^2 = n^2 + 3n + 1$ is the number of components of the regressor $\varphi(k-1)$. Such a condition may be ensured by chosing an external input sufficiently rich of order m, i.e. it consists of at least $m/2$ frequencies in the frequency domain (Ioannou & Sun, 1996). ***

4. Stability Analysis

The plant discretized model can be written as follows,

$$y(k) = \hat{y}(k) + e(k) = \hat{\theta}^T(k-1)\varphi(k-1) + e(k) = -\sum_{i=1}^{n} \hat{a}_i(k-1)y(k-i) + \sum_{i=1}^{n+1} \hat{b}_i(k-1)u(k-i) + e(k) \quad (18)$$

and the adaptive control law as,

$$\begin{aligned} u(k) = \frac{1}{\hat{b}_1(k)} \Bigg\{ & \sum_{i=1}^{n} \left(\hat{s}_1(k-1)\hat{a}_i(k-1) - \hat{s}_{i+1}(k-1)\right) y(k-i) - \sum_{i=1}^{n} \left(\hat{s}_1(k-1)\hat{b}_i(k-1) + \hat{b}_{i+1}(k-1)\right) u(k-i) \\ & - \hat{s}_1(k-1)\hat{b}_{n+1}(k-1)u(k-n-1) + \sum_{i=1}^{n+1} b_{m_i} c(k-i+1) \Bigg\} - \frac{\hat{s}_1(k)}{\hat{b}_1(k)} e(k) + \delta(k) \end{aligned} \quad (19)$$

where (12) has been used with $R(q)$ and $S(q)$ substituted, respectively, by time-varying polynomials $\hat{R}(z,k) = \hat{B}(z,k)$ and $\hat{S}(z,k)$, which is the solution of the equation (14) for the adaptive case, and,

$$\begin{aligned} \delta(k) = \frac{1}{\hat{b}_1(k)} \Bigg\{ & \sum_{i=1}^{n} \left[\left(\hat{s}_1(k) - \hat{s}_1(k-1)\right)\hat{a}_i(k-1) - \left(\hat{s}_{i+1}(k) - \hat{s}_{i+1}(k-1)\right) \right] y(k-i) \\ & - \sum_{i=1}^{n} \left[\left(\hat{s}_1(k) - \hat{s}_1(k-1)\right)\hat{b}_i(k-1) + \left(\hat{b}_{i+1}(k) - \hat{b}_{i+1}(k-1)\right) \right] u(k-i) \\ & - \left(\hat{s}_1(k) - \hat{s}_1(k-1)\right)\hat{b}_{n+1}(k-1)u(k-n-1) \Bigg\} \end{aligned} \quad (20)$$

By combining (18) and (19), the discrete-time closed-loop system can be written as:

$$x(k) = \Lambda(k-1)\, x(k-1) + \Psi_1 e(k) + \Psi_2 \vartheta(k) \tag{21}$$

where $\vartheta(k) = \dfrac{1}{\hat{b}_1(k)}\left(\sum_{i=1}^{n+1} b_{m_i} c(k-i+1) - \hat{s}_1(k)\, e(k)\right) + \delta(k)$ and,

$x(k-1) = [y(k-1)y(k-2)\cdots y(k-n)u(k-1)u(k-2)\cdots u(k-n-1)]$

$\psi_1 = [1\,0\cdots 0]^T \in \Re^{(2n+1)x1}$; $\psi_2 = \left[0\,0\cdots 0\underset{n+1}{\underset{\downarrow}{1}}0\cdots 0\right]^T \in \Re^{(2n+1)x1}$

$$\Lambda(k-1) = \begin{bmatrix} -\hat{a}_1(k-1) & -\hat{a}_2(k-1) & \cdots & -\hat{a}_{n-1}(k-1) & -\hat{a}_n(k-1) & \hat{b}_1(k-1) & \hat{b}_2(k-1) & \cdots & \hat{b}_n(k-1) & \hat{b}_{n+1}(k-1) \\ 1 & 0 & \cdots & 0 & 0 & 0 & 0 & \cdots & 0 & 0 \\ 0 & 1 & \cdots & \vdots & 0 & 0 & 0 & \cdots & 0 & 0 \\ \vdots & \vdots & \ddots & 0 & \vdots & \vdots & \vdots & \ddots & \vdots & \vdots \\ 0 & 0 & \cdots & 1 & 0 & 0 & 0 & \cdots & 0 & 0 \\ \dfrac{\hat{f}_1(k-1)}{\hat{b}_1(k)} & \dfrac{\hat{f}_1(k-1)}{\hat{b}_1(k)} & \cdots & \dfrac{\hat{f}_{n-1}(k-1)}{\hat{b}_1(k)} & \dfrac{\hat{f}_n(k-1)}{\hat{b}_1(k)} & \dfrac{\hat{h}_1(k-1)}{\hat{b}_1(k)} & \dfrac{\hat{h}_2(k-1)}{\hat{b}_1(k)} & \cdots & \dfrac{\hat{h}_n(k-1)}{\hat{b}_1(k)} & \dfrac{\hat{h}_{n+1}(k-1)}{\hat{b}_1(k)} \\ 0 & 0 & \cdots & 0 & 0 & 1 & 0 & \cdots & 0 & 0 \\ 0 & 0 & \cdots & 0 & 0 & 0 & 1 & \cdots & 0 & 0 \\ \vdots & \vdots & \ddots & \vdots & \vdots & \vdots & \vdots & \ddots & \vdots & \vdots \\ 0 & 0 & \cdots & 0 & 0 & 0 & 0 & \cdots & 1 & 0 \end{bmatrix} \tag{22}$$

with $\hat{f}_i(k-1) = \hat{s}_1(k-1)\hat{a}_i(k-1) - \hat{s}_{i+1}(k-1)$, $\hat{h}_i(k-1) = -\left(\hat{s}_i(k-1)\hat{b}_i(k-1) + \hat{b}_{i+1}(k-1)\right)$, for $i \in \{1, 2, \ldots, n\}$, and $\hat{h}_{n+1}(k-1) = -\hat{s}_1(k-1)\hat{b}_{n+1}(k-1)$.

Note that $\hat{a}_i(k-1)$ and $\hat{b}_i(k-1) = \sum_{j=1}^{N} \hat{b}_{i,j}(k-1)\hat{\alpha}_j(k-1)$ are uniformly bounded from Lemma 1 (properties ii and iii). Also, $\hat{b}_1(k) \neq 0$ since the adaptation of the multirate gains makes such a parameter fixed to a prefixed one which is suitably chosen and $\hat{s}_i(k-1)$ is uniformly bounded from the resolution of a equation being similar to that of (14) replacing polynomials $A(z)$ and $S(z)$ by time-varying polynomials $\hat{A}(z,k-1)$ and $\hat{S}(z,k-1)$, respectively.

The following theorem, whose proof is presented in Appendix B, establishes the main stability result of the adaptive control system.

Theorem 1. ***Main stability result.***

(i) The adaptive control law stabilizes the discrete-time plant model (6) in the sense that $\{u(k)\}$ and $\{y(k)\}$ are bounded for all finite initial states and any uniformly bounded reference input sequence $\{c(k)\}$ subject to Assumptions 1,

(ii) $\{y(k)\}$ converges to $\{y_m(k)\}$ as k tends to infinity, and

(iii) the continuous plant input and output signals, $u(t)$ and $y(t)$, are bounded for all t. ***

5. Simulations Results

Some simulation results which illustrate the effectiveness of the proposed method are shown in the current section. A continuous-time unstable plant of transfer function $G(s)=\frac{s-2}{(s-1)(s+3)}$ with an unstable zero, and whose internal representation is defined by the matrices $A=\begin{bmatrix}-3 & 0\\ 0 & 1\end{bmatrix}$, $B=\begin{bmatrix}1 & 1\end{bmatrix}^T$ and $C=\begin{bmatrix}1.25 & -0.25\end{bmatrix}$, is considered. A suitable multirate scheme with fast input sampling through a FROH device is used to place the zeros of the discretized plant within the stability region and a discrete-time controller is synthesized so that the discrete-time closed-loop system matches a reference model. The results for the case of known plant parameters are presented in a first example and then two more examples with the described adaptive control strategies are considered. The difference among such adaptive control strategies relies on the way of updating the multirate gains for ensuring the stability of the estimated discretized plant zeros.

5.1. Known Plant Parameters

The discretization of the continuous-time plant with a multirate, $N=3$, and a FROH device with $\beta=0.7$ for a slow sampling time $T=0.3$ is performed leading to the discrete transfer function $H(z)=\frac{B(z)}{A(z)}=\frac{b_1(g)z^2+b_2(g)z+b_3(g)}{z(z^2-1.7564z+0.5488)}$ where $b_1(g)=0.0307\alpha_1+0.0693\alpha_2+0.13\alpha_3$, $b_2(g)=-(0.0788\alpha_1+0.1488\alpha_2+0.2631\alpha_3)$ and $b_3(g)=0.0083\alpha_1+0.0343\alpha_2+0.0797\alpha_3$ are the coefficients of the transfer function numerator of the discretized model. Such coefficients depend on the multirate gains α_i, for $i\in\{1,\ 2,\ 3\}$, included as components in the vector g. The zeros of such a discretized plant can be fixed within the stability domain via a suitable choice of the multirate gains. In this example such gains are $\alpha_1=-621.8706$, $\alpha_2=848.4241$ and $\alpha_3=-297.4867$ so that $B(z)=B'(z)=z^2+z+0.25$ and then both zeros are placed at $z_0=-0.5$. The control objective is the matching of the reference model defined by the transfer function $G_m(z)=\frac{z^2+z-0.272}{(z+0.2)^3}$. For such a purpose, the controller has to cancel the discretized plant zeros, which are stable, and add those of the reference model to the discrete-time closed-loop system. The values of the control parameters to meet such an objective are $s_1=2.3564$, $s_2=-0.4288$ and $s_3=0.008$. A unitary step is considered as external input signal. Figure 1 displays the time evolution of the closed-loop system output, its values at the slow sampling instants and the sequence of the discrete-time reference model output. Figure 2 shows the plant input signal. Note that perfect model matching is achieved, at the slow sampling instants, without any constraints in the choice of the zeros of the reference model $G_m(z)$, in spite of the continuous-time plant possesses an unstable zero. Furthermore, the continuous-time output and input signals are maintained bounded for all time.

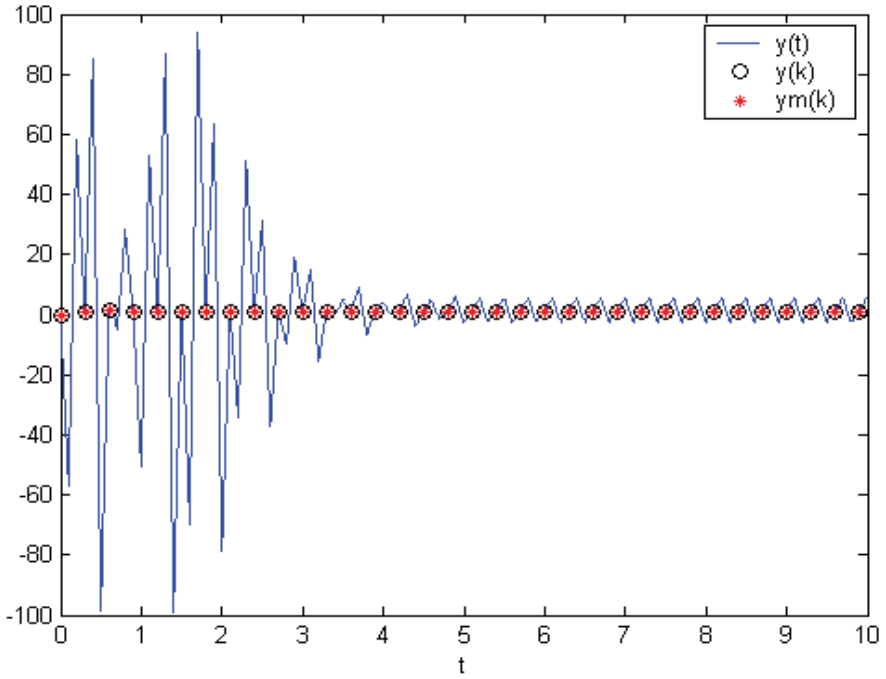

Fig. 1. Plant and reference model output signals

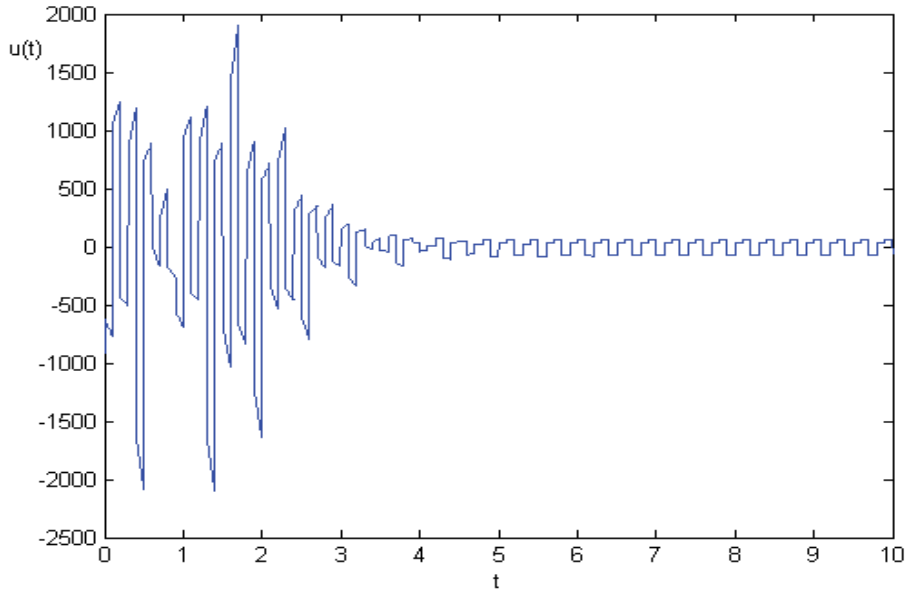

Fig. 2. Plant input signal

5.2. Unknown Plant Parameters

An adaptive version of the discrete-time controller designed in the previous example is considered with the parameters estimation algorithm being initialized with $\hat{\theta}^0(0) = 10^{-2} \times \left[263.46 \quad -82.32 \quad 4.61 \quad 10.39 \quad 19.51 \quad -11.82 \quad -22.33 \quad -39.46 \quad 1.25 \quad 5.15 \quad 11.95\right]^T$ and $P(0) = 1000 \cdot I_{11}$. Furthermore, the values $\delta = \delta_0 = 10^{-6}$ are chosen for the modification algorithm included in such an estimation process. Two different methods are considered to update the multirate gains. The first one consists of updating such gains at all the slow sampling instants so that the discretized zeros are maintained constant within the stability domain (Algorithm 1). The second one consists of changing the value of the multirate gains only when at least one of the discretized zeros, which are time-varying, is going out of the stability domain. Otherwise, the values for the multirate gains are maintained equal to those of the previous slow sampling instant (Algorithm 2).

5.2.1. Algorithm 1: Discretized plant zeros are maintained constant

Figure 3 displays the time evolution of the closed-loop adaptive control system output, its values at the slow sampling instants and the sequence of the discrete-time reference model output under a unitary step as external input signal. Note that the discrete-time model matching is reached after a transient time interval. Figures 4 and 5 show, respectively, the plant output signal and the input signal generated from the multirate with the FROH applied to the control sequence $\{u(k)\}$. It can be observed that both signals are bounded for all time. Finally, Figures 6 and 7 display, respectively, the time evolution of the multirate gains and the adaptive controller parameters. Note that the multirate gains and the adaptive control parameters are time-varying until they converge to constant values.

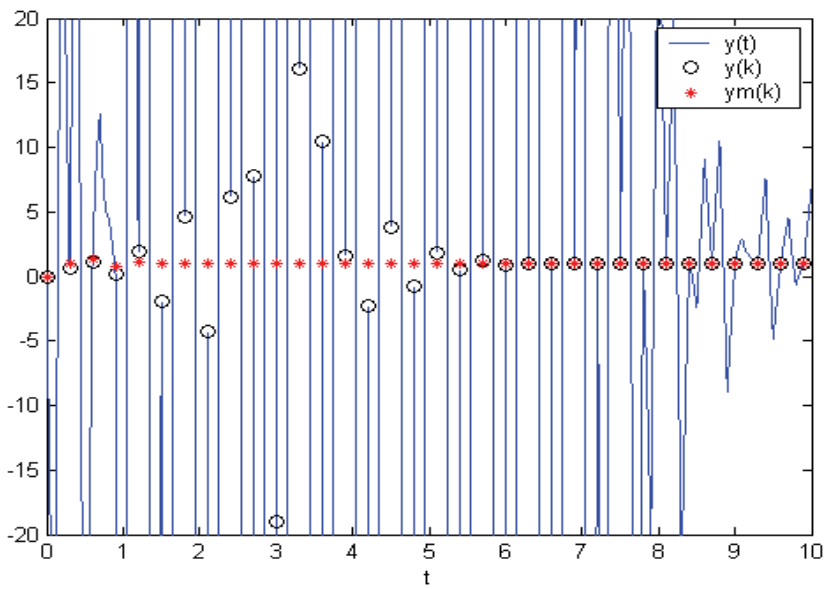

Fig. 3. Plant and reference model output signals

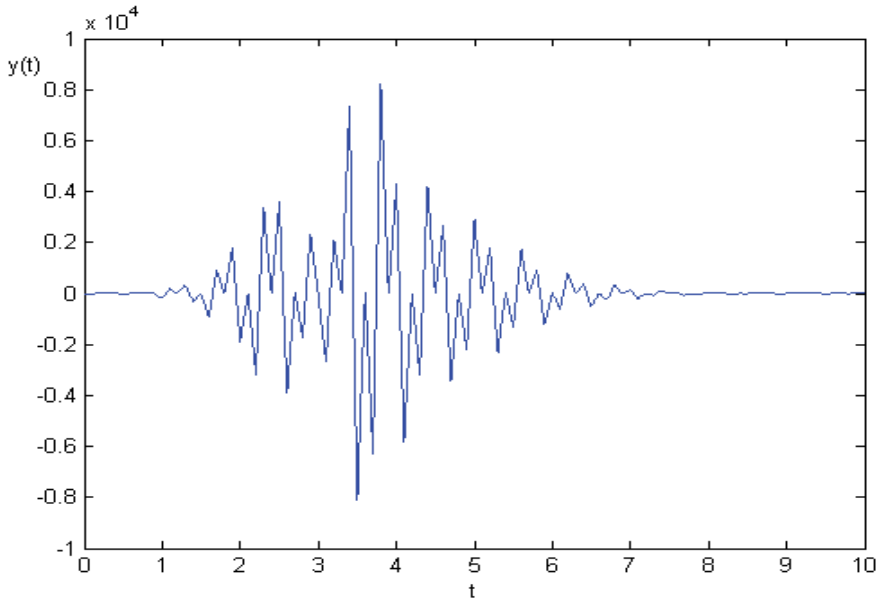

Fig. 4. Plant output signal

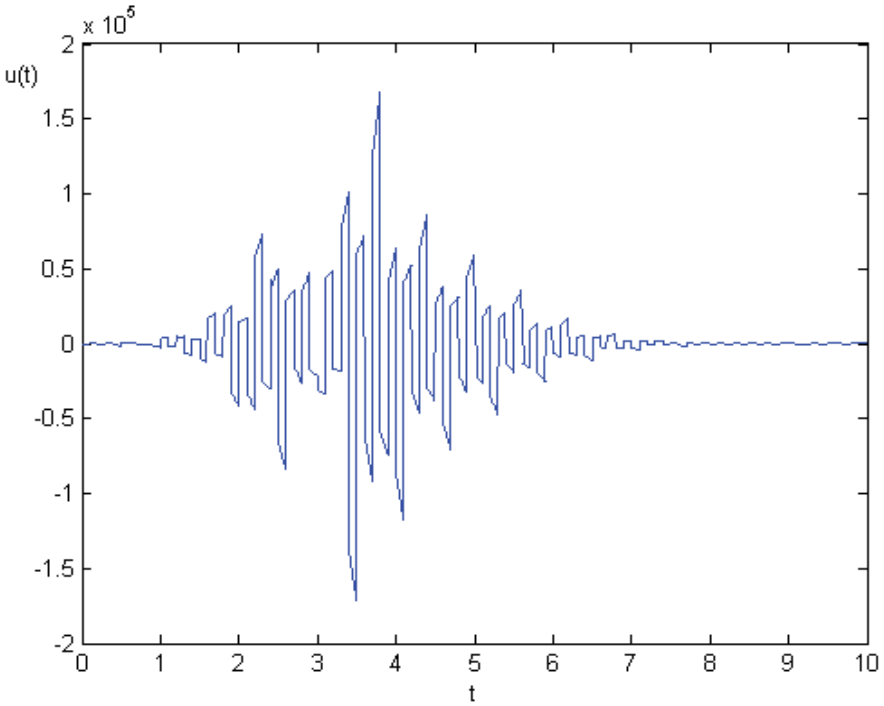

Fig. 5. Plant input signal

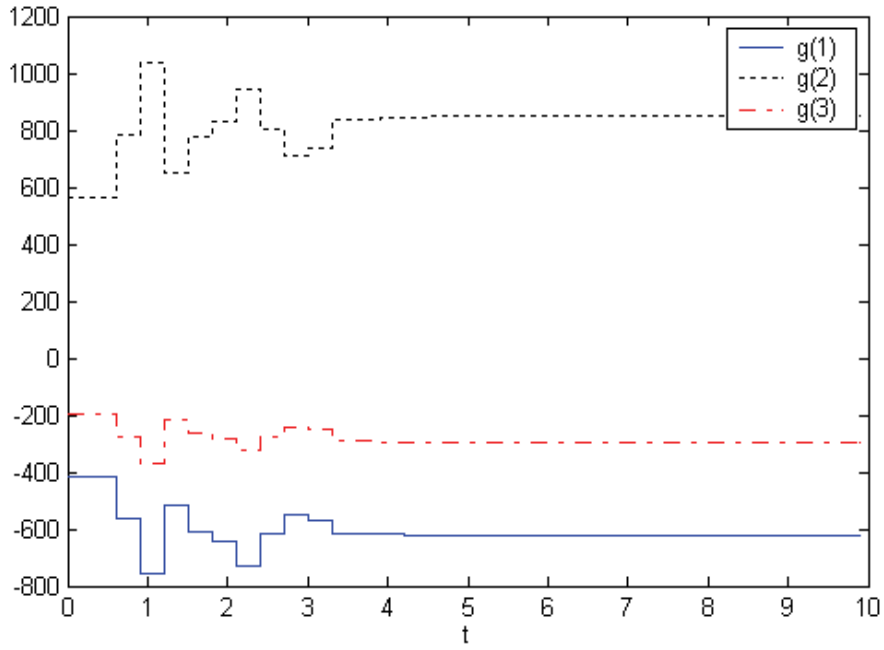

Fig. 6. Multirate gains

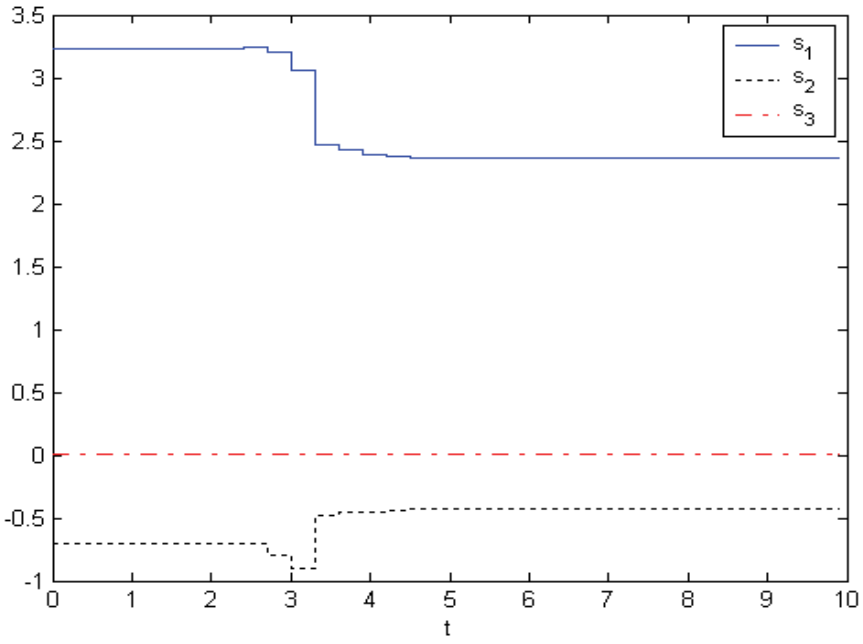

Fig. 7. Adaptive control parameters

5.2.2. Algorithm 2: Discretized plant zeros are time-varying

The multirate gains are maintained constant to their values at the previous slow sampling instant until at least one of the discretized plant zeros is going out of the stability domain. In this sense, note that the discretized zeros vary when the values of the multirate gains are maintained constant and eventually they can go out of the stability domain. When this happens such gains are again calculated to place both discretized zeros at $z_0 = -0.5$. The discrete-time model matching is reached after a transient time interval and the continuous-time plant output and input signals are bounded for all time as it can be observed from Figures 8, 9 and 10 where the response to a unitary step is shown. The maximum values reached by both continuous-time output and input signals are larger than those obtained with the previous method (Algorithm 1) for updating the multirate gains. Figures 11 and 12 display, respectively, the evolution of the multirate gains and the controller parameters. The adaptive control parameters are time-varying until they converge to constant values while the multirate gains are piecewise constant and also they converge to constant values. Note that this second method ensures a small number of changes in the values of the multirate gains compared with the first method since such gains only vary when it is necessary to maintain the zeros within the stability domain. This fact gives place to a less computational effort to generate the control law than that required with the first method. However, the behaviour of the continuous-time plant output and input signals is worse with the use of this second alternative in this particular example. Finally, the evolution of the modules of the discretized plant zeros and the coefficients of the time-varying numerator of such an estimated model are, respectively, shown in Figures 13 and 14.

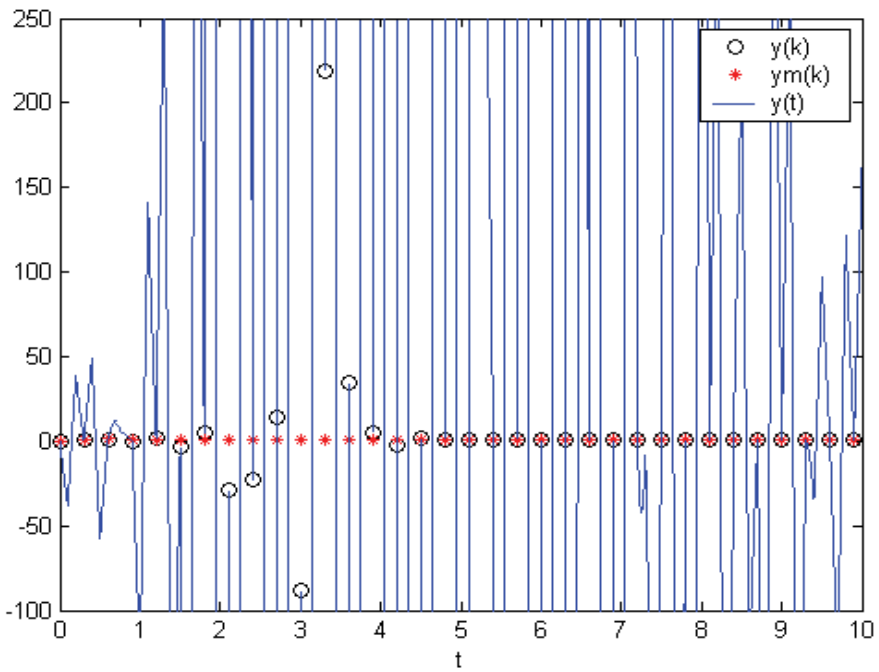

Fig. 8. Plant and reference model output signals

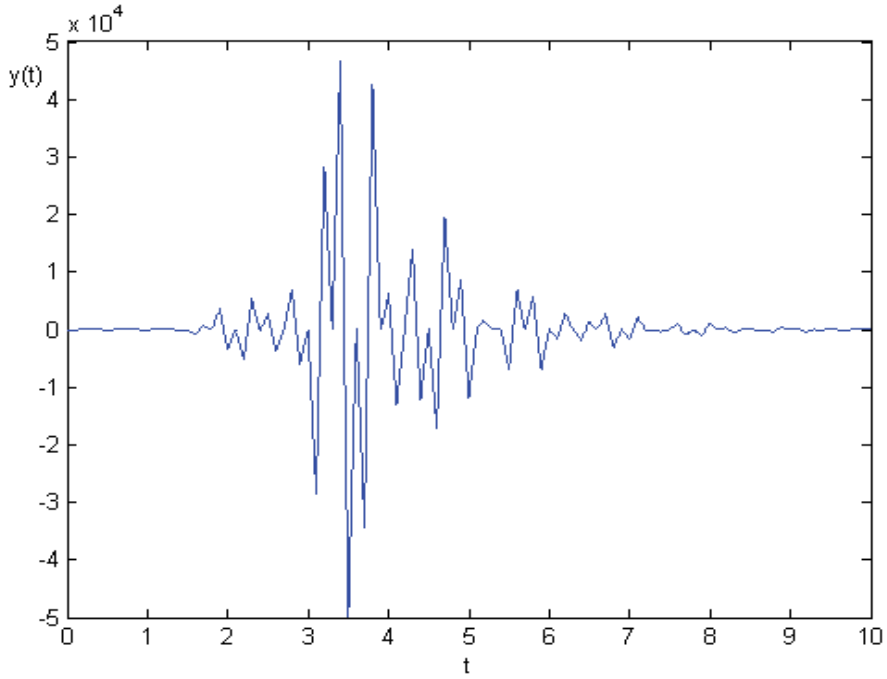

Fig. 9. Plant output signal

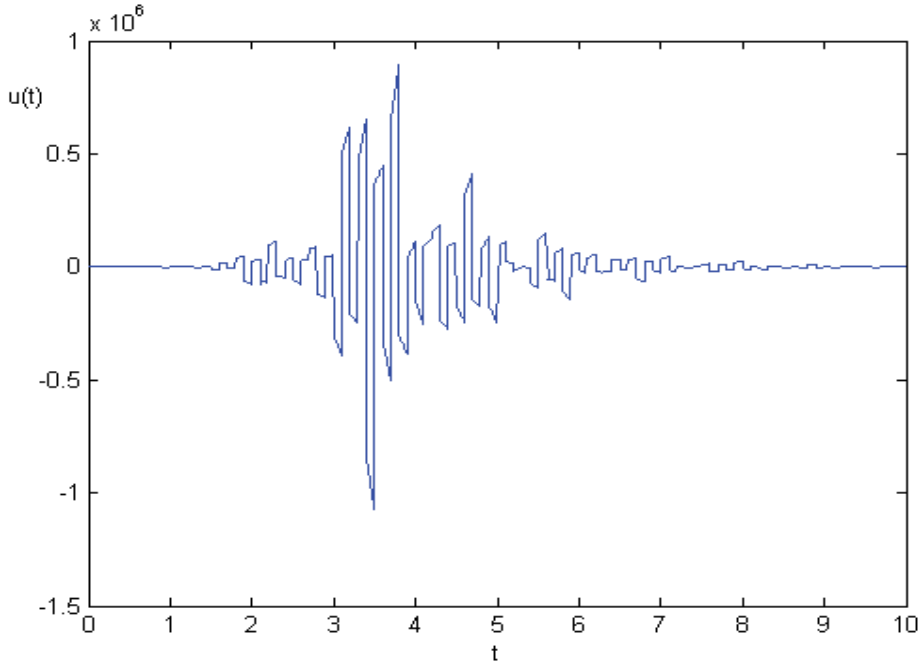

Fig. 10. Plant input signal

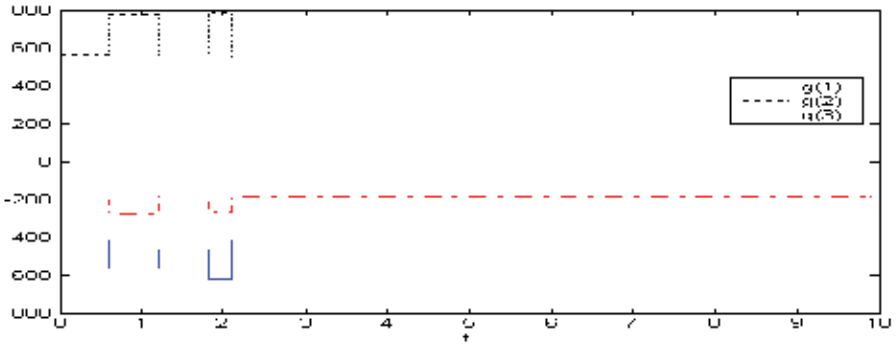

Fig. 11. Multirate gains

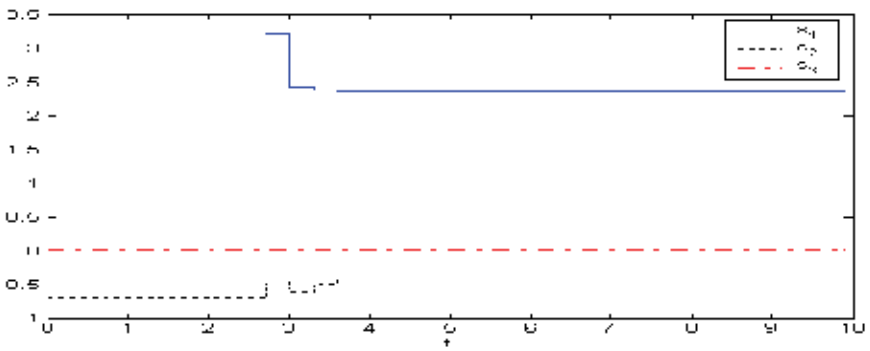

Fig. 12. Adaptive control parameters

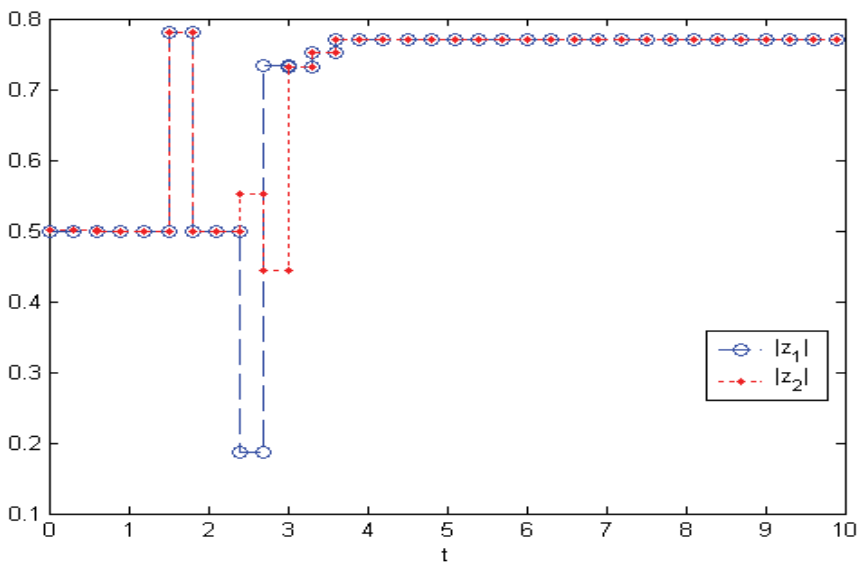

Fig. 13. Modules of the estimated discretized plant zeros

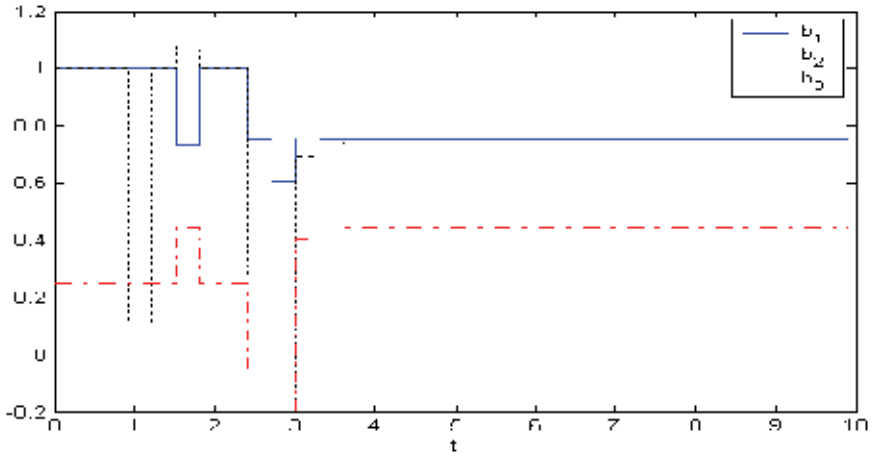

Fig. 14. Coefficients of the estimated discretized plant numerator

6. Conclusion

This paper deals with the stabilization of an unstable and possibly non-inversely stable continuous-time plant. The mechanism used to fulfill the stabilization objective consists of two steps. The first one is the discretization of the continuous-time plant by using a FROH device combined with a multirate input in order to obtain an inversely stable discretized model of the plant. Then, a discrete-time controller is designed to match a discrete-time reference model by such a discretized plant. There is not any restriction in the choice of the reference model since the zeros of the discretized plant model are guaranteed to be stable by the fast sampled input generated by the multirate sampling device.

An adaptive version of such a controller constitutes the main contribution of the present manuscript. The model matching between the discretized plant and the discrete-time reference model is asymptotically reached in the adaptive case of unknown plant. Also, the boundedness of the continuous-time plant input and output signals are ensured, as it is illustrated by means of some simulation examples. In this context, the behaviour of the designed adaptive control system in the inter-samples period may be improved. In this sense, an improvement in such a behaviour has been already reached with a multi-estimation scheme where several discretization/estimation processes, each one with its proper FROH and multirate device, are working in parallel providing different discretized plant estimated models (Alonso-Quesada & De la Sen, 2007). Such a scheme is completed with a supervisory system which activates one of the discretization/estimation processes. Such a process optimizes a performance index related with the inter-sample behaviour. In this sense, each of the discretization/estimation processes gives a measure of its quality by means of such an index which may measure the size of the tracking-error and/or the size of the plant input for the inter-sample period. The supervisor switches on-line from the current process to a new one when the last is better than the former, i.e. the performance index of the new process is smaller than that of the current one. Moreover, the supervisor has to guarantee a minimum residence time between two consecutive switches in order to ensure the stability of the adaptive control system.

7. Appendix A. Proof of Lemma 1

(i) $P(k)$ is a monotonic non-increasing matrix sequence since $P(k)-P(k-1)\le 0$ for all integer $k>0$ from (16). Moreover, if $P(k_1)=0$ for any integer $k_1>0$ then $P(k_1+1)-P(k_1)=0$ from (16) and then $P(k)=0$ for all integer $k\ge k_1$. Thus, $0\le P(k)\le P(0)$ and $P(k)$ asymptotically converges to a finite limit as $k\to\infty$.

(ii) By considering the non-negative sequence $V(k)=\tilde{\theta}^{0T}(k)P^{-1}(k)\tilde{\theta}^{0}(k)$ and applying the matrix inversion lemma (Goodwin & Sin, 1984) to (16) it follows that,

$$V(k)-V(k-1)=-\frac{\left(e^{0}(k)\right)^2}{1+\varphi^{T}(k-1)P(k-1)\varphi(k-1)}\le 0 \tag{23}$$

where (16) and the definition of the estimation error have been used. Then, $V(k)\le V(0)$ and $\left\|\tilde{\theta}^{0}(k)\right\|\le\frac{\lambda_{max}\{P(0)\}}{\lambda_{min}\{P(0)\}}\left\|\tilde{\theta}^{0}(0)\right\|<\infty$ where $\lambda_{max}\{P(0)\}$ and $\lambda_{min}\{P(0)\}$ denote the maximum and the minimum eigenvalues of $P(0)$, respectively. It implies that $\tilde{\theta}^{0}(k)$, and then also $\hat{\theta}^{0}(k)$, is uniformly bounded. Then, $\hat{\theta}(k)$ is also bounded since the modification algorithm guarantees the boundedness of $\hat{M}(k)$ provided that $\hat{\theta}^{0}(k)$ is bounded. On other hand, $V(k)$ asymptotically converges to a finite limit as $k\to\infty$ from its definition and the fact that such a sequence is non-negative and monotonic non-increasing. Then, $\tilde{\theta}^{0}(k)$, and also $\hat{\theta}^{0}(k)$, converges to a finite limit as $k\to\infty$ since $P(k)$ also converges as it has been proved in (i). Then, $\hat{M}(k)$ and $\hat{\theta}(k)$ also converge to finite limits as $k\to\infty$.

(iii) The boundedness and convergence of the estimation model parameters vector together with the non-singularity of the matrix $\hat{M}(k)$, guaranteed by the modification algorithm, implies the boundedness and convergence of the vector $\hat{g}(k)$ obtained by resolution of equation (17).

(iv) It follows that $\sum_{i=1}^{k}\frac{\left(e^{0}(i)\right)^2}{1+\varphi^{T}(i-1)P(i-1)\varphi(i-1)}=V(0)-V(k)\le V(0)<\infty$ from (23), then $\frac{\left(e^{0}(k)\right)^2}{1+\varphi^{T}(k-1)P(k-1)\varphi(k-1)}$ is uniformly bounded and it converges to zero as $k\to\infty$.

(v) It follows that $\lim_{k\to\infty}\left\{e^{0}(k)\right\}=0$ irrespective of the boundedness of $\varphi(k-1)$ from the fact that $\lim_{k\to\infty}\left\{\frac{\left(e^{0}(k)\right)^2}{1+\varphi^{T}(k-1)P(k-1)\varphi(k-1)}\right\}=0$. On one hand, if $\varphi(k-1)$ is bounded then

$\lim_{k\to\infty}\left\{\frac{\left(e^0(k)\right)^2}{1+\varphi^T(k-1)P(k-1)\varphi(k-1)}\right\}=0$ implies directly that $\lim_{k\to\infty}\left\{e^0(k)\right\}=0$. On the other hand, if $\varphi(k-1)$ is unbounded then $\lim_{k\to\infty}\left\{\frac{\left(e^0(k)\right)^2}{1+\varphi^T(k-1)P(k-1)\varphi(k-1)}\right\}=0$ implies that $\lim_{k\to\infty}\left\{\frac{\left\|\tilde{\theta}^0(k-1)\right\|^2}{\left\|P(k-1)\right\|^2}\right\}=0$ since $e^0(k)=\tilde{\theta}^{0T}(k-1)\varphi(k-1)$ and then $\lim_{k\to\infty}\left\{\left\|\tilde{\theta}^0(k-1)\right\|^2\right\}=0$ from the fact that $P(k)$ is uniformly bounded. Thus, $\lim_{k\to\infty}\left\{e^0(k)\right\}=0$.

(vi) Provided that the external input sequence $\{c(k)\}$ is sufficiently rich such that $\varphi(k-1)$ is persistently exciting, $\hat{\theta}^0(k)$ tends to the true parameters vector θ as $k\to\infty$ (Goodwin & Sin, 1984). Then, $\hat{M}(k)$ tends to $\hat{M}^0(k)$ from the modification algorithm and, consequently, $\hat{\theta}(k)$ tends to $\hat{\theta}^0(k)$ and $e(k)$ tends to zero as $k\to\infty$. ***

8. Appendix B. Proof of Theorem 1

(i) $\Lambda(k)$ is bounded since the estimation model parameters $\hat{a}_i(k)$ and $\hat{b}_j(k)$, and the controller parameters $\hat{s}_j(k)$, for $i\in\{1, 2, \ldots, n\}$ and $j\in\{1, 2, \ldots, n+1\}$, are bounded thanks to the estimated parameters vector $\hat{\theta}(k)$ and the multirate gains vector $\hat{g}(k)$ are bounded for all integer $k\geq 0$. The eigenvalues of $\Lambda(k)$ are in $|z|<1$ since they are the roots of $A_m(z)$ and $A_s(z)$, due to the designed control law, and the roots of $\hat{B}(z,k)$ which are within the unit circle due to the suitable adaptation of the multirate gains. Besides,

$$\sum_{k'=k_0+1}^{k}\left\|\Lambda(k')-\Lambda(k'-1)\right\|^2\leq\gamma_0+\gamma_1(k-k_0) \tag{24}$$

for all integers k and k_0 such that $k>k_0\geq 0$, and some sufficiently small positive real constants γ_0 and γ_1 (Bilbao-Guillerna et al., 2005). Note that (24) is fulfilled with a slow enough estimation rate via a suitable choice of $P(0)$ in (16) so that γ_1 is sufficiently small. Thus, the time-varying homogeneous system $x(k)=\Lambda(k-1)\,x(k-1)$ is exponentially stable and its transition matrix $\phi(k,k')=\prod_{j=k'}^{k-1}\Lambda(j)$ satisfies $\left\|\phi(k,k')\right\|\leq\rho_1\sigma_0^{k-k'}$ for all $k\geq k'$ where $\sigma_0\in(0,1)$ and ρ_1 is a non-dependent constant (Alonso-Quesada & De la Sen, 2004). It follows from (21) that:

$$x(k) = \phi(k,k_0)\, x(k_0) + \sum_{k'=k_0}^{k} \phi(k,k')\left(\Psi_1 e(k') + \Psi_2 \vartheta(k')\right) \tag{25}$$

for all integer $k \geq k_0 \geq 0$. Then,

$$\|x(k)\| = \rho_1 \sigma_0^{k-k_0} \|x(k_0)\| + \sum_{k'=k_0}^{k} \rho_1 \sigma_0^{k-k'} \left(\rho_2 + \rho_3 |e(k')| + \rho_4 |\delta(k')|\right) \tag{26}$$

for some positive real constants ρ_2, ρ_3 and ρ_4, provided that the input reference sequence $\{c(k)\}$ is bounded. It follows that $\lim_{k\to\infty} |\hat{a}_i(k) - \hat{a}_i(k-1)| = 0$ and $\lim_{k\to\infty} |\hat{b}_j(k) - \hat{b}_j(k-1)| = 0$ for all $i \in \{1, 2, \ldots, n\}$ and $j \in \{1, 2, \ldots, n+1\}$ from the convergence property of the estimation algorithm. Then, $\lim_{k\to\infty} |\hat{s}_i(k) - \hat{s}_i(k-1)| = 0$ as it follows from the adaptive control resolution. Consequently, $\lim_{k\to\infty} |\delta(k)| = 0$. Besides, $\lim_{k\to\infty} |e(k)| = 0$ from the estimation algorithm. Then, $x(k)$ is bounded from (26), which implies that sequences $\{u(k)\}$ and $\{y(k)\}$ are also bounded.

(ii) On one hand, the adaptive control law ensures that the estimated sequence $\{\hat{y}(k)\}$ matches the reference model one $\{y_m(k)\}$ for all integer $k \geq 0$. On the other hand, the estimation algorithm guarantees the asymptotic convergence of the estimation error $e(k)$ to zero. Then, the output sequence $\{y(k)\}$ tends to $\{y_m(k)\}$ asymptotically as $k \to \infty$.

(iii) The adaptive control algorithm ensures that there is no finite escapes. Then, the boundedness of the sequences $\{u(k)\}$ and $\{y(k)\}$ implies that the plant input and output continuous-time signals $u(t)$ and $y(t)$ are bounded for all t.

9. Acknowledgment

The authors are very grateful to MCYT by its partial support through grants DPI 2003-0164 and DPI2006-00714.

10. References

Alonso-Quesada, S. & De la Sen, M. (2004). Robust adaptive control of discrete nominally stabilizable plants. *Appl. Math. Comput.*, Vol. 150, pp. 555-583.

Alonso-Quesada, S. & De la Sen, M. (2007). A discrete multi-estimation adaptive control scheme for stabilizing non-inversely stable continuous-time plants using fractional holds, *Proceedings of 46th IEEE Conference on Decision and Control,* pp. 1320-1325, ISBN: 1-4244-1498-9, New Orleans, LA, USA, December 2007, Publisher: Omnipress.

Arvanitis, K. G. (1999). An algorithm for adaptive pole placement control of linear systems based on generalized sampled-data hold functions. *J. Franklin Inst.,* Vol. 336, pp. 503-521.

Aström, K. J. & Wittenmark, B. (1997). *Computer Controlled Systems: Theory and Design*, Prentice-Hall Inc., ISBN: 0-13-736787-2, New Jersey.

Bárcena, R., De la Sen, M. and Sagastabeitia, I. (2000). Improving two stability properties of the zeros of sampled systems with fractional order hold, *IEE Proceedings - Control Theory and Applications*, Vol. 147, No. 4, pp. 456-464.

Bilbao-Guillerna, A., De la Sen, M., Ibeas, A. and Alonso-Quesada, S. (2005). Robustly stable multiestimation scheme for adaptive control and identification with model reduction issues. *Discrete Dynamics in Nature and Society*, Vol. 2005, No. 1, pp. 31-67.

Blachuta, M. J. (1999). On approximate pulse transfer functions. *IEEE Transactions on Automatic Control*, Vol. 44, No. 11, pp. 2062-2067.

De la Sen, M & Alonso-Quesada, S. (2007). Model matching via multirate sampling with fast sampled input guaranteeing the stability of the plant zeros. Extensions to adaptive control. *IET Control Theory Appl.,* Vol. 1, No. 1, pp. 210-225.

Goodwin, G. C. & Sin, K. S. (1984). *Adaptive Filtering, Prediction and Control*, Prentice-Hall Inc., ISBN: 0-13-004069-X, New Jersey.

Goodwin, G. C. & Mayne, D. Q. (1987). A parameter estimation perspective of continuous-time model reference adaptive control. *Automatica*, Vol. 23, No. 1, pp. 57-70.

Ioannou, P. A. & Sun, J. (1996). *Robust Adaptive Control*, Prentice-Hall Inc., ISBN: 0-13-439100-4, New Jersey.

Liang, S., Ishitobi M. & Zhu, Q. (2003). Improvement of stability of zeros in discrete-time multivariable systems using fractional-order hold, *International Journal of Control,* Vol. 76, No. 17, pp. 1699-1711.

Liang, S. & Ishitobi, M. (2004). Properties of zeros of discretised system using multirate input and hold, *IEE Proc. – Contr. Theory Appl.,* Vol. 151, No. 2, pp. 180-184.

Narendra, K. S. & Annaswamy, A. M. (1989). *Stable Adaptive Systems*, Prentice-Hall Inc., ISBN: 0-13-840034-2, New Jersey.

6

Hybrid Schemes for Adaptive Control Strategies

Ricardo Ribeiro & Kurios Queiroz
Federal University of Rio Grande do Norte
Brazil

1. Introduction

The purpose of this chapter is to redesign the standard adaptive control schemes by using hybrid structure composed by Model Reference Adaptive Control (MRAC) or Adaptive Pole Placement Control (APPC) strategies, associated to Variable Structure (VS) schemes for achieving non-standard robust adaptive control strategies. The both control strategies is now on named VS-MRAC and VS-APPC. We start with the theoretical base of standard control strategies APPC and MRAC, discussing their structures, as how their parameters are identified by adaptive observers and their robustness properties for guaranteeing their stability. After that, we introduce the sliding mode control (variable structure) in each control scheme for simplifying their design procedure. These design procedure are based on stability analysis of each hybrid robust control scheme. With the definition of both hybrid control strategies, it is analyzed their behavior when controlling system plants with unmodeled disturbances and parameter variation. It is established how the adaptive laws compensates these unmodeled dynamics. Furthermore, by using simple systems examples it is realized a comparison study between the hybrid structures VS-APPC and VSMRAC and the standard schemes APPC and MRAC. As the hybrid structures use switching laws due to the sliding mode scheme, the effect of chattering is analyzed on the implementation and consequently effects on the digital control hardware where sampling times are limiting factor. For reducing these drawbacks it is also discussed possibilities which kind of modifications can employ. Finally, some practical considerations are discussed on an implementation on motor drive systems.

2. Variable Structure Model Reference Adaptive Controller (VS-MRAC)

The *VS-MRAC* was originally proposed in (Hsu *et al.*, 1989) and extensively discussed in (Hsu *et al.*, 1994). The main features of this control scheme are the robustness of parameters uncertainties and unmodeled disturbances, as well as good transitory response.
Consider the following first order plant

$$W(s) = \frac{y}{u} = \frac{b_p}{s + a_p} \ , \tag{1}$$

where b_p and a_p are unknown or known with limited uncertainties. Admitting a reference model given by

$$M(s) = \frac{y_m}{r} = \frac{b_m}{s + a_m}, \tag{2}$$

in which $k_m > 0$ and $a_m > 0$, the following output error variable can be defined as

$$e_0 = y - y_m . \tag{3}$$

The control objective is to force $y(t)$ to asymptotically track the reference output signal, $y_m(t)$, by regulating e_0 to be zero, while keeping all the closed-loop signals uniformly bounded. The control law used for accomplished this is

$$u = \theta_1 y + \theta_2 r , \tag{4}$$

which is the same as used in traditional model reference adaptive control. However, instead of the integral adaptive laws for the controller parameters, switching laws are proposed in order to improve the system transient performance and its robustness.

If b_p and a_p are known, the ideal controller parameters (θ_1^* and θ_2^*) can be founded using the following condition

$$\frac{y}{r} = \frac{y_m}{r} , \tag{5}$$

which means that our control objective is achieved, i.e., the closed-loop system behaves like the open-loop reference model. Consequently, the control law equation can be rewritten as

$$u = \theta_1^* y + \theta_2^* r . \tag{6}$$

Analyzing (1) and (2) in the time domain, we get

$$\dot{y} = -a_p y + k_p u , \tag{7}$$

$$\dot{y}_m = -a_m y_m + k_m r . \tag{8}$$

Adding and subtracting terms related to the ideal control parameters in (4),

$$u = \theta_1 y + \theta_2 r - \theta_1^* y - \theta_2^* r + \theta_1^* y + \theta_2^* r , \tag{9}$$

and then grouping some terms

$$u = (\theta_1 - \theta_1^*)y + (\theta_2 - \theta_2^*)r + \theta_1^* y + \theta_2^* r\,, \tag{10}$$

we have

$$u = \tilde{\theta}_1 y + \tilde{\theta}_2 r + \theta_1^* y + \theta_2^* r\,, \tag{11}$$

in which terms $\tilde{\theta}_1$ and $\tilde{\theta}_2$ are deviations of ideal controller parameters θ_1 and θ_2. Substituting the resulting equation (11) in (7),

$$\dot{y} = -a_p y + b_p(\tilde{\theta}_1 y + \tilde{\theta}_2 r + \theta_1^* y + \theta_2^* r)\,, \tag{12}$$

we can rewrite this equation as

$$\dot{y} = -a_p y + b_p \theta_1^* y + b_p \theta_2^* r + b_p(\tilde{\theta}_1 y + \tilde{\theta}_2 r)\,, \tag{13}$$

which results in

$$\dot{y} = -(a_p - b_p \theta_1^*)y + b_p \theta_2^* r + b_p(\tilde{\theta}_1 y + \tilde{\theta}_2 r)\,. \tag{14}$$

From (6), the model input r can be defined as

$$r = \frac{u - \theta_1^* y}{\theta_2^*}\,. \tag{15}$$

Therefore, using (11) and (15) in (8), we get

$$\dot{y}_m = -a_m y + b_m r + \frac{b_m}{\theta_2^*}(\tilde{\theta}_1 y + \tilde{\theta}_2 r)\,. \tag{16}$$

Finally, comparing (14) and (16) due to the condition (5), we have the desired controller parameters

$$\theta_1^* = \frac{a_p - a_m}{b_p}\,, \tag{17}$$

$$\theta_2^* = \frac{b_m}{b_p}. \tag{18}$$

The above desired controller parameters assure that plant output converges to its reference model, because b_p and a_p are known. This design criteria is named as *The Matching Conditions*.
However, our interests are concerned with unknown plant parameters or with known plant parameters with uncertainties, which require the use of adaptive laws for adjusting controller parameters. Derivating the output error equation given in (3),

$$\dot{e}_0 = \dot{y} - \dot{y}_m \tag{19}$$

and using the condition (5), with equations (8), (16) and (19), we get

$$\dot{e}_0 = -a_m y + b_m r + \frac{b_m}{\theta_2^*}(\tilde{\theta}_1 y + \tilde{\theta}_2 r) - (-a_m y_m + b_m r), \tag{20}$$

which can be rearranged as

$$\dot{e}_0 = -a_m (y - y_m) + \frac{b_m}{\theta_2^*}(\tilde{\theta}_1 y + \tilde{\theta}_2 r). \tag{21}$$

Thus,

$$\dot{e}_0 = -a_m e_0 + \frac{b_m}{\theta_2^*}(\tilde{\theta}_1 y + \tilde{\theta}_2 r). \tag{22}$$

Now, consider the Lyapunov function candidate given by

$$V(e_0) = \frac{1}{2} e_0^2 > 0, \tag{23}$$

and its respective first time derivative

$$\dot{V}(e_0) = e_0 \dot{e}_0. \tag{24}$$

By substituting (22) in (24), we obtain the following equation

$$\dot{V}(e_0) = \left[-a_m e_0 + \frac{b_m}{\theta_2^*}(\tilde{\theta}_1 y + \tilde{\theta}_2 r) \right] e_0 \ , \tag{25}$$

that can be rewritten as

$$\dot{V}(e_0) = -a_m e_0^2 + \frac{b_m}{\theta_2^*}\left[\left(\theta_1 - \theta_1^* \right) e_0 y + \left(\theta_2 - \theta_2^* \right) e_0 r \right]. \tag{26}$$

Using the switching laws,

$$\theta_1 = -\overline{\theta}_1 sgn(e_0 y) \, , \tag{27}$$

$$\theta_2 = -\overline{\theta}_2 sgn(e_0 r) \, , \tag{28}$$

we obtain,

$$\dot{V}(e_0) = -a_m e_0^2 - \frac{b_m}{\theta_2^*}\left[\left(\overline{\theta}_1 \mid e_0 y \mid + \theta_1^* e_0 y \right) + \left(\theta_2 \mid e_0 r \mid + \theta_2^* e_0 r \right) \right]. \tag{29}$$

If the conditions $\overline{\theta}_1 > \mid \theta_1^* \mid$ and $\overline{\theta}_2 > \mid \theta_2^* \mid$ are satisfied, the terms with indefinite signals in (29) are dominated, and then

$$\dot{V}(e_0) \leq -a_m e_0^2 < 0 \tag{30}$$

which guarantees that $e_0 = 0$ is a globally asymptotically stable (GAS) equilibrium point, because (30) is a negative definite function.

3. Variable Structure Adaptive Pole Placement Control (VS-APPC)

As the VS-MRAC, the VS-APPC is the hybrid control structure obtained from the association of Pole Placement Control (PPC) together with Variable Structure (VS). Therefore, the theoretical development of this section starts from PPC control scheme and then we introduce the VS concepts for achieving the proposed VS-APPC.
Considering the single input/single output (SISO) LTI plant

$$y = G(s)u \, , \tag{31}$$

in which

$$G(s) = \frac{Z(s)}{R(s)} = \frac{b_{n-1}s^{n-1} + ... + b_1 s + b_0}{s^n + a_{n-1}s^{n-1} + ... + a_1 s + a_0}\,, \tag{32}$$

there are, as plant parameters, 2*n* elements, which are the coefficients of the numerator and denominator of transfer function $G(s)$. We can define the vector θ^* as

$$\theta^* = \begin{bmatrix} b_{n-1} & . & . & . & b_1 & b_0 & a_{n-1} & . & . & . & a_1 & a_0 \end{bmatrix}^T. \tag{33}$$

From this, the following constraints must be observed:

S1. $R(s)$ is a monic polynomial whose degree n is known.

S2. $Z(s)$, $R(s)$ are coprime and degree$(Z) < n$.

Assumptions (S1) and (S2) allow $Z(s)$, $R(s)$ to be non-Hurwitz in contrast to the MRC (Model Reference Control) case, where $Z(s)$ is required to be Hurwitz.

We can also extend the PPC scheme for including the tracking objective, where output y is required to follow a certain class of reference signals r, by using the internal model principle (Ioannou & Sun, 1996). The uniformly bounded reference signal is assumed to satisfy

$$Q_m(s)r = 0\,, \tag{34}$$

where $Q_m(s)$, the internal model of r, is a known monic polynomial of degree q with non-repeated roots on the $j\omega$-axis and satisfies

S3. $Q_m(s)$, $Z(s)$ are coprime.

Considering the control law given by

$$Q_m(s)L(s)u = -P(s)y + M(s)r\,, \tag{35}$$

where $P(s)$, $M(s)$, $L(s)$ are polynomials (with $L(s)$ monic) of degree $q + n - 1$, $q + n - 1$ e $n - 1$, respectively, and $Q_m(s)$ satisfies (34) and assumption (S3).

Applying (35) to the plant (31), we obtain the closed-loop plant equation

$$y = \frac{Z(s)M(s)}{Q_m(s)L(s)R(s) + P(s)Z(s)}r\,, \tag{36}$$

whose characteristic equation is

$$Q_m(s)L(s)R(s) + P(s)Z(s) = 0\,, \tag{37}$$

and has order $2n + q - 1$. The objective now is chosen $P(s)$, $L(s)$ such that

$$Q_m(s)L(s)R(s) + P(s)Z(s) = A^*(s) \tag{38}$$

is satisfied for a given monic Hurwitz polynomial $A^*(s)$ of degree $2n + q - 1$. Because of assumptions S2 e S3 which guarantee that $Q_m(s)$, $R(s)$, $Z(s)$ are coprime, there is a solution so that $L(s)$ and $P(s)$ satisfy (38) and this solution is unique (Ioannou & Sun, 1996).
Using (38), the closed-loop is described by

$$y = \frac{Z(s)M(s)}{A^*(s)}r\,. \tag{39}$$

Similarly, from the plant (31) and the control law (35) and (38), we obtain

$$u = \frac{R(s)M(s)}{A^*(s)}r\,. \tag{40}$$

Because r is uniformly bounded and $\frac{Z(s)M(s)}{A^*(s)}$, $\frac{R(s)M(s)}{A^*(s)}$ are proper with stable poles, y and u remain bounded whenever $t \to \infty$ for any polynomial $M(s)$ of degree $n + q - 1$ (Ioannou & Sun, 1996). Therefore, the pole placement objective is achieved by the control law (35) without having any additional restrictions in $M(s)$ and $Q_m(s)$. When $r = 0$, (39) and (40) imply that y and u converge to zero exponentially fast. On the other hand, when $r \neq 0$, the tracking error $e = y - r$ is given by

$$e = \frac{Z(s)M(s) - A^*(s)}{A^*(s)}r = \frac{Z(s)}{A^*(s)}[M(s) - P(s)]r - \frac{L(s)R(s)}{A^*(s)}Q_m(s)r\,. \tag{41}$$

In order to obtain zero tracking error, the equation above suggests the choice of $M(s) = P(s)$ to cancel its first term, while the second term can be canceled by using (34). Therefore, the pole placement and tracking objective are achieved by using the control law

$$Q_m(s)L(s)u = -P(s)(y - r)\,, \tag{42}$$

which is implemented as shown in Fig. 1 using $n+q-1$ integrators for the controller realization. An alternative realization of (42) is obtained by rewriting it as

$$u = \frac{\Lambda - LQ_m}{\Lambda} u - \frac{P}{\Lambda}(y - r)\,, \tag{43}$$

where Λ is any monic Hurwitz polynomial of degree $n+q-1$.

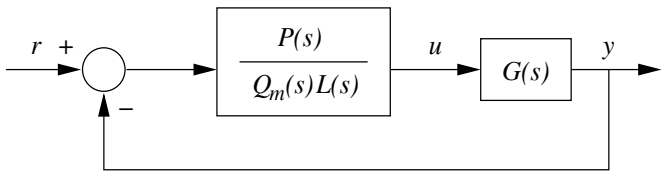

Fig. 1. Block diagram of pole placement control.

The PPC design supposes that the plant parameters are known, what not always is true or possible. Therefore, integral adaptive laws can be proposed for estimating these parameters and then used with PPC schemes. This new strategy is called Adaptive Pole Placement Controller (APPC), where the *certainty equivalence principle* guarantees that the output plant tracks the reference signal r, if the estimates converge to the desired values. In this section, instead of these traditional adaptive laws, switching laws will be used for the the first order plant case, according to (Silva *et al.*, 2004).
Consider the plant,

$$y = \frac{b}{s+a} u\,, \tag{44}$$

and its respective time domain equation,

$$\dot{y} = -ay + bu\,, \tag{45}$$

where the parameters a and b are unknown or known with uncertainties. Let be a_m a positive constant, we may write (45) by adding and subtracting the term $a_m y$,

$$\dot{y} = -a_m y + (a_m - a)y + bu\,. \tag{46}$$

A model for the plant may be written as

$$\dot{\hat{y}} = -a_m \hat{y} + (a_m - \hat{a})y + \hat{b}u\,, \tag{47}$$

where $\hat{a}$ and $\hat{b}$ are estimates for a and b, respectively (Ioannou & Sun, 1996).
We define the estimation error e_0 as

$$e_0 = y - \hat{y}\,, \tag{48}$$

and with (46) and (47), we get

$$\dot{e}_0 = -a_m e_0 + \tilde{a}y - \tilde{b}u\,, \tag{49}$$

where

$$\tilde{a} = \hat{a} - a\ , \tag{50}$$
$$\tilde{b} = \hat{b} - b\ . \tag{51}$$

Choosing the following Lyapunov function candidate,

$$V(e_0) = \frac{1}{2}{e_0}^2 > 0\,, \tag{52}$$

we have

$$\dot{V}(e_0) = e_0\dot{e}_0\ , \tag{53}$$

which can be rewritten using (49),

$$\dot{V}(e_0) \ = -a_m{e_0}^2 + \tilde{a}e_0 y - \tilde{b}e_0 u\,. \tag{54}$$

Expanding the above equation with (50) and (51),

$$\dot{V}(e_0) \ = -a_m{e_0}^2 + (\hat{a} - a)e_0 y - (\hat{b} - b)e_0 u\,, \tag{55}$$

and then using the switching laws,

$$\hat{a} = -\overline{a}\,\mathrm{sgn}(e_0 y)\,, \tag{56}$$
$$\hat{b} = \overline{b}\,\mathrm{sgn}(e_0 u)\,, \tag{57}$$

we get,

$$\dot{V}(e_0) \;= -a_m {e_0}^2 - (\overline{a}\left|e_0 y\right| + a e_0 y) - (\overline{b}\left|e_0 u\right| - b e_0 u)\,. \tag{58}$$

Finally, if the conditions $\overline{a} > \left|a\right|$ and $\overline{b} > \left|b\right|$ are satisfied,

$$\dot{V}(e_0) \le -a_m {e_0}^2 < 0\,, \tag{59}$$

which guarantees that $e_0 = 0$ is a globally asymptotic stable (GAS) equilibrium point. Moreover, if we follow a similar procedure described in (Hsu & Costa, 1989), we can prove that $e_0 = 0$ reaches the sliding surface in a finite time t_f ($e_0 = 0\,,\ \forall t > t_f$).

4. Application on a Current Control Loop of an Induction Machine

To evaluate the performance of both proposed hybrid adaptive schemes, we use an induction machine voltage x current model as an experimental plant. The voltage equations of the induction machine on arbitrary reference frame can be presented by the following equations:

$$v_{sd}^g \;= \left(r_s + \frac{l_s - \sigma l_s}{\tau_r}\right) i_{sd}^g + \sigma l_s \frac{di_{sd}^g}{dt} \;- \omega_g \sigma l_s i_{sq}^g - \left(\frac{l_s - \sigma l_s}{l_m}\right)\left(\omega_r \phi_{rq}^g + \frac{\phi_{rd}^g}{\tau_r}\right), \tag{60}$$

$$v_{sq}^g \;= \left(r_s + \frac{l_s - \sigma l_s}{\tau_r}\right) i_{sq}^g + \sigma l_s \frac{di_{sq}^g}{dt} \;+ \omega_g \sigma l_s i_{sd}^g + \left(\frac{l_s - \sigma l_s}{l_m}\right)\left(\omega_r \phi_{rd}^g - \frac{\phi_{rq}^g}{\tau_r}\right), \tag{61}$$

where v_{sd}^g, v_{sq}^g, i_{sd}^g and i_{sq}^g are *dq* axis stator voltages and currents in a generic reference frame, respectively; r_s, l_s and l_m are the stator resistance, stator inductance and mutual inductance, respectively; ω_g and ω_r are the angular frequencies of the *dq* generic reference frame and rotor reference frame, respectively; $\sigma = 1 - l_m^2 \,/\, l_s l_r$ and $\tau_r = l_r \,/\, r_r$ are the leakage factor and rotor time constant, respectively.

The above model can be simplified by choosing the stator reference frame ($\omega_g = 0$). Therefore, equations (60) and (61) can be rewritten as

$$v_{sd}^s = r_{sr} i_{sd}^s + \sigma l_s \frac{di_{sd}^s}{dt} + e_{sd}^s\,, \tag{62}$$

$$v_{sq}^{s} = r_{sr} i_{sq}^{s} + \sigma l_s \frac{di_{sq}^{s}}{dt} + e_{sq}^{s} \ , \tag{63}$$

where s is the superscript related to the stator reference frame, $r_{sr} = r_s + (l_s - \sigma l_s) / \tau_r$, e_{sd}^{s} and e_{sq}^{s} are *fcems* of the *dq* machine phases given by

$$e_{sd}^{s} = -\left(\omega_r \phi_{rq}^{s} + \frac{\phi_{rd}^{s}}{\tau_r} \right) \frac{(l_s - \sigma l_s)}{l_m}, \tag{64}$$

and

$$e_{sq}^{s} = \left(\omega_r \phi_{rd}^{s} - \frac{\phi_{rq}^{s}}{\tau_r} \right) \frac{(l_s - \sigma l_s)}{l_m}, \tag{65}$$

The current x voltage transfer function of the induction machine can be obtained from (62) and (63) as

$$\frac{I_{sd}^{s}(s)}{V_{sd}^{s'}(s)} = \frac{I_{sd}^{s}(s)}{V_{sd}^{s'}(s)} = \frac{1 / r_{sr}}{s\tau_s + 1}, \tag{66}$$

where $\tau_s = \sigma l_s / r_{sr}$, $V_{sd}^{s'}(s) = V_{sd}^{s}(s) - E_{sd}^{s}(s)$ and $V_{sq}^{s'}(s) = V_{sq}^{s}(s) - E_{sq}^{s}(s)$. The *fcems* $E_{sd}^{s}(s)$ and $E_{sq}^{s}(s)$ are considered unmodeled disturbances to be compensated by the control scheme.

Analyzing the current x voltage transfer functions of a standard machine, we can observe that the time constant τ_s has parameters which vary with the dynamic behavior of machine. Moreover, this plant has also unmodeled disturbances. This justifies the use of this control plant for evaluating the performance of proposed control schemes.

5. Control System

Fig. 2 presents the block diagram of a standard vector control strategy, in which the proposed control schemes are employed for induction motor drive. Block *RFO* realizes the vector rotor field oriented control strategy. It generates the stator reference currents i_{sd}^{s*} and i_{sq}^{s*}, angular stator frequency ω_o^* of stator reference currents from desired reference torque T_e^*, and reference rotor flux ϕ_r^*, respectively. Blocks *VS-ACS* implement the proposed robust adaptive current control schemes that could be the *VS-MRAC* strategy or the *VS-*

APPC strategy. Both current controllers are implemented on the stator reference frame. Block $dq^s / 123$ transforms the variables from dq^s stationary reference frame into 123 stator reference frame.
Generically, the current-voltage transfer function given by equation (66) can be rewritten as

$$W^s_{isdq}(s) = \frac{I^s_{sd}(s)}{V'^s_{sd}(s)} = \frac{I^s_{sq}(s)}{V'^s_{sq}(s)} = \frac{b_s}{s + a_s}, \tag{67}$$

in which $b_s = 1 / \sigma l_s$ and $a_s = 1 / \tau_s$. In this model, the *fcems* e^s_{sd} and e^s_{sq} are considered unmodeled disturbances to be compensated by current controllers. The parameters a_s and b_s are known with uncertainties that can be introduced by machine saturation, temperature changes or loading variation.

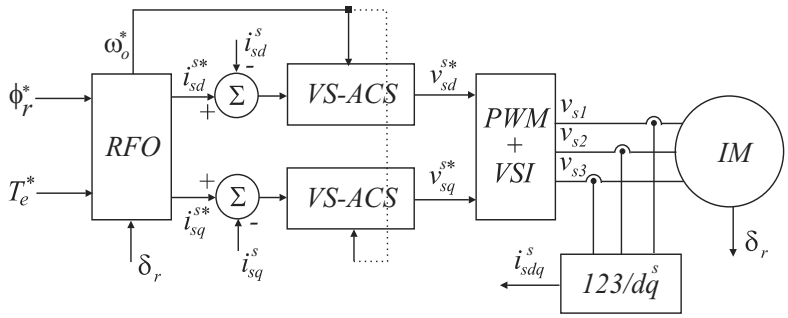

Fig. 2. Block diagram of the proposed *IM* motor drive system.

5.1 VS-MRAC Scheme

Consider that the linear first order plant of induction machine current-voltage transfer function W^s_{isdq} given by (67) and a reference model characterized by transfer function

$$M^s_{isdq}(s) = k_m \frac{N_m(s)}{D_m(s)} = \frac{b_e}{s + a_e}, \tag{68}$$

which attends for the stability constraints that is the constant b_s in (67) and b_e should have positive sign, as mentioned before. The output error can be defined as

$$e^s_{0sdq} = i^s_{sdq} - i^s_{mdq}, \tag{69}$$

where i^s_{mdq} (i^s_{md} and i^s_{mq}) are the outputs of the reference model. The tracking of the model control signal ($i^s_{sd} = i^s_{md}$ or $i^s_{sq} = i^s_{mq}$) is reached if the input of the control plant is defined as

$$v^s_{sdq} = \theta^*_{1dq} i^s_{sdq} + \theta^*_{2dq} i^{s*}_{sdq} \tag{70}$$

where θ^*_{1d} (θ^*_{1q}) and θ^*_{2d} (θ^*_{2q}) are the ideal controller parameters, that can be only determined if $W^s_{isdq}(s)$ is known. According to section 2, they can be determined as

$$\theta^*_{1d} = \theta^*_{1q} = \frac{a_s - a_e}{b_s}, \tag{71}$$

and

$$\theta^*_{2d} = \theta^*_{2q} = \frac{b_e}{b_s}. \tag{72}$$

Once $W^s_{isdq}(s)$ is not known, the controllers parameters $\theta_{1dq}(t)$ and $\theta_{2dq}(t)$ are updated by using switching laws as

$$\theta_{idq} = -\overline{\theta}_{idq} sgn(e^s_{0sdq} y^s_{isdq}) \tag{73}$$

where $i = [1,2]$ and y^s_{sdq} is the reference currents i^{s*}_{sdq} or the output currents i^s_{sdq}, and $\overline{\theta}_{idq} > \left|\theta^*_{idq}\right|$ are upper bounds which are assumed to be known, and the signal-function *sgn* is defined as

$$sgn(x) = \begin{cases} 1 & if \quad x > 0 \\ -1 & if \quad x < 0 \end{cases}. \tag{74}$$

Introducing nominal values of controller parameters $\theta_{idq(nom)}$ (ideally $\theta_{idq(nom)} = \theta^*_{idq}$). It is convenient to modify the control plant input given by (70) for the following

$$v_{sdq}^{s} = \theta^{T}\begin{bmatrix} v_{1dq} \\ i_{sdq}^{s} \\ v_{2dq} \\ i_{sdq}^{s*} \end{bmatrix} + \theta_{nom}^{T}\begin{bmatrix} i_{sdq}^{s} \\ i_{sdq}^{s*} \end{bmatrix}, \tag{75}$$

with $\theta^{T} = \begin{bmatrix} \theta_{v1dq} & \theta_{s1dq} & \theta_{v2dq} & \theta_{s2dq} \end{bmatrix}$, $\theta_{nom}^{T} = \begin{bmatrix} \theta_{s1dq(nom)} & \theta_{s2dq(nom)} \end{bmatrix}$ and

$$\begin{aligned} \dot{v}_{1dq} &= \Lambda v_{1dq} + v_{sdq}^{s} \\ \dot{v}_{2dq} &= \Lambda v_{2dq} + i_{sdq}^{s} \end{aligned}, \tag{76}$$

in which

$$\begin{aligned} \theta_{s1dq} &= -\overline{\theta}_{s1dq} sgn(e_{0sdq}^{s} i_{sdq}^{s}) + \theta_{s1dq(nom)} \\ \theta_{s2dq} &= -\overline{\theta}_{s2dq} sgn(e_{0sdq}^{s} i_{sdq}^{s*}) + \theta_{s2dq(nom)} \end{aligned}, \tag{77}$$

and

$$\begin{aligned} \theta_{v1dq} &= -\overline{\theta}_{v1dq} sgn(e_{0sdq}^{s} v_{1dq}) \\ \theta_{v2dq} &= -\overline{\theta}_{v2dq} sgn(e_{0sdq}^{s} v_{2dq}) \end{aligned}, \tag{78}$$

where θ_{s1dq}, θ_{s2dq}, θ_{v1dq} and θ_{v2dq} are the controller parameters, $\theta_{s1dq(nom)}$ and $\theta_{s2dq(nom)}$ are the nominal parameters of the controller, and v_{1dq} and v_{2dq} are the system plant input and output filtered signals, respectively. The constants $\overline{\theta}_{s1dq}$ or $\overline{\theta}_{s2dq}$ is chosen by considering that

$$\begin{aligned} \overline{\theta}_{s1dq} &> \left| \theta_{s1dq}^{*} - \theta_{s1dq(nom)} \right| \\ \overline{\theta}_{s2dq} &> \left| \theta_{s2dq}^{*} - \theta_{s2dq(nom)} \right| \end{aligned}, \tag{79}$$

The input and output filters given by equation (76) are designed as proposed in (Narendra & Annaswamy, 1989). The filter parameter Λ is chosen such that $N_{m}(s)$ is a factor of $\det(sI - \Lambda)$. Conventionally, these filters are used when the system plant is the second order or higher. However, it is used in the proposed controller to get two more parameters for minimizing the tracking error e_{0sdq}^{s}.

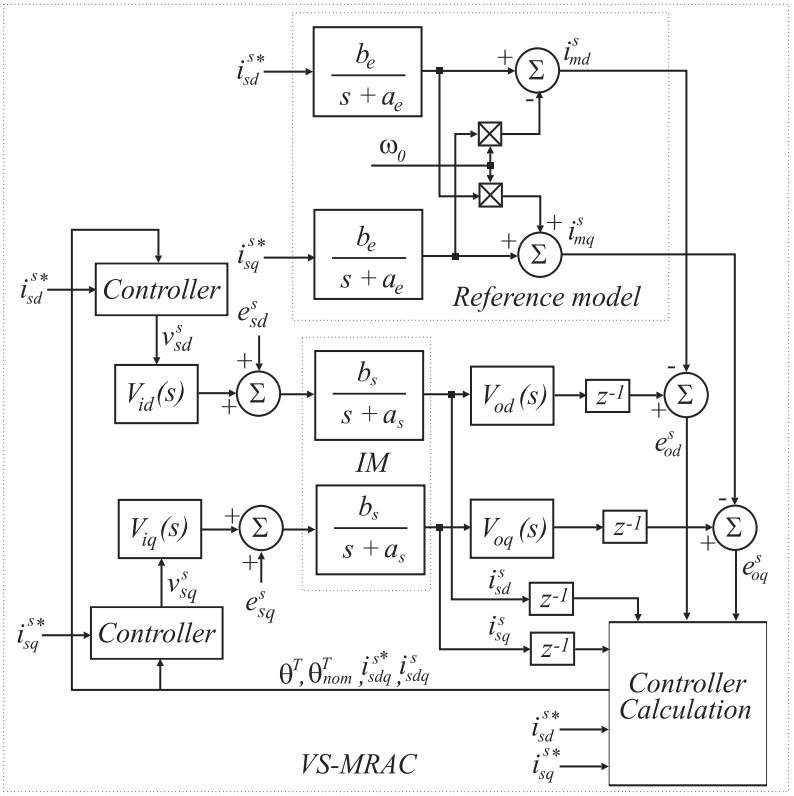

Fig. 3. Block diagram of proposed *VS-MRAC* current controller.

The block diagram of the *VS-MRAC* control algorithm is presented in Fig. 3. The proposed control scheme is composed by *VS* for calculating the controller parameters and a *MRAC* for determining the system desired performance. The *VS* is implemented by the block *Controller Calculation*, in which Equations (77) and (78) together are employed for determining θ_{s1dq}, θ_{s2dq}, θ_{v1dq} and θ_{v2dq}. These parameters are used by *Controller* blocks for generating the control signals v_{sdq}^{s}. To reduce the chattering at the output of controllers, input filters, represented by blocks $V_{id}(s)$ and $V_{iq}(s)$ are employed. They use filter model represented by Eqs. (76). These filtered voltages feed the *IM* which generates phase currents i_{sdq}^{s} which are also filtered by filter blocks $V_{od}(s)$ and $V_{oq}(s)$ and then, compared with the reference model output i_{mdq}^{s} for generating the output error e_{0sdq}^{s}. The reference models are implemented by two blocks which implements transfer functions (68). The output of these blocks is interconnected by coupling terms $-\omega_o I_{mq}^{s}$ and $\omega_o I_{md}^{s}$, respectively. This

approach used to avoid the phase delay between the input (I_{sdq}^{s*}) and output (I_{mdq}^{s*}) of the reference model.

5.1.1 Design of the Controller

To design the proposed *VS-MRAC* controller, initially is necessary to choose a suitable reference model $M_{isdq}^{s}(s)$. Based on the parameters of the induction machine used in present study, given in Table 1, the reference model employed is

$$M_{isdq}^{s}(s) = \frac{550}{s + 550}, \tag{80}$$

From this reference model, the nominal values can be determined by using equations (71) and (72) which results in $\theta_{1sd(nom)} = \theta_{1sq(nom)} = 3.7$ and $\theta_{2sd(nom)} = \theta_{2sq(nom)} = 55$. Considering the restrictions given by (79), the parameters $\overline{\theta}_{s1dq}$ and $\overline{\theta}_{s2dq}$, chosen for achieving a control signal with minimum amplitude are $\overline{\theta}_{s1dq} = 0.37$ and $\overline{\theta}_{s2dq} = 5.5$. It is important to highlight that choice criteria determines how fast the system converges to their references. Moreover, it also determines the level of the chattering verified at the control system after its convergence. As mentioned before the use of input and output filters are not required for control plant of fist order. They are used here for smoothing the control signal. Their parameters was determined experimentally, which results in $\Lambda = 1, \theta_{v1d} = \theta_{v1d} = 2.0$ and $\theta_{v2d} = \theta_{v2q} = 0.1$. This solution is not unique and different adjust can be employed on these filters setup which addresses to different overall system performance.

5.2 VS-APPC Scheme

The first approach of *VS-APPC* in (Silva *et al.*, 2004) does not deal with unmodeled disturbances occurred at the system control loop like machine *fems*. To overcome this, a modified *VS-APPC* is proposed here.

Let us consider the first order *IM* current-voltage transfer function given by equation (67). The main objective is to estimate parameters a_s and b_s to generate the inputs v_{sd} and v_{sq} so that the machine phase currents i_{sd}^{s} and i_{sq}^{s} following their respective reference currents i_{sd}^{s*} and i_{sd}^{s*} and, the closed loop poles are assigned to those of a Hurwitz polynomials $A_s^*(s)$ given by

$$A^*(s) = s^3 + \alpha_2^* s^2 + \alpha_1^* s + \alpha_0^* , \tag{81}$$

where coefficients α_2^*, α_1^* and α_0^* determine the closed-loop performance requirements. To estimate the parameters a_s and b_s, the respective switching laws are used

$$\hat{a}_s = -\overline{a}_s sgn(e^s_{0sdq} i^s_{sdq}), \tag{82}$$

$$\hat{b}_s = \overline{b}_s sgn(e^s_{0sdq} v^s_{sdq}), \tag{83}$$

with the restrictions $\overline{a}_s > |a_s|$ and $\overline{b}_s > |b_s|$ satisfied, as mentioned before. The pole placements and the tracking objectives of proposed *VS-APPC* are achieved, if the following control law is employed

$$Q_m(s)L(s)V^s_{sdq}(s) = -P(s)(I^s_{sdq} - I^{s*}_{sdq}) \tag{84}$$

which addresses to the implementation of the controller transfer function

$$C_{sd}(s) = C_{sq}(s) = \frac{P(s)}{Q_m(s)L(s)}. \tag{85}$$

The polynomial $Q_m(s)$ is choose to satisfy $Q_m(s)I^{s*}_{sd}(s) = Q_m(s)I^{s*}_{sq}(s) = 0$. For the *IM* current-voltage control plant (see equation (67)) and considering that the *VS-APPC* control algorithms are implemented on the stator reference frame, which results in sinusoidal reference currents, a suitable choice for the controller polynomials are $Q_m(s) = s^2 + \omega_o^{*2}$ (internal model of sinusoidal reference signals i^*_{sd} and i^*_{sq}), $L(s) = 1$ and $P(s) = \hat{p}_2 s^2 + \hat{p}_1 s + \hat{p}_0$, where ω_o^* is the angular frequency of reference currents. This choice results in a current controller with the following transfer functions

$$C_{sd}(s) = C_{sq}(s) = \frac{\hat{p}_2 s^2 + \hat{p}_1 s + \hat{p}_0}{s^2 + \omega_o^{*2}} \tag{86}$$

where angular frequency ω_o^* is generated by vector *RFO* control scheme and coefficients $\hat{p}_2$, $\hat{p}_1$ and $\hat{p}_0$ are determined by solving the Diophantine equation for desired Hurwitz polynomial A_s^* (see equation (81)) as follows

$$\hat{p}_2 = \frac{\alpha_2^* - \hat{a}_s}{\hat{b}_s} \tag{87}$$

$$\hat{p}_1 = \frac{\alpha_1^* - \omega_o^{*2}}{\hat{b}_s} \tag{88}$$

$$\hat{p}_0 = \frac{\alpha_0^* - \omega_o^{*2}\hat{a}_s}{\hat{b}_s} \tag{89}$$

To avoid zero division on the equation (87)-(89), the switching law (83) is modified by

$$\hat{b}_s = \overline{b}_s sgn(e^s_{0sdq} v^s_{sdq}) + b_{s(nom)} \tag{90}$$

in which $b_{s(nom)}$ is the nominal values of b_s and the stability restriction becomes $\overline{b}_s > \left| b_s - b_{s(nom)} \right|$.

The control signals v^s_{sd} and v^s_{sq} generated at the output of the proposed controller *VS-APPC* can be derived from equation (86) which results in the following state-space model

$$\dot{x}^s_{1sdq} = x^s_{2sdq} + \hat{p}_1 \varepsilon^s_{sdq} \tag{91}$$

$$\dot{x}^s_{2sdq} = -\omega_o^2 x^s_{1sdq} + (\hat{p}_0 - \omega_o^2 \hat{p}_2)\varepsilon^s_{sdq} \tag{92}$$

$$v^s_{sdq} = x^s_{1sdq} + \hat{p}_2 \varepsilon^s_{sdq} \tag{93}$$

where $\varepsilon^s_{sdq}(t) = i^{s*}_{sdq} - i^s_{sdq}$ is the current error that is calculated from the measured quantities issued by data acquisition plug-in board as described next. Therefore, to generate the output signal of the controllers it is necessary to solve the equations (91)-(93).

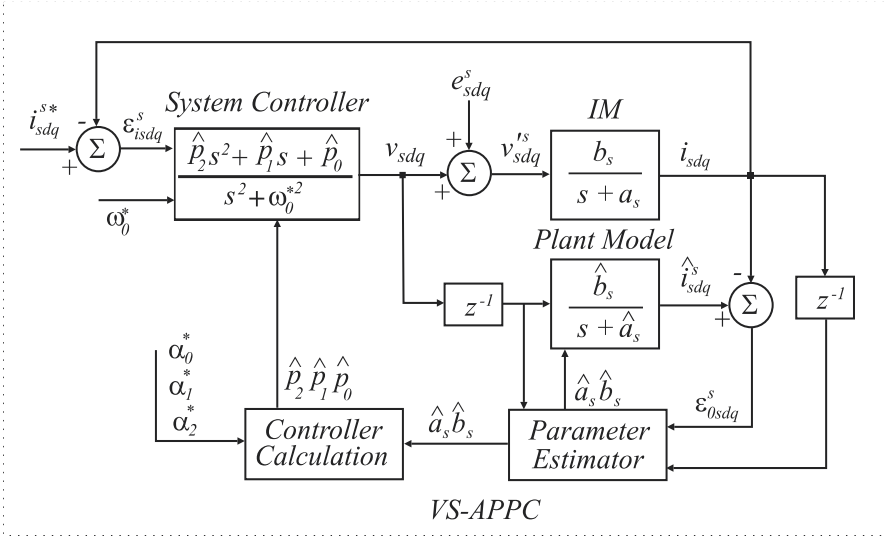

Fig. 4. Block diagram of proposed *VS-APPC* current controller.

The block diagram of the *VS-APPC* control algorithm for the machine current control loop is presented in Fig. 4. The proposed adaptive control scheme is composed a *SMC* parameter estimator and a machine current control loop subsystems. The *SMC* composed by blocks system controller and plant model identifies the dynamic of the *IM* current-voltage model. The output of this system generates the estimative of machine phase currents $\hat{i}^s_{sd}$ and $\hat{i}^s_{sq}$. The control loop subsystem composed by system controller and *IM* regulates the machine phase currents i^s_{sd} and i^s_{sq} and compensate the disturbances e^s_{sd} and e^s_{sq}. The comparison between the estimative currents ($\hat{i}^s_{sd}$ and $\hat{i}^s_{sq}$) and the machine phase currents (i^s_{sd} and i^s_{sq}) determines the estimation errors e^s_{0sd} and e^s_{0sq}. These errors together with machine voltages v^s_{sd} and v^s_{sq}, and *VS-APPC* algorithm set points $\overline{a}_s$, $\overline{b}_s$ and $\overline{b}_{s(nom)}$ are used for calculating parameter estimative $\hat{a}_s$ and $\hat{b}_s$, from the use of equations (82) and (90). These estimates update the plant model of the *IM* and are used by the controller calculation for together with, the coefficients of the desired polynomial A^*_s and angular frequency ω^*_o, determine the parameters of the system controller $\hat{p}_2$, $\hat{p}_1$ and $\hat{p}_0$. The introduction of the *IMP* into the controller modeling avoids the use of stator to synchronous reference frame transformations. With this approach, the robustness for unmodeled disturbances is achieved.

5.2.1 Design of the Controller

To design the proposed *VS-APPC* controller is necessary to choose a suitable polynomial and to determine the controllers coefficients $\hat{p}_2$, $\hat{p}_1$, and $\hat{p}_0$. A good choice criteria for

accomplishing the bound system conditions, is to define a polynomial which roots are closed to the control plant time constants. The characteristics of *IM* used in this work are listed in the Table 1. The current-voltage transfer functions for *dq* phases are given by

$$\frac{I_{sdq}^{s}(s)}{V_{sdq}^{s}(s)} = \frac{10}{s + 587} \tag{94}$$

A possible choice for suitable polynomial $A_s^*(s)$ can be

$$A_s^*(s) = (s + 587)^3 \tag{95}$$

According to Equations (82), (90) and (87)-(89), and based on the desired polynomial (95), the estimative of the parameters of *VS-APPC* current controllers can be obtained as

$$\hat{p}_2 = \frac{1761 - \hat{a}_s}{\hat{b}_s} \tag{96}$$

$$\hat{p}_1 = \frac{1033707 - \omega_o^2}{\hat{b}_s} \tag{97}$$

$$\hat{p}_0 = \frac{202262003 - \omega_o^2 \hat{a}_s}{\hat{b}_s} \tag{98}$$

To define the coefficients of the switching laws it is necessary to take into account together the stability restrictions $\overline{a}_s > \left|a_s\right|$ and $\overline{b}_s > \left|b_s - b_{s(nom)}\right|$. Based on the simulation and the theoretical studies, it can be observed that the magnitude of the respective switching laws ($\overline{a}_s$ and $\overline{b}_s$) determine how fast the *VS-APPC* controllers converge to their respective references. However, the choice of greater values, results in controllers outputs (v_{sd} and v_{sq}) with high amplitudes, which can address to the operation of system with nonlinear behavior. Thus, a good design criteria is to choose the parameters closed to average values of control plant coefficients a_s and b_s. Using this design criteria for the *IM* employed in this work, the following values are obtained $b_{s(nom)} = 9$, $\overline{b}_s = 2$ and $\overline{a}_s = 600$. This solution is not unique and different design adjusts can be tested for different induction machines. The performance of these controllers is evaluated by simulation and experimental results as presented next.

$r_s = 31.0\Omega$	$r_r = 27.2\Omega$	$l_s = 0.8042H$	$l_r = 0.7992H$
$l_m = 0.7534H$	$J = 0.0133kg.m^2$	$F = 0.0146kg.m$	$P = 2$

Table 1. *IM* nominal parameters

6. Experimental Results

The performance of the proposed *VS-MRAC* and *VS-APPC* adaptive controllers was evaluated by experimental results. To realize these tests, an experimental platform composed by a microcomputer equipped with a specific data acquisition card, a control board, *IM* and a three-phase power converter was used. The data of the *IM* used in this platform, are listed in Table 1. The command signals of three-phase power converter are generated by a microcomputer with a sampling time of 100 μs . The data acquisition card employs Hall effect sensors and *A/D* converters, connected to low-pass filters with cutoff frequency of $f_c = 2.5kHz$. Figures 5(a) and 5(b) show the experimental results of *VS-MRAC* control scheme. In these figures are present the graphs of the reference model phase currents i^s_{md} and i^s_{mq} superimposed to the machine phase currents i^s_{sd} and i^s_{sq} . In this experiment, the reference model currents are settled initially in $I^s_{mdq} = 0.8A$ and $f_s = 30Hz$. At the instant $t = 0.15s$, each reference model phase currents is changed by $I^s_{mdq} = 0.2A$. In these results it can be observed that the machine phase currents follow the model reference currents with a good transient response and a current ripple of $\Delta i^s_{sdq} \simeq 0.05A$. Figures 6-7 present the experimental results of *VS-APPC* control scheme. In the Fig. 6(a) are shown the graph of reference phase current i^{s*}_{sd} superimposed by its estimation phase current $\hat{i}^s_{sd}$. In this test, similar to the experiment realized to the *VS-MRAC*, the magnitude of the reference current is settled in $I^{s*}_{sdq} = 0.8A$ and at instant $t = 0.15s$, it is changed by $I^{s*}_{sdq} = 0.2A$. These results show that the estimation scheme employed in the *VS-APPC* estimates the machine phase current with small current ripple. Figure 6(b) shows the graphs of the reference phase current i^{s*}_{sd} superimposed by its corresponded machine phase current i^s_{sd} . In this result, it can be verified that the machine phase current converges to its reference current imposed by *RFO* vector control strategy. Similar to the results presented before, Fig. 7(a) presents the experimental results of reference phase current i^{s*}_{sq} superimposed by its estimation phase current $\hat{i}^s_{sq}$ and Fig. 7(b) shows the reference phase current i^{s*}_{sq} superimposed by its corresponded machine phase current i^s_{sq} . These results show that the *VS-APPC* also demonstrates a good performance. In comparison to the VS-MRAC, the machine phase currents of the *VS-APPC* present small current ripple.

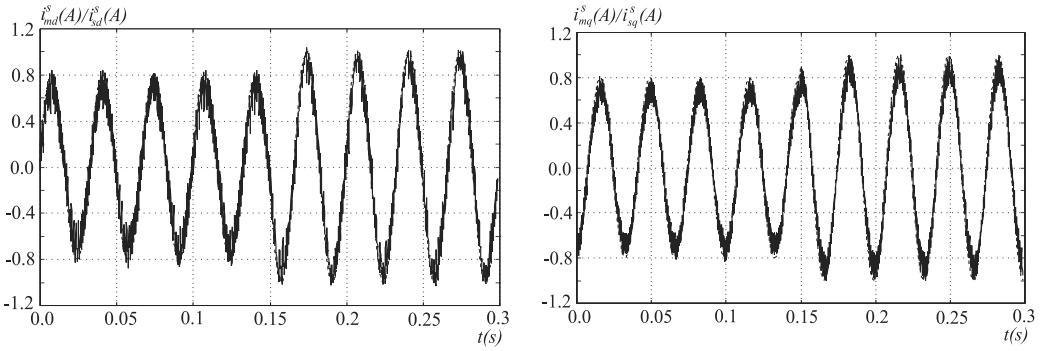

Fig. 5. Experimental results of *VS-MRAC* phase currents i^s_{md} (a) and i^s_{mq} (b) superimposed to *IM* phase currents i^s_{sd} (a) and i^s_{sd} (b), respectively.

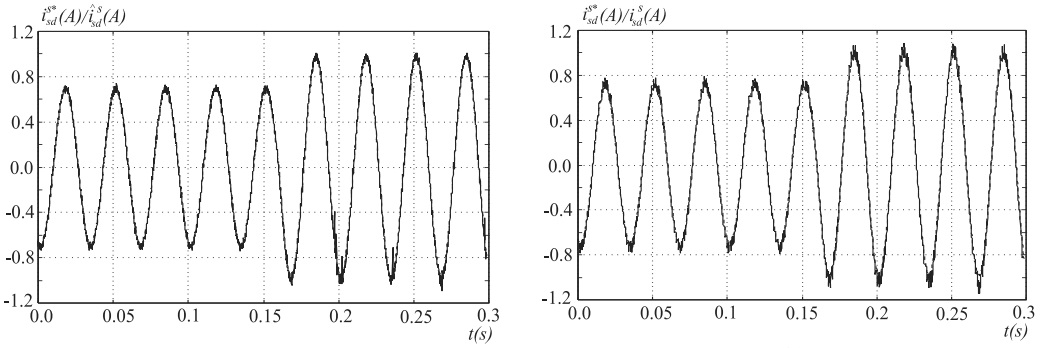

Fig. 6. Experimental results of *VS-APPC* reference phase current i^{s*}_{sd} superimposed to estimation *IM* phase current $\hat{i}^s_{sd}$ (a) and *IM* phase current i^s_{sd} (b).

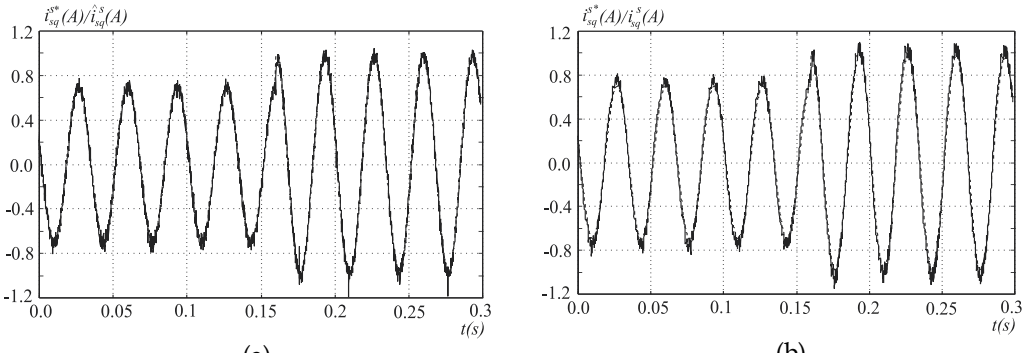

Fig. 7. Experimental results of *VS-APPC* reference phase current i^{s*}_{sq} superimposed to estimation *IM* phase current $\hat{i}^s_{sq}$ (a) and *IM* phase current i^s_{sq} (b).

7. References

Hsu, L. & Costa, R. R. (1989). Variable structure model reference adaptive control using only input and output measurement: part I. *International Journal of Control*, Vol.49, No. 1, pp. 399-416.

Hsu, L. (1990). Variable Structure model reference adaptive control using only Input and output measurements - general case. *IEEE Transactions on Automatic Control*, Vol.35, pp. 1238-1243.

Hsu, L.; Araújo, A. D. de & Costa, R. R. (1994). Analysis and design of i/o based variable structure adaptive control. *IEEE Transactions on Automatic Control*, Vol. 39, No. 1, pp. 4-21.

Ioannou, P. A. & Kokotovic, P. V. (1984). Instability analysis and improvement of robustness of adaptive control. *Automatica*, Vol. 20, pp. 583-594.

Ioannou, P. A. & Tsakalis, K. S. (1986). Robust direct adaptive controller. *IEEE Transactions on Automatic Control*, Vol. AC-31, pp. 1033-1043.

Ioannou, P. A. & Sun, J. (1996). *Robust adaptive control*. Prentice Hall, New Jersey, USA.

Kazmierkowski, M. P. & Malesani, L. (1998). Current control techniques for three-phase voltage-source pwm converters: a survey. *IEEE Transactions on Industry Applications*, Vol. 45, No 5, pp. 601-703.

Malesani, L.; Mattavelly, P. & Tomasin, P. (1997) . Improved constant-frequency hysteresis current control of vsi inverters with simple feedforward bandwith prediction. *IEEE Transactions on Industry Applications*, Vol. 33, No. 5, pp. 1194-1202.

Naik, S. M., Kumar, P. R. & Ydstie, B. E. (1992). Robust continuous-time adaptive control by parameter projection. *IEEE Transactions on Automatic Control*, Vol. AC-37, pp. 182-197.

Narendra , K. S. & Valavani, L. S. (1978). Stable adaptive controller design-direct control. *IEEE Transactions on Automatic Control*, Vol. AC-23, pp. 570-583.

Narendra , K. S., Lin, Y. H. & Valavani, L. S. (1980). Stable adaptive controller design, part II: proof of stability. *IEEE Transactions on Automatic Control*, Vol. AC-25, pp. 440-448.

Narendra, K. & Annaswamy, A. (1989). *Stable adaptive control*. Englewood Cliffs and NJ: Prentice-Hall.

P. Vas (1998). *Sensorless vector and direct torque control*. Oxford University Press.

Plunkett, B. (1979). A current controlled pwm transistor inverter drive. *In Proceedings of the IEEE Industry Applications Society Annual Meeting*, pp. 785-792.

Sastry, S. S. & Bodson, N. M. (1989). *Adaptive control: stability, convergence and robustness*. Prentice-Hall, New Jersey.

Silva Jr, F. C; Araújo, A. D. de & Oliveira, J. B. (2004). A proposal for a variable structure adaptive pole placement control. *In Proceedings of the IEEE Workshop on Variable Structure Systems*, 2004.

Utkin, V. I. (1977). Variable structure system with sliding mode. *IEEE Transactions on Automatic Control*, Vol.AC- 22, pp. 212-222.

Utkin, V. I. (1978). *Sliding modes and their application in variable structure systems.* Mir Publishers, Moscow.

Utkin, V. I. (1992). *Sliding Modes in Control and Optimization.* Spring-Verlag, New York.

Wishart, M. T. & Harley, R. G. (1995). Identication and control of induction machine using articial neural networks. *IEEE Transactions on Industry Applications*, Vol. 31, No. 3, pp. 612-619.

Zhang, C. J. & Dunnigan, M. W. (2003). Robust adaptive stator current control for an induction machine. *In Proceedings of the IEEE Conference Control Applications*, pp. 779-784.

7

Adaptive Control for Systems with Randomly Missing Measurements in a Network Environment

Yang Shi[1] and Huazhen Fang[1]
[1]*Department of Mechanical Engineering, University of Saskatchewan*
Canada

1. Introduction

Networked control systems (NCSs) are a type of distributed control systems, where the information of control system components (reference input, plant output, control input, etc.) is exchanged via communication networks. Due to the introduction of networks, NCSs have many attractive advantages, such as reduced system wiring, low weight and space, ease of system diagnosis and maintenance, and increased system agility, which motivated the research in NCSs. The study of NCSs has been an active research area in the past several years, see some recent survey articles (Chow & Tipsuwan, 2001; Hespanha & Naghshtabrizi, 2007; Yang, 2006) and the references therein. On the other hand, the introduction of networks also presents some challenges such as the limited feedback information caused by packet transmission delays and packet loss; both of them are due to the sharing and competition of the transmission medium, and bring difficulties for analysis and design for NCSs. The information transmission delay arises from by the limited capacity of the communication network used in a control system, whereas the packet loss is caused by the unavoidable data losses or transmission errors. Both the information transmission delay and packet loss may result in randomly missing output measurements at the controller node, as shown in Fig. 1. So far different approaches have been used to characterize the limited feedback information. For example, the information transmission delay and packet losses have been modeled as Markov chains (Zhang et al., 2006). The binary Bernoulli distribution is used to model the packet losses in (Sinopoli et al., 2004; Wang et al., 2005 a & 2005 b).

The main challenge of NCS design is the limited feedback information (information transmission delays and packet losses), which can degrade the performance of systems or even cause instability. Various methodologies have been proposed for modeling, stability analysis, and controller design for NCSs in the presence of limited feedback information. A novel feedback stabilization solution of multiple coupled control systems with limited communication is proposed by bringing together communication and control theoretical issues in (Hristu & Morgansen, 1999). Further the control and communication codesign methodology is applied in (Hristu-Varsakelis, 2006; Zhang & Hristu-Varsakelis, 2006) – a method of stabilizing linear NCSs with medium access constraints and transmission delays by designing a delay-compensated feedback controller and an accompanying medium

access policy is presented. In (Zhang et al., 2001), the relationship of sampling time and maximum allowable transfer interval to keep the systems stable is analyzed by using a stability region plot; the stability analysis of NCSs is addressed by using a hybrid system stability analysis technique. In (Walsh et al., 2002), a new NCS protocol, try-once-discard (TOD), which employs dynamic scheduling method, is proposed and the analytic proof of global exponential stability is provided based on Lyapunov's second method. In (Azimi-Sadjadi, 2003), the conditions under which NCSs subject to dropped packets are mean square stable are provided. Output feedback controller that can stabilize the plant in the presence of delay, sampling, and dropout effects in the measurement and actuation channels is developed in (Naghshtabrizi & Hespanha, 2005). In (Yu et al., 2004), the authors model the NCSs with packet dropout and delays as ordinary linear systems with input delays and further design state feedback controllers using Lyapunov-Razumikhin function method for the continuous-time case, and Lyapunov-Krasovskii based method for the discrete-time case, respectively. In (Yue et al., 2004), the time delays and packet dropout are simultaneously considered for state feedback controller design based on a delay-dependent approach; the maximum allowable value of the network-induced delays can be determined by solving a set of linear matrix inequalities (LMIs). Most recently, Gao, et al., for the first time, incorporate simultaneously three types of communication limitation, e.g., measurement quantization, signal transmission delay, and data packet dropout into the NCS design for robust H_∞ state estimation (Gao & Chen, 2007), and passivity based controller design (Gao et al., 2007), respectively. Further, a new delay system approach that consists of multiple successive delay components in the state, is proposed and applied to network-based control in (Gao et al., 2008).

However, the results obtained for NCSs are still limited: Most of the aforementioned results assume that the plant is given and model parameters are available, while few papers address the analysis and synthesis problems for NCSs whose plant parameters are unknown. In fact, while controlling a real plant, the designer rarely knows its parameters accurately (Narendra & Annaswamy, 1989). To the best of our knowledge, adaptive control for systems with unknown parameters and randomly missing outputs in a network environment has not been fully investigated, which is the focus of this paper.

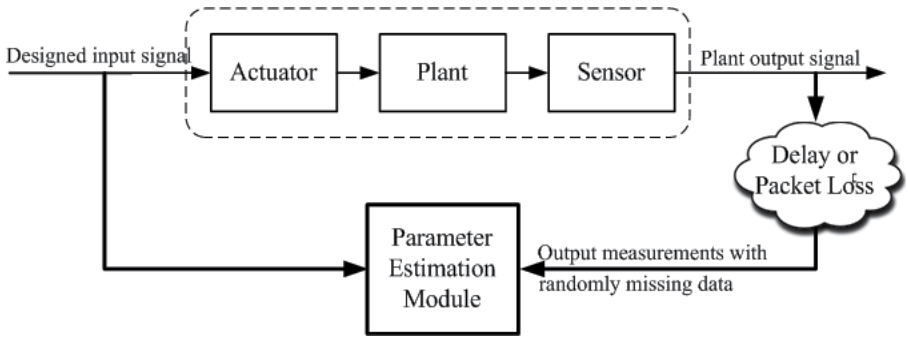

Fig. 1. An NCS with randomly missing outputs.

It is worth noting that systems with regular missing outputs – a special case of those with randomly missing outputs – can also be viewed as multirate systems which have uniform

but various input/output sampling rates (Chen & Francis, 1995). Such systems may have regular-output-missing feature. In (Ding & Chen, 2004a), Ding, et al. use an auxiliary model and a modified recursive least squares (RLS) algorithm to realize simultaneous parameter and output estimation of dual-rate systems. Further, a least squares based self-tuning control scheme is studied for dual-rate linear systems (Ding & Chen, 2004b) and nonlinear systems (Ding et al., 2006), respectively. However, network-induced limited feedback information unavoidably results in randomly missing output measurements. To generalize and extend the adaptive control approach for multirate systems (Ding & Chen, 2004b; Ding et al., 2006) to NCSs with randomly missing output measurements and unknown model parameters is another motivation of this work.

In this paper, we first model the availability of output as a Bernoulli process. Then we design an output estimator to online estimate the missing output measurements, and further propose a novel Kalman filter based method for parameter estimation with randomly output missing. Based on the estimated output or the available output, and the estimated model parameters, an adaptive control is proposed to make the output track the desired signal. Convergence of the proposed output estimation and adaptive control algorithms is analyzed.

The rest of this paper is organized as follows. The problem of adaptive control for NCSs with unknown model parameters and randomly missing outputs is formulated in Section 2. In Section 3, the proposed algorithms for output estimation, model parameter estimation, and adaptive control are presented. In Section 4, the convergence properties of the proposed algorithms are analyzed. Section 5 gives several illustrative examples to demonstrate the effectiveness of the proposed algorithms. Finally, concluding remarks are given in Section 6.

Notations: The notations used throughout the paper are fairly standard.' E ' denotes the expectation. The superscript ' T ' stands for matrix transposition; $\lambda_{\max/\min}(X)$ represents the Maximum/minimum eigenvalue of X; $|X|=\det(X)$ is the determinant of a square matrix X; $\|X\|^2 = tr(XX^T)$ stands forthe trace of XX^{T}. If $\exists\, \delta_0 \in \mathrm{R}^+$ and $k_0 \in \mathrm{Z}^+$, $|f(k)| \le \delta_0 g(k)$ for $k \ge k_0$, then $f(k) = O(g(k))$; if $f(k)/g(k) \to 0$ for $k \to \infty$, then $f(k) = o(g(k))$.

2. Problem Formulation

The problem of interest in this work is to design an adaptive control scheme for networked systems with unknown model parameters and randomly missing outputs. In Fig. 2, the output measurements y_k could be unavailable at the controller node at some time instants because of the network-induced limited feedback information, e.g., transmission delay and/or packet loss. The data transmission protocols like TCP guarantee the delivery of data packets in this way: When one or more packets are lost the transmitter retransmits the lost packets. However, since a retransmitted packet usually has a long delay that is not desirable for control systems, the retransmitted packets are outdated by the time they arrive at the controller (Azimi-Sadjadi, 2003; Hristu-Varsakelis & Levine, 2005). Therefore, in this paper, it is assumed that the output measurements that are delayed in transmission are regarded as missed ones.

The availability of y_k can be viewed as a random variable γ_k. γ_k is assumed to have Bernoulli distribution:

$$\mathrm{E}(\gamma_k\gamma_s) = \mathrm{E}\gamma_k\mathrm{E}\gamma_s \text{ for } k \neq s, \tag{1}$$
$$\mathrm{Prob}(\gamma_k) = \begin{cases} \mu_k, \text{ if } \gamma_k = 1, \\ 1-\mu_k, \text{ else if } \gamma_k = 0, \end{cases}$$

where $0 < \mu_k \leq 1$.

Consider a single-input-single-output (SISO) process (Fig. 2):

$$\mathrm{A}_z x_k = B_z u_k, \quad y_k = x_k + v_k \tag{2}$$

where u_k is the system input, y_k the output and v_k the disturbing white noise with variance r_v. A_z and B_z are two backshift polynomials defined as

$$A_z = 1 + a_1 z^{-1} + a_2^{-2} + \cdots + a_{n_a} z^{-n_a},$$
$$B_z = b_0 + b_1 z^{-1} + b_2 z^{-2} + \cdots + b_{n_b} z^{-n_b}.$$

The polynomial orders n_a and n_b are assumed to be given. Eqn. (2) can be written equivalently as the following linear regression model:

$$y_k = \varphi_{0k}^{\mathrm{T}}\theta + v_k, \tag{3}$$

where

$$\varphi_{0k} = \left[-x_{k-1} - x_{k-2} \cdots - x_{k-n_a} u_k u_{k-1} \cdots u_{k-n_b}\right]^{\mathrm{T}},$$
$$\theta = \left[a_1\ a_2 \cdots a_{n_a}\ b_0\ b_1 \cdots b_{n_b}\right]^{\mathrm{T}}.$$

Vector φ_{0k} represents system's excitation and response information necessary for parameter estimation, while vector θ contains model parameters to be estimated.

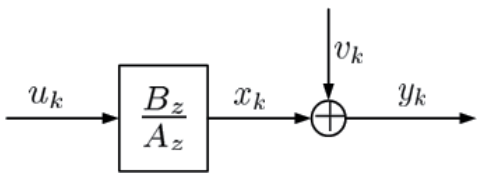

Fig. 2. Output-error (OE) model structure.

For a system with the output-error (OE) model placed in a networked environment subject to randomly missing outputs, the objectives of this paper are:

1. Design an output estimator to online estimate the missing output measurements.
2. Develop a recursive Kalman filter based identification algorithm to estimate unknown model parameters.

3. Propose an adaptive tracking controller to make the system output track a given desired signal.
4. Analyze the convergence properties of the proposed algorithms.

3. Parameter Estimation, Output Estimation, and Adaptive Control Design

There are two main challenges of the adaptive control design for a networked system as depicted in Fig. 1: (1) randomly missing output measurements; (2) unknown system model parameters. Therefore, in this section, we first propose algorithms for missing output estimation and unknown model parameter estimation, and then design the adaptive control scheme.

3.1 Parameter estimation and missing output estimation

Consider the model in (3). It is shown by (Cao & Schwartz, 2003) and (Guo, 1990) that the corresponding Kalman filter can be conveniently used for parameter estimation. In combination with an auxiliary model, the Kalman filter based parameter estimation algorithm for an OE model is given by

$$\hat{\theta}_k = \hat{\theta}_{k-1} + K_{a,k}(y_k - \varphi_{a,k}^{\mathrm{T}}\hat{\theta}_{k-1}), \tag{4}$$

$$K_{a,k} = \frac{P_{a,k-1}\varphi_{a,k}}{r_v + \varphi_{a,k}^{\mathrm{T}}P_{a,k-1}\varphi_{a,k}}, \tag{5}$$

$$P_{a,k} = P_{a,k-1} - \frac{P_{a,k-1}\varphi_{a,k}\varphi_{a,k}^{\mathrm{T}}P_{a,k-1}}{r_v + \varphi_{a,k}^{\mathrm{T}}P_{a,k-1}\varphi_{0k}}, \tag{6}$$

$$x_{a,k} = \phi_{a,k}^{\mathrm{T}}\hat{\theta}_k, \tag{7}$$

$$\varphi_{a,k} = \left[-x_{a,k-1} - x_{a,k-2}\cdots - x_{a,k-n_a}\ u_k\ u_{k-1}\cdots u_{k-n_b}\right]^{\mathrm{T}}, \tag{8}$$

where $\hat{\theta}_k$ represents the estimated parameter vector at time instant k.

It is worth to note that the above algorithm as shown in (4)-(8) cannot be *directly* applied to the parameter estimation of systems with randomly missing outputs in a network environment, as y_k in (4) may not be available. This motivates us to develop a new algorithm that can simultaneously online estimate the unavailable missing output and estimate system parameters under the network environment. The proposed algorithm consists of two steps.

Step 1: Output estimation

Albertos, et al. propose a simple algorithm that uses the input-output model, replacing the unknown past values by estimates when necessary (Albertos et al., 2006). Inspired by this work, we design the following output estimator:

$$z_k = \gamma_k y_k + (1-\gamma_k)\hat{y}_k, \tag{9}$$

with

$$\hat{y}_k = \varphi_k^{\mathrm{T}} \hat{\theta}_{k-1}.$$

In (9), γ_k is a Bernoulli random variable used to characterize the availability of y_k at time instant k at the controller node, as defined in (1). With the time-stamp technique, the controller node can detect the availability of the output measurements, and thus, the values of γ_k (either 1 or 0) are known. The knowledge of their corresponding probability μ_k is not used in the designed estimator. The structure of the designed output estimator is intuitive and simple yet very effective, which will be seen soon from the simulation examples.

Step 2: Model parameter estimation
Replacing y_k in the algorithm (4)-(8) by z_k, defining a new φ_k, and considering the random variable γ_k, we readily obtain the following algorithm:

$$\hat{\theta}_k = \hat{\theta}_{k-1} + K_k(z_k - \varphi_k^{\mathrm{T}} \hat{\theta}_{k-1}), \tag{10}$$

$$K_k = \frac{P_{k-1}\varphi_k}{r_v + \varphi_k^{\mathrm{T}} P_{k-1}\varphi_k}, \tag{11}$$

$$P_k = P_{k-1} - \gamma_k \frac{P_{k-1}\varphi_k\varphi_k^{\mathrm{T}} P_{k-1}}{r_v + \varphi_k^{\mathrm{T}} P_{k-1}\varphi_k}, \tag{12}$$

$$x_{b,k} = \varphi_k^{\mathrm{T}} \hat{\theta}_k, \tag{13}$$

$$\varphi_k = \left[-x_{b,k-1} - x_{b,k-2} \cdots - x_{b,k-n_a}\ u_k\ u_{k-1} \cdots u_{k-n_b}\right]^{\mathrm{T}}. \tag{14}$$

Remark 3.1. *Consider two extreme cases. If the availability sequence* $\{\gamma_1, \cdots, \gamma_k\}$ *constantly assumes 1, then no output measurement is lost, and the algorithm above will reduce to the algorithm (4)-(6). On the other hand, if the availability sequence* γ_k *constantly takes 0, then all output measurements are lost, and the parameter estimates just keep the initial values.*

3.2 Adaptive control design

Consider the tracking problem. Let $y_{r,k}$ be a desired output signal, and define the output tracking error

$$\zeta_k := y_k - y_{r,k}.$$

If the control law u_k is appropriately designed such that $y_{r,k} = \varphi_{0k}^{\mathrm{T}}\theta$, then the average tracking error z_k approaches zero finally. Replacing θ by $\hat{\theta}_{k-1}$ and φ_{0k} by φ_k yields

$$\begin{aligned} y_{r,k} &= \varphi_k^{\mathrm{T}}\hat{\theta}_{k-1} = -\sum_{i=1}^{n_a}\hat{\theta}_{i,k-1}x_{k-i} + \sum_{i=0}^{n_b}\hat{\theta}_{n_a+i+1,k-1}u_{k-i} \\ &= -\hat{a}_{1,k-1}x_{b,k-1} - \cdots - \hat{a}_{n_a,k-1}x_{b,k-n_a} + \hat{b}_{0,k-1}u_k + \cdots + \hat{b}_{n_b,k-1}u_{k-n_b}. \end{aligned}$$

Therefore, the control law can be designed as

$$u_k = \frac{1}{\hat{b}_{0,k-1}}\left[y_{r,k} + \sum_{i=1}^{n_a}\hat{a}_{i,k-1}x_{k-i} - \sum_{i=1}^{n_b}\hat{b}_{i,k-1}u_{k-i} \right]. \tag{15}$$

The proposed adaptive control scheme consists of the missing output estimator [Equation (9)], model parameter estimator [Equations (10-14)], and the adaptive control law [Equation (15)]. The overall control diagram is shown in Fig. 3.

4. Convergence Analysis

This section focuses on the analysis of some convergence properties. Some preliminaries are first summarized to facilitate the following convergence analysis of parameter estimation in (10)-(12) and of output estimation in (9). Inspired by the work in (Chen & Guo, 1991; Ding & Chen, 2004a; Ding et al., 2006), the convergence analysis is carried out under the stochastic framework.

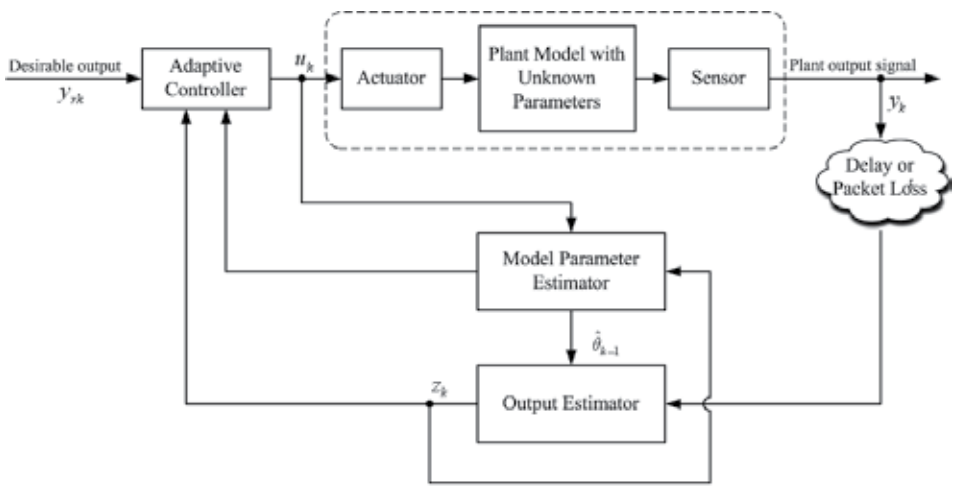

Fig. 3. Adaptive control diagram.

4.1 Preliminaries

To facilitate the convergence analysis, directly applying the matrix inversion formula (Horn

& Johnson, 1991)

$$(A+BCD)^{-1} = A^{-1} - A^{-1}B(C^{-1}+DA^{-1}B)^{-1}DA^{-1},$$

the proposed parameter estimation algorithm in Section 3.1 [(10)-(12] can be equivalently rewritten as:

$$\hat{\theta}_k = \hat{\theta}_{k-1} + r_v^{-1}P_k\varphi_k(z_k - \varphi_k^{\mathrm{T}}\hat{\theta}_{k-1}), \tag{16}$$

$$P_k^{-1} = P_{k-1}^{-1} + r_v^{-1}\gamma_k\varphi_k\varphi_k^{\mathrm{T}}. \tag{17}$$

Suppose that P_k is initialized by $p_0 I$, where p_0 is a positive real value large enough, and define $r_k = \mathrm{tr}(P_k^{-1})$. The relation between r_k and $|P_k^{-1}|$ can be established in the following lemma.

Lemma 4.1. *The following relation holds:*

$$\ln \mathrm{E}\,|P_k^{-1}| = O(\ln \mathrm{E} r_k). \tag{18}$$

Proof: Using the formulae

$$\mathrm{tr}(X) = \sum_{i=1}^{n}\lambda_i(X) \ \text{ and } |X| = \prod_{i=1}^{n}\lambda_i(X),$$

where n is the dimension of X, we have

$$\mathrm{E}\,|P_k^{-1}| \le (\mathrm{E} r_k)^n.$$

This completes the proof.

The next lemma shows the convergence of two infinite series that will be useful later.

Lemma 4.2. *The following inequalities hold:*

$$\sum_{i=1}^{t}\mu_i r_v^{-1}\mathrm{E}\left(\varphi_i^{\mathrm{T}}P_i\varphi_i\right) \le \ln \mathrm{E}\,|P_k^{-1}| + n_0 \ln p_0 \ \text{a.s.}, \tag{19}$$

$$\sum_{i=1}^{\infty}\mu_i r_v^{-1}\frac{\mathrm{E}\left(\varphi_i^{\mathrm{T}}P_i\varphi_i\right)}{\left(\ln \mathrm{E}\,|P_i^{-1}|\right)^c} < \infty \ \text{a.s.}, \tag{20}$$

where $c > 1$.

Proof: The proof can be done along the similar way as Lemma 2 in (Ding & Chen, 2004b) and is omitted here. □

The following is the well-known martingale convergence theorem that lays the foundation for the convergence analysis of the proposed algorithms.

Theorem 4.1. (Goodwin & Sin, 1984) *Let* $\{X_k\}$ *be a sequence of nonnegative random variables adapted to an increasing* σ *-algebras* $\{F_k\}$ *. If*

$$E(X_{k+1} \mid F_k) \le (1+\check{n}_k)X_k - \alpha_k + \beta_k, \text{ a.s.},$$

where $\alpha_k \ge 0$, $\beta_k \ge 0$, $EX_0 < \infty$, $\sum_{i=0}^{\infty} |\varepsilon_i| < \infty$ *and* $\sum_{i=0}^{\infty} \beta_i < \infty$ *almost surely (a.s.), then* X_k *converges a.s. to a finite random variable and*

$$\lim_{N\to\infty} \sum_{i=0}^{N} \alpha_i < \infty, \text{ a.s.}$$

4.2 Convergence analysis

To carry out the convergence analysis of the proposed algorithms, it is essential to appropriately construct a martingale process satisfying the conditions of Theorem 4.1. Main results on the convergence properties of the proposed algorithm are summarized in the following Theorem.

Theorem 4.2. *For the system considered in (3), assume that*

(A1) $\{v_k, F_k\}$ *is a martingale difference sequence satisfying*

$$E(v_k \mid F_{k-1}) = 0, \text{ a.s.}, \tag{21}$$

$$E(v_k^2 \mid F_{k-1}) = r_v < \infty, \text{ a.s.}; \tag{22}$$

(A2) $\frac{1}{A_z} - \frac{1}{2}$ *is strictly positive real;*

(A3) B_z *is stable; i.e., zeros o f* B_z *are inside the closed unit disk.*

Suppose the desired output signal is bounded: $|y_{r,k}| < \infty$ *. Applying the missing output estimator [Equation (9)], model parameter estimator [Equations (10-14)], and the adaptive control law [Equation (15)], then the output tracking error has the property of minimum variance, i.e.,*

$$(1)\ \lim_{k\to\infty} \frac{1}{k} \sum_{i=1}^{k} (y_{r,i} - y_i + v_i)^2 = 0, \text{ a.s.};$$

$$(2)\ \lim_{k\to\infty} \frac{1}{k} \sum_{i=1}^{k} \mu_i E\{(z_i - y_{r,i})^2 \mid F_{i-1}\} = r_v < \infty, \text{ a.s.}$$

Proof: As pointed out in (Goodwin & Sin, 1984; Chen & Guo, 1991), from (A2) it follows that

$$\frac{1}{k} \sum_{i=1}^{k} u_i^2 \le O(1) + O\left(\frac{c_1}{k} \sum_{i=1}^{k} y_i^2\right), \text{ a.s.} \tag{23}$$

Here, c_1 is a positive constant. Define the following vectors:

$$e_k = z_k - \varphi^{\mathrm{T}}\hat{\theta}_{k-1},$$

$$\overline{\eta}_k = y_k - x_{b,k},$$

$$\eta_k = \gamma_k \overline{\eta}_k,$$

$$\overline{\tau}_k = y_{r,k} - y_k + v_k,$$

$$\tau_k = \gamma_k \overline{\tau}_k.$$

From (2), (3), (16) and (16), it follows that

$$\eta_k = \gamma_k (x_k - x_{b,k} + v_k), \tag{24}$$

$$\eta_k = (1 + r_v^{-1}\varphi_k^{\mathrm{T}} P_{k-1}\varphi_k)^{-1} e_k, \tag{25}$$

$$e_k = -\tau_k + \gamma_k v_k. \tag{26}$$

Also define the parameter estimation error vector and a Lyapunov-like function as

$$\tilde{\theta}_k = \hat{\theta}_k - \theta,$$
$$V_k = \tilde{\theta}_k^{\mathrm{T}} P_k^{-1} \tilde{\theta}_k.$$

From (9), (16) and (25), we obtain

$$\tilde{\theta}_k = \tilde{\theta}_{k-1} + r_v^{-1} P_k \varphi_k e_k = \tilde{\theta}_{k-1} + r_v^{-1} P_{k-1} \varphi_k \eta_k. \tag{27}$$

With (17) and (27), V_k can be further evaluated as

$$V_k = V_{k-1} + r_v^{-1}\gamma_k (\varphi_k^{\mathrm{T}}\tilde{\theta}_k)^2 + 2 r_v^{-1}\varphi_k^{\mathrm{T}}\tilde{\theta}_k \eta_k - r_v^{-2}\varphi_k^{\mathrm{T}} P_k \varphi_k (1 - r_v^{-1}\varphi_k^{\mathrm{T}} P_k \varphi_k) e_k^2.$$

Let us define

$$\tilde{u}_k = -\varphi_k^{\mathrm{T}}\tilde{\theta}_k,$$

$$\tilde{y}_k = \frac{1}{2}\varphi_k^{\mathrm{T}}\tilde{\theta}_k + (\overline{\eta}_k - v_k).$$

Then we have

$$\begin{aligned} V_k &= V_{k-1} - 2r_v^{-1}\gamma_k\tilde{u}_k\tilde{y}_k + 2r_v^{-1}\gamma_k\varphi_k^{\mathrm{T}}\tilde{\theta}_k v_k - r_v^{-2}\varphi_k^{\mathrm{T}}P_k\varphi_k(1-r_v^{-1}\varphi_k^{\mathrm{T}}P_k\varphi_k)e_k^2 \\ &= V_{k-1} - 2r_v^{-1}\gamma_k\tilde{u}_k\tilde{y}_k + 2r_v^{-1}\gamma_k\varphi_k^{\mathrm{T}}\tilde{\theta}_{k-1}v_k + 2r_v^{-2}\varphi_k^{\mathrm{T}}P_k\varphi_k\left[(e_k-\gamma_k v_k)^{\mathrm{T}}v_k + \gamma_k v_k^2\right] \\ &\quad -r_v^{-2}\varphi_k^{\mathrm{T}}P_k\varphi_k(1-r_v^{-1}\varphi_k^{\mathrm{T}}P_k\varphi_k)\tau_k^2 + 2r_v^{-2}\varphi_k^{\mathrm{T}}P_k\varphi_k(1-r_v^{-1}\varphi_k^{\mathrm{T}}P_k\varphi_k)\tau_k v_k \\ &\quad -r_v^{-2}\varphi_k^{\mathrm{T}}P_k\varphi_k(1-r_v^{-1}\varphi_k^{\mathrm{T}}P_k\varphi_k)v_k^2 \\ &\le V_{k-1} - 2r_v^{-1}\gamma_k\tilde{u}_k\tilde{y}_k + 2r_v^{-1}\gamma_k\varphi_k^{\mathrm{T}}\tilde{\theta}_{k-1}v_k + 2r_v^{-2}\varphi_k^{\mathrm{T}}P_k\varphi_k\left[(e_k-\gamma_k v_k)^{\mathrm{T}}v_k + \gamma_k v_k^2\right] \\ &\quad -r_v^{-2}\varphi_k^{\mathrm{T}}P_k\varphi_k(1-r_v^{-1}\varphi_k^{\mathrm{T}}P_k\varphi_k)\tau_k^2 + 2r_v^{-2}\varphi_k^{\mathrm{T}}P_k\varphi_k(1-r_v^{-1}\varphi_k^{\mathrm{T}}P_k\varphi_k)\tau_k v_k. \end{aligned} \tag{28}$$

Note that $\varphi_k^{\mathrm{T}}\tilde{\theta}_{k-1}$, $e_k-\gamma_k v_k$, $\varphi_k^{\mathrm{T}}P_k\varphi_k$ and τ_k are uncorrelated with v_k and F_{k-1}-measurable. Thus taking the conditional expectation of both sides of (28) with respect to F_{k-1} gives

$$\begin{aligned} \mathrm{E}(V_k \mid \mathrm{F}_{k-1}) &\le V_{k-1} - 2r_v^{-1}\mu_k\mathrm{E}(\tilde{u}_k\tilde{y}_k) + 2r_v^{-1}\mu_k\mathrm{E}(\varphi_k^{\mathrm{T}}P_k\varphi_k) \\ &\quad -r_v^{-2}\mu_k\mathrm{E}\left[\varphi_k^{\mathrm{T}}P_k\varphi_k(1-r_v^{-1}\varphi_k^{\mathrm{T}}P_k\varphi_k)\right]\bar{\tau}_k^2. \end{aligned} \tag{29}$$

Consider that

$$\begin{aligned} A_z(\bar{\eta}_k - v_k) &= A_z(y_k - x_{b,k}) \\ &= B_z u_k - A_z x_{b,k} \\ &= -\varphi_k^{\mathrm{T}}\tilde{\theta}_k = \tilde{u}_k. \end{aligned}$$

Therefore, we have

$$\tilde{y}_k = \left(\frac{1}{A_z} - \frac{1}{2}\right)\tilde{u}_k.$$

In (A2), it is assumed that $\left(\frac{1}{A_z} - \frac{1}{2}\right)$ is positive real, which indicates

$$S_k := 2r_v^{-1}\sum_{i=1}^{k}\mu_k\tilde{u}_k\tilde{y}_k \ge 0, \text{ a.s.} \tag{30}$$

Adding S_k to both sides of (29) yields

$$\begin{aligned} \mathrm{E}(V_k + S_k \mid \mathrm{F}_{k-1}) &\le V_{k-1} + S_{k-1} + 2r_v^{-1}\mu_k\mathrm{E}(\varphi_k^{\mathrm{T}}P_k\varphi_k) \\ &\quad -r_v^{-2}\mu_k\mathrm{E}\left[\varphi_k^{\mathrm{T}}P_k\varphi_k(1-r_v^{-1}\varphi_k^{\mathrm{T}}P_k\varphi_k)\right]\bar{\tau}_k^2. \end{aligned} \tag{31}$$

Define a new sequence:

$$W_k = \frac{V_k + S_k}{\left(\ln \mathrm{E}\,|\,P_k^{-1}\,|\right)^c},\ c > 1. \tag{32}$$

Since $\ln \mathrm{E}\,|\,P_k^{-1}\,|$ is nondecreasing and $\varphi_k^{\mathrm{T}} P_k \varphi_k = o(1)$, there exists a k_0 such that if $k \geq k_0$ we have

$$\begin{aligned} \mathrm{E}\left(W_k \,|\, \mathrm{F}_{k-1}\right) \;\leq\; & \frac{V_{k-1} + S_{k-1}}{\left(\ln \mathrm{E}\,|\,P_k^{-1}\,|\right)^c} + \frac{2 r_v^{-1} \mu_k \mathrm{E}\left(\varphi_k^{\mathrm{T}} P_k \varphi_k\right)}{\left(\ln \mathrm{E}\,|\,P_k^{-1}\,|\right)^c} \\ & - \frac{r_v^{-2} \mu_k \mathrm{E}\left[\varphi_k^{\mathrm{T}} P_k \varphi_k (1 - r_v^{-1} \varphi_k^{\mathrm{T}} P_k \varphi_k)\right] \overline{\tau}_k^2}{\left(\ln \mathrm{E}\,|\,P_k^{-1}\,|\right)^c} \\ \leq\; & W_{k-1} + \frac{2 r_v^{-1} \mu_k \mathrm{E}\left(\varphi_k^{\mathrm{T}} P_k \varphi_k\right)}{\left(\ln \mathrm{E}\,|\,P_k^{-1}\,|\right)^c} \\ & - \frac{r_v^{-2} \mu_k \mathrm{E}\left(1 - r_v^{-1} \varphi_k^{\mathrm{T}} P_k \varphi_k\right) \overline{\tau}_k^2}{\left(\ln \mathrm{E}\,|\,P_k^{-1}\,|\right)^c}. \end{aligned} \tag{33}$$

From (12) we have

$$\mathrm{E}\left(1 - r_v^{-1} \varphi_k^{\mathrm{T}} P_k \varphi_k\right) > 0.$$

Also note that by Lemma 4.2 the summation of the third term in (33) from 0 to ∞ is finite. Therefore, Theorem 4.1 is applicable, and it gives

$$\sum_{k=1}^{\infty} \frac{r_v^{-2} \mu_k \mathrm{E}\left(1 - r_v^{-1} \varphi_k^{\mathrm{T}} P_k \varphi_k\right) \overline{\tau}_k^2}{\left(\ln E\,|\,P_k^{-1}\,|\right)^c} < \infty \ \text{ a.s.} \tag{34}$$

Further, Lemma 4.1 indicates

$$\sum_{k=1}^{\infty} \frac{r_v^{-2} \mu_k \mathrm{E}\left(1 - r_v^{-1} \varphi_k^{\mathrm{T}} P_k \varphi_k\right) \overline{\tau}_k^2}{\left(\ln \mathrm{E} r_k\right)^c} < \infty \ \text{ a.s.} \tag{35}$$

As $\left[1 - r_v^{-1} \mathrm{E}\left(\varphi_k^{\mathrm{T}} P_k \varphi_k\right)\right]$ is positive and nondecreasing, it holds that $1 = O\left[1 - r_v^{-1} \mathrm{E}\left(\varphi_k^{\mathrm{T}} P_k \varphi_k\right)\right]$. Hence,

$$\sum_{i=1}^{\infty} \frac{\overline{\tau}_i^2}{\left(\ln \mathrm{E} r_i\right)^c} < \infty \ \text{ a.s.} \tag{36}$$

Since $\lim_{k \to \infty} \ln \mathrm{E} r_k = \infty$, then from the Kronecker lemma [15] it follows that

$$\lim_{k\to\infty}\Delta_k = 0, \text{ a.s.},$$

where

$$\Delta_k := \frac{1}{(\ln \mathrm{E} r_k)^c}\sum_{i=1}^{k}\bar{\tau}_i^2.$$

With

$$r_k = \frac{n}{p_0} + \sum_{i=1}^{k} r_v^{-1}\gamma_i\varphi_i^{\mathrm{T}}\varphi_i$$

and (23), we obtain

$$\begin{aligned}\frac{1}{k}\sum_{i=1}^{k}\bar{\tau}_i^2 &= \frac{\Delta_k}{k}O\left[(\ln \mathrm{E} r_k)^c\right]\\ &= \frac{\Delta_k}{k}O\left[\mathrm{E}(r_k)\right]\\ &= \frac{\Delta_k}{k}O\left(\frac{n}{p_0} + n_a\sum_{i=1}^{k}\mu_i\mathrm{E}^2(z_i) + n_b\sum_{i=1}^{k}u_i^2\right)\\ &= \Delta_k O\left(\frac{1}{k}\sum_{i=1}^{k}y_i^2\right)\end{aligned} \tag{37}$$

By (22) we have

$$\frac{1}{k}\sum_{i=1}^{k}y_i^2 = O(1) + O\left(\frac{1}{k}\sum_{i=1}^{k}\eta_i^2\right). \tag{38}$$

Substituting (37) into (38) gives

$$\frac{1}{k}\sum_{i=1}^{k}y_i^2 = O(1), \text{ a.s.},$$

which implies together with (37) that

$$\lim_{k\to\infty}\frac{1}{k}\sum_{i=1}^{k}\bar{\tau}_i^2 = 0, \text{ a.s.},$$

or equivalently

$$\lim_{k\to\infty}\frac{1}{k}\sum_{i=1}^{k}(y_{r,i}-y_i+v_i)^2=0,\ \text{a.s.} \tag{39}$$

Since

$$\begin{aligned}\mathrm{E}\left\{(y_{r,k}-y_k+v_k)^2\,|\,\mathrm{F}_{k-1}\right\} &= \mathrm{E}[(y_{r,k}-y_k)^2+2y_{r,k}v_k\ -2y_kv_k+v_k^2\,|\,\mathrm{F}_{k-1}]\\ &= \mathrm{E}[(y_{r,k}-y_k)^2\,|\,\mathrm{F}_{k-1}]+0-2r_v+r_v\\ &= \mathrm{E}[(y_{r,k}-y_k)^2\,|\,\mathrm{F}_{k-1}]-r_v,\ \text{a.s.},\end{aligned}$$

and $\gamma_k z_k=\gamma_k y_k$, we have

$$\lim_{k\to\infty}\frac{1}{k}\sum_{i=1}^{k}\mu_i\mathrm{E}\left\{(z_i-y_{r,i})^2\,|\,\mathrm{F}_{i-1}\right\}=\lim_{k\to\infty}\frac{1}{k}\sum_{i=1}^{k}\mu_i\mathrm{E}\left\{(y_i-y_{r,i})^2\,|\,\mathrm{F}_{i-1}\right\}=r_v,\ \text{a.s.}$$

This completes the proof. □

5. Illustrative Examples

In this section, we give three examples to illustrate the adaptive control design scheme proposed in the previous sections.
The OE model shown in Fig. 2 in the simulation is chosen as

$$y_k=\frac{b_0+b_1z^{-1}+b_2z^{-2}}{1+a_1z^{-1}+a_2z^{-2}}u_k+v_k,$$

which is assumed to be placed in a network environment (Fig. 1) with randomly missing output measurements and unknown model parameters. $\{v_k\}$ is a Gaussian white noise sequence with zero mean and variance $r_v=0.05^2$. The parameter vector $\theta=[a_1\ a_2\ b_0\ b_1\ b_2]^{\mathrm{T}}$ is to be estimated. Here, true values of θ are

$$\theta=[-0.3\ 0.6\ 0.5\ 0.2\ 0.34]^{\mathrm{T}}.$$

For simulation purposes, we assume that: (1) θ is unknown and initialized by ones; (2) the output measurement $\{y_k\}$ is subject to randomly missing when transmitted to the controller node; (3) the availability of the output measurements (y_k) at the controller node is characterized by the probability μ_k; (4) The desired output signal to be tracked is a square wave alternating between -1 and 1 with a period of 1000. Mathematically, it is given by

$$y_{r,(500i+j)}=(-1)^{i+1},\ i=0,1,2,\cdots,\ j=1,2,...500.$$

In the following simulation studies, we carry out experiments for three different scenarios

regarding the availability of the output measurements at the controller node and the parameter variation, and examine the control performance, respectively. According to the proposed adaptive control scheme shown in Fig. 3, we apply the algorithms of the missing output estimator, model parameter estimator, and the adaptive control law to the networked control system.

Example 1: $\mu_k = 0.85$. In the first example, 85% of all the measurements are available at the controller node after network transmission from the sensor to the controller. The output response is shown in Fig. 4, from which it is observed that the output tracking performance is satisfactory. In order to take a closer observation on the model parameter estimation and output estimation, we define the relative parameter estimation error as

$$\delta_{par}\% = \frac{|\hat{\theta}_k - \theta|}{|\theta|} \times 100\%.$$

It is shown in Fig. 5 (solid blue curve) that $\delta_{par}\%$ is becoming smaller with k increasing. Comparison between the estimated outputs and true outputs during the time range $501 \le t \le 550$ is illustrated in Fig. 6: The dashed lines are corresponding to the time instants when data missing occurs, and the small circles on the top of the dashed lines represent the estimated outputs at these time instants. From Fig. 6 it can be found that the missing output estimation also exhibits good performance.

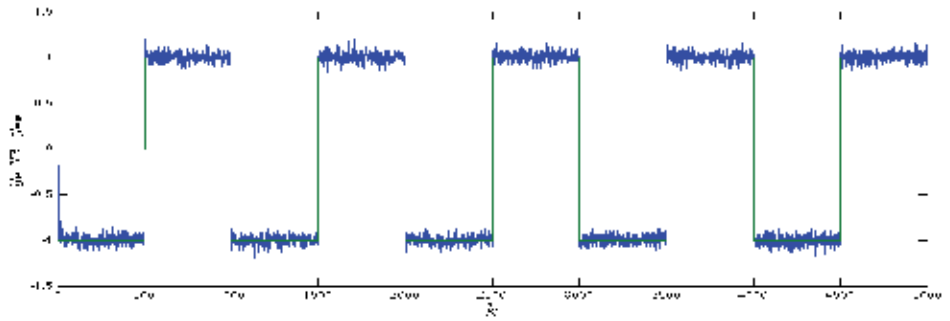

Fig. 4. Example 1: Output response when $\mu_k = 0.85$.

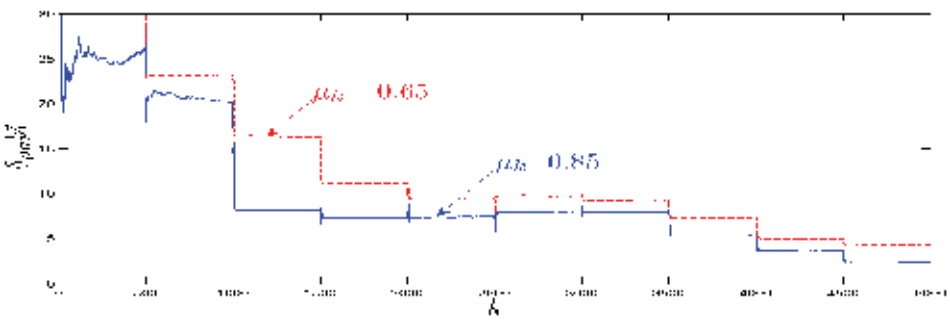

Fig. 5. Comparison of relative Parameter estimation errors for Example 1 and Example 2:

Blue solid line for Example 1; red dotted line for Example 2.

Example 2: $\mu_k = 0.65$. In the second example, a worse case subject to more severe randomly missing outputs is examined: Only 65% of all the measurements are available at the controller node. The output response is shown in Fig. 7. Even though the available output measurements are more scarce than those in Example 1, it is still observed that the output is tracking the desired signal with satisfactory performance. The relative parameter estimation error, $\delta_{par}\%$, is shown in Fig. 5 (dashed red curve). Clearly, it is decreasing when k is increasing. The estimated outputs and the true outputs are illustrated in Fig. 8, from which we can see good output estimation performance.

For the comparison purpose, the relative parameter estimation errors of these two examples are shown in Figure 5. We can see that the parameter estimation performance when $\mu_k = 0.85$ is better than that when $\mu_k = 0.65$ .It is no doubt that the estimation performance largely depends on data completeness that is characterized by μ_k .

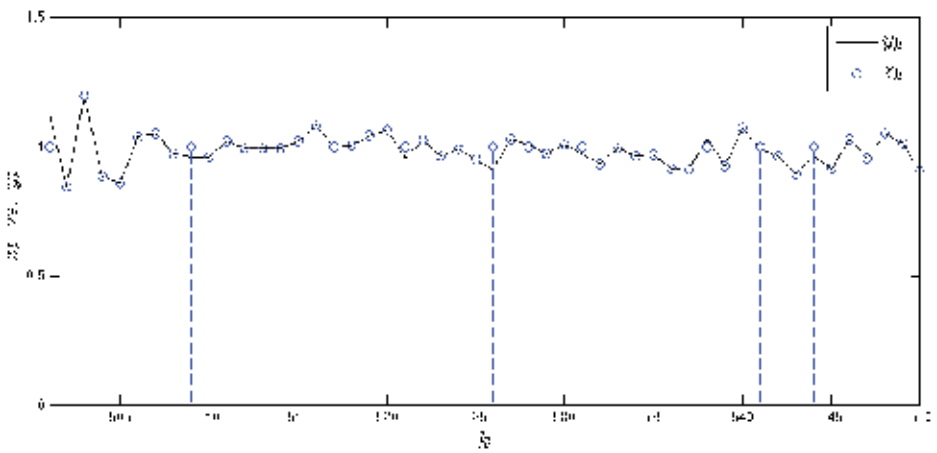

Fig. 6. Example 1: Comparison between estimated and true outputs when $\mu_k = 0.85$ (The dashed line represents output missing).

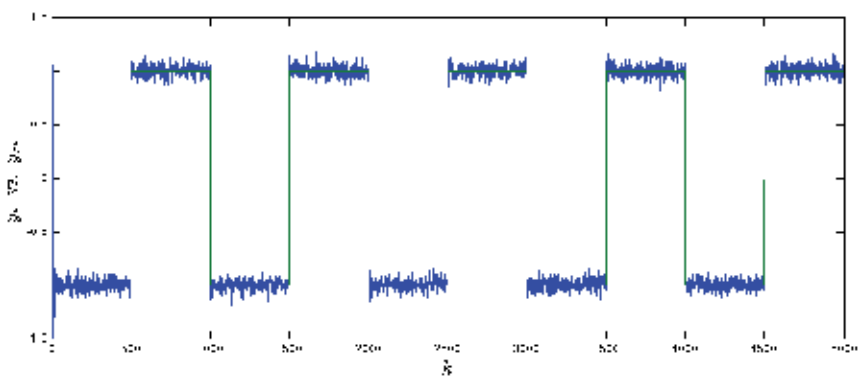

Fig. 7. Example 2: Output response when $\mu_k = 0.65$.

Example 3: Output tracking performance subject to parameter variation. In practice, the model parameters may vary during the course of operation due to the change of load, external disturbance, noise, and so on. Hence, it is also paramount to explore the robustness of the designed controller against he influence of parameter variation. In this example, we assume that at $k = 2500$, model parameters are all increased by 50%. The output response is shown in Fig. 9. It can be seen that: At $k = 2500$, the output response has a big overshoot because of the parameter variation; however, the adaptive control scheme quickly forces the system output to track the desired signal again.

Observing Figs. 4, 7, and 9 in three examples, we notice that the tracking error and oscillation still exist. This is mainly due to (1) the missing output measurements, and, (2) the relatively high noise-signal ratio (around 25%). On the other hand, it is desirable to develop new control schemes to further improve the control performance for networked systems subject to limited feedback information, which is worth to do extensive research.

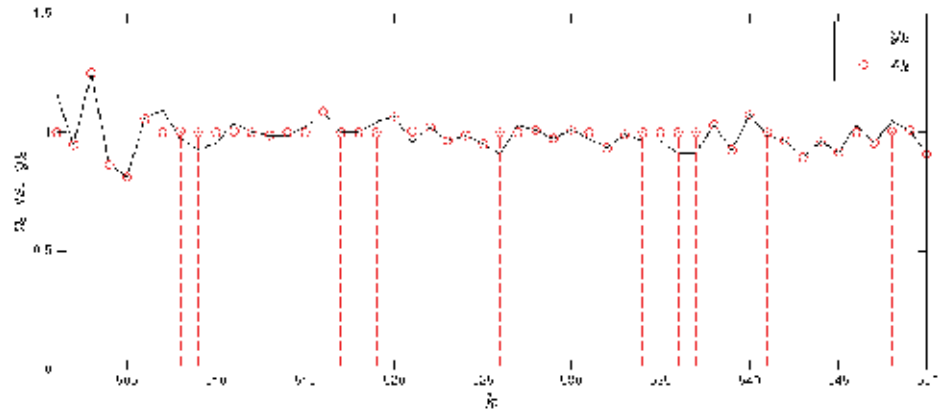

Fig. 8. Example 2: Comparison between estimated and true outputs when $\mu_k = 0.65$ (The dashed line represents output missing).

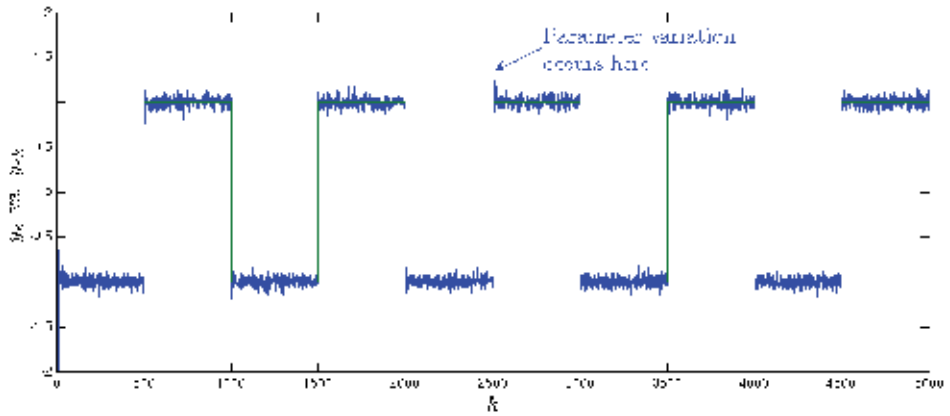

Fig. 9. Example 3: Output response subject to parameter variation: At time instant $k = 2500$, all parameters are increased by 50%.

6. Conclusion

This paper has investigated the problem of adaptive control for systems with SISO OE models placed in a network environment subject to unknown model parameters and randomly missing output measurements. The missing output estimator, Kalman filter based model parameter estimator, and adaptive controller have been designed to achieve output tracking. Convergence performance of the proposed algorithms is analyzed under the stochastic framework. Simulation examples verify the proposed methods. It is worth mentioning that the proposed scheme is developed for SISO systems in this work, and the extension to multi-input-multi-output (MIMO) systems is a subject worth further researching

7. References

Albertos, P.; Sanchis, R. & Sala A. (1999). Output prediction under scarce data operation: control applications. *Automatica*, Vol. 35, No. 10, page numbers (1671–1681), ISSN 0005-1098.

Azimi-Sadjadi, B. (2003). Stability of networked control systems in the presence of packet losses. *Proceedings of 42nd IEEE Conf. Decision & Control*, pp. 676–681, Hyatt Regency Maui, December 2003.

Branicky, M. S.; Liberatore, V. & Phillips, S. M. (2003). Networked control system co-simulation for co-design, *Proceedings of Amer. Control Conf.*, pp. 3341–3346, Denver, June 2003.

Cao, L. & Schwartz, H. M. (2003). Exponential convergence of the Kalman filter based parameter estimation algorithm. *Int. J. Adapt. Contr. & Signal Process.,* Vol. 17, No. 10, page numbers (763–784), ISSN 1099-1115.

Chen, H. F. & Guo, L. (1991). *Identification and Stochastic Adaptive Control*, Birkhauser, ISBN 0-8176-3597-1, Boston.

Chen J. M. & Chen B. S. (2000). System parameter identification with input/output noisy data and missing measurements. *IEEE Trans. Signal Processing,* Vol. 48, No. (6), page numbers (1548–1558), ISSN 1053-587X.

Chen, T. & Francis, B. (1995). *Optimal Sampled-data Control Systems*, Springer, ISBN 3-540-19949-7, London.

Chow, M. Y. & Tipsuwan, Y. (2001). Network based control systems: a tutorial, *Proceedings of IECON01: 27th Ann. Conf. IEEE Industrial Electronics Soc.*, pp. 1593–1602, Denver, Nov 2001.

Ding, F. & Chen, T. (2004a). Combined parameter and output estimation of dual-rate systems using an auxiliary model. *Automatica,*Vol. 40, No. 10, page numbers (1739–1748), ISSN 0005-1098.

Ding, F. & Chen, T. (2004b). Identification of dual-rate systems based on finite impulse response models. *Int. J. Adapt. Contr. & Signal Process.,* Vol. 18. No. 7, page numbers (589–598), ISSN 1099-1115.

Ding, F.; Chen, T. & Iwai, Z. (2006). Adaptive digital control of Hammerstein nonlinear systems with limited output sampling. *SIAM J. Control Optim.*, Vol. 45, No. 6, page numbers (2257–2276), ISSN 1095-7138.

Gao, H. & Chen, T. (2007). H_∞ estimation for uncertain systems with limited communication capcaity. *IEEE Trans. Automat. Contr.,* Vol. 52, No. 11, page numbers (2070–2084), ISSN 0018-9286.

Gao, H.; Chen, T. & Chai, TY. (2007). Passivity and passification for networked control systems. *SIAM J. Control Optim.*, Vol. 46, No. 4, page numbers (1299–1322), ISSN 1095-7138.

Gao, H.; Chen, T. & Lam, J. (2008). A new delay system approach to network-based control. *Automatica*, Vol. 44, No. 1, page numbers (39–52), ISSN 0005-1098.

Goodwin, G. C. & Sin, K. S. (1984) *Adaptive Filtering, Prediction and Control*, Prentice Hall, ISBN-13: 978-0130040695, Englewood Cliffs.

Guo, L. (1990). Estimating time-varying parameters by the Kalman filter based algorithm: stability and convergence. *IEEE Trans. Automat. Contr.,* Vol. 35, No. 2, page numbers (141–147), ISSN 0018-9286.

Hespanha, J. P.; Naghshtabrizi, P. & Xu, P. (2007). A survery of recent results in networked control systems. *Proc. of the IEEE*, Vol. 95, No. 1, page numbers (138–162), ISSN 0018- 9219.

Horn, R. A. & Johnson, C. R. (1991). *Topics in Matrix Analysis*, Cambridge University Press, ISBN-13: 9780521467131, Cambridge.

Hristu, D. & Morgansen, K. (1999). Limited communication control. *Systems & Control Letters,* Vol. 37, No. 4, page numbers (193–205), ISSN 0167-6911.

Hristu-Varsakelis, D. & Levine, W. S. (2005). *Handbook of Networked and Embedded Control Systems,* Birkhauser, ISBN: 978-0-8176-3239-7.

Hristu-Varsakelis, D. (2006). Stabilization of networked control systems with access constraints and delays. *Proceedings of 45th IEEE Conf. Decision & Control,* pp. 1123–1128, San Diego, December 2006.

Isaksson, A. J. (1993). Identification of ARX-models subject to missing data. *IEEE Trans. Automat. Contr,* Vol. 38, No. 5, page numbers (813–819), ISSN 0018-9286.

Kao, C. Y. & Lincoln, B. (2004). Simple stability criteria for systems with time-varying delays, *Automatica,* Vol. 40, No. 8, page numbers (1429–1434), ISSN 0005-1098.

Lian, F. L.; Moyne, J. & Tilbury, D. (2002). Network design consideration for distributed control systems. *IEEE Trans. Contr. Syst. Technol,* Vol. 10, No. 2, page numbers (297–307), ISSN 1558-0865.

Naghshtabrizi, P. & Hespanha, J. P. (2005). Designing an observer-based controller for a network control system. *Proceedings of 44th IEEE Conf. Decision & Control, and European Control Conf.,* pp. 848–853, Seville December 2005.

Narendra, K. S. & Annaswamy, A. M. (1989). *Stable Adaptive Systems*, Dover Publications, ISBN 9780486442266.

Nilsson, J. (1998). *Real-time Control Systems with Delays*, Ph.D. Thesis, Lund Institute of Technology.

Shi, Y.; Fang, H. & Yan, M. (2008). Kalman filter-based adaptive control for networked systems with unknown parameters and randomly missing outputs. *Int. J. Robust Nonlinear Contol*. In press, DOI: 10.1002/rnc.1390.

Sinopoli, B.; Schenato, L.; Franceschetti, M.; Poolla, K.; Jordan, M. I. & Sastry, S. S. (2004). Kalman filtering with intermittent observations. *IEEE Trans. Autom. Contr*. Vol. 49, No. 9, page numbers (1453–1464), ISSN 1558-0865.

Wallin, R.; Isaksson, A. J. & Noreus, O. (2001). Extension to "Output prediction under scarce data operation: control applications". *Automatica*, Vol. 37, No. 12, page numbers (2069–2071), ISSN 0005-1098.

Walsh, G. C. & Ye, H. (2001). Scheduling of networked control systems. *IEEE Control Syst. Mag.* Vol. 21, No. 1, page numbers (57-65), ISSN 0272-1708.

Walsh, G. C.; Ye, H. & Bushnell, L. G. (2002). Stability analysis of networked control systems. *IEEE Trans. Contr. Syst. Technol.*, Vol. 10, No. 3, page numbers (438–446), ISSN 1558-0865.

Wang, Z. D.; Yang, F.; Ho, D. W. C. & Liu, X. (2005a). Robust finite-horizon filtering for stochastic systems with missing measurements. *IEEE Signal Process. Lett.,* Vol. 12, No. 6, page numbers (437–440), ISSN: 1558-2361.

Wang, Z. D.; Yang, F.; Ho, D. W. C. & Liu, X. (2005b). Variance-constrained control for uncertain stochastic systems with missing measurement. *IEEE Trans. Syst. Man Cybern. A, Syst. Humans*, Vol. 35, No. 5, page numbers (746–753), ISSN: 1083-4427.

Wu, J. & Chen, T. (2007). Design of networked control systems with packet dropouts. *IEEE Trans. Automat. Contr.*, Vol. 52, No. 7, page numbers (1314–1319), ISSN 1558-0865.

Yang, T. C. (2006). Networked control system: a brief survey. *IEE Proc. Contr. Theory Appl.*, Vol. 153, No. 4, page numbers (403–412), ISSN 1350-2379.

Yu, M.; Wang, L.; Chu, T. & Hao, F. (2004). An LMI approach to networked control systems with data packet dropout and transmission delays, *Proceedings of 45th IEEE Conf. Decision & Control,* pp. 3545–3550, San Diego, December 2005.

Yue, D.; Han, Q. L. & Peng, C. (2004). State feedback controller design of networked control systems. *IEEE Trans. Circuits Syst. II*, Vol. 51, No. 11, page numbers (640–644), ISSN 1549-7747.

Zhang, L. & Hristu-Varsakelis, D. (2006). Communication and control co-design for networked control systems. *Automatica*, Vol. 42, No. 6, page numbers (953–958), ISSN 0005-1098.

Zhang, L.; Shi, Y.; Chen, T. & Huang, B. (2005). A new method for stabilization of networked control systems with random delays. *IEEE Trans. Automat. Contr.*, Vol. 50, No. 8, page numbers (1177–1181), ISSN 1558-0865.

Zhang, W.; Branicky, M. S. & Phillips S. M. (2001). Stability of networked control systems. *IEEE Control Syst. Mag.*, Vol. 21, No. 1, page numbers (84–99), ISSN 0272-1708.

8

Adaptive Control Based On Neural Network

Sun Wei, Zhang Lujin, Zou Jinhai and Miao Siyi
College of Electrical and Information Engineering, Hunan University
Changsha City, Hunan Province, P. R. China

1. Introduction

Neural network has good nonlinear function approximation ability. It can be widely used to identify the model of controlled plant. In this chapter, the theories of modeling uncertain plant by using two kinds of neural networks: feed-forward neural network and recurrent neural network are introduced. And two adaptive control strategies for robotic tracking control are developed. One is recurrent fuzzy neural network based adaptive control (RFNNBAC), and another is neural network based adaptive robust control (NNBARC). In RFNNBAC, a kind of recurrent fuzzy neural network (RFNN) is constructed by using recurrent neural network to realize fuzzy inference, In which, temporal relations are embedded in the network by adding feedback connections on the first layer of the network. Two RFNNs are used to identify and control plant respectively. Base on the Lyapunov stability approach, the convergence of the proposed RFNN is analyzed. In NNBARC, A robust controller and a neural network are combined into an adaptive robust robotic tracking control scheme. Neural network is used to approximate the modeling uncertainties in robotic system. Then the disadvantageous effects on tracking performance, due to the approximating error of the neural network and non-measurable external disturbances in robotic system, are attenuated to a prescribed level by robust controller. The robust controller and the adaptation law of neural network are designed based on Hamilton-Jacobi-Issacs (HJI) inequality theorem. The weights of NN are easily tuned on-line by a simple adaptation law, with no need of a tedious and lengthy off-line training phase.
This chapter is organized in the following manner. In the first section a robust robotic tracking controller based on neural network is designed and its effectiveness is proved by applying it to control the trajectories of a two-link robot. Secondly, a recurrent fuzzy neural network based adaptive control is proposed and simulation experiments are made by applying it on robotic tracing control problem to confirm its effectiveness. Finally, some conclusions are drawn.

2. A robust robotic tracking controller based on neural network

In the past decades, there has been much research on the applications of nonlinear control theory to control robots, and many useful properties of robot dynamics such as the skew-symmetry property were discovered. There are basically two strategies to control such uncertain nonlinear systems: the robust control strategy and the adaptive control strategy. A

convenient point of robust control strategy is that it can attenuate disadvantageous effects of various uncertainties (e.g., structured parametric uncertainties and unstructured disturbances) to a required level, provided that the upper bound of uncertainties is well known (Abdallah et al. 1991). However, since this strategy use max-min method to design the controller, it can not yield good transient performance. On the other hand, regressor matrixes are always used in the design of adaptive control systems for robot manipulators (Ortega & Spong 1989). In this situation, the unknown nonlinear dynamics of robotic systems are always assumed to be linearly parametrisable. However, there are some potential difficulties associated with this classical adaptive control design. For example, the unknown parameters may be quickly varying, the linear parametrisable property may not hold, computation of the regressor matrix is a time-consuming task, and implementation also requires a precise knowledge of the structure of the entire robot dynamic model (Saad et al. 1994; Sanner & Slotine 1998; Spooner & Passino 1996).

It has been shown that multi-layer neural networks can approximate any continuous function as accurately as possible. Based on this universal approximation property, many important adaptive neural-network-based control schemes have been developed to solve highly nonlinear control problem (Sanner & Slotine 1998; Spooner & Passino 1996; Narenra & Parthasarathy 1990; Polycarpou 1996). But most of these schemes use grads-descent method to train the weights, which can not ensure the stability of whole closed-loop system. In the recent years, researchers began to develop the neural-network-based controller with closed-loop stability based on the Lyapunov method. A controller based on forward propagation network was developed in (Carelli et al. 1995), but it didn't consider the effects of uncertainties. An adaptive neural network control strategy with guaranteed stability was proposed in (Behera et al. 1996) on the assumption that the approximation error of the neural network is known and bounded.

In the first part of this chapter, we will propose a neural-network-based robust robotic tracking controller according to HJI inequation theorem presented by Shen in (Shen 1996). A neural network equipped with a robust learning algorithm is introduced firstly to learn the modeling uncertainties in robotic system. Then the disadvantageous effects on tracking performance caused by neural network approximating error and non-measurable external disturbances in robotic system will be attenuated to a prescribed level by the designing a robust controller.

This section is organized as follows. In subsection 2.1, HJI inequation theorem is introduced. In subsection 2.2 the dynamics of robot system and its properties are described. The neural network based robust control strategy is proposed in subsection 2.3, where the structure of robust controller and the robust learning algorithm of neural network are derived. Simulations for a two-link robot are presented in subsection 2.4.

2.1 HJI inequation theorem

A system with non-measurable disturbance d can be formulated as:

$$\dot{x} = f(x) + g(x)d \tag{1}$$

For evaluating the disturbance restraint performance of system (1), an evaluation signal $z = h(x)$ is introduced to represent the signals need to be concerned, such as error. And a

performance index signal can be defined as:

$$J = \sup_{\|d\|_2 \neq 0} \frac{\|z\|_2}{\|d\|_2} \tag{2}$$

Obviously, smaller J means better disturbance restraint performance. The robust design problem of system (1) can be solved by designing a controller to make J less than a prescribed level.

HJI(Hamilton-Jacobi-Isaacs)InequationTheorem: Given an positive constant $\gamma > 0$, if there exists an derivable function, V(x)≥0, which satisfies the following HJI inequation:

$$\dot{V} = \frac{\partial V}{\partial x}\dot{x} = \frac{\partial V}{\partial x}f(x) + \frac{\partial V}{\partial x}g(x)d \le \frac{1}{2}\left\{\gamma^2\|d\|^2 - \|z\|^2\right\}, \forall d \tag{3}$$

then the performance index signal of system (1) is less than γ, that is to say, $J \le \gamma$.

2.2 Problem statement

The kinetics equation of a robotic manipulator with uncertainties can be expressed as:

$$M(q)\ddot{q} + V(q,\dot{q})\dot{q} + G(q) + \Delta T(q,\dot{q}) + d_R = T \tag{4}$$

where $q, \dot{q}, \ddot{q} \in R^n$ is the joint position, velocity, and acceleration vectors; $M(q) \in R^{n\times n}$ denotes the moment of inertia; $V(q,\dot{q})\dot{q}$ are the Coriolis and centripetal forces; $G(q)$ includes the gravitational forces; T is the applied torque; $\Delta T(q,\dot{q})$ represents the modelling uncertainties in robotic system, and d_R is external non-measurable disturbance.

It is well known that the robot dynamics has the following properties.

Property 1— Boundedness of the Inertia matrix: The inertia matrix $M(q)$ is symmetric and positive definite, and satisfies the following inequalities:

$$0 < \lambda_m I \le M(q) \le \lambda_M I \tag{5}$$

where λ_m and λ_M are known positive constants.

Property 2—Skew symmetry: The inertia and centripetal-Coriolis matrices have the following property:

$$\xi^T\{\dot{M}(q) - 2V(q,\dot{q})\}\xi = 0, \forall \xi \in R^n \tag{6}$$

Property 1 is very important in generating a positive definite function to prove the stability of the closed-loop system. Property 2 will help in simplifying the controller.

The aim of this paper is to design a neural-network-based robust controller (NNBRC) for the robot system under uncertainties, such that closed-loop system is guaranteed to be stable

and the joint position $q(t)$ can track the desired trajectory $q_d(t)$ rapidly and accurately.

2.3 Design of NNBRC

A NNBRC is proposed in this section. In the proposed strategy, a neural network (NN) is firstly used for identifing modelling uncertainties $\Delta T(q,\dot{q})$, then, a robust learning algorithm and a robust controller are designed based on HJI equation theorem to counteract the disadvantageous effects caused by approximation error of the NN and external disturbance d_R.

2.3.1 Construction of the neural network

A three-layer NN is shown in Fig.1.Using $u_i^{(1)}, o_i^{(1)}$ to denote the input and output of the ith node in the lth layer separately, the signal propagation and the operation functions of the nodes in each layer are introduced as follows.

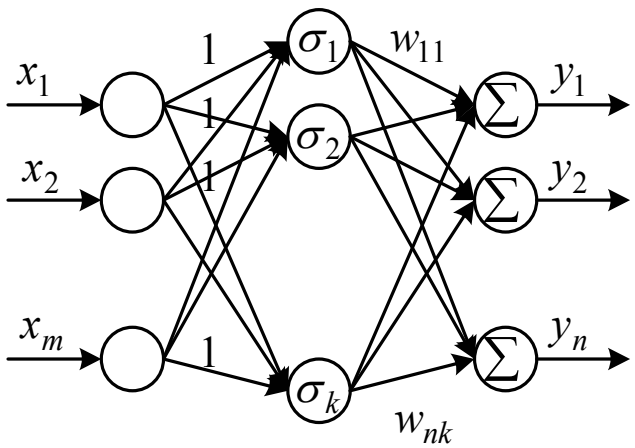

Fig. 1. Structure of three-layer NN

Layer 1 – Input Layer:

$$o_i^{(1)} = u_i^{(1)} = x_i, i = 1,2,\cdots,m \tag{7}$$

Layer 2 – Hidden Layer:

$$u_j^{(2)} = \sum_{i=1}^{m} o_i^{(1)}, \ j = 1,2,\cdots,k \tag{8}$$

$$o_j^{(2)} = \sigma_j = 1/[1+\exp(-u_j^{(2)})], j = 1,2,\cdots,k \tag{9}$$

Layer 3 – Output Layer:

$$y_h = o_h^{(3)} = u_h^{(3)} = \sum_{j=1}^{k} w_{hj} \cdot o_j^{(2)}, h = 1,2,\cdots,n \tag{10}$$

Let

$$W = \begin{bmatrix} w_{11} & w_{12} & \cdots & w_{1k} \\ w_{21} & w_{22} & \cdots & w_{2k} \\ \vdots & \vdots & \vdots & \vdots \\ w_{n1} & w_{n2} & \cdots & w_{nk} \end{bmatrix}, \sigma = \begin{bmatrix} \sigma_1 \\ \sigma_2 \\ \vdots \\ \sigma_k \end{bmatrix}, Y = \begin{bmatrix} y_1 \\ y_2 \\ \vdots \\ y_n \end{bmatrix}$$

then the outputs of the three-layer NN can be written as:

$$Y = W\sigma \tag{11}$$

In this paper, the three-layer NN described above will be used to identify the modeling uncertainties $\Delta T(q,\dot{q})$ in robotic system. Using ε_T to denote the network approximation error, then the modeling uncertainties can be denoted by:

$$\Delta T\ (q,\dot{q}) = W_T\sigma_T + \varepsilon_T \Delta T(q,\dot{q}) \tag{12}$$

where W_T is the weight matrix, σ_T is the activation function vector.
Substitute (12) into (4), then the dynamics of the robot manipulator with a NN identifier can be formulated as:

$$M(q)\ddot{q} + V(q,\dot{q})\dot{q} + G(q) + W_T\sigma_T + \varepsilon_T + d_R = T \tag{13}$$

Regarding ε_T as another external disturbance of robotic system, and using $\varepsilon_R = \varepsilon_T + d_R$, then (13) can be rewritten as:

$$M(q)\ddot{q} + V(q,\dot{q})\dot{q} + G(q) + W_T\sigma_T + \varepsilon_R = T \tag{14}$$

For attenuating disadvantageous effects caused by ε_R to a prescribed level, a robust learning algorithm of NN and a robust controller can be designed based on HJI equation as below 2.3.2.

2.3.2 Robust controller and NN learning algorithm

At first, we introduce a control signal u, which satisfies:

$$M(q)\ddot{q}_d + V(q,\dot{q})\dot{q}_d + G(q) + u = T \tag{15}$$

where $q_d, \dot{q}_d, \ddot{q}_d \in R^n$ is desired joint position, velocity, and acceleration vectors separately.

Thus, the closed-loop robot control system can be constructed by substituting (15) into (14). Let $e = q - q_d$, the closed-loop system can be formulated as:

$$M(q)\ddot{e} + V(q,\dot{q})\dot{e} + W_T\sigma_T + \varepsilon_R = u \tag{16}$$

By regarding ε_R as external disturbance and introducing the evaluation signal $z_R = pe$, where p is a positive constant, we can define the index signal as:

$$J_R = \sup_{\|\varepsilon_R\|_2 \neq 0} \frac{\|z_R\|_2}{\|\varepsilon_R\|_2} \tag{17}$$

The idea of NNBRC is to design controller u and the NN learning algorithm $\dot{W}_T$ such that J_R is less than a prescribed level, γ.
Define two state variables as:

$$\begin{cases} x_1 = e \\ x_2 = \dot{e} + \alpha e \end{cases} \tag{18}$$

where α is an prescribed positive constant. Thus, system (16) can be rewritten as:

$$\begin{cases} \dot{x}_1 = x_2 - \alpha x_1 \\ M\dot{x}_2 = -Vx_2 + \omega - W_T\sigma_T - \varepsilon_R + u \end{cases} \tag{19}$$

where $\omega = M\alpha\dot{e} + V\alpha e$, W_T is a $n \times k$ matrix that can be described as:

$$W_T = \begin{bmatrix} w_{T11} & w_{T12} & \cdots & w_{T1k} \\ w_{T21} & w_{T22} & \cdots & w_{T2k} \\ \vdots & \vdots & \vdots & \vdots \\ w_{Tn1} & w_{Tn2} & \cdots & w_{Tnk} \end{bmatrix} = \begin{bmatrix} w_{T1} & w_{T2} & \cdots & w_{Tk} \end{bmatrix}$$

Theorem 1: Considering system (19), if the learning algorithm of NN is:

$$\dot{W}_T = -\eta W_T \tag{20}$$

The controller u is designed as:

$$u = -x_1 - \omega + W_T\sigma_T - \left(\varepsilon_2 + \frac{1}{2Y^2}\right)x_2 \tag{21}$$

and the parameter p in the *evaluation signal*, $z_R = pe = px_1$, satisfies:

$$\alpha - \frac{1}{2}p^2 = \varepsilon_1 \tag{22}$$

where $\varepsilon_1, \varepsilon_2$ and η are all prescribed positive constant, then the disturbance restraint index signal of system (19), J_R, is less than γ.

Proof: Considering system (19), we define the following derivable function:

$$L = \frac{1}{2}\cdot x_1^T \cdot x_1 + \frac{1}{2}\cdot x_2^T \cdot M \cdot x_2 + \frac{1}{2}\cdot \|W_T\|^2 \tag{23}$$

Thus,

$$\begin{aligned}\dot{L} &= x_1^T \dot{x}_1 + x_2^T M \dot{x}_2 + \frac{1}{2}x_2^T \dot{M} x_2 + \sum_{i=1}^{m} w_{Ti}^T \dot{w}_{Ti} \\ &= x_1^T (x_2 - \alpha x_1) + x_2^T (\omega - W_T \sigma_T - \varepsilon_R + u) \\ &\quad + \frac{1}{2}x_2^T (\dot{M} - 2V) x_2 + \sum_{i=1}^{m} w_{Ti}^T \dot{w}_{Ti}\end{aligned}$$

According to Property 2 of the robot dynamics, the above equation can be rewritten as:

$$\begin{aligned}\dot{L} &= x_1^T (x_2 - \alpha x_1) + x_2^T (\omega - w_T \sigma_T - \varepsilon_R + u) + \sum_{i=1}^{m} w_{Ti}^T \dot{w}_{Ti} \\ &= -x_1^T \alpha x_1 + x_2^T (x_1 + \omega - w_T \sigma_T - \varepsilon_R + u) + \sum_{i=1}^{m} w_{Ti}^T \dot{w}_{Ti}\end{aligned}$$

Substituting (20) into above equation, then

$$\dot{L} = -x_1^T \alpha x_1 + x_2^T (x_1 + \omega - W_T \sigma_T - \varepsilon_R + u) - \eta \|W_T\|^2$$

Regarding ε_R as external disturbance, let

$$\begin{aligned}H &= \dot{L} - \frac{1}{2}\gamma^2 \|\varepsilon_R\|^2 + \frac{1}{2}\|z_R\|^2 \\ &= -\alpha \|x_1\|^2 + x_2^T (x_1 + \omega - W_T \sigma_T + u) - x_2^T \varepsilon_R \\ &\quad - \eta \|W_T\|^2 - \frac{1}{2}\gamma^2 \|\varepsilon_R\|^2 + \frac{1}{2}p^2 \|x_1\|^2 \\ &= -\left(\alpha - \frac{1}{2}p^2\right)\|x_1\|^2 + x_2^T (x_1 + \omega - W_T \sigma_T + u) \\ &\quad - x_2^T \varepsilon_R - \eta \|W_T\|^2 - \frac{1}{2}\gamma^2 \|\varepsilon_R\|^2\end{aligned}$$

$$\because -2x_2^T\varepsilon_R - \gamma^2\|\varepsilon_R\|^2 = -\left\{2x_2^T\varepsilon_R + \gamma^2\|\varepsilon_R\|^2\right\}$$

$$= -\left\{\frac{1}{\gamma^2}\|x_2\|^2 + 2x_2^T\varepsilon_R + \gamma^2\|\varepsilon_R\|^2 - \frac{1}{\gamma^2}\|x_2\|^2\right\}$$

$$= -\left\{\left\|\frac{1}{\gamma}x_2 + \gamma\varepsilon_R\right\|^2 - \frac{1}{\gamma^2}\|x_2\|^2\right\}$$

$$= -\left\|\frac{1}{\gamma}x_2 + \gamma\varepsilon_R\right\|^2 + \frac{1}{\gamma^2}\|x_2\|^2$$

$$\le \frac{1}{\gamma^2}\|x_2\|^2$$

$$\therefore -x_2^T\varepsilon_R - \frac{1}{2}\gamma^2\|\varepsilon_R\|^2 \le \frac{1}{2\gamma^2}\|x_2\|^2$$

$$H \le -\left(\alpha - \frac{1}{2}p^2\right)\|x_1\|^2 + x_2^T\left(x_1 + \omega - W_T\sigma_T + u\right) - \eta\|W_T\|^2 + \frac{1}{2\gamma^2}\|x_2\|^2$$

$$= -\left(\alpha - \frac{1}{2}p^2\right)\|x_1\|^2 + x_2^T\left(x_1 + \omega - W_T\sigma_T + u + \frac{1}{2\gamma^2}x_2\right) - \eta\|W_T\|^2$$

Substituting (21), (22) into above inequation, then

$$H \le -\varepsilon_1\|x_1\|^2 - \varepsilon_2\|x_2\|^2 - \eta\|W_T\|^2 \le 0$$

$$\therefore \dot{L} \le \frac{1}{2}\left\{\gamma^2\|\varepsilon_R\|^2 - \|z_R\|^2\right\}$$

According to HJI equation theorem, we can conclude that the disturbance restraint performance index signal of system (19), J_R, is less than γ. The structure of the proposed neural network based robust control strategy is illustrated in Fig. 2.

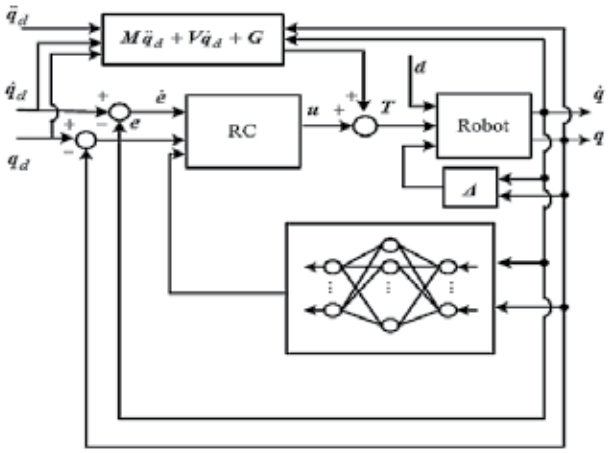

Fig. 2. Structure of the NN-based robust tracking control system

2.4 Simulation example

In this section, the proposed control strategy will be applied to control the trajectory of a two-link robot (see Fig. 3) for proving its effectiveness.

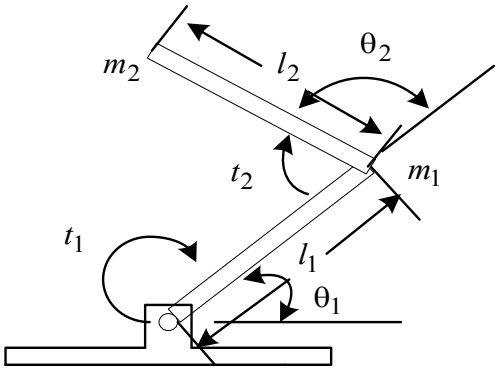

Fig. 3. Two-link robot

In Fig.3, m1and m2 are masses of arm1 and arm2 respectively; l1 and l2 are lengths of arm1 and arm2; t1 and t2 are torques on arm1 and arm2; θ_1 and θ_2 are positions of arm1 and arm2. The dynamics model of two-link robot is same as (4).
Let

$$q = [\theta_1 \quad \theta_2]^T,\ \dot{q} = [\dot{\theta}_1 \quad \dot{\theta}_2]^T \tag{24}$$

$$\ddot{q} = [\ddot{\theta}_1 \quad \ddot{\theta}_2]^T,\ T = [t_1 \quad t_2]^T \tag{25}$$

$$c_i \equiv \cos\theta_i,\ s_i \equiv \sin\theta_i,\ c_{ij} \equiv \cos(\theta_i + \theta_j) \tag{26}$$

then M, V,G in (4) can de described as:

$$M(q) = \begin{bmatrix} m_1 l_1^2 + m_2(l_1^2 + l_2^2 + 2l_1 l_2 c_2) & m_2 l_2^2 + m_2 l_1 l_2 c_2 \\ m_2 l_2^2 + m_2 l_1 l_2 c_2 & m_2 l_2^2 \end{bmatrix} \tag{27}$$

$$V(q,\dot{q}) = \begin{bmatrix} -2m_2 l_1 l_2 s_2 \dot{q}_2 & -m_1 l_1 l_2 s_2 \dot{q}_2 \\ m_2 l_1 l_2 s_2 \dot{q}_1 & 0 \end{bmatrix} \tag{28}$$

$$G(q) = \begin{bmatrix} m_2 l_2 g c_{12} + (m_1 + m_2) l_1 g c_1 \\ m_2 l_2 g c_{12} \end{bmatrix} \tag{29}$$

In this paper, the parameters of the two-link robot are $m_1 = 10$ kg, $m_2 = 2$ kg, $l_1 = 1.1$ m, and $l_2 = 0.8$ m. The Initial states are $q(0) = [0.5 \quad 0.5]$ rad, $\dot{q}(0) = [0 \quad 0]^T$ rad/s, and $\ddot{q}(0) = [0 \quad 0]^T$ rad/s². The desired trajectories can be described as:

$$q_d(t) = [\sin(2\pi t) \quad \cos(2\pi t)]^T \text{ rad} \tag{30}$$

$$\dot{q}_d(t) = [2\pi\cos(2\pi t) \quad -2\pi\sin(2\pi t)]^T \text{ rad/s} \tag{31}$$

$$\ddot{q}_d(t) = [-4\pi^2\sin(2\pi t) \quad -4\pi^2\cos(2\pi t)]^T \text{ rad/s}^2 \tag{32}$$

The model error due to friction is assumed as:

$$\Delta T = \begin{bmatrix} 0.5\,\text{sign}(\dot{e}_1)[0.1 + \exp(-|\dot{e}_1|)] \\ \text{sign}(\dot{e}_2)[0.2 + \exp(-|\dot{e}_2|)] \end{bmatrix} \text{ N·m} \tag{33}$$

The external disturbance, $d_R = [d_1 \quad d_2]^T$ is a random signal which amplitude is less than 10N·m. In simulations, the NNBRC can be designed based on (21), in which $\alpha = 50$, $\varepsilon_1 = 0.1$, $\varepsilon_2 = 0.1$, $\gamma = 0.05$, $p = 9$. The NN learning algorithm is designed according to (20), where $\eta = 0.1$.

Fig.4 and Fig.5 present the simulation experiment results, in which, proposed control strategy is compared to traditional robust control (TRC) strategy. From these results, we can conclude that the NN-based robust tracking control strategy proposed in this paper can counteract disadvantageous effects caused by uncertainties in robotic system efficiently, and can achieve better transient performance than traditional robust control.

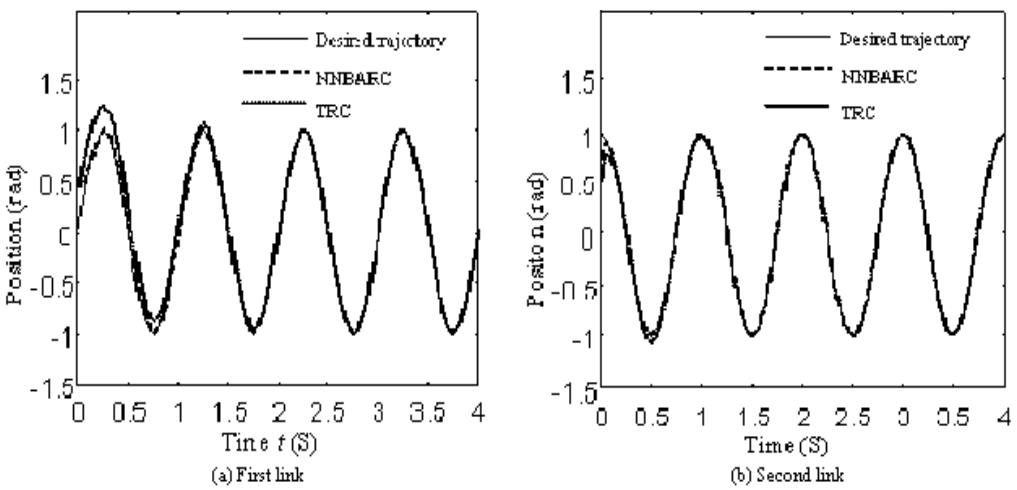

Fig. 4. Robot trajectories

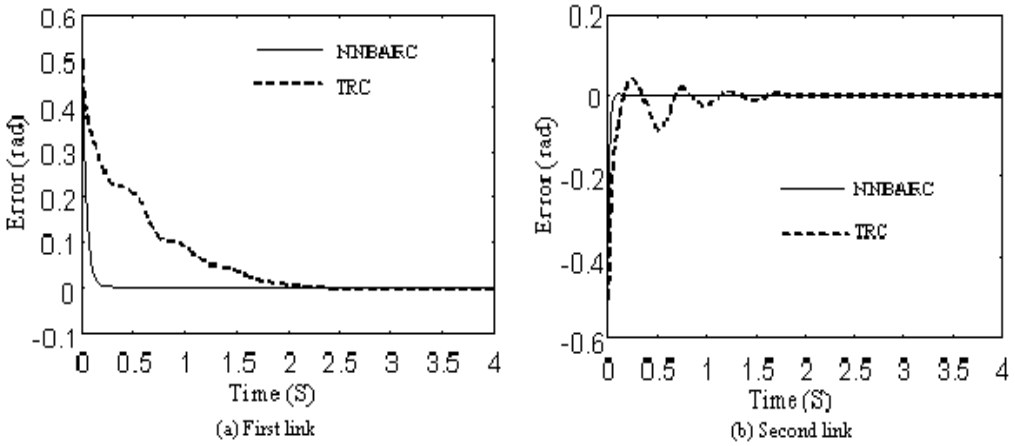

Fig. 5. Robot tracking errors

3. A Recurrent Fuzzy Neural Network Based Adaptive Control

Recently, much research has been done on using neural networks (NN) to identify and control dynamic systems (Park et al. 1996; Narendra & Parthasarathy 1990; Brdys & Kulawski 1999). NN can be classified as feed forward neural networks and recurrent neural networks. Feed forward neural networks can approximate a continuous function to an arbitrary degree of accuracy. However, feed forward neural network is a static mapping; it can not represent a dynamic mapping. Although this problem can be solved by using tapped delays, feed forward neural network requires a large number of neurons to represent dynamical responses in the time domain. Moreover, since the weight updates of feed forward neural network is irrelative to the internal information of neural network, the function approximation is sensitive to the training data. On the other hand, recurrent neural networks (Ku & Lee 1995; Ma & Ji 1998; Sundareshan & Condarcure 1998; Liang & Wang 2000) are able to represent dynamic mapping very well and store the internal information for updating weights later. Recurrent neural network has an internal feedback loop; it captures the dynamical response of a system without external feedback through delays. Recurrent neural network is a dynamic mapping and demonstrates good performance in the presence of uncertainties, such as parameter variations, external disturbance, unmodeled and nonlinear dynamics. However, the drawbacks of recurrent neural network, which are same as neural network, are that the function of the network is difficult to interpret and few efficient constructive methods can be found for choosing network structure and determining the parameters of neurons.

As is widely known, both fuzzy logic systems and neural network systems are aimed at exploiting human-like knowledge processing capability. In recent years, researchers started to recognize that fuzzy control has some similarities to neural network (Jang & Sun 1993; Hunt et al. 1996; Buckley et al. 1993; Reyneri 1999). Fuzzy neural network (FNN), which uses NN to realize fuzzy inference, combines the capability of fuzzy reasoning in handling uncertain information and the capability of neural networks in learning from processes. It is

possible to train NN using the experience of human operators expressed in term of linguistic rules, and interpret the knowledge that NN acquired from training data in linguistic form. And it is very easy to choose the structure of NN and determine the parameters of neurons from linguistic rules. However, a major drawback of the FNN is that its application domain is limited to static problems due to its feed forward network structure.

Recurrent fuzzy neural network (RFNN) is a modified version of FNN, which use recurrent network for realizing fuzzy inference and can be constructed from a set of fuzzy rules. It inherits all characteristics of FNN such as fuzzy inference, universal approximation and convergence properties. Moreover, with its own internal feedback connections, RFNN can temporarily store dynamic information and cope with temporal problems efficiently. For this ability to temporarily store information, the structure of RFNN is much simpler than FNN. Fewer nodes are required in RFNN for system identification.

In this section, a recurrent fuzzy neural network structure is proposed, in which, the temporal relations are embedded by adding feedback connections on the first layer of FNN. Back propagation algorithm is used to train the proposed RFNN. To guarantee the convergence of the RFNN, the Lyapunov stability approach is applied to select appropriate learning rates. For control problem, an adaptive control scheme is proposed, in which, two proposed RFNN are used to identify and control plant respectively. Finally, simulation experiments are made by applying proposed adaptive control scheme on robotic tracking control problem to confirm its effectiveness.

This section is organized as follows. In subsection 3.2, RFNN is constructed. The construction of RFNNBAC is presented in subsection 3.3. Learning algorithms of RFNN are derived in subsection 3.4. Stability of RFNN is analyzed in subsection 3.5. In subsection 3.6 proposed RFNNBAC is applied on robotic tracking control and simulation results are given. Finally, some conclusions are drawn in subsection 3.7.

3.1 Construction of RFNN

The structure of the proposed RFNN is shown in Fig. 6, which comprises n input variables, m term nodes for each input variable, l rule nodes, and p output nodes. This RFNN thus consists of four layers and $n + (n \times m) + l + p$ nodes.

Using u_i^k , O_i^k to denote the input and output of the ith node in the kth layer separately, the signal propagation and the operation functions of the nodes in each layer are introduced as follows.

Layer 1 (Input Layer): This layer accepts input variables. Its nodes transmit input values to the next layer. Feedback connections are added in this layer to embed temporal relations in the network. For every node in this layer, the input and output are represented as:

$$u_i^1(k) = x_i^1(k) + w_i^1 O_i^1(k-1), O_i^1(k) = u_i^1(k), i = 1,2,\cdots,n \tag{34}$$

where k is the number of iterations; w_i^1 is the recurrent weights.

Layer 2 (Membership Layer): Nodes in this layer represent the terms of respective linguistic variables. Each node performs a Gaussian membership function

$$u_{ij}^2 = -\frac{(O_i^1 - a_{ij})^2}{(b_{ij})^2}, O_{ij}^2 = \exp(u_{ij}^2) \tag{35}$$

where $i = 1,2,\cdots,n$, $j = 1,2,\cdots,m$; a_{ij} and b_{ij} are the mean and the standard deviation of the Gaussian membership function; the subscript ij indicates the jth term of the ith input variable.

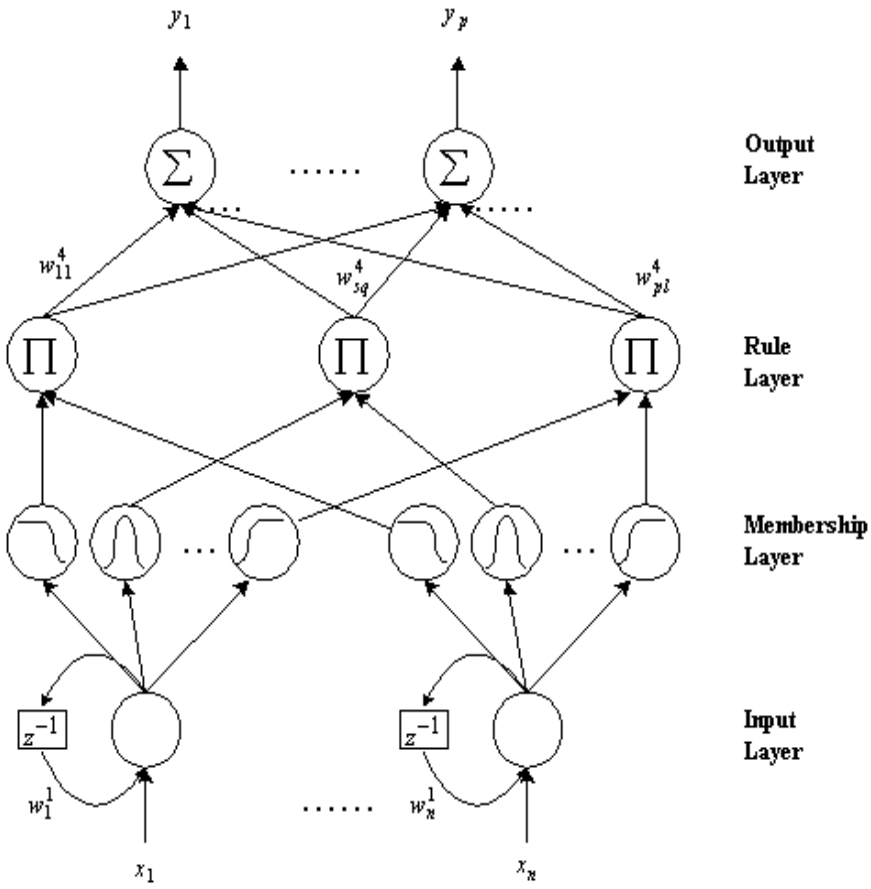

Fig. 6. Structure of four-layer RFNN

Layer 3(Rule Layer): This layer forms the fuzzy rule base and realizes the fuzzy inference. Each node is corresponding to a fuzzy rule. Links before each node represent the preconditions of the corresponding rule, and the node output represents the "firing strength" of corresponding rule.
If the qth fuzzy rule can be described as:

qth rule: if x_1 is A_1^q, x_2 is A_2^q, … , x_n is A_n^q then y_1 is B_1^q, y_2 is B_2^q, … , y_p is B_p^q, where A_i^q is the term of the ith input in the qth rule; B_j^q is the term of the jth output in the qth rule.

Then, the qth node of layer 3 performs the AND operation in qth rule. It multiplies the input signals and output the product.

Using $O_{iq_i}^2$ to denote the membership of x_i to A_i^q, where $q_i \in \{1,2,\cdots,m\}$, then the input and output of qth node can be described as:

$$u_q^3 = \prod_i O_{iq_i}^2 \ , O_q^3 = u_q^3, i = 1,2,\cdots,n; q = 1,2,\cdots,l \tag{36}$$

Layer 4(Output Layer): Nodes in this layer performs the defuzzification operation. the input and output of sth node can be calculated by:

$$u_s^4 = \sum_q w_{sq}^4 O_q^3 \ , \ O_s^4 = \frac{u_s^4}{\sum_q O_q^3} \tag{37}$$

where $s = 1,2,\cdots,p$, $q = 1,2,\cdots,l$, w_{sq}^4 is the center of B_j^q , which represents the output action strength of the sth output associated with the qth rule.

From the above description, it is clear that the proposed RFNN is a fuzzy logic system with memory elements in first layer. The RFNN features dynamic mapping with feedback and more tuning parameters than the FNN. In the above formulas, if the weights in the feedback unit w_i^1 are all equal to zero, then the RFNN reduces to an FNN. Since a fuzzy system has clear physical meaning, it is very easy to choose the number of nodes in each layer of RFNN and determine the initial value of weights. Note that the parameters w_i^1 of the feedback units are not set from human knowledge. According to the requirements of the system, they will be given proper values representing the memorized information. Usually the initial values of them are set to zero.

3.2 Structure of RFNNBAC

In this section, the structure of RFNNBAC will be developed below, in which, two proposed RFNN are used to identify and control plant respectively.

3.2.1 Identification based on RFNN

Resume that a system to be identified can be modeled by an equation of the following form:

$$y(k) = f\left(y(k-1),\cdots y\left(k-n_y\right), u(k),\cdots, u\left(k-n_u\right)\right) \tag{38}$$

where u is the input of the system, n_y is the delay of the output, and n_u is the delay of the input.
Feed forward neural network can be applied to identify above system by using y(k-1),… ,y(k-n-1), u(k), … , u(k-m) as inputs and approximating the function f.
For RFNN, the overall representation of inputs x and the output y can be formulated as

$$y(k) = g(O_1^1(k), \cdots, O_n^1(k)) \tag{39}$$

Where

$$\begin{aligned} O_i^1(k) &= x_i(k) + w_i^1(k) O_i^1(k-1) \\ &= x_i(k) + w_i^1(k)\left[x_i(k-1) + w_i^1(k-1) O_i^1(k-2)\right] \\ &\quad \vdots \\ &= x_i(k) + w_i^1(k) x_i(k-1) + w_i^1(k) w_i^1(k-1) x_i(k-2) + \cdots \\ &\quad + w_i^1(k) w_i^1(k-1) \cdots w_i^1(1) x_i(0) \end{aligned}$$

Using the current input u(k) and the most recent output y(k-1) of the system as the inputs of RFNN, (39) can be modified as:

$$\hat{y}(k) = \hat{f}(y(k-1), \cdots, y(0), u(k), \cdots, u(0)) \tag{40}$$

By training the RFNN according to the error e(k) between the actual system output and the RFNN output, the RFNN will estimate the output trajectories of the nonlinear system (38). The training model is shown in Fig.7.

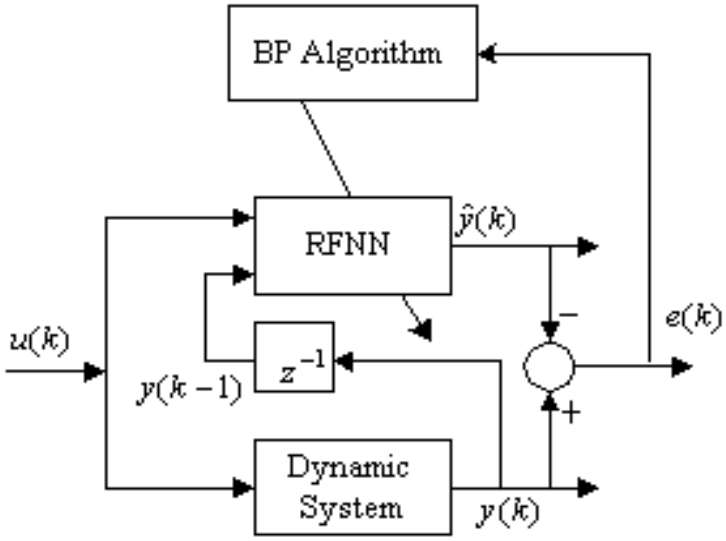

Fig. 7. Identification of dynamic system using RFNN

From above description, For Using RFNN to identify nonlinear system, only y(k-1) and u(k) need to be fed into the network .This simplifies the network structure, i. e., reduces the number of neurons

3.2.2 RFNNBAC

The block diagram of RFNNBAC is shown in Fig. 8. In this scheme, two RFNNs are used as controller (RFNNC) and identifier (RFNNI) separately. The plant is identified by RFNNI, which provides the information about the plant to RFNNC. The inputs of RFNNC are e(k) and $\dot{e}(k)$. e(k) is the error between the desired output r(t) and the actual system output y(k). The output of RFNNC is the control signal u(k), which drives the plant such that e(k) is minimized. In the proposed system, both RFNNC and RFNNI have same structure.

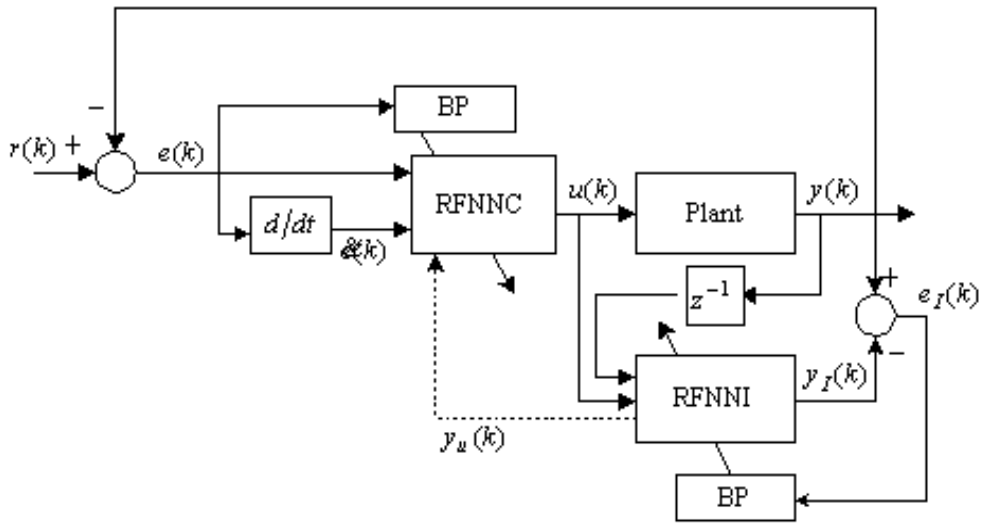

Fig. 8. Control system based on RFNNs

3.3 Learning Algorithm of RFNN

For parameter learning, we will develop a recursive learning algorithm based on the back propagation method

3.3.1 Learning algorithm for identifier

For training the RFNNI in Fig.8, the cost function is defined as follows:

$$J_I(k)=\frac{1}{2}\sum_{s=1}^{p}(e_{Is}(k))^2=\sum_{s=1}^{p}(y_s(k)-y_{Is}(k))^2 \tag{41}$$

where $y_s(k)$ is the sth output of the plant, $y_{Is}(k)=O_s^4$ is the sth output of RFNNI, and $e_{Is}(k)$ is the error between $y_s(k)$ and $y_{Is}(k)$ for each discrete time k.

By using the back propagation (BP) algorithm, the weights of the RFNNI is adjusted such

that the cost function defined in (41) is minimized. The BP algorithm may be written briefly as:

$$\begin{aligned} W_I(k+1) &= W_I(k) + \Delta W_I(k) \\ &= W_I(k) + \eta_I\left(-\frac{\partial J_I(k)}{\partial W_I(k)}\right) \end{aligned} \tag{42}$$

where η_I represents the learning rate and W_I represents the tuning weights, in this case, which are w^4_{Isq}, a_{Iiq_i}, b_{Iiqi}, and w^1_{Ii}. Subscript I represents RFNNI.

According to the RFNNI structure (34)~(37), cost function (41) and BP algorithm (42), the update rules of RFNNI weights are

$$w^4_{Isq}(k+1) = w^4_{Isq}(k) - \eta_I^{w4}\frac{\partial J_I(k)}{\partial w^4_{Isq}(k)} \tag{43}$$

$$a_{Iiq_i}(k+1) = a_{Iiq_i}(k) - \eta_I^{a}\frac{\partial J_I(k)}{\partial a_{Iiq_i}(k)} \tag{44}$$

$$b_{Iiq_i}(k+1) = b_{Iiq_i}(k) - \eta_I^{b}\frac{\partial J_I(k)}{\partial b_{Iiq_i}(k)} \tag{45}$$

$$w^1_{Ii}(k+1) = w^1_{Ii}(k) - \eta_I^{w1}\frac{\partial J_I(k)}{\partial w^1_{Ii}(k)} \tag{46}$$

Where

$$\frac{\partial J_I(k)}{\partial w^4_{Isq}(k)} = -e_{Is}(k)\frac{O^3_{Iq}}{\sum_q O^3_{Iq}}$$

$$\frac{\partial J_I(k)}{\partial a_{Iiq_i}(k)} = -\sum_s e_{Is}(k)\cdot\frac{w^4_{Isq} - O^4_{Is}}{\sum_q O^3_{Iq}}\cdot O^3_{Iq}\cdot\frac{2\left(O^1_{Ii} - a_{Iiq_i}\right)}{\left(b_{Iiq_i}\right)^2}$$

$$\frac{\partial J_I(k)}{\partial b_{Iiq_i}(k)} = -\sum_s e_{Is}(k)\cdot\frac{w^4_{Isq} - O^4_{Is}}{\sum_q O^3_{Iq}}\cdot O^3_{Iq}\cdot\frac{2\left(O^1_{Ii} - a_{Iiq_i}\right)^2}{\left(b_{Iiq_i}\right)^3}$$

$$\frac{\partial J_I(k)}{\partial w^1_{Ii}(k)} = -\sum_q\sum_s e_{Is}(k)\cdot\frac{w^4_{Isq} - O^4_{Is}}{\sum_q O^3_{Iq}}\cdot O^3_{Iq}\cdot\frac{-2\left(O^1_{Ii} - a_{Iiq_i}\right)}{\left(b_{Iiq_i}\right)^2}\cdot O^1_{Ii}(k-1)$$

3.3.2 Learning algorithm for controller

For training RFNNC in Fig. 8, the cost function is defined as

$$J_C(k)=\frac{1}{2}\sum_{s=1}^{p}(e_s(k))^2=\sum_{s=1}^{p}(r_s(k)-y_s(k))^2 \tag{47}$$

where $r_s(k)$ is the sth desired output, $y_s(k)$ is the sth actual system output and $e_s(k)$ is the error between $r_s(k)$ and $y_s(k)$.

Then, the gradient of J_C is

$$\begin{aligned}\frac{\partial J_C}{\partial W_C}&=\sum_s\frac{\partial J_C}{\partial y_s}\cdot\frac{\partial y_s}{\partial W_C}\\&=\sum_s-e_s(k)\frac{\partial y_s(k)}{\partial u_o(k)}\cdot\frac{\partial u_o(k)}{\partial W_C},\\&=\sum_s-e_s(k)yu_{so}(k)\cdot\frac{\partial u_o(k)}{\partial W_C}\end{aligned} \tag{48}$$

where u_o is the oth control signal, which is also the oth output of RFNNC, and $yu_{so}(k)=\partial y_s(k)/\partial u_o(k)$ denotes the system sensitivity. Thus the parameters of the RFNNC can be adjusted by

$$\begin{aligned}W_C(k+1)&=W_C(k)+\Delta W_C(k)\\&=W_C(k)+\eta_C(-\frac{\partial J_C(k)}{\partial W_C(k)})\end{aligned} \tag{49}$$

Note that the convergence of the RFNNC cannot be guaranteed until $yu_{so}(k)$ is known. Obviously, the RFNNI can provide $yu_{so}(k)$ to RFNNC. Resume that the oth control signal is also the oth input of RFNNI, then $yu_{so}(k)$ can be calculated by

$$\begin{aligned}\frac{\partial y_s(k)}{\partial u_o(k)}&=\sum_q\frac{\partial O_{Is}^4}{\partial O_{Iq}^3}\cdot\frac{\partial O_{Iq}^3}{\partial O_{Ioq_o}^2}\cdot\frac{\partial O_{Ioq_o}^2}{\partial O_{Io}^1}\cdot\frac{\partial O_{Io}^1}{\partial u_o}\\&=\sum_q\frac{w_{Isq}^4-O_{Is}^4}{\sum_q O_{Iq}^3}\cdot O_{Iq}^3\cdot\frac{-2(O_{Io}^1-a_{Ioq_o})}{(b_{Ioq_o})^2}\end{aligned} \tag{50}$$

3.4 Stability analysis of the RFNN

Choosing an appropriate learning rate η is very important for the stability of RFNN. If the value of the learning rate η is small, convergence of the RFNN can be guaranteed, however,

the convergence speed may be very slow. On the other hand, choosing a large value for the learning rate can fasten the convergence speed, but the system may become unstable.

3.4.1 Stability analysis for identifier

For choosing the appropriate learning rate for RFNNI, discrete Lyapunov function is defined as

$$L_I(k) = J_I(k) = \frac{1}{2}\sum_s (e_{Is}(k))^2 \tag{51}$$

Thus the change of the Lyapunov function due to the training process is

$$\begin{aligned}
\Delta L_I(k) &= L_I(k+1) - L_I(k) \\
&= \frac{1}{2}\sum_s (e_{Is}(k+1))^2 - \frac{1}{2}\sum_s (e_{Is}(k))^2 \\
&= \frac{1}{2}\sum_s \left[(e_{Is}(k+1))^2 - (e_{Is}(k))^2\right] \\
&= \frac{1}{2}\sum_s \left[(e_{Is}(k+1) + e_{Is}(k)) \cdot (e_{Is}(k+1) - e_{Is}(k))\right] \\
&= \frac{1}{2}\sum_s \left[(2e_{Is}(k) + \Delta e_{Is}(k)) \cdot \Delta e_{Is}(k)\right] \\
&= \frac{1}{2}\sum_s \left[(\Delta e_{Is}(k))^2 + 2e_{Is}(k)\Delta e_{Is}(k)\right] \\
&= \frac{1}{2}\sum_s (\Delta e_{Is}(k))^2 + \frac{1}{2}\sum_s \left[2e_{Is}(k)\Delta e_{Is}(k)\right]
\end{aligned} \tag{52}$$

The error difference due to the learning can be represented by

$$\Delta e_{Is}(k) = e_{Is}(k+1) - e_{Is}(k) \approx \frac{\partial e_{Is}(k)}{\partial W_I(k)} \cdot \Delta W_I(k) \tag{53}$$

Where

$$\begin{aligned}
\Delta W_I(k) &= -\eta_I \frac{\partial J_I(k)}{\partial W_I(k)} = -\eta_I \sum_s \frac{\partial J_I(k)}{\partial e_{Is}(k)} \cdot \frac{\partial e_{Is}(k)}{\partial W_I(k)} \\
&= -\eta_I \sum_s e_{Is}(k) \cdot \frac{\partial e_{Is}(k)}{\partial W_I(k)}
\end{aligned}$$

So (52) can be modified as

$$\begin{aligned}\Delta L(k) &= \frac{1}{2}\sum_s\left[\frac{\partial e_{Is}(k)}{\partial W_I(k)}\cdot\left(-\eta_I\frac{\partial J_I(k)}{\partial W_I(k)}\right)\right]^2+\frac{1}{2}\sum_s\left[2e_{Is}(k)\cdot\frac{\partial e_{Is}(k)}{\partial W_I(k)}\cdot\left(-\eta_I\frac{\partial J_I(k)}{\partial W_I(k)}\right)\right]\\ &= \frac{1}{2}\left(\eta_I\frac{\partial J_I(k)}{\partial W_I(k)}\right)^2\sum_s\left(\frac{\partial e_{Is}(k)}{\partial W_I(k)}\right)^2-\eta_I\frac{\partial J_I(k)}{\partial W_I(k)}\cdot\sum_s\left(e_{Is}(k)\cdot\frac{\partial e_{Is}(k)}{\partial W_I(k)}\right)\\ &= \frac{1}{2}\left(\eta_I\frac{\partial J_I(k)}{\partial W_I(k)}\right)^2\sum_s\left(\frac{\partial e_{Is}(k)}{\partial W_I(k)}\right)^2-\eta_I\left(\frac{\partial J_I(k)}{\partial W_I(k)}\right)^2\\ &= \frac{1}{2}\eta_I\left(\frac{\partial J_I(k)}{\partial W_I(k)}\right)^2\left[\eta_I\sum_s\left(\frac{\partial e_{Is}(k)}{\partial W_I(k)}\right)^2-2\right]\end{aligned} \tag{54}$$

To guarantee the convergence of RFNNI, the change of Lyapunov function $\Delta L_I(k)$ should be negative. So learning rate must satisfy the following condition:

$$0<\eta_I(k)<2\Big/\sum_s\left(\frac{\partial e_{Is}(k)}{\partial W_I(k)}\right)^2. \tag{55}$$

For the learning rate of each weight in RFNNI, the condition (22) can be modified as

$$0<\eta_I^{w4}(k)<2\Big/\max_q\left\{\sum_s\left(\frac{\partial e_{Is}(k)}{\partial w^4_{Isq}(k)}\right)^2\right\} \tag{56}$$

$$0<\eta_I^{a}(k)<2\Big/\max_{q,i}\left\{\sum_s\left(\frac{\partial e_{Is}(k)}{\partial a_{Iiq_i}(k)}\right)^2\right\} \tag{57}$$

$$0<\eta_I^{b}(k)<2\Big/\max_{q,i}\left\{\sum_s\left(\frac{\partial e_{Is}(k)}{\partial b_{Iiq_i}(k)}\right)^2\right\} \tag{58}$$

$$0<\eta_I^{w1}(k)<2\Big/\max_i\left\{\sum_s\left(\frac{\partial e_{Is}(k)}{\partial w^1_{Ii}(k)}\right)^2\right\}. \tag{59}$$

3.4.2 Stability analysis for controller

Similar to (51), the Lyapunov function for RFNNC can be defined as

$$L_C(k) = J_C(k) = \frac{1}{2}\sum_s (e_s(k))^2 \tag{60}$$

So, similar to (56)-(59), the learning rates for training RFNNC should be chosen according to the following rules:

$$0 < \eta_C^{w4}(k) < 2 \Big/ \max_q \left\{ \sum_s \left(\frac{\partial e_s(k)}{\partial w^4_{C\,sq}(k)} \right)^2 \right\} \tag{61}$$

$$0 < \eta_C^{a}(k) < 2 \Big/ \max_{q,i} \left\{ \sum_s \left(\frac{\partial e_s(k)}{\partial a_{C\,iq_i}(k)} \right)^2 \right\} \tag{62}$$

$$0 < \eta_C^{b}(k) < 2 \Big/ \max_{q,i} \left\{ \sum_s \left(\frac{\partial e_s(k)}{\partial b_{C\,iq_i}(k)} \right)^2 \right\} \tag{63}$$

$$0 < \eta_C^{w1}(k) < 2 \Big/ \max_{i} \left\{ \sum_s \left(\frac{\partial e_s(k)}{\partial w^1_{C\,i}(k)} \right)^2 \right\} \tag{64}$$

3.5 Simulation Experiments

Dynamics of robotic manipulators are highly nonlinear and may contain uncertain elements such as friction and load. Many efforts have been made in developing control schemes to achieve the precise tracking control of robot manipulators. Among available options, neural networks and fuzzy systems (Er & Chin 2000; Llama et al. 2000; Wang & Lin 2000; Huang & Lian 1997) are used more and more frequently in recent years. In the simulation experiments of this chapter, the proposed RFNNBAC is applied to control the trajectory of the two-link robotic manipulator described in chapter 2.4 to prove its effectiveness.

In the simulation, the parameters of manipulator are m_1 =4 *kg*, m_2 =2 kg, l_1 =1 *m*, l_2 =0.5 *m*, *g* =9.8 *N/kg*. Initial conditions are given as $\theta_1(0)$ =0 *rad*, $\theta_2(0)$ =1 *rad*, $\dot{\theta}_1(0)$ =0, and $\dot{\theta}_2(0)$ =0 *rad/s*. The desired trajectory is given by $\hat{\theta}_1(t) = \sin(2\pi t)$ and $\hat{\theta}_2(t) = \cos(2\pi t)$. The friction and disturbance terms in (4) are assumed to be

$$d_R = \begin{bmatrix} 5\cos(5t) \\ 5\cos(5t) \end{bmatrix} Nm,\ \Delta T(q, \dot{q}) = 0.5\,\mathrm{sign}(\dot{q})\, Nm.$$

Simulation results are shown in Fig.9 ~Fig.14. Fig.9 and Fig.10 illustrate the trajectories of two joints; the two outputs of identifier (RFNNI) are shown in Fig.11 and Fig.12 separately; the cost function for RFNNC is shown in Fig.13; and Fig.14 shows the cost function for RFNNI.

From simulation results, it is obvious that the proposed RFNN can identify and control the robot manipulator very well.

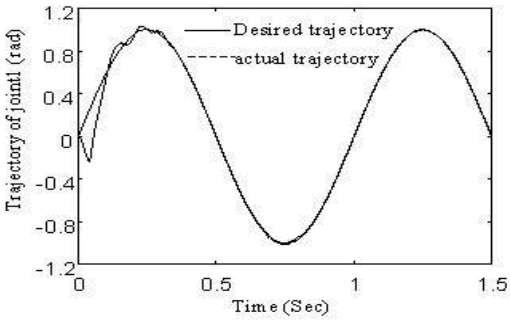

Fig. 9. Trajectory of joint1

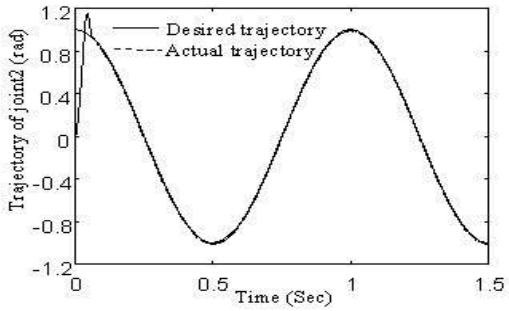

Fig. 10. Trajectory of joint2

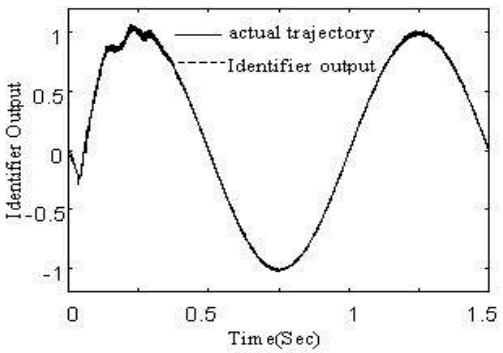

Fig. 11. Identifier (RFNNI) output1

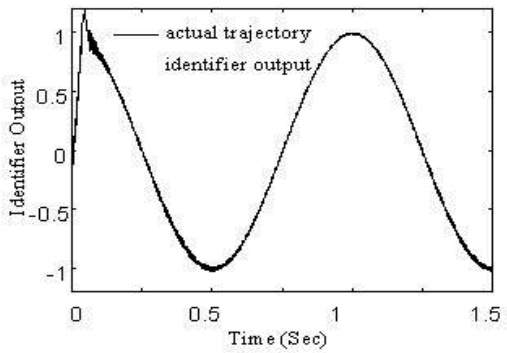

Fig. 12. Identifier (RFNNC) output2

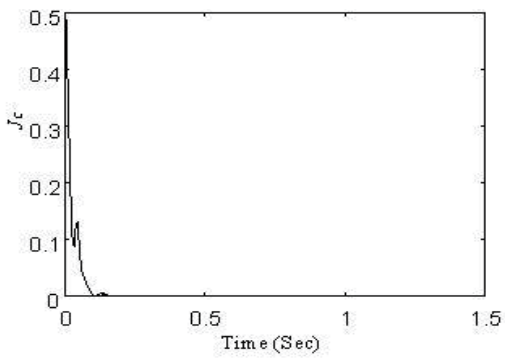

Fig. 13. Cost function for RFNNC

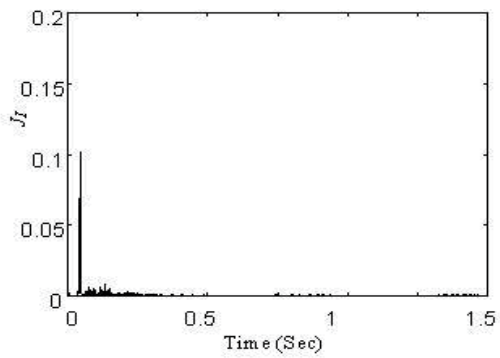

Fig. 14. Cost function for RFNNI

4. Conclusion

In this paper, the adaptive control based on neural network is studied. Firstly, a neural network based adaptive robust tracking control design is proposed for robotic systems under the existence of uncertainties. In this proposed control strategy, the NN is used to identify the modeling uncertainties, and then the disadvantageous effects caused by neural network approximating error and external disturbances in robotic system are counteracted by robust controller. Especially the proposed control strategy is designed based on HJI inequation theorem to overcome the approximation error of the neural network bounded issue. Simulation results show that proposed control strategy is effective and has better performance than traditional robust control strategy. Secondly, an RFNN for realizing fuzzy inference using the dynamic fuzzy rules is proposed. The proposed RFNN consists of four layers and the feedback connections are added in first layer. The proposed RFNN can be used for the identification and control of dynamic system. For identification, RFNN only needs the current inputs and most recent outputs of system as its inputs. For control, two RFNNs are used to constitute an adaptive control system, one is used as identifier (RFNNI) and another is used as controller (RFNNC). Also to prove the proposed RFNN and control strategy robust, it is used to control the robot manipulator and simulation results verified their effectiveness.

5. References

Abdallah, C., Dawson, D., Dorato, P. & Jamshidi, M. (1991). Survey of the robust of rigid robots, *IEEE Control Systems Magazine,* Vol. 11, No. 2, pp. 24-30.

Ortega, R. & Spong, M. W. (1989). Adaptive motion control of rigid robots: a tutorial, *Automatica,* Vol. 25, No. 3, pp. 877-888.

Saad, M., Dessaint, L. A., Bigras, P. & Haddad, K. (1994). Adaptive versus neural adaptive control: application to robotics, *International Journal of Adaptive Control and Signal Processing,* Vol. 8, No. 2, pp. 223-236.

Sanner, R. M. & Slotine, J. J. E. (1992). Gaussian networks for direct adaptive control, *IEEE Transactions on. Neural Network,* Vol. 3, No. 4, pp. 837-863.

Spooner, J. T. & Passino, K. M. (1996). Stable adaptive control using fuzzy systems and neural networks, *IEEE Transactions on Fuzzy system,* Vol. 4, No. 2, pp. 339-359.

Narenra, K. S. & Parthasarathy, K. (1990). Identification and control of dynamical systems using neural networks, *IEEE Transactions on Neural networks,* Vol. 1, No. 1, pp. 4-27.

Polycarpou, M. M. (1996). Stable adaptive neural control scheme for nonlinear systems, *IEEE Transactions on Automatic Control,* Vol. 41, No. 2, pp. 447-451.

Carelli, R., Camacho, E. F. & Patino, D. (1995). A neural network based feedforward adaptive controller for robot, *IEEE Transactions on Systems, Mman and Cybernetics, Part B: Cybernetics,* Vol. 25, No. 6, pp. 1281-1288.

Behera, L., Chaudhury, S. & Gopal, M. (1996). Neuro-adaptive hybrid controller for robot-manipulator tracking control, *IEE Proceedings Control Theory Applications,* Vol.143, No.1, pp.2710-275.

Shen, T. L. (1996). *H∞ control theory and its applications*, ISBN 7302022151, Tsinghua Press, Beijin, China.

Park, Y. M., Choi, M. S. & Lee, K. Y. (1996). An optimal tracking neuro-controller for nonlinear dynamic systems, *IEEE Transactions on Neural Networks,* Vol. 7, No. 5, pp. 1099-1110.

Narendra, K. S. & Parthasarathy, K. (1990). Identification and control of dynamical systems using neural networks, *IEEE Transactions on Neural Networks,* Vol. 1, No. 1, pp. 4-27.

Brdys, M. A. & Kulawski, G. J. (1999). Dynamic neural controllers for induction motor, *IEEE Transactions on Neural Networks,* Vol. 10, No. 2, pp. 340-355.

Ku, C. C. & Lee, K. Y. (1995). Diagonal recurrent neural networks for dynamic systems control, *IEEE Transactions on Neural Networks,* Vol. 6, No. 1, pp. 144-156.

Ma, S. & Ji, C. (1998). Fast training of recurrent neural networks based on the EM algorithm, *IEEE Transactions on Neural Networks,* Vol. 9, No. 1, pp. 11-26.

Sundareshan, M. K. & Condarcure, T. A. (1998). Recurrent neural-network training by a learning automation approach for trajectory learning and control system design, *IEEE Transactions on Neural Networks,* Vol. 9, No. 3, pp. 354-368.

Liang, X. B. & Wang, J. (2000). A recurrent neural network for nonlinear optimization with a continuously differentiable objective function and bound constraints, *IEEE Transactions on Neural Networks,* Vol. 11, No. 6, pp. 1251-1262.

Jang, J. S. R. & Sun, C. T. (1993). Functional equivalence between radial basis function networks and fuzzy inference systems, *IEEE Transactions on Neural Networks*, Vol. 4, No. 1, pp. 156-159.

Hunt, K. J., Hass, R. & Munay-Smith, R. (1996). Extending the functional equivalence of radial basis function networks and fuzzy inference systems, *IEEE Transactions on Neural Networks*, Vol. 7, No. 3, pp. 776-781.

Buckley, J. J., Hayashi, Y. & Czogala, E. (1993). On the equivalence of neural nets and fuzzy expert systems, *Fuzzy Sets and Systems*, Vol. 53, No. 2, pp. 129-134.

Reyneri, L. M. (1999). Unification of neural and wavelet networks and fuzzy systems, *IEEE Transactions on Neural Networks*, Vol. 10, No. 4, pp. 801-814.

Er, M. J. & Chin, S. H. (2000). Hybrid adaptive fuzzy controller of robot manipulators with bounds estimation, *IEEE Transactions on Industrial Electronics*, Vol. 47, No. 5, pp. 1151-1160.

Llama, M. A., Kelly, R. & Santibanez, V. (2000). Stable computed-torque control of robot manipulator via fuzzy self-tuning, *IEEE Transactions on Systems, Man and Cybernetics, Part B: Cybernetics*, Vol. 30, No. 1, pp. 143-150.

Wang, S. D. & Lin, C. K. (2000). Adaptive tuning of the fuzzy controller for robots, *Fuzzy Sets Systems,* Vol. 110, No. 3, pp. 351-363.

Huang, S. J. & Lian, R. J. (1997). A hybrid fuzzy logic and neural network algorithm for robot motion control, *IEEE Transactions on Industrial Electronics*, Vol. 44, No. 3, pp. 408-417.

9

Adaptive control of the electrical drives with the elastic coupling using Kalman filter

Krzysztof Szabat and Teresa Orlowska-Kowalska
Wroclaw University of Technology
Poland

1. Introduction

The control problem of the two-mass system originally derives from rolling-mill drives (Sugiura & Hori, 1996), (Ji & Sul, 1995), (Szabat & Orlowska-Kowalska, 2007). Large inertias of the motor, rolls and long shaft create an elastic system. The motor speed is different from the load side and the shaft undergoes large torsional torque. A similar problem exists in the field of conveyer drives (Hace et al., 2005). Also the performance of the machines used in textile industry is reduced by the non-ideal characteristics of the shaft (Beineke et al., 1997), (Wertz et al., 1999). An analogous problem appears in the paper machine sections (Valenzuela et al., 2005) and in modern servo-drives (Vukosovic & Stojic, 1998), (O'Sullivan et al., 2007), (Shen & Tsai, 2006). Moreover, torsional vibrations decrease the performance of the robot arms (Ferretti et al., 2004), (Huang & Chen, 2004). This problem is especially important in the field of space robot manipulators. Due to the cost of transport, the total weight of the machine must be drastically reduced. This reduces the stiffness of the mechanical connections which in turn influences the performance of the manipulator in a negative way (Katsura & Ohnishi, 2005), (Ferretti et al., 2005). The elasticity of the shaft worsens the performance of the position control of deep-space antenna drives (Gawronski et al., 1995). Vibrations affect the dynamic characteristics of computer hard disc drives (Ohno & Hara, 2006) and (Horwitz et al., 2007).
Torsional vibrations can appear in a drive system due to the following reasons:
- changeability of the reference speed;
- changeability of the load torque;
- fluctuation of the electromagnetic torque;
- limitation of the electromagnetic torque;
- mechanical misalignment between the electrical motor and load machine;
- variations of load inertia
- unbalance of the mechanical masses;
- system nonlinearities, such as friction torque and backlash.

The simplest method to eliminate the oscillation problem (occurring while the reference speed changes) is a slow change of the reference velocity. Nevertheless, it causes the decrease of the drive system dynamics and does not protect it against oscillations appearing when the disturbance torque changes. The conventional control structure based on the PI

speed controller, tuned by the classical symmetric criterion, with a single feedback from the motor speed is not effective in damping the speed oscillations. One of the simplest ways to improve the torsional vibrations ability of the classical structure is presented in (Zhang & Furusho, 2000). It is based on the suitable selection of the system closed-loop poles. However, this method improves the drive performance only for a limited range of the system parameters.

When the resonant frequency of the system excides hundreds of Hertz, the application of the digital filters is an industrial standard. The Notch-filter is usually mentioned as a tool ensuring the damping of the oscillations (Vukosovic & Stojic, 1998), (Ellis & Lorenz, 2000). Rarely a low-pass filter or Bi-filter is used. The digital filters can damp the torsional vibration, yet the dynamics of the system may be affected.

To improve performances of the classical control structure with the PI controller, the additional feedback loop from one selected state variable can be used. The additional feedback allows setting the desired value of the damping coefficient, but the free value of the resonant frequency cannot be achieved simultaneously (Szabat & Orłowska-Kowalska, 2007). According to the literature, the application of the additional feedback from the shaft torque is very common (Szabat & Orłowska-Kowalska, 2007). The design methodology of that system can be divided into two groups. In the first framework the shaft torque is treated as the disturbance. The simplest approach relies on feeding back the estimated shaft torque to the control structure, with the gain less than one. The more advanced methodology, called Resonance Ratio Control (RRC) is presented in (Hori et al., 1999). The system is said to have good damping ability when the ratio of the resonant to antiresonant frequency has a relatively big value (about 2). The second framework consists in the application of the modal theory. Parameters of the control structure are calculated by comparison of the characteristic equation of the whole system to the desired polynomial. To obtain a free design of the control structure parameters, i.e. the resonant frequency and the damping coefficient, the application of two feedbacks from different groups is necessary. The design methodology of this type of the systems is presented in (Szabat & Orłowska-Kowalska, 2007).

The control structures presented so far are based on the classical cascade compensation schemes. Since the early 1960s a completely different approach to the analysis of the system dynamics has been developed – the state space methodology (Michels et al., 2006). The application of the state-space controller allows to place the system poles in an arbitrary position so theoretically it is possible to obtain any dynamic response of the system. The suitable location of the closed-loop system poles becomes one of the basic problems of the state space controller application. In (Ji & Sul, 1995) the selection of the system poles is realized through LQ approach. The authors emphasize the difficulty of the matrices selection in the case of the system parameter variation. The influence of the closed-loop location on the dynamic characteristics of the two-mass system is analyzed in (Qiao et al., 2002), (Suh et al., 2001). In (Suh et al., 2001) it is stated that the location of the system poles in the real axes improve the performance of the drive system and makes it more robust against the parameter changing.

In the case of the system with changeable parameters more advanced control concepts have been developed. In (Gu et al., 2005), (Itoh et al., 2004) the applications of the robust control theory based on the H_∞ and μ-*synthesis* frameworks are presented. The implementation of the genetic algorithm to setting of the control structure parameter is shown in (Itoh et al., 2004). The author reports good performance of the system despite the variation of the inertia

of the load machine. The next approach consists in the application of the sliding-mode controller. For example, in paper (Erbatur et al., 1999) this method is applied to controlling the SCARA robot. A design of the control structure is based on the Lyapunov function. The similar approach is used in (Hace et al., 2005) where the conveyer drive is modelled as the two-mass system. The authors clam that the design structure is robust to the parameter changes of the drive and external disturbances. Other application examples of the sliding-mode control can be found in (Erenturk, 2008). The next two frameworks of control approach relies on the use of the adaptive control structure. In the first framework the controller parameters are adjusted on-line on the basis of the actual measurements. For instance in (Wang & Frayman, 2004) a dynamically generated fuzzy-neural network is used to damp torsional vibrations of the rolling-mill drive. In (Orlowska-Kowalska & Szabat, 2008b) two neuro-fuzzy structures working in the MRAS structure are compare. The experimental results show the robustness of the proposed concept against plant parameter variations. In the other framework changeable parameters of the plant are identified and then the controller is retuned in accordance with the currently identified parameters. The Kalman filter is applied in order to identify the changeable value of the inertia of the load machine (Orlowska-Kowalska & Szabat, 2008a). This value is used to correct the parameters of the PI controller and two additional feedbacks. A similar approach is presented in (Hirovonen et al., 2006). In the paper (Cychowski et al., 2008) the model predictive controller is applied o ensure the optimal control of the system states taking the system constrains into consideration. In order to reduce the computational complexity the explicit version of the controller is suggested to real-time implementation.
This paper is divided into seven sections. After an introduction, the mathematical model of the two-mass drive system and utilised control structure are described. In section IV, the mathematical model of the NEKF is presented. The simulation results of the non-adaptive and adaptive NEKF are demonstrated in sections V. The proposed adaptation mechanism is described and the analysed algorithms are compared. After a short description of the laboratory set-up, the experimental results are presented in section VI. Conclusions are presented at the end of the paper.

2. The mathematical model of the two-mass system and the control structure

In technical papers there exist many mathematical models, which can be used for the analysis of the plant with elastic couplings. In many cases the drive system can be modelled as a two-mass system, where the first mass represents the moment of inertia of the drive and the second mass refers to the moment of inertia of the load side. The mechanical coupling is treated as an inertia free. The internal damping of the shaft is sometimes also taken into consideration. Such a system is described by the following state equation (Szabat & Orlowska-Kowalska, 2007) (with non-linear friction neglected):

$$\frac{d}{dt}\begin{bmatrix}\Omega_1(t)\\ \Omega_2(t)\\ M_s(t)\end{bmatrix}=\begin{bmatrix}\frac{-D}{J_1} & \frac{D}{J_1} & \frac{-1}{J_1}\\ \frac{D}{J_2} & \frac{-D}{J_2} & \frac{1}{J_2}\\ K_c & -K_c & 0\end{bmatrix}\begin{bmatrix}\Omega_1(t)\\ \Omega_2(t)\\ M_s(t)\end{bmatrix}+\begin{bmatrix}\frac{1}{J_1}\\ 0\\ 0\end{bmatrix}[M_e]+\begin{bmatrix}0\\ \frac{-1}{J_2}\\ 0\end{bmatrix}[M_L] \tag{1}$$

where: Ω_1- motor speed, Ω_2- load speed, M_e– motor torque, M_s– shaft (torsional) torque, M_L– load torque, J_1 – inertia of the motor, J_2– inertia of the load machine, K_c– stiffness coefficient, D – internal damping of the shaft.
The described model is valid for the system in which the moment of inertia of the shaft is much smaller than the moment of the inertia of the motor and the load side. In other cases a more extended model should be used, such as the Rayleigh model of the elastic coupling or even a model with distributed parameters. The suitable choice of the mathematical model is a compromise between the accuracy and calculation complexity. As can be concluded from the literature, nearly in all cases the simplest shaft-inertia-free model has been used.
To simplify the comparison of the dynamical performances of the drive systems of different power, the mathematical model (1) is expressed in per unit system, using the following notation of new state variables:

$$\omega_1 = \frac{\Omega_1}{\Omega_N}\ \omega_2 = \frac{\Omega_2}{\Omega_N}\ m_e = \frac{M_e}{M_N}\ m_s = \frac{M_s}{M_N}\ m_L = \frac{M_L}{M_N} \tag{2}$$

where: Ω_N – nominal speed of the motor, M_N – nominal torque of the motor, ω_1, ω_2 – motor and load speeds, m_e, m_s, m_L – electromagnetic, shaft and load torques in per unit system.
The mechanical time constant of the motor – T_1 and the load machine – T_2 are thus given as:

$$T_1 = \frac{\Omega_N J_1}{M_N}\quad T_2 = \frac{\Omega_N J_2}{M_N} \tag{3}$$

The stiffness time constant – T_c and internal damping of the shaft – d can be calculated as follows:

$$T_c = \frac{M_N}{K_c \Omega_N}\quad d = \frac{\Omega_N D}{M_N} \tag{4}$$

Taking into account the equations (3)-(5) the state equation of the two-mass system in per-unit value is represented as:

$$\frac{d}{dt}\begin{bmatrix}\omega_1(t)\\ \omega_2(t)\\ m_s(t)\end{bmatrix} = \begin{bmatrix}\frac{-d}{T_1} & \frac{d}{T_1} & \frac{-1}{T_1}\\ \frac{d}{T_2} & \frac{-d}{T_2} & \frac{1}{T_2}\\ \frac{1}{T_c} & \frac{-1}{T_c} & 0\end{bmatrix}\begin{bmatrix}\omega_1(t)\\ \omega_2(t)\\ m_s(t)\end{bmatrix} + \begin{bmatrix}\frac{1}{T_1} & 0\\ 0 & \frac{-1}{T_2}\\ 0 & 0\end{bmatrix}\begin{bmatrix}m_e\\ m_L\end{bmatrix} \tag{5}$$

Usually, due to its small value the internal damping of the shaft d is neglected in the analysis of the two-mass drive system.

3. Adaptive control structure

A typical electrical drive system is composed of a power converter-fed motor coupled to a

mechanical system, a microprocessor-based controllers, current, rotor speed and/or position sensors used as feedback signals. Typically, cascade speed control structure containing two major control loops is used, as presented in Fig 1.

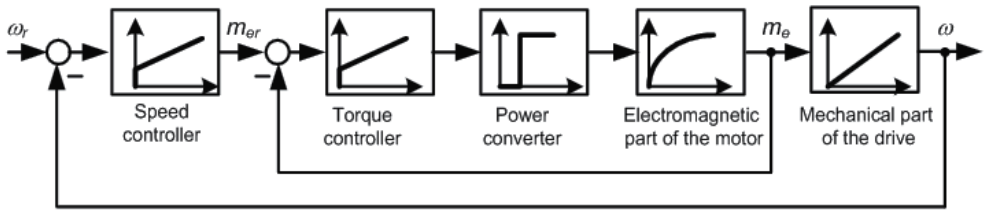

Fig. 1. The classical cascade control structure of the two-mass system

The inner control loop performs a motor torque regulation and consists of the power converter, electromagnetic part of the motor, current sensor and respective current or torque controller. As this control loop is designed to provide sufficiently fast torque control, it can be approximated by an equivalent first order term with small time constant. If the control is ensured, the driven machine could be an AC or DC motor, with no difference in the outer speed control loop. The outer loop consists of the mechanical part of the motor, speed sensor, speed controller, and is cascaded to the inner loop. It provides speed control according to the reference value (Szabat & Orlowska-Kowalska, 2007).

Such a classical structure in not effective enough in the case of the two-mass system. To improve the dynamical characteristics of the drive, the modification of the cascade structure is necessary. In this paper the structure with the state controller which allows the free location of the closed-loop poles is considered. So it requires the additional information of the shaft torque and the load speed. The parameters of the control structures are set using pole-placement methods, with the methodology presented in (Szabat & Orlowska-Kowalska, 2007), according to the following equations:

$$k_I = T_1 T_2 T_c \omega_0^4 \tag{6}$$

$$k_1 = 4 T_1 \xi_r \omega_0 \tag{7}$$

$$k_2 = T_1 T_c \left(2\omega_0^2 + 4\xi_r^2 \omega_0^2 - \frac{1}{T_2 T_c} - \frac{1}{T_1 T_c} \right) \tag{8}$$

$$k_3 = k_1 \left(\omega_0^2 T_2 T_c - 1 \right) \tag{9}$$

where: ξ_r - required damping coefficient, ω_0- required resonant frequency of the system.

In the industrial applications, the direct measurement of the shaft torque m_s and the load speed ω_2 is very difficult. For that reason, in this paper the Nonlinear Extended Kalman Filter (NEKF) is used to provide the information about non-measurable mechanical state variables. Additionally, the time constant T_2 of the load side is also estimated and used to on-line retuning the control structure parameters, according to Eq. (6)-(9). The estimated

value of T_{2e} is also used to change the element q_{55} of the covariance matrix **Q** in the way presented in the next section (Eq. (21)). The considered control structure is presented in Fig. 2. The proposed adaptive control structure ensure the desired characteristic of the drives despite the changes of the time constant of the load machine.

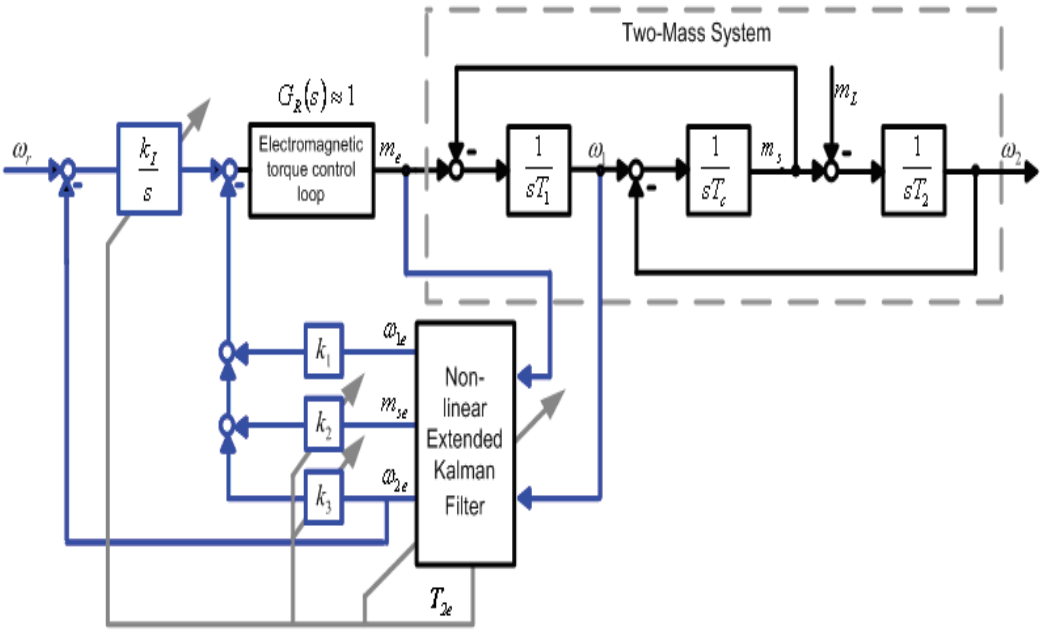

Fig. 2. The block diagram of the state-feedbacks adaptive control structure

3. Mathematical model of the nonlinear extended Kalman filter (NEKF)

In the presence of the time-varying load machine inertia T_2, there is a need to extend the two-mass system state vector (1) with the additional element $1/T_2$ and non-measurable load torque m_L :

$$\mathbf{x_R}(t) = \left[\omega_1(t) \;\; \omega_2(t) \;\; m_s(t) \;\; m_L(t) \;\; \frac{1}{T_2}(t) \right]^T . \tag{10}$$

The extended, nonlinear state and output equations can be written in the following form:

$$\frac{d}{dt}\mathbf{x_R}(t) = \mathbf{A_R}\left(\frac{1}{T_2}(t)\right)\mathbf{x_R}(t) + \mathbf{B_R}\,\mathbf{u}(t) + \mathbf{w}(t) = \mathbf{f_R}\left(\mathbf{x_R}(t), \mathbf{u}(t)\right) + \mathbf{w}(t) \tag{11a}$$

$$\mathbf{y_R}(t) = \mathbf{C_R}\mathbf{x_R}(t) + \mathbf{v}(t) \tag{11b}$$

where matrices of the system are defined as follows (in [p.u.]):

$$\mathbf{A_R}\left(\frac{1}{T_2}(t)\right)=\begin{bmatrix} 0 & 0 & \frac{-1}{T_1} & 0 & 0 \\ 0 & 0 & \frac{1}{T_2}(t) & \frac{-1}{T_2}(t) & 0 \\ \frac{1}{T_c} & \frac{-1}{T_c} & 0 & 0 & 0 \\ 0 & 0 & 0 & 0 & 0 \\ 0 & 0 & 0 & 0 & 0 \end{bmatrix} \mathbf{B_R}=\begin{bmatrix} \frac{1}{T_1} \\ 0 \\ 0 \\ 0 \\ 0 \end{bmatrix} \mathbf{C_R}=\begin{bmatrix} 1 \\ 0 \\ 0 \\ 0 \\ 0 \end{bmatrix}^T \tag{12}$$

and **w**(t), **v**(t) - represent process and measurement errors (Gaussian white noise), according to the Kalman Filter (KF) theory.
The matrix $\mathbf{A}_R$ depends on the changeable parameter T_2. It means that in every calculation step this matrix must be updated due to the estimated value of T_2. The input and the output vectors of the drive system (and NEKF) are electromagnetic torque and motor speed respectively:

$$\mathbf{u}=m_e \quad \mathbf{y}=\omega_1 \tag{13}$$

After the discretization of Eq. (11) with T_p sampling step, the state estimation using NEKF algorithm is calculated:

$$\hat{\mathbf{x}}_\mathbf{R}(k+1/k+1)=\hat{\mathbf{x}}_\mathbf{R}(k+1/k)+\mathbf{K}(k+1)\left[\mathbf{y}_\mathbf{R}(k+1)-\mathbf{C}_\mathbf{R}(k+1)\hat{\mathbf{x}}_\mathbf{R}(k+1/k)\right] \tag{14}$$

where the gain matrix **K** is obtained by the suitable numerical procedure.
In the first step the estimation of the filter covariance matrix is calculated:

$$\mathbf{P}(k+1/k)=\mathbf{F}_\mathbf{R}(k)\mathbf{P}(k)\mathbf{F}_\mathbf{R}^\mathbf{T}(k)+\mathbf{Q}(k) \tag{15}$$

where:

$$\mathbf{F}_\mathbf{R}(k)=\left.\frac{\partial \mathbf{f}_\mathbf{R}\left(\mathbf{x}_\mathbf{R}(k/k),\mathbf{u}(k),k\right)}{\partial x_\mathrm{P}(k/k)}\right|_{\mathbf{x}_\mathbf{R}=\hat{\mathbf{x}}_\mathbf{R}(k/k)} \tag{16}$$

and **Q** is a state noise covariance matrix. $\mathbf{F}_R$ is the state matrix of the nonlinear dynamical system (11) after its linearization in the actual operating point, which must be updated in every calculation step:

$$\mathbf{F}_\mathbf{R}(k)=\begin{bmatrix} 1 & 0 & \frac{-1}{T_1}T_p & 0 & 0 \\ 0 & 1 & \frac{1}{T_2}(k)T_p & \frac{-1}{T_2}(k)T_p & T_p(m_s(k)-m_L(k)) \\ \frac{1}{T_c}T_p & \frac{-1}{T_c}T_p & 1 & 0 & 0 \\ 0 & 0 & 0 & 1 & 0 \\ 0 & 0 & 0 & 0 & 1 \end{bmatrix} \tag{17}$$

The filter gain matrix **K** of the NEKF and the update of the covariance matrix of the state estimation error **P** are calculated using the following equations:

$$\mathbf{K}(k+1)=\mathbf{P}(k+1/k)\mathbf{C}_{\mathbf{R}}^{\mathrm{T}}(k+1)\left[\mathbf{C}_{\mathbf{R}}(k+1)\mathbf{P}(k+1/k)\mathbf{C}_{\mathbf{R}}^{\mathrm{T}}(k+1)+\mathbf{R}(k)\right]^{-1} \tag{18}$$

$$\mathbf{P}(k+1/k+1)=\left[\mathbf{I}-\mathbf{K}(k+1)\mathbf{C}_{\mathbf{R}}(k+1)\right]\mathbf{P}(k+1/k) \tag{19}$$

where: **R** – the output noise covariance matrix.
The quality of the state estimation depends on the suitable choice of the covariance matrices **Q** and **R**. However, according to the technical literature, the analytical guidelines which ensure proper setting of these matrices do not exist. Usually the trial and error procedure is used. However, this process is time-consuming and does not ensure the optimal performances of NEKF. In this paper elements of covariance matrices have been set using the genetic algorithm (Szabat & Orlowska-Kowalska, 2008), with the following cost function:

$$F=\left(\sum_{1}^{j}|m_s-m_{se}|\right)\left(\sum_{1}^{j}|\omega_2-\omega_{2e}|\right)\left(\sum_{1}^{j}|m_L-m_{Le}|\right)\left(\sum_{1}^{j}|T_2-T_{2e}|\right) \tag{20}$$

where: m_s, ω_2, m_L, T_2 –real variables and parameter of the two-mass system; m_{se}, ω_{2e} , m_{Le}, T_{2e} –estimated variables and parameter, j – total number of samples. The cost function defined in this way ensures the optimal setting of covariance matrices **Q** and **R** for changeable time constant of the load machine.

4. Simulation results

4.1 Open-loop system

In simulation tests the estimation quality of all system state variables is investigated. The shaft torque and the load speed are taken for the closed-loop structure with the direct feedback from system state variables (Fig.1). The electromagnetic torque and the motor speed, used as the input and output vectors of NEKF, are disturbed with white noises. In Fig. 3. the transients of the electromagnetic torque and motor speed are presented.

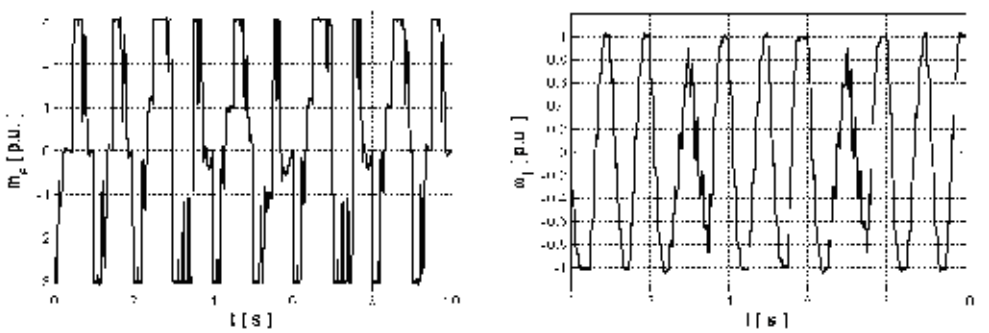

a) b)

Fig. 3. Transients of the electromagnetic torque (a) and the motor speed (b)

The drive system works in the reverse condition with the electromagnetic torque limit set to 3 [p.u.] in the considered case is tested. The state estimator working outside the control structure is tested. The transients of all the real and estimated variables and theirs estimation errors are demonstrated In Fig 4.

The NEKF starts work with a misidentified value of the time constant of the load machine (initial value of the T_2 is set to101.5ms – Fig 4.g). Then at the time t_1=2s the time constant of the load machine T_2 and the load torque m_L begin to change (Fig. 4c,g). Those two variables vary in a smooth sinusoidal way. The NEKF estimates all the system states simultaneously. As can be seen from Fig. 4, the transients of all estimates contain high-frequency noises. The steady state level of the estimation error is about 0.02 (Fig. 4e) for the load speed and about 0.10 (Fig. 4e) for the shaft torque. The biggest errors exist in the transients of the load torque and of time constant of the load machine (Fig. 4h). The initial estimation error of T_2, cause by the misidentified value of the time constant of the load machine is eliminated after 500ms. The typical disruptions can be seen in the estimated transient. They appear when the direction of the motor speed is rapidly changed. The characteristic feature of the NEKF is the fact that the estimation of the time constant of the load machine is only possible when the load speed is changing. Therefore, the biggest estimation errors occurs when the time constant of the load side is varied and the load speed is constant (Fig. 4g,h). The next NEKF feature is that the estimate of the T_2 contains bigger frequency noises in the case when the real value of the T_2 is larger. Because the load torque and time constant of the load machine have been varied in a smooth way good estimation accuracy has been achieved in the simultaneous estimation of all the states.

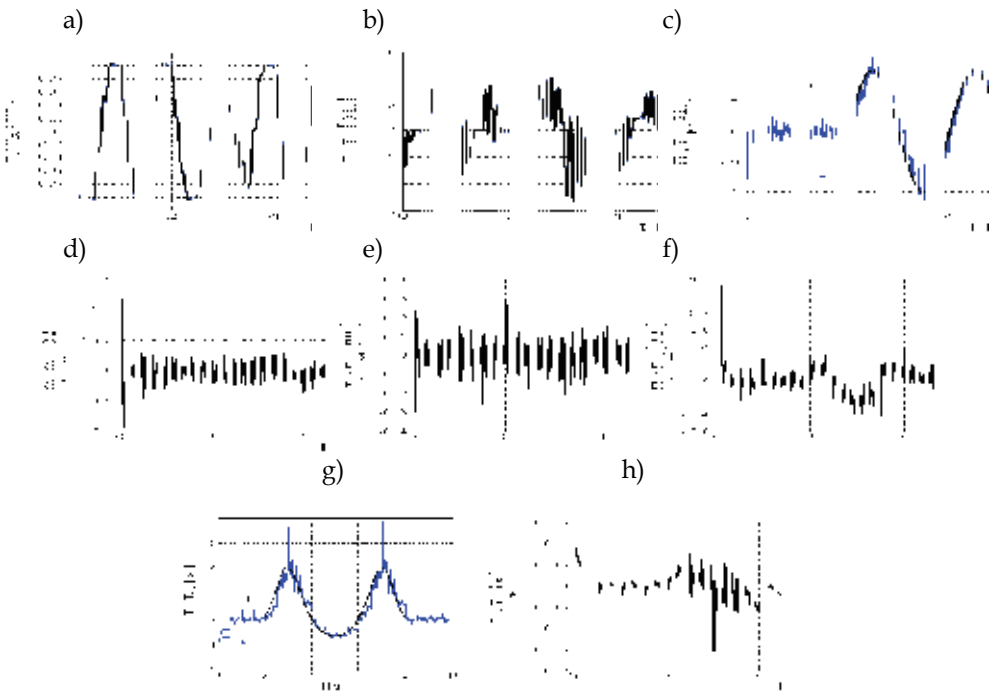

Fig. 4. Transients of the real and estimated state variables and their estimation errors: load speed (a,d) shaft torque (b,e), load torque (c,f) and time constant of the load side (g,h)

Then the case of the rapid changing of the load torque and time constant of the load machine is considered. The input (electromagnetic torque) and output vector (motor speed) of the NEKF are presented In Fig. 5. As the previously the drive is working under reverse condition and the limit level of the electromagnetic torque is also set to 3 [p.u.]. The electromagnetic torque and the motor speed are disrupted by white noises, which emulate the measurements noises. The real and estimated variables and their estimation errors for rapid changes of the load torque and the load side inertia are presented in Fig. 6.
Similarly as in the previous case, the drive system starts working with a misidentified time constant of the load machine T_2=101.5ms (Fig. 6g). Then at the time t=1s and 3s the time constant of the load machine and the load torque change rapidly (Fig. 6c,g). Next, at the time t=5, 6 and 8s only the load torque and at the time t= 4, 6.5 and 8.5s only the time constant of the load machine vary quickly. The following work cycle allows to examine the quality of the variables estimation under different conditions. The average level of the estimation error is about 0.014 (Fig. 6e) for the load speed and about 0.06 for the shaft torque (Fig. 6f). However, the simultaneous alternation of the load torque and time constant of the load machine bring about the rise of the big, quickly damped estimation errors of the load speed (Fig. 6b) and shaft torque (Fig. 6d). A single change of the above-mentioned variables cause the increase of the estimation errors, but for a smaller extent than in the pervious case. The last two estimated variables, i.e. the load torque and the time constant of the load machine depend on each other significantly. The rapid change of one variable brings about a significant increase of the estimation error of the other variable (Fig. 6f,h).

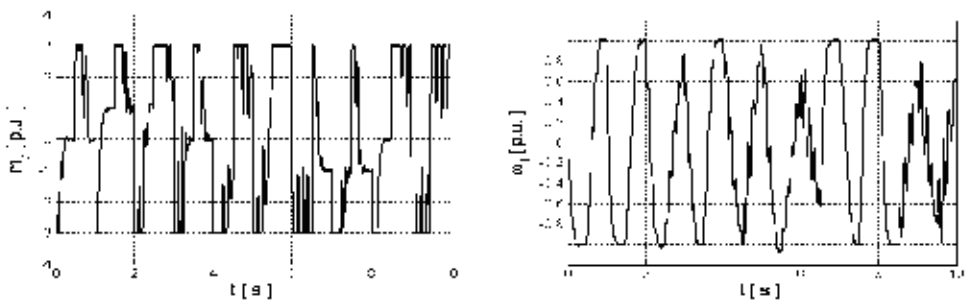

a) b)

Fig. 5. Transients of the electromagnetic torque (a) and the motor speed (b)

Similarly as in the previous case, the drive system starts working with a misidentified time
From the transients presented in Fig. 4 and Fig. 6 the following remarks can be formulated:
-the estimation of the time constant of the load machine is possible only when the motor speed is changing;
-the estimates of the load torque and the time constant of the load machine are correlated: the change of the load torque causes the rise of the error of the load machine time constant and vice versa. This is especially clearly visible in the transient presented in Fig. 6;
-the noise level of the of the estimated load machine time constant of the strictly depends on the actual value of the real time constant and the value of the covariance matrix element q_{55}; when of the value of the T_2 is smaller, the element q_{55} should have a bigger value and vice versa.

The dynamic characteristics of the non-adaptive NEKF strictly depends on the proper setting of the covariance matrix values. In the case of the changeable time constant of the load machine the element q_{55} is a compromise between the slow covariance for a small value of T_2 and a large noise level when value of T_2 is big. The modification of the estimating procedure is related to this feature. Because the noise level in the estimated variable depends on the real value of the T_2, the NEKF with the changeable element q_{55} of the correlation matrix **Q** is proposed. The element q_{55} adopts to the estimating value of the time constant of the load machine according to the following formula:

$$q_{55} = q_{55N}\left(\frac{T_{2N}}{T_{2e}}\right)^n \tag{21}$$

where: q_{55N}- the value of q_{55} selected for the nominal parameters of the drive (using genetic algorithm), T_{2N} – nominal time constant of the load machine, T_{2e} – estimated time constant of the load machine, n – power factor.

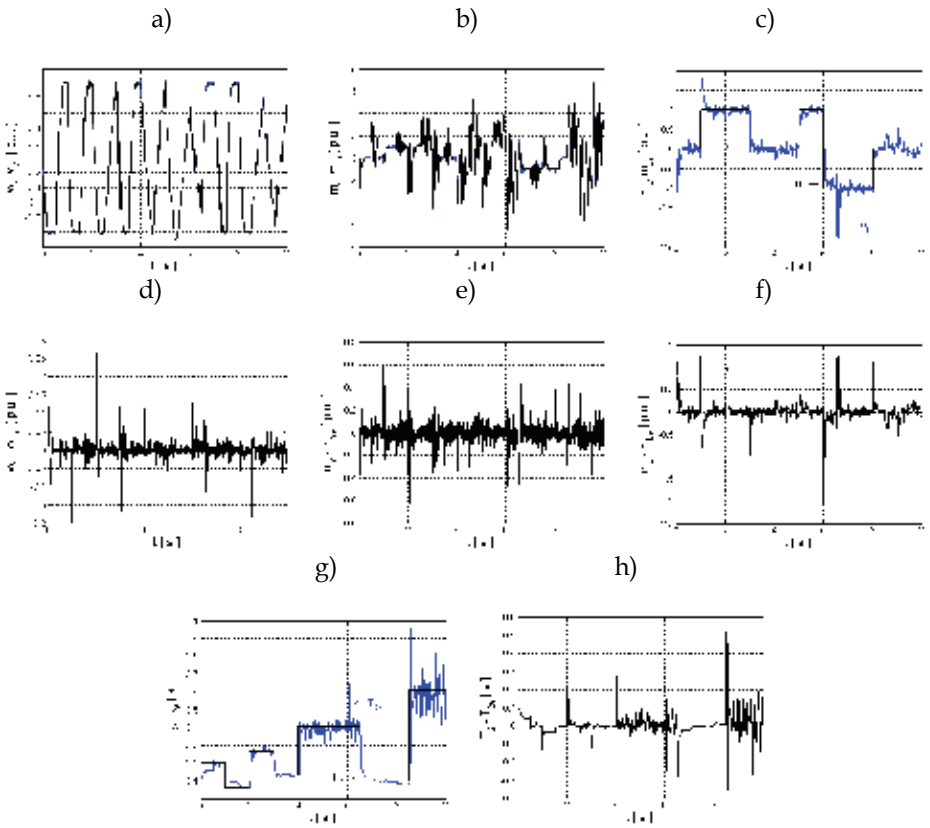

Fig. 6. Transients of the real and estimated state variables and their estimation errors: load speed (a,d)shaft torque (b,e), load torque (c,f) and time constant of the load side (g,h)

Then the adaptive NEKF is tested under the same conditions as previously but with the adaptation formula (21). Because the biggest difference is visible in the time constant of the load machine only the transients of those variables are presented below. In Fig 7 the transients for smooth (case 1- a) and rapid (case 2- b) changes of the load torque and time constant of the load machine for power factor n=3 are presented.
The difference between the non-adaptive and adaptive NEKF algorithm is clearly visible when the Fig. 4, 6 and 7 are compared. The estimate of T_2 has a smaller estimation error and noise level than for the non-adaptive NEKF. The rapid changing of the load torque does not influence the estimate of T_2 so significantly as in the previous non-adaptive NEKF case. Also the estimate of the load torque has better accuracy in the adaptive NEKF case. Similarly, the fast variation of the time constant of the load machine causes a smaller error in the estimate of load torque in the adaptive NEKF.

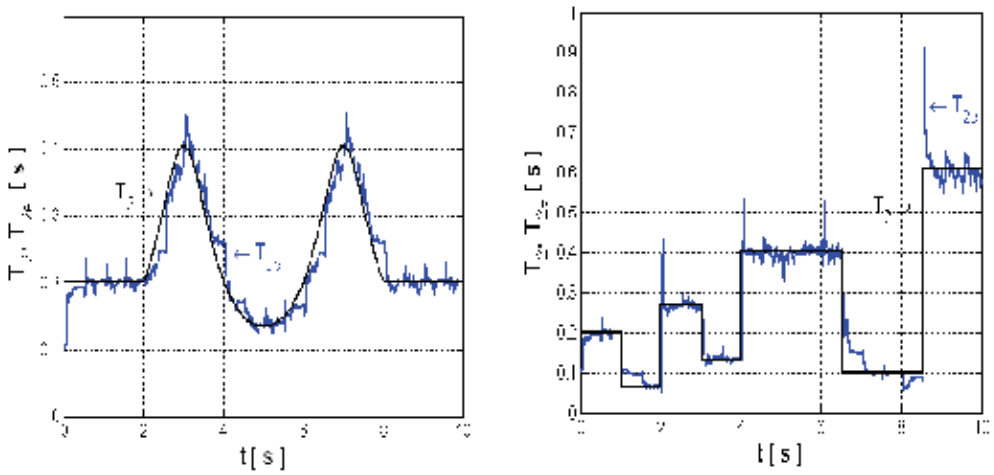

a) b)

Fig. 7. Transients of the real and estimated time constant of the load side for the adaptive NEKF with power factor n=3, case-1 (a), case-2 (b)

In order to compare the performance of the non-adaptive and adaptive NEKFs, the estimation errors of all estimated have been calculated using of the following equation:

$$\Delta_v = \frac{\sum_{i=1}^{N} |v - v_e|}{N} \tag{22}$$

where: N – total number of samples, v – real variable,
v_e – estimating variable.

The estimation errors of all state variables for non-adaptive (n=0) and adaptive NEKF (n =3) are presented in the Table 1.

	$\Delta\omega_2$	Δm_s	ΔT_2	Δm_L
Case 1 n=0	0.0092	0.0456	0.0180	0.0942
Case 1 n=3	0.0086	0.0442	0.0159	0.0907
Case 2 n=0	0.0140	0.0605	0.0301	0.1073
Case 2 n=3	0.0123	0.0570	0.0224	0.0975

Table 1. The estimation errors of the state variables for the case 1 and case 2 for the adaptive and non-adaptive NEKF

The application of the adaptation mechanism decreases the estimation error in all estimated variables. This feature is especially evident when the time constant of the load machine and the load torque change rapidly (case -2). For instance, the application of the adaptation mechanism ensures the reduction of estimation error of the T_{2e} by approximately 25%.

3.2 Closed-loop system

First, the effectiveness of the proposed control structure has been investigated in the simulation study. The non-measurable state variables, e.g. shaft torque, load speed and load torque, are delivered to the control structure by the NEKF.

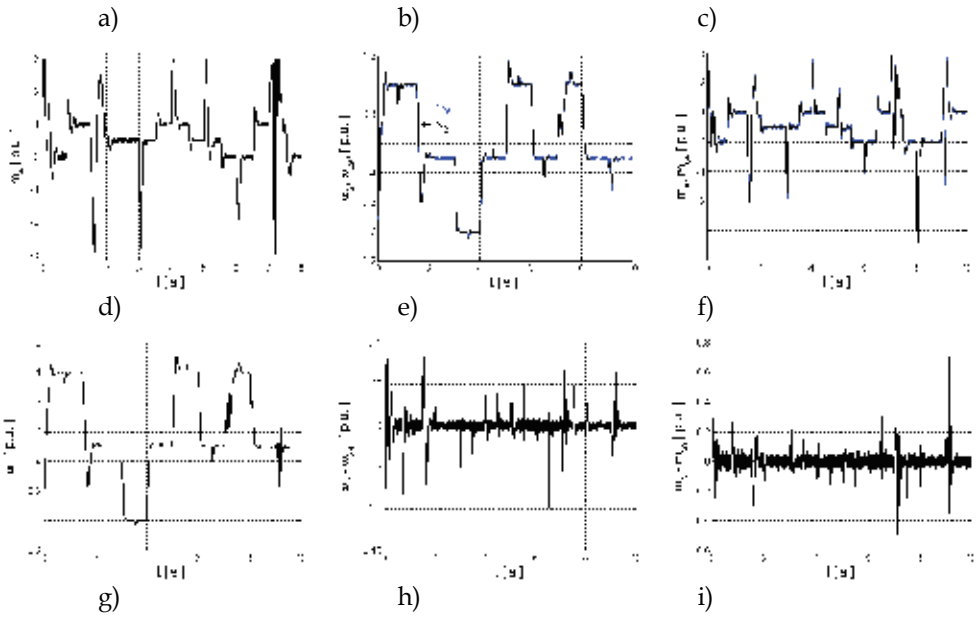

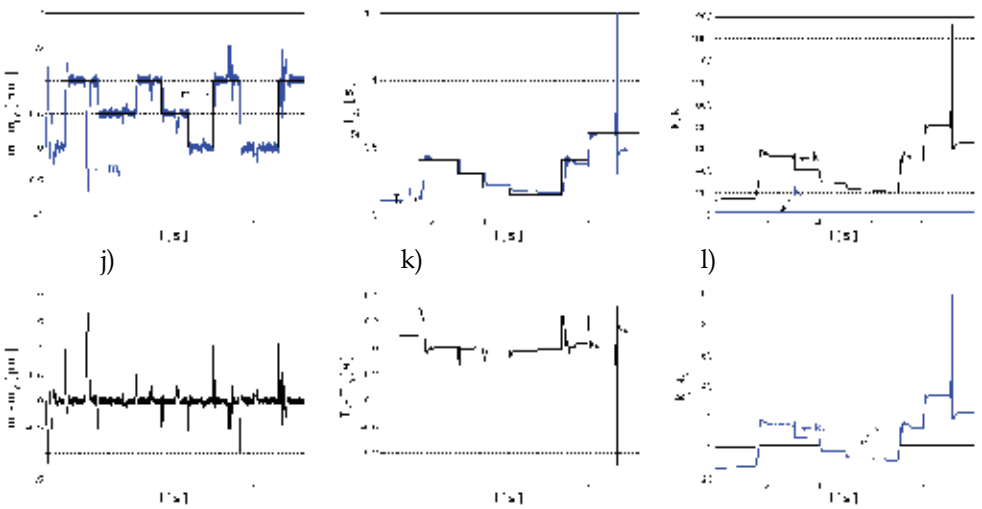

Fig. 8. Transients of the electromagnetic torque (a), motor speed (d), real and estimated state variables and their estimation errors: load speed (b,e), shaft torque (c,f), load torque (g,j), time constant of the load machine (h,k) adaptive control structure parameters (i,l) in the control structure with simultaneous estimation of the time constant of the load machine and load torque

The estimated time constant of the load machine is used in the adaptation law in order to retune the control structure coefficients in accordance with (6)-(9). The adaptation formula (21) is used to improve the NEKF performance. However, in order to ensure the stable work of the control structure the coefficients of the covariance matrices are decreased in comparison to the previous section. The desired values of the resonant frequency of the system and the damping coefficient are ω_0=45s^{-1} and ξ_r=0.7 respectively. The transients of the system states as well as the control structure coefficient are presented In Fig 8.

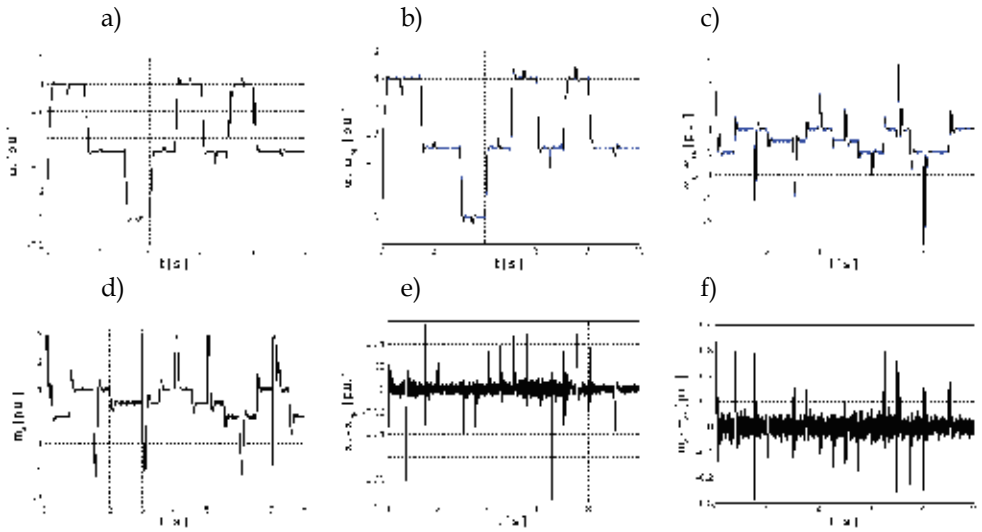

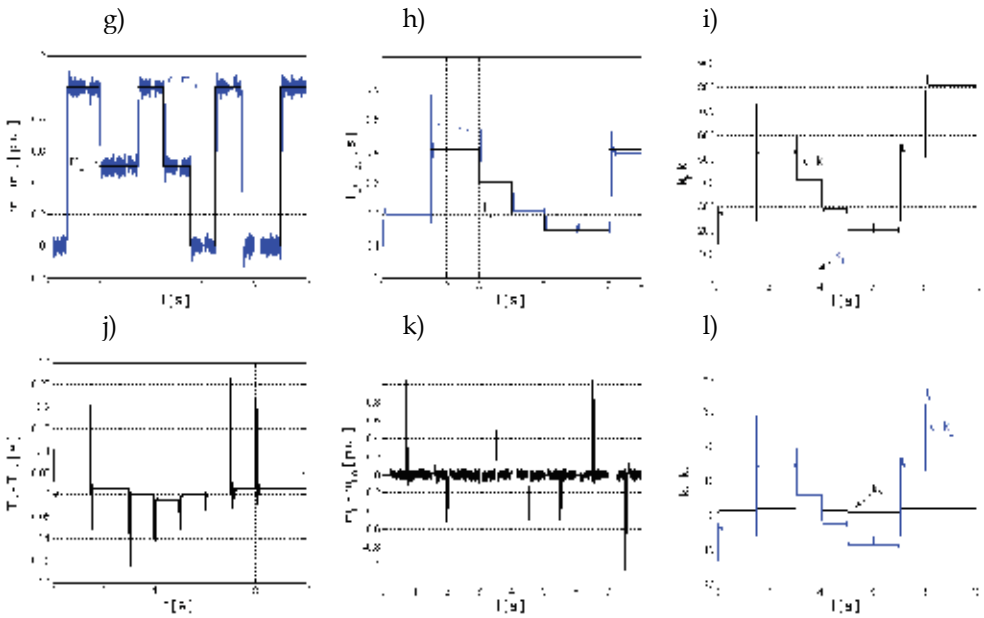

Fig. 9. Transients of the electromagnetic torque (a), motor speed (d), real and estimated state variables and their estimation errors: load speed (b,e), shaft torque (c,f), load torque (g,j), time constant of the load machine (h,k) adaptive control structure parameters (i,l) in the control structure with modified estimation algorithm

The system starts work with a misidentified value of the time constant of the load machine T_{2e} =101ms (Fig. 8h) which results oscillations in the estimated load torque transient. Despite this no visible oscillations appear in the transients of the load speed. After 2s, the estimate of the time constant of the load machine reaches its real value. The rapid changing of the load torque causes the oscillations in the estimate of T_{2e} which are noticeable visible at the time t=9s. Still, a such big estimation error can not be accepted in the high performance drive system

In order to improve the control structure performance the following modifications of the standard NEKF algorithm improving the quality of the estimation have been implemented. Firstly, the estimation of the time constant T_2 is active only when the motor speed is changing. Secondly, during this time the estimation of the load torque m_L is blocked. In the NEKF algorithm the last estimated value of the m_L is used. Also, when motor speed is not changing, the estimate of T_2 is stopped and the estimate of the m_L becomes active. During this time, the last estimated value of the time constant T_2 is utilized in the algorithm. This modification allows to increase the values of the covariance matrices of the NEKF.
All system states are reconstructed well and their estimation errors are very small and do not influence the system dynamics negatively (Fig. 9). The time constant of the load machine is estimated accurately with a small steady-stay error. The moments when the estimate of m_{Le} is stopped are visible in the load torque transient (Fig. 9g). Thus, the adaptive system with adaptive NEKF work properly.

5. Experimental results

All theoretical considerations have been confirmed experimentally in the laboratory set-up composed of a 0.5kW DC-motor driven by a static converter. The motor is coupled to a load machine by an elastic shaft (a steel shaft of 5mm diameter and 600mm length). The speed and position of the driven and loading motors have been measured by incremental encoders (36000 pulses per rotation). The mechanical system has a natural frequency of approximately 9.5Hz. The nominal parameters of the system are T_1=203ms, T_2=203ms, T_c =2.6ms. The picture of the experimental set-up is presented in Fig. 10.

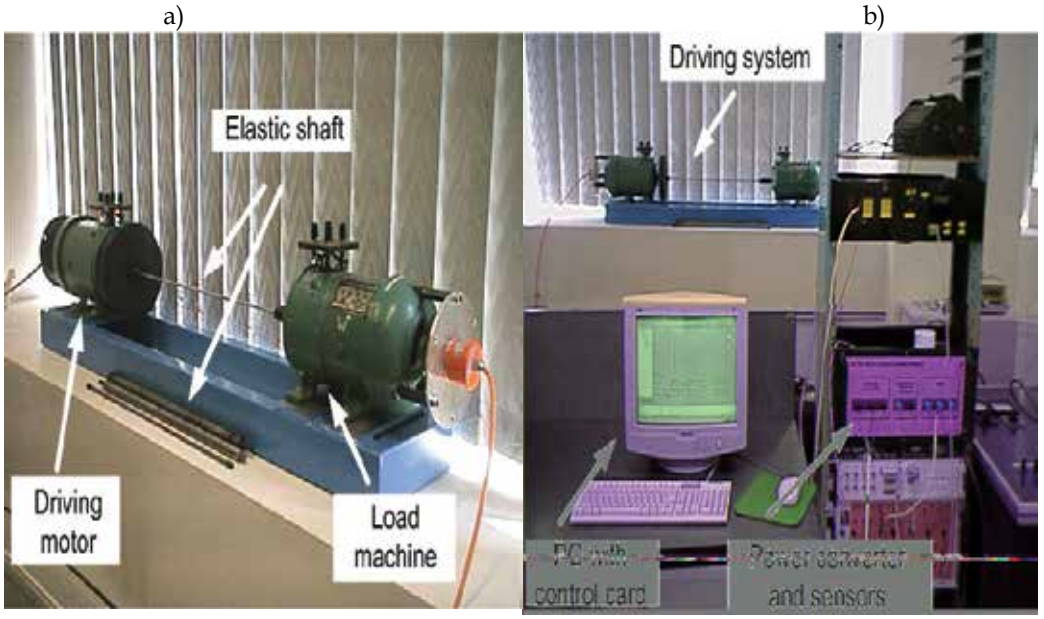

Fig. 10. The mechanical part of the laboratory set-up (a) and the general view of the laboratory set-up (b)

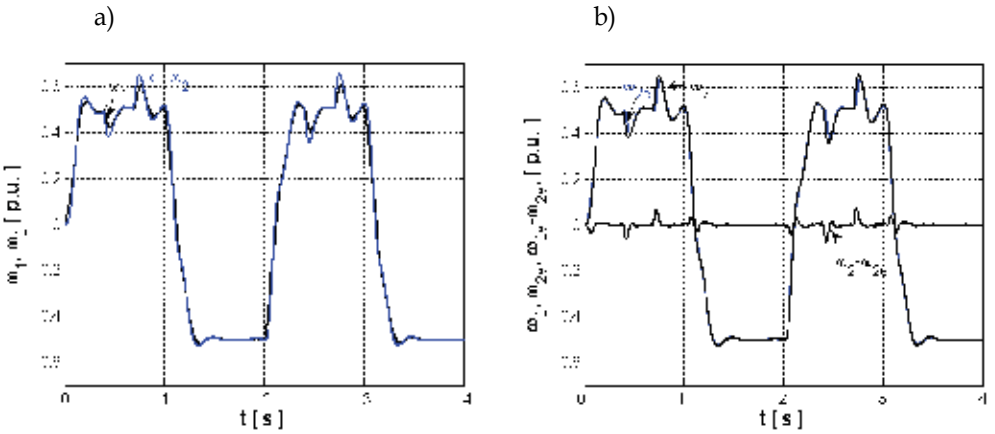

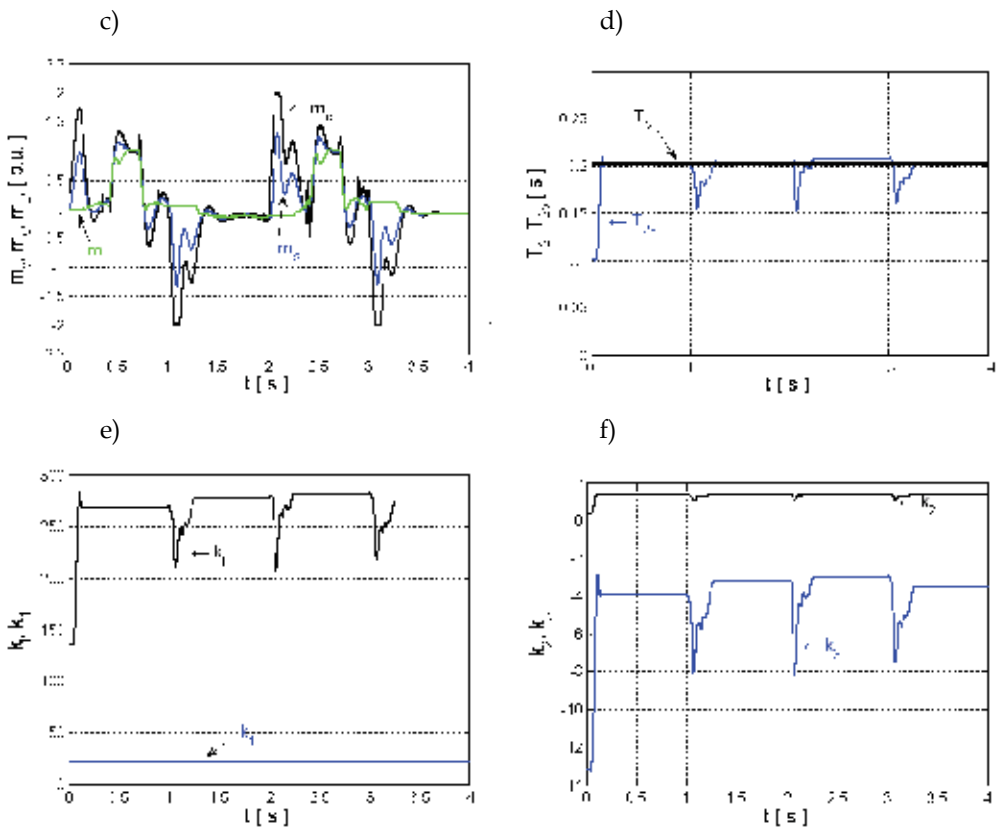

Fig. 11. Real transients of the: motor and load speeds (a), real and estimated load speeds and its estimation error (b), electromagnetic and estimated shaft and load torque (c), estimated time constant of the load side (d), control structure parameters (e,f) –for the reference value of the speed ω_r=0.5

First the performance of the drive system has been tested for the nominal value of the time constant of the load machine T_2=0.203s. The electromagnetic torque limit has been set to 2.

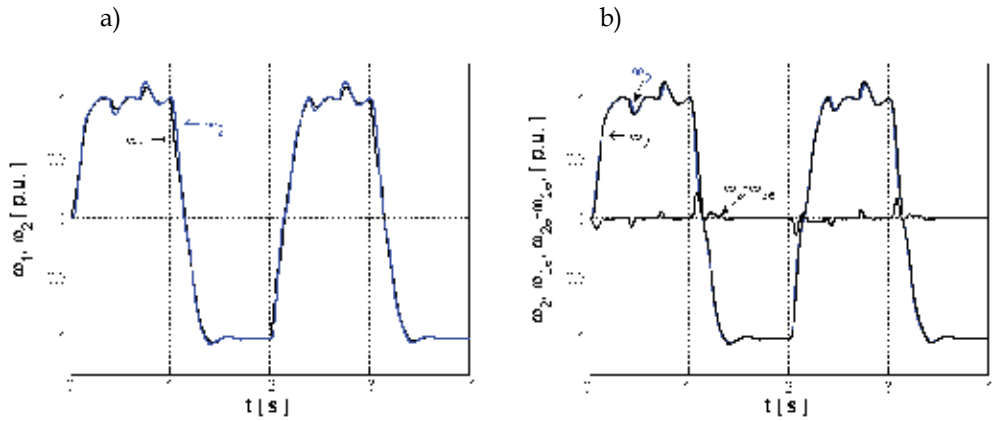

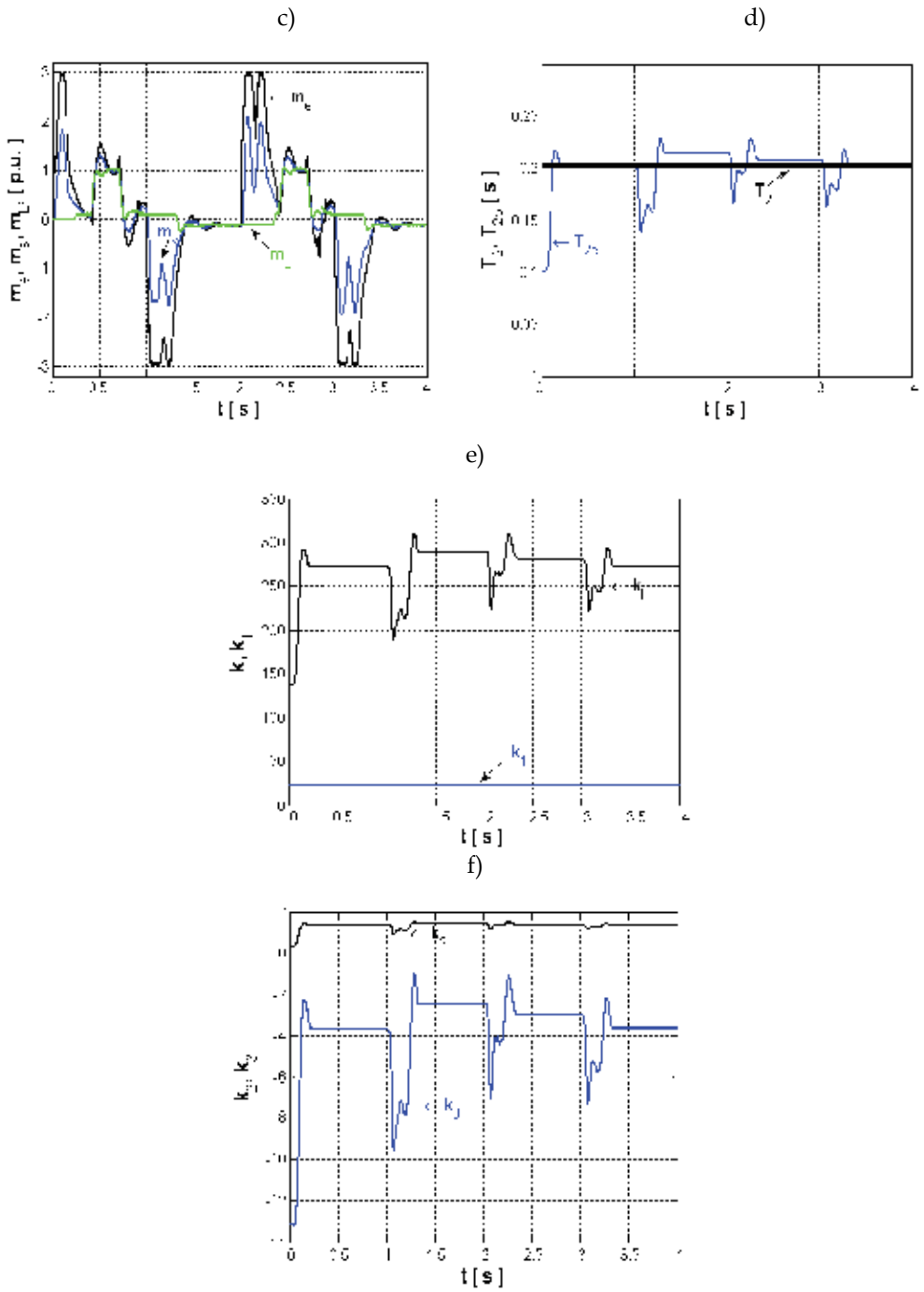

Fig. 12. Real transients of the: motor and load speeds (a), real and estimated load speeds and its estimation error (b), electromagnetic and estimated shaft and load torque (c), estimated time constant of the load side (d), control structure parameters (e,f) –for the reference value of the speed ω_r=1

The system works with the reference value of the speed set to 0.5. According to the adaptation procedure described in the previous section during start-up the estimate of the m_{Le} is blocked and the estimate of the T_{2e} is activated which is observable in Fig. 11c,d. When the control error decreases below 0.05, the estimate T_{2e} is blocked and the m_{Le}. At the time t_1=0.4s the nominal load torque is applied to the system. This affects the system speed in a negative way and some disruption is visible in its transients. The load torque is switched off at the time t_2=0.8s and the non-zero value of the estimate of the m_{Le} comes from the friction torques. At the time t_3=1s the system begins to reverse. When the value of the system speed is negative, no external torque is applied to the system. The drive reverses again at the time t_4=2s and then the work cycle is repeated. Clearly, the adaptive control structure with the NEKF works properly. The load speed as well as the time constant of the load machine are estimated with small errors. The transients of the control structure parameters are presented in Fig. 11 e,f. They vary (except k_1) with the estimated value of the T_{2e}.
Next the control structure with the electromagnetic torque limit set to 3 has been examined. The work cycle is identical as previously. But the reference speed is set to the nominal value. The transients of the system are presented in Fig. 12.
Similarly as before, the initial value of the time constant of the load machine is set to T_{2e}=0.1015s. After the start-up it reaches its real value almost without an error. During the next reversal the estimate of the T_2 oscillates around the real value. However, it should be pointed out that the estimation error does not exceed a few percent of the real value. The estimate of the T_2 is reconstructed very well. Small errors appear in its transient during the time when the load torque is switched on and off and during the reversal. The adaptive control structure with the state controller works in a stable way.

6. Conclusion

In order to damp the torsional vibrations, which could destroy the mechanical coupling between the driven and loading machine, the control structure with state controller is applied. The control structure coefficients depend on the time constant of the load side machine. In the case of the system with changeable load side inertia, there is a need to estimate this parameter and adapt the control structure gains in accordance with the actual estimated value. The application of the adaptive control structure ensures the required transient of the load speed despite the changeable load side inertia. In order to use the adaptive control structure, there is a need to choose a state estimator, which has to estimate the non-measurable system state variables and changeable parameters of the system. In this paper, the non-adaptive and adaptive nonlinear extended Kalman filter (NEKF) is tested. Parameters of the covariance matrices **Q** and **R** are selected using the genetic algorithm with special cost function. The application of the global optimization technique allows to reach the global solution according to the defined cost function. However, the application of the genetic algorithm is possible only as an off-line process due to a long calculation time. To ensure the optimal values of the covariance matrix **Q**, despite the load side parameter changes, the adaptation mechanism is developed. The suitable on-line change of the covariance matrix element q_{55} is proposed, according to the estimated value of the load side time constant. It is proved by simulation and experimental tests that the proposed control structure is effective for damping the torsional oscillation of two-mass drive system, also in

the case of wide range changes of load side inertia.

7. References

Beineke, S., Schütte, F. & Grotstollen H. (1997). Comparison of Methods for State Estimation and On-Line Identification in Speed and Position Control Loops, *Proc. of the Intern. Conf. European Power Electronics EPE'97*, pp. 3.364-3.369, Norway.

Cychowski M. T., Delaney K. and Szabat K. (2008), Explicit Model Predictive Control of the Drive System with Elastic Coupling, *Proc. of 13th International Conference on Power Electronics and Motion Control EPE-PEMC 2008*, on. cd, Poland

Erbatur, K., Kaynak, O. & Sabanovic A. (1999). A Study on Robustness Property of Sliding Mode Controllers: A Novel Design and Experimental Investigations, *IEEE Transaction on Industrial Electronics,* Vol. 46, No. 5 , pp. 1012-1018.

Erenturk, K. (2008). Nonlinear two-mass system control with sliding-mode and optimised proportional and integral derivative controller combined with a grey estimator, *Control Theory & Applications, IET*, Vol. 2, No. 7, pp. 635 – 642.

Ellis, G. & Lorenz, R.D. (2000), Resonant load control methods for industrial servo drives. *Proc. of the IEEE Industry Application Society Annual Meeting,* pp. 1438-1445.

Ferretti, G., Magnoni, G. A. & Rocco, P. (2004). Impedance Control for Elastic Joint Industrial Manipulators, *IEEE Trans. on Robotics and Automation*, Vol. 20, pp. 488-498.

Ferretti, G., Magnoni, G. A., Rocco, P., Vigano, L. & Rusconi, A. (2005). On the Use of Torque Sensors in a Space Robotics Application, : *Proc. on the IEEE/RSJ International Conference on Intelligent Robots and Systems IROS 2005*, pp. 1947- 1952, Canada.

Gawronski, W., Racho, C. S. & Mellstrom, J. A. (1995). Application of the LQG and Feedforward Controllers to the Deep Space Network Antennas, *IEEE Trans. on Control System Technology*, Vol. 3, No. 4, pp. 417-421.

Gu D. W., Petkov P. H., Konstantinov M. M. (2005). Robust Control Design with Matlab®, *Springer*.

Hace. A., Jezernik, K. & Sabanovic, A. (2005). Improved Design of VSS Controller for a Linear Belt-Driven Servomechanism, *IEEE/ASME Trans. on Mechatronic,* Vol. 10, No. 4, pp. 385-390.

Hirovonen, M., Pyrhonen, O. & Handroos H. (2006). Adaptive nonlinear velocity controller for a flexible mechanism of a linear motor, Mechatronic, *Elsevier,* Vol. 16, No. 5, pp. 279-290.

Hori, Y., Sawada, H. & Chun, Y. (1999). Slow resonance ratio control for vibration suppression and disturbance rejection in torsional system, *IEEE Trans. on Industrial Electronics,* Vol. 46, No. 1, pp. 162-168.

Horwitz, R., Li, Y., Oldham, K., Kon, S. & Huang, X. (2007), Dual-stage servo systems and vibration compensation in computer hard disk drives, *Control Engineering Practice*, Vol. 15, pp. 291-305.

Huang, A.,C. & Chen, Y., C. (2004). Adaptive Sliding Control for Single-Ling Flexible-Joint Robot With Mismatched Uncertainties, *IEEE Trans. on Control System Technology,* Vol. 12, pp. 770-775.

Itoh D., Iwasaki M., Matsui N. (2004). Optimal Design of Robust Vibration Suppression Controller Using Genetic Algorithms, *IEEE Transaction on Industrial Electronics*, Vol. 51, No. 5, pp. 947-953.

Ji, J. K. & Sul, S. K. (1995). Kalman Filter and LQ Based Speed Controller for Torsional Vibration Suppression in a 2-Mass Motor Drive System, *IEEE Trans. on Industrial Electronics*, Vol. 42, No. 6, pp. 564-571.

Katsura, S. & Ohnishi, K. (2005). Force Servoing by Flexible Manipulator Based on Resonance Ratio Control, *Proc. of the IEEE International Symposium on Industrial Electronics ISIE 2005*, pp. 1343-1348, Croatia.

Michels, K., Klawonn, F., Kruse, R. & Nürnberger, A. (2006). Fuzzy Control – Fundamentals, Stability and Design of Fuzzy Controllers, *Springer*.

Ohno, K. & Hara, T. (2006). Adaptive Resonant Mode Compensation for hard Dick Drives, , *IEEE Trans. on Industrial Electronics,* Vol. 53, No. 2, pp. 624-629.

Orlowska-Kowalska, T. & Szabat, K. (2008). Damping of Torsional Vibrations in Two-Mass System Using Adaptive Sliding Neuro-Fuzzy Approach, *IEEE Transactions on Industrial Informatics*, Vol. 4, No. 1, pp. 47-57.

O'Sullivan, T., Bingham, C. C. & Schofield, N. (2007), Enhanced Servo-Control Performance of Dual-Mass System, *IEEE Trans. on Ind. Electronics*, Vol. 54, No. 3, pp. 1387-1398.

Qiao, R., Zhu, Q. M., Li, S. Y. & Winfield, A. (2002). Torsional Vibration Suppression of a 2-Mass Main Drive System of Rolling Mill with KF Enhanced Pole Placement, *Proc. of the 4th World Congress on Intelligent Control and Automation*, pp. 206-210, China.

Shen, B. H. & Tsai, M. C. (2006) Robust dynamic stiffness design of linear servomotor drives, *Control Engineering Practice*, Vol. 14, pp. 1325-1336.

Sugiura, K. & Hori, Y. (1996). Vibration Suppression in 2- and 3-Mass System Based on the Feedback of Imperfect Derivative of the Estimated Torsional Torque, *IEEE Trans. on Industrial Electronics,* Vol. 43, No. 2, pp. 56-64.

Suh, G., Hyun, D. S., Park, J. I., Lee, K. D. & Lee, S. G. (2001), Design of a Pole Placement Controller for Reducing Oscillation and Settling Time in a Two-Inertia System, *Proc. of 24th Annual Conference of the IEEE Industrial Electronics Society IECON'01*,pp. 1439-1444, USA.

Szabat, K. & Orłowska-Kowalska, T. (2007). Vibration Suppression in Two-Mass Drive System using PI Speed Controller and Additional Feedbacks – Comparative Study, *IEEE Trans. on Industrial Electronics,* Vol. 54, No. 2, pp.1193-1206.

Szabat, K. & Orlowska-Kowalska, T. (2008). Performance Improvement of Industrial Drives With Mechanical Elasticity Using Nonlinear Adaptive Kalman Filter, *IEEE Transactions on Industrial Electronics*, Vol. 55, No. 3, pp. 1075-1084.

Valenzuela, M. A., Bentley, J. M. & Lorenz, R. D. (2005). Evaluation of Torsional Oscillations in Paper Machine Sections, *IEEE Trans. on Industrial Applications*, Vol. 41, No. 2, pp. 493-501.

Vukosovic, S., N. & Stojic, M. R., (1998). Suppression of Torsional Oscillations in a High-Performance Speed Servo Drive, *IEEE Trans. on Industrial Electronic*, Vol. 45, No. 1, pp. 108-117.

Wertz H., Beineke S., Frőhleke N., Bolognani S., Unterkofler K., Zigliotto M. & Zordan M. (1999) Computer Aided Commissioning of Speed and Position Control for Electrical Drives with Identification of Mechanical Load, *Proc. of the Thirty-Fourth IAS Annual Meeting Industry Applications Conference,* pp. 4.1372-4.2379, USA.

Wang L., Frayman Y. (2002). A Dynamically Generated Fuzzy Neural Network and its Application to Torsional Vibration Control of Tandem Cold Rolling Mill Spindles, *Engineering Applications of Artificial Intelligence,* Vol.15, No. 6, pp. 541-550.

Zhang, G. & Furusho, J. (2000). Speed Control of Two-Inertia System by PI/PID Control, *IEEE Trans. on Industrial Electronics*, Vol. 47, No. 3, pp. 603-609.

10

Adaptive Control of Dynamic Systems with Sandwiched Hysteresis Based on Neural Estimator

Yonghong Tan[1], Ruili Dong[1,2] & Xinlong Zhao[3]
1. Shanghai Normal University 2. Shanghai Jiaotong University &
3. Zhejiang Sci-Tech University
China

1. Introduction

The so-called Sandwich system with hysteresis is a class of systems in which a hysteretic subsystem is sandwiched between two smooth dynamic blocks. In engineering, many practical processes can be considered as the sandwich systems with hysteresis. In the following, two typical examples will be presented.

1.1 Ultra-precision moving positioning stage

A typical ultra-precision moving positioning stage is often used in ultra-precision manufacturing system for its nanometer displacement and fast linear moving speed. Usually, such platform consists of electric amplifiers, piezoelectric actuators and loads. As hysteresis is inherent in piezoelectric actuator, the amplifier and load can be considered as smooth dynamic subsystems. Therefore, this platform can be considered as a typical sandwich system with hysteresis. Fig.1 shows the architecture of such system.

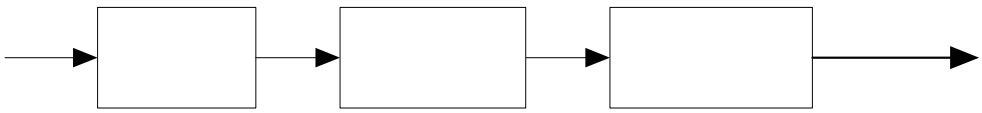

Fig. 1. Architecture of ultra-precision moving stage with piezoelectric actuator

1.2 Mechanical Transmission System

Mechanical transmission system often exists in machine tools or many other mechanical systems. A typical mechanical transmission system is shown in Fig.2. In this system, the servomotor is used to drive a gearbox connected with a mechanical work platform through a screw. In this system, u is the servomotor angle, x is the angle of the gearbox, and y is the displacement of the work platform. The servomotor and the work platform can be considered as smooth dynamic subsystems. However, the gearbox and screw in this system is a typical hysteresis nonlinearity due to the tear and wear of the gear teeth. Obviously, this mechanical system can be described by the sandwich system with hysteresis.

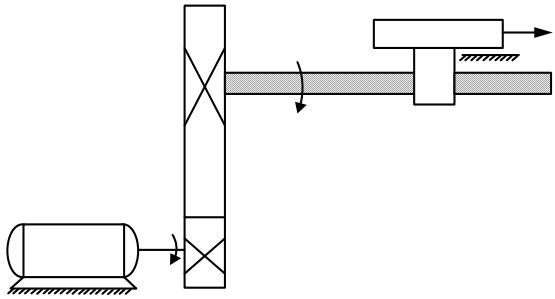

Fig. 2. Mechanical transmission system

Although, sandwich systems with hysteresis often exist in engineering practice, there are only several research reports found on the control of them. Taware & Tao (1999) presented an analysis on the control of such systems with backlash-type hysteresis. Tao & Ma (2001) proposed an optimal control for the systems with sandwiched backlash. In their methods, an optimal control scheme is employed for backlash compensation. Then, the nonlinear feedback control law is used for the control of nonlinear dynamics. Zhao & Tan (2006) proposed a neural adaptive control for sandwich systems with hysteresis. The neural network based hysteresis compensator is developed to compensate for the effect of the hysteresis. Furthermore, Zhao et. al. (2007) presented an adaptive control strategy for sandwich systems with dynamic hysteresis based on Duhem hysteretic operator. Corradini et. al. (2007) proposed a variable structure control of nonlinear uncertain sandwich systems with hysteretic block. Therefore, the control of sandwich systems with hysteresis has become one of the interesting topics in control engineering domain.

It is known that the existence of hysteresis in actuators often leads to oscillation and undesirable inaccuracy. Therefore, the main purpose of design a control scheme for sandwich system with hysteresis is to eliminate the side effect of hysteresis inherent in the system and force the system to track the reference trajectory. Note that hysteresis is a non-differentiable nonlinear system with multi-valued mapping. Moreover the structure of the sandwich system is rather complex. Hence, it is not easy to construct a compensator for the hysteresis in such system. Therefore it is a real challenge to develop a control strategy for the dynamic systems with sandwiched hysteresis.

In this chapter, a mathematical description of the sandwich systems with hysteresis will be described in section 2. Then, in section 3, the control architecture for the sandwich systems with hysteresis will be illustrated. In this architecture, a neural network based inverse model is constructed to cancel the effect of the first dynamic block of sandwich system. Then, the sandwich system can be transformed to a nonlinear system preceded by hysteresis which can be described by a Hammerstein model with hysteresis. In Section 4, a neural network based estimator will be developed in terms of a proposed expanded input space with hysteretic operator. The developed neural hysteretic estimator can be used to compensate for the system residual caused by the effect of hysteresis. Section 5 will present an adaptive control strategy based on pseudo inverse control technique for the obtained Hammerstein system with hysteresis. One of advantages of the controller is that it does not need to construct the hysteresis inverse to cancel hysteretic effect. The neural control strategy and the corresponding adaptive law based on the Lyapunov stability theory will be developed.

Furthermore, Comparison of the simulation results between the proposed method and the PID control strategy will be illustrated in Section 6. Section 7 will present the remarks and conclusions of this Chapter.

2. Mathematical Description of Sandwich Systems with Hysteresis

The structure of the sanwich system with hysteresis is shown in Fig.3. Suppose the nonlinear single-input-single-output (SISO) system with sandwiched hysteresis is described by

$$L_i:\ f_i[v^{(n)}, v^{(n-1)}, \cdots, v^{(1)}, v, r^{(m)}, r^{(m-1)}, \cdots, r^{(1)}, r] = 0 \tag{1}$$

where r is the input, v is the output, $v^{(n)}$ is the *n-th* order derivative of v, $r^{(m)}$ is *m-th* order derivative of r, m and n $(m \le n)$ are the orders of the input and output respectively.

$$H:\ u = H(v) \tag{2}$$

where H presents the hysteresis nonlinearity.

$$L_o: \begin{cases} \dot{x}_1 = x_2 \\ \dot{x}_2 = x_3 \\ \cdots \\ \dot{x}_{n-1} = x_n \\ \dot{x}_n = f_o(x) + g_o(x)u \end{cases} \tag{3}$$

and

$$y = x_1 \tag{4}$$

where $x = [x_1, x_2, \cdots, x_n]^T$ is the system state vector, u is the input, y is the output, v is the control input and u is the actuator output. It is assumed that $f_o(x)$ and $g_o(x)$ are sufficiently smooth but unknown functions and satisfy $\frac{\partial f_o}{\partial u} \neq 0$ and $\frac{\partial g_o}{\partial u} \neq 0$. Moreover, assume that f_o is invertible. Notation $H[.]$ denotes that the hysteresis nonlinearity is not dependent on an instantaneous value $v(t)$ but the trajectory, $v(t) \in C^0[0,t]$. Assume that all the control and input variables, i.e. $v^{(n)}, v^{(n-1)}, \cdots, v^{(1)}, v, r^{(m)}, r^{(m-1)}, \cdots, r^{(1)}, r$ are known.

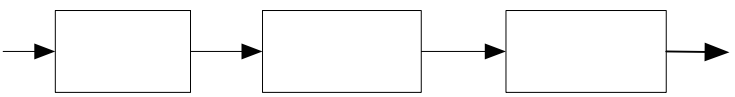

Fig. 3. The structure of sandwich system with hysteresis

3. Control Architecture for Sandwich System with Hysteresis

From Fig. 3, it is known that the architecture of the sandwich system with hysteresis is rather complex. It would be convenient for us to design a control strategy for such system if we could find a method to simplify the structure of the system. In this section, a control architecture for the sandwich system will be discussed. In this architecture, a neural networks (NN) based inverse system $\hat{L}_i^{-1}$ will be constructed. By connecting the NN based inverse with the system L_i can form an approximate pseudo-linear unit compensator which leads to $\hat{L}_i^{-1}L_i \approx 1$. Then the sandwich system can be transform to a pseudo-linear unit system connected with a nonlinear system preceded with hysteresis nonlinearity which is shown in Fig.4. The obtained the system can be considered as a Hammerstein System with hysteresis.

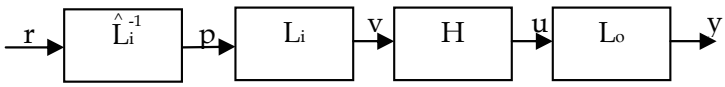

Fig. 4. The sandwich system with a pseudo-linear unit compensation

With the above-mentioned NN based inverse, the effect of L_i would be cancelled. So we can design the controller for the system L_o preceded by a hysteresis nonlinearity. Usually, the model uncertainty of the neural network based compensator exists. That implies the NN based compensator cannot completely compensate for the effect of L_i. Therefore, a model residual should be added to system L_o. That is $\hat{L}_i^{-1}L_i = 1+\xi$, where ξ is a bounded modeling error. Hence, the obtained system preceded by a hystersis can be described as follows:

$$H: u = H(v) \ , \tag{5}$$

$$L_o: \begin{cases} \dot{x}_1 = x_2 \\ \dot{x}_2 = x_3 \\ \cdots \\ \dot{x}_{n-1} = x_n \\ \dot{x}_n = f_o(x) + g_o(x)u + \xi \end{cases} , \tag{6}$$

and

$$y = x_1 \ . \tag{7}$$

The control objective is to design a control law $v(t)$ to force $y(t)$, the plant output, to track a smooth prescribed trajectory $y_d(t)$ with an acceptable accuracy. The desired state vector is defined as $x_d(t) = [y_d, \dot{y}_d, \cdots y_d^{(n-1)}]^T$ where $y_d^{(n-1)}$ is the $(n-1)th$ order derivative. Moreover, the tracking error vector is defined as $e = x - x_d$. It is assumed that the desired states are

bounded, i.e. $\|x_d\| \le X_d$. Moreover, ξ denotes bounded disturbance caused by NN based inverse, where $|\xi| \le \xi_N$, and $\xi_N > 0$.
Define the filtered tracking error as

$$\tau = [\lambda_1, \lambda_2 \cdots \lambda_{n-1}, 1]e = [\Lambda^T, 1]e \tag{8}$$

where $\Lambda = [\lambda_1, \lambda_2 \cdots \lambda_{n-1}]^T$ is a parameter vector to be designed. Suppose
$s^{n-1} + \lambda_{n-1}s^{n-2} + \cdots + \lambda_1$
is Hurwitz. Differentiating (8) and using (6), it results in

$$\dot{\tau} = \dot{x}_n - y_d^n + [0, \Lambda^T]e = f_o(x) + g_o(x)u - y_d^n + [0, \Lambda^T]e + \xi \tag{9}$$

As u is the output of hysteresis which is usually unknown, an invertible function $\hat{f}(x,v)$ is introduced to approximate $f_o(x) + g_o(x)u$. Adding and subtracting $\hat{f}(x,v)$ to and from the right hand side of (9), it yields

$$\begin{aligned} \dot{\tau} &= \delta + f_o(x) + g_o(x)u - \hat{f}(x,v) - y_d^{(n)} + [0, \Lambda^T]e + \xi \\ &= \delta + F(x,u) - \hat{f}(x,v) - y_d^{(n)} + [0, \Lambda^T]e + \xi \\ &= \delta + \tilde{f}(x,v,u) - y_d^{(n)} + [0, \Lambda^T]e + \xi \end{aligned} \tag{10}$$

where $\delta = \hat{f}(x,v)$ is the so called pseudo-control (Calis & Hovakimyan, 2001) and (Hovakimyan & Nandi ,2002), $F(x,u) = f_o(x) + g_o(x)u$ and $\tilde{f}(x,v,u) = F(x,u) - \hat{f}(x,v)$ is the system residual. As $\hat{f}(x,v)$ is invertible with respect to v and satisfies (Calis & Hovakimyan, 2001):

$$1.\ \operatorname{sgn}\frac{\partial F}{\partial u}\frac{\partial u}{\partial v} = \operatorname{sgn}\frac{\partial \hat{f}}{\partial v}, \tag{11}$$

and

$$2.\ \left|\frac{\partial \hat{f}}{\partial v}\right| > \frac{1}{2}\left|\frac{\partial F}{\partial u}\frac{\partial u}{\partial v}\right| > 0\ . \tag{12}$$

In order to design the corresponding control strategy, the approximation of the nonlinear residual $\tilde{f}(x,v,u)$ is required. Neural networks would be one of the recommended alternatives to model this residual. However, $\tilde{f}(x,v,u)$ involves the characteristic of

hysteresis, the traditional nonlinear identification methods such as neural modeling technique usually cannot be directly applied to the modeling of it since the hysteresis is a non-linearity with multi-valued mapping (Adly & Abd-El-Hafiz, 1998). In Section 4, we will present a method to construct the neural estimator for $\tilde{f}(x,v,u)$ to compensate for the effect of hysteresis. Moreover, a corresponding adaptive control method based on the control archieture stated-above will be illustrated in Section 5.

4. Neural Estimator for System Residual

In order to approximate the system residual, neural network can be considered as an alternative. However, the system residual contains the characteristic of hysteresis which is a system with multi-valued mapping. In this section, a hysteretic operator is proposed to construct an expanded input space so as to transform the multi-valued mapping of hysteresis into a one-to-one mapping (Zhao & Tan, 2008). Thus, the neural networks can be used for modeling of hysteresis based on the expanded input space with the hysteretic operator. The proposed hysteretic operator is defined as:

$$h(x) = (1 - e^{-|x - x_p|})(x - x_p) + h(x_p), \tag{13}$$

where x is the current input, $h(x)$ is the current output, x_p is the dominant extremum adjacent to the current input x. $h(x_p)$ is the output of the operator when the input is x_p.

Lemma 1: Let $x(t) \in C(R^+)$, where $R^+ = \{t \mid t \geq 0\}$ and $C(R^+)$ are the sets of continuous functions on R^+. If there exist two time instants t_1, t_2 and $t_1 \neq t_2$, such that $x(t_1) = x(t_2)$, $x(t_1)$ and $x(t_2)$ are not the extrema, then $h[x(t_1)] \neq h[x(t_2)]$.

Proof: For $x(t)$ decreases or increases monotonically, (13) becomes

$$h(x) = \begin{cases} h_{in}(x) = [1 - e^{-(x - x_p)}](x - x_p) + h(x_p), & \dot{x}(t) > 0 \\ h_{de}(x) = (1 - e^{x - x_p})(x - x_p) + h(x_p), & \dot{x}(t) < 0 \end{cases} \tag{14}$$

$$\begin{aligned} h'_{in}(x) &= e^{-(x - x_p)} \cdot (x - x_p) + [1 - e^{-(x - x_p)}] \\ &= 1 - [1 - (x - x_p)] / e^{x - x_p} \\ &> 1 - 1 / e^{x - x_p} > 0 \end{aligned} \tag{15}$$

Therefore, $h_{in}(x)$ is monotonic. Similarly one can obtain that $h_{de}(x)$ is monotonic. It is noted that $h_{in}(x)$ is obtained from $h_{in0}(x) = (1 - e^{-x})x \quad (x \geq 0)$. That means its origin moves from $(0,0)$ to $(x_p, h(x_p))$. Similarly $h_{de}(x)$ is obtained from $h_{de0}(x) = (1 - e^{x})x \quad (x \leq 0)$. It represents that its origin moves from $(0,0)$ to $(x_p, h(x_p))$. As $h_{in0}(-x) = -h_{de0}(x)$, it implies

that $h_{in}(x)$ and $h_{de}(x)$ are antisymmetric. Therefore it can be concluded that $h_{in}(x)$ and $h_{de}(x)$ intersect only at extrumum point $(x_p, h(x_p))$. That is, if $x(t_1)$ and $x(t_2)$ are not the extrema, $x(t_1) = x(t_2)$, then $h\left[x(t_1)\right] \neq h\left[x(t_2)\right]$.

Remark: If both $h(x)$ and $H[\cdot]$ are fed with the same input $v(t)$, the curve of $h[v(t)]$ exhibits similarity to that of $H[v(t)]$ such as ascending, turning and descending. Moreover, since $x(t_1) = x(t_2)$, $x(t_1)$ and $x(t_2)$ are not the extrema, $h\left[x(t_1)\right] \neq h\left[x(t_2)\right]$, the pair $(v(t), h[v(t)])$ will uniquely correspond to one of the output values of hysteresis $H[v(t)]$.

Lemma 2: If there exist two time instants t_1, t_2 and $t_1 \neq t_2$, such that $h[x(t_1)] - h[x(t_2)] \to 0$, then $x(t_1) - x(t_2) \to 0$.

Proof:

$$\frac{h_{in}\left[x(t_1)\right] - h_{in}\left[x(t_2)\right]}{x(t_1) - x(t_2)} = k, \quad k \in (0, +\infty), \tag{16}$$

and

$$x(t_1) - x(t_2) = \frac{h_{in}\left[x(t_1)\right] - h_{in}\left[x(t_2)\right]}{k}. \tag{17}$$

It is clear that if $h_{in}\left[x(t_1)\right] - h_{in}\left[x(t_2)\right] \to 0$, then $x(t_1) - x(t_2) \to 0$. Similarly, it is obtained that if $h_{de}\left[x(t_1)\right] - h_{de}\left[x(t_2)\right] \to 0$, then $x(t_1) - x(t_2) \to 0$. Thus, it leads to the following theorem, i.e.:

Theorem 1: For any hysteresis, there exists a continuous one-to-one mapping $\Gamma : R^2 \to R$, such that $H[v(t)] = \Gamma(v(t), h[v(t)])$, where $\{v(t), h[v(t)]\}$ is an expanded input space with hysteresis operator.

Proof: The proof can be divided into two cases, i.e.

Case 1: If $v(t)$ is not the extrema. Based on Lemma1, if there exist two time instants t_1, t_2 and $t_1 \neq t_2$, then $(v(t_1), h\left[v(t_1)\right]) \neq (v(t_2), h\left[v(t_2)\right])$. Therefore, the pair $(v(t), h[v(t)])$ uniquely corresponds to an output value of $H[v(t)]$.

Case 2: If $v(t)$ is the extrema, then $(v(t_1), h\left[v(t_1)\right]) = (v(t_2), h\left[v(t_2)\right])$. According to the principle of the classical Preisach modeling, i.e. $H[v(t_1)] = H[v(t_2)]$, then the pair [redacted] uniquely corresponds to an output value of $H[v(t)]$.

Combining the above-mentioned two cases, there exists a mapping $\Gamma : R^2 \to R$ such that $H[v(t)] = \Gamma(v(t), h[v(t)])$.

In theorem 1, the obtained mapping $\Gamma(.)$ is a continuous function. According to Lemma 2, from $v(t_1) - v(t_2) \to 0$, it leads to $H[v(t_1)] - H[v(t_2)] \to 0$. Also, from $h\left[v(t_1)\right] - h\left[v(t_2)\right] \to 0$, it

yields $v(t_1)-v(t_2)\to 0$. Then, it results in $H[v(t_1)]-H[v(t_2)]\to 0$. Therefore, it is derived that Γ is a continuous function. Moreover, Theorem1 indicates that the multi-valued mapping of hysteresis can be transformed to a one-to-one mapping. It can be proved that the obtained mapping is a continuous mapping, i.e.

Let $T=[t_0,\infty)\in R$, $V=\{v\mid T\xrightarrow{v}R\}$. Also let $F=\{h\mid T\xrightarrow{h}R\}$ be the input sets. Given $t_i\in T$ it is obvious that $v(t_i)<+\infty$ and $h[v(t_i)]<+\infty$. So that $(v(t_i),h[v(t_i)])\in R^2$. Thus, it is obtained that $\Phi=\{(v(t_i),h[v(t_i)])\mid v(t_i)\in V,h[v(t_i)]\in F\}$ is a compact set .

Hence, it provides a premise to apply neural networks to modeling of the behavior of hysteresis. Based on the proposed expanded input space with hysteretic operator, a neural network is used to approximate the system residual, i.e. $\tilde{f}(x,v,u)$:

$$\tilde{f}(x.v,u)=W^T\sigma(V^Tx_{nn})+\varepsilon(x_{nn}) \tag{18}$$

where $\sigma(\cdot)$ is activation function, V is the first-to-second layer interconnection weights, W is the second-to-third layer interconnection weights, $x_{nn}=(x^T,\delta,u)$, ε is the NN functional reconstruction error, $\|\varepsilon(x_{nn})\|\le\varepsilon_N$, and $\varepsilon_N>0$.

The above-mentioned neural network based on the expanded input space with hysteretic operator can be used to construct the corresponding neural estimator for the system residual $\tilde{f}(x,v,u)$. Thus, it can be used for the compensation for the effect of the hysteresis inherent in the sandwich system.

5. Adaptive Control Strategy

In section 3, we introduce an architecture of the control strategy for the sandwich system with hysteresis. In the control structure, a neural inverse model is used to compensate for the effect of L_i in the architecture of the sandwich system with hysteresis. After the compensation, the sandwich system with hysteresis is approximately tranformed into a Hammerstein system with hysteresis. In this section, an adaptive control strategy is developed for the obtained Hammerstein system with hysteresis.

Assumption 1: If the weight matrices, i.e. V and W of the neural estimator are respectively bounded by $V_p>0$ and $W_p>0$, i.e. $\|W\|_F\le W_p$ and $\|V\|\le V_p$,where $\|\cdot\|_F$ represents Frobenius norm. Then, the corresponding pseudo-control can be chosen as

$$\delta=y_d^{(n)}-K\tau-[0,\Lambda^T]e-v_{ad}+v_r \tag{19}$$

where v_r is the term for robust design, K is a design parameter, v_{ad} is the output of neural network, i.e. $v_{ad}=\hat{W}^T\sigma(\hat{V}^Tx_{nn})$ where $\hat{W}$ and $\hat{V}$ are the estimated values of W and V .

From (10) and (19), notice that $\tilde{f}(x,v,u)$ depends on v_{ad} through δ. However, v_{ad} has to be designed to cancel the effect of $\tilde{f}(x,v,u)$. This should assume that the mapping $\delta_{ad} \mapsto \tilde{f}$ is a contraction over the entirely interested input domain. It has been proven by Hovakimyan and Nandi (2002) that the assumption is held when (11) and (12) are satisfied. Using (18) and (19), (10) can be written as

$$\dot{\tau} = -K\tau - \hat{W}^T\sigma(\hat{V}^T x_{nn}) + W^T\sigma(V^T x_{nn}) + v_r + \varepsilon + \xi \,. \tag{20}$$

Difine

$$\tilde{V} = V - \hat{V} \text{ and } \tilde{W} = W - \hat{W} \quad . \tag{21}$$

The Taylor series expansion of $\sigma(Vx_{nn})$ for a given x_{nn} can be written as

$$\sigma(Vx_{nn}) = \sigma(\hat{V}x_{nn}) + \sigma'(\hat{V}x_{nn})\tilde{V}x_{nn} + o(\tilde{V}x_{nn})^2 \tag{23}$$

where $\sigma'(\hat{z}) = d\sigma(z)/dz\,|_{z=\hat{z}}$ and $o(\tilde{z})^2$ is the term of order two. Denoting $\sigma = \sigma(V^T x_{nn})$, $\hat{\sigma} = \sigma(\hat{V}^T x_{nn})$, and $\hat{\sigma}' = \sigma'(\hat{V}^T x_{nn})$, with the procedure as Appendix, we have

$$\dot{\tau} = -K\tau + \tilde{W}^T(\hat{\sigma} - \hat{\sigma}'\hat{V}^T x_{nn}) + \hat{W}^T\hat{\sigma}'\tilde{V}^T x_{nn} + v_r + \varepsilon + \xi + w \tag{24}$$

where

$$w = W^T(\sigma - \hat{\sigma}) + W^T\hat{\sigma}'\hat{V}^T x_{nn} - \hat{W}^T\hat{\sigma}'V^T x_{nn} \,. \tag{25}$$

An upper bound for w can be presented as:

$$\|w\| \le \|W\|_1 + \|W\|\left\|\hat{\sigma}'\hat{V}^T x_{nn}\right\| + \|V\|_F \left\|x_{nn}\hat{W}^T\hat{\sigma}'\right\|_F \tag{26}$$

or

$$\|w\| \le \rho_w \vartheta_w(\hat{W},\hat{V},x_{nn}) \tag{27}$$

where $\vartheta_w = 1 + \left\|\hat{\sigma}'\hat{V}^T x_{nn}\right\| + \left\|x_{nn}\hat{W}^T\hat{\sigma}'\right\|_F$ and $\rho_w = \max(\|W\|_1, \|W\|, \|V\|_F)$.

Theorem 2: Let the desired trajectory be bounded. Consider the system represented by (5), (6) and (7), if the control law and adaptive law are given by

$$v = \hat{f}^{-1}(x, \delta) \tag{28}$$

$$\delta = y_d^{(n)} - K\tau - [0, \Lambda^T]e - v_{ad} + v_r \tag{29}$$

$$\dot{\hat{W}} = F[(\hat{\sigma} - \hat{\sigma}'\hat{V}^T x_{nn})\tau - k\hat{W}\|\tau\|] \tag{30}$$

$$\dot{\hat{V}} = R[x_{nn}\hat{W}^T\hat{\sigma}'\tau - k\hat{V}\|\tau\|] \tag{31}$$

$$\dot{\hat{\phi}} = \gamma[\|\tau\|(\vartheta_w + 1) - k\|\tau\|\hat{\phi}] \tag{32}$$

and

$$v_r = \begin{cases} -\hat{\phi}(\vartheta_w + 1)\dfrac{\tau}{\|\tau\|}, & \|\tau\| \neq 0 \\ 0, & \|\tau\| \neq 0 \end{cases} \tag{33}$$

where $F = F^T > 0$, $R = R^T > 0$, $\gamma > 0$, $\phi = \max[\rho_w, (\varepsilon_N + \xi_N)]$, and $\tilde{\phi} = \phi - \hat{\phi}$; then the signals e, $\hat{W}$, $\hat{V}$, and $\hat{\phi}$ in the closed-loop system are ultimately bounded.

Proof: Consider the following Lyapunov function candidate, i.e.

$$L = \frac{1}{2}\tau^2 + \frac{1}{2}tr(\tilde{W}^T F^{-1}\tilde{W}) + \frac{1}{2}tr(\tilde{V}^T R^{-1}\tilde{V}) + \frac{1}{2}\tilde{\phi}^T\gamma^{-1}\tilde{\phi} \tag{34}$$

The derivative of L will be

$$\dot{L} = \tau\dot{\tau} + tr(\tilde{W}^T F^{-1}\dot{\tilde{W}}) + tr(\tilde{V}^T R^{-1}\dot{\tilde{V}}) + \tilde{\phi}^T\gamma^{-1}\dot{\tilde{\phi}} \tag{35}$$

Substituting (20) into (35), it yields

$$\begin{aligned}\dot{L} = &-K\tau^2 + \tau v_r + \tau(w + \varepsilon + \xi) + \tilde{\phi}^T\gamma^{-1}\dot{\tilde{\phi}} + tr\tilde{W}^T[F^{-1}\dot{\tilde{W}} + (\hat{\sigma} - \hat{\sigma}'\hat{V}^T x_{nn})\tau] \\ &+ tr\tilde{V}^T(R^{-1}\dot{\tilde{V}} + x_{nn}\tau\hat{W}^T\hat{\sigma}')\end{aligned}. \tag{36}$$

Substituting $\dot{\tilde{W}} = -\dot{\hat{W}}$ and $\dot{\tilde{V}} = -\dot{\hat{V}}$ into (30) and (31), (36) can be rewritten as

$$\dot{L} = -K\tau^2 + \tau v_r + \tau(w + \varepsilon + \xi) + \tilde{\phi}^T\gamma^{-1}\dot{\tilde{\phi}} + k|\tau|[tr(\tilde{W}^T\hat{W}) + tr(\tilde{V}^T\hat{V})] \ . \tag{37}$$

Considering (27) and $\phi = \max[\rho_w, (\varepsilon_N + \xi_N)]$,we obtain

$$\dot{L} \le -K\tau^2 + \tau v_r + |\tau|\phi(\vartheta_w + 1) - \tilde{\phi}\gamma^{-1}\dot{\hat{\phi}} + k|\tau|[tr(\tilde{W}^T\hat{W}) + tr(\tilde{V}^T\hat{V})]. \tag{38}$$

Substituting (32) and (33) into (38), it results in

$$\dot{L} \le -K\tau^2 + k\|\tau\|[tr(\tilde{W}^T\hat{W}) + tr(\tilde{V}^T\hat{V}) + \tilde{\phi}^T\hat{\phi}] \quad . \tag{39}$$

Defining

$$\tilde{Z} = \begin{bmatrix} \tilde{W} & 0 & 0 \\ 0 & \tilde{V} & 0 \\ 0 & 0 & \tilde{\phi} \end{bmatrix}, \ \hat{Z} = \begin{bmatrix} \hat{W} & 0 & 0 \\ 0 & \hat{V} & 0 \\ 0 & 0 & \hat{\phi} \end{bmatrix} \text{ and } Z = \begin{bmatrix} W & 0 & 0 \\ 0 & V & 0 \\ 0 & 0 & \phi \end{bmatrix}, \tag{39}$$

can be rewritten as

$$\dot{L} \le -K\tau^2 + k\|\tau\| tr(\tilde{Z}^T\hat{Z}) . \tag{40}$$

As $tr(\tilde{Z}^T\hat{Z}) \le \|\tilde{Z}\|_F \|Z\|_F - \|\tilde{Z}\|_F^2$,

it leads to

$$\dot{L} \le -K\tau^2 + k\|\tau\|(\|\tilde{Z}\|_F \|Z\|_F - \|\tilde{Z}\|_F^2) . \tag{41}$$

That is

$$\dot{L} \le -\|\tau\|[K\|\tau\| + k(\|\tilde{Z}\|_F - \frac{\|Z\|_F}{2})^2 - \frac{k\|Z\|_F^2}{4}] . \tag{42}$$

Thus, $\dot{L}$ is negative as long as either $\|\tau\| > \frac{k\|Z\|_F^2}{4K}$ or $\|\tilde{Z}\|_F > \|Z\|_F$. This demonstrate that τ, $\tilde{W}$, $\tilde{V}$, and $\tilde{\phi}$ are ultimately bounded. According to Assumption 1 and the definition of τ and ϕ, we can obtain that the variables e, $\hat{W}$, $\hat{V}$ and $\hat{\phi}$ in the closed-loop system are ultimately bounded.

6. Simulation

In order to illustrate that the proposed approach is applicable to nonlinear system with sandwiched hysteresis, we consider the following nonlear system:

L_i , $\dot{v} = -0.2(\sin v - \cos v) - \frac{v}{1+v^2} + (0.4 \sin v \cos v^2 + 0.8)r$, $v(0) = 0$

H , The hysteresis is generated by the sum of $N = 50$ backlash operators, i.e. ,

$u = H[v(t)] = \sum_{i=1}^{N} u_i$, and

$$\dot{u}_i = \begin{cases} \dot{v}(t) & \dot{v}(t) > 0, u_i(t) = v(t) - \frac{d_i}{2} \\ \dot{v}(t) & \dot{v}(t) < 0, u_i(t) = v(t) + \frac{d_i}{2} \\ 0 & \text{otherwise} \end{cases}$$

where u_i and d_i are respectively the output and the dead-band width of i - th backlash operator where $i = 1, 2, \cdots N$ ($N > 0$ is a positive integer).The values of the dead-band widths are evenly distributed within $[0.02, 1]$. All the initial outputs of the operators are set to zero. Fig. 5 shows the response of the hysteresis contained in the system.

$$L_o : \begin{cases} \dot{x}_1 = x_2 \\ \dot{x}_2 = (1 - x_1^2)x_2 - x_1 + u \end{cases}$$

and

$y = x_1$.

The design procedure of the controller for the snadwich system with hysteresis will be shown in the following.

1) *Construction of nerual network based L_i inverse.* An artificial neural network unit inverse , i.e. $\hat{L}_i^{-1}$ is constructed to cancel the effect of the first dynamic block, i.e. L_i . The system is excited by the input $r_l(t) = \sin 2t + \cos t$. Then, 500 input/output pairs of data $\{r_l, (v_l, \dot{v}_l)\}$ are obtained. Using these data as learning samples, a neural network based inverse $\hat{L}_i^{-1}$ is constructed. The architecture of neural network based inverse model consists of 2 input nodes, 10 hidden neurons and 1 output neuron. The sigmoid function and linear function are respectively used as activation function in the hidden layer and the output layer. The conjugate gradient algorithm with Powell-Beale restarted method (Powell, 1977) is used to

train the neural network. The compensation result of the NN based $\hat{L}_i^{-1}$ is shown in Fig. 6. It is known that there are some larger error happened in the beginning. Then it is gradually reduced as the control proceeded.

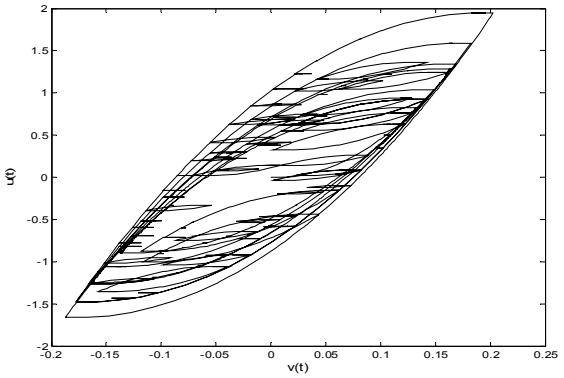

Fig. 5. The hysteresis in the system

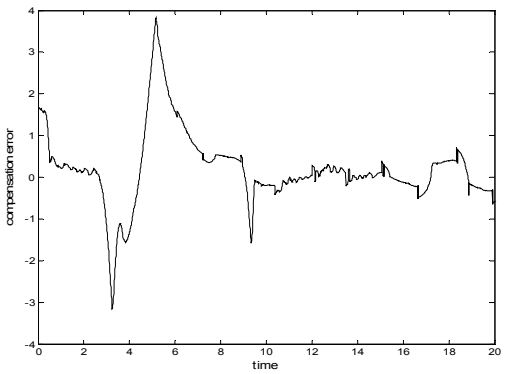

Fig. 6. The compensation error of NN based $\hat{L}_i^{-1}$

2) Neural approximator of system residual: The neural network used to approximate $\tilde{f}(x,v,u)$ consists of 4 input nodes, 35 hidden neurons and 1 output neuron. The input of the NN is $x_{nn} = (x^T, \delta, u)$. The activation function is $\sigma(x) = \dfrac{1}{1+e^x}$.

3) The selection of the controller parameters: The other parameters of the controller are respectively chosen as $\lambda_1 = 2$, $K = 11$, $k = 0.001$, $\gamma = 0.1$, $\hat{f}(x,v) = v$, $F = 8I$, and $R = 5I$, where I is the unit matrix.

4) PID control for comparison: In order to compare the control performance of the proposed control strategy with the PID controller , we choose

$$v(t) = -22e_1 + \int_0^t e_1 dt - 13e_2$$

where $e_1 = y - y_d$, $e_2 = \dot{y} - \dot{y}_d$. Moreover, the desired output of the system is $y_d(t) = 0.1\pi[\sin 2t - \cos t]$.

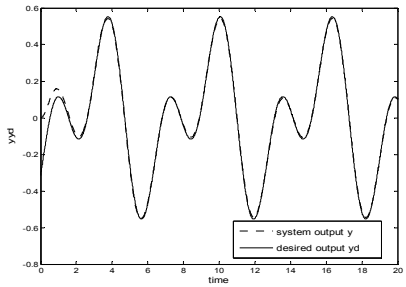

Fig. 7. The control response of the proposed method

From Fig.7, it is known that the control performance of the proposed controller has achieved good control response. Also, Fig.8 illustrates the control performance of the PID controller. It can be seen that the PID control strategy has led to larger control error when the reference signal achieves its local extreme. However, the proposed control strategy obtained better control performance. It can obviously derive more accurate control result.

7. Conclusions

An adaptive control strategy for nonlinear dynamic systems with sandwich hysteresis is presented. In the proposed control scheme, a neural network unit inverse is constructed to compensate for the effect of the first smooth dynamic subsystem. Thus, the sandwich system with hysteresis can be transformed to a Hammerstein type nonlinear dynamic system preceded by hysteresis. Considering the modified structure of the sandwich system, an adaptive controller based on the pseduo-control technique is developed. In our method, a neural network is used to approximate the system residual based on the proposed expanded input space with hysteretic operator. The advantage of this method can avoid constructing the hysteresis inverse. Then, the adaptive control law is derived in terms of the Lyapunov stability theorem. It has been proved that the ultimate boundedness of the closed-loop control error is guaranteed. Simulation results have illustrated that the proposed scheme has obtained good control performance.

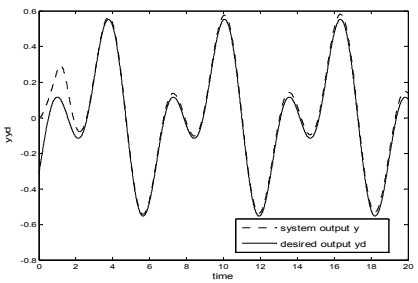

Fig. 8. The control response of the PID control method

8. Appendix

From (20), the approximation error can be written as:

$$\begin{aligned} & W^T\sigma - \hat{W}^T\hat{\sigma} \\ &= W^T\sigma - \hat{W}^T\sigma + \hat{W}^T\sigma - \hat{W}^T\hat{\sigma} \\ &= \tilde{W}^T\sigma + \hat{W}^T(\sigma - \hat{\sigma}) \end{aligned} \tag{A1}$$

Substituting (23) into (A1), it yields

$$\begin{aligned} & W^T\sigma - \hat{W}^T\hat{\sigma} \\ &= \tilde{W}^T(\hat{\sigma} + \hat{\sigma}'\tilde{V}^T x_{nn} + o(\tilde{V}^T x_{nn})^2) + \hat{W}^T(\hat{\sigma}'\tilde{V}^T x_{nn} + o(\tilde{V}^T x_{nn})^2) \\ &= \tilde{W}^T\hat{\sigma} + \tilde{W}^T\hat{\sigma}'\tilde{V}^T x_{nn} + \hat{W}^T\hat{\sigma}'\tilde{V}^T x_{nn} + W^T o(\tilde{V}^T x_{nn})^2 \\ &= \tilde{W}^T\hat{\sigma} + \tilde{W}^T\hat{\sigma}'V^T x_{nn} - \tilde{W}^T\hat{\sigma}'\hat{V}^T x_{nn} + \hat{W}^T\hat{\sigma}'\tilde{V}^T x_{nn} + W^T o(\tilde{V}^T x_{nn})^2 \\ &= \tilde{W}^T(\hat{\sigma} - \hat{\sigma}'\hat{V}^T x_{nn}) + \tilde{W}^T\hat{\sigma}'V^T x_{nn} + \hat{W}^T\hat{\sigma}'\tilde{V}^T x_{nn} + W^T o(\tilde{V}^T x_{nn})^2 . \end{aligned} \tag{A2}$$

Defining $w = \tilde{W}^T\hat{\sigma}'V^T x_{nn} + W^T o(\tilde{V}^T x_{nn})^2$, (A2) becomes

$$\begin{aligned} & W^T\sigma - \hat{W}^T\hat{\sigma} \\ &= \tilde{W}^T(\hat{\sigma} - \hat{\sigma}'\hat{V}^T x_{nn}) + \hat{W}^T\hat{\sigma}'\tilde{V}^T x_{nn} + w . \end{aligned}$$

So that

$$\begin{aligned} w &= W^T\sigma - \hat{W}^T\hat{\sigma} - \tilde{W}^T(\hat{\sigma} - \hat{\sigma}'\hat{V}^T x_{nn}) - \hat{W}^T\hat{\sigma}'\tilde{V}^T x_{nn} \\ &= W^T\sigma - W^T\hat{\sigma} + \tilde{W}^T\hat{\sigma}'\hat{V}^T x_{nn} - \hat{W}^T\hat{\sigma}'\tilde{V}^T x_{nn} \\ &= W^T(\sigma - \hat{\sigma}) + W^T\hat{\sigma}'\hat{V}^T x_{nn} - \hat{W}^T\hat{\sigma}'\hat{V}^T x_{nn} - \hat{W}^T\hat{\sigma}'\tilde{V}^T x_{nn} \\ &= W^T(\sigma - \hat{\sigma}) + W^T\hat{\sigma}'\hat{V}^T x_{nn} - \hat{W}^T\hat{\sigma}'V^T x_{nn} \end{aligned}$$

9. Acknowledgement

This research is partially supported by the Innovation Program of Shanghai Municipal Education Commission (Grant No.:09ZZ141), the National Science Foundation of China (NSFC Grant No.: 60572055) and the Advanced Research Grant of Shanghai Normal University (Grant No: DYL200809).

10. References

Taware, A. & Tao, G. (1999). Analysis and control of sandwich systems, *Proceeding of the 38th conference on decision and control,* pp.1156-1161, Phoenix, Arizona, USA, December 1999

Tao, G. & Ma, X.(2001).Optimal and nonlinear decoupling control of system with sandwiched backlash, *Automatica*, Vol.37, No.1, 165-176.

Hovakimyan, N.& Nandi, F.(2002). Adaptive output feedback control of uncertain nonlinear systems using single-hidden-layer neural networks, IEEE Transactions on Neural Networks, Vol.13, No.6, 1420-1431

Calis, A.& Hovakimyan, N. (2001). Adaptive output feedback control of nonlinear systems using neural networks, *Automatica*, Vol. 37, 1201-1211.

Powell, M.(1977). Restart procedures for the conjugate gradient method, *Mathematical Programming,* Vol. 12, 241-254.

Zhao, X.; Tan, Y. & Zhao, T.(2008). Adaptive control of nonlinear system with sandwiched hysteresis using Duhem operator, *Control and Decision,* Vol. 22, No. 10, 1134-1138

Corradini, M., Manni, A & Parlangeli, G. (2007). Variable structure control of nonlinear uncertain sandwich systems with nonsmooth nonlinearities,*Proceedings of the 46th IEEE Conference on Decision and Control*, pp. 2023-2038

Zhao, X. & Tan, Y.(2006). Neural adaptive control of dynamic sandwich systems with hysteresis, *Proceedings of the 2006 IEEE International Symposium on Intelligent Control,* pp. 82-87

Adly, A.A.& Abd-El-Hafiz, S.K. (1998). Using neural networks in the identification of Preisach-type hysteresis models. *IEEE Trans. on Magnetics,* Vol. 34, No.3, 629-635

Zhao, X. & Tan, Y. (2008). Modeling hysteresis and its inverse model using neural networks based on expanded input space method,*IEEE Transactions on Control Systems Technology*, Vol. 16, No. 3, pp. 484-490

11

High-Speed Adaptive Control Technique Based on Steepest Descent Method for Adaptive Chromatic Dispersion Compensation in Optical Communications

Ken Tanizawa and Akira Hirose
Department of Electronic Engineering, The University of Tokyo
Japan

1. Introduction

The traffic volume of the data transmission is increasing each year with the explosive growth of the Internet. The networking technologies supporting the data transmission are optical fiber transmission technologies. In the physical layer, the networks are classified into three networks, the long-haul network that connects city to city, the metropolitan area network that connects the central station in the city to the neighboring base station, and the access network that connects the base station to the home. In order to adapt to the increase of the data transmission, we need to achieve high-speed transmission and increase the capacity of transmission in each network.

In the access network, many kinds of passive optical networks (PON) are studied to offer a high-speed access to the Internet at low cost. In the metropolitan area network, we contemplate the update of the network structure from the conventional peer-to-peer transmission to the ring or mesh structure for the high-capacity and highly reliable networks. In the long-haul network, the study on multilevel modulation such as the differential quadrature phase shift keying (DQPSK) is a recent popular topic for the high-capacity transmission because the multilevel modulation utilizing the phase information offers high-speed transmission without increasing the symbol rate. Other modulation and multiplexing technologies are also studied for the high-capacity networks. The orthogonal frequency division multiplexing (OFDM) is one of the wavelength division multiplexing methods and achieves high spectral efficiency by the use of orthogonal carrier frequencies. The optical code division multiple access (OCDMA) is a multiplexing technique in the code domain. These techniques are developed in the wireless communication and modified for the optical transmission technologies in these days.

In the long-haul and the metropolitan area networks whose transmission distance is over 10 km in 40 Gb/s, chromatic dispersion (CD) is one of the main factors which limits the transmission speed and the advances of the network structure. The CD is a physical phenomenon that the group velocity of light in the fiber depends on its wavelength (Agrawal, 2002). The CD causes the degradation of the transmission quality as the optical

signals having a spectral range are distorted by the difference of the transmission speed in the wavelength domain. The effect of dispersion increases at a rate proportional to the square of the bit-rate.
In the high-speed optical transmission over 40 Gb/s, we have to compensate for the CD variation caused by the change of strain and temperature adaptively in addition to the conventional static CD compensation because the dispersion tolerance is very small in such a high-speed transmission. Also, in metropolitan area networks employing reconfigurable networking technology such as the mesh or ring network, the transmission route changes adaptively depending on the state of traffic and the network failure. As the CD value depends on the length of the transmission fiber, we have to compensate for the relatively large CD variation caused by the change of the transmission distance.
With the aforementioned background, many researches and demonstrations have been conducted in the field of the adaptive CD compensation since around 2000 (Ooi et al., 2002; Yagi et al., 2004). The adaptive compensations are classified into two major groups, the optical compensations and the electrical compensations. In the electrical compensation, we utilize the waveform equalizer such as the decision feedback equalizer (DFE), the feed forward equalizer (FFE) or the maximum likelihood sequence equalizer (MLSE) after detection (Katz et al., 2006). These equalizers are effective for the adaptive CD compensation because they act as a waveform reshaping. The compensation based on DEF and FFE has advantages that the equalization circuit is compact and implemented at low cost. However, the compensation range is limited because the phase information of the received signal is lost by the direct detection. The MLSE scheme is very effective in 10 Gb/s transmission. However it is difficult to upgrade high bit-rate over 40 Gb/s because the scheme requires high-speed A/D converter in implementation.
In the optical domain, the adaptive CD compensation is achieved by the iterative feedback control of a tunable CD compensator with a real-time CD monitoring method as shown in Fig. 1. Many types of tunable CD compensators are researched and developed recently. The tunable CD compensator is implemented by the devices generating arbitral CD value. Also, many kinds of CD monitoring methods are studied and demonstrated for the feedback control of tunable CD compensators. While the compensation devices and the dispersion monitoring methods are studied with keen interest, the adaptive control algorithm, how to control the tunable CD compensator efficiently, has not been fully studied yet in the optical domain CD compensation. When the tunable CD compensator is controlled iteratively for the adaptive CD compensation, the control algorithm affects the speed of the compensation to a great degree as well as the response time of the compensation devices and the monitorings. Although the simple hill-climbing method and the Newton method are employed as a control algorithm in many researches and demonstrations, these algorithms are not always the best control algorithm for the adaptive CD compensation.

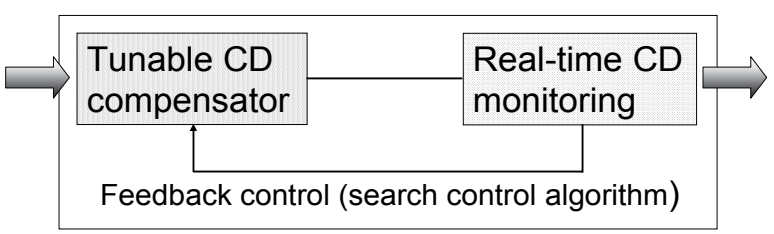

Fig. 1. Adaptive CD compensation in the receiver.

In this chapter, we report the adaptive CD compensation employing adaptive control technique in optical fiber communications. We propose a high-speed and low cost adaptive control algorithm based on the steepest descent method (SDM) for feedback control of the tunable CD compensator. The steepest descent approach has an ability to decrease the iteration number for the convergence. We conducted transmission simulations for the evaluation of the proposed adaptive control technique, and the simulation results show that the proposed technique achieves high-speed compensation of the CD variation caused by the change of the transmission distance in 40 Gb/s transmission.
The organization of this chapter is as follows. In Section 2, we explain the fundamentals of CD and adaptive CD compensation in optical fiber communications for the background knowledge of this research. Then we propose the adaptive control technique based on the SDM for adaptive CD compensation in Section 3. In Section 4, we show the demonstrations and performance analysis of the proposed technique in 40 Gb/s transmission by simulations. Finally, we summarize and conclude this paper in Section 5.

2. Chromatic Dispersion in Optical Fiber Communications

2.1 Fundamental of chromatic dispersion

The group velocity of the light depends on its wavelength when the light is propagating in mediums. This phenomenon is called CD or group velocity dispersion (GVD). In optical communications utilizing the optical fiber as a transmission medium, the optical pulse is affected by the CD as the propagation time depends on the constituent wavelength of the optical pulse as shown in Fig. 2. The CD has two contributions, material dispersion and waveguide dispersion in a single mode fiber (SMF). The material dispersion is attributed to the characteristics of silica that the refractive index changes with the optical wavelength. The waveguide dispersion is caused by the structure of optical fiber, the core radius and the index difference.
Considering optical propagation in the fiber, the propagation constant β is a function of the angular frequency ω and expanded by Taylor expansion as follows.

$$\beta(\omega) = \beta_0 + \beta_1(\omega - \omega_0) + \frac{1}{2}\beta_2(\omega - \omega_0)^2 + \frac{1}{6}\beta_3(\omega - \omega_0)^3 + \cdots \quad (1)$$

Here, ω_0 is a center angular frequency, and β_0, β_1, β_2, and β_3 are Taylor's coefficients. The time required for the propagation of unit length τ is obtained by differentiating partially the propagation constant β as follows.

$$\tau(\omega) = \beta_1 + \beta_2(\omega - \omega_0) + \frac{1}{2}\beta_3(\omega - \omega_0)^2 + \cdots \quad (2)$$

It is confirmed from (2) that the required time is angular frequency dependent; the propagation time of optical pulse depends on the wavelength in optical communications. The coefficients β_2 and β_3 are first-order and second-order constants indicating the degree of the angular frequency dependence, respectively. Assuming that the second-order CD is negligible, the CD parameter is defined as

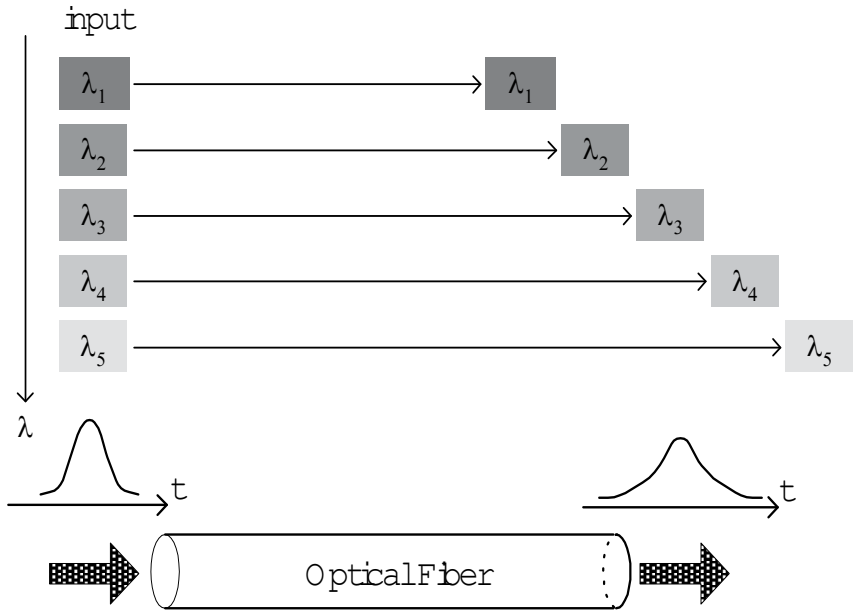

Fig. 2. Schematic diagram of chromatic dispersion.

$$D = \frac{d\tau}{d\lambda} = -\frac{2\pi c}{\lambda^2}\beta_2 \tag{3}$$

where c is the speed of light. The unit of the CD parameter is ps/nm/km.
In SMF, the CD parameter is zero at around 1300 nm and about 20 ps/nm/km at the typical wavelength used for optical communications, around 1550 nm. We have many characteristics of optical fibers such as dispersion shifted fiber (DSF) whose CD parameter is zero at around 1550 nm for the reduction of CD effect in optical fiber communications, and dispersion compensating fibers (DCF) whose CD parameter is minus value for the purpose of static CD compensation.
In optical fiber communications, the optical pulse is affected by the CD as it has relatively wide spectral range corresponding to the bit-rate. Assuming that the optical pulse is a Gaussian waveform for the simplicity, the waveform in time-domain is expressed as

$$U(0,T) = \exp\left(-\frac{T^2}{2T_0^2}\right) \tag{4}$$

where T_0 is a full width at half maximum (FWHM) of the pulse. When the pulse is transmitted for arbitral distance z, the waveform is affected by the CD and distorted as

$$U(z,T) = \frac{T_0}{(T_0^2 - j\beta_2 z)^{1/2}} \exp\left(-\frac{T^2}{2(T_0^2 - j\beta_2 z)}\right) \tag{5}$$

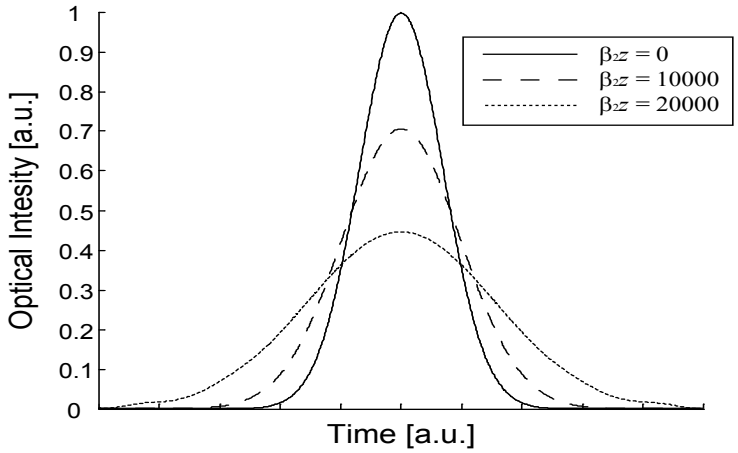

Fig. 3. Optical pulses affected by chromatic dispersion.

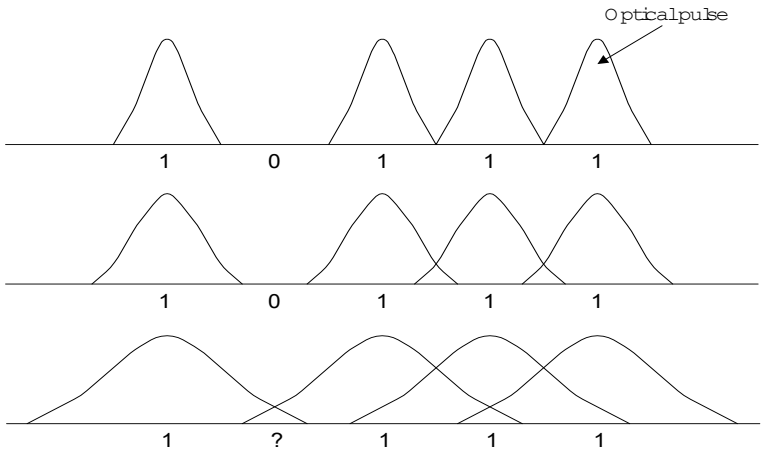

Fig. 4. Interference of neighboring pulses in optical communication.

where we neglect the second-order CD for simplicity as the first-order CD is dominant.
Figure 3 shows the waveforms of optical pulse when we change the product of β_2 and z under the condition that T_0=100 ps. The larger the product of β_2 and z is, the wider the FWHM of the transmitted waveform is; the effect of CD is larger in the case that the transmission distance is longer and the CD parameter is larger. If the FWHM of the optical pulse gets wider, the possibility of the inter symbol interference (ISI) is higher as shown in Fig. 4. As the ISI causes code error in optical communications, the transmission distance is limited by the CD. Also, the maximum transmission distance is reduced according to the bit rate of the transmission B because the FWHM of the optical pulse T_0 is decreased when the bit rate increases. We can also understand it from the fact that the spectral width is wide in short optical pulse. The effect of CD on the bit rate B can be estimated and the CD tolerance D_T, the limitation of CD that the quality of the transmission is assured, is expressed as

$$\left|D_T\right| < \frac{1}{Bz\Delta\lambda} \tag{6}$$

where $\Delta\lambda$ is the range of wavelength in the optical pulse. The CD tolerance is inversely proportional to the bit rate and the transmission distance and the wavelength range of the input pulse.

2.2 Adaptive chromatic dispersion compensation

As mentioned in Section 1, the adaptive CD compensation is an essential technology for high-speed optical fiber communications as the CD tolerance is very small in the systems whose transmission speed is over 40 Gb/s. Many researches have been conducted for the adaptive CD compensation in optical communications. The principle of the CD compensation is very simple as shown in Fig. 5. We can achieve the CD compensation by placing a transmission medium which has the inverse CD value of the transmission fiber in the transmission line. The adaptive CD compensation is achieved by changing the compensating CD value adaptively according to the CD in the transmission fiber. The conventional setup of the adaptive CD compensation is shown in Fig. 1; the tunable CD compensator is feedback controlled with the real-time CD monitoring. In this section, tunable CD compensators and CD monitoring techniques are briefly introduced for the background information of the adaptive control algorithm to be proposed.

We have many types of tunable CD compensators for the adaptive compensation. They are basically implemented by the dispersive medium with the function of tunability, for example, chirped fiber Bragg grating (CFBG) with heater elements (Matsumoto et al., 2001; Eggleton et al., 2000), micro-electro mechanical system (MEMS) (Sano et al., 2003), ring resonator (Takahashi et al., 2006), and so on. We adopt a virtually imaged phased array (VIPA) compensator in the following research. The VIPA compensator is a tunable CD compensator, which is consisted of the combination of a VIPA plate and a three dimensional adjustable surface mirror (Shirasaki, 1997; OOi et al., 2002). The VIPA plate operates as a grating, and the specific spectral components of light is reflected by the mirror to induce CD.

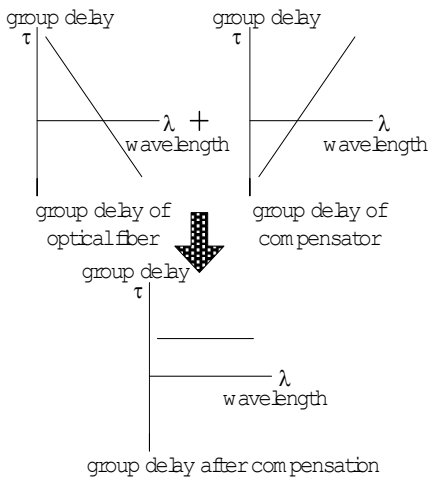

Fig. 5. Principle of chromatic dispersion compensation.

	Response time	Cost	Relationship between transmission quality and monitoring signal	Monitoring range	Pilot signal
Clock power level monitoring method	Good	Good	Fair	Good	Not required
Clock phase detection method	Good	Fair	Good	Poor	Not required
Eye-diagram	Good	Fair	Excellent	Good	Not required
BER	Fair	Poor	Excellent	Good	Required

Table 1. Performances of feedback signals in adaptive CD compensation

We can generate arbitral CD value as the change of the geometry of the three dimensional mirror. In the VIPA compensator, wide compensation range, ±1800 ps/nm in 10 and 40 Gb/s, is achieved by the appropriate design of the three dimensional mirror.
Also, many kinds of CD monitoring methods are studied and demonstrated for the feedback control of the tunable CD compensators. The typical monitoring signals are bit error rate (BER), eye-diagram, clock power level (Sano et al., 2001), and phase difference of clock signals (Qian et al., 2002). We show the performance comparison of the feedback signals for adaptive control of the tunable CD compensator in Table 1. The requirement of pilot signal is the disadvantage for the BER as the monitoring signal. If we consider each characteristic of the feedback signal, the extracted-clock power level or the eye-diagram is better for the feedback signal in adaptive CD compensation. We adopt the eye-opening value obtained from the eye-diagram as the feedback signal in the adaptive control method to be proposed.

3. High-Speed Adaptive Control Method Based on Steepest Descent Method

In this section, we propose a method of high-speed adaptive control of tunable CD compensator for adaptive CD compensation. We apply the steepest descent method to the adaptive control algorithm in order to reduce the compensation time. The approximation of partial derivative for the steepest descent approach is proposed and applied to the control of the VIPA compensator.

3.1 Steepest descent-based control algorithm for adaptive chromatic dispersion compensation

The adaptive control system must be low cost, high-speed, and applicable to wide dispersion ranges for the adaptive CD compensation in optical communications. Most control systems require high-cost measuring instruments for the CD monitoring. We therefore propose the feedback control method that does not require high-cost CD monitoring. In our proposal, the feedback signal is a received waveform in the time domain. The tunable CD compensator is controlled repeatedly to reshape the waveform. The measurement of the waveform is relatively easy and uninfluential in the transmission

conditions such as pilot-signal requirements. Conventional feedback control is based on the hill-climbing method, which requires a lot of time for optimization. We have therefore applied the steepest descent method to the feedback control for high-speed compensation.
Figure 6 shows an optical dynamic routing network with the adaptive CD compensation. Transmitted signals are passed through a route that is chosen arbitrarily among optical paths, being affected by the CD. In the receiver part, the degraded signals are fed into the tunable CD compensator and the dispersion is compensated. The adaptive dispersion compensation is achieved by the combination of a tunable CD compensator and a controller. The compensated signals are received by a photodiode and demodulated.

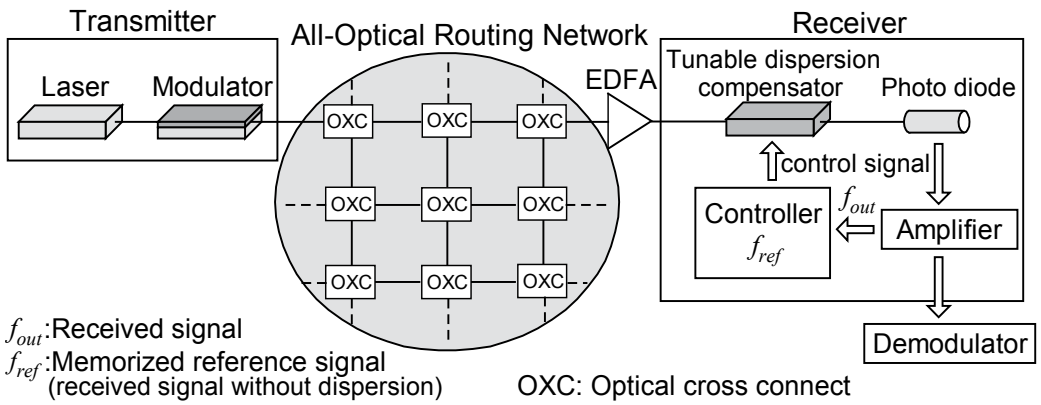

Fig. 6. Schematic diagram of all-optical dynamic routing network with the adaptive dispersion compensation technique.

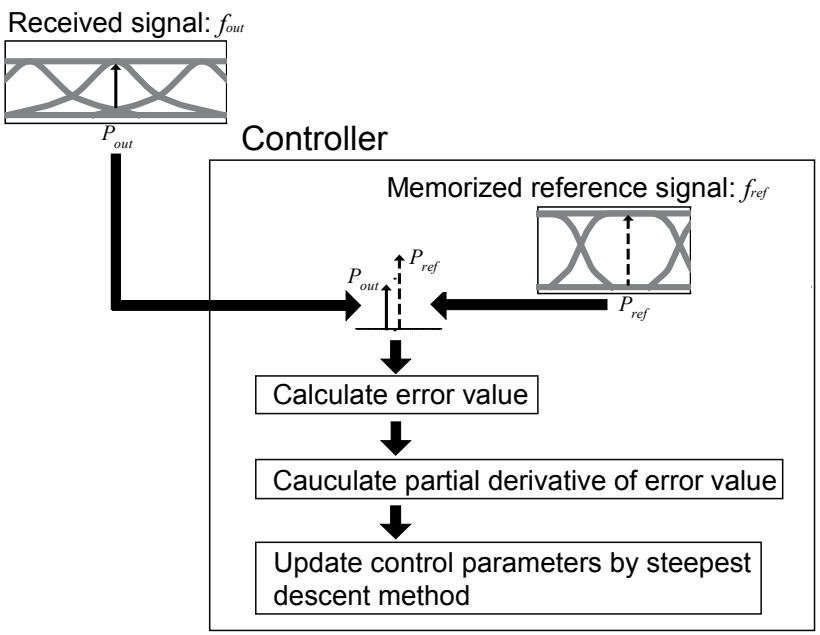

Fig. 7. Procedure of proposed steepest-descent-based control.

The tunable compensator is controlled by our proposed adaptive control method based on the steepest descent method. The proposed procedure of the controller is shown in Fig. 7, where P_{out} and P_{ref} are the eye-opening values (normalized as P_{ref} = 1) of the received and reference signals, f_{out} and f_{ref} respectively. In this method, we measure and register the reference signal, f_{ref} which is a received signal unaffected by the CD. The reference signal is determined from the characteristics of the transmitter-receiver set. Therefore, we can copy the reference signal to other receivers after it has been measured once.
The first step is a calculation of an error value: *Er*. The error value is defined as the difference between the eye-opening values, P_{out} and P_{ref}.

$$Er = \frac{1}{2}\left(P_{ref} - P_{out}\right)^2 \tag{7}$$

The next step is a calculation of partial derivatives of *Er* in terms of the control parameters, x_i (i=1,2,…, n), for the update based on the steepest descent method.

$$\frac{\partial Er}{\partial x_i} = \left(P_{out} - P_{ref}\right)\frac{\partial P_{out}}{\partial x_i} \tag{8}$$

We need to measure small changes in P_{out} when x_i changes slightly in order to get the accurate partial derivatives of P_{out} with respect to x_i. However, this is unrealistic as it takes a lot of time for the measurement and our goal is to achieve quick CD compensation. Therefore, we approximate the partial derivatives of P_{out} with respect to x_i. The approximation is to be mentioned at the next subsection.
In the final step, the control parameters are update as

$$x_i \Rightarrow x_i - \varepsilon\frac{\partial Er}{\partial x_i} \tag{9}$$

where ε is an appropriate constant concerning the speed and accuracy of the convergence. We repeat this procedure until the transmission quality becomes optimal. The required number of update iterations is fewer than that of the normal feedback control based on the hill-climbing method due to the steepest descent approach. In practical all-optical dynamic routing networks, the procedure is repeated all the time as the transmission route changes at frequent intervals.

3.2 Approximation of partial derivatives for steepest descent approach

To approximate the partial derivatives of P_{out} with respect to x_i, we need to know the change in one-bit waveforms of the received signal, $w_{out}(t)$, caused by the change in x_i. When we assume that the waveform of the transmitted signal is a Gaussian-like pulse (the peak level is unity) just like in the approximation in return-to-zero transmissions and that the transmission is affected only by the CD, the waveform, $w_{out}(t)$ is calculated analytically in terms of the CD values of the transmission fiber, D_{fiber} ps/nm and TDC, D_{TDC} ps/nm, as

$$w_{out}(t) = v_{peak}\,\mathbf{exp}\left(-\frac{{v_{peak}}^2 t^2}{{T_{FWHM}}^2}\right) \tag{10}$$

$$v_{peak}^2 = \frac{{T_{FWHM}}^2}{{T_{FWHM}}^2 + \left(\frac{\lambda^2}{2\pi c} D_{fiber} + \frac{\lambda^2}{2\pi c} D_{TDC}\right)^2} \tag{11}$$

where T_{FWHM} is the FWHM of the transmitted signal, λ is the center wavelength , t is time, and c is the speed of light. The partial derivative of $w_{out}(t)$ with respect to x_i is calculated from (10) and (11).

$$\frac{\partial w_{out}(t)}{\partial x_i} = \pm\frac{{v_{peak}}^2}{{T_{FWHM}}^2}\sqrt{1-{v_{peak}}^2}\left(\frac{2t^2{v_{peak}}^2}{{T_{FWHM}}^2}-1\right)\mathbf{exp}\left(\frac{-t^2{v_{peak}}^2}{{T_{FWHM}}^2}\right)\cdot\frac{\lambda^2}{2\pi c}\frac{\partial D_{TDC}}{\partial x_i} \tag{12}$$

Equation (10) shows that the value v_{peak} is the peak level of $w_{out}(t)$. We can measure it in a practical system. Therefore, (12) shows that we can obtain the approximated partial derivative of $w_{out}(t)$ with respect to x_i because T_{FWHM} and λ are known parameters. We obtain the partial derivative of the peak value in $w_{out}(t)$ by substituting 0 for t.

$$\left.\frac{\partial w_{out}(t)}{\partial x_i}\right|_{t=0} = \frac{\partial v_{peak}}{\partial x_i} = \pm\frac{{v_{peak}}^2}{{T_{FWHM}}^2}\sqrt{1-{v_{peak}}^2}\cdot\frac{\lambda^2}{2\pi c}\frac{\partial D_{TDC}}{\partial x_i} \tag{13}$$

The value of v_{peak} corresponds to the eye-opening value in nonreturn-to-zero (NRZ) transmission approximately. Therefore, the partial derivative of P_{out} with respect to x_i is approximated as follows.

$$\frac{\partial P_{out}}{\partial x_i} = \pm\frac{{P_{out}}^2}{{T_{FWHM}}^2}\sqrt{1-{P_{out}}^2}\cdot\frac{\lambda^2}{2\pi c}\frac{\partial D_{TDC}}{\partial x_i} \tag{14}$$

3.3 Detailed control algorithm for VIPA compensator

In the simulations described in the next section, we employ a VIPA compensator as the tunable CD compensator. The VIPA compensator has a single control parameter, i.e. CD S ps/nm. The detailed control procedure of the VIPA compensator is as follows. In general, we can apply the proposed method to any kind of tunable CD compensators.

(i) Initialize the parameter of the VIPA compensator: S ps/nm

$$S = 0 \text{ ps/nm} \tag{15}$$

(ii) Calculate the error value: Er

The error value, *Er*, is derived from (7).
If P_{out} is zero, we go to (iii), otherwise to (iv).

(iii) Update *S* by the hill-climbing method

$$S \Rightarrow S - \Delta S \tag{16}$$

where ΔS ps/nm is an appropriate small constant. We then go on to (v).

(iv) Update *S* by the steepest descent method
We calculate the partial derivative of *Er* from (8) and (14).
The partial derivative of P_{out} with respect to *S* is approximated as

$$\frac{\partial P_{out}}{\partial S} = \pm \frac{{P_{out}}^2}{{T_{FWHM}}^2} \sqrt{1 - {P_{out}}^2} \cdot \frac{\lambda^2}{2\pi c} \tag{17}$$

The parameter *S* is updated as

$$S \Rightarrow S - \varepsilon \frac{\partial Er}{\partial S} \tag{18}$$

where ε is an appropriate constant. We then go to (v).

(v) Judge the error value: *Er*

We calculate *Er* again by using (7). If *Er* increases or becomes small enough, the procedure stops. Otherwise, we go back to (ii) and repeat the same process. However, in practical all-optical dynamic routing networks, the compensation process is repeated all the time as the dispersion value changes frequently.

4. Transmission Simulations at 40 Gb/s

4.1 Simulation results in NRZ-OOK transmission at 40 Gb/s

Numerical transmission simulations using OptiSystem were conducted to verify the application of the proposed technique to 40 Gb/s optical fiber transmission system. In the proposed control method, we have to set the constants for search, ε and ΔS, appropriately. They were adjusted for the 40 Gb/s transmission and set at 3×10^5 and 30, respectively. The output power of a distributed feedback laser diode (DFB-LD) at the transmitter was 0 dBm. We supposed that the modulation format were NRZ-OOK. The central wavelength of the transmitted signal was 1550 nm. The transmission path was a non-zero dispersion shifted fiber (NZ-DSF). We assumed that CD, polarization mode dispersion (PMD), self-phase modulation (SPM), and other nonlinearity affect the transmitted signal. The power loss was amplified to 0 dBm by an erbium-doped fiber amplifier (EDFA) after both of the fiber transmission and the dispersion compensation by the VIPA compensator. The EDFA, the

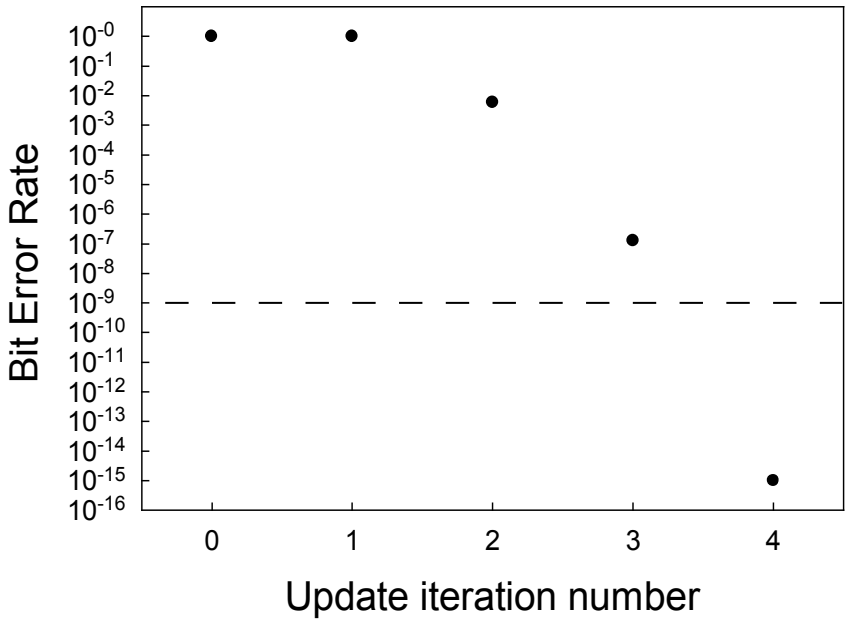

(a)

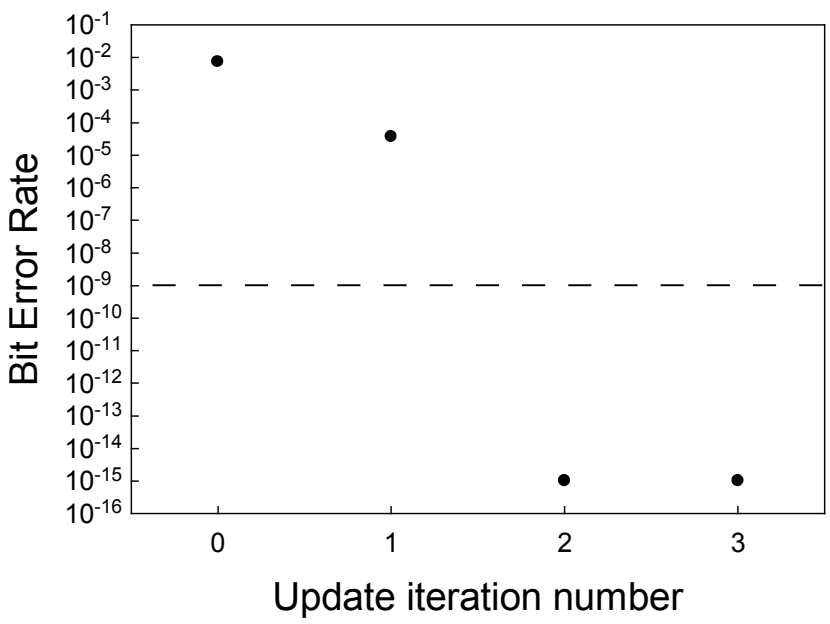

(b)

Fig. 8. BERs at every update of the compensator (a) 0→20km, (b) 20→25km.

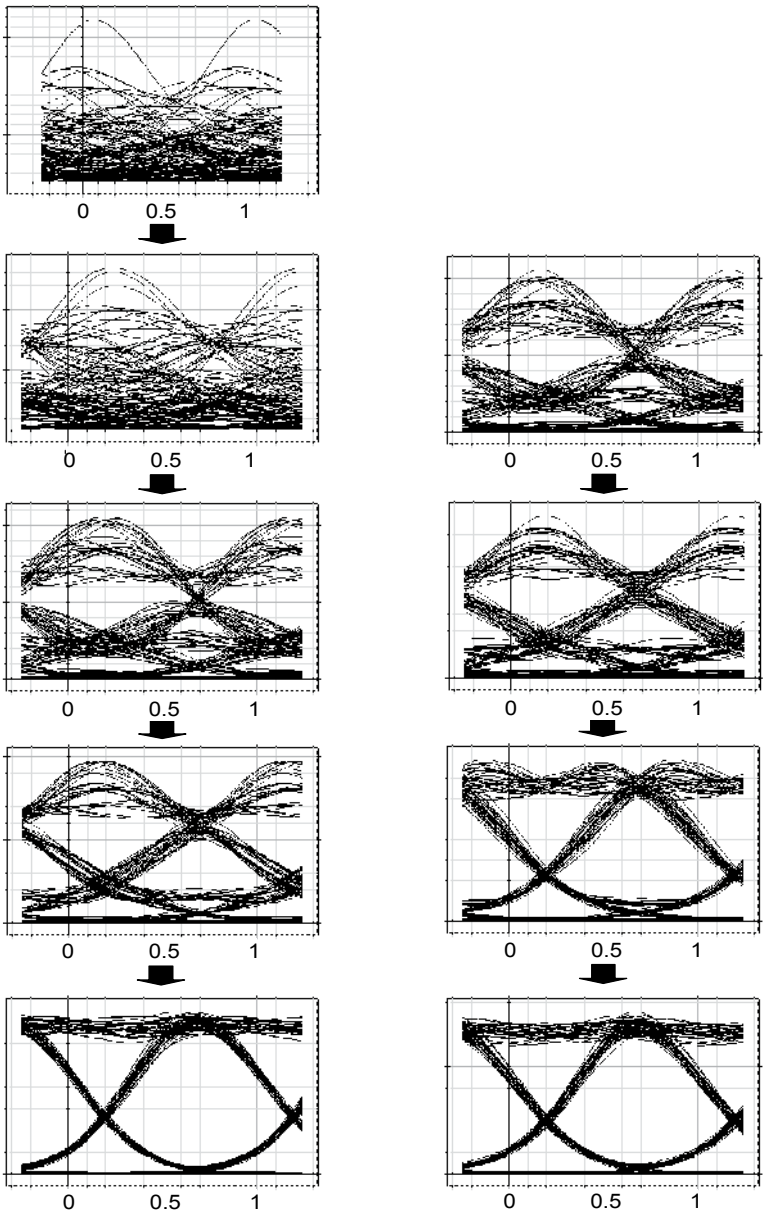

Fig. 9. Eye-diagrams at every update of the compensator (a) 0→20km, (b) 20→25km.

receiver, and other optical components were assumed to have moderate levels of noise.

Transmission simulation results are shown in Fig. 8 and Fig. 9. In these simulations, the initial value of S was set at 0. Fig. 8 shows the BERs at every update of the VIPA compensator when the transmission distance changes (a) from 0 to 20 km (dispersion: 0 →

100 ps/nm) and (b) from 20 to 25 km (dispersion: 100 → 125 ps/nm). The compensation improved the BER (a) from 1.0×10^{0} to 1.0×10^{-15} and (b) from 7.41×10^{-3} to 1.0×10^{-15}, respectively. As shown in Fig. 9, the eye-diagrams measured by a sampling oscilloscope were found reshaped. These results show that the CD compensation with the proposed control method improve the transmission quality.

The update iteration number to achieve a sufficiently low BER ($<10^{-9}$) were four and two, respectively in these two cases. A single calculation of the next dispersion value requires less than 10 ms. The response time of the VIPA compensator is 2 ms for every 1 ps/nm compensation. Therefore, the time required for ±400 ps/nm CD compensation is about 1 s, which is determined practically by the response time of the VIPA compensator. This technique achieves a high-speed adaptive control of a tunable CD compensator in 40 Gb/s transmission since the update iteration number is small and the calculation time with the proposed approximation is short enough. The proposed technique is more effective if the response time of the tunable CD compensator is faster as the required iteration number is decreased by our proposed adaptive control technique based on the steepest descent method.

4.2 Compensation range and required iteration number

Figure 10 shows the compensation range of the proposed method at 40 Gb/s. We measured BERs before and after compensation when the CD value changed from 0 ps/nm to arbitrary value. The compensation range in which the BER after compensation is less than 10^{-9} is about from −450 to 450 ps/nm, corresponding to a NZ-DSF path-length change of about ±90 km. This range is wide enough for compensating the change of CD caused by dynamic routing. In this wide compensation range, the iteration number required for error free transmission ($BER<10^{-9}$) is less than 15. The fast adaptive CD compensation is also achieved by the proposed adaptive control technique as the required iteration number is small.

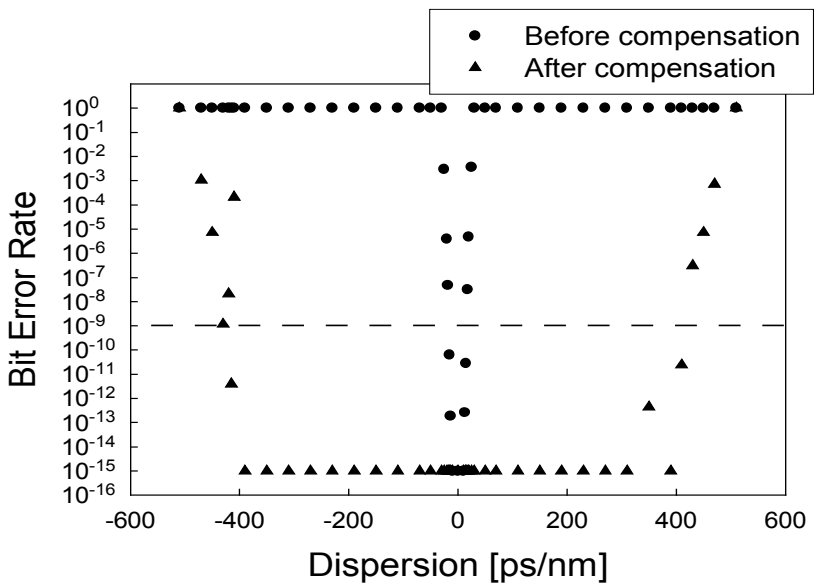

Fig. 10. Compensation range of the proposed method at 40 Gb/s.

5. Conclusion

In this chapter, we have proposed high-speed adaptive CD compensation with the adaptive control method based on the steepest descent method and reported the performances evaluated by numerical simulations.
The simulation results show that the proposed control method based on the steepest descent method controls the tunable CD compensator quickly and effectively for a wide dispersion range in 40 Gb/s transmission. The range is up to ±450 ps/nm, and the required compensation time is about 1 s for the CD variation within ±400 ps/nm at 40 Gb/s. These achievements are valuable for the future optical networks employing dynamic routing technique.

6. References

Agrawal, G. (2002). *Fiber-Optic Communication Systems,* Wiley-Interscience, ISBN 0-471-21571-6, USA

Eggleton, B. J.; Ahuja, A.; Westbrook, P. S.; Rogers, J. A.; Kuo, P.; Nielsen, T. N. & Mikkelsen, B. (2000). Integrated Tunable Fiber Gratings for Dispersion Management in High-Bit Rate Systems. *IEEE/OSA Journal of Lightwave Technology,* Vol. 18, No. 10, (Oct. 2000) pp. 1418-1432

Katz, G.; Sadot, D. & Tabrikian, J. (2006). Electrical Dispersion Compensation Equalizers in Optical Direct- and Coherent-Detection Systems. *IEEE Transanctions on Communications,* Vol. 54, No. 11, (Nov. 2006) pp. 2045-2050

Matsumoto, S.; Ohira, T.; Takabayashi, M.; Yoshiara, K. & Sugihara, T. (2001). Tunable Dispersion Equalizer with a Divided Thin-Film Heater for 40-Gb/s RZ Transmission. *IEEE Photonics Technology Letters,* Vol. 13, (Aug. 2001) pp. 827-829

Ooi, H.; Nakamura, K.; Akiyama, Y.; Takahara, T.; Terahara, T.; Kawahata, Y.; Isono, H. & Ishikawa, G. (2002). 40-Gb/s WDM Transmission With Virtually Imaged Phased Array (VIPA) Variable Dispersion Compensators. *IEEE/OSA Journal of Lightwave Technology,* Vol. 20, (Dec. 2002) pp. 2196-2203

Sano, T.; Iwashima, T.; Katayama, M.; Kanie, T.; Harumoto, M.; Shigehara, M.; Suganuma, H.; & Nishimura, M. (2003). Novel Multichannel Tunable Chromatic Dispersion Compensator Based on MEMS and Diffraction Grating. *IEEE Photonics Technology Letters,* Vol. 15, No. 8, (Aug. 2003) pp. 1109-1111

Shirasaki, M. (1997). Chromatic-Dispersion Compensator Using Virtually Imaged Phased Array. *IEEE Photonics Technology Letters,* Vol. 9, No. 12, (Dec. 1997) pp. 1598-1600

Tanizawa, K. & Hirose, A. (2007). Adaptive Control of Tunable Dispersion Compensator That Minimizes Time-Domain Waveform Error by Steepest Descent Method. *IEEE Photonics Technology Letters,* Vol. 18, No. 13, (Jul. 2006) pp. 1466-1468

Tanizawa, K. & Hirose, A. (2007). Performance Analysis of Steepest-Descent-Based Feedback Control of Tunable Dispersion Compensator for Adaptive Dispersion Compensation in All-Optical Dynamic Routing Networks. *IEEE/OSA Journal of Lightwave Technology,* Vol. 24, No. 4, (Apr. 2007) pp. 1086-1094

Yagi, M.; Satomi, S.; Tanaka, S.; Ryu, S.; & Asano, S. (2005). Field Trial of Automatic Chromatic Dispersion Compensation for 40-Gb/s-Based Wavelength Path

Protection. *IEEE Photonics Technology Letters,* Vol. 17, No. 1, (Jan. 2005) pp. 229-231

12

Adaptive Control of Piezoelectric Actuators with Unknown Hysteresis

Wen-Fang Xie, Jun Fu, Han Yao and, C.-Y. Su
Department of Mechanical & Industrial Engineering
Concordia University
Canada

1. Introduction

Hysteresis phenomenon occurs in all smart material-based sensors and actuators, such as shape memory alloys, piezoceramics and magnetostrictive actuators (Bank & Smith, 2000; Tan & Baras, 2004). In order to study this phenomenon, different models were proposed (Brokate & Sprekels, 1996; Visintin, 1994). Normally, hysteresis models are classified into two categories, physics-based model such as Jiles-Atherton model (Jiles & Atherton, 1986) and phenomenology-based model such as Preisach operator (Brokate & Sprekels, 1996; Visintin, 1994) and Duhem model (Visintin, 1994). From control systems point of view, hysteresis is generally non-differentiable, nonlinear, and unknown. As a result, systems with hysteresis usually exhibit undesirable inaccuracies or oscillation and even instability. Mitigating the effect of hysteresis becomes necessary and important, thus it has received increasing attention in recent years (Tao & Kokotovic, 1995, Su, et al, 2000, Su, et al, 2005). Many of these studies are related to modeling of hysteresis and their control issues.

With the development of artificial intelligent (AI), AI is being applied to dealing with nonlinearities in systems (Ge & Wang, 2002). Only a few studies have been carried out by using NN to tackle hysteresis modeling and compensation (Makaveev, et al, 2002; Kuczmann & Ivanyi, 2002; Beuschel et al, 1998; Zhao & Tan, 2006). In the paper (Makaveev, et al, 2002), a NN model is used to describe the hysteresis behavior in different frequencies with the knowledge of some properties of magnetic materials, such as loss separation property to allow the separate treatment of quasi-static and dynamic hysteretic effects. Beuschel et al used (Beuschel et al, 1998) a modified Luenberger observer and NN are used to identify a general model of hysteresis. These researches demonstrate that NN can work as an unknown function approximator to describe the characteristics of hysteresis. Recently, two papers (Zhao & Tan, 2006; Lin et al 2006) applied the approximation property of NN to coping with the identification of Preisach-type hysteresis in piezoelectric actuator, and the hysteresis estimation problem for piezo-positioning mechanism based on hysteresis friction force function, respectively. It should be noted that the aforementioned results share a common assumption that the output of hysteresis is measurable.

In practical systems, smart actuators are integrated into the systems, which makes the measurement of output of hysteresis hard. Hence it is a challenge to design an observer for

the unavailable output of hysteresis. Due to the unavailability of the output of hysteresis, the major obstacle of pre-inversion compensator for hysteresis is the lack of effective observer design methods for piezoelectric actuators. Especially, the traditional "Luenberger-type" nonlinear observer design (Krener & Isidori, 1983) or the "high-gain" observer (Krener & Kang, 2003) cannot be applied directly, since the hysteresis is highly nonlinear. The sliding-mode observer was developed to estimate the internal friction states of LuGre model for the servo actuators with friction (Xie, 2007). This observer needs a low-pass filter to remove the high-frequency components in the estimated state variable, which is not applicable in this paper. Yang and Lin (Yang & Lin, 2004) proposed homogeneous observers design for a class of n-dimensional inherently nonlinear systems whose Jacobian linearization is neither controllable nor observable.

Inspired by NN's universal approximation property, and the aforementioned facts in observer design, we propose an observer-based adaptive control of piezoelectric actuators with unknown hysteresis in this paper. The main contribution of this paper is the following: First, it applies the NN to on-line approximate complicated piecewise continuous unknown nonlinear functions in the explicit solution to Duhem model. Second, an observer is designed to estimate the output of hysteresis of piezoelectric actuator based on the system input and output. Third, the stability of the controlled piezoelectric actuator with the observer is guaranteed by using Lyapunov extension (Kuczmann & Ivanyi, 2002).

The organization of the paper is as follows. In Section II, a Duhem model of hysteresis and the problem statement are given. The main results on NN-based compensator for hysteresis are presented in Section III. Section IV provides an example to show the feasibility of the proposed method. Conclusions are given in Section V.

2. Preliminaries

2.1 Duhem model of hysteresis

Many different mathematic models are built to describe the hysteresis behavior, such as Preisach model, Prandtl-Ishlinkii model and Duhem model (Coleman & Hodgdon, 1987; Macki et al, 1993). Considering its capability of providing a finite-dimensional differential model of hysteresis, we adopt classical Duhem model to develop the adaptive controller for the piezoelectric actuator.

The Duhem model is a rate independent operator, with input signal v , $\dot{v}$ and output signal τ . The Duhem model describes hysteresis $H(t)$ by the following mathematical model (Coleman & Hodgdon, 1987; Macki et al, 1993).

$$\frac{d\tau}{dt} = \alpha \cdot \left|\frac{dv}{dt}\right| \cdot [f(v) - \tau] + \frac{dv}{dt} \cdot g(v) \tag{1}$$

where α is a positive number, $f(v)$ and $g(v)$ are prescribed real-valued functions on $(-\infty,+\infty)$.

It can also be represented as (Coleman & Hodgdon, 1987; Macki et al, 1993):

$$\frac{d\tau}{dv} = \begin{cases} \alpha \cdot [f(v) - \tau] + g(v), & \dot{v} > 0 \\ -\alpha \cdot [f(v) - \tau] + g(v), & \dot{v} < 0 \end{cases} \tag{2}$$

where α is the same positive number in (1), $g(v)$ is the slope of the model, and $f(v)$ is the average value of the difference between upward side and downward side.

Property 1 (Coleman & Hodgdon, 1987; Macki et al, 1993): $f(v)$ is a piecewise smooth, monotone increasing, odd function with a derivative $f'(v)$, which is not identically zero. For large value of input $v(t)$, there exists a finite limit $f'(\infty)$;

$$f(v) = -f(-v),\ \lim_{v\to\infty} f'(v) < \infty \tag{3}$$

Property 2 (Coleman & Hodgdon, 1987; Macki et al, 1993): $g(v)$ is a piecewise continuous, even function with

$$g(v) = g(-v),\ \lim_{v\to\infty} g'(v) < \infty \tag{4}$$

It has been shown that Duhem model can describe a large class of hysteresis in various smart materials, such as ferromagnetically soft material, or piezoelectric actuator by appropriately choosing $f(v)$ and $g(v)$ (Coleman & Hodgdon, 1987; Macki et al, 1993). One widely used pair of functions of $f(v)$ and $g(v)$ are

$$f(v) = \begin{cases} a_1 \cdot v_s + a_2(v - v_s) & for \quad v > v_s \\ a_1 \cdot v & for \quad |v| \le v_s \\ -a_1 \cdot v_s + a_2(v + v_s) & for \quad v < -v_s \end{cases} \tag{5},$$

$$g(v) = a_3 \tag{6}$$

where $v_s > 0$, $a_1 > 0$, $a_2 > 0$, $1 > a_3 > 0$, a_1 and a_2 satisfy $a_1, a_2 \in [a_{\min} \quad a_{\max}]$, $a_{\min}$ and $a_{\max}$ are known constants. Substituting the $f(v)$ and $g(v)$ into (2), we have

$$\dot{\tau} = \begin{cases} \alpha \cdot \dot{v}[a_1 \cdot v_s + a_2(v - v_s) - \tau] + a_3 \cdot \dot{v} & v > v_s, \dot{v} > 0 \\ \alpha \cdot \dot{v}[a_1 \cdot v - \tau] + a_3 \cdot \dot{v} & 0 < v \le v_s, \dot{v} > 0 \\ \alpha \cdot \dot{v}[\tau - a_1 \cdot v] + a_3 \cdot \dot{v} & -v_s \le v < 0, \dot{v} < 0 \\ \alpha \cdot \dot{v}[a_1 \cdot v_s - a_2(v + v_s) + \tau] + a_3 \cdot \dot{v} & v < -v_s, \dot{v} < 0 \end{cases} \tag{7}$$

The above equation can be solved for τ

$$\tau = \begin{cases} a_2 \cdot v - f_{21} & v > v_s, \dot{v} > 0 \\ a_1 \cdot v - f_{22} & 0 < v \le v_s, \dot{v} > 0 \\ a_1 \cdot v - f_{23} & -v_s \le v < 0, \dot{v} < 0 \\ a_2 \cdot v - f_{24} & v < -v_s, \dot{v} < 0 \end{cases} \tag{8}$$

with

$$\begin{cases} f_{21}=(a_2\cdot v_0-\tau_0)\cdot e^{-\alpha(v-v_0)}-e^{-\alpha\cdot v}\int_{v_0}^{v}(a_3-a_2)\cdot e^{\alpha\cdot\zeta}d\zeta-(a_1-a_2)\cdot v_s & v>v_s,\dot{v}>0 \\ f_{22}=(a_1\cdot v_0-\tau_0)\cdot e^{-\alpha(v-v_0)}-e^{-\alpha\cdot v}\int_{v_0}^{v}(a_3-a_1)\cdot e^{\alpha\cdot\zeta}d\zeta & 0<v\le v_s,\dot{v}>0 \\ f_{23}=(a_1\cdot v_0-\tau_0)\cdot e^{\alpha(v-v_0)}-e^{\alpha\cdot v}\int_{v_0}^{v}(a_3-a_1)\cdot e^{-\alpha\cdot\zeta}d\zeta & -v_s\le v<0,\dot{v}<0 \\ f_{24}=(a_2\cdot v_0-\tau_0)\cdot e^{\alpha(v-v_0)}-e^{\alpha\cdot v}\int_{v_0}^{v}(a_3-a_2)\cdot e^{-\alpha\cdot\zeta}d\zeta+(a_1-a_2)\cdot v_s & v<-v_s,\dot{v}<0 \end{cases} \tag{9}$$

In order to describe the piezoelectric actuator, we choose the same functions $f(v)$ and $g(v)$ as those in (Banning, et al, 2001), which is a special case of the foregoing choice of $f(v)$ and $g(v)$, i.e. $a_1=a$, $a_2=0$ and $a_3=\bar{b}$ when $|v|\le v_s$.

$$f(v)=\begin{cases} a\cdot v_s & for \quad v>v_s \\ a\cdot v & for \quad |v|\le v_s \\ -a\cdot v_s & for \quad v<-v_s \end{cases} \tag{10}$$

$$g(v)=\begin{cases} 0 & for \quad v>v_s \\ \bar{b} & for \quad |v|\le v_s \\ 0 & for \quad v<-v_s \end{cases} \tag{11}$$

where $v_s>0$, $a>0$, $\bar{b}>0$ and $a>\bar{b}\ge a/2$. Suppose the parameter a satisfies $a\in[a_{\min}\quad a_{\max}]$, $a_{\min}$ and $a_{\max}$ are known constants.

Substituting (5) and (6) into (1), we have

$$\dot{\tau}=\begin{cases} \alpha\cdot\dot{v}[a\cdot v_s-\tau] & v>v_s,\dot{v}>0 \\ \alpha\cdot\dot{v}[a\cdot v-\tau]+\bar{b}\cdot\dot{v} & 0<v\le v_s,\dot{v}>0 \\ \alpha\cdot\dot{v}[\tau-a\cdot v]+\bar{b}\cdot\dot{v} & -v_s\le v<0,\dot{v}<0 \\ \alpha\cdot\dot{v}[a\cdot v_s+\tau] & v<-v_s,\dot{v}<0 \end{cases} \tag{12}$$

Equation (7) can be solved for τ

$$\tau=\begin{cases} -f_{21} & v>v_s,\dot{v}>0 \\ a\cdot v-f_{22} & 0<v\le v_s,\dot{v}>0 \\ a\cdot v-f_{23} & -v_s\le v<0,\dot{v}<0 \\ -f_{24} & v<-v_s,\dot{v}<0 \end{cases} \tag{13}$$

where

$$\begin{cases} f_{21}=-\tau_0 e^{-\alpha(v-v_0)_1}-av_s & v>v_s,\dot{v}>0 \\ f_{22}=(a\cdot v_0-\tau_0)\cdot e^{-\alpha(v-v_0)}-e^{-\alpha v}\cdot\int_{v_0}^{v}(\bar{b}-a)\cdot e^{\alpha\zeta}d\zeta & 0<v\le v_s,\dot{v}>0 \\ f_{23}=(a\cdot v_0-\tau_0)\cdot e^{\alpha(v-v_0)}-e^{-\alpha v}\cdot\int_{v_0}^{v}(\bar{b}-a)\cdot e^{-\alpha\zeta}d\zeta & -v_s\le v<0,\dot{v}<0 \\ f_{24}=-\tau_0 e^{-\alpha(v-v_0)_1}+av_s & v<-v_s,\dot{v}<0 \end{cases} \tag{14}$$

Equation (8) can be also expressed as:

$$\tau=a\cdot\chi_1\cdot v-(f_{21}\cdot\chi_2\cdot\chi_3+f_{22}\cdot\chi_1\cdot\chi_3+f_{23}\cdot\chi_1\cdot\chi_4+f_{24}\cdot\chi_2\cdot\chi_4) \tag{15}$$

where $\chi_i(i=1,2\cdots4)$ are indicator functions defined as:

$$\chi_1=\begin{cases}1 & |v|\le v_s\\ 0 & |v|>v_s\end{cases},\ \chi_2=\begin{cases}0 & |v|\le v_s\\ 1 & |v|>v_s\end{cases},\ \chi_3=\begin{cases}1 & \dot{v}\ge 0\\ 0 & \dot{v}<0\end{cases},\ \chi_4=\begin{cases}0 & \dot{v}\ge 0\\ 1 & \dot{v}<0\end{cases}.$$

Following the definition of the indicator functions, we get

$$\chi_1\cdot\chi_2=0,\ \chi_1+\chi_2=1,\ \chi_3\cdot\chi_4=0,\ \chi_1+\chi_2=1,\ \chi_k^2=\chi_k, k=1,2,3,4$$

By defining $\dot{\chi}_1=\dot{\chi}_2=0$, we have

$$\dot{\tau}=a\cdot\chi_1\cdot\dot{v}-(\dot{f}_{21}\cdot\chi_2\cdot\chi_3+\dot{f}_{22}\cdot\chi_1\cdot\chi_3+\dot{f}_{23}\cdot\chi_1\cdot\chi_4+\dot{f}_{24}\cdot\chi_2\cdot\chi_4)$$

Let

$$F_2=\dot{f}_{21}\cdot\chi_2\cdot\chi_3+\dot{f}_{22}\cdot\chi_1\cdot\chi_3+\dot{f}_{23}\cdot\chi_1\cdot\chi_4+\dot{f}_{24}\cdot\chi_2\cdot\chi_4$$

and $K_a=a\chi_1$. We can also write the derivative of τ as

$$\dot{\tau}=K_a\dot{v}-F_2 \tag{16}$$

2.2 Augmented Multilayer Perceptron (MLP) Neural Network

The MLP NN has been explored to approximate any function with arbitrary degree of accuracy (Hornik et al, 1989). However, it needs a large number of NN nodes and training iterations to approximate non-smooth functions (i.e. piecewise continuous), such as friction, hysteresis, backlash and other hard nonlinearities. For these piecewise continuous functions, the MLP needs to be augmented to work as a function approximator. Results for approximation of piecewise continuous functions or functions with jumps are given in the

paper (Selmic & Lewis, 2000). We use the augmented NN to approximate the piecewise continuous function in hysteresis model.

Let S be a compact set of R^n and define $C^n(S)$ be the space such that the map $f(x) : S \to R^n$ is piecewise continuous. The NN can approximate a function $f(x) \in C^n(S)$, $x \in R^n$, which has a jump at $x = c$ and is continuous from the right as

$$f(x) = W^T \cdot \sigma(V^T \cdot x) + W_f{}^T \cdot \varphi[V_f{}^T \cdot (x - c)] + \varepsilon(x) \tag{17}$$

where $\varepsilon(x)$ is a functional restructure error vector, W^T, $W_f{}^T$ and V^T, $V_f{}^T$ are nominal constant weight matrices. $\sigma(\cdot)$ and $\varphi(\cdot)$ are activation functions for hidden neurons.

For the hysteresis model (16), the piecewise continuous function F2 will be approximated by the augmented NN. In this paper, it is assumed that there exists weight matrix W such that $\|\varepsilon(x)\| \le \varepsilon_N$ with constant $\varepsilon_N > 0$, for all $x \in R^n$, and the Frobenius norm of each matrix is bounded by a known constant $\|W\| \le W_N$ with $W_N > 0$.

3. NN-based compensator and controller design

Given the augmented MLP NN and hysteresis model, a NN-based pre-inversion compensator for the hysteresis is designed to cancel out the effect of hysteresis. In this section, a novel approach is developed to compensate the hysteretic nonlinearity and to guarantee the stability of integrated piezoelectric actuator control system.

3.1 Problem statement

Consider a piezoelectric actuator subject to a hysteresis nonlinearities described by Duhem model. It can be identified as a second-order linear model preceded by hysteretic nonlinearity as follows:

$$\begin{aligned} m \cdot \ddot{y}(t) + b \cdot \dot{y}(t) + k \cdot y(t) &= k \cdot c \cdot \tau_{pr}(t) \\ \tau_{pr}(t) &= H[v(t)] \end{aligned} \tag{18}$$

where v(t) is the input to piezoelectric actuator, $y(t)$ denotes the position of piezoelectric actuator, m, b, k denote the mass, damping and stiffness coefficients, respectively, $H(\bullet)$ represents the Duhem model (1).

In order to eliminate the effect of hysteresis on the piezoelectric actuator system, a NN-based hysteresis compensator is designed to make the output from hysteresis model τ_{pr} approach the designed control signal τ_{pd}. After the hysteresis is compensated by the NN, an

adaptive control for piezoelectric actuator is to be designed to ensure the stability of the overall system and the boundedness of output tracking error of the piezoelectric actuator with unknown hysteresis.

We consider the tracking problem, in which $y(t)$ is to asymptotically track a reference signal $y_d(t)$ having the properties that $y_d(t)$ and its derivatives up to second derivative are bounded, and $\ddot{y}_d(t)$ is piecewise continuous, for all $t \geq 0$. The tracking error of the piezoelectric actuator is defined as

$$e_p(t) = y_d(t) - y(t) . \tag{19}$$

A filtered error is defined as

$$r_p(t) = \dot{e}_p(t) + \lambda_p \cdot e_p(t) \tag{20}$$

where $\lambda_p > 0$ is a designed parameter.

Differentiating $r_p(t)$ and combining it with the system dynamics Eq. (18), one may obtain:

$$\begin{aligned} \frac{m}{k \cdot c} \cdot \dot{r}_p = & -\frac{b}{k \cdot c} \cdot r_p - \tau_{pr} + \frac{m}{k \cdot c} \cdot (\ddot{y}_d + \lambda_p \cdot \dot{e}_p) \\ & + \frac{b}{k \cdot c} \cdot (\dot{y}_d + (\lambda_p - \frac{k}{b}) \cdot e_p) + \frac{1}{c} \cdot y_d . \end{aligned} \tag{21}$$

The tracking error dynamics can be written as

$$\frac{m}{k \cdot c} \cdot \dot{r}_p = -\frac{b}{k \cdot c} \cdot r_p - \tau_{pr} + Y_d{}^T \cdot \theta_p \tag{22}$$

where $Y_d = \left[\ddot{y}_d + (\Lambda_p - \frac{k}{b}) \cdot \dot{e}_p \quad \dot{y}_d + \Lambda_p \cdot e_p \quad y_d \right]^T$ is a regression vector and $\theta_p = \left[\frac{m}{k \cdot c} \quad \frac{b}{k \cdot c} \quad \frac{1}{c} \right]^T \in R^3$ is a unknown parameter vector with $\theta_{p\min} \leq \theta_{pi} \leq \theta_{p\max} \quad i = 1, 2, 3$ where $\theta_{p\min}$ and $\theta_{p\max}$ are some known real numbers.

3.2 NN-based Compensator for Hysteresis

In presence of the unknown hysteresis nonlinearity, the desired control signal τ_{pd} for the piezoelectric actuator is different from the real control signal τ_{pr} . Define the error as

$$\tilde{\tau}_p = \tau_{pd} - \tau_{pr} \tag{23}$$

Differentiating (23), yields

$$\dot{\tilde{\tau}}_p = \dot{\tau}_{pd} - \dot{\tau}_{pr} \tag{24}$$

thus, we have

$$\dot{\tilde{\tau}}_p = \dot{\tau}_{pd} - K_a \dot{v} + F_2 \tag{25}$$

Here we utilize a second first-layer-fixed MLP to approximate the nonlinear function F_2.

$$\begin{aligned} F_2 = {} & W_2^T \cdot \sigma(V_2^T \cdot h) + W_{f21}^T \cdot \varphi_{21} \cdot [V_{f21}^T \cdot (h - c_{21})] \\ & + W_{f22}^T \cdot \varphi_{22} [V_{f22}^T \cdot (h - c_{22})] \\ & + W_{f23}^T \cdot \varphi_{23} [V_{f23}^T \cdot (h - c_{23})] + \varepsilon_2(h) \end{aligned} \tag{26}$$

where $h = \begin{bmatrix} \tau_{pd} & \tau_{p0} & v & \dot{v} & 1 \end{bmatrix}^T$, τ_{p0} is the initial value of the control signal, V_2^T, V_{f21}^T, V_{f22}^T, and V_{f23}^T are input-layer weight matrices, W_2^T, W_{f21}^T, W_{f22}^T, and W_{f23}^T are output-layer weight matrices, 0, v_s, and $-v_s$ are jump points on the output layer, and $\sigma(\cdot)$, $\varphi_{21}(\cdot)$, $\varphi_{21}(\cdot)$, and $\varphi_{23}(\cdot)$ are the activation functions, and $\varepsilon_1(h)$ is the functional restructure error in which inversion error is included. Output-layer weight matrices W_2^T, W_{f21}^T, W_{f22}^T and W_{f23}^T are trained so that the output of NN approximates to the nonlinear function F_2.

Let

$$\Theta(h,v_s) = [\sigma(V_2^T \cdot h) \quad \varphi_{21}(V_{f21}^T \cdot h) \quad \varphi_{22}(V_{f22}^T \cdot h - v_s) \quad \varphi_{23}(V_{f23}^T \cdot h + v_s)]^T$$

and $W_1^T = [W_2^T \quad W_{f21}^T \quad W_{f22}^T \quad W_{f23}^T]$. The nonlinear function F_2 is expressed as:

$$F_2 = W_1^T \Theta(h, v_s) + \varepsilon_1(h) \tag{27}$$

It is assumed that the Frobenius norm of weight matrix W1 is bounded by a known constant $\|W_1\| \le W_{1N}$ with $W_{1N} > 0$ and $\|\varepsilon_1(h)\| \le \varepsilon_{1N}$ with constant $\varepsilon_{1N} > 0$, for all $x \in R^n$.

The estimated nonlinear function $\hat{F}_2$ is constructed by using the neural network with the weight matrix $\hat{W}_1$:

$$\hat{F}_2 = \hat{W}_1^T \Theta(h, v_s).$$

Hence the restructure error between the nonlinear functions F_2 and $\hat{F}_2$ is derived as:

$$\tilde{F}_2 = F_2 - \hat{F}_2 = \tilde{W}_1^T \Theta(h, v_s) + \varepsilon_1(h) .$$

"where $\tilde{W}_1^T = W_1^T - \hat{W}_1^T$."

Remark 1 When the input changes its sign derivative (Beuschel et al, 1998), the augmented MLP can approximate the piecewise continuous functions. In the process, the "jump functions" leads to vertical segments in the feed-forward pre-inversion compensation, where the "functional restructure error" can be confronted by the adaptive controller in Section III.C (Selmic & Lewis, 2000).

A hysteresis pre-inversion compensator is designed:

$$\dot{v} = \hat{\mu} \cdot \{k_b \cdot \tilde{\tau}_p + \dot{\tau}_{pd} + \hat{W}_1^T \cdot \Theta(h, v_s) + r_p\} \tag{28}$$

where $\hat{\mu} = \frac{a_{\min}}{\hat{a}}$ is an estimated constant, which satisfies $0 < \hat{\mu} \le 1$ with the known boundary of $a \in [a_{\min} \quad a_{\max}]$, k_b is a positive constant, $\hat{a}$ is the estimated values of a, and $\hat{W}_1^T = [\hat{W}_2^T \quad \hat{W}_{f21}^T \quad \hat{W}_{f22}^T \quad \hat{W}_{f23}^T]$ is the estimated output-layer weight matrix W_1^T.

Define error matrix as:

$$\tilde{W}_1^T = W_1^T - \hat{W}_1^T .$$

Inserting (26), (28) into (25), we obtain

$$\begin{aligned} \dot{\tilde{\tau}}_p = & -k_b \cdot \hat{\mu} \cdot K_a \cdot \tilde{\tau}_p + (1 - \hat{\mu} \cdot K_a) \cdot \dot{\tau}_{pd} + (1 - \hat{\mu} \cdot K_a) \\ & \cdot \hat{W}_1^T \cdot \Theta(h, v_s) - \hat{\mu} \cdot K_a \cdot r_p + \tilde{W}_1^T \cdot \tilde{\Theta}(h, v_s) + \varepsilon_1(h) \end{aligned} \tag{29}$$

We choose weight matrix update rule as

$$\dot{\hat{W}}_1 = \Gamma \Theta(h, v_s) \cdot \tilde{\tau}_p + k_{p1} \left| \tilde{\tau}_p \right| \cdot \hat{W}_1 \tag{30}$$

where Γ is a positive adaptation gain diagonal matrix, and k_{p1} is a positive constant.

Design the update rule of parameter $\hat{\mu}$ in pre-inversion compensator $\dot{v}$ as

$$\dot{\hat{\mu}} = Proj(\hat{\mu}, \quad \eta \cdot \tilde{\tau}_p \cdot [\dot{\tau}_{pd} + \hat{W}_1^T \Theta(h, v_s) + r_p] \tag{31}$$

where η is positive constant, Proj(.) is a projection operator, which is defined as follows:

$$\dot{\hat{\mu}} = \Pr oj(\hat{\mu}, \quad -\eta \cdot \tilde{\tau}_{pr} \cdot \hat{\mu} \cdot [\dot{\tau}_{pd} + \hat{\Theta}(h, v_s)] =$$

$$\begin{cases} 0 & if \quad \hat{\mu}=1 \quad and \quad \eta\cdot\tilde{\tau}_{pr}\cdot[\dot{\tau}_{pd}+\hat{\Theta}(h,v_s)]<0 \\ & if \quad \left(\frac{a_{\min}}{a_{\max}}\right)^2<\hat{\mu}<1 \\ -\eta\cdot\tilde{\tau}_{pr}\cdot\hat{\mu}\cdot[\dot{\tau}_{pd}+\hat{\Theta}(h,v_s)] & or \quad \hat{\mu}=1 \quad and \quad \eta\cdot\tilde{\tau}_{pr}\cdot[\dot{\tau}_{pd}+\hat{\Theta}(h,v_s)]\geq 0 \\ & or \quad \hat{\mu}=\left(\frac{a_{\min}}{a_{\max}}\right)^2 \quad and \quad \eta\cdot\tilde{\tau}_{pr}\cdot[\dot{\tau}_{pd}+\hat{\Theta}(h,v_s)]\leq 0 \\ 0 & if \quad \hat{\mu}=\left(\frac{a_{\min}}{a_{\max}}\right)^2 \quad and \quad \eta\cdot\tilde{\tau}_{pr}\cdot[\dot{\tau}_{pd}+\hat{\Theta}(h,v_s)]>0 \end{cases} \tag{32}$$

The adaptive NN-based pre-inversion compensator $\dot{v}$ is developed to drive the adaptive control signal τ_{pd} to approach the output of hysteresis model τ_{pr} so that the hysteretic effect is counteracted.

3.3 Controller Design Using Estimated Hysteresis Output

It is noticed that the output of hysteresis is not normally measurable for the plant subject to unknown hysteresis. However, considering the whole system as a dynamic model preceded by Duhem model, we could design an observer to estimate the output of hysteresis based on the input and output of the plant.

The velocity of the actuator $\dot{y}(t)$ is assumed measurable. Define the error between the outputs of actuator and observer as

$$e_1 = y - \hat{y} \tag{33}$$

The observed output of hysteresis is denoted as $\hat{\tau}_{pr}$ and the error between the output of hysteresis τ_{pr} and the observed $\hat{\tau}_{pr}$ is defined as $e_2 = \tau_{pr} - \hat{\tau}_{pr}$. Then the observer is designed as:

$$\dot{\hat{y}} = \dot{y} + L_1 e_1 \tag{34}$$

$$\dot{\hat{\tau}}_{pr} = \hat{K}_a \dot{v} - \hat{F}_2 + L_2 e_1 - K_{pr}\hat{\tau}_{pr} \tag{35}$$

The error dynamics of the observer is obtained based on the actuator model and hysteresis model.

$$\begin{aligned} \dot{e}_1 &= -L_1 e_1 = -L_1 e_1 \\ \dot{e}_2 &= \tilde{K}_a \dot{v} - \tilde{F}_2 - L_2 e_1 + K_{pr}\hat{\tau}_{pr} \end{aligned} \tag{36}$$

where the parameter error is defined as $\tilde{K}_a = K_a - \hat{K}_a$.

By using the observed hysteresis output $\hat{\tau}_{pr}$, we may define the signal error between the adaptive control signal τ_{pd} and the estimated hysteresis output as:

$$\tilde{\tau}_{pe} = \tau_{pd} - \hat{\tau}_{pr} \tag{37}$$

The derivative of the signal error is:

$$\dot{\tilde{\tau}}_{pe} = \dot{\tau}_{pd} - \hat{K}_a \dot{v} + \hat{F}_2 - L_2 e_1 + K_{pr} \hat{\tau}_{pr} . \tag{38}$$

A hysteresis pre-inversion compensator is designed:

$$\dot{v} = \hat{\mu} \cdot \{ k_b \cdot \tilde{\tau}_{pe} + \dot{\tau}_{pd} + \hat{F}_2 + r_p \} . \tag{39}$$

By substituting the neural network output $\hat{F}_2 = \hat{W}_1^T \Theta(h, v_s)$ and pre-inversion compensator output into the derivative of the signal error, one obtains:

$$\dot{\tilde{\tau}}_{pe} = (1 - \hat{K}_a \hat{\mu}) \dot{\tau}_{pd} - \hat{K}_a \hat{\mu} \cdot k_b \tilde{\tau}_{pe} + (1 - \hat{K}_a \hat{\mu}) \hat{W}_1^T \Theta(h, v_s) - \hat{K}_a \hat{\mu} \cdot r_p - L_2 e_1 + K_{pr} \hat{\tau}_{pr} \tag{40}$$

The weight matrix update rule is chosen as:

$$\dot{\hat{W}}_1 = \Gamma \Theta(h, v_s) \cdot \tilde{\tau}_{pe} + k_{p1} \left| \tilde{\tau}_{pe} \right| \cdot \hat{W}_1 \tag{41}$$

And the update rule of parameter $\hat{\mu}$ in pre-inversion compensator $\dot{v}$ is designed with the same projection operator as (32):

$$\dot{\hat{\mu}} = Proj(\hat{\mu}, \quad \eta \cdot \tilde{\tau}_{pe} \cdot [\dot{\tau}_{pd} + \hat{W}_1^T \Theta(h, v_s) + r_p]) . \tag{42}$$

The update rule of parameter $\hat{K}_a$ in the observer (35) is designed with the same projection operator as (32):

$$\dot{\hat{K}}_a = Proj(\hat{K}_a, \quad \gamma \cdot \hat{\mu} \cdot \tilde{\tau}_{pe} \cdot [\dot{\tau}_{pd} + \hat{W}_1^T \Theta(h, v_s) + r_p] + \dot{v} \cdot \tilde{\tau}_{pe}) . \tag{43}$$

Hence we design the adaptive controller and update rule of control parameter as:

$$\tau_{pd} = k_{pd} \cdot r_p + Y_d^T \cdot \hat{\theta}_p \tag{44}$$

$$\dot{\hat{\theta}}_p = Proj_{\hat{\theta}_p} (\hat{\theta}_p, \quad \beta \cdot Y_d \cdot r_p) \tag{45}$$

where the projection operator is

$$\{Proj_{\hat{\theta}_p}(\hat{\theta}_p, \quad \beta \cdot Y_d \cdot r_p)\}_i =$$

$$\begin{cases} 0 & if \quad \hat{\theta}_{pi} = \theta_{p\max} \; and \quad \beta \cdot (Y_d \cdot r_p)_i < 0 \\ & if \quad \theta_{p\min} < \hat{\theta}_{pi} < \theta_{p\max} \\ \beta \cdot (Y_d \cdot r_p)_i & or \quad \hat{\theta}_{pi} = \theta_{p\max} \; and \quad \beta \cdot (Y_d \cdot r_p)_i \geq 0 \\ & or \quad \hat{\theta}_{pi} = \theta_{p\min} \; and \quad \beta \cdot (Y_d \cdot r_p)_i \leq 0 \\ 0 & if \quad \hat{\theta}_{pi} = \theta_{p\min} \; and \quad \beta \cdot (Y_d \cdot r_p)_i > 0 \end{cases}$$

With the adaptive robust controller, pre-inversion hysteresis compensator and hysteresis observer, the overall control system of integrated piezoelectric actuator is shown in Fig. 3. The stability and convergence of the above integrated control system are summarized in Theorem 1.

Theorem 1 For a piezoelectric actuator system (18) with unknown hysteresis (1) and a desired trajectory $y_d(t)$, the adaptive robust controller (44), NN based compensator (39) and hysteresis observer (34) and (35) are designed to make the output of actuator to track the desired trajectory $y_d(t)$. The parameters of the adaptive robust controller and the NN based compensator are tuned by the updating rules (41)-(43) and (45). Then, the tracking error $e_p(t)$ between the output of actuator and the desired trajectory $y_d(t)$ converge to a small neighborhood around zero by appropriately choosing suitable control gains k_{pd}, k_b and observer gains L_1, L_2 and K_{pr}.

Proof: Define a Lyapunov function

$$V_2 = \frac{1}{2} \cdot \frac{m}{k \cdot c} \cdot r_p{}^2 + \frac{1}{2} \tilde{\tau}_{pe}{}^2 + \frac{1}{2} \cdot tr(\tilde{W}_1^T \Gamma^{-1} \tilde{W}_1) + \frac{1}{2 \cdot \eta K_a} (1 - \hat{\mu} K_a)^2$$

$$+ \frac{1}{2 \cdot \gamma} (K_a - \hat{K}_a)^2 + \frac{1}{2\beta} \cdot (\theta_p - \hat{\theta}_p)^T \cdot (\theta_p - \hat{\theta}_p) + \frac{1}{2} e_1^2 + \frac{1}{2} e_2^2$$

The derivative of Lyapunov function is obtained:

$$\dot{V}_2 = \frac{m}{k \cdot c} \cdot r_p \dot{r}_p + \tilde{\tau}_{pe} \cdot \dot{\tilde{\tau}}_{pe} - tr(\dot{\tilde{W}}_1^T \Gamma^{-1} \tilde{W}_1) - \frac{1}{\eta} (1 - \hat{\mu} K_a) \dot{\hat{\mu}} - \frac{1}{\gamma} (K_a - \hat{K}_a) \dot{\hat{K}}_a$$

$$- \frac{1}{\beta} \cdot (\theta_p - \hat{\theta}_p)^T \cdot \dot{\hat{\theta}}_p + e_1 \dot{e}_1 + e_2 \dot{e}_2$$

Introducing control strategies (39), (44) and the update rules (41)-(43), (45) into above equation, one obtains

$$\dot{V}_2 = -(\frac{b}{k \cdot c} + k_{pd}) \cdot r_p^2 - k_b \cdot \hat{\mu} \cdot \hat{K}_a \cdot \tilde{\tau}_{pe}{}^2 + \varepsilon_1(h) \tilde{\tau}_{pe} - k_{p1} \left| \tilde{\tau}_{pe} \right| tr(\tilde{W}_1^T \hat{W}_1)$$

$$- e_2 r_p - L_2 e_1 \tilde{\tau}_{pe} + K_{pr} \hat{\tau}_{pr} \tilde{\tau}_{pe} - L_1 e_1^2 - (L_2 e_1 + \tilde{F}_2) e_2 + K_{pr} \hat{\tau}_{pr} e_2$$

By using $\hat{\tau}_{pr} = \tau_{pr} - e_2$, $\left| \tilde{F} \right| \leq \varepsilon_{1N}$ and inequality: $\pm ab \leq \frac{1}{2} a^2 + \frac{1}{2} b^2$, one has:

$$\begin{aligned}\dot{V}_2 &= -(\frac{b}{k\cdot c}+k_{pd})\cdot r_p^2 - k_b\cdot\hat{\mu}\cdot\hat{K}_a\cdot\tilde{\tau}_{pe}^{\ 2} + \varepsilon_1(h)\tilde{\tau}_{pe} - k_{p1}\left|\tilde{\tau}_{pe}\right| tr(\tilde{W}_1^T\hat{W}_1)\\ &+\frac{1}{2}e_2^2+\frac{1}{2}r_p^2+\frac{1}{2}L_2^2e_1^2+\frac{1}{2}\tilde{\tau}_{pe}^2+\frac{1}{2}\tilde{\tau}_{pe}^2+\frac{1}{2}K_{pr}^2\tau_{pr}^2+\frac{1}{2}K_{pr}^2\tilde{\tau}_{pe}^2+\frac{1}{2}e_2^2\\ &-L_1e_1^2+\frac{1}{2}(L_2e_1+\varepsilon_{1N})^2+\frac{1}{2}e_2^2+K_{pr}\tau_{pr}e_2-K_{pr}e_2^2\end{aligned} \tag{46}$$

By using the inequality $\frac{1}{2}(a+b)^2 \le a^2+b^2$, we can derive the following inequality:

$$\begin{aligned}\dot{V}_2 &\le -(\frac{b}{k\cdot c}+k_{pd}-\frac{1}{2})\cdot r_p^{\ 2} - (k_b\cdot\hat{\mu}\cdot\hat{K}_a-\frac{1}{2}K_{pr}^2-1)\cdot\tilde{\tau}_{pe}^{\ 2}+\left|\tilde{\tau}_{pe}\right|\cdot\varepsilon_{1N}\\ &-k_{p1}\cdot\left|\tilde{\tau}_{pe}\right|\cdot\left\|\tilde{W}_1\right\|(W_{1N}-\left\|\tilde{W}_1\right\|)-(L_1-\frac{3}{2}L_2^{\ 2})e_1^2-(K_{pr}-2)e_2^2+\varepsilon_{1N}^2+K_{pr}^2\tau_{pr}^2\end{aligned}$$

From the Property 1 of Chapter 2 in the recent book (Ikhouane & Rodellar, 2007), we know τ_{pr}^2 is bounded (say, $\tau_{pr}^2 \le M^2$ where M is a constant), and then define a constant $\delta = \varepsilon_{1N}^2 + K_{pr}^2M^2 > \varepsilon_{1N}^2 + K_{pr}^2\tau_{pr}^2$ such that

$$\begin{aligned}\dot{V}_2 &\le -(\frac{b}{k\cdot c}+k_{pd}-\frac{1}{2})\cdot r_p^{\ 2} - (k_b\cdot\hat{\mu}\cdot\hat{K}_a-\frac{1}{2}K_{pr}^2-1)\cdot\tilde{\tau}_{pe}^{\ 2}+\left|\tilde{\tau}_{pe}\right|\cdot\varepsilon_{1N}\\ &-k_{p1}\cdot\left|\tilde{\tau}_{pe}\right|\cdot\left\|\tilde{W}_1\right\|(W_{1N}-\left\|\tilde{W}_1\right\|)-(L_1-\frac{3}{2}L_2^{\ 2})e_1^2-(K_{pr}-2)e_2^2+\delta\end{aligned} \tag{47}$$

We select the control parameters k_{pd} , k_b and observer parameters L_1 , L_2 and K_{pr} satisfying the following inequalities:

$$\frac{b}{k\cdot c}+k_{pd}-\frac{1}{2}>0,$$

$$K_{pr}>2,$$

$$k_b\cdot a_{\max}\cdot\hat{K}_a-\frac{1}{2}K_{pr}^2-1>0,$$

$$L_1>\frac{3}{2}L_2^{\ 2}.$$

Let $k_m = k_b\cdot a_{\max}\cdot\hat{K}_a-\frac{1}{2}K_{pr}^2-1$. If we have

$$\left|\tilde{\tau}_{pe}\right| > \frac{-k_{p1}\cdot W_{1N}^{\ 2}/4+\varepsilon_{1N}}{k_m},$$

$$\left\|\tilde{W}_1\right\| > W_{1N}/2+\sqrt{W_{1N}^2/4-\varepsilon_{1N}/k_{p1}} \tag{48}$$

we can easily conclude that the closed-loop system is semi-globally bounded (Su & Stepanenko, 1998).

Hence, the following inequality holds

$$\frac{-k_{p1}\cdot W_{1N}{}^{2}/4+\varepsilon_{1N}}{k_m}<b_r$$

where $b_r>0$ represents the radius of a ball inside the compact set C_r of the tracking error $\tilde{\tau}_{pe}(t)$.

Thus, any trajectory $\tilde{\tau}_{pe}(t)$ starting in compact set $C_r=\{r|\|r\|\le b_r\}$ converges within C_r and is bounded. Then the filtered error of system $r_p(t)$ and the tracking error of the hysteresis $\tilde{\tau}_{pe}(t)$ converge to a small neighborhood around zero. According to the standard Lyapunov theorem extension (Kuczmann & Ivanyi, 2002), this demonstrates the UUB (uniformly ultimately bounded) of $r_p(t)$, $\tilde{\tau}_{pe}(t)$, $\tilde{W}_1$, e_1 and e_2.

Remark 2 It is worth noting that our method is different from (Zhao & Tan, 2006; Lin et al 2006) in terms of applying neural network to approximate hysteresis. The paper (Zhao & Tan, 2006) transformed multi-valued mapping of hysteresis into one-to-one mapping, whereas we sought the explicit solution to the Duhem model so that augmented MLP neural networks can be used to approximate the complicated piecewise continuous unknown nonlinear functions. Viewed from a wavelet radial structure perspective, the WNN in the paper (Lin et al 2006) can be considered as radial basis function network. In our scheme, the unknown part of the solution was approximated by an augmented MLP neural network.

4. Simulation studies

In this section, the effectiveness of the NN-based adaptive controller is demonstrated on a piezoelectric actuator described by (18) with unknown hysteresis. The coefficients of the dynamic system and hysteresis model are m =0.016kg, b =1.2Ns/μm, k =4500N/ μm, c =0.9 μm /V, a =6, $\bar{b}$ =0.5, v_s =6 μm /s, $\beta=0.1$, $k_{pd}=50$.

The input reference signal is chosen as the desired trajectory: $y_d=3\cdot\sin(0.2\pi t)$. The control objective is to make the output signal y follow the given desired trajectory y_d. From Fig. 1, one may notice that relatively large tracking error is observed in the output response due to the uncompensated hysteresis.

The Neural Network has 10 hidden neurons for the first part of neural network and 5 hidden neurons for the rest parts of neural network with three jumping points (0, v_s, $-v_s$). The gains for updating output weight matrix are all set as $\Gamma=diag\{10\}_{25X25}$. The activation function $\sigma(\cdot)$ is a sigmoid basis function and activation function $\varphi(\cdot)$ has the definition $\varphi(\cdot)=\left(\frac{1-e^{-\alpha x}}{1+e^{-\alpha x}}\right)^k$ $x\ge 0$, otherwise zero. The parameters for the observer are set as: $K_a=20$, $k_b=100$, $\eta=0.1$, $\gamma=0.1$, $K_{pr}=10$, $L_1=100$, $L_2=1$ and initial

conditions are $\hat{y}(0) = 0$, $\hat{\tau}(0) = 0$. The system responses are shown in Fig.2, from which it is observed that the tracking performance is much better than that of adaptive controlled piezoelectric actuator without hysteretic compensator.

The input and output maps of NN-based pre-inversion hysteresis compensator and hysteresis are given in Fig. 3, respectively. The desired control signal and real control signal map (Fig. 3c) shows that the curve is approximate to a line which means the relationship between two signals is approximately linear with some deviations.

In order to show the effectiveness of the designed observer, we compare the observed hysteresis output $\hat{\tau}_{pr}$ and the real hysteresis output τ_{pr} in Fig. 4. The simulation results show that the observed hysteresis output signal can track the real hysteresis output. Furthermore, the output of adaptive hysteresis pre-inversion compensator $v(t)$ is shown in Fig.5. The signal is shown relatively small and bounded.

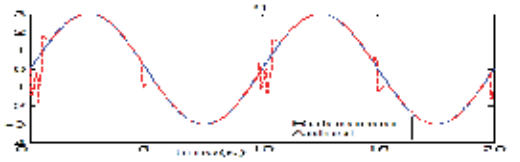

(a)

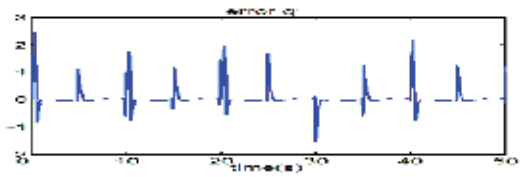

(b)

Fig. 1 Performance of NN controller without hysteretic compensator (a) The actual control signal (dashed line) with reference (solid) signal; (b) Error $y_1 - y_d$

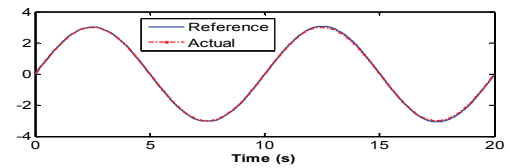

(a)

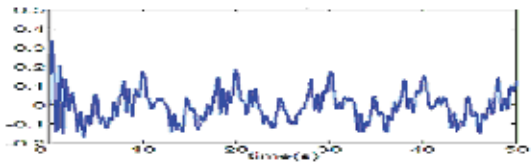

(b)

Fig. 2. Performance of NN controller with hysteresis, its compensator and observer (a) The actual control signal (dashed line) with reference (solid) signal; (b) Error $y_1 - y_d$

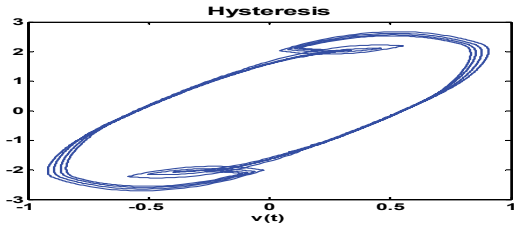

(a)

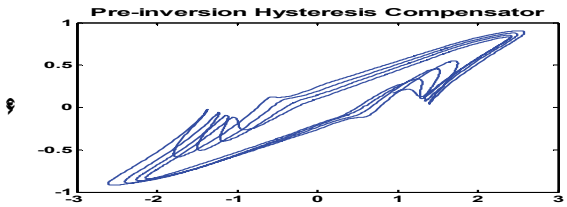

(b)

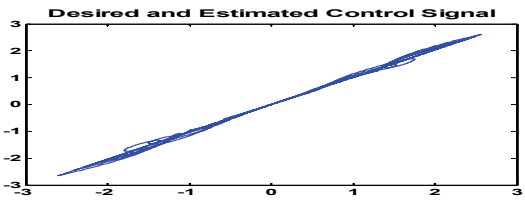

(c)

Fig. 3. (a) Hysteresis's input and output map $\tau_{pr}\ vs.\ v$; (b) Pre-inversion compensator's input and output map $v\ vs.\ \tau_{pd}$; (c) Desired control signal and Observed control signal curve $\hat{\tau}_{pr}\ vs.\ \tau_{pd}$.

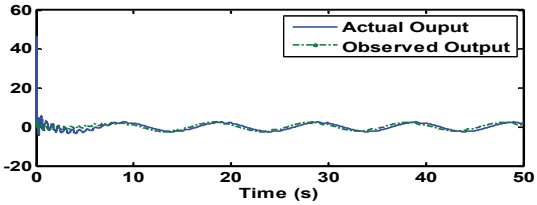

Fig. 4. Observed Hysteresis Ouput $\hat{\tau}_{pr}$ and Real Hysteresis Output τ_{pr}

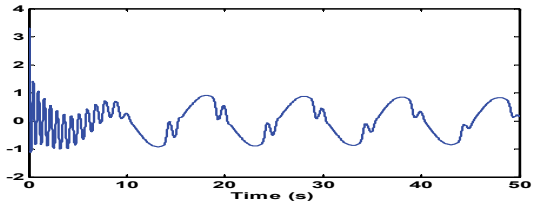

Fig. 5. Adaptive Hysteresis Pre-inversion Compensator $v(t)$

5. Conclusion

In this paper, an observer-based controller for piezoelectric actuator with unknown hysteresis is proposed. An augmented feed-forward MLP is used to approximate a complicated piecewise continuous unknown nonlinear function in the explicit solution to the differential equation of Duhem model. The adaptive compensation algorithm and the weight matrix update rules for NN are derived to cancel out the effect of hysteresis. An observer is designed to estimate the value of hysteresis output based on the input and output of the plant. With the designed pre-inversion compensator and observer, the stability of the integrated adaptive system and the boundedness of tracking error are proved. Future work includes the compensator design for the rate-dependent hysteresis.

6. References

Banks, H. T. & Smith, R. C. (2000). Hysteresis modeling in smart material systems, *J. Appl. Mech. Eng*, Vol. 5, pp. 31-45.

Tan, X. & Baras, J. S. (2004). Modelling and control of hysteresis in magnetostrictive actuators, *Automatica*, Vol. 40, No. 9, pp. 1469-1480.

Brokate, M. & Sprekels, J. (1996). *Hysteresis and Phase Transitions*, New York: Springer-Verlag.

Visintin, A. (1994). *Differential Models of Hysteresis*, New York: Springer-Verlag.

Jiles, D. C. & Atherton, D. L. (1986). Theory of ferromagnetic hysteresis, *J. Magnet. Magn. Mater*, Vol. 61, pp. 48-60.

Tao, G. & Kokotovic, P. V. (1995). Adaptive control of Plants with Unknown Hysteresis, *IEEE Transactions on Automatic Control*, Vol. 40, No. 2, pp. 200-212.

Su, C. Y.; Stepanenko, Y.; Svoboda, J. & Leung, T. P. (2000). Robust Adaptive Control of a Class of Nonlinear Systems with Unknown Backlash-Like Hysteresis, *IEEE Transactions on Automatic Control*, Vol. 45, No. 12, pp. 2427-2432.

Su, C. Y.; Wang, Q.; Chen, K. & Rakheja, S. (2005). Adaptive Variable Structure Control of a Class of Nonlinear Systems with Unknown Prandtl-Ishlinskii Hysteresis, *IEEE Transactions on Automatic Control,* Vol. 50, No. 12, pp. 2069-2074.

Tan, X. & Baras, J. S. (2005). Adaptive Identification and Control of Hysteresis in Smart Materials, *IEEE Transactions on Automatic Control,*Vol.50, No.(6), pp. 827-839.

Ge, S. S. & Wang, C. (2002). Direct adaptive NN control of a class of nonlinear systems, *IEEE Transactions on Neural Networks*, Vol. 13, No. 1, pp. 214-221.

Makaveev, D.; Dupre, L, & Melkebeek, J. (2002). Neural-Network-Based Approach to Dynamic Hysteresis for Circular and Elliptical Magnetization in Electrical Steel Sheet, *IEEE Transactions on Magnetics,* Vol. 38, No.5, pp. 3189-3191.

Kuczmann, M. &Ivanyi, A. (2002). A New Neural-Network-Based Scalar Hysteresis Model, *IEEE Transactions on Magnetics,* Vol. 38, No.2, pp. 857-860.

Beuschel, M.; Hangl, F, & Schroder, D. (1998). A General Approach for Hysteresis Modeling and Identification Using Neural Networks, *Proceeding of the 1998 IEEE world Congress on Computational Intelligence & The 1998 IEEE International Joint Conference,* Vol.3, pp. 2425-2428.

Zhao, X. & Tan, Y. (2006). Neural network based identification of Preisach-type hysteresis in piezoelectric actuator using hysteretic operator, *Sensors and Actuators A: Physical*, Vol.126, pp.306-311.

Lin, F.; Shieh, H. & Huang P. (2006). Adaptive Wavelet Neural Network Control with Hysteresis Estimation for Piezo-Positioning Mechanism, *IEEE Transactions on Neural Network*, Vol. 17, No. 2, pp. 432-444.

Yang, B. & Lin, W. (2004). Homogeneous Observers, Iterative Design, and Global Stabilization of High-Order Nonlinear Systems by Smooth Output Feedback, *IEEE Transactions on Automatic Control*, Vol. 49, No. 7, pp. 1069-1080.

Krener, A. J. & Isidori, A. (1983). Linearization by output injection and nonlinear observer, *Systems & Control Letters*, Vol.3, pp. 47-52.

Krener, A. J. & Kang, W. (2003). Locally convergent nonlinear observers, *SIAM J. Control Optim.*, Vol. 42, No. 1, pp. 157-177.

Xie, W. F. (2007). Sliding-Mode-Observer-Based Adaptive Control for Servo Actuator with Friction, *IEEE Transactions on Industrial Electronics*, Vol. 54, No. 3, pp. 1517-1528.

Kuczmann, M. & Ivanyi, A. (2002). A New Neural-Network-Based Scalar Hysteresis Model, *IEEE Transactions on Magnetics*, Vol.38, No. 2, pp. 857-860.

Coleman, B. D. & Hodgdon, M. L. (1987). On a class of constitutive relations for ferromagnetic hysteresis, *Arch. Rational Mech. Anal.*, pp: 375-396.

Macki, J. W.; Nistri, P. & Zecca, P. (1993). Mathematical models for hysteresis, *SIAM Review*, Vol.35, No. 1, pp. 94-123.

Banning, R.; Koning, W. L.; Adriaens, J. J. & Koops, R. K. (2001). State-space analysis and identification for a class of hysteretic systems, *Automatica*, Vol. 37, No. 4, pp. 1883-1892.

Hornik, K.; Stinchcombe, M. & White, H. (19989). Multilayer feedforward networks are universal approximators, *Neural Networks*, Vol.2, pp. 359-366.

Selmic, R. R. & Lewis, F. L. (2000). Deadzone Compensation in Motion Control Systems Using Dynamical Neural Networks, *IEEE Transactions on Automatic Control*, Vol.45, No. 4, pp. 602-613.

Ikhouane, F. & Rodellar, J. (2007). *Systems with Hysteresis-Analysis, Identification and Control using the Bouc-Wen Model*, England: John Wiley.

Su, C. Y. & Stepanenko, Y. (1998). Redesign of hybrid adaptive/robust motion control of rigid-link electrically-driven robot manipulators, *IEEE Transactions on Robotics and Automation*, Vol.14, No. 4, pp. 651-655.

13

On the Adaptive Tracking Control of 3-D Overhead Crane Systems

Yang, Jung Hua
National Pingtung University of Science and Technology
Pingtung, Taiwan

1. Introduction

For low cost, easy assembly and less maintenance, overhead crane systems have been widely used for material transportation in many industrial applications. Due to the requirements of high positioning accuracy, small swing angle, short transportation time, and high safety, both motion and stabilization control for an overhead crane system becomes an interesting issue in the field of control technology development. Since the overhead crane system is underactuated with respect to the sway motion, it is very difficult to operate an overhead traveling crane automatically in a desired manner. In general, human drivers, often assisted by automatic anti-sway system, are always involved in the operation of overhead crane systems, and the resulting performance, in terms of swiftness and safety, heavily depends on their experience and capability. For this reason, a growing interest is arising about the design of automatic control systems for overhead cranes. However, severely nonlinear dynamic properties as well as lack of actual control input for the sway motion might bring about undesired significant sway oscillations, especially at take-off and arrival phases. In addition, these undesirable phenomena would also make the conventional control strategies fail to achieve the goal. Hence, the overhead crane systems belong to the category of incomplete control system, which only allow a limited number of inputs to control more outputs. In such a case, the uncontrollable oscillations might cause severe stability and safety problems, and would strongly constrain the operation efficiency as well as the application domain. Furthermore, an overhead crane system may experience a range of parameter variations under different loading condition. Therefore, a robust and delicate controller, which is able to diminish these unfavorable sway and uncertainties, needs to be developed not only to enhance both efficiency and safety, but to make the system more applicable to other engineering scopes.

The overhead crane system is non-minimum phase (or has unstable zeros in linear case) if a nonlinear state feedback can hold the system output identically zero while the internal dynamics become unstable. Output tracking control of non-minimum phase systems is a highly challenging problem encountered in many practical engineering applications such as aircraft control [1], marine vehicle control [2], flexible link manipulator control [3], inverted pendulum system control [4]. The non-minimum phase property has long been recognized to be a major obstacle in many control problems. It is well known that unstable zeros cannot

be moved with state feedback while the poles can be arbitrarily placed (if completely controllable). In most standard adaptive control as well as in nonlinear adaptive control, all algorithms require that the plant to be minimum phase. This chapter presents a new procedure for designing output tracking controller for non-minimum phase systems (The overhead crane systems).

Several researchers have dealt with the modeling and control problems of overhead crane system. In [5], a simple proportional derivative (PD) controller is designed to asymptotically regulate the overhead crane system to the desired position with natural damping of sway oscillation. In [6], the authors propose an output feedback proportional derivative controller that stabilizes a nonlinear crane system. In [7], the authors proposed an indirect adaptive scheme, based on dynamic feedback linearization techniques, which was applied to overhead crane systems with two control input. In [8], Li *et al* attacked the under-actuated problem by blending four local controllers into one overall control strategy; moreover, experimental results delineating the performance of the controller were also provided. In [9], a nonlinear controller is proposed for the trolley crane systems using Lyapunov functions and a modified version of sliding-surface control is then utilized to achieve the objective of cart position control. However, the sway angle dynamics has not been considered for stability analysis. In [10], the authors proposed a saturation control law based on a guaranteed cost control method for a linearized version of 2-DOF crane system dynamics. In [11], the authors designed a nonlinear controller for regulating the swinging energy of the payload. In [12], a fuzzy logic control system with sliding mode Control concept is developed for an overhead crane system. Y. Fang *et al*. [13] develop a nonlinear coupling control law to stabilize a 3-DOF overhead crane system by using LaSalle invariance theorem. However, the system parameters must be known in advance. Ishide *et al.* [14] train a fuzzy neural network control architecture for an overhead traveling crane by using back-propagation method. However, the trolley speed is still large even when the destination is arrived, which would result in significant residual sway motion, low safety, and poor positioning accuracy. In the paper [15], a nonlinear tracking controller for the load position and velocity is designed with two loops: an outer loop for position tracking, and an inner loop for stabilizing the internally oscillatory dynamics using a singular perturbation design. But the result is available only when the sway angle dynamics is much faster than the cart motion dynamics. In the paper [16], a simple control scheme, based on second-order sliding modes, guarantees a fast precise load transfer and swing suppression during the load movement, despite of model uncertainties. In the paper [17], it proposes a stabilizing nonlinear control law for a crane system having constrained trolley stroke and pendulum length using the Lyapunov's second method and performs some numerical experiments to examine the validity of the control law. In the paper [18], the variable structure control scheme is used to regulate the trolley position and the hoisting motion towards their desired values. However the input torques exhibit a lot of chattering. This chattering is not desirable as it might shorten the lifetime of the motors used to drive the crane. In the paper [19], a new fuzzy controller for anti-swing and position control of an overhead traveling crane is proposed based on the Single Input Rule Modules (SIRMs). Computer simulation results show that, by using the fuzzy controller, the crane can be smoothly driven to the

destination in a short time with low swing angle and almost no overshoot. D. Liu *et al.* [20] present a practical solution to analyze and control the overhead crane. A sliding mode fuzzy control algorithm is designed for both X-direction and Y-direction transports of the overhead crane. Incorporating the robustness characteristics of SMC and FLC, the proposed control law can guarantee a swing-free transportation. J.A. Mendez *et al.* [21] deal with the design and implementation of a self-tuning controller for an overhead crane. The proposed neurocontroller is a self-tuning system consisting of a conventional controller combined with a **NN** to calculate the coefficients of the controller *on-line.* The aim of the proposed scheme is to reduce the training-time of the controller in order to make the real-time application of this algorithm possible. Ho-Hoon Lee *et al.* [22] proposes a new approach for the anti-swing control of overhead cranes, where a model-based control scheme is designed based on a V-shaped Lyapunov function. The proposed control is free from the conventional constraints of small load mass, small load swing, slow hoisting speed, and small hoisting distance, but only guarantees asymptotic stability with all internal signals bounded. This paper also proposes a practical trajectory generation method for a near minimum-time control, which is independent of hoisting speed and distance. In this paper [23], robustness of the proposed intelligent gantry crane system is evaluated. The evaluation result showed that the intelligent gantry crane system not only has produced good performances compared with the automatic crane system controlled by classical PID controllers but also is more robust to parameter variation than the automatic crane system controlled by classical PID controllers. In this paper [24], the I-PD and PD controllers designed by using the CRA method for the trolley position and load swing angle of overhead crane system have been proposed. The advantage of CRA method for designing the control system so that the system performances are satisfied not only in the transient responses but also in the steady-state responses, have also been confirmed by the simulation results.

Although most of the control schemes mentioned above have claimed an adaptive stabilizing tracking/regulation for the crane motion, the stability of the sway angle dynamics is hardly taken into account. Hence, in this chapter, a nonlinear control scheme which incorporates both the cart motion dynamics and sway angle dynamics is devised to ensure the overall closed-loop system stability. Stability proof of the overall system is guaranteed via Lyapunov analysis. To demonstrate the effectiveness of the proposed control schemes, the overhead crane system is set up and satisfactory experimental results are also given.

2. Dynamic Model of Overhead Crane

The aim of this section is to drive the dynamic model of the overhead crane system. The model is dived using Lagrangian method. The schematic plotted in Figure 1 represents a three degree of freedom overhead crane system. To facilitate the control development, the following assumptions with regard to the dynamic model used to describe the motion of overhead crane system will be made. The dynamic model for a three degree of freedom (3-DOF) overhead crane system (see Figure 1) is assumed to have the following postulates.

A1: The payload and the gantry are connected by a mass-less, rigid link.

A2: The angular position and velocity of the payload and the rectilinear position and

velocity of the gantry are measurable.
A3: The payload mass is concentrated at a point and the value of this mass is exactly known; moreover, the gantry mass and the length of the connecting rod are exactly known.
A4: The hinged joint that connects the payload link to the gantry is frictionless.

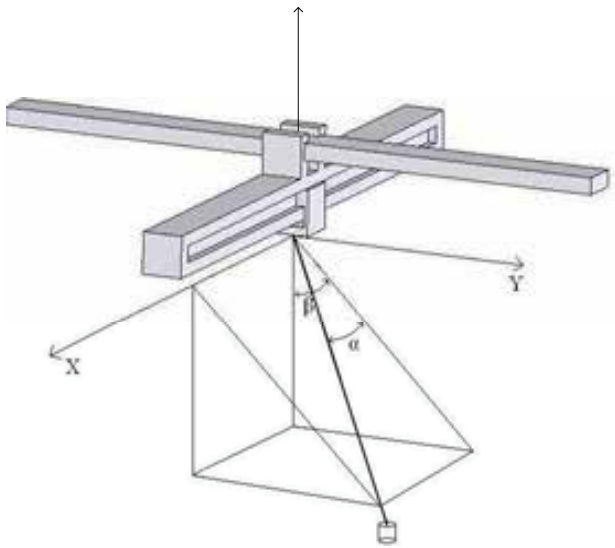

Fig. 1. 3-D Overhead Crane System

The 3-D crane system will be derived based on Lagrange-Euler approach. Consider the 3-dimensional overhead crane system as shown in Figure 1. The cart can move horizontally in x-y plane, in which the moving distance of the cart along the X-rail is denoted as *x(t)* and the distance on the Y-rail measured from the initial point of the construction frame is denoted as *y(t)*. The length of the lift line is denoted as *l*. Define the angle between the lift line and its projection on the y-z plane as $\alpha(t)$ and the angle between the projection line and the negative axis as $\beta(t)$. Then the kinetic energy and potential energy of the system can be found in Equation (1.1) and (1.2), respectively and be expressed as the following equations.

$$K = \frac{1}{2}m_1\dot{x}^2 + \frac{1}{2}(m_1 + m_2)\dot{y}^2 + \frac{1}{2}m_c(\dot{x}_c^2 + \dot{y}_c^2 + \dot{z}_c^2) \tag{1}$$

$$V = -mgl\cos\alpha\cos\beta \tag{2}$$

where x_c, y_c are the related positions of the load described in the Cartesian coordinate, which can be mathematically written as

$$x_c = x + l\,sin\,\alpha \tag{3}$$

$$y_c = y + l\cos\alpha\sin\beta \tag{4}$$

$$z_c = -l\cos\alpha\cos\beta \tag{5}$$

The following equations express the velocities by taking the time derivative of above equations

$$\dot{x}_c = \dot{x} + l\dot{\alpha}\cos\alpha \tag{6}$$

$$\dot{y}_c = \dot{y} - l\dot{\alpha}\sin\alpha\sin\beta + l\dot{\beta}\cos\alpha\cos\beta \tag{7}$$

$$\dot{z}_c = -l\dot{\alpha}\sin\alpha\cos\beta - l\dot{\beta}\cos\alpha\sin\beta \tag{8}$$

By using the Lagrange-Euler formulation,

$$\frac{d}{dt}\left(\frac{\partial L}{\partial \dot{q}_i}\right) - \frac{\partial L}{\partial q_i} = \tau_i, i = 1,2,3,4. \tag{9}$$

where $L = K - V$, q_i is the element of vector $q = [x \quad y \quad \alpha \quad \beta]^T$ and τ_i is the corresponding external input to the system, we have the following mathematical representation which formulates the system motion

$$M(q)\ddot{q} + C(q,\dot{q}) + G(q) = \tau \tag{10}$$

where $M(q) \in R^{4\times4}$ is inertia matrix of the crane system, $C(q,\dot{q}) \in R^{4\times1}$ is the nonlinear terms coming from the coupling of linear and rotational motion, $G(q) \in R^{4\times1}$ is the terms due to gravity, and $\tau = [u_x \quad u_y \quad 0 \quad 0]^T$ is the input vector.

As mentioned previously, the dynamic equation of motion described the overhead crane system also have the same properties as follows

P1: The inertia matrix $M(q)$ is symmetric and positive definite for all $q \in R^n$.

P2: There exists a matrix $B(q,\dot{q})$ such that $C(q,\dot{q}) = B(q,\dot{q})\dot{q}$, and $\forall x \in R^4$ $x^T(\dot{M} - 2B)x = 0$, i.e., $\dot{M} - 2B$ is skew-symmetric. $B(q,\dot{q}_x)\dot{q}_y = B(q,\dot{q}_y)\dot{q}_x$.

P3: The parameters of the system can be linearly extracted as

$$M(q)\ddot{q} + C(q,\dot{q}) + G(q) = W_f(q,\dot{q},\ddot{q})\Phi_f \tag{11}$$

where $W_f(q,\dot{q},\ddot{q})$ is the regressor matrix and Φ_f is a vector containing the system parameters.

Dynamic Model of Overhead Crane

In this section, an adaptive control scheme will be developed for the position tracking of an overhead crane system.

2.1 Model formulation

For design convenience, a general coordinate is defined as follows

$q^T = [q_p^T \quad q_\theta^T]$

where

$q_p^T = [x \quad y]$, $q_\theta^T = [\alpha \quad \beta]$

and using the relations in **P2,** the dynamic equation of an overhead crane (10) is partitioned in the following form

$$\begin{bmatrix} M_{pp} & M_{p\theta} \\ M_{p\theta}^T & M_{\theta\theta} \end{bmatrix} \begin{bmatrix} \ddot{q}_p \\ \ddot{q}_\theta \end{bmatrix} + \begin{bmatrix} B_{pp} & B_{p\theta} \\ B_{\theta p} & B_{\theta\theta} \end{bmatrix} \begin{bmatrix} \dot{q}_p \\ \dot{q}_\theta \end{bmatrix} + \begin{bmatrix} G_p(q) \\ G_\theta(q) \end{bmatrix} = \begin{bmatrix} u_p \\ 0 \end{bmatrix} \tag{12}$$

where M_{pp}, $M_{p\theta}$, $M_{\theta\theta}$, B_{pp}, $B_{p\theta}$, $B_{\theta p}$, $B_{\theta\theta}$ are 2×2 matrices partitioned from the inertia matrix $M(q)$ and the matrix $B(q,\dot{q})$, respectively, G_p, G_θ are 2×1 vectors, and $u_p^T = [u_x \quad u_y]$. Before investigating the controller design, let the error signals be defined as

$$e = q - q_d = [e_p^T \quad e_\theta^T]^T \tag{13}$$

and the stable hypersurface plane is defined as

$$s = \dot{e} + Ke = \begin{bmatrix} \dot{e}_p + K_p e_p \\ \dot{e}_\theta + K_\theta e_\theta \end{bmatrix} = \begin{bmatrix} s_p \\ s_\theta \end{bmatrix} \tag{14}$$

where

$$e_p = q_p - q_{pd} = [x - x_d \quad y - y_d]^T \equiv [e_x \quad e_y]^T,$$

$$e_\theta = q_\theta - q_{\theta d} = [\alpha - \alpha_d \quad \beta - \beta_d]^T \equiv [e_\alpha \quad e_\beta]^T,$$

$$K_p = \begin{bmatrix} k_1 & 0 \\ 0 & k_2 \end{bmatrix}, \; K_\theta = \begin{bmatrix} k_3 & 0 \\ 0 & k_4 \end{bmatrix}$$

and x_d, y_d, α_d and β_d are defined trajectories of x, y, α and β respectively, and K_p, K_θ are some arbitrary positive definite matrices.

Then, after a lot of mathematical arrangements, the dynamics of the newly defined signal vectors s_p, s_θ can be derived as

$$\begin{bmatrix} M_{PP} & M_{P\theta} \\ M_{P\theta}^T & M_{\theta\theta} \end{bmatrix} \begin{bmatrix} \dot{s}_p \\ \dot{s}_\vartheta \end{bmatrix} + \begin{bmatrix} B_{PP} & B_{P\theta} \\ B_{\theta P} & B_{\theta\theta} \end{bmatrix} \begin{bmatrix} s_p \\ s_\theta \end{bmatrix} = \begin{bmatrix} \tau_p + u_P \\ \tau_\theta \end{bmatrix} \tag{15}$$

where

$$\tau_p = M_{pp}(-\ddot{q}_{pd} + k_p \dot{e}_p) + M_{p\theta}(-\ddot{q}_\theta + k_\theta \dot{e}_\theta) + B_{pp}(-\dot{q}_{pd} + k_p e_p) + B_{p\theta}(-\dot{q}_\theta + k_p e_\theta) \tag{16}$$

$$\tau_\theta = M_{\theta p}(-\ddot{q}_{pd} + k_p \dot{e}_p) + M_{\theta\theta}(-\ddot{q}_\theta + k_\theta \dot{e}_\theta) + B_{\theta p}(-\dot{q}_{pd} + k_p e_p) + B_{\theta\theta}(-\dot{q}_\theta + k_\theta e_\theta) \tag{17}$$

Remark 1: The desired trajectories x_d, y_d, α_d and β_d should be carefully chosen so as to satisfy the internal dynamics, as shown in the lower part of equation (15), when the control objective is achieved, i.e.,

$$M_{P\theta}^T(q_d)\begin{bmatrix} \ddot{x}_d \\ \ddot{y}_d \end{bmatrix} + M_{\theta\theta}(q_d)\begin{bmatrix} \ddot{\alpha}_d \\ \ddot{\beta}_d \end{bmatrix} + B_{\theta P}(q,\dot{q})\begin{bmatrix} \dot{x}_d \\ \dot{y}_d \end{bmatrix} + B_{\theta\theta}(q,\dot{q})\begin{bmatrix} \dot{\alpha}_d \\ \dot{\beta}_d \end{bmatrix} + G_\theta(q) = 0 \tag{18}$$

Without loss of generality, we always choose an exponentially-convergent trajectories with final constant values for x_d, y_d and zero for α_d, β_d.

2.2 Adaptive Controller Design

In this subsection, an adaptive nonlinear control will be presented to solve the tracking control problem.

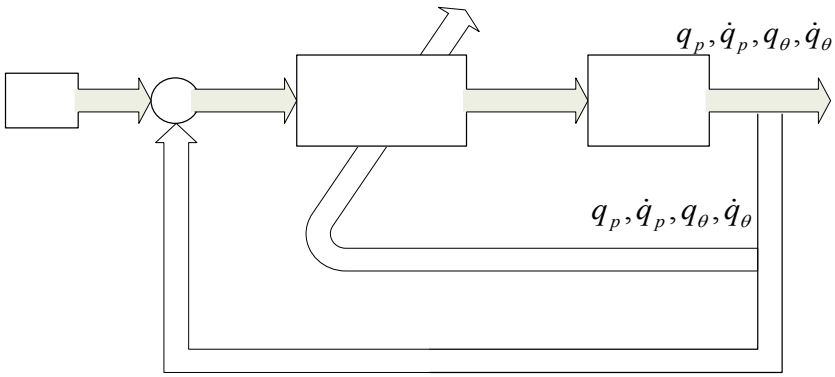

Fig. 2. An Adaptive Self-tuning Controller Block Diagram

As indicated by property **P3** in section 1.2, the dynamic equations of an overhead crane have the well-known linear-in-parameter property. Thus, we define

$$\omega_1\phi_1 = M_{pp}(\ddot{q}_{pd} + k_p\dot{e}_p) + M_{p\theta}(-\ddot{q}_{\theta d}k_\theta\dot{e}_\theta) + B_{pp}(\dot{q}_{pd} + k_p e_p) + B_{p\theta}k_p e_p \tag{19}$$

$$\omega_2\phi_2 = M_{\theta p}(\ddot{q}_{pd} + k_p\dot{e}_p) + M_{\theta\theta}(k_\theta\dot{e}_\theta) + B_{\theta p}(\dot{q}_{pd} + k_p e_p) + B_{\theta\theta}k_\theta e_\theta \tag{20}$$

where ω_1, ω_2 are regressor matrices with appropriate dimensions, and ϕ_1, ϕ_2 are their corresponding vectors of unknown constant parameters, respectively. As a majority of the adaptive controller, the following signal is defined

$$\dot{Z}_x = \begin{cases} 2(\sqrt{Z}_x a_x(t) + b_x(t)), & Z_x(t) > 0 \\ 2b_x(t), Z_x(t) = 0, & b_x(t) > 0 \\ \delta_x, Z_x(t) = 0, & b_x(t) \le 0 \end{cases} \tag{21}$$

where δ_x is some small positive constant and

$$a_x(t) = \frac{\|s_p\|^2}{\|s_p\|^2 + \varepsilon}(-s_\theta{}^T\omega_2\hat{\phi}_2 - s_\theta{}^T K_{v\theta}s_\theta) \tag{22}$$

$$b_x(t) = \frac{\varepsilon}{\|s_p\|^2 + \varepsilon}(-s_\theta{}^T\omega_2\hat{\phi}_2 - s_\theta{}^T K_{v\theta}s_\theta) \tag{23}$$

Remark 2: Note that (21) is simply to define a differential equation of which its variable $Z_x(t)$ remains positive. Let another signal *k(t)* be defined to be its positive root, i.e., $k = \sqrt{Z_x}$, It can be shown that

$$\dot{k}(t) = \frac{1}{k(t)}\left(\frac{k\|s_p\|^2 + \varepsilon}{\|s_p\|^2 + \varepsilon}\right)(-s_\theta^T\omega_2\hat{\phi}_2 - s_\theta^T K_{v\theta}s_\theta) \qquad k \neq 0 \tag{24}$$

In the sequel, we will first assume that there exists a measure zero set of time sequences $\{t_i\}_{i=1}^{\infty}$ such that $Z(t_i) = 0$ or $k(t_i) = 0$, $i = 1,2,3,...\infty$, and then, verify the existence assumption valid.

Now let the adaptive control law be designed as

$$u_P = -\omega_1\hat{\phi}_1 - \tau_v - K_{vp}s_p \tag{25}$$

$$\tau_v = \left[\frac{(k-1)s_p}{\|s_p\|^2 + \varepsilon} (-s_\theta{}^T \omega_2 \hat{\phi}_2 - s_\theta{}^T K_{v\theta} s_\theta) \right] \tag{26}$$

where

$$\omega_1 \hat{\phi}_1 = \hat{M}_{pp}(\ddot{q}_{pd} + k_p \dot{e}_p) + \hat{M}_{p\theta}(k_\theta \dot{e}_\theta) + \hat{B}_{pp}(\dot{q}_{pd} + k_p e_p) + \hat{B}_{p\theta} k_p e_p \tag{27}$$

$$\omega_2 \hat{\phi}_2 = \hat{M}_{\theta p}(\ddot{q}_{pd} + k_p \dot{e}_p) + \hat{M}_{\theta\theta}(k_\theta \dot{e}_\theta) + \hat{B}_{\theta p}(\dot{q}_{pd} + k_p e_p) + \hat{B}_{\theta\theta} k_\theta e_\theta \tag{28}$$

and $\hat{\phi}_1, \hat{\phi}_2$ are the estimates of ϕ_1, ϕ_2 respectively, then the error dynamics can be obtained as

$$\begin{bmatrix} M_{PP} & M_{P\theta} \\ M_{P\theta}^T & M_{\theta\theta} \end{bmatrix} \begin{bmatrix} \dot{s}_p \\ \dot{s}_\vartheta \end{bmatrix} + \begin{bmatrix} B_{PP} & B_{P\theta} \\ B_{\theta P} & B_{\theta\theta} \end{bmatrix} \begin{bmatrix} s_p \\ s_\theta \end{bmatrix} + \begin{bmatrix} K_{vp} & 0 \\ 0 & K_{v\theta} \end{bmatrix} \begin{bmatrix} s_p \\ s_\theta \end{bmatrix} = \begin{bmatrix} \omega_1 \tilde{\phi}_1 - \tau_v \\ \omega_2 \phi_2 + K_{v\theta} s_\theta \end{bmatrix} \tag{29}$$

or more compactly as

$$M(q)\dot{s} + h(q, \dot{q})s + Ks = \begin{bmatrix} \omega_1 \tilde{\phi}_1 - \tau_v \\ \omega_2 \phi_2 + K_{v\theta} s_\theta \end{bmatrix} \tag{30}$$

where

$$\begin{bmatrix} \tilde{\phi}_1 \\ \tilde{\phi}_2 \end{bmatrix} = \begin{bmatrix} \hat{\phi}_1 - \phi_1 \\ \hat{\phi}_2 - \phi_2 \end{bmatrix} \tag{31}$$

Moreover, let the adaptation laws be chosen as

$$\begin{aligned} \dot{\hat{\phi}}_1 &= -k_a \omega_1 s_p \\ \dot{\hat{\phi}}_2 &= -k_b \omega_2 s_\theta \end{aligned} \tag{32}$$

where k_a, k_b are some positive definite gain matrices. In what follows we will show that the error dynamics (30) along with the adaptive laws (32) constitutes an asymptotically stable closed-loop dynamic system. This is exactly stated in the following theorem.

Theorem : *Consider the 3-D overhead crane system as mathematically described in (10) or (12) with all the system parameters unknown. Then, by applying control laws (25)-(28) and adaptive laws (32), the objective for the tracking control problem can be achieved, i.e., all signals inside the closed-loop system (29) are bounded and* $e_x, e_\alpha, e_y, e_\beta \to 0$ *asymptotically in the sense of Lyapunov.*

Proof: Define the Lyapunov function candidate as

$$V(t) = \frac{1}{2}s^T M(q)s + \frac{1}{2}\tilde{\phi}_1^T k_a^{-1}\tilde{\phi}_1 + \frac{1}{2}\tilde{\phi}_2^T k_b^{-1}\tilde{\phi}_2 + \frac{1}{2}Z_x$$
$$= \frac{1}{2}s^T M(q)s + \frac{1}{2}\tilde{\phi}_1^T k_a^{-1}\tilde{\phi}_1 + \frac{1}{2}\tilde{\phi}_2^T k_b^{-1}\tilde{\phi}_2 + \frac{1}{2}k^2$$

It is obvious that, due to the quadratic form of system states as well as the definition of $Z_x(t)$, *V(t)* is always positive-definite and indeed a Lyapunov function candidate. By taking the time derivative of V we get

$$\dot{V}(t) = s^T M(q)\dot{s} + \frac{1}{2}s^T \dot{M}(q)s + \dot{\tilde{\phi}}_1^T k_a^{-1}\tilde{\phi}_1 + \dot{\tilde{\phi}}_2^T k_b^{-1}\tilde{\phi}_2 + k\dot{k}$$

$$= s^T(-B(q,\dot{q})s - K_{vp}s + \begin{bmatrix} -\omega_1\tilde{\phi}_1 - \tau_v \\ \omega_2\phi_2 + K_{v\theta}s_\theta \end{bmatrix}) + \frac{1}{2}s^T\dot{M}(q)s + s_p^T\omega_1\tilde{\phi}_1 + s_\theta^T\omega_2\tilde{\phi}_2$$

$$+ (\frac{k\|s_p\|^2 + \varepsilon}{\|s_p\|^2 + \varepsilon})(-s_\theta^T\omega_2\hat{\phi}_2 - s_\theta^T K_{v\theta}s_\theta)$$

$$= -sKs - s_p^T\omega_1\tilde{\phi}_1 - (\frac{(k-1)\|s_p\|^2}{\|s_p\|^2 + \varepsilon})(-s_\theta^T\omega_2\hat{\phi}_2 - s_\theta^T K_{v\theta}s_\theta) + s_\theta^T\omega_2\phi_2 + s_p^T\omega_1\tilde{\phi}_1$$

$$+ (\frac{k\|s_p\|^2 + \varepsilon}{\|s_p\|^2 + \varepsilon})(-s_\theta^T\omega_2\hat{\phi}_2 - s_\theta^T K_{v\theta}s_\theta) + s_\theta^T\omega_2\tilde{\phi}_2 + s_\theta^T K_{v\theta}s_\theta$$

$$= -s^T Ks \tag{33}$$

It is clear that $\dot{V}(t) < 0$ as long as $K > 0$, which then implies $s, k, \tilde{\phi}_1, \tilde{\phi}_2 \in L_\infty$ Now, assume that $k(t) = 0$ instantaneously at t_i. Because the solution $Z_x(t)$ of the equation (21) is well defined and is continuous for all $t \geq 0$, k(t) is continuous at t_i, i.e., $k(t_i-) = k(t_i+)$. Since V is a continuous function of k, it is clear that $V(t)$ remains to be continuous at t_i, i.e. , $V(t_i-) = V(t_i+)$. Form then hypothesis, $\dot{V}(t_i^-) < 0$ and $\dot{V}(t_i^+) < 0,$ we hence can conclude that V is nonincreasing in t including t_i, which then readily implies that $s, k \in L_\infty$. Therefore, e, τ_v and $\tau_\theta \in L_\infty$ directly from equation (13) and definitions of τ_v and τ_θ. It then follows from (30) that $\dot{s} \in L_\infty$. On the other hand, if the set of time instants $\{t_i\}_{i=1}^{\infty}$ is measure zero, then $-\int_0^\infty \dot{V} dt = V(0) - V(\infty) < \infty$ or equivalently that $-\int_0^\infty \|s\|^2 dt < \infty$ so that $s \in L_2$. Form the error dynamics, we can further conclusion that $\dot{s} \in L_\infty$. Then by Barbalat's lemma we readily obtain that $s \to 0$ as $t \to \infty$ asymptotically as $t \to \infty$ and therefore, $e, \dot{e} \to 0$ as $t \to \infty$ Note that in the above proof we have used the property $(\dot{M}(q) - 2B(q, \dot{q}))$ is skew- symmetric. Finally, to complete the proof in theory, we need to show that the above hypothesis that the set of time instants $\{t_i\}_{i=1}^{\infty}$ is indeed measure zero. However, it is quite straightforward to conclude the result from (21) by simply using the fact that all signals are bounded. This completes our proof.

Remark 3: From the robustness point of view, it would be better if additional feedback term $-k_q s_\theta$ is included in the control law (24). With such an inclusion, the sway stabilization result subject to external disturbance can also be maintained as the cart arrived at its destination. This can be easily checked from the stability proof given in the theorem.

Proof: Let the Lyapunov function candidate be chosen as

$$V(t) = \frac{1}{2} s^T M(q) s + \frac{1}{2} \tilde{\phi}_1^T k_a^{-1} \tilde{\phi}_1 + \frac{1}{2} \tilde{\phi}_2^T k_b^{-1} \tilde{\phi}_2 + \frac{1}{2} Z_x$$

$$= \frac{1}{2} s^T M(q) s + \frac{1}{2} \tilde{\phi}_1^T k_a^{-1} \tilde{\phi}_1 + \frac{1}{2} \tilde{\phi}_2^T k_b^{-1} \tilde{\phi}_2 + \frac{1}{2} k^2$$

and take the time derivative of V to get

$$\dot{V}(t) = s^T M(q) \dot{s} + \frac{1}{2} s^T \dot{M}(q) s + \dot{\tilde{\phi}}_1^T k_a^{-1} \tilde{\phi}_1 + \dot{\tilde{\phi}}_2^T k_b^{-1} \tilde{\phi}_2 + k\dot{k}$$

$$= s^T \left(-B(q, \dot{q}) s - K_{vp} s + \begin{bmatrix} -\omega_1 \tilde{\phi}_1 - \tau_v - k_q s_\theta \\ \omega_2 \phi_2 + K_{v\theta} s_\theta \end{bmatrix}\right) + \frac{1}{2} s^T \dot{M}(q) s + s_p^T \omega_1 \tilde{\phi}_1 + s_\theta^T \omega_2 \tilde{\phi}_2$$

$$+\left(\frac{k\left\|s_p\right\|^2+\varepsilon}{\left\|s_p\right\|^2+\varepsilon}\right)\left(-s_\theta{}^T\omega_2\hat{\phi}_2-s_\theta{}^T K_{v\theta}s_\theta\right)$$

$$=-s^T Ks-k_q s_\theta s_p$$

$$\dot{V}(t)=-s^T K_v s-k_q s_\theta s_p$$

$$\dot{V}(t)\le-\lambda_{\min}(K_v)(s_p{}^2+s_\theta{}^2)+\frac{1}{2}k_q(s_p{}^2+s_\theta{}^2)$$

$$=-(\lambda_{\min}(K_v)-\frac{1}{2}k_q)(s_p{}^2+s_\theta{}^2)$$

Thus, the same conclusion can be made as preciously if

$$\lambda_{\min}(K_v)>\frac{1}{2}k_q$$

3. Computer Simulation

In this subsection, several simulations are performed and the results also confirm the validity of our proposed controller. The desired positions for *X* and *Y* axes are 1 m. Figure 3 shows the time response of X-direction. Figure 5 show the time responses of Y-direction. It can be seen that the cart can simultaneously achieve the desired positions in both X and Y axes in approximately 6 seconds with the sway angles almost converging to zero at the same time. Figure 4 and Figure 6 show the response of the sway angle with the control scheme. Figure 7 and Figure 8 show the velocity response of both X-direction and Y-direction. Figure 9 and Figure 10 show the control input magnitude. In Figure 11~14, the parameter estimates are seen to converge to some constants when error tends to zero asymptotically and the time response of the tuning function *k(t)* is plotted in Figure 15.
The control gains are chosen to be

$$k_p=\begin{bmatrix}1.5 & 0\\ 0 & 1\end{bmatrix},k_\theta=\begin{bmatrix}2.35 & 0\\ 0 & 1\end{bmatrix},$$

$$k_{vp} = \begin{bmatrix} 1.5 & 0 \\ 0 & 1.8 \end{bmatrix}, k_{v\theta} = \begin{bmatrix} 1.35 & 0 \\ 0 & 1.2 \end{bmatrix}$$

The corresponding adaptive gains are set to be $k_a = k_b = 1$

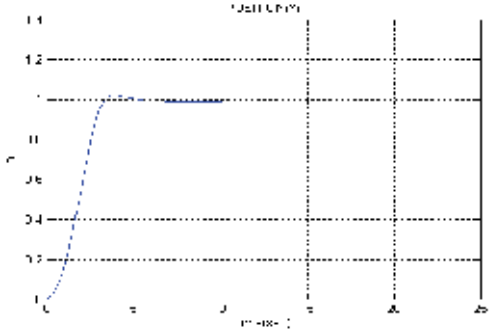

Fig. 3. Gantry Tracking Response $x(t)$ with Adaptive Algorithm

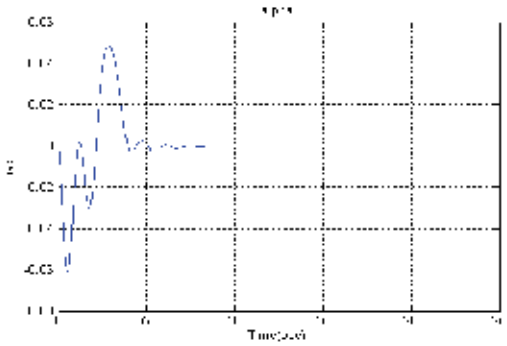

Fig. 4. Sway Angle Response $\alpha(t)$ with Adaptive Algorithm

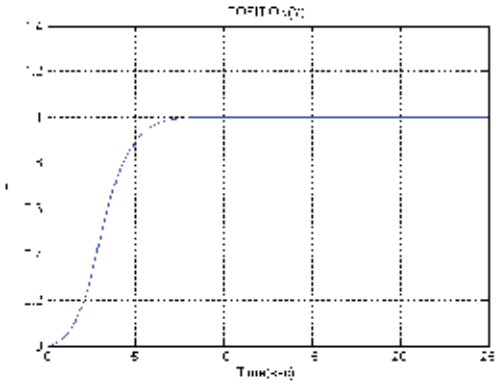

Fig. 5. Gantry Tracking Response $y(t)$ with Adaptive Algorithm

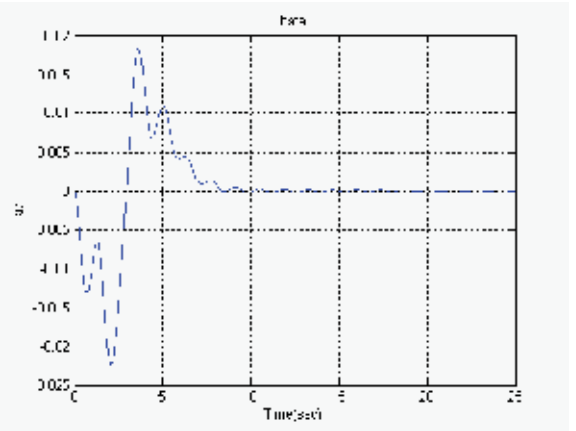

Fig. 6. Sway Angle Response $\beta(t)$ with Adaptive Algorithm

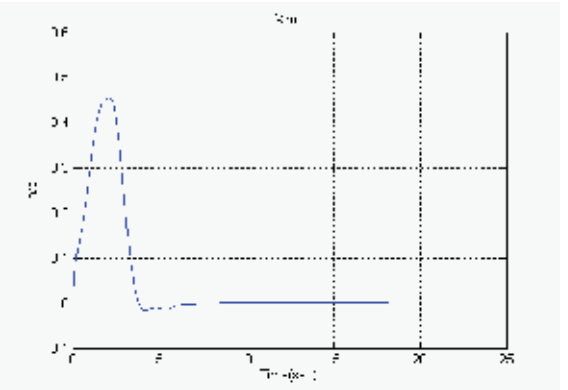

Fig. 7. Gantry Velocity Response $\dot{x}(t)$ with Adaptive Algorithm

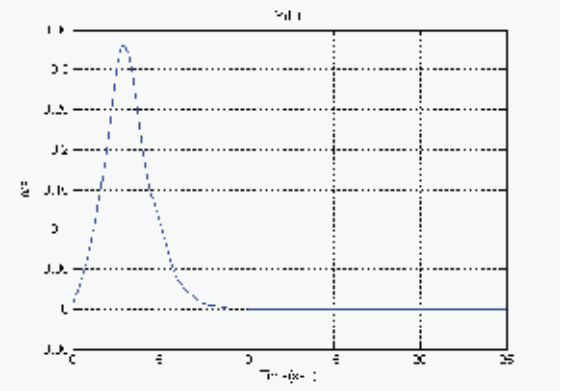

Fig. 8. Gantry Velocity Response $\dot{y}(t)$ with Adaptive Algorithm

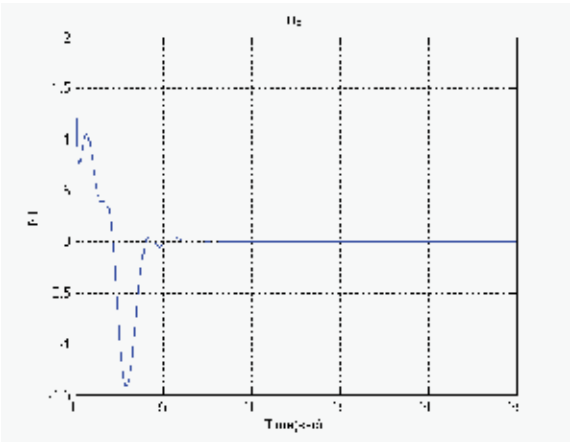

Fig. 9. Force Input u_x

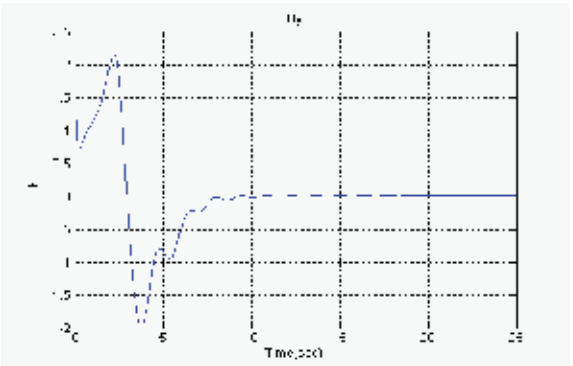

Fig. 10. Force Input u_y

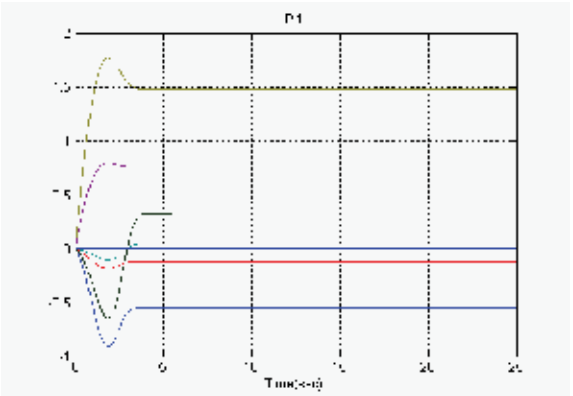

Fig. 11. Estimated Parameters $\phi_{1x}(t)$

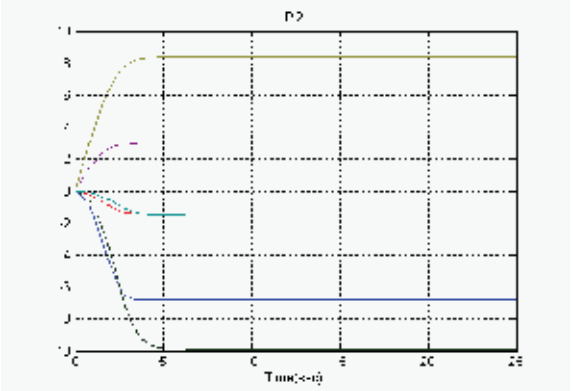

Fig. 12. Estimated Parameters

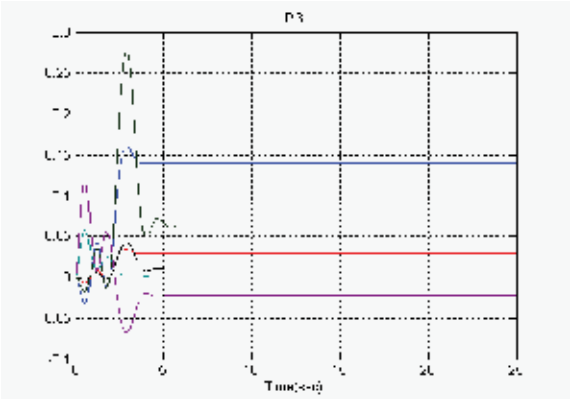

Fig. 13. Estimated Parameters $\phi_{1y}(t)$

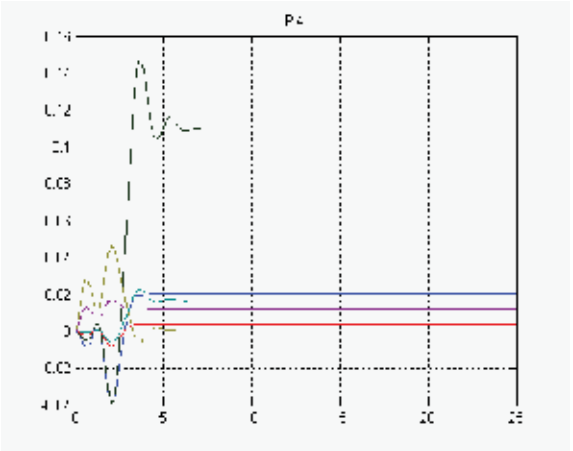

Fig. 14. Estimated Parameters $\phi_{2\alpha}(t)$

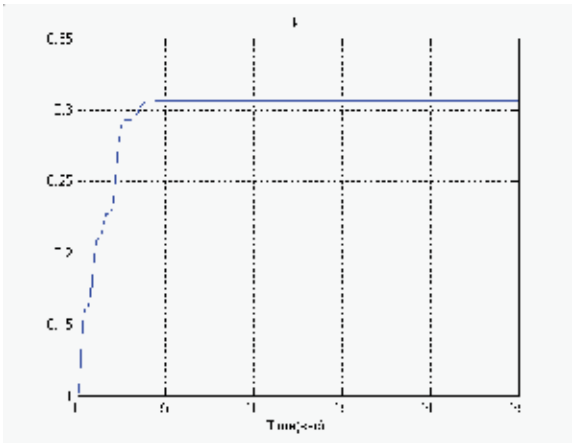

Fig. 15. Response Trajectory of $k(t)$

4. Experimental Verification

In this section, to validate the practical application of the proposed algorithms, a three degree-of-freedom overhead crane apparatus, is built up as shown in Figure 16. Several experiments are also performed and indicated in the subsequent section for demonstration of the effectiveness of the proposed controller.

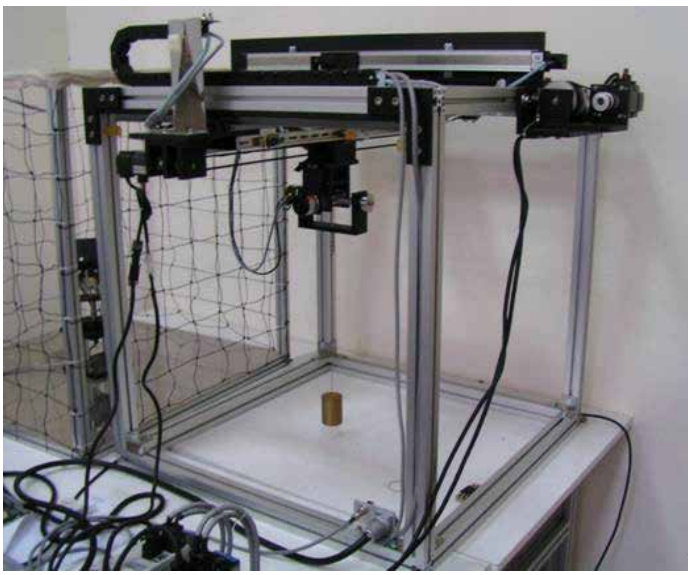

Fig. 16. Experimental setup for the overhead crane system

The control algorithm is implemented on a xPC Target for use with real time Workshop® manufactured by The Math Works, Inc., and the xPC target is inserted in a Pentium4

2.4GHz PC running under the Windows operating system. The sensing system includes the two photo encoders and two linear position sensors. The cart motion X-direction and Y-direction motion measured by linear potentiometer. Two potentiometers are connected to the travel direction and the traverse direction. An AC servo motor with 0.95 N-m maximum torque and 3.8N-m maximum torque output is used to drive the cart motion X direction and Y direction. The servomotors are set in torque control mode so as to output the desired torques.

In the experimental study, the proposed control algorithms have been tested and compared with the conventional PD controller. From the experimental results, it is found that our proposed algorithms indeed outperform the conventional control scheme in all aspects. A schematic description of the experimental system is draw in Figure 17.

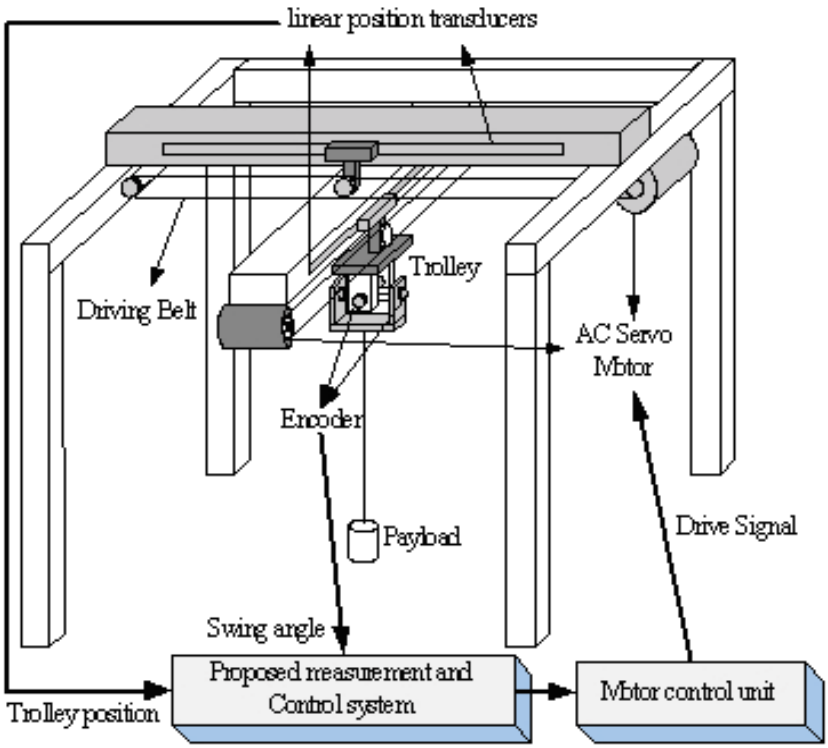

Fig. 17. A Schematic Overview of the Experimental Setup

4.1 Experiments for Conventional PD control as a comparative study

In the experiments, a simple PD control scheme with only position and velocity feedback is first tested for the crane control. Figure 18 and Figure 20 show the control responses. From Figure 19 and Figure 21 it is observed that the sway oscillation can not be rapidly damped by using only conventional PD control, although the tracking objective is ultimately achieved.

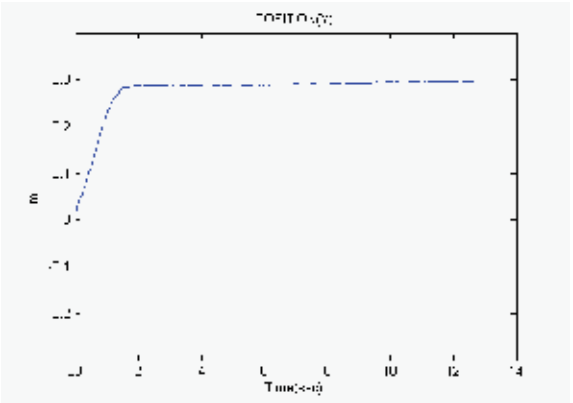

Fig. 18. Gantry Tracking Response $x(t)$ with Conventional PD Control

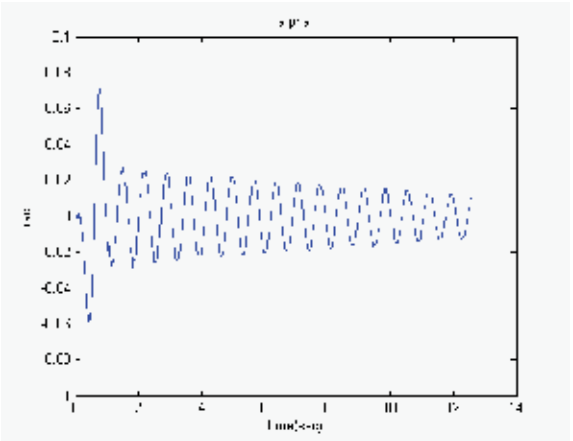

Fig. 19. Sway Angle Response $\alpha(t)$ with Conventional PD Control

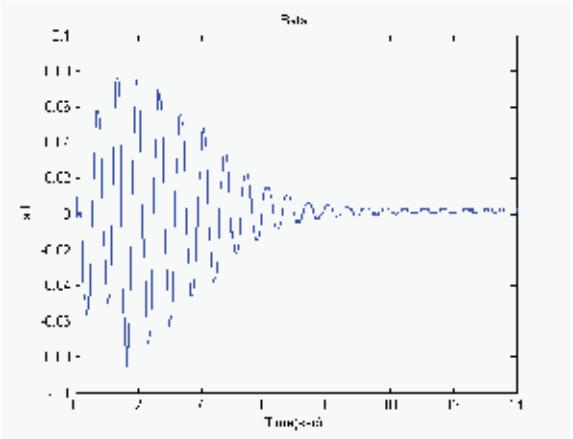

Fig. 21. Sway Angle Response $\beta(t)$ with Conventional PD Control

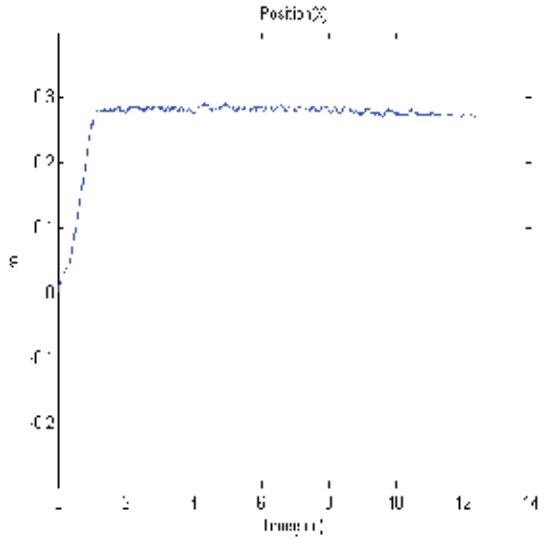

Fig. 20. Gantry Tracking Response $y(t)$ with Conventional PD Control

4.2 Experiments for the Proposed Adaptive Control Method with Set-point Regulation

In the subsection, the developed adaptive controller is applied. The following controlled gains are chosen for experiments.

$$k_p = \begin{bmatrix} 2 & 0 \\ 0 & 1 \end{bmatrix}, k_\theta = \begin{bmatrix} 3 & 0 \\ 0 & 1 \end{bmatrix},$$
$$k_{vp} = \begin{bmatrix} 1.5 & 0 \\ 0 & 3 \end{bmatrix}, k_{v\theta} = \begin{bmatrix} 1.35 & 0 \\ 0 & 2 \end{bmatrix}$$

The corresponding adaptive gains are set to be 1 *i.e.,* $k_a = k_b = 1$. Figure 22~31 depict the experimental results for the crane system with the adaptive control law. Figure 22 and Figure 24 demonstrate the tracking performance in X and Y directions. It is experimentally demonstrated that the sway angle can be actively damped out by using our proposed adaptive schemes, as shown in Figure 23 and Figure 25 with maximum swing angle about 0.05 rad and 0.06 rad, respectively. Figure 26 and Figure 27 show the input torques from each AC servo motors, whereas Figure 28~30 plot the associated adaptive gain turning trajectories. The trajectory of coupling gain *k(t)* is also in Figure 31 with initial value 0.05. The initial values of other state variable are all zero. Apparently the tracking and damping performances by applying the adaptive control algorithm are much better than the ones resulting from the PD control.

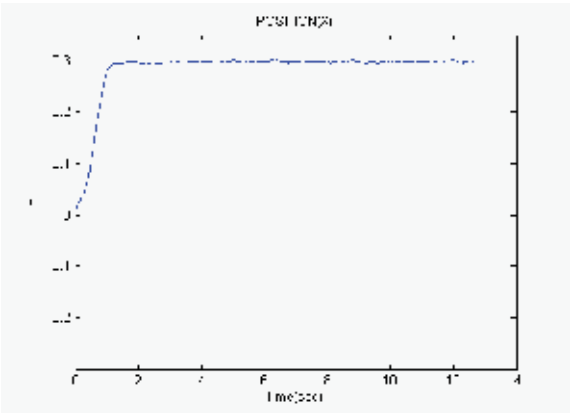

Fig. 22. Gantry Tracking Response with Adaptive Algorithm X(t)

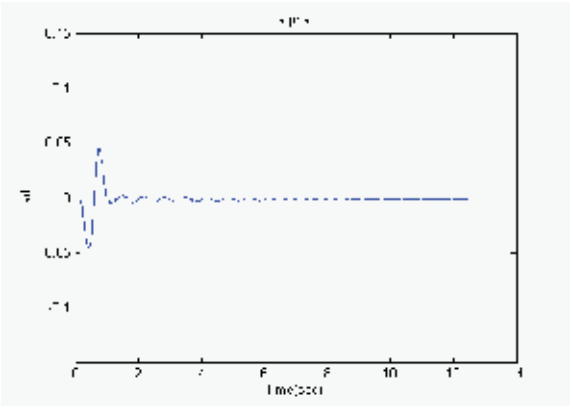

Fig. 23. Sway Angle Response with Adaptive Algorithm α (t)

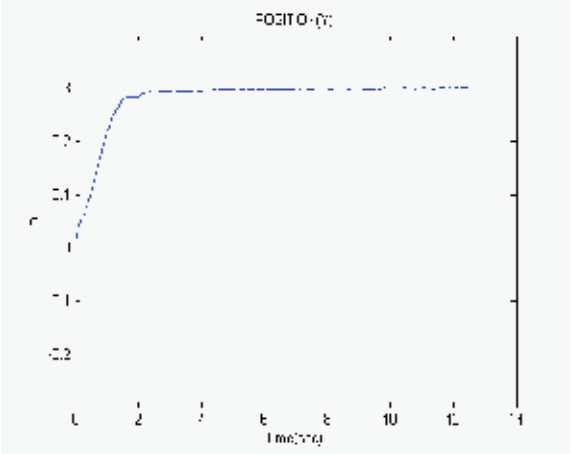

Fig. 24. Gantry Tracking Response with Adaptive Algorithm Y(t)

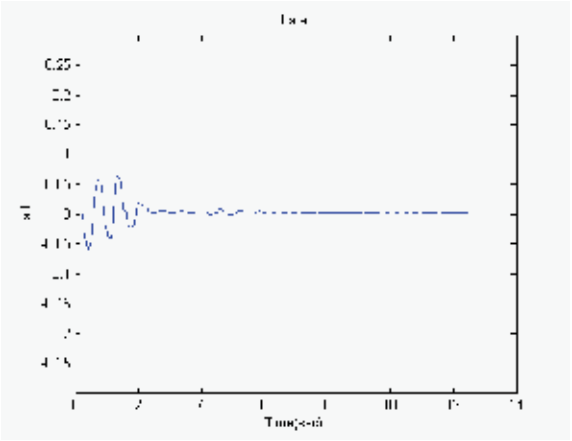

Fig. 25. Sway Angle Response with Adaptive Algorithm β (t)

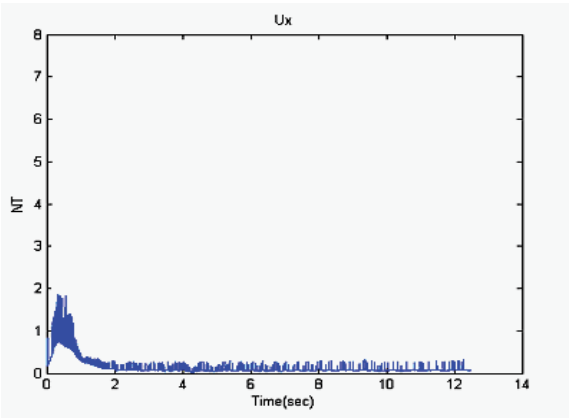

Fig. 26. Force Input Ux

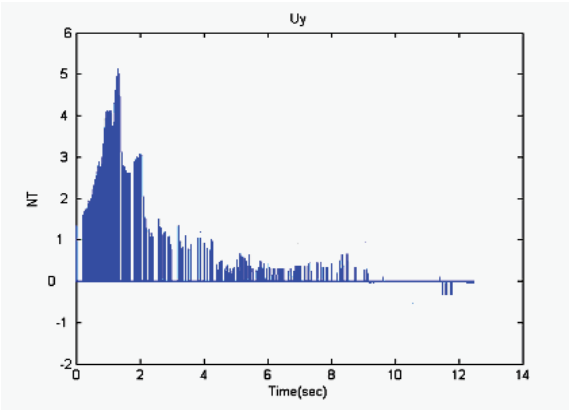

Fig. 27. Force Input Uy

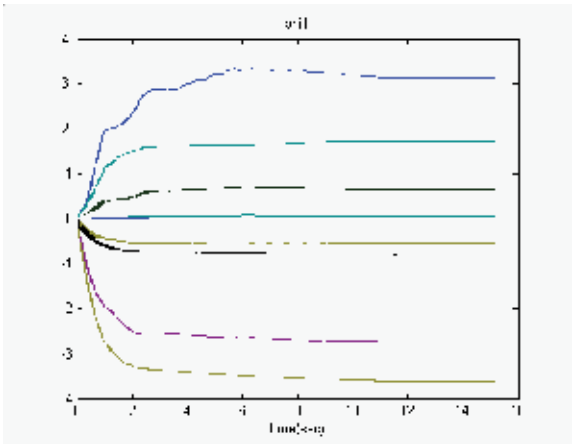

Fig. 28. Estimated Parameters ϕ_{1x} (t)

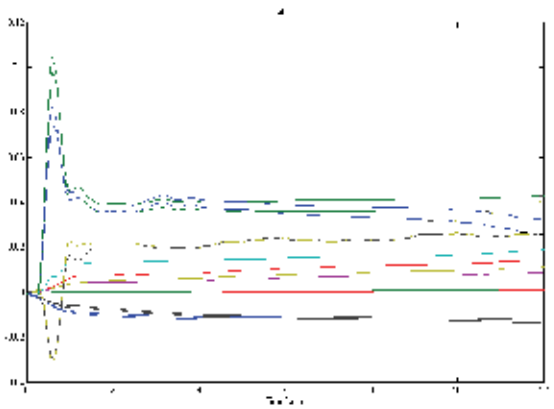

Fig. 30. Estimated Parameters $\phi_{2\alpha}$ (t) and $\phi_{2\beta}$ (t)

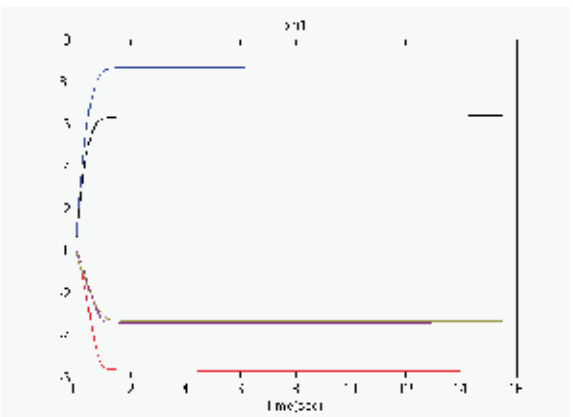

Fig. 29. Estimated Parameters ϕ_{1y} (t)

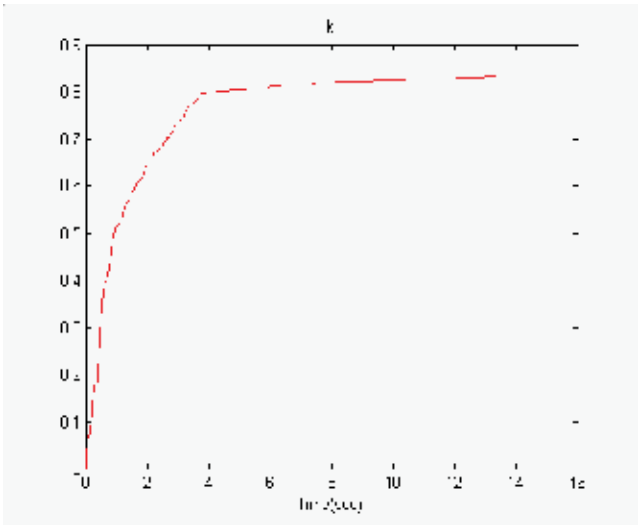

Fig. 31. Trajectory of k (t)

4.3 Experiments for the Proposed Adaptive Control with Square Wave Tracking

To prove the prevalence of our controllers, experiments on the tracking of square wave, as shown in Figure 6, is also conducted. The gains are kept the same as in the previous experiments. Figure 6(a) and Figure 6(c) demonstrate the tracking performance in X and Y directions, respectively while Figure 6(b) and Figure 6(d) show the suppression results of sway angles. It is found that good performance can still be preserved is spite of the sudden change of desired position.

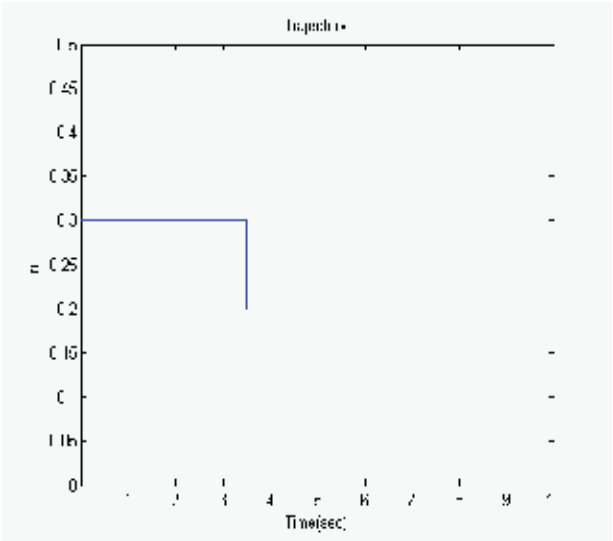

Fig. 32. Desired Trajectory

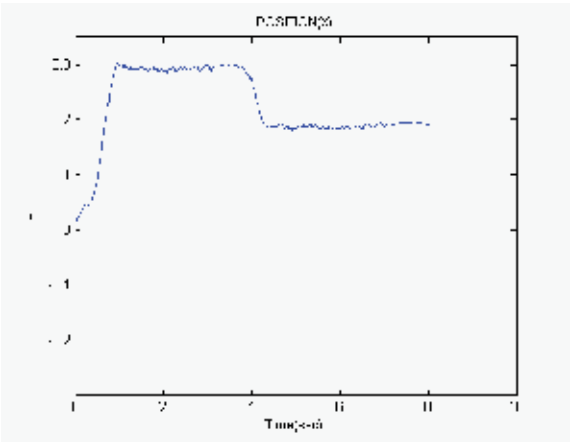

Fig. 33. Tracking Response $x(t)$ with Adaptive Algorithm

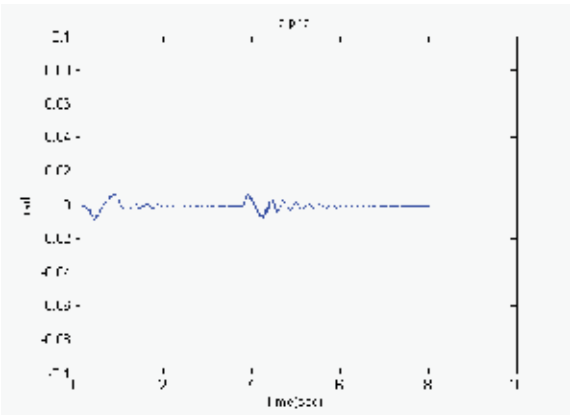

Fig. 34. Sway Angle Response $\alpha(t)$ with Adaptive Algorithm

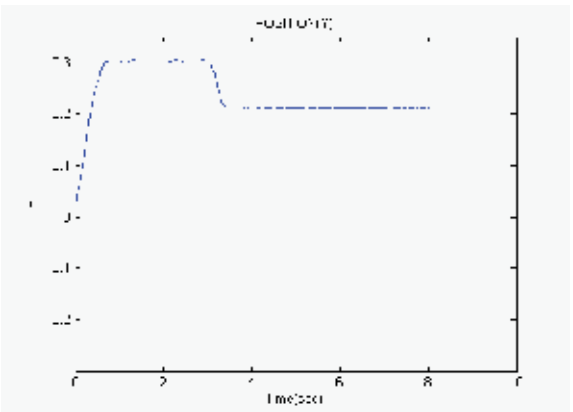

Fig. 35. Tracking Response $y(t)$ with Adaptive Algorithm

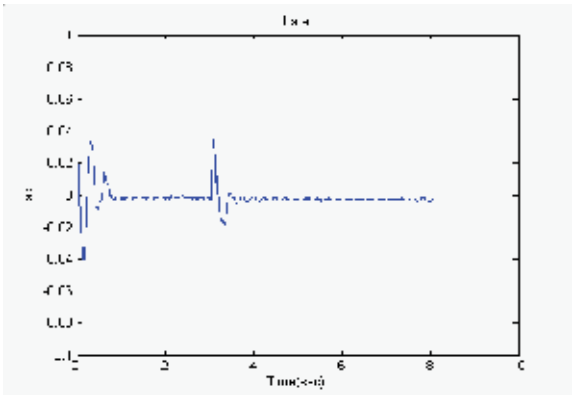

Fig. 36. Sway Angle Response $\beta(t)$ with Adaptive Algorithm

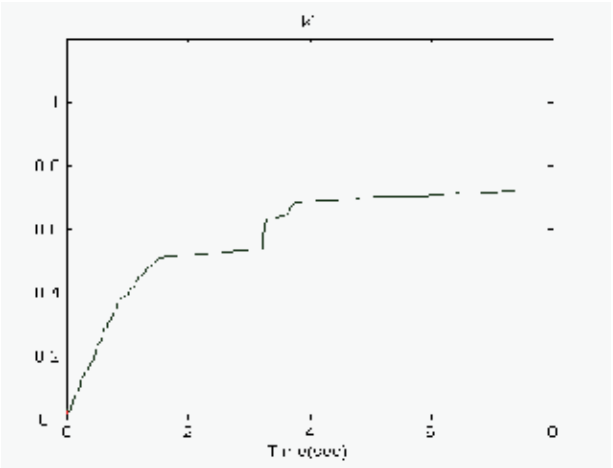

Fig. 37. Trajectory of k(t)

5. Conclusion

In this chapter, a nonlinear adaptive control law has been presented for the motion control of overhead crane. By utilizing a Lyapunov-based stability analysis, we can achieve asymptotic tracking of the crane position and stabilization of payload sway angle for an overhead crane system which is subject to both underactuation and parametric uncertainties. Comparative simulation studies have been performed to validate the proposed control algorithm. To practically validate the proposed adaptive schemes, an overhead crane system is built up and experiments are also conducted. Both simulations and experiments show better performance in comparison with the conventional PD control.

6. References

Philippe Martin, Santosh Devasia, and Brad Paden, 1996, "A Different Look at Output

Tracking: Control of a VTOL Aircraft." *Automatica*, Vol. 32, No. 1, pp. 101-107.

Yannick Morel, and Alexander Leonessa, 2003, "Adaptive Nonlinear Tracking Control of an Underactuated Nonminimum Phase Model of a Marine Vehicle Using Ultimate Boundedness." *Proc. of the 42nd IEEE Conference on Decision and Control, Maui, Hawaii USA*, pp. 3097-3102.

Xuezhen Wang, and Degang Chen, 2006, "Output Tracking Control of a One-Link Flexible Manipulator via Causal Inversion." *IEEE Transactions on Control Systems Technology*, Vol. 14, No. 1, pp. 141-148.

Qiguo Yan, 2003, "Output Tracking of Underactuated Rotary Inverted Pendulum by Nonlinear Controller." *Proc. of the 42nd IEEE Conference on Decision and Control, Maui, Hawaii USA*, pp. 2395-2400.

Y. Fang, E. Zergeroglu, W. E. Dixon, and D.M. Dawson, 2001, "Nonlinear Coupling Control Laws for an Overhead Crane System." *Proc. of the 2001 IEEE International Conference on Control Applications*, pp. 639-644.

B. Kiss, J. Levine, and Ph. Mullhaupt, 2000, "A Simple Output Feedback PD controller for Nonlinear Cranes." *Proc. of the 39th IEEE Conference on Decision and Control, Sydney, Australia*, pp. 5097-5101.

F. Boustany, and B. d'Andrea-Novel, 1992, "Adaptive Control of an Overhead Crane Using Dynamic Feedback Linearization and Estimation Design." *Proc. of the 1992 IEEE International conference on Robotics and Automation*, pp. 1963-1968.

W. Li, and Q. Tang, 1993, "Control Design for a Highly Nonlinear System." *Proc. of the ASME Annual Winter Meeting, Vol. 50, Symposium on Mechatronics, New Orleans, LA*, pp. 21-26.

Barmeshwar Vikramaditya, and Rajesh Rajamani, 2000, "Nonlinear Control of a trolley crane system." *Proc. of the American Control Conference Chicago, Illinois*, pp. 1032-1036.

Kazunobu Yoshida, and Hisashi Kawabe, 1992, "A Design of Saturating Control with a Guaranteed Cost and Its Application to the Crane Control System." *IEEE Transactions on Automatic Control*, Vol. 37, No. 1, pp. 121-127.

Chung Choo Chung, and John Hauser, 1995, "Nonlinear Control of a Swinging Pendulum." *Automatica*, Vol. 31, No. 6, pp. 851-862.

Dian-Tong Liu, Jian-Qiang Yi, and Dong-Bin Zhao, 2003, "Fuzzy tuning sliding mode control of transporting for an overhead crane." *Proc. the second International Conference on Machine Learning and Cybernetics, Xian, China*, pp. 2541-2546.

Y. Fang, W. E. Dixon, D. M. Dawson, and E. Zergeroglu, 2001, "Nonlinear coupling control laws for 3-DOF overhead crane system." *Proc. the 40th IEEE Conference on Decision and Control, Orlando, Florida, USA*, pp. 3766-3771.

T. Ishide, H. Uchida, and S. Miyakawa, 1991, "Application of a fuzzy neural network in the automation of crane system." *Proc. of the 9th Fuzzy System Symposium,* pp. 29-33.

J. Yu, F. L. Lewis, and T. Huang, 1995, "Nonlinear feedback control of a gantry crane." *Proc. of the American Control Conference, Seattle, Washington, USA*, pp. 4310-4315.

Giorgio Bartolini, Alessandro Pisano, and Elio Usai, 2002, "Second-order sliding-mode control of container cranes." *Proc. of the 38th Automatica,* pp. 1783-1790.

Kazunobu Yoshida, 1998, "Nonlinear control design for a crane system with state constraints." *Proc. of the American Control Conference, Philadelphia, Pennsylvania*, pp. 1277-1283.

M. J. Er, M. Zribi, and K. L. Lee, 1988, "Variable Structure Control of Overhead Crane." *Proc. of the 1998 IEEE International Conference on Control Applications, Trieste, Italy*, pp.398-402.

Jianqiang Yi, Naoyoshi Yubazaki, and Kaoru Hirota, 2003, "Anti-swing and positioning control of overhead traveling crane." *Proc. of the Information Sciences 155,* pp. 19-42.

Diantong Liu, Jianqiang Yi, Dongbin Zhao, and Wei Wang, 2004, "Swing-Free Transporting of Two-Dimensional Overhead Crane Using Sliding Mode Fuzzy Control." *Proc. of the 2004 American Control Conference, Boston, Massachusetts*, pp. 1764-1769.

J.A. Mendez, L. Acosta, L. Moreno, A. Hamilton, and G.N. Marichal, 1998, "Design of a Neural Network Based Self-Tuning Controller for an overhead crane." *Proc. of the 1998 IEEE International Conference on Control Applications*, pp. 168-171.

Ho-Hoon Lee, and Seung-Gap Choi, 2001, "A Model-Based Anti-Swing Control of Overhead Cranes with High Hoisting Speeds." *Proc. of the 2001 IEEE International Conference on Robotics and Automation, Seoul, Korea*, pp. 2547-2552.

Wahyudi, and J. Jalani, 2006, "Robust Fuzzy Logic Controller for an Intelligent Gantry Crane System." *First International Conference on Industrial and Information Systems*, pp. 497-502.

Wanlop Sridokbuap, Songmoung Nundrakwang, Taworn Benjanarasuth, Jongkol Ngamwiwit and Noriyuki Komine, 2007, "I-PD and PD Controllers Designed by CRA for Overhead Crane System." *International Conference on Control, Automation and Systems, COEX, Seoul, Korea*, pp. 326-330.

APPENDIX A

Mathematical Description of The Dynamic Model

The dynamic equation of the 3D overhead crane system can be derived by using

Largrange-Euler formula and shown in the following

$$M(q)\ddot{q} + C(q,\dot{q}) + G(q) = \tau$$

where

$$M(q) = \begin{bmatrix} m_1 + m_c & 0 & m_c l\cos\alpha & 0 \\ 0 & m_1 + m_2 + m_c & -m_c l\sin\alpha\sin\beta & m_c l\cos\alpha\cos\beta \\ m_c l\cos\alpha & -m_c l\sin\alpha\sin\beta & m_c l^2 & 0 \\ 0 & m_c l\cos\alpha\cos\beta & 0 & m_c l^2\cos^2\alpha \end{bmatrix}$$

$$C(q,\dot{q}) = \begin{bmatrix} -m_c l\dot{\alpha}^2 \sin\alpha \\ -m_c l(\dot{\alpha}^2 + \dot{\beta}^2)\cos\alpha \sin\beta - 2m_c l\dot{\alpha}\dot{\beta}\sin\alpha\cos\beta \\ m_c l^2 \dot{\beta}^2 \sin\alpha\cos\alpha \\ -2m_c l^2 \dot{\alpha}\dot{\beta}\sin\alpha\cos\alpha \end{bmatrix}$$

$$G(q) = \begin{bmatrix} 0 \\ 0 \\ -m_c gl\sin\alpha\cos\beta \\ -m_c gl\cos\alpha\sin\beta \end{bmatrix}$$

$$\tau = \begin{bmatrix} u_x & u_y & 0 & 0 \end{bmatrix}^T$$
$$q = \begin{bmatrix} x & y & \alpha & \beta \end{bmatrix}^T$$

To satisfy property P2 as stated in section 2 the vector $C(q,\dot{q})$ can be re-arranged as $C(q,\dot{q}) = B(\dot{q},q)\dot{q}$ where

$$B(q,\dot{q}) = \begin{bmatrix} 0 & 0 & -m_c l\dot{\alpha}^2 \sin\alpha & 0 \\ 0 & 0 & -m_c l\dot{\alpha}\cos\alpha\sin\beta - m_c l\dot{\beta}\sin\alpha\cos\beta & -m_c l\dot{\alpha}\sin\alpha\cos\beta - m_c l\dot{\beta}\cos\alpha\sin\beta \\ 0 & 0 & 0 & m_c l^2 \sin\alpha\cos\beta \\ 0 & 0 & -m_c l^2 \dot{\beta}\sin\alpha\cos\beta & -m_c l^2 \dot{\alpha}\sin\alpha\cos\beta \end{bmatrix}$$

It can be easily checked that

$$\dot{M} - 2C = \begin{bmatrix} 0 & 0 \\ 0 & 0 \\ -m_c l\dot{\alpha}\sin\alpha & -m_c l\dot{\alpha}\cos\alpha\sin\beta - m_c l\dot{\beta}\sin\alpha\cos\beta \\ 0 & 0 \end{bmatrix}$$

$$\begin{bmatrix} m_c l\dot{\alpha}\sin\alpha & 0 \\ m_c l\dot{\alpha}\cos\alpha\sin\beta + m_c l\dot{\beta}\sin\alpha\cos\beta & 0 \\ 0 & -2m_c l^2\dot{\beta}\sin\alpha\cos\beta \\ 2m_c l^2\dot{\beta}\sin\alpha\cos\beta & 0 \end{bmatrix}$$

which is skew-symmetrical matrix.

14

Adaptive Inverse Optimal Control of a Magnetic Levitation System

Yasuyuki Satoh[1], Hisakazu Nakamura[1],
Hitoshi Katayama[2] and Hirokazu Nishitani[1]
[1]*Nara Institute of Science and Technology,* [2]*Shizuoka University*
Japan

1. Introduction

In recent years, control Lyapunov functions (CLFs) and CLF-based control designs have attracted much attention in nonlinear control theory. Particularly, CLF-based inverse optimal controllers are some of the most effective controllers for nonlinear systems [Sontag (1989); Freeman & Kokotović (1996); Sepulchre et al. (1997); Li & Krstić (1997); Krstić & Li (1998)]. These controllers minimize a meaningful cost function and guarantee the optimality and a stability margin. Moreover, we can obtain the optimal controller without solving the Hamilton-Jacobi equation. An inverse optimal controller with input constraints has also been proposed [Nakamura et al. (2007)]. On the other hand, these controllers assume that the desired state of the controlled system is an equilibrium state. Then, if the controlled system does not satisfy the assumption, we have to use a pre-feedback control design method to the assumption is virtually satisfied. However, a pre-feedback control design causes the luck of robustness. This implies that a stability margin of inverse optimal controllers is lost. Hence the designed controller does not asymptotically stabilize the system if there exists a parameter uncertainty in the system.

In this article, we study how to guarantee a stability margin when the pre-feedback controller design is used. We consider a magnetic levitation system as an actual control example and propose an adaptive inverse optimal controller which guarantees a gain margin for the system. The proposed controller consists of a conventional inverse optimal controller and a pre-feedback compensator with an adaptive control mechanism. By introducing adaptive control law based on adaptive control Lyapunov functions (ACLFs), we can successfully guarantee the gain margin for the closed loop system. Furthermore, we apply the proposed method to the actual magnetic levitation system and confirm its effectiveness by experiments.

This article is organized as follows. Section 2 introduces some mathematical notation and definitions, and outlines the previous results of CLF-based inverse optimal control design. Section 3 describes the experimental setup of the magnetic levitation system and its mathematical model. In section 4, we design an inverse optimal controller with a pre-feedback compensator for the magnetic levitation system. The problem with the designed controller is demonstrated by the experiment in section 5. To deal with the problem, we

propose an adaptive inverse optimal controller in section 6. The effectiveness of the proposed controller is confirmed by the experiment in section 7. Section 8 is devoted to concluding remarks.

2. Preliminaries

In this section, we introduce some mathematical definitions and preliminary results of CLF-based inverse optimal control. We also refer to ACLF-based adaptive control techniques.

2.1 Mathematical notations and definitions

We use the notation $R_{\geq 0} := [0, \infty)$.

Definition 1 A function $\mathrm{sgn}(y)$ is defined for $y \in R$ by the following equation:

$$\mathrm{sgn}(y) = \begin{cases} -1 & (y < 0) \\ 0 & (y = 0) \\ 1 & (y > 0). \end{cases} \tag{1}$$

In this section, we consider the following input affine nonlinear system:

$$\dot{x} = f(x) + g(x)u, \tag{2}$$

where $x \in R^n$ is a state vector, $u \in U \subseteq R^m$ is an input vector and U is a convex subspace containing the origin $u = 0$. We assume that $f : R^n \to R^n$ and $g : R^n \to R^{n \times m}$ are continuous vector fields, and $f(0) = 0$. Let $L_f V$ and $L_g V$ be the Lie derivative of $f(x)$ and $g(x)$ respectively, which are defined by

$$L_f V(x) = \frac{\partial V}{\partial x} f(x), \tag{3}$$

$$L_g V(x) = \frac{\partial V}{\partial x} g(x). \tag{4}$$

For simplicity of notations, we shall drop (x) in the remaining of this article. We suppose that a local control Lyapunov function is given for system (2).

Definition 2 A smooth proper positive-definite function $V : X \to R_{\geq 0}$ defined on a neighborhood of the origin $X \subset R^n$ is said to be a local control Lyapunov function (local CLF) for system (2) if the condition

$$\inf_{u \subset U} \{L_f V + L_g V \cdot u\} < 0 \tag{5}$$

is satisfied for all $x \in X \setminus \{0\}$. Moreover, $V(x)$ is said to be a control Lyapunov function (CLF) for system (2) if $V(x)$ is a function defined on entire R^n and condition (3) is satisfied for all $x \in R^n \setminus \{0\}$.

If there exists no input constraint ($U = R^m$), a smooth proper positive-definite function $V : R^n \to R_{\geq 0}$ is a CLF if and only if

$$L_g V = 0 \Rightarrow L_f V < 0, \forall x \neq 0. \tag{6}$$

In this article, we guarantee the robustness of controllers by sector margins and gain margins.

Definition 3 A locally Lipschitz continuous mapping $\phi(u) \in R^m$ is said to be a sector nonlinearity in (α, β) with respect to $u \in R^m$ if the following conditions are satisfied:

$$\begin{aligned} \alpha u^T u < u^T \phi(u) < \beta u^T u, \forall u \neq 0, \\ \phi(0) = 0. \end{aligned} \tag{7}$$

Definition 4 System (2) is said to have a sector margin (α, β) with respect to $u \in R^m$ if the closed system

$$\dot{x} = f(x) + g(x)\phi(u) \tag{8}$$

is asymptotically stable, where $\phi(u)$ is any sector nonlinearity in (α, β) with respect to $u \in R^m$.

Definition 5 System (2) is said to have a gain margin (α, β) with respect to $u \in R^m$ if the closed system (8) is asymptotically stable, when $\phi(u)$ is given as follows:

$$\phi(u) = \kappa u, \kappa \in (\alpha, \beta). \tag{9}$$

By the definition, gain margins are the special case of sector margins. If system (2) has a sector margin (α, β), it also has a gain margin (α, β).

2.2 Inverse optimal controller

We introduce the inverse optimal controller proposed by Nakamura et al [Nakamura et al. (2007)]. The following results are obtained for system (2) with input constraint

$$U_k^C := \left\{ u \in R^m \middle| \|u\|_k = \left(\sum_{i=1}^{m} |u_i|^k \right)^{\frac{1}{k}} < C(x) \right\}, \tag{10}$$

where $1 < k < \infty$ is a constant and $C(x) > 0$ is continuous on R^n.

Theorem 1 We consider system (2) with input constraint (10). Let $V(x)$ be a local CLF for system (2) and $a_1 > 0$ be the maximum number satisfying

$$\begin{aligned} &\inf_{u \in U_k^C} \{L_f V + L_g V \cdot u\} < 0, \\ &\forall x \in W_1 := \{x \mid V(x) < a_1\}. \end{aligned} \tag{11}$$

Then, W_1 is a domain in which the origin is asymptotically stabilizable. If $V(x)$ is a CLF, then $a_1 = \infty$ and $W_1 = R^n$.

Theorem 2 We consider system (2) with input constraint (10) . Let $V(x)$ be a local CLF for system (2) , $P(x)$ be a function defined by

$$P(x) = \frac{L_f V}{C(x) \left\| L_g V \right\|_{\frac{k}{k-1}}}, \tag{12}$$

and $a_r \in (0, a_1)$ be the maximum number such that the condition

$$\begin{aligned} &\inf_{u \in U_k^C} \left\{ L_f V + \frac{k-1}{k} L_g V \cdot u \right\} < 0, \\ &\forall x \in W_r := \{x \mid V(x) < a_r\} \end{aligned} \tag{13}$$

is satisfied, and d be a positive constant. Then, input

$$u_i = -\frac{1}{R(x)} \left| L_{g_i} V^{\frac{1}{k-1}} \right| \operatorname{sgn}(L_{g_i} V) \qquad (i = 1, \ldots, m), \tag{14}$$

$$R(x) = \begin{cases} \dfrac{(2 + q(x) \left\| L_g V \right\|_{\frac{k}{k-1}}^{\frac{1}{k-1}}) \left\| L_g V \right\|_{\frac{k}{k-1}}^{\frac{1}{k-1}}}{\dfrac{k}{k-1}(P + |P|) + q(x) \left\| L_g V \right\|_{\frac{k}{k-1}}^{\frac{1}{k-1}}} & (L_g V \neq 0) \\ \dfrac{2}{q(x)} & (L_g V = 0), \end{cases} . \tag{15}$$

$$q(x) = d C^{\frac{1}{k-1}}(x) \tag{16}$$

asymptotically stabilizes the origin in W_r, and minimizes the cost function:

$$J = \int_0^\infty \left\{ l(x) + \frac{R^{k-1}(x)}{k} \|u\|_k^k \right\} dt,$$
$$l(x) = \frac{k-1}{k} \cdot \frac{1}{R(x)} \left\| L_g V \right\|_{\frac{k}{k-1}}^{\frac{k}{k-1}} - L_f V. \tag{17}$$

Moreover, it achieves at least a sector margin (α, β) in W_r.

2.3 Adaptive control problem

We consider an adaptive control problem for nonlinear systems. In this section, we introduce some definitions and properties. We consider the following input affine nonlinear system:

$$\dot{x} = f_0(x) + f_1(x)\theta + g(x)u, \tag{18}$$

where $x \in R^n$ is a state vector, $u \in R^m$ is an input vector, and $\theta \in R^p$ is a constant unknown parameter vector. We assume that $f_0 : R^n \to R^n$, $g : R^n \to R^{n \times m}$ and $f_1 : R^n \to R^{n \times p}$ are continuous vector fields, and $f_0(0) = 0$. Note that there exists no input constraint.
The stabilizability of the system with unknown parameters is defined as the following.

Definition 6 Let $\hat{\theta}$ be an estimate of θ. We say that (18) is globally adaptively stabilizable if there exist a function $\alpha(x, \hat{\theta})$ continuous on $R^n \setminus \{0\} \times R^p$ with $\alpha(0, \hat{\theta}) \equiv 0$, a continuous function $\tau(x, \hat{\theta})$, and a positive definite symmetric $p \times p$ matrix Γ, such that the dynamic controller

$$u = \alpha(x, \hat{\theta}), \tag{19}$$

$$\dot{\hat{\theta}} = \Gamma \tau(x, \hat{\theta}) \tag{20}$$

guarantees that the solution $(x, \hat{\theta})$ is globally bounded, and $x \to 0$ as $t \to \infty$ for any value of the unknown parameter $\theta \in R^p$.
For the stabilization problem, we introduce an adaptive control Lyapunov function (ACLF) as the following.

Definition 7 We consider system (18) and assume that $V_a(x, \theta)$ is a CLF for system (18). Then, $V_a(x, \theta)$ is called an adaptive control Lyapunov function (ACLF) for system (18) if there exists a positive-definite symmetric matrix Γ such that for each $\theta \in R^p$, V_a is a CLF for the modified system

$$\dot{x} = f_0(x) + f_1(x)\left(\theta + \Gamma\left(\frac{\partial V_a}{\partial \theta}\right)^T\right) + g(x)u. \tag{21}$$

Krstić et al. (1995) proved the following theorem.

Theorem 3 The following two statements are equivalent:

(1) There exists a triple (α, V_a, Γ) such that $\alpha(x, \hat{\theta})$ globally asymptotically stabilizes (21) at $x = 0$ for each $\theta \in R^p$ with respect to the Lyapunov function $V_a(x, \theta)$.

(2) There exists an ACLF $V_a(x, \theta)$ for system (18).

3. Magnetic Levitation System

3.1 System configuration

We consider a stabilization problem of a magnetic levitation system shown in Fig. 1[Mizutani et al. (2004)]. The system consists of a magnet with a disk, a glass guide rod, upper and lower magnetic drive coils that generate a magnetic field in response to a DC current and two laser-based sensors that measure the magnetic position using the reflection of the disk surface.

3.2 Mathematical model of the system

In this article, we control the position of the magnet using attractive force generated by the upper drive magnetic coil. The force diagram is illustrated in Fig. 2. ξ is the position of the magnet from the upper coil, and F_u is an attractive force for the magnet generated by the upper drive magnetic coil.

The dynamical equation for the magnet is described by

$$m\ddot{\xi} = F_u - m\mu\dot{\xi} - mg_0, \tag{22}$$

where m is the mass of the magnet, μ is a friction constant. g_0 is the gravitational acceleration.

Fig. 1. Magnetic levitation system

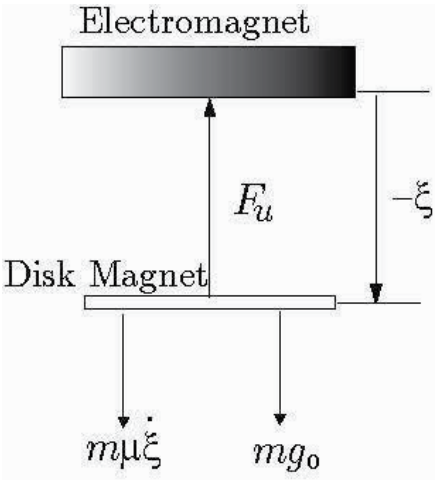

Fig. 2. Force diagram of the magnetic levitation system

Here, F_u is modeled by

$$F_u = \frac{u}{a(-\xi + b)^4}, \tag{23}$$

where a and b are constants determined by numerical modeling of the magnetic configuration, and u is a control input voltage for the upper coil. The position ξ is measured by the upper laser sensor.
Let ξ^* be the desired position of the magnet, $x_1 = \xi - \xi^*$, and $x_2 = \dot{x}_1$. We set $x = [x_1, x_2]^T$. Then we obtain the following state equation:

$$\dot{x} = f(x) + g(x)u, \tag{24}$$

where $f(x)$ and $g(x)$ are defined as

$$f(x) = \begin{bmatrix} x_2 \\ -\mu x_2 - g_0 \end{bmatrix}, g(x) = \begin{bmatrix} 0 \\ \dfrac{1}{ma(-x_1 - \xi^* + b)^4} \end{bmatrix}. \tag{25}$$

The system parameters are shown in Table 1.

m [kg]	μ [-]	g_0 [m/s²]	a [V/N·m⁴]	b [m]
0.12	4.5	9.80665	40118.9	0.056464

Table 1. Parameter values of the magnetic levitation system

There exists the following input constraint in system (24):

$$\|u\|_2 = \sqrt{u^2} < 5\,[\mathrm{V}]. \tag{26}$$

By the above discussion, the control problem is reduced to the stabilization problem of system (24) with the input constraint (26).

4. Pre-feedback Gravity Compensation

In system (2), we assume that $f(0) = 0$. However, $f(0) \neq 0$ in system (24). Therefore, we cannot directly apply the inverse optimal controller (14) to system (24). To achieve $f(0) = 0$, we design a controller to compensate for gravity by a pre-feedback input.
We consider the following gravity compensation input $u_c(x)$ as

$$u_c(x) = mg_0 a(-x_1 - \xi^* + b)^4. \tag{27}$$

Substituting (27) into (24), the gravitational acceleration g_0 is successfully canceled. Then, we split the input $u(x)$ using $u_c(x)$ as

$$u(x) = u_c(x) + u_s(x), \tag{28}$$

where u_s is an asymptotic stabilizing input for system (24) when $g_0 = 0$.
By using (26) and (28), the input constraint is rewritten to

$$\|u(x)\|_2 = \|u_c(x) + u_s(x)\|_2 < 5. \tag{29}$$

To handle input constraint (29) as a norm constraint, we rewrite (29) as

$$\|u_s(x)\| < \left\| 5 - |u_c(x)| \right\|_2 := C(x). \tag{30}$$

(30) represents a constraint depending on the state. Note that constraint (30) is more severe than the original constraint (29). The problem of designing controller (28) is reduced to the problem of designing controller $u_s(x)$ with input constraint $\|u_s(x)\|_2 < C(x)$.
To apply inverse optimal controller (14), we construct a CLF for system (24). In general, the controller performance often depends on a CLF. However, it is unclear which CLF achieves the best control performance. Hence, we construct a CLF with a design parameter. Using the integrator backstepping method, a CLF $V(x)$ can be carried out as

$$V(x) = \frac{1}{2}(r^2 + 1){x_1}^2 + r x_1 x_2 + \frac{1}{2}{x_2}^2, \tag{31}$$

where r is a positive constant and also a design parameter.
Now, we construct input u_s. Let $f_0(x)$ be the function defined by

$$f_0(x) = f(x)|_{g_0=0} = \begin{bmatrix} x_2 \\ -\mu x_2 \end{bmatrix}. \tag{32}$$

By using (31), we can calculate $L_{f_0}V$ and L_gV as

$$L_{f_0}V = \{(r^2+1) - \mu r\}x_1x_2 + (r-\mu){x_2}^2, \tag{33}$$

$$L_gV = \frac{rx_1 + x_2}{ma(-x_1 - \xi^* + b)^4}. \tag{34}$$

Substituting (33) and (34) into (14) and (15), we get the following input $u_s(x)$.

$$u_s(x) = -\frac{1}{R_1(x)}L_gV, \tag{35}$$

$$R_1(x) = \begin{cases} \dfrac{(2+q(x)\|L_gV\|_2)\|L_gV\|_2}{2(P_1+|P_1|)+q(x)\|L_gV\|_2} & (L_gV \neq 0) \\ \dfrac{2}{q(x)} & (L_gV = 0), \end{cases} \tag{36}$$

$$P_1(x) = \frac{L_{f_0}V}{C(x)\|L_gV\|_2}, \tag{37}$$

$$q(x) = dC(x) = d\|5 - |u_c(x)|\ \|_2. \tag{38}$$

According to Theorem 2, $u_s(x)$ has a sector margin $(1/2, \infty)$.
Finally, the following controller $u(x)$ is obtained:

$$u(x) = mg_0a(-x_1 - \xi^* + b)^4 - \frac{1}{R_1(x)}L_gV. \tag{39}$$

5. Experiment 1

We apply controller (39) to the magnetic levitation system. We set $x(0) = [-1.4, 0.0]^T$ and $\xi^* = -2.0$ [cm]. The controller is implemented by MATLAB/SIMULINK. The sampling

interval is 1×10^{-3} [sec] and control parameters are $r=8$ and $d=1.25\times10^{-4}$, respectively.
The time response of the controlled system is shown in Fig. 3. Although the velocity x_2 vibrates due to sensor noise, the input constraint (26) is satisfied. However, the position x_1 does not converge to zero (an offset error remains). Then, the actual magnetic levitation system is not asymptotically stabilized by the proposed controller (39).
The biggest reason for the offset error is the lack of robustness with respect to u_c. If there exists a parameter uncertainty in $g(x)$, the gravitational acceleration g_0 is not completely canceled by the pre-feedback $u_g(x)$. Therefore, the proposed controller $u(x)$ does not guarantee the robustness for the system (24) even if the stabilizing input $u_s(x)$ guarantees the sector margin $(1/2,\infty)$ for the system

$$\dot{x}=f_0(x)+g(x)u_s. \tag{40}$$

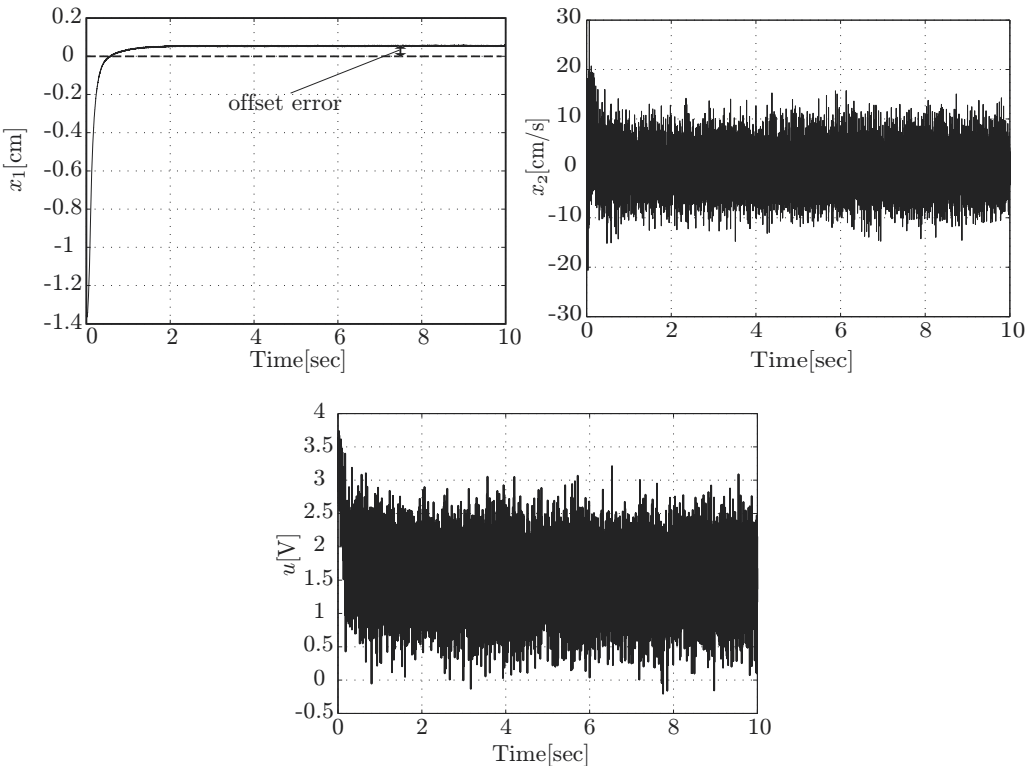

Fig. 3. Experimental result of controller (39)

6. Adaptive Inverse Optimal Controller Design

6.1 Robustness recovery via adaptive control

To solve the problem stated in section 5, we propose a controller that guarantees a gain

margin for u. We apply an adaptive control technique to achieve a gain margin for input u. Before applying the adaptive controller, we rewrite the system (24) to

$$\dot{x} = f_0(x) + f_1(x)g_0 + g(x)u \ , \tag{41}$$

where $f_0(x)$ is defined by (31) and $f_1(x) = [0,-1]^T$. Additionally, to consider a gain margin for (41), we rewrite the system to

$$\dot{x} = f_0(x) + \kappa f_1(x)\theta + \kappa g(x)u \ , \tag{42}$$

where κ is an unknown constant and $\theta := g_0 / \kappa$ is a constant unknown parameter. Note that the range of κ, in which the origin of the system (42) is asymptotically stable, is a gain margin for input u. Furthermore, we consider the following input:

$$u(x,\hat{\theta}) = u_c(x,\hat{\theta}) + u_s'(x,\hat{\theta}), \tag{43}$$

where $\hat{\theta} := g_0 / \hat{\kappa}$ and $\hat{\kappa}$ is an estimate of κ. We suppose that input $u_s'(x,\hat{\theta})$ asymptotically stabilizes the system (40) and guarantees the gain margin $(1/2,\infty)$. Let $u_g(x,\hat{\theta})$ be a gravity compensation input defined as follows:

$$u_c(x,\hat{\theta}) = ma\hat{\theta}(-x_1 - \xi^* + b)^4. \tag{44}$$

Remark 1 In this section, we do not mention whether the input constraints exist or not.

Then, we construct an adaptive law $\dot{\hat{\theta}}$ such that the input (43) stabilizes the system (42) and show the input (43) has a gain margin $(1/2,\infty)$.
In this section, we use an ACLF to construct an adaptive law. The following lemma is available for constructing an ACLF.

Lemma 1 We consider system (42). Let $V(x)$ be a CLF for system (41). Then, $V(x)$ is an ACLF for system (42).

Proof: If $V(x)$ is an ACLF for system (42), $V(x)$ is a CLF for the following system:

$$\dot{x} = f_0(x) + \kappa f_1(x)\left(\theta + \gamma \frac{\partial V}{\partial \theta}\right) + \kappa g(x)u, \tag{45}$$

where γ is a positive constant. Note that $\partial V / \partial \theta = 0$, the above system is rewritten to

$$\dot{x} = f_0(x) + \kappa f_1(x)\theta + \kappa g(x)u. \tag{46}$$

Sytem (46) is asymptotically stabilized by the input

$$u(x) = \theta u_c(x) + u_s(x), \tag{47}$$

where $u_c(x)$ and $u_s(x)$ are defined by (27) and (35) respectively. This implies all CLFs for system (41) are ACLFs for system (42).

By Lemma 1, CLF (31) is applicable to an ACLF for system (42).

Lemma 2 We consider system (42) and assume that an ACLF $V(x)$ for (42) is obtained. Let $V'(x,\hat{\theta})$ be a function defined by

$$V'(x,\hat{\theta}) = V(x) + \frac{\kappa}{2\gamma}(\theta - \hat{\theta})^2 = V(x) + \frac{\kappa}{2\gamma}\tilde{\theta}^2, \tag{48}$$

where $1/2 < \kappa < \infty$ and $\tilde{\theta} := \theta - \hat{\theta}$. Let the adaptive law $\dot{\hat{\theta}}$ be

$$\dot{\hat{\theta}} = \gamma\tau(x) = \gamma\frac{\partial V}{\partial x} f_1(x). \tag{49}$$

Then, $V'(x,\hat{\theta})$ is a Lyapunov function for the closed loop system of (42).

Proof: Let the origin of system (42) be $(x,\hat{\theta}) = (0,\theta)$. Then, V' is a positive definite function. Assume u is input (43) and note that $\dot{\tilde{\theta}} = -\dot{\hat{\theta}}$. Then,

$$\begin{aligned} \dot{V}'(x,\hat{\theta}) &= \frac{\partial V}{\partial x}\left[f_0(x) + \kappa\left\{f_1(x)\hat{\theta} + g(x)\left(u_c(x,\hat{\theta}) + u_s'(x,\hat{\theta})\right)\right\}\right] \\ &= \frac{\partial V}{\partial x}\left[f_0(x) + \kappa g(x)u_s'(x,\hat{\theta})\right] \le 0. \end{aligned} \tag{50}$$

Since the input $u_s'(x,\hat{\theta})$ has a gain margin $(1/2,\infty)$, $\dot{V}'(x,\hat{\theta})$ is less than or equal to zero. Then $V'(x,\hat{\theta})$ is a Lyapunov function for the closed loop system of (42) and the origin $(x,\hat{\theta}) = (0,\theta)$ is stable.

Remark 2 Lyapunov function (48) contains an unknown constant κ. However, it does not become a problem because both input (43) and adaptive law (49) do not contain κ.

Lemma 3 We consider system (42) and assume that an ACLF $V(x)$ for (42) is obtained. Then, if $1/2 < \kappa < \infty$, $x \to 0 (t \to \infty)$ and $\hat{\theta} \to \theta (t \to \infty)$ are achieved by input (43) and adaptive law (49).

Proof: By Lemma 2, we can construct a Lyapunov function $V'(x,\hat{\theta})$ (47) for system (41). The input and the adaptive law are given by (42) and (48), respectively. Then, we obtain $\dot{V}'(x,\hat{\theta}) \le 0 (x \ne 0)$ because the input $u_s'(x,\hat{\theta})$ has a gain margin $(1/2,\infty)$. Let S be a set defined by

$$\begin{aligned} S &:= \{(x,\hat{\theta}) \left| \dot{V}'(x,\hat{\theta}) = 0, x \in R^n, \hat{\theta} \in R \right.\}, \\ &= \{(x,\hat{\theta}) \left| x = 0, \hat{\theta} \in R \right.\}. \end{aligned} \tag{51}$$

We show that the largest invariant set contained in S consists of only a point $(x,\hat{\theta}) = (0,\theta)$. Consider the following solution of (42) belonging to S:

$$x(t) \equiv 0, t \ge 0. \tag{52}$$

Note that $u_s'(0,\hat{\theta}) = 0$, we obtain the following equation for (42):

$$\begin{aligned} \dot{x} &= f_0(0) + \kappa \{ f_1(0)\theta + g(0)u(0,\hat{\theta}) \}, \\ &= \kappa \{ f_1(0)\theta + g(0)u_c(x,\hat{\theta}) \}, \\ &= \kappa f_1(\theta - \hat{\theta}) \equiv 0, \end{aligned} \tag{53}$$

where $\kappa \ne 0$ and $f_1(0) \ne 0$, we obtain $\hat{\theta} \equiv \theta$. On the other hand, if $x = 0$ and $\hat{\theta} \ne \theta$, we obtain $\dot{x} \ne 0$ by (50). Therefore, the largest invariant set contained in S is a set $\{(0,\theta)\}$. Finally, we obtain $x \to 0$ and $\hat{\theta} \to \theta$ when $t \to \infty$ by LaSalle's invariance principle [Khalil (2002)].

The following theorem is obtained by Lemmas 2 and 3.

Theorem 4 We consider system (42), controller (43) and adaptive law (49). Then, the controller has a gain margin $(1/2,\infty)$.

6.2 Adaptive inverse optimal controller

We calculate $\dot{\hat{\theta}}$ of (49) by using CLF (31) as:

$$\begin{aligned} \dot{\hat{\theta}} &= \gamma \begin{bmatrix} (r^2+1)x_1 + rx_2 & rx_1 + x_2 \end{bmatrix} \begin{bmatrix} 0 \\ -1 \end{bmatrix} \\ &= -\gamma(rx_1 + x_2). \end{aligned} \tag{54}$$

Furthermore, taking into consideration the input constraint, we obtain the following controller:

$$u(x,\hat{\theta}) = u_c(x,\hat{\theta}) + u_s'(x,\hat{\theta}) = ma\hat{\theta}(-x_1 - \xi^* + b)^4 + u_s'(x,\hat{\theta}), \tag{55}$$

$$u_s'(x,\hat{\theta}) = -\frac{1}{R_2(x,\hat{\theta})} L_g V, ' \tag{56}$$

$$R_2(x,\hat{\theta}) = \begin{cases} \dfrac{(2+q(x,\hat{\theta})\|L_g V\|_2)\|L_g V\|_2}{2(P_2 + |P_2|) + q(x,\hat{\theta})\|L_g V\|_2} & (L_g V \neq 0) \\ \dfrac{2}{q(x,\hat{\theta})} & (L_g V = 0), \end{cases} \tag{57}$$

$$P_2(x,\hat{\theta}) = \frac{L_{f_0} V}{C(x,\hat{\theta})\|L_g V\|_2}, \tag{58}$$

$$q(x,\hat{\theta}) = dC(x,\hat{\theta}), \tag{59}$$

$$C(x,\hat{\theta}) = \left\| 5 - \left| u_c(x,\hat{\theta}) \right| \right\|_2, \tag{60}$$

where we use $u_s(x)$ given by (35) as $u_s'(x,\hat{\theta})$. Then, note that the input constraint $C(x)$ is rewritten to $C(x,\hat{\theta})$ given by (60). According to Lemma 2 and the result of [Nakamura et al. (2007)], we can show the input $u_s'(x,\hat{\theta})$ minimizes the following cost function:

$$J = \int_0^\infty l(x,\hat{\theta}) + \frac{R_2(x,\hat{\theta})}{2} u_s'^2 dt, \tag{61}$$

where

$$l(x,\hat{\theta}) = \frac{1}{2R_2(x,\hat{\theta})} \|L_g V\|_2^2 - L_{f_0} V. \tag{62}$$

It is obvious that a gain margin $(1/2, \infty)$ is guaranteed for controller (55) at least in the neighborhood of the origin.

7. Experiment 2

In this section, we apply controller (55) to the magnetic levitation system and confirm its effectiveness by the experiment. To consider the input constraint, we employ the following adaptive law with projection instead of (54):

$$\dot{\hat{\theta}} = \begin{cases} 0 & \hat{\theta} = 2g_0, rx_1 + x_2 > 0 \\ 0 & \hat{\theta} = 0, rx_1 + x_2 < 0 \\ -\gamma(rx_1 + x_2) & otherwise \end{cases} . \tag{63}$$

We set the adaptation gain $\gamma = 160$ and the initial value of the estimate $\hat{\theta}(0) = 820$. The other experimental conditions and control parameters are the same as in section 5. The experimental result is shown in Fig. 5. Position x_1 converges to zero without any tuning of control parameters. The gain margin guaranteed by the adaptive law seems quite effective. We can observe that the input is larger than the non-adaptive controller (39), however, the input constraint is satisfied. The parameter estimate $\hat{\theta}$ also tends to converge to the true value θ. As a result, the effectiveness of the proposed controller (55) is confirmed.

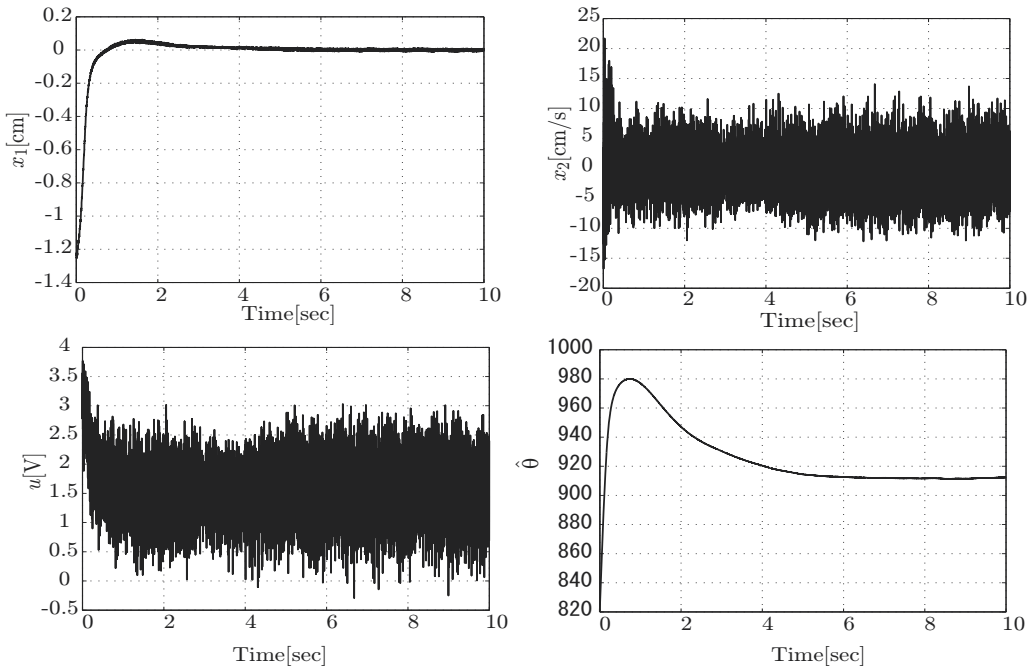

Fig. 4. Experimental result of controller (55)

8. Conclusion

In this article, we proposed an adaptive inverse optimal controller for the magnetic levitation system. First, we designed an inverse optimal controller with a pre-feedback gravity compensator and applied it to the magnetic levitation system. However, this controller cannot guarantee any stability margin. We demonstrated that the controller did not work well (offset error remained) in the experiment. Hence, we proposed an improved controller via an adaptive control technique to guarantee the stability margin. Finally, we

confirmed the effectiveness of the proposed adaptive inverse optimal controller by the experiment. As a result, we achieved offset-free control performance.

9. References

Freeman, R.A. & Kokotović, P.V. (1996). *Robust Nonlinear Control Design. State-space and Lyapunov Techniques*. Birkhäuser, Boston.

Khalil, H.K. (2007). *Nonlinear systems*, 3rd ed. Prentice Hall, Upper Saddle River, New Jersey.

Krstić, M.; Kanellakopoulos, I. & Kokotović, P. (1995). Nonlinear and Adaptive Control Design. Wiley-Interscience, New York.

Krstić, M. & Li, Z. (1998). Inverse optimal design of input-state-stabilizing nonlinear controllers. *IEEE Transaction on Automatic Control*, 43, 3, 336-350.

Li, Z. & Krstić, M. (1997). Optimal design of adaptive tracking controllers for non-linear systems. *Automatica*, 33, 8, 1459-1473

Mizutani, T.; Katayama, H. & Ichikawa A. (2004). Tracking control of a magnetic levitation system by feedback linearization. *Proceedings of SICE Annual Conference 2004*, 121-126.

Nakamura, N. ; Nakamura, H.; Yamashita, Y. & Nishitani, H. (2007). Inverse optimal control for nonlinear systems with input constraints. *Proceedings of the European Control Conference 2007 (CD-ROM).*

Sepulchre, R.; Janković, M. & Kokotović, P.V. (1997). *Constructive Nonlinear Control*. Springer, London.

Sontag, E.D. (1989). A universal construction of Artstein's theorem on nonlinear stabilization. *System & Control Letters,* 13, 117-123.

15

Adaptive Precision Geolocation Algorithm with Multiple Model Uncertainties

Wookjin Sung , Kwanho You
Sungkyunkwan University, Department of Electrical Engineering
Korea

1. Introduction

In the unmanned ground vehicle (UGV) case, the estimation of a future position with a present one is one of the most important techniques (Madhavan & Schlenoff, 2004). Generally, the famous global positioning system (GPS) has been widely used for position tracking because of its good performance (Torrieri, 1984; Kim et al., 2006). However, there exist some defects. For example, it needs a separate receiver and it must have at least three available satellite signals. Moreover it is also vulnerable to the indoor case (Gleanson, 2006) or the reflected signal fading.

There have been many researches to substitute or to assist the GPS. One of them is the method of using the time difference of arrival (TDoA) which needs no special equipment and can be operated in indoor multipath situation (Najar & Vidal, 2001). The TDoA means an arrival time difference of signals transmitted from a mobile station to each base station. It is the basic concept of estimation that the position of a mobile station can be obtained from the crossing point of hyperbolic curves which are derived from the definition of TDoA. Including some uncertainties, there have been several approaches to find the solution of TDoA based geolocation problem using the least square method, for example, Tayler series method (Xiong et al., 2003), Chan's method (Ho & Chan, 1993), and WLS method (Liu et al., 2006). However in case of a moving source, it demands a huge amount of computational efforts each step, so it is required to use a method which demands less computational time. As a breakthrough to this problem, the application of EKF can be reasonable.

The modeling errors happen in the procedure of linear approximation for system behaviors to track the moving source's position. The divergence caused from the modeling errors is a critical problem in Kalman filter applications (Julier & Uhlmann, 2004). The standard Kalman filter cannot ensure completely the error convergence because of the limited knowledge of the system's dynamical model and the measurement noise. In real circumstances, there are uncertainties in the system modeling and the noise description, and the assumptions on the statistics of disturbances could be restrictive since the availability of a precisely known model is very limited in many practical situations. In practical tracking filter designs, there exist model uncertainties which cannot be expressed by the linear state-space model. The linear model increases modeling errors since the actual mobile station moves in a non-linear process. Especially even with a little priori knowledge it is quite

valuable concerning the strategy.
Hence, the compensation of model uncertainties is an important task in the navigation filter design. In modeling or formulating the mathematical equations, the possible prediction errors are approximated or assumed as a model uncertainty. The facts discussed above leads to unexpected deterioration of the filtering performance. To prevent the divergence problem due to modeling errors in the EKF approach, the adaptive filter algorithm can be one of the good strategies for estimating the state vector. This chapter suggests the adaptive fading Kalman filter (AFKF) (Levy, 1997; Xia et al., 1994) approach as a robust solution. The AFKF essentially employs suboptimal fading factors to improve the tracking capability. In AFKF method, the scaling factor is introduced to provide an improved state estimation. The traditional AFKF approach for determining the scaling factors mainly depends on the designer's experience or computer simulation using a heuristic searching plan. In order to resolve this defect, the fuzzy adaptive fading Kalman filter (FAFKF) is proposed and used as an adaptive geolocation algorithm. The application of fuzzy logic to adaptive Kalman filtering gains more interests. The fuzzy logic adaptive system is constructed so as to obtain the suitable scaling factors related to the time-varying changes in dynamics. In the FAFKF, the fuzzy logic adaptive system (FLAS) is used to adjust the scaling factor continuously so as to improve the Kalman filter performance.
In this chapter, we also explain how to compose the FAFKF algorithm for TDoA based position tracking system. Through the comparison using the simulation results from the EKF and FAFKF solution under the model uncertainties, it shows the improved estimation performance with more accurate tracking capability.

2. Geolocation with TDoA analytical methods

When the mobile station (MS: the unknown position) sends signals to each base station (BS: the known position), there is a time difference because of the BS's isolated location from MS. The fundamental principle of position estimation is to use the intersection of hyperbolas according to the definition of TDoA as shown in Fig. 1.
The problem of geolocation can be formulated as

$$\begin{aligned} d_i &= \|s - b_i\| \\ d_{i1} &= ct_{i1} = ct_i - ct_1 \\ b_i &= col\{x_i, y_i\},\ i = 1, 2, 3, \cdots, m \\ s &= col\{x, y\} \end{aligned} \tag{1}$$

where b_i is the known position of *i*-th signal receiver (BS), s is the unknown position of signal source (MS), and c is the propagation speed of signal. In Eq. (1), d_i means the distance between MS and *i*-th BS and t_i is the time of signal arrival (ToA) (Schau & Robinson, 1987) from MS to *i*-th BS. Hence t_{i1} becomes the time difference of arrival (TDoA) which is the difference of ToA between t_i (from MS to the *i*-th BS) and t_1 (from

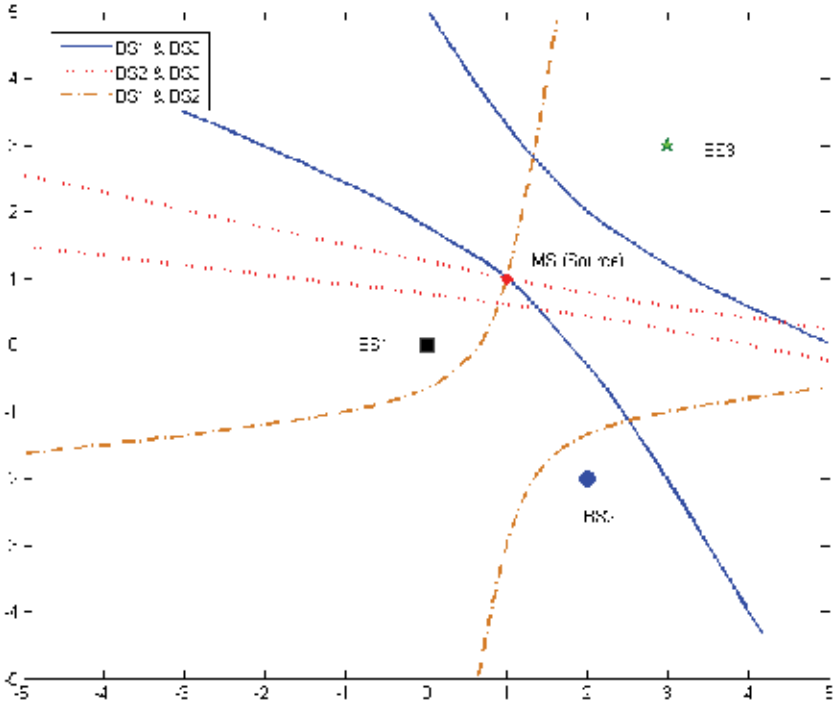

Fig. 1. Geometric method using hyperbolas.

MS to the first BS). The distance difference of d_{i1} results from the multiplication of TDoA and *c*.

Generally it is possible to estimate the source location if the values of ToA could be provided exactly. However, it is required to be synchronized for all MS and BS's in this case. To find the TDoA of acknowledgement signal from MS to BS's, the time delay estimation can be used. As shown in Fig. 1, the estimation of geolocation can be obtained by solving the nonlinear hyperbolic equation from the relation of TDoA. If there are three BS's as in Fig. 1, we can draw three distinct hyperbolic curves using distance difference from TDoA signal. It is the principle of geometric method that the cross point becomes the position estimation of MS.

To find the position estimation (*s*) of the unknown MS in an analytical method, let's rewrite the distance difference equation (1) as

$$d_i = d_1 + d_{i1}, \; i = 2, 3, \cdots, m. \tag{2}$$

By squaring Eq. (2) with the relation of $(d_i)^2 = \langle s - b_i, s - b_i \rangle$, the nonlinear equation for positional vector of *s* can be formulated as following.

$$\|s\|^2 - 2b_i^T s + \|b_i\|^2 = \|s\|^2 - 2b_1^T s + \|b_1\|^2 + 2d_1 d_{i1} + (d_{i1})^2, \;\; i = 2, \cdots, m \tag{3}$$

To represent the solution in linear matrix equality form, Eq. (3) can be simplified as

$$\|b_1\|^2 - \|b_i\|^2 + (d_{i1})^2 = 2\langle b_1 - b_i, s\rangle - 2d_1 d_{i1},\ i = 2,\cdots,\ m \tag{4}$$

Using the distance from MS to the first BS, $(d_1)^2 = (x - x_1)^2 + (y - y_1)^2$, and with b_1 as the origin of coordinates, i.e., $b_1 = col\{0, 0\}$, we can obtain the position estimation from the following two nonlinear constraints.

$$\begin{aligned} &\frac{1}{2}(-\|b_i\|^2 + (d_{i1})^2) = -\langle b_i, s\rangle - d_1 d_{i1},\ i = 2,3,\cdots,m \\ &x^2 + y^2 - (d_1)^2 = 0 \end{aligned} \tag{5}$$

To find the solution of s, Eq. (5) is rewritten in linear matrix equation. Now the source vector s can be acquired by solving the following MS geolocation problem.

$$\begin{aligned} &\mathbf{G}s = \mathbf{h} + \boldsymbol{\rho} d_1 \\ &(d_1)^2 = \langle s, s\rangle \\ &\mathbf{h} = \frac{1}{2}\begin{bmatrix} \|b_2\|^2 - (d_{21})^2 \\ \vdots \\ \|b_m\|^2 - (d_{m1})^2 \end{bmatrix} = \frac{1}{2}(\mathbf{d} - \boldsymbol{\rho} \bullet \boldsymbol{\rho}) \\ &\boldsymbol{\rho} = -\begin{bmatrix} d_{21} \\ \vdots \\ d_{m1} \end{bmatrix},\ \mathbf{d} = \begin{bmatrix} \langle b_2, b_2\rangle \\ \vdots \\ \langle b_m, b_m\rangle \end{bmatrix} \end{aligned} \tag{6}$$

where $\mathbf{G} = [b_2 \cdots b_m]^T$ and $\bullet$ means the Hadamar operator.

3. Geolocation with model uncertainty

This section describes the geolocation using the estimation filter in state-space. As stated in the section 2, the conventional analytical methods are focused on solving the nonlinear hyperbolic equations. In this section, we introduce the fuzzy adaptive fading Kalman filter to get the precision estimation for multiple model uncertainties.

3.1 System modeling

In the real case, TDoA signal can be distorted by the timing error due to non-line-of sight or by additive white Gaussian noise. To find the precision geolocation in real case, the system modeling must include the model uncertainty. Let t_o be the ideal TDoA signal and Δt is

the distorted amount by external noises. The real value of TDoA is changed as $t = t_o + \Delta t$.
If the real value of TDoA is used in Eq. (6), it becomes more complicated nonlinear equation and this complexity may cause huge computational efforts in the real-time process. As a breakthrough to this problem, the Kalman filter which needs relatively less computational time can be an alternative solution.
Since the hyperbolic equation of TDoA is nonlinear, the extended Kalman Filter (EKF) can be used as a nonlinear state estimator. The basic algorithm of EKF is shown as in Fig. 2.

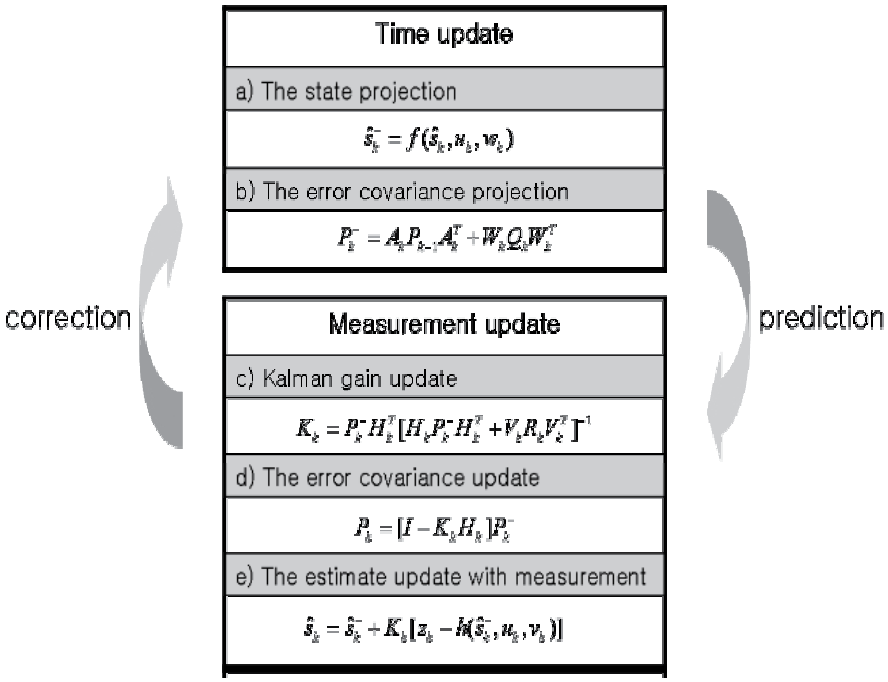

Fig. 2. Flow chart of extended Kalman filter.

The first step is the time update in which it predicts the state of next steps from processing model and it compares the real measurement with the prediction measurement of $\hat{s}$ obtained by time update process. For TDoA based geolocation using extended Kalman filter, the discrete state-equation of the processing and measurement model for MS can be formulated as

$$s_{k+1} = As_k + Bu_k + w_k$$
$$A = \begin{bmatrix} 1 & 0 & \Delta & 0 \\ 0 & 1 & 0 & \Delta \\ 0 & 0 & 0 & 0 \\ 0 & 0 & 0 & 0 \end{bmatrix}, \quad B = \begin{bmatrix} 0 & 0 \\ 0 & 0 \\ 1 & 0 \\ 0 & 1 \end{bmatrix} \tag{7}$$

where $s(k) = [x \ y \ \dot{x} \ \dot{y}]^T$, u_k is the known velocity of moving MS, Δ is the time interval of sampling, w_k is an additive white Gaussian noise (AWGN).
From the definition of TDoA, the measurement model can be written as

$$\begin{aligned} z_k &= h(s_k, v_k) \\ &= \frac{1}{c}(\| Ms_k - b_i \| - \| Ms_k - b_j \|) + v_k \\ M &= \begin{bmatrix} 1 & 0 & 0 & 0 \\ 0 & 1 & 0 & 0 \end{bmatrix} \end{aligned} \tag{8}$$

where v_k is the measurement noise in AWGN.
The output result of z_k which is the TDoA signal provides the information of MS position. As an accurate geolocation method, the frequency difference (FDoA) resulted from Doppler shifts observation can be added in the state equation. However, to make the problem more simple, we consider only the TDoA signal as an output measurement in this section.
Since the measurement model z_k is nonlinear equation, the linear approximation using partial differential method should be done for the use of EKF.

$$\begin{aligned} z_k &= z_{k-1} + H_k s_k + V_k \\ H_k &\approx \frac{\partial h_k}{\partial s_k}, \quad V_k \approx \frac{\partial h_k}{\partial v_k} \end{aligned} \tag{9}$$

3.2 Geolocation using fuzzy adaptive fading Kalman filter (FAFKF)

EKF is a very useful method for nonlinear state estimation. However, as EKF is based on the linearization of nonlinear system using partial differential method, the modeling errors can easily lead to the divergence problem. To solve this problem, an adaptive fading Kalman filter (AFKF) with a fading factor can be applied. The application of AFKF to geolocation estimation is given in the following mathematical expression.
Basically, the fading factor λ_k is added in the error covariance projection during the time update process.

$$P_k^- = \lambda_k A_k P_{k-1} A_k^T + W_k Q_k W_k^T \tag{10}$$

where $\lambda_k = diag(\lambda_1, \lambda_2, \cdots, \lambda_m)$. In normal case of $\lambda_k = 1$, it means the general EKF. If the estimated value approaches to the steady-state value, the fading factor λ_k becomes less than 1. If λ_k is greater than 1, the divergence could happen. This iterative process is called as the adaptive fading loop given as follows.

$$
\begin{aligned}
\lambda_{k+1} &= \max\left\{1, \frac{\alpha \cdot tr[F_k]}{tr[E_k]}\right\} \\
F_k &= C_0 - R_k - H_k Q_k H_k^T \\
E_k &= H_k A_k P_k A_k^T H_k^T \\
C_0 &= \begin{cases} \dfrac{\phi_0 \phi_0^T}{2}, & k = 0 \\ \dfrac{\lambda_k \phi_k \phi_k^T}{1+\lambda_k}, & k \geq 1 \end{cases} \\
\phi_k &= z_k - \hat{z}_k, \quad \hat{z}_k = h(\hat{s}_k, v_k)
\end{aligned}
\tag{11}
$$

where α is a scaling factor and $tr[\cdot]$ is the trace of a matrix.

Moreover the measurement estimation of $\hat{z}_k$ is predicted through the estimation of $\hat{s}_k$. That is, if we get more accurate $\hat{s}_k$, then the more accurate $\hat{z}_k$ can be obtained. As the error of output measurement is within the ε – neighborhood i.e., $\| z_k - \hat{z}_k \| \leq \varepsilon_k$ and $\varepsilon_k - \varepsilon_{k-1} \leq 0$, it is confirmed that the present estimation performance is guaranteed and the fading factor becomes $\lambda_{k+1} \leq 1$.

The fuzzy logic adaptive system (FLAS) offers an effective method when the problem is too complicated or hard to be analyzed in mathematical way. The procedure of general fuzzy system can be classified as three parts; fuzzification, fuzzy inference, and defuzzification. The first step of fuzzification is to make linguistic variables from inputs and outputs. The second step of fuzzy inference is to make rules using *if-then* expression. Finally the third step of defuzzification is to decide the degree of the output value.

Using the scaling factor (α) as an output from FLAS, the fading factor in FAFKF is updated as $\lambda_{k+1} = \alpha \cdot tr[F_k] / tr[E_k]$. According to the following two degree of divergence (DoD) parameters from the innovation covariance matrix and the trace of innovation covariance matrix, it is possible to identify the changing degree in dynamics of MS. The first DoD parameter δ is defined as the ratio of the trace of innovation covariance matrix at present state and the number of measurements used for estimating location.

$$
\delta = \frac{\phi_k{}^T \phi_k}{m} \tag{12}
$$

where $\phi_k = [\phi_1 \ \phi_2 \cdots \phi_m]^T$, m is the number of measurements (number of TDoA signals).

The second DoD parameter σ is defined as the average of the absolute value of the measurement error ϕ_k.

$$
\sigma = \frac{1}{m} \sum_{i=1}^{m} | \phi_i | \tag{13}
$$

The fading factor λ_k updated through the adaptive fading loop is used to change the error covariance P_k.

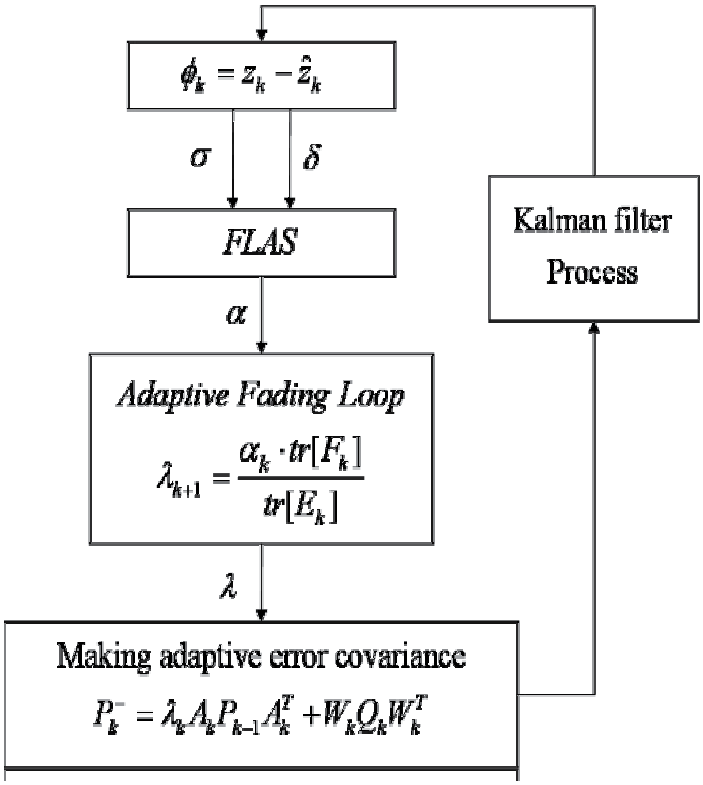

Fig. 3. Flow chart of the fuzzy adaptive fading Kalman filter process.

Fig. 3 shows how the FAFKF works for TDoA geolocation problem. As a first step in the process of FAFKF, the two DoD parameters (δ, σ) are obtained from measurement difference between the real value (z_k) and the estimation result ($\hat{z}_k$). These DoD parameters are used as the inputs for the fuzzy system. Finally the FLAS is employed for determining the scaling factor α from the innovation information. According to the scaling factor α, the estimation accuracy is determined. Using the fuzzy logic system, we can adjust the fading factors adaptively to improve the estimation performance.

4. Simulation results

The basic circumstance to be used in the simulation is shown in Fig. 4. There are two BS's and the signal source of MS is supposed to move at a constant speed but changes its direction every 2.5 sec. In Fig. 4, the dotted line is an ideal path of MS with no external forces. The solid line is the real path which is affected by the multiple noises such as the

measurement noise v_k and the process noise w_k. The thick solid line is the path of MS estimated by the standard EKF with no adaptive method. Fig. 4 shows that the performance of EKF is restricted especially when the MS changes the direction. The accumulated position error is increased as the MS changes its direction frequently.
To prove the effectiveness of the adaptive fading factor in TDoA gelocation, the simulation parameters are set close to the real values. Table 1 shows the simulation parameters.

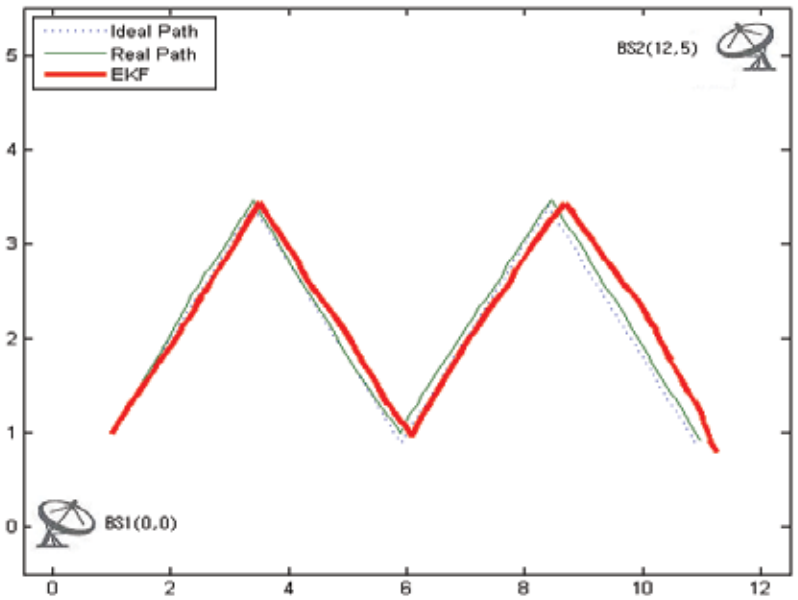

Fig. 4. Simulation circumstance for MS

The FLAS consists of the following 9 rules and is represented in the following *if-then* form. The membership functions of input fuzzy variable (DoD parameters: δ and σ) and output (scaling factor: α) are shown in Fig. 5.

i. if δ is n (negative) and σ is n, then α is nb (negative big).
ii. if δ is z (zero) and σ is n, then α is ns (negative small).

	EKF	**AFKF**	**FAFKF**
Speed	Constant	Constant	Constant.
□ (time interval)	0.1 sec	0.1 sec	0.1 sec
α (scaling factor)	None	0.12	FLAS output
λ (fading factor)	None	Constant	Fuzzy based

Table 1. Parameters for the TDoA geolocation simulation

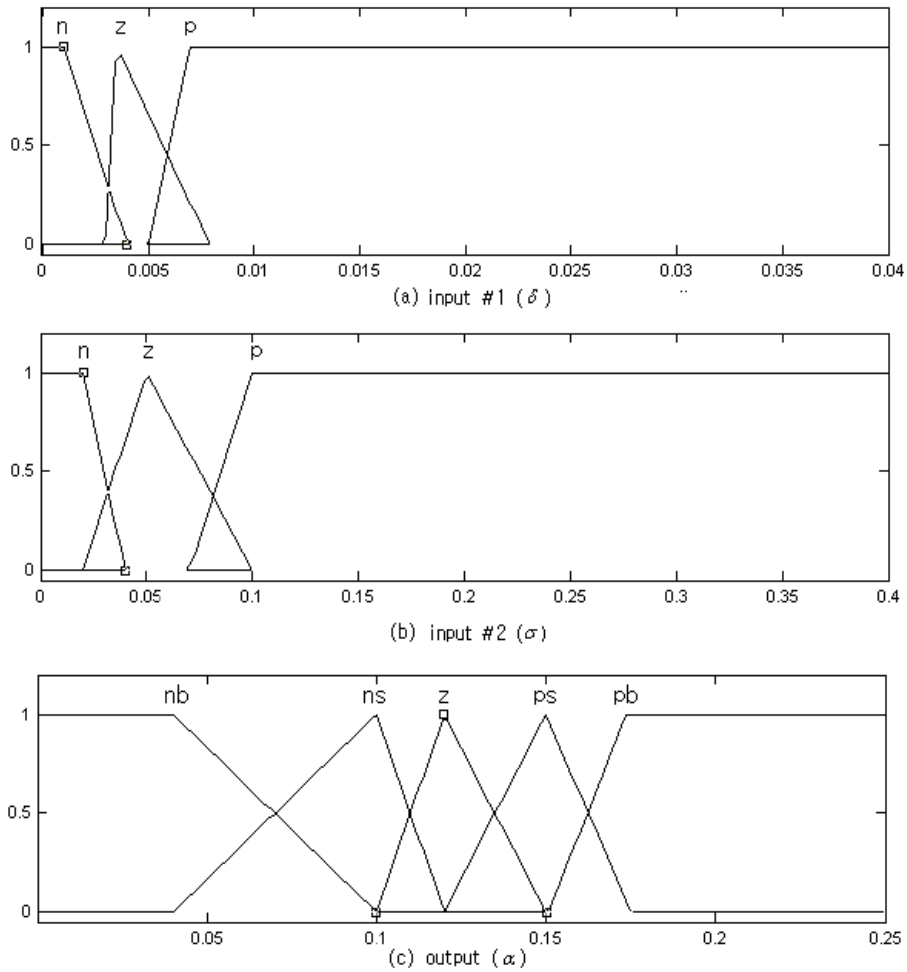

Fig. 5. Membership functions in FLAS

iii.	if δ is p (positive) and σ is n,	then α is z.
iv.	if δ is n and σ is z,	then α is ns.
v.	if δ is z and σ is z,	then α is z.
vi.	if δ is p and σ is z,	then α is ps (positive small).
vii.	if δ is n and σ is p,	then α is z.
viii.	if δ is z and σ is p,	then α is ps.
ix.	if δ is p and σ is p,	then α is pb (positive big).

As the DoD parameter (δ) and the averaged magnitude (σ) of $\phi(k)$ change within 0.003~0.007 and 0.03~0.1 respectively, we define those range as zero for δ and σ. The output of the scaling factor (α) is determined as 0.12 following that of AFKF in the

associated range. Other values can be determined from experiential way. The simulation result of FLAS and adaptive fading loop is given in Fig. 6.

Fig. 6 shows the change of the scaling factor α_k and the fading factor λ_k. The values of α_k and λ_k change very steeply to correct the position error from the beginning and the estimate $\hat{s}_k$ gets close to the real value within ε-neighborhood about after 1 sec since the fading factor becomes small.

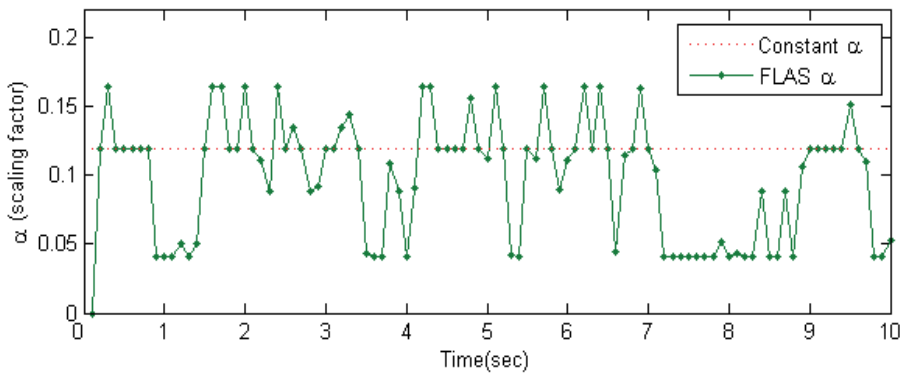

(a) Change of Scaling factor

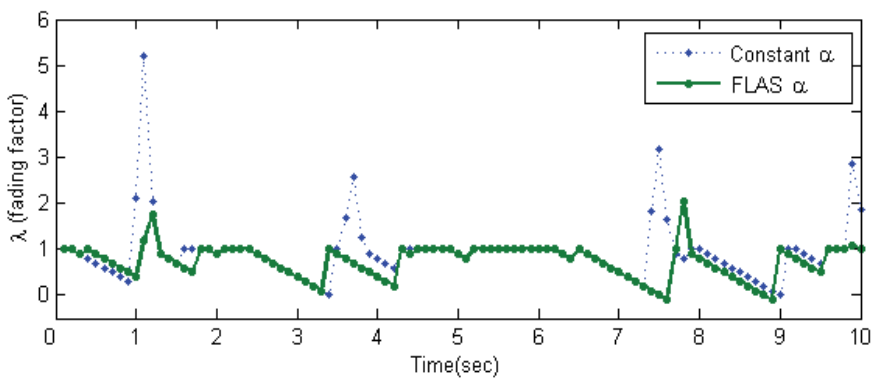

(b) Change of Fading factor

Fig. 6. Change of scaling factor (α) and fading factor (λ).

Fig. 7 shows the performance of the proposed geolocation algorithm (FAFKF) through the comparison with AFKF and EKF. The performance is measured in terms of the norm of positioning error, i.e. $\|s_k - \hat{s}_k\|$. As shown in Fig. 7, the positioning error of FAFKF is much smaller than that of EKF. It can be confirmed that the difference of position error between EKF and FAFKF is increased as the MS changes its direction more frequently. It means that the position estimation with FAFKF is tracking more precisely to the real value of s_k than

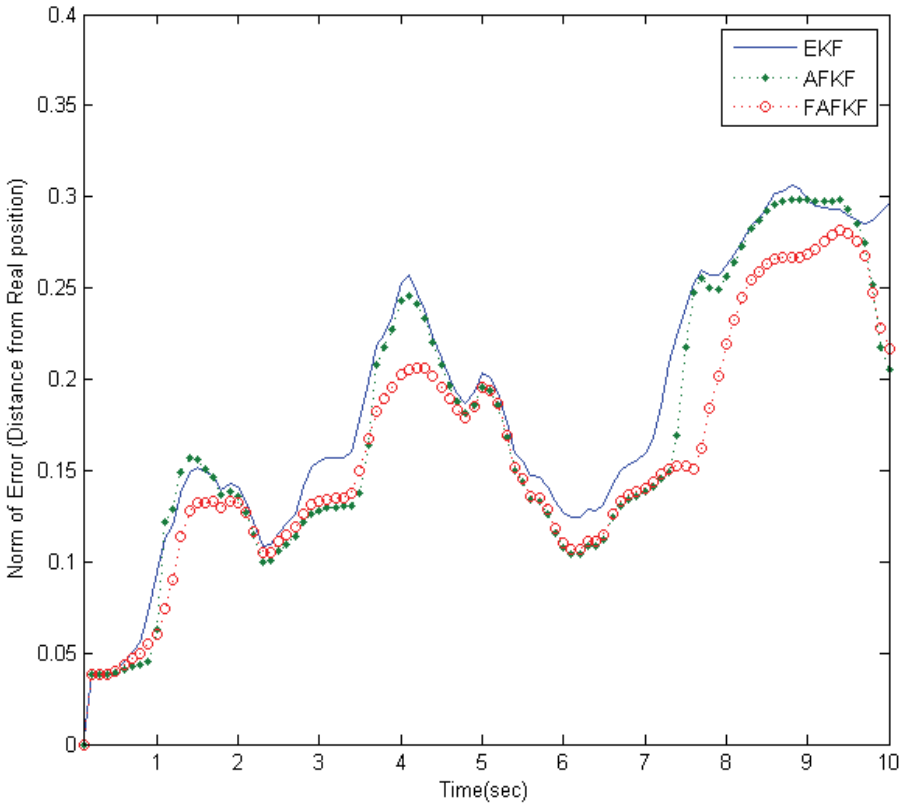

Fig. 7. Comparison of error performance

AFKF or the standard EKF.

Fig. 8 indicates the path estimation performance of the proposed geolocation algorithm through the comparison with AFKF and EKF under the situation of Fig. 4. As the adaptive fading factor takes the sub-optimal value at each iteration, the error covariance has been updated and is used to modify the Kalman filter gain adaptively. As shown in Fig. 8, the trajectory estimation using FAFKF is close to the real value under noise added real circumstance.

5. Conclusion

In this chapter, we introduced TDoA geolocation algorithm to reduce the position estimation error. To be more similar to real circumstance, the MS is supposed to change its direction periodically. The standard EKF which solves a huge computational problem of TDoA based geolocaion can estimate the location of source through the linearization of nonlinear measurement equation. However, the linearization from partial differentiation causes a divergence problem which restricts the performance of the EKF.

To solve this problem, we applied FAFKF algorithm which changes the error covariance using an adaptive fading factor (λ) from fuzzy logic. The scaling factor α which is used

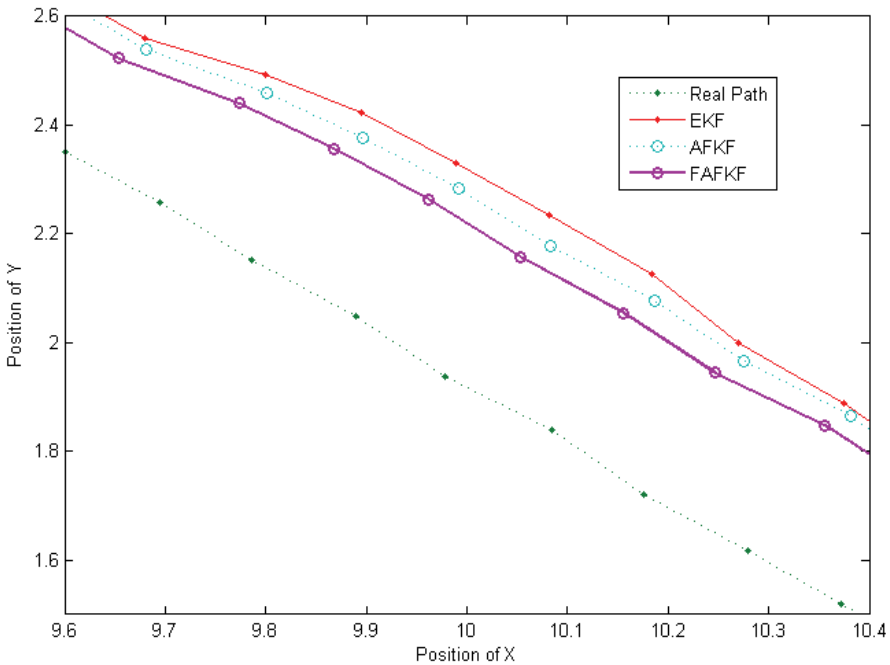

Fig. 8. Comparison of path estimation.

to update the fading factor has been decided by the fuzzy logic to minimize the estimation error. Through the simulation results, it is confirmed that the trajectory estimation using FAFKF follows the real one more precisely than EKF. The positioning error from FAFKF is less than that performed by AFKF.

6. References

Gleason, C.P. (2006). *Tracking human movement in an indoor environment using mobility profiles*, M.S. thesis, University of Nebraska-Lincoln, August, 2006.

Ho, K.C. & Chan, Y.T. (1993). Solution and performance analysis of geolocation by TDoA, *IEEE Tr. Aerospace & Electronic Systems,* Vol. 29, No. 4, pp. 1311-1322, 1993.

Julier, S.J. & Uhlmann, J.K. (2004). Unscented filtering and nonlinear estimation, *IEEE Review*, Vol. 92, No. 3, pp. 401-422, 2004.

Kim K.H., Lee, J.G. & Park, C.G. (2006). Adaptive two-stage EKF for INS-GPS loosely coupled system with unknown fault bias, *Jour. of Global Positioning System,* Vol. 5, pp. 62-69, 2006.

Levy, L.J. (1997). The Kalman filter: navigation's integration workhorse, *Annual report in Applied Physics Laboratory*, Johns Hopkins University, 1997.

Liu, J.M., Zhang, C. & Liu, S. (2006). A TDOA location algorithm based on data fusion, *Frontiers of Electronical and Electronic Engineering in China*, Vol. 1, No.3, pp. 330-333, 2006.

Madhavan, R. & Schlenoff, C. (2004). The effect of process models on short-term prediction of moving objects for unmanned ground vehicles, *International IEEE Conf. Intelligent Transportation Systems*, Vol. 1, pp. 471-476, 2004.

Najar, M. & Vidal, J. (2001). Kalman tracking based on TDOA for UMTS mobile location, *IEEE International Symp. Personal, Indoor and Mobile Radio Communications*, Vol. 1, pp. B45-B49, 2001.

Schau, H.C. & Robinson, A.Z. (1987). Passive source localization employing intersecting spherical surfaces from Time-of-Arrival differences, *IEEE Tr. Acoustics, Speech, & Signal Processing*, Vol. ASSP-35, No. 8, pp. 1223-1225, 1987.

Torrieri, D.J. (1984). Statistical theory of passive location systems, *IEEE Tr. on Aerospace and Electronic Systems,* Vol. AES-20, No. 2, pp. 183-197, 1984.

Xia, Q., Rao, M., Ying, Y. & Shen, X. (1994). Adaptive fading Kalman filter with an application, *Automatica*, Vol. 30, No. 8, pp. 1333-1338, 1994.

Xiong, J.Y., Wang, W. & Zhu, Z.L. (2003). An improved Taylor algorithm inTDOA subscriber position location, *Proc. of ICCT*, Vol. 2, pp. 981-984, 2003.

16

Adaptive Control for a Class of Non-affine Nonlinear Systems via Neural Networks

Zhao Tong
School of Automatization and Electronic Engineering, Qingdao University of Science and Technology
China

1. Introduction

Adaptive control of highly uncertain nonlinear dynamic systems has been an important research area in the past decades, and in the meantime neural networks control has found extensive application for a wide variety of areas and has attracted the attention of many control researches due to its strong approximation capability. Many significant results on these topics have been published in the literatures (Lewis et al., 1996 ; Yu & Li 2002; Yesidirek & Lewis 1995). It is proved to be successful that neural networks are used in adaptive control. However, most of these works are applicable for a kind of affine systems which can be linearly parameterized. Little has been found for the design of specific controllers for the nonlinear systems, which are implicit functions with respect to control input. We can find in literatures available there are mainly the results of Calise et al. (Calise & Hovakimyan 2001) and Ge et al. (Ge et al. 1997). Calise et al. removed the affine in control restriction by developing a dynamic inversion based control architecture with linearly parameterized neural networks in the feedback path to compensate for the inversion error introduced by an approximate inverse. However, the proposed scheme does not relate to the properties of the functions, therefore, the special properties are not used in design. Ge, S.S. et al., proposed the control schemes for a class of non-affine dynamic systems, using mean value theorem, separate control signals from controlled plant functions, and apply neural networks to approximate the control signal, therefore, obtain an adaptive control scheme.
Furthermore, when controlling large-scale and highly nonlinear systems, the presupposition of centrality is violated due to either due to problems in data gathering when is spread out or due to the lack of accurate mathematical models. To avoid the difficulties, the decentralized control architecture has been tried in controller design. Decentralized control systems often also arise from various complex situations where there exist physical limitations on information exchange among several subsystems for which there is insufficient capability to have a single central controller. Moreover, difficulty and uncertainty in, measuring parameter values within a large-scale system may call for adaptive techniques. Since these restrictions encompass a large group of applications, a variety of decentralized adaptive techniques have been developed (Ioannou 1986).

Earlier literature on the decentralized control methods were focused on control of large-scale linear systems. The pioneer work by Siljak (Siljak 1991) presents stability theorems of interconnected linear systems based on the structure information only. Many works consider subsystems which are linear in a set of unknown parameters (Ioannou 1986 ; Fu 1992 ; Sheikholeslam & Desor 1993 ; Wen 1994 ; Tang et al. 2000), and these results were focused on systems with first order interconnections. When the subsystems has nonlinear dynamics or the interconnected is entered in a nonlinear fashion, the analysis and design problem becomes even challenging.

The use of neural networks' learning ability avoids complex mathematical analysis in solving control problems when plant dynamics are complex and highly nonlinear, which is a distinct advantage over traditional control methods. As an alternative, intensive research has been carried out on neural networks control of unknown nonlinear systems. This motivates some researches on combining neural networks with adaptive control techniques to develop decentralized control approaches for uncertain nonlinear systems with restrictions on interconnections. For example, in (Spooner & Passino 1999), two decentralized adaptive control schemes for uncertain nonlinear systems with radial basis neural networks are proposed, which a direct adaptive approach approximates unknown control laws required to stabilize each subsystem, while an indirect approach is provided which identifies the isolated subsystem dynamics to produce a stabilizing controller. For a class of large scale affine nonlinear systems with strong interconnections, two neural networks are used to approximate the unknown subsystems and strong interconnections, respectively (Huang & Tan 2003), and Huang & Tan (Huang & Tan 2006) introduce a decomposition structure to obtain the solution to the problem of decentralized adaptive tracking control a class of affine nonlinear systems with strong interconnections. Apparently, most of these results are likewise applicable for affine systems described as above. For the decentralized control research of non-affine nonlinear systems, many results can be found from available literatures. Nardi et al. (Nardi & Hovakimyan 2006) extend the results in Calise et al. (Calise & Hovakimyan 2001) to non-affine nonlinear dynamical systems with first order interconnections. Huang (Huang & Tan 2005) apply the results in (Ge & Huang 1999) to a class of non-affine nonlinear systems with strong interconnections.

Inspired by the above researches, in this chapter, we propose a novel adaptive control scheme for non-affine nonlinear dynamic systems. Although the class of nonlinear plant is the same as that of Ge et al. (Ge et al. 1997), utilizing their nice reversibility, and invoking the concept of pseudo-control and inverse function theorem, we find the equitation of error dynamics to design adaptation laws. Using the property of approximation of two-layer neural networks (NN), the control algorithm is gained. Then, the controlled plants are extended to large-scale decentralized nonlinear systems, which the subsystems are composed of the class of non-affine nonlinear functions. Two schemes are proposed, respectively. The first scheme designs a RBFN-based (radial basis function neural networks) adaptive control scheme with the assumption which the interconnections between subsystems in entire system are bounded linearly by the norms of the tracking filtered error. In the scheme, unlike most of other approaches in available literatures, the weight of BBFN and center and width of Gaussian function are tuned adaptively. In another scheme, the interconnection is assumed as stronger nonlinear function. Moreover, in the former, in every subsystem, a RBFN is adopted which is used to approximate unknown function, and in the latter, in every subsystem, two RBFNs are respectively utilized to approximate unknown

function and uncertain strong interconnection function. For those complicated large-scale decentralized dynamic systems, in order to decrease discontinuous factors and make systems run smooth, unlike most of control schemes, the hyperbolic tangent functions are quoted in the design of robust control terms, instead of sign function. Otherwise, the citation of the smooth function is necessary to satisfy the condition of those theorems.
The rest of the paper is organized as follows. Section 2 gives the normal form of a class of non-affine nonlinear systems. Section 3 proposes a novel adaptive control algorithm, which is strictly derived from some mathematical and Lyapunov stability theories, and the effectiveness of the scheme is validated through simulation. Extending the above-mentioned result, Section 4 discusses two schemes of decentralized adaptive neural network control for the class of large-scale nonlinear systems with linear function interconnections and nonlinear function interconnections, respectively. Finally, the Section 5 is concluding remarks.

2. Problem Statement

We consider a general analytic system

$$\begin{cases} \dot{\zeta} = \mathbf{g}(\zeta, u), \quad \zeta \in R^n, \quad u \in R \\ y = h(\zeta), \qquad y \in R. \end{cases} \tag{1}$$

where $\mathbf{g}(\cdot,\cdot)$ is a smooth vector fields and $h(\cdot)$ is a scalar function. In practice, many physical systems such as chemical reactions, PH neutralization and distillation columns are inherently nonlinear, whose input variables may enter in the systems nonlinearly as described by the above general form (Ge et al. 1998). Then, the Lie derivative (Tsinias & Kalouptsidis 1983) of $h(\zeta)$ with respect to $\mathbf{g}(\zeta,u)$ is a scalar function defined by $L_{\mathbf{g}}h = [\partial h(\zeta)/\partial\zeta]\mathbf{g}(\zeta,u)$. Repeated Lie derivatives can be defined recursively as $L_{\mathbf{g}}^{i}h = L_{\mathbf{g}}(L_{\mathbf{g}}^{i-1}h), \quad for \quad i = 1, 2\cdots$. The system (1) is said to have relative degree α at $(\zeta_{\mathbf{0}}, u_0)$, if there exists a smallest positive integer α such that $\partial L_{\mathbf{g}}^{i}h/\partial u = 0$, $\partial L_{\mathbf{g}}^{\alpha}h/\partial u \neq 0, \quad i = 1,\cdots,\alpha-1$.

Let $\Omega_\zeta \subset R^n$ and $\Omega_u \subset R$ be compact subsets containing $\zeta_{\mathbf{0}}$ and u_0 , respectively. System (1) is said to have a strong relative degree α in a compact set $D = \Omega_\zeta \times \Omega_u$, if it has relative degree α at every point $(\zeta_{\mathbf{0}}, u_0) \in D$. Therefore, system (1) is feedback linearizable and the mapping $\Phi(\zeta) = [\phi_1(\zeta), \phi_2(\zeta), \cdots \phi_n(\zeta)]$, with $\phi_j(\zeta) = L_{\mathbf{g}}^{j-1}h, \quad j = 1, 2, \cdots \alpha$ has a Jacobian matrix which is nonsingular for all $\mathbf{x} \in \Phi(\zeta)$, system (1) can be transformed into a normal form

$$\begin{cases} \dot{x}_1 = x_2 \\ \dot{x}_2 = x_3 \\ \quad \vdots \\ \dot{x}_n = f(x,u) \\ y = x_1 \end{cases} \tag{2}$$

where $f(x,u) = L_{\mathbf{g}}^{n} h$ and $x = \Phi^{-1}(\boldsymbol{\zeta})$ with $x = [x_1, x_2, \cdots, x_n]^T$. Define the domain of normal system (2) as $\bar{D} \triangleq \left\{ (x,u) \middle| x \in \Phi(\Omega_{\zeta}); u \in \Omega_u \right\}$.

3. Adaptive Control for a Class of Non-affine Nonlinear Systems via Two-Layer Neural Networks

Now we consider the $n-th$ order nonlinear systems of the described form as (2). For the considered systems in the chapter, we may make the following assumptions.

Assumption 1. $\partial f(x,u)/\partial u \neq 0$ for all $(x,u) \in \Omega \times R$.

Assumption 2. $f(\cdot): R^{n+1} \to R$, is an unknown continuous function and $f(x,u)$ a smooth function with respect to control input u.

The control objective is: determine a control law, force the output, y, to follow a given desired output, x_d with an acceptable accuracy, while all signals involved must be bounded.

Assumption 3. The desired signals $x_d(t) = [y_d, y_d^{(1)}, \cdots, y_d^{(n-1)}]$, and $X_d = [x_d^T, y_d^{(n)}]^T$ are bounded, with $\|X_{\mathbf{d}}\| \leq \bar{X}_d$, $\bar{X}_d$ a known positive constant.

Define the tracking error vector as

$$e = x - x_d, \tag{3}$$

and a filtered tracking error as

$$\tau = [\Lambda^T \quad 1] e, \tag{4}$$

with Λ a gain parameter vector selected so that $e(t) \to 0$ as $\tau \to 0$. Differentiating (4), the filtered tracking error can be written as

$$\dot{\tau} = \dot{x}_n - x_d^{(n)} + [0 \quad \Lambda^T]\mathbf{e}. \tag{5}$$

Define a continuous function

$$\delta = -k\tau + x_d^{(n)} - [0 \quad \Lambda^T]\mathbf{e}. \tag{6}$$

where k is a positive constant. We know $\partial f(x,u)/\partial u \neq 0$ (Assumption 1), thus, $\partial[f(x,u)-\delta]/\partial u \neq 0$. Considering the fact that $\partial\delta/\partial u = 0$, we invoke the implicit function theorem (Lang 1983), there exists a continuous ideal control input u^* in a neighborhood of $(x,u) \in \Omega \times R$, such that $f(x,u^*)-\delta = 0$, i.e. $\delta = f(x,u^*)$ holds. $\delta = f(x,u^*)$ may represent ideal control inverse.

Adding and subtracting δ to the right-hand side of $\dot{x}_n = f(x,u)$ of (2), one obtains

$$\dot{x}_n = f(x,u) - \delta - k\tau + x_d^{(n)} - [0 \quad \Lambda^T]e, \tag{7}$$

and yields

$$\dot{\tau} = -k\tau + f(x,u) - \delta. \tag{8}$$

Considering the following state dependent transformation $\psi = \dot{x}_n$, where ψ is commonly referred to as the pseudo-control (Calise & Hovakimyan 2001). Apparently, the pseudo-control is not a function of the control u but rather a state dependent operator. Then, $\partial\psi/\partial u = 0$, from Assumption 1, $\partial f(x,u)/\partial u \neq 0$ thus $[\psi - f(x,u)]/\partial u \neq 0$. With the implicit function theorem, for every $(x,u) \in \Omega \times R$, there exists a implicit function such that $\psi - f(x,u) = 0$ holds, i.e. $\psi = f(x,u)$. Therefore, we have

$$\psi = f(x,u). \tag{9}$$

Furthermore, using inverse function theorem, with the fact that $[\psi - f(x,u)]/\partial u \neq 0$ and $f(x,u)$ is a smooth with respect to control input, u, then, $f(x,u)$ defines a local diffeomorphism (Slotine & Li 1991), such that, for a neighborhood of u, there exists a smooth inverse function and $u = f^{-1}(x,\psi)$ holds. If the inverse is available, the control problem is easy. But this inverse is not known, we can generally use some techniques, such as neural networks, to approximate it. Hence, we can obtain an estimated function, $\hat{u} = f^{-1}(x,\hat{\psi})$. This result in the following equation holding:

$$\hat{\psi} = f(x,\hat{u}), \tag{10}$$

where $\hat{\psi}$ may be referred to as approximation pseudo-control input which represents actual dynamic approximation inverse.

Remark 1. According to the above-mentioned conditions, when one designs the pseudo-control signal, $\hat{\psi}$, must be a smooth function. Therefore, in order to satisfy the condition, we adopt hyperbolic tangent function, instead of sign function in design of input. This also makes control signal tend smooth and system run easier. The hyperbolic tangent function has a good property as follows (Polycarpou 1996) :

$$0 < |\eta| - \eta \tanh(\frac{\eta}{\alpha}) \le \varsigma\alpha , \tag{11}$$

with $\varsigma = 0.2785$, α any positive constant. Moreover, theoretically, $\hat{\psi}$ is approximation inverse, generally a nonlinear function, but it must be bounded and play a dynamic approximation role and make system stable. Hence, it represents actual dynamic approximation inverse.

Based on the above conditions, in order to control the system and make it be stable, we design the approximation pseudo-control input $\hat{\psi}$ as follows:

$$\hat{\psi} = f(x, u^*) + u_{ad} + v_r , \tag{12}$$

where u_{ad} is output of a neural network controller, which adopts a two-layer neural network, v_r is robustifying control term designed in stability analysis.

Adding and subtracting $\hat{\psi}$ to the right-hand side of (8), with $\delta = f(x, u^*)$, we have

$$\begin{aligned} \dot{\tau} &= -k\tau + f(x,u) + \hat{\psi} - f(x,u^*) - u_{ad} - v_r - \delta \\ &= -k\tau + \tilde{\Delta}(x,u,u^*) + \hat{\psi} - \delta - u_{ad} - v_r , \end{aligned} \tag{13}$$

where $\tilde{\Delta}(x,u,u^*) = f(x,u) - f(x,u^*)$ is error between nonlinear function and its ideal control function, we can use the neural network to approximate it.

3.1 Neural network-based approximation

A two-layer NN consists of two layers of tunable weights, a hidden layer and an output layer. Given a $\varepsilon > 0$, there exists a set of bounded weights M and N such that the nonlinear error $\tilde{\Delta} \in C(\Omega)$, with Ω compact subset of R^n , can be approximated by a two-layer neural network, i.e.

$$\tilde{\Delta} = M^T \sigma(N^T x_{nn}) + \varepsilon(x_{nn}) , \tag{14}$$

with $x_{nn} = [1, x_d^T, e^T, \hat{\psi}]$ input vector of NN.

Assumption 4. The approximation error ε is bounded as follows:

$$|\varepsilon| \le \varepsilon_N, \tag{15}$$

where $\varepsilon_N > 0$ is an unknown constant.

Let $\hat{M}$ and $\hat{N}$ be the estimates respectively of M and N. Based on these estimates, let u_{ad} be the output of the NN

$$u_{ad} = \hat{M}^T \sigma(\hat{N}^T x_{nn}). \tag{16}$$

Define $\tilde{M} = M - \hat{M}$ and $\tilde{N} = N - \hat{N}$, where we use notations: $Z = diag[M, N]$, $\tilde{Z} = diag[\tilde{M}, \tilde{N}]$, $\hat{Z} = diag[\hat{M}, \hat{N}]$ for convenience. Then, the following inequality holds:

$$tr(\tilde{Z}^T \hat{Z}) \le \|\tilde{Z}\|_F \|Z\|_F - \|\tilde{Z}\|_F^2. \tag{17}$$

The Taylor series expansion of $\sigma(N^T x_{nn})$ for a given x_{nn} can be written as:

$$\sigma(N^T x_{nn}) = \sigma(\hat{N}^T x_{nn}) + \sigma'(\hat{N}^T x_{nn}) \tilde{N}^T x_{nn} + O(\tilde{N}^T x_{nn})^2, \tag{18}$$

with $\hat{\sigma} := \sigma(\hat{N}^T x_{nn})$ and $\hat{\sigma}'$ denoting its Jacobian, $O(\tilde{N}^T x_{nn})^2$ the term of order two. In the following, we use notations: $\sigma := \sigma(N^T x_{nn})$, $\tilde{\sigma} := \sigma(\tilde{N}^T x_{nn})$.

With the procedure as Appendix A, the approximation error of function can be written as

$$M^T \sigma(N^T x_{nn}) - \hat{M}^T \sigma(\hat{N}^T x_{nn}) = \tilde{M}^T (\hat{\sigma} - \hat{\sigma}' \hat{N}^T x_{nn}) + \hat{M}^T \hat{\sigma}' \tilde{N}^T x_{nn} + \omega, \tag{19}$$

and the disturbance term ω can be bounded as

$$|\omega| \le \|N\|_F \left\| x_{nn} \hat{M}^T \hat{\sigma}' \right\|_F + \|M\| \left\| \hat{\sigma}' \hat{N}^T x_{nn} \right\| + \|M\|_1, \tag{20}$$

where the subscript "F" denotes Frobenius norm, and the subscript "1" the 1-norm. Redefine this bound as

$$|\omega| \le \rho_\omega \vartheta_\omega(\hat{M}, \hat{N}, x_{nn}), \tag{21}$$

where $\rho_\omega = \max\{\|M\|, \|N\|_F, \|M\|_1\}$ and $\vartheta_\omega = \left\|x_{nn}\hat{M}^T\hat{\sigma}'\right\|_F + \left\|\hat{\sigma}'\hat{N}^T x_{nn}\right\| + 1$. Notice that ρ_ω is an unknown coefficient, whereas ϑ_ω is a known function.

3.2 Parameters update law and stability analysis

Substituting (14) and (16) into (13), we have

$$\dot{\tau} = -k\tau + M^T\sigma(N^T x_{nn}) - \hat{M}^T\sigma(\hat{N}^T x_{nn}) + \psi - v_r - \delta + \varepsilon(x_{nn}). \tag{22}$$

Using(19), the above equation can become

$$\dot{\tau} = -k\tau + \tilde{M}^T(\hat{\sigma} - \hat{\sigma}'\hat{N}^T x_{nn}) + \hat{M}^T\hat{\sigma}'\tilde{N}^T x_{nn} + \psi - \delta - v_r + \omega + \varepsilon. \tag{23}$$

Theorem 1. Consider the nonlinear system represented by Eq. (2) and let Assumption 1-4 hold. If choose the approximation pseudo-control input $\hat{\psi}$ as Eq.(12), use the following adaptation laws and robust control law

$$\begin{aligned}
\dot{\hat{M}} &= F\left[(\hat{\sigma} - \hat{\sigma}'Nx_{nn})\tau - k_1\hat{M}|\tau|\right], \\
\dot{\hat{N}} &= R\left[x_{nn}\hat{M}^T\hat{\sigma}'\tau - k_1\hat{N}|\tau|\right], \\
\dot{\hat{\phi}} &= \gamma\left\{\tau(\vartheta_\omega + 1)\tanh\left[\frac{\tau(\vartheta_\omega + 1)}{\alpha}\right] - \lambda\hat{\phi}\right\} \\
v_r &= -\hat{\phi}(\vartheta_\omega + 1)\tanh\left[\frac{\tau(\vartheta_\omega + 1)}{\alpha}\right]
\end{aligned} \tag{24}$$

where $F = F^T > 0, R = R^T > 0$ are any constant matrices, $k_1 > 0$ and $\gamma > 0$ are scalar design parameters, $\hat{\phi}$ is the estimated value of the uncertain disturbance term $\phi = \max(\rho_\omega, \varepsilon_N)$, defining $\tilde{\phi} = \phi - \hat{\phi}$ with $\tilde{\phi}$ error of ϕ, then, guarantee that all signals in the system are uniformly bounded and that the tracking error converges to a neighborhood of the origin.

Proof. Consider the following positive define Lyapunov function candidate as

$$L = \frac{1}{2}\tau^2 + \frac{1}{2}tr(\tilde{M}^T F^{-1}\tilde{M}) + \frac{1}{2}tr(\tilde{N}^T R^{-1}\tilde{N}) + \frac{1}{2}\gamma^{-1}\tilde{\phi}^2 \tag{25}$$

The time derivative of the above equation is given by

$$\dot{L} = \dot{\tau}\tau + tr(\tilde{M}^T F^{-1}\dot{\tilde{M}}) + tr(\tilde{N}^T R^{-1}\dot{\tilde{N}}) + \gamma^{-1}\tilde{\phi}\dot{\tilde{\phi}} \tag{26}$$

Substituting (23) and the anterior two terms of (24) into (26), after some straightforward manipulations, we obtain

$$\begin{aligned}\dot{L} &= -k\tau^2 + \tau[\tilde{M}^T(\hat{\sigma} - \hat{\sigma}'\hat{N}^T x_{nn}) + \hat{M}^T\hat{\sigma}'\tilde{N}^T x_{nn} + (\hat{\psi} - \delta) - v_r + \omega + \varepsilon] \\ &\quad + tr(\tilde{M}^T F^{-1}\dot{\tilde{M}}) + tr(\tilde{N}^T R^{-1}\dot{\tilde{N}}) + \gamma^{-1}\tilde{\phi}\dot{\tilde{\phi}} \\ &= -k\tau^2 + \tau(\hat{\psi} - \delta) - \tau v_r + \tau(\omega + \varepsilon) + \gamma^{-1}\tilde{\phi}\dot{\tilde{\phi}} + k_1|\tau|tr(\tilde{Z}^T\hat{Z}). \\ &\le -k\tau^2 + \tau(\hat{\psi} - \delta) - \tau v_r + |\tau|\phi(\vartheta_\omega + 1) + \gamma^{-1}\tilde{\phi}\dot{\tilde{\phi}} + k_1|\tau|tr(\tilde{Z}^T\hat{Z}).\end{aligned} \tag{27}$$

With (4),(6),(12),(16) and the last two equations of (24), the approximation error between actual approximation inverse and ideal control inverse is bounded by

$$|\hat{\psi} - \delta| \le c_1 + c_2|\tau| + c_3\left\|\tilde{Z}\right\|_F, \tag{28}$$

where c_1, c_2, c_3 are positive constants.

Using (11) and the last two terms of (24), we obtain

$$\begin{aligned}\dot{L} &\le -k\tau^2 + \tau(\hat{\psi} - \delta) - \tau\hat{\phi}(\vartheta_\omega + 1)\tanh\left[\frac{\tau(\vartheta_\omega + 1)}{\alpha}\right] \\ &\quad + |\tau|\phi(\vartheta_\omega + 1) - \tilde{\phi}\left\{\tau(\vartheta_\omega + 1)\tanh\left[\frac{\tau(\vartheta_\omega + 1)}{\alpha}\right] - \lambda\hat{\phi}\right\} + k_1|\tau|tr(\tilde{Z}^T\hat{Z}) \\ &\le -k\tau^2 + \tau(\hat{\psi} - \delta) + \varsigma\phi\alpha + \lambda\tilde{\phi}\hat{\phi} + k_1|\tau|tr(\tilde{Z}^T\hat{Z})\end{aligned} \tag{29}$$

Applying (17),(28) , and $\tilde{\phi}\hat{\phi} \le |\tilde{\phi}||\phi| - |\tilde{\phi}|^2$, after completing square, we have the following inequality

$$\dot{L} \le -(k - c_2)|\tau|^2 + D_1|\tau| + D_2 \tag{30}$$

where $D_1 = c_1 + \frac{k_1}{4}(Z_M + \frac{c_3}{k_1})^2, D_2 = \frac{1}{4}\lambda\phi^2 + \varsigma\phi\alpha$.

Let $D_3 = \sqrt{D_1^2 + 4D_2(k - c_2)} + D_1$, thus, as long as $|\tau| \ge D_3/[2(k - c_2)]$, and $k > c_2$, then $\dot{L} \le 0$ holds.

Now define

$$\Omega_\phi = \left\{\tilde{\phi}\ \middle|\ |\tilde{\phi}| \le \phi\right\},\ \ \Omega_Z = \left\{\tilde{Z}\ \middle|\ \|\tilde{Z}\|_F \le \frac{1}{k_1}(k_1 Z_M + c_3)\right\},\ \ \Omega_\tau = \left\{\tau\ \middle|\ |\tau| \le \frac{1}{2(k-c_2)} D_3\right\}. \quad (31)$$

Since $Z_M, k_1, k, D_1, D_2, D_3, c_2, c_3$ are positive constants, as long as k is chosen to be big enough, such that $k > c_2$ holds, we conclude that Ω_ϕ, Ω_Z and Ω_τ are compact sets. Hence $\dot{L}$ is negative outside these compacts set. According to a standard Lyapunov theorem, this demonstrates that $\tilde{\phi}, \tilde{Z}$ and τ are bounded and will converge to Ω_ϕ, Ω_Z and Ω_τ, respectively. Furthermore, this implies e is bounded and will converge to a neighborhood of the origin and all signals in the system are uniformly bounded.

3.3 Simulation Study

In order to validate the performance of the proposed neural network-based adaptive control scheme, we consider a nonlinear plant, which described by the differential equation

$$\begin{aligned} \dot{x}_1 &= x_2 \\ \dot{x}_2 &= -\omega^2 x_1 - 0.02(\omega + x_1^2)x_2 + u^3 + (x_1^2 + x_2^2)\sigma(u) + \tanh(0.2u) + d \end{aligned} \quad (32)$$

where $\omega = 0.4\pi$, $\sigma(u) = (1-e^{-u})/(1+e^{-u})$ and $d = 0.2$. The desired trajectory $x_d = 0.1\pi[\sin(2t) - \cos(t)]$.

To show the effectiveness of the proposed method, two controllers are studied for comparison. A fixed-gain PD control law is first used as Polycarpou, (Polycarpou 1996). Then, the adaptive controller based on NN proposed is applied to the system.

Input vector of neural network is $x_{nn} = [1, x_d^T, e^T, \hat{\psi}]$, and number of hidden layer nodes 25. The initial weight of neural network is $\hat{M}(0) = (0), \hat{N}(0) = (0)$. The initial condition of controlled plant is $x(0) = [0.1, 0.2]^T$. The other parameters are chosen as follows: $k_1 = 0.01, \gamma = 0.1, \lambda = 0.01, \alpha = 10$, $\Lambda = 2, F = 8I_M$, $R = 5I_N$, with I_M, I_N corresponding identity matrices.

Fig.1, 2, and 3 show the results of comparisons, the PD controller and the adaptive controller based on NN proposed, of tracking errors, output tracking and control input, respectively. These results indicate that the adaptive controller based on NN proposed presents better control performance than that of the PD controller. Fig.4 depicts the results of output of NN, norm values of $\hat{M}, \hat{N}$, respectively, to illustrate the boundedness of the estimates of $\hat{M}, \hat{N}$ and the control role of NN. From the results as figures, it can be seen that the learning rate of neural network is rapid, and tracks objective in less than 2 seconds. Moreover, as desired, all signals in system, including control signal, tend to be smooth.

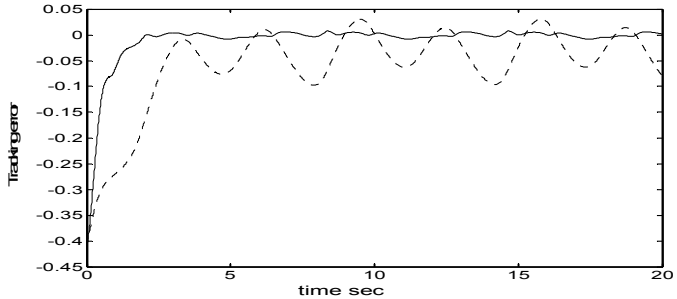

Fig. 1. Tracking errors: PD(dot) and NN(solid).

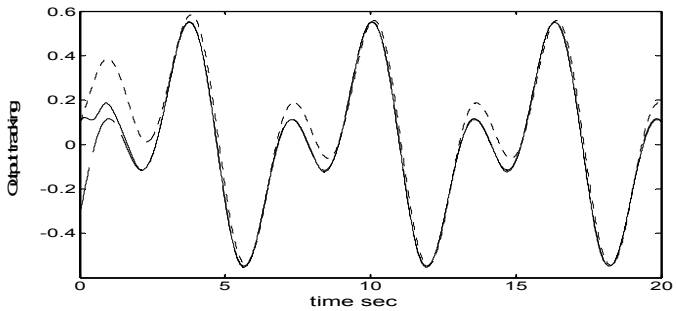

Fig. 2. Output tracking: desired (dash), NN(solid) and PD(dot).

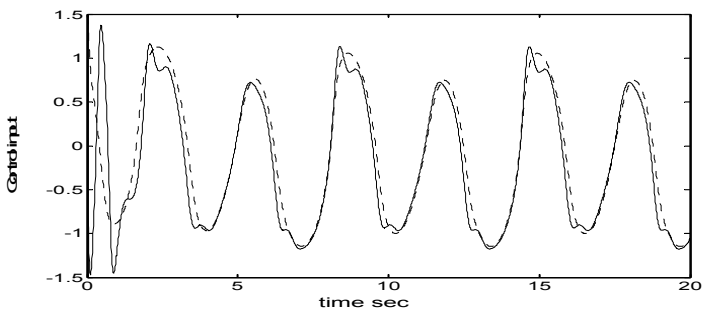

Fig. 3. Control input: PD (dash), NN(solid)

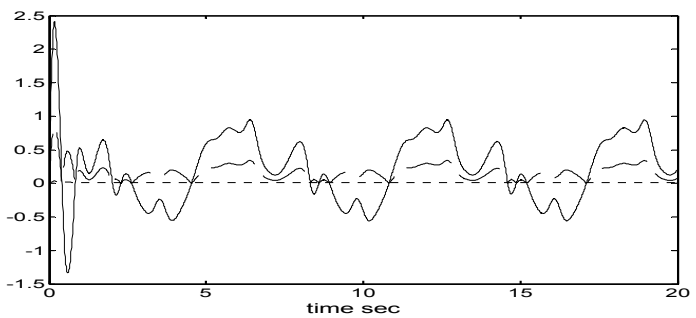

Fig. 4. $\|\hat{M}\|$ (dash), $\|\hat{N}\|$ (dot), output of NN(solid)

4. Decentralized Adaptive Neural Network Control of a Class of Large-Scale Nonlinear Systems with linear function interconnections

In the section, the above proposed scheme is extended to large-scale decentralized nonlinear systems, which the subsystems are composed of the class of the above-mentioned non-affine nonlinear functions. Two schemes are proposed, respectively. The first scheme designs a RBFN-based adaptive control scheme with the assumption which the interconnections between subsystems in entire system are bounded linearly by the norms of the tracking filtered error. In another scheme, the interconnection is assumed as stronger nonlinear function.

We consider the differential equations in the following form described, and assume the large-scale system is composed of the nonlinear subsystems:

$$\begin{cases} \dot{x}_{i1} = x_{i2} \\ \dot{x}_{i2} = x_{i3} \\ \quad \vdots \\ \dot{x}_{il_i} = f_i(x_{i1}, x_{i2}, \cdots, x_{il_i}, u_i) + g_i(x_1, x_2, \cdots, x_n) \\ y_i = x_{i1} \end{cases} \quad (33)$$
$$i = 1, 2, \cdots n,$$

where $x_i \in R^{l_i}$ is the state vector, $x_i = [x_{i1}, x_{i2}, \cdots, x_{il_i}]^T$, $u_i \in R$ is the input and $y_i \in R$ is the output of the $i-th$ subsystem.

$f_i(x_i, u_i) : R^{li+1} \to R$ is an unknown continuous function and implicit and smooth function with respect to control input u_i .

Assumption 5. $\partial f_i(x_i, u_i) / \partial u_i \neq 0$ for all $(x_i, u_i) \in \Omega_i \times R$.

$g_i(x_1, x_2, \cdots, x_n)$ is the interconnection term. In according to the distinctness of the interconnection term, two schemes are respectively designed in the following.

4.1 RBFN-based decentralized adaptive control for the class of large-scale nonlinear systems with linear function interconnections

Assumption 6. The interconnection effect is bounded by the following function:

$$\left| g_i(x_1, x_2, \cdots, x_n) \right| \leq \sum_{j=1}^{n} \gamma_{ij} \left| \tau_j \right|, \quad (34)$$

where γ_{ij} are unknown coefficients, τ_j is a filtered tracking error to be defined shortly .

The control objective is: determine a control law, force the output, y_i , to follow a given desired output, x_{di} , with an acceptable accuracy, while all signals involved must be bounded.

Define the desired trajectory vector $x_{di} = [y_{di}, \dot{y}_{di}, \cdots, y_{di}^{l_i-1}]^T$ and $X_{di} = \left[y_{di}, \dot{y}_{di}, \cdots, y_{di}^{(l_i)} \right]^T$, tracking error $e_i = x_i - x_{di} = [e_{i1}, e_{i2}, \cdots, e_{il_i}]^T$, thus, the filter tracking error can be written as

$$\tau_i = [\Lambda_i^T \quad 1]\mathbf{e}_i = k_{i,1}e_i + k_{i,2}\dot{e}_i + \cdots + k_{i,l_i-1}e_i^{(l_i-2)} + e_i^{(l_i-1)}, \tag{35}$$

where the coefficients are chosen such that the polynomial $k_{i,1} + k_{i,2}s + \cdots + k_{i,l_i-1}s^{(l_i-2)}$ $+s^{(l_i-1)}$ is Hurwitz.

Assumption 7. The desired signal $x_{di}(t)$ is bounded, so that $\left\| X_{di} \right\| \le \overline{X}_{di}$, where $\overline{X}_{di}$ is a known constant.

For an isolated subsystem, without interconnection function, by differentiating (35), the filtered tracking error can be rewritten as

$$\dot{\tau}_i = \dot{x}_{il_l} - x_{di}^{(l_i)} + [0 \quad \Lambda_i^T]e_i = f_i(x_i, u_i) + Y_{di} \tag{36}$$

with $Y_{di} = -x_{di}^{(l_i)} + [0 \quad \Lambda_i^T]e_i$.

Define a continuous function

$$\delta_i = -k_i\tau_i - Y_{di} \tag{37}$$

where k_i is a positive constant. With Assumption 5, we know $\partial f(x_i, u_i)/\partial u_i \neq 0$, thus, $\partial[f(x_i, u_i) - \delta_i]/\partial u_i \neq 0$. Considering the fact that $\partial\delta_i/\partial u_i = 0$, we invoke the implicit function theorem, there exists a continuous ideal control input u_i^* in a neighborhood of $(x_i, u_i) \in \Omega_i \times R$, such that $f(x_i, u_i^*) - \delta_i = 0$, i.e. $\delta_i = f_i(x_i, u_i^*)$ holds. $\delta_i = f_i(x_i, u_i^*)$ represents ideal control inverse.

Adding and subtracting δ_i to the right-hand side of $\dot{x}_{il_i} = f_i(x_i, u_i) + g_i$ of (33), one obtains

$$\dot{x}_{il_i} = f_i(x_i, u_i) + g_i - \delta_i - k_i\tau_i - Y_{di}, \tag{38}$$

and yields

$$\dot{\tau}_i = -k_i\tau_i + f_i(x_i, u_i) + g_i - \delta_i \ . \tag{39}$$

In the same the above-discussed manner as equations (9)-(10) , we can obtain the following equation:

$$\hat{\psi}_i = f_i(x_i, \hat{u}_i) \, . \tag{40}$$

Based on the above conditions, in order to control the system and make it be stable, we design the approximation pseudo-control input $\hat{\psi}_i$ as follows:

$$\hat{\psi}_i = -k_i\tau_i - Y_{di} + u_{ci} + v_{ri} \, , \tag{41}$$

where u_{ci} is output of a neural network controller, which adopts a RBFN, v_{ri} is robustifying control term designed in stability analysis.

Adding and subtracting $\hat{\psi}_i$ to the right-hand side of (39), with $\delta_i = -k_i\tau_i - Y_{di} = f_i(x_i, u_i^*)$, we have

$$\dot{\tau}_i = -k_i\tau_i + \tilde{\Delta}_i(x_i, u_i, u_i^*) - u_{ci} + \hat{\psi}_i - \delta_i - v_{ri} + g_i \, , \tag{42}$$

where $\tilde{\Delta}_i(x_i, u_i, u_i^*) = f_i(x_i, u_i) - f_i(x_i, u_i^*)$ is error between nonlinear function and its ideal control function, we can use the RBFN to approximate it.

4.1.1 Neural network-based approximation

Given a multi-input-single-output RBFN, let n_{1i} and m_{1i} be node number of input layer and hidden layer, respectively. The active function used in the RBFN is Gaussian function, $S_l(\mathbf{x}) = \exp[-0.5(\|z_i - \mu_{lk}\|^2)/\sigma_k^2]$, $l = 1, \cdots, n_{1i}$, $k = 1, \cdots, m_{1i}$ where $z_i \in R^{n_{1i}\times 1}$ is input vector of the RBFN, $\mu_i \in R^{n_{1i}\times m_{1i}}$ and $\sigma_i \in R^{m_{1i}\times 1}$ are the center matrix and the width vector.

Based on the approximation property of RBFN, $\tilde{\Delta}_i(x_i, u_i, u_i^*)$ can be written as

$$\tilde{\Delta}_i(x_i, u_i, u_i^*) = W_i^T S_i(z_i, \mu_i, \sigma_i) + \varepsilon_i(z_i) \, , \tag{43}$$

where $\varepsilon_i(z_i)$ is approximation error of RBFN, $W_i \in R^{m_{1i}\times 1}$.

Assumption 8. The approximation error $\varepsilon(x_{nn})$ is bounded by $|\varepsilon_i| \le \varepsilon_{Ni}$, with $\varepsilon_{Ni} > 0$ is an unknown constant.

The input of RBFN is chosen as $z_i = [x_i^T, \tau_i, \hat{\psi}_i]^T$. Moreover, output of RBFN is designed as

$$u_{ci} = \hat{W}_i^T S_i(z_i, \hat{\mu}_i, \hat{\sigma}_i). \tag{44}$$

Define $\hat{W}_i, \hat{\mu}_i, \hat{\sigma}_i$ as estimates of ideal W_i, μ_i, σ_i, which are given by the RBFN tuning algorithms.

Assumption 9. The ideal values of W_i, μ_i, σ_i satisfy

$$\|W_i\| \le W_{iM}, \quad \|\mu_i\|_F \le \mu_{iM}, \quad \|\sigma_i\| \le \sigma_{iM}, \tag{45}$$

where $W_{iM}, \mu_{iM}, \sigma_{iM}$ are positive constants. $\|\cdot\|_F$ and $\|\cdot\|$ denote Frobenius norm and 2-norm, respectively. Define their estimation errors as

$$\tilde{W}_i = W_i - \hat{W}_i, \quad \tilde{\mu}_i = \mu_i - \hat{\mu}_i, \quad \tilde{\sigma}_i = \sigma_i - \hat{\sigma}_i. \tag{46}$$

Using the notations: $Z_i = diag[W_i, \mu_i, \sigma_i], \tilde{Z}_i = diag[\tilde{W}_i, \tilde{\mu}_i, \tilde{\sigma}_i], \hat{Z}_i = diag[\hat{W}_i, \hat{\mu}_i, \hat{\sigma}_i]$ for convenience.

The Taylor series expansion for a given μ_i and σ_i is

$$S_i(z_i, \mu_i, \sigma_i) = S_i(z_i, \hat{\mu}_i, \hat{\sigma}_i) + \hat{S}'_{\mu i}\tilde{\mu}_i + \hat{S}'_{\sigma i}\tilde{\sigma}_i + O(\tilde{\mu}_i, \tilde{\sigma}_i)^2 \tag{47}$$

where $\hat{S}'_{\mu i} \triangleq \partial S_k(z_i, \hat{\mu}_i, \hat{\sigma}_i)/\partial \mu_i, \quad \hat{S}'_{\sigma i} \triangleq \partial S_k(z_i, \hat{\mu}_i, \hat{\sigma}_i)/\partial \sigma_i$ evaluated at $\mu_i = \hat{\mu}_i$, $\sigma_i = \hat{\sigma}_i, O(\tilde{\mu}_i, \tilde{\sigma}_i)^2$ denotes the terms of order two. We use notations: $\hat{S}_i := S_i(z_i, \hat{\mu}_i, \hat{\sigma}_i)$, $\tilde{S}_i := S_i(z_i, \tilde{\mu}_i, \tilde{\sigma}_i)$, $S_i := S_i(z_i, \mu_i, \sigma_i)$.

Following the procedure in Appendix B, it can be shown that the following operation. The function approximation error can be written as

$$W_i^T S_i - \hat{W}_i^T \hat{S}_i = \tilde{W}_i^T (\hat{S}_i - \hat{S}'_{\mu i}\hat{\mu}_i - \hat{S}'_{\sigma i}\hat{\sigma}_i) + \hat{W}_i^T (\hat{S}'_{\mu i}\tilde{\mu}_i + \hat{S}'_{\sigma i}\tilde{\sigma}_i) + \omega_i(t), \tag{48}$$

The disturbance term $\omega_i(t)$ is given by

$$\omega_i(t) = W_i^T (S_i - \hat{S}_i) + W_i^T (\hat{S}'_{\mu i}\hat{\mu}_i + \hat{S}'_{\sigma i}\hat{\sigma}_i) - \hat{W}_i^T (\hat{S}'_{\mu i}\mu_i + \hat{S}'_{\sigma i}\sigma_i) \tag{49}$$

Then, the upper bound of $\omega_i(t)$ can be written as

$$|\omega_i(t)| \le \|W_i\|(\|\hat{S}'_{\mu i}\hat{\mu}_i\|_F + \|\hat{S}'_{\sigma i}\hat{\sigma}_i\|_F) + \|\hat{W}_i^T \hat{S}'_{\mu i}\|_F \|\mu_i\|_F + \|\hat{W}_i^T \hat{S}'_{\sigma i}\|_F \|\sigma_i\| + 2\|W_i\|_1 \le \rho_{\omega i}\vartheta_{\omega i} \tag{50}$$

where $\rho_{\omega i} = \max(\|W_i\|, \|\mu_i\|_F, \|\sigma_i\|, 2\|W_i\|_1)$, $\vartheta_{\omega i} = \left\|\hat{S}'_{\mu i}\hat{\mu}_i\right\|_F + \left\|\hat{S}'_{\sigma i}\hat{\sigma}_i\right\|_F + \left\|\hat{W}_i^T\hat{S}'_{\mu i}\right\|_F + \left\|\hat{W}_i^T\hat{S}'_{\sigma i}\right\|_F + 1$, with $\|\cdot\|_1$ 1 norm. Notice that $\rho_{\omega i}$ is an unknown coefficient, whereas $\vartheta_{\omega i}$ is a known function.

4.1.2 Controller design and stability analysis

Substituting (43) and (44) into (42), we have

$$\dot{\tau}_i = -k_i\tau_i + W_i^T S_i - \hat{W}_i^T\hat{S}_i + \hat{\psi}_i - \delta_i - v_{ri} + g_i + \varepsilon_i(z_i), \tag{51}$$

using (48), the above equation can become

$$\begin{aligned}\dot{\tau}_i = &-k_i\tau_i + \tilde{W}_i^T(\hat{S}_i - \hat{S}'_{\mu i}\hat{\mu}_i - \hat{S}'_{\sigma i}\hat{\sigma}_i) + \hat{W}_i^T(\hat{S}'_{\mu i}\tilde{\mu}_i + \hat{S}'_{\sigma i}\tilde{\sigma}_i)\\ &+\hat{\psi}_i - \delta_i - v_{ri} + g_i + \varepsilon_i(z_i) + \omega_i(t).\end{aligned} \tag{52}$$

Theorem 2. Consider the nonlinear subsystems represented by Eq. (33) and let assumptions hold. If choose the pseudo-control input $\hat{\psi}_i$ as Eq.(41), and use the following adaptation laws and robust control law

$$\dot{\hat{W}}_i = F_i\left[(\hat{S}_i - \hat{S}'_{\mu i}\hat{\mu}_i - \hat{S}'_{\sigma i}\hat{\sigma}_i)\tau_i - \gamma_{Wi}\hat{W}_i|\tau_i|\right], \tag{53}$$

$$\dot{\hat{\mu}}_i = G_i\left[\hat{S}'^{\,T}_{\mu i}\hat{W}_i\tau_i - \gamma_{Wi}\hat{\mu}_i|\tau_i|\right], \tag{54}$$

$$\dot{\hat{\sigma}}_i = H_i\left[\hat{S}'^{\,T}_{\sigma i}\hat{W}_i\tau_i - \gamma_{Wi}\hat{\sigma}_i|\tau_i|\right], \tag{55}$$

$$\dot{\hat{\phi}}_i = \gamma_{\phi i}\left[\tau_i\vartheta^*_{\omega i}\tanh(\frac{\tau_i\vartheta^*_{\omega i}}{\alpha_i}) - \lambda_{\phi i}\hat{\phi}_i|\tau_i|\right], \tag{56}$$

$$\dot{\hat{d}}_i = \gamma_{di}(\tau_i^2 - \lambda_{di}\hat{d}_i|\tau_i|), \tag{57}$$

$$v_{ri} = \hat{\phi}_i\vartheta^*_{\omega i}\tanh(\frac{\tau_i\vartheta^*_{\omega i}}{\alpha_i}) + \hat{d}_i\tau_i\ , \tag{58}$$

where $\vartheta_{\omega i}^{*} = \vartheta_{\omega i} + 1$, $F_i = F_i^T > 0, G_i = G_i^T > 0, H_i = H_i^T > 0$ are any constant matrices, $\gamma_{Wi}, \gamma_{\phi i}, \gamma_{di}, \lambda_{\phi i}, \lambda_{di}$ and α_i are positive design parameters, $\hat{\phi}_i$ is the estimated value of the uncertain disturbance term $\phi_i = \max(\rho_{\omega i}, \varepsilon_{Ni})$, defining $\tilde{\phi}_i = \phi_i - \hat{\phi}_i$ with $\tilde{\phi}_i$ error, $d_i > 0$ is used to estimate unknown positive number to shield interconnection effect, $\hat{d}_i$ is its estimated value, with $\tilde{d}_i = d_i - \hat{d}_i$ estimated error, then, guarantee that all signals in the system are bounded and the tracking error e_i will converge to a neighborhood of the origin.

Proof. Consider the following positive define Lyapunov function candidate as

$$L_i = \frac{1}{2}\tau_i^2 + \frac{1}{2}\left[tr(\tilde{W}_i^T F_i^{-1} \tilde{W}_i) + tr(\tilde{\mu}_i^T G_i^{-1} \tilde{\mu}_i) + tr(\tilde{\sigma}_i^T H_i^{-1} \tilde{\sigma}_i) + \gamma_{\phi i}^{-1} \tilde{\phi}_i^2 + \gamma_{di}^{-1} \tilde{d}_i^2 \right] \quad (59)$$

The time derivative of the above equation is given by

$$\dot{L}_i = \tau_i \dot{\tau}_i + tr(\tilde{W}_i^T F_i^{-1} \dot{\tilde{W}}_i) + tr(\tilde{\mu}_i^T G_i^{-1} \dot{\tilde{\mu}}_i) + tr(\tilde{\sigma}_i^T H_i^{-1} \dot{\tilde{\sigma}}_i) + \gamma_{\phi i}^{-1} \tilde{\phi}_i \dot{\tilde{\phi}}_i + \gamma_{di}^{-1} \tilde{d}_i \dot{\tilde{d}}_i \quad (60)$$

Applying(52) to (60), we have

$$\begin{aligned} \dot{L}_i = \tau_i & \begin{bmatrix} -k_i \tau_i + \tilde{W}_i^T (\hat{S}_i - \hat{S}'_{\mu i} \hat{\mu}_i - \hat{S}'_{\sigma i} \hat{\sigma}_i) + \hat{W}_i^T (\hat{S}'_{\mu i} \tilde{\mu}_i + \hat{S}'_{\sigma i} \tilde{\sigma}_i) \\ + \hat{\psi}_i - \delta_i - v_{ri} + g_i + \varepsilon_i + \omega_i \end{bmatrix} \\ & + tr(\tilde{W}_i^T F_i^{-1} \dot{\tilde{W}}_i) + tr(\tilde{\mu}_i^T G_i^{-1} \dot{\tilde{\mu}}_i) + tr(\tilde{\sigma}_i^T H_i^{-1} \dot{\tilde{\sigma}}_i) + \gamma_{\phi i}^{-1} \tilde{\phi}_i \dot{\tilde{\phi}}_i + \gamma_{di}^{-1} \tilde{d}_i \dot{\tilde{d}}_i \end{aligned} \quad (61)$$

Substituting the adaptive laws (53), (54) and (55) into (61), and $\left(\dot{\div}\right) = -\left(\dot{\div}\right)$,yields

$$\begin{aligned} \dot{L}_i &= \tau_i \left[-k_i \tau_i + \hat{\psi}_i - \delta_i - v_{ri} + g_i + \varepsilon_i + \omega_i \right] + \gamma_{Wi} |\tau_i| tr(\tilde{Z}_i^T \hat{Z}_i) + \gamma_{\phi i}^{-1} \tilde{\phi}_i \dot{\tilde{\phi}}_i + \gamma_{di}^{-1} \tilde{d}_i \dot{\tilde{d}}_i \\ &\le -k_i \tau_i^2 + \tau_i (\hat{\psi}_i - \delta_i) - v_{ri} \tau_i + \tau_i g_i + |\tau_i| (\rho_{\omega i} \vartheta_{\omega i} + \varepsilon_{Ni}) \\ &\quad + \gamma_{Wi} |\tau_i| tr(\tilde{Z}_i^T \hat{Z}_i) + \gamma_{\phi i}^{-1} \tilde{\phi}_i \dot{\tilde{\phi}}_i + \gamma_{di}^{-1} \tilde{d}_i \dot{\tilde{d}}_i \\ &\le -k_i \tau_i^2 + \tau_i (\hat{\psi}_i - \delta_i) - v_{ri} \tau_i + \tau_i g_i + |\tau_i| \phi_i \vartheta_{\omega i}^{*} \\ &\quad + \gamma_{Wi} |\tau_i| tr(\tilde{Z}_i^T \hat{Z}_i) + \gamma_{\phi i}^{-1} \tilde{\phi}_i \dot{\tilde{\phi}}_i + \gamma_{di}^{-1} \tilde{d}_i \dot{\tilde{d}}_i \end{aligned} \quad (62)$$

Inserting (56) and (58) into the above inequality, we obtain

$$\begin{aligned}\dot{L}_i \le & -k_i\tau_i^2 + \tau_i(\hat{\psi}_i - \delta_i) + \tau_i g_i + |\tau_i|\phi_i\vartheta_{\omega i}^* - \tau_i\hat{\phi}_i\vartheta_{\omega i}^* \tanh(\frac{\tau_i\vartheta_{\omega i}^*}{\alpha_i}) \\ & - \tilde{\phi}_i\left[\tau_i\vartheta_{\omega i}^* \tanh(\frac{\tau_i\vartheta_{\omega i}^*}{\alpha_i}) - \lambda_{\phi i}\hat{\phi}_i|\tau_i|\right] - \hat{d}_i\tau_i^2 \\ & - \tilde{d}_i(\tau_i^2 - \lambda_{di}\hat{d}_i|\tau_i|) + \gamma_{Wi}|\tau_i| tr(\tilde{Z}_i^T\hat{Z}_i) \\ = & -k_i\tau_i^2 + \tau_i(\hat{\psi}_i - \delta_i) + \phi_i\left[|\tau_i|\vartheta_{\omega i}^* - \tau_i\vartheta_{\omega i}^* \tanh(\frac{\tau_i\vartheta_{\omega i}^*}{\alpha_i})\right] + \lambda_{\phi i}|\tau_i|\tilde{\phi}_i\hat{\phi}_i \\ & - d_i\tau_i^2 + \tau_i g_i + \lambda_{di}|\tau_i|\tilde{d}_i\hat{d}_i + \gamma_{Wi}|\tau_i| tr(\tilde{Z}_i^T\hat{Z}_i)\end{aligned} \tag{63}$$

Using (11), (63) becomes

$$\begin{aligned}\dot{L}_i \le & -k_i\tau_i^2 + \tau_i(\hat{\psi}_i - \delta_i) + \phi_i\varsigma_i\alpha_i - d_i\tau_i^2 + \tau_i g_i \\ & + |\tau_i|\left[\lambda_{\phi i}\tilde{\phi}_i\hat{\phi}_i + \lambda_{di}\tilde{d}_i\hat{d}_i + \gamma_{Wi} tr(\tilde{Z}_i^T\hat{Z}_i)\right]\end{aligned} \tag{64}$$

By completing square, we have

$$\begin{aligned}\dot{L}_i \le & -k_i\tau_i^2 + \tau_i(\hat{\psi}_i - \delta_i) + \phi_i\varsigma_i\alpha_i + \frac{g_i^2}{4d_i} \\ & + |\tau_i|\left[\lambda_{\phi i}\tilde{\phi}_i\hat{\phi}_i + \lambda_{di}\tilde{d}_i\hat{d}_i + \gamma_{Wi} tr(\tilde{Z}_i^T\hat{Z}_i)\right]\end{aligned} \tag{65}$$

With (41), (44), (53)-(58), approximation error between actual approximation inverse and ideal control inverse is bounded by

$$|\hat{\psi}_i - \delta_i| \le c_{1i} + c_{2i}|\tau_i| + c_{3i}\left\|\tilde{Z}_i\right\|_F, \tag{66}$$

where c_{1i}, c_{2i}, c_{3i} are positive constants.

$$\begin{aligned}\dot{L}_i \le & -(k_i - c_{2i})\tau_i^2 + |\tau_i|\left(c_{1i} + c_{3i}\left\|\tilde{Z}_i\right\|_F\right) + \phi_i\varsigma_i\alpha_i \\ & + \frac{g_i^2}{4d_i} + |\tau_i|\left[\lambda_{\phi i}\tilde{\phi}_i\hat{\phi}_i + \lambda_{di}\tilde{d}_i\hat{d}_i + \gamma_{Wi} tr(\tilde{Z}_i^T\hat{Z}_i)\right]\end{aligned} \tag{67}$$

Since $tr(\tilde{Z}_i^T\hat{Z}_i) \le \left\|\tilde{Z}_i\right\|_F \|Z_i\|_F - \left\|\tilde{Z}_i\right\|_F^2$, $\tilde{\phi}_i\hat{\phi}_i \le |\tilde{\phi}_i||\phi_i| - |\tilde{\phi}_i|^2$, $\tilde{d}_i\dot{\tilde{d}}_i \le |\tilde{d}_i||d_i| - |\tilde{d}_i|^2$ hold, the

above inequality can be written as

$$\begin{aligned}\dot{L}_i \le & -\left(k_i - c_{2i}\right)\tau_i^{\,2} + \left|\tau_i\right|\left(c_{1i} + c_{3i}\left\|\tilde{Z}_i\right\|_F\right) + \phi_i\varsigma_i\alpha_i + \frac{g_i^{\,2}}{4d_i} \\ & + \left|\tau_i\right|\left[\lambda_{\phi i}\left(\left|\tilde{\phi}_i\right|\left|\phi_i\right| - \left|\tilde{\phi}_i\right|^2\right) + \lambda_{di}\left(\left|\tilde{d}_i\right|\left|d_i\right| - \left|\tilde{d}_i\right|^2\right) + \gamma_{Wi}\left(\left\|\tilde{Z}_i\right\|_F\left\|Z_i\right\|_F - \left\|\tilde{Z}_i\right\|_F^2\right)\right]\end{aligned} \tag{68}$$

By completing square for (68), we get

$$\dot{L}_i \le -\left(k_i - c_{2i}\right)\tau_i^{\,2} + c_{5i}\left|\tau_i\right| + \left|\phi_i\right|\varsigma_i\alpha_i + \frac{g_i^{\,2}}{4d_i} \tag{69}$$

where $c_{5i} = c_{1i} + c_{4i}$,with $c_{4i} = \dfrac{\lambda_{\phi i}}{4}\left|\phi_i\right|^2 + \dfrac{\lambda_{di}}{4}\left|d_i\right|^2 + \dfrac{\left(\gamma_{Wi}\left\|Z_i\right\|_F + c_{3i}\right)^2}{4}$.

For the overall system, it can be derived that the bound as

$$\dot{L} = \sum_{i=1}^{n}\dot{L}_i \le \sum_{i=1}^{n}\left\{-\left(k_i - c_{2i}\right)\tau_i^{\,2} + c_{5i}\left|\tau_i\right| + \left|\phi_i\right|\varsigma_i\alpha_i + \frac{g_i^{\,2}}{4d_i}\right\} \tag{70}$$

According to (34), $\left|g_i\right| \le \sum_{j=1}^{n}\gamma_{ij}\left|\tau_j\right| = \chi^T\Gamma_i$, define $\chi = [|\tau_1|, |\tau_2|, \cdots |\tau_n|]^T$, $\Gamma_i = [\gamma_{i1}, \gamma_{i2}, \cdots \gamma_{in}]^T$, $K = diag[k_1 - c_{21}, k_2 - c_{22}, \cdots, k_n - c_{2n}]$, $C = [c_{51}, c_{52}, \cdots, c_{5n}]^T$, $D = \sum_{i=1}^{n}\left(\left|\phi_i\right|\varsigma_i\alpha_i\right)$, the above inequality can be rewritten as

$$\begin{aligned}\dot{L} &\le -\chi^T\left(K - \frac{1}{4d_i}\Gamma_i\Gamma_i^{\,T}\right)\chi + C^T\chi + D = -\chi^T E\chi + C^T\chi + D \\ &\le -\lambda_{\min}(E)\left\|\chi\right\|^2 + \left\|C\right\|\left\|\chi\right\| + D\end{aligned} \tag{71}$$

where $E = K - (4d_i)^{-1}\Gamma_i\Gamma_i^{\,T}$, $\lambda_{\min}(E)$ the minimum singular value of E . Then $\dot{L} \le 0$, as long as $k_i > c_{2i}$ and sufficiently large d_i , E would be positive definite, and

$$\|\chi\| \geq \sqrt{\frac{\|C\|^2 + D\lambda_{\min}(E)}{4\lambda^2{}_{\min}(E)}} + \frac{\|C\|}{2\lambda_{\min}(E)} = A,$$
$$\left|\tilde{\phi}_i\right| \geq |\phi_i|, \left|\tilde{d}_i\right| \geq |d_i|, \left\|\tilde{Z}_i\right\|_F \geq \frac{1}{\gamma_{Wi}}\left(\gamma_{Wi}\|Z_i\|_F + c_{3i}\right) \tag{72}$$

Now, we define

$$\Omega_\chi = \left\{\chi \mid \|\chi\| \leq A\right\}, \Omega_{\phi_i} = \left\{\tilde{\phi}_i \mid \left|\tilde{\phi}_i\right| \leq |\phi_i|\right\},$$
$$\Omega_{d_i} = \left\{\tilde{d}_i \mid \left|\tilde{d}_i\right| \leq |d_i|\right\}, \Omega_{Z_i} = \left\{\left\|\tilde{Z}_i\right\|_F \mid \left\|\tilde{Z}_i\right\|_F \leq \frac{1}{\gamma_{Wi}}\left(\gamma_{Wi}\|Z_i\|_F + c_{3i}\right)\right\} \tag{73}$$

Since $\|Z_i\|_F, \phi_i, d_i, \gamma_{Wi}, c_{3i}$ are positive constants, we conclude that Ω_χ , Ω_{Zi} , Ω_{ϕ_i} and Ω_{d_i} are compact sets. Hence $\dot{L}$ is negative outside these compacts set. According to a standard Lyapunov theorem, this demonstrates that $\tilde{Z}_i, \tilde{\phi}_i, \tilde{d}_i$ and χ are bounded and will converge to Ω_χ , Ω_{Zi} , Ω_{ϕ_i} and Ω_{d_i} , respectively. Furthermore, this implies e_i is bounded and will converge to a neighborhood of the origin and all signals in the system are bounded.

4.1.3 Simulation Study

In order to validate the effectiveness of the proposed scheme, we implement an example, and assume that the large-scale system is composed of the following two subsystems defined by

$$\textit{Subsystem}\quad 1: \begin{cases} \dot{x}_{11} = x_{12} \\ \dot{x}_{12} = -\omega^2 x_{11} + 0.02(\omega - x_{11}^2)x_{12} + u_1 \\ \qquad + (x_{11}^2 + x_{12}^2)\sigma(u_1) + 0.2 + \sin(0.2x_{21}) \end{cases} \tag{74}$$

$$\textit{Subsystem}\quad 2: \begin{cases} \dot{x}_{21} = x_{22} \\ \dot{x}_{22} = x_{21}^2 + 0.1(1 + x_{22}^2)u_2 + \tanh(0.1u_2) \\ \qquad + 0.15u_2{}^3 + \tanh(0.1x_{11}) \end{cases} \tag{75}$$

where $\omega = 0.4\pi$, $\sigma(u_1) = (1 - e^{-u_1})/(1 + e^{-u_1})$. The desired trajectory $x_{d11} = 0.1\pi[\sin(2t) - \cos(t)]$, $x_{d21} = 0.1\pi\cos(2t)$.

Input vectors of neural networks are $z_i = [x_i^T, \tau_i, \hat{\psi}_i]^T$, $i = 1, 2$, and number of hidden layer nodes both 8. The initial weight of neural network is $\hat{W}_i(0) = (0)$. The center values and the widths of Gaussian function are initialized as zeroes, and $\sqrt{5}$, respectively. The initial condition of controlled plant is $x_1(0) = [0.1, 0.2]^T$ $x_2(0) = [0, 0]^T$. The other parameters are chosen as follows:

$\Lambda_i = 5, k_i = 5$ $\gamma_{Wi} = 0.001, \gamma_{\phi i} = 1, \gamma_{di} = 1, \lambda_{\phi i} = 0.01, \lambda_{di} = 0.01$, $\alpha_i = 10$, $F_i = 10 I_{Wi}$, $G = 2I_{\mu i}, H = 2I_{\sigma i}$, with $I_{Wi}, I_{\mu i}, I_{\sigma i}$ corresponding identity matrices.

Fig.5 shows the results of comparisons of tracking errors of two subsystems. Fig.6 gives control input of two subsystems, Fig.7 and Fig.8 the comparison of tracking of two subsystems, respectively. Fig.9 and Fig.10 illustrate outputs of two RBFNs and the change of norms of $\hat{W}, \hat{\mu}, \hat{\sigma}$, respectively. From these results, it can be seen that the effectiveness of the proposed scheme is validated, and tracking errors converge to a neighborhood of the zeroes and all signals in system are bounded. Furthermore, the learning rate of neural network controller is rapid, and can track the desired trajectory in about 1 second. From the results of control inputs, after shortly shocking, they tend to be smoother, and this is because neural networks are unknown for objective in initial stages.

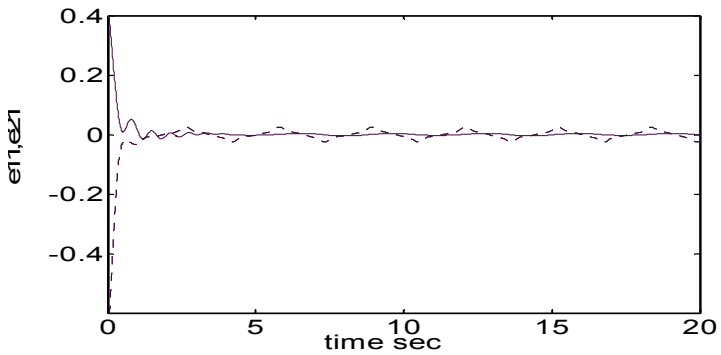

Fig. 5. Tracking error of two subsystems: 1(solid), 2(dot)

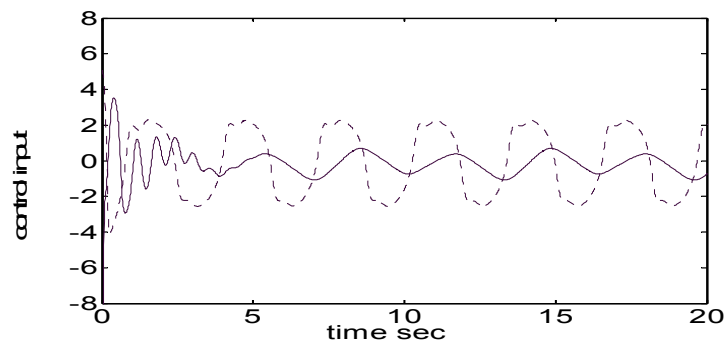

Fig. 6. Control input of two subsystems: 1(solid), 2(dot)

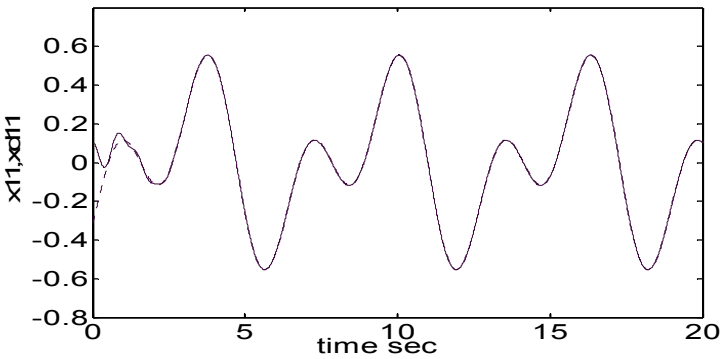

Fig. 7. Comparison of the tracking of subsystem 1: x_{11} (solid) and x_{d11} (dot)

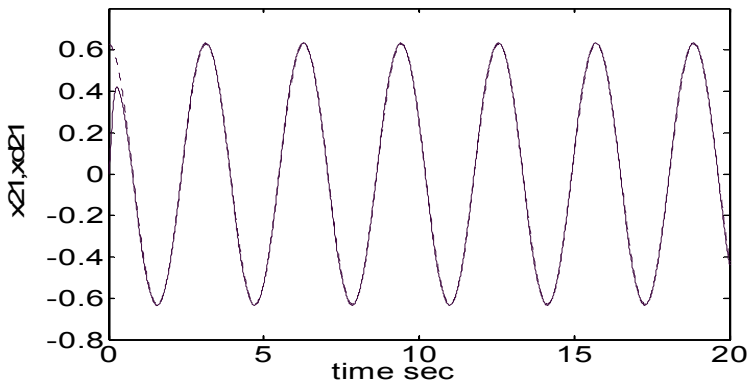

Fig. 8. Comparison of the tracking of subsystem 2: x_{21} (solid) and x_{d21} (dot)

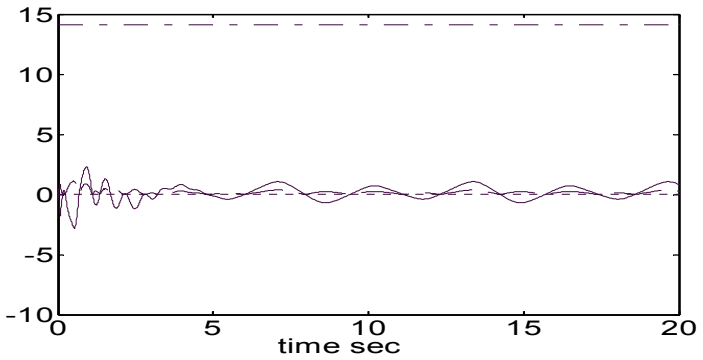

Fig. 9. Subsystem 1: Output of RBFN (solid), norms of $\hat{W}$ (dash), $\hat{\mu}$ (dot), $\hat{\sigma}$ (dash-dot)

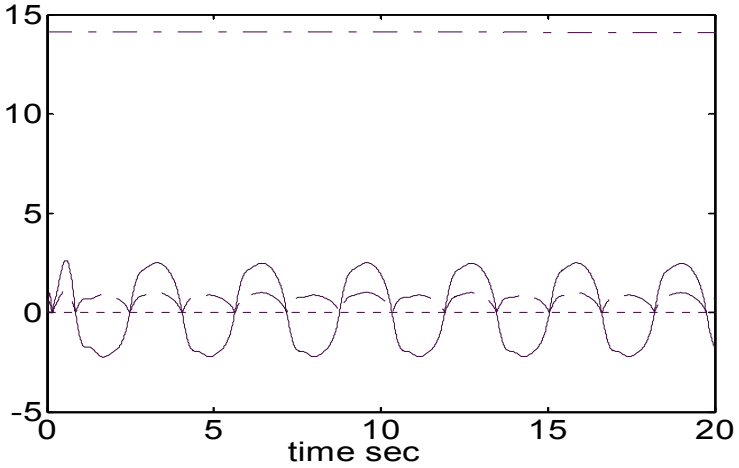

Fig. 10. Subsystem 2: Output of RBFN (solid), norms of $\hat{W}$ (dash), $\hat{\mu}$ (dot), $\hat{\sigma}$ (dash-dot)

4.2 RBFN-based decentralized adaptive control for the class of large-scale nonlinear systems with nonlinear function interconnections

Assumption 10. The interconnection effect is bounded by the following function:

$$\left|g_i(x_1, x_2, \cdots, x_n)\right| \le \sum_{j=1}^{n} \xi_{ij}(|\tau_j|), \tag{76}$$

where $\xi_{ij}(|\tau_j|)$ are unknown smooth nonlinear function, τ_j are filtered tracking errors to be defined shortly .

The control objective is: determine a control law, force the output, y_i , to follow a given desired output, x_{di} , with an acceptable accuracy, while all signals involved must be bounded.

Define the desired trajectory vector $x_{di} = [y_{di}, \dot{y}_{di}, \cdots, y_{di}^{l_i-1}]^T$, $X_{di} = [y_{di}, \dot{y}_{di}, \cdots, y_{di}^{(l_i)}]^T$ and tracking error $e_i = x_i - x_{di} = [e_{i1}, e_{i2}, \cdots, e_{il_i}]^T$, thus, the filter tracking error can be written as

$$\tau_i = [\Lambda_i^T \quad 1]e_i = k_{i,1}e_i + k_{i,2}\dot{e}_i + \cdots + k_{i,l_i-1}e_i^{(l_i-2)} + e_i^{(l_i-1)}, \tag{77}$$

where the coefficients are chosen such that the polynomial $k_{i,1} + k_{i,2}s + \cdots + k_{i,l_i-1}s^{(l_i-2)} + s^{(l_i-1)}$ is Hurwitz.

Assumption 11. The desired signal $x_{di}(t)$ is bounded, so that $\left\|X_{di}\right\| \le \overline{X}_{di}$, with $\overline{X}_{di}$ a known constant.

For an isolated subsystem, without interconnection function, by differentiating (77), the filtered tracking error can be rewritten as

$$\dot{\tau}_i = \dot{x}_{il_i} - y_{di}^{(l_i)} + [0 \quad \Lambda_i^T]e_i = f_i(x_i, u_i) + Y_{di} \,, \tag{78}$$

with $Y_{di} = -y_{di}^{(l_i)} + [0 \quad \Lambda_i^T]e_i$.
Define a continuous function

$$\delta_i = k_i \tau_i + Y_{di}, \tag{79}$$

where k_i is a positive constant. With Assumption 5, we know $\partial f(x_i, u_i)/\partial u_i \neq 0$, thus, $\partial[f(x_i, u_i) - \delta_i]/\partial u_i \neq 0$. Considering the fact that $\partial \delta_i / \partial u_i = 0$, with the implicit function theorem, there exists a continuous ideal control input u_i^* in a neighborhood of $(x_i, u_i) \in \Omega_i \times R$, such that $f(x_i, u_i^*) - \delta_i = 0$, i.e. $\delta_i = f_i(x_i, u_i^*)$ holds. Here, $\delta_i = f_i(x_i, u_i^*)$ represents an ideal control inverse. Adding and subtracting δ_i to the right-hand side of $\dot{x}_{il_i} = f_i(x_i, u_i) + g_i$ of (33), one obtains

$$\dot{x}_{il_i} = f_i(x_i, u_i) + g_i + \delta_i - Y_{di} - k_i \tau_i, \tag{80}$$

and yields

$$\dot{\tau}_i = -k_i \tau_i + f_i(x_i, u_i) + g_i + \delta_i, \tag{81}$$

Similar to the above-mentioned equation (40), $\hat{\psi}_i = f_i(x_i, \hat{u}_i)$ holds.
Based on the above conditions, in order to control the system and make it be stable, we design the approximation pseudo-control input $\hat{\psi}_i$ as follows:

$$\hat{\psi}_i = -k_i \tau_i - Y_{di} - u_{ci} - \hat{W}_{gi}^T S_{gi}(|\tau_i|)\tau_i - v_{ri}, \tag{82}$$

where u_{ci} is output of a neural network controller, which adopts a RBFN, v_{ri} is robustifying control term designed in stability analysis, $\hat{W}_{gi}^T S_{gi}(|\tau_i|)$ is used to compensate the interconnection nonlinearity (we will define later).
Adding and subtracting $\hat{\psi}_i$ to the right-hand side of (81), with $\delta_i = k_i \tau_i + Y_{di} = f_i(x_i, u_i^*)$, we have

$$\dot{\tau}_i = -k_i \tau_i + \tilde{\Delta}_i(x_i, u_i, u_i^*) - u_{ci} - \hat{W}_{gi}^T S_{gi}(|\tau_i|)\tau_i + \delta_i - \hat{\psi}_i - v_{ri} + g_i, \tag{83}$$

where $\tilde{\Delta}_i(x_i, u_i, u_i^*) = f_i(x_i, u_i) - f_i(x_i, u_i^*)$ is error between the nonlinear function and its ideal control function, we can use the RBFN to approximate it.

4.2.1 Neural network-based approximation

Based on the approximation property of RBFN, $\tilde{\Delta}_i(x_i, u_i, u_i^*)$ can be written as

$$\tilde{\Delta}_i(x_i, u_i, u_i^*) = W_i^T S_i(z_i) + \varepsilon_i(z_i), \tag{84}$$

where W_i is the weight vector, $S_i(z_i)$ is Gaussian basis function, $\varepsilon_i(z_i)$ is the approximation error and the input vector $z_i \in R^q$, q the number of input node.

Assumption 12. The approximation error $\varepsilon_i(z_i)$ is bounded by $|\varepsilon_i| \leq \varepsilon_{Ni}$, with $\varepsilon_{Ni} > 0$ is an unknown constant. The input of the RBFN is chosen as $z_i = [x_i^T, \tau_i, \hat{\psi}_i]^T$. Moreover, output of the RBFN is designed as

$$u_{ci} = \hat{W}_i^T S_i(z_i). \tag{85}$$

Define $\hat{W}_i$ as estimates of ideal W_i, which are given by the RBFN tuning algorithms.

Assumption 13. The ideal value of W_i satisfies

$$\| W_i \| \leq W_{iM}, \tag{86}$$

where W_{iM} is positive known constant, with estimation errors as $\tilde{W}_i = W_i - \hat{W}_i$.

4.2.2 Controller design and stability analysis

Substituting (84) and (85) into (83), we have

$$\dot{\tau}_i = -k_i \tau_i + \tilde{W}_i^T S_i + \delta_i - \hat{\psi}_i - v_{ri} + g_i - \hat{W}_{gi}^T S_{gi}(|\tau_i|)\tau_i + \varepsilon_i(z_i) \tag{87}$$

Theorem 3. Consider the nonlinear subsystems represented by Eq. (33) and let assumptions hold. If choose the pseudo-control input $\hat{\psi}_i$ as Eq.(82), and use the following adaptation laws and robust control law

$$\dot{\hat{W}}_i = F_i[S_i \tau_i - \gamma_{Wi} \hat{W}_i |\tau_i|], \tag{88}$$

$$\dot{\hat{W}}_{gi} = G_i[S_{gi}(|\tau_i|)\tau_i^2 - \gamma_{gi}\hat{W}_{gi}|\tau_i|], \tag{89}$$

$$\dot{\hat{\phi}}_i = \lambda_{\phi i}[\tau_i(|\tau_i|+1)\tanh(\tau_i/\alpha_i) - \gamma_{\phi i}\hat{\phi}_i|\tau_i|], \tag{90}$$

$$v_{ri} = \hat{\phi}_i(|\tau_i|+1)\tanh(\tau_i/\alpha_i), \tag{91}$$

where $F_i = F_i^T > 0$, $G_i = G_i^T > 0$ are any constant matrices, $\lambda_{\phi i}, \gamma_{Wi}, \gamma_{gi}, \gamma_{\phi i}$ and α_i are positive design parameters, $\hat{\phi}_i$ is the estimated value of the unknown approximation errors, which will be defined shortly, then, guarantee that all signals in the system are bounded and the tracking error e_i will converge to a neighborhood of the origin.

Proof. Consider the following positive define Lyapunov function candidate as

$$2L_i = \tau_i^2 + \tilde{W}_i^T F_i^{-1}\tilde{W}_i + \tilde{W}_{gi}{}^T G_i^{-1}\tilde{W}_{gi} + \lambda_{\phi i}^{-1}\tilde{\phi}_i^2 \tag{92}$$

The time derivative of the above equation is given by

$$\dot{L}_i = \tau_i\dot{\tau}_i + \tilde{W}_i^T F_i^{-1}\dot{\tilde{W}}_i + \tilde{W}_{gi}{}^T G_i^{-1}\tilde{W}_{gi} + \lambda_{\phi i}^{-1}\tilde{\phi}_i\dot{\tilde{\phi}}_i \tag{93}$$

Applying (87) and(53) to (59) and $(\dot{\tilde{\cdot}}) = -(\dot{\hat{\cdot}})$, we have

$$\begin{aligned}\dot{L}_i = \tau_i[&-k_i\tau_i + \delta_i - \hat{\psi}_i - v_{ri} + g_i - \hat{W}_{gi}^T S_{gi}(|\tau_i|)\tau_i + \varepsilon_i] \\ &+ \gamma_{Wi}\tilde{W}_i^T\hat{W}_i|\tau_i| + \tilde{W}_{gi}{}^T G_i^{-1}\dot{\tilde{W}}_{gi} + \lambda_{\phi i}^{-1}\tilde{\phi}_i\dot{\tilde{\phi}}_i\end{aligned} \tag{94}$$

Using (76), (94) is rewritten as

$$\begin{aligned}\dot{L}_i \le &-k_i\tau_i^2 + \tau_i(\delta_i - \hat{\psi}_i) - v_{ri}\tau_i + \tau_i[\textstyle\sum_{j=1}^n \xi_{ij}(|\tau_j|) - \hat{W}_{gi}^T S_{gi}(|\tau_i|)\tau_i] \\ &+ |\tau_i|\varepsilon_{Ni} + \lambda_{\phi i}^{-1}\tilde{\phi}_i\dot{\tilde{\phi}}_i + \gamma_{Wi}\tilde{W}_i^T\hat{W}_i|\tau_i| + \tilde{W}_{gi}{}^T G_i^{-1}\dot{\tilde{W}}_{gi}\end{aligned} \tag{95}$$

Since $\xi_{ij}(\cdot)$ is a smooth function, there exists a smooth function $\zeta_{ij}(|\tau_j|), (1 \le i, j \le n)$ such that $\xi_{ij}(|\tau_j|) = |\tau_j|\zeta_{ij}(|\tau_j|)$ hold. Thus, we have

$$\begin{aligned}\dot{L}_i \le & -k_i\tau_i^2 + \tau_i(\delta_i - \hat{\psi}_i) - v_{ri}\tau_i + \tau_i^2[\sum_{j=1}^{n}\zeta_{ij}(|\tau_j|) - \hat{W}_{gi}^T S_{gi}(|\tau_i|)] \\ & + |\tau_i|\varepsilon_{Ni} + \lambda_{\phi i}^{-1}\tilde{\phi}_i\dot{\tilde{\phi}}_i + \gamma_{Wi}\tilde{W}_i^T\hat{W}_i|\tau_i| + \tilde{W}_{gi}{}^T G_i^{-1}\dot{\tilde{W}}_{gi}\end{aligned} \tag{96}$$

Since the function $d_i(|\tau_i|) = \sum_{i=1}^{n}\zeta_{ij}(|\tau_i|)$ is smooth and τ_i is on a compact set, $d_i(|\tau_i|)$ can be approximated via a RBFN, i.e., $d_i(|\tau_i|) = W_{gi}^T S_{gi}(|\tau_i|) + \varepsilon_{gi}$, with bounded approximation error ε_{gi}, $|\varepsilon_{gi}| \le \varepsilon_{gNi}$. $\hat{W}_{gi}$ is estimate of ideal W_{gi}, with boundedness $\|W_{gi}\| \le W_{gMi}$, $W_{gMi} > 0$ a known constant, and the estimation errors as $\tilde{W}_{gi} = W_{gi} - \hat{W}_{gi}$. Then, (96) becomes

$$\begin{aligned}\dot{L}_i \le & -k_i\tau_i^2 + \tau_i(\delta_i - \hat{\psi}_i) - v_{ri}\tau_i + \tau_i[\sum_{j=1}^{n}\xi_{ij}(|\tau_j|) - \hat{W}_{gi}^T S_{gi}(|\tau_i|)\tau_i] \\ & + |\tau_i|\varepsilon_{Ni} + \lambda_{\phi i}^{-1}\tilde{\phi}_i\dot{\tilde{\phi}}_i + \gamma_{Wi}\tilde{W}_i^T\hat{W}_i|\tau_i| + \tilde{W}_{gi}{}^T G_i^{-1}\dot{\tilde{W}}_{gi} \\ \le & -k_i\tau_i^2 + \tau_i(\delta_i - \hat{\psi}_i) - v_{ri}\tau_i + \tau_i^2\tilde{W}_{gi}^T S_{gi}(|\tau_i|) + \varepsilon_{gi}\tau_i^2 + |\tau_i|\varepsilon_{Ni} \\ & + \lambda_{\phi i}^{-1}\tilde{\phi}_i\dot{\tilde{\phi}}_i + \gamma_{Wi}\tilde{W}_i^T\hat{W}_i|\tau_i| + \tilde{W}_{gi}{}^T G_i^{-1}\dot{\tilde{W}}_{gi}\end{aligned} \tag{97}$$

Substituting the adaptive law (89), we obtain

$$\begin{aligned}\dot{L}_i \le & -k_i\tau_i^2 + \tau_i(\delta_i - \hat{\psi}_i) - v_{ri}\tau_i + \varepsilon_{gNi}\tau_i^2 + |\tau_i|\varepsilon_{Ni} + \lambda_{\phi i}^{-1}\tilde{\phi}_i\dot{\tilde{\phi}}_i \\ & + \gamma_{Wi}\tilde{W}_i^T\hat{W}_i|\tau_i| + \gamma_{gi}\tilde{W}_{gi}{}^T\hat{W}_{gi}|\tau_i|\end{aligned} \tag{98}$$

Define $\phi_i = \max(\varepsilon_{Ni}, \varepsilon_{gNi})$, with $\hat{\phi}_i$ is its estimate, and $\tilde{\phi}_i = \phi_i - \hat{\phi}_i$ with $\tilde{\phi}_i$ error. (98) can be rewritten as

$$\begin{aligned}\dot{L}_i \le & -k_i\tau_i^2 + \tau_i(\delta_i - \hat{\psi}_i) - v_{ri}\tau_i + \phi_i(\tau_i^2 + |\tau_i|) \\ & + \lambda_{\phi i}^{-1}\tilde{\phi}_i\dot{\tilde{\phi}}_i + \gamma_{Wi}\tilde{W}_i^T\hat{W}_i|\tau_i| + \gamma_{gi}\tilde{W}_{gi}{}^T\hat{W}_{gi}|\tau_i|\end{aligned} \tag{99}$$

Applying the adaptive law (56) and robust control term (58), we have

$$\begin{aligned}\dot{L}_i &\le -k_i\tau_i^2 + \tau_i(\delta_i - \hat{\psi}_i) - \hat{\phi}_i\tau_i(|\tau_i|+1)\tanh(\tau_i/\alpha_i) + \phi_i|\tau_i|(|\tau_i|+1)\\ &\quad - \tilde{\phi}_i\tau_i(|\tau_i|+1)\tanh(\tau_i/\alpha_i) + \gamma_{Wi}\tilde{W}_i^T\hat{W}_i|\tau_i| + \gamma_{gi}\tilde{W}_{gi}{}^T\hat{W}_{gi}|\tau_i| + \lambda_{\phi i}\tilde{\phi}_i\hat{\phi}_i|\tau_i|\\ &= -k_i\tau_i^2 + \tau_i(\delta_i - \hat{\psi}_i) + \phi_i|\tau_i|(|\tau_i|+1) - \phi_i\tau_i(|\tau_i|+1)\tanh(\tau_i/\alpha_i)\\ &\quad + \gamma_{Wi}\tilde{W}_i^T\hat{W}_i|\tau_i| + \gamma_{gi}\tilde{W}_{gi}{}^T\hat{W}_{gi}|\tau_i| + \lambda_{\phi i}\tilde{\phi}_i\hat{\phi}_i|\tau_i|\\ &= -k_i\tau_i^2 + \tau_i(\delta_i - \hat{\psi}_i) + \phi_i(|\tau_i|+1)\left[|\tau_i| - \tau_i\tanh(\tau_i/\alpha_i)\right]\\ &\quad + \gamma_{Wi}\tilde{W}_i^T\hat{W}_i|\tau_i| + \gamma_{gi}\tilde{W}_{gi}{}^T\hat{W}_{gi}|\tau_i| + \lambda_{\phi i}\tilde{\phi}_i\hat{\phi}_i|\tau_i|\end{aligned} \tag{100}$$

Using (11), we get

$$\begin{aligned}\dot{L}_i &\le -k_i\tau_i^2 + \tau_i(\delta_i - \hat{\psi}_i) + \phi_i(|\tau_i|+1)\varsigma\alpha_i\\ &\quad + \gamma_{Wi}\tilde{W}_i^T\hat{W}_i|\tau_i| + \gamma_{gi}\tilde{W}_{gi}{}^T\hat{W}_{gi}|\tau_i| + \gamma_{\phi i}\tilde{\phi}_i\hat{\phi}_i|\tau_i|\end{aligned} \tag{101}$$

With (82), (85), and (88)-(91), the approximation error between the ideal control inverse and the actual approximation inverse is bounded by $|\delta_i - \hat{\psi}_i| \le c_{1i} + c_{2i}|\tau_i| + c_{3i}\|\tilde{W}_i\| + c_{4i}\|\tilde{W}_{gi}\|$, with $c_{1i}, c_{2i}, c_{3i}, c_{4i}$ positive constants. Moreover, we utility the facts, $\tilde{a}^T\hat{a} \le \|\tilde{a}\|\|a\| - \|\tilde{a}\|^2$, (101) can be rewritten as

$$\begin{aligned}\dot{L}_i &\le -(k_i - c_{2i})\tau_i^2 + |\tau_i|\left(c_{1i} + c_{3i}\|\tilde{W}_i\| + c_{4i}\|\tilde{W}_{gi}\|\right) + |\tau_i|\begin{bmatrix}\gamma_{Wi}\|\tilde{W}_i\|(\|W_i\| - \|\tilde{W}_i\|)\\ +\gamma_{gi}\|\tilde{W}_{gi}\|(\|W_{gi}\| - \|\tilde{W}_{gi}\|)\\ +\lambda_{\phi i}|\tilde{\phi}_i|(|\phi_i| - |\tilde{\phi}_i|)\end{bmatrix} + \phi_i\varsigma_i\alpha_i\\ &\le -(k_i - c_{2i})\tau_i^2 + c_{1i}|\tau_i| + \phi_i\varsigma_i\alpha_i + |\tau_i|\begin{Bmatrix}\left[-\gamma_{Wi}\|\tilde{W}_i\|^2 + (\|W_i\| + c_{3i})\|\tilde{W}_i\|\right]\\ +\left[-\gamma_{gi}\|\tilde{W}_{gi}\|^2 + (\|W_{gi}\| + c_{4i})\|\tilde{W}_{gi}\|\right]\\ -\lambda_{\phi i}|\tilde{\phi}_i|^2 + |\phi_i||\tilde{\phi}_i|\end{Bmatrix}\end{aligned} \tag{102}$$

Completing square for (102), we have

$$\dot{L}_i \le -(k_i - c_{2i})\tau_i^2 + c_{8i}|\tau_i| + \phi_i\varsigma_i\alpha_i \tag{103}$$

with $c_{5i} = \gamma_{Wi} \| W_i \| + c_{3i}, c_{6i} = \gamma_{gi} \| W_{gi} \| + c_{4i}$, $c_{7i} = \phi_i^2 / 4\lambda_{\phi i} + c_{6i}^2 / 4\gamma_{gi} + c_{5i}^2 / 4\gamma_{Wi}$, $c_{8i} = c_{1i} + \phi_i \varsigma_i \alpha_i + c_{7i}$.

For the overall system, we have

$$\dot{L} = \sum_{i=1}^{n} \dot{L}_i \le \sum_{i=1}^{n} [-(k_i - c_{2i}) \tau_i^2 + c_{8i} | \tau_i | + \phi_i \varsigma_i \alpha_i] \tag{104}$$

Now, define $\chi = [| \tau_1 |, \cdots | \tau_n |]^T$, $K = diag[k_1 - c_{21}, \cdots, k_n - c_{2n}]$, $C = [c_{81}, c_{82}, \cdots, c_{8n}]^T$, $D = \sum_{i=1}^{n} (\phi_i \varsigma_i \alpha_i)$. (104) can be rewritten as

$$\dot{L} \le -\chi^T K \chi + C^T \chi + D \le -\lambda_{\min}(K) \| \chi \|^2 + \| C \| \| \chi \| + D \tag{105}$$

By completing square, yields

$$\dot{L} \le -\lambda_{\min}(K) \left(\| \chi \| - \frac{\| C \|}{2\lambda_{\min}(K)} \right)^2 + \frac{\| C \|^2}{4\lambda_{\min}(K)} + D \tag{106}$$

Clearly, $\dot{L} \le 0$, as long as $k_i > c_{2i}$, and

$$\| \chi \| \ge A, \ \left| \tilde{\phi}_i \right| \ge \lambda_{\phi i}^{-1} | \phi_i |, \ \left\| \tilde{W}_i \right\| \ge c_{5i} \gamma_{Wi}^{-1} \| W_i \|, \ \left\| \tilde{W}_{gi} \right\| \ge c_{6i} \gamma_{gi}^{-1} \left\| W_{gi} \right\| \tag{107}$$

where $A = \sqrt{[\| C \|^2 + D\lambda_{\min}(K)] / [4\lambda_{\min}^2(K)]} + \| C \| / [2\lambda_{\min}(K)]$ with $\lambda_{\min}(K)$ the minimum singular value of K.
Now, we define

$$\begin{aligned} &\Omega_\chi = \left\{ \chi \mid \| \chi \| \le A \right\}, \Omega_{\phi_i} = \left\{ \tilde{\phi}_i \mid \left| \tilde{\phi}_i \right| \le \lambda_{\phi i}^{-1} | \phi_i | \right\}, \\ &\Omega_{W_i} = \left\{ \left\| \tilde{W}_i \right\| \mid \left\| \tilde{W}_i \right\| \le c_{5i} \gamma_{Wi}^{-1} \| W_i \| \right\}, \Omega_{Wg_i} = \left\{ \left\| \tilde{W}_{gi} \right\| \mid \left\| \tilde{W}_{gi} \right\| \le c_{6i} \gamma_{gi}^{-1} \left\| W_{gi} \right\| \right\}, \end{aligned} \tag{108}$$

Since $\| W_i \|, \left\| W_{gi} \right\|, \phi_i, \gamma_{\phi i}, \gamma_{Wi}, \gamma_{Wgi}, c_{5i}, c_{6i}$ are positive constants, we conclude that Ω_χ , Ω_{ϕ_i} , $\Omega_{W i}$ and Ω_{Wg_i} are compact sets. Hence $\dot{L}$ is negative outside these compacts set. According to a standard Lyapunov theorem, this demonstrates that $\tilde{W}_i, \tilde{W}_{gi}, \tilde{\phi}_i$ and χ are bounded and will converge to Ω_χ , Ω_{ϕ_i} , $\Omega_{W i}$ and Ω_{Wg_i} , respectively.

Furthermore, this implies e_i is bounded and will converge to a neighborhood of the origin and all signals in the system are bounded.

4.2.3 Simulation Study

In order to validate the effectiveness of the proposed scheme, we implement an example, and assume that the large-scale system is composed of the following two subsystems defined by

$$Subsystem\ \ 1:\begin{cases}\dot{x}_{11}=x_{12}\\ \dot{x}_{12}=-\omega^2 x_{11}+0.02(\omega-x_{11}^2)x_{12}+u_1+(x_{11}^2+x_{12}^2)\sigma(u_1)\\ \qquad +0.1\|x_2\|\exp(0.5\|x_2\|)\end{cases} \tag{109}$$

$$Subsystem\ \ 2:\begin{cases}\dot{x}_{21}=x_{22}\\ \dot{x}_{22}=x_{21}^2+0.1(1+x_{22}^2)u_2+\tanh(0.1u_2)+0.15{u_2}^3\\ \qquad +0.2\|x_2\|\exp(0.1\|x_2\|)\end{cases} \tag{110}$$

where $\omega=0.4\pi$, $\sigma(u_1)=(1-e^{-u_1})/(1+e^{-u_1})$. The desired trajectory $x_{d11}=0.1\pi[\sin(2t)-\cos(t)]$, $x_{d21}=0.1\pi\sin(2t)$. For the RBFNs as (84), input vectors are chosen as $z_i=[x_i^T,\tau_i,\hat{\psi}_i]^T$, $i=1,2$ and number of hidden layer nodes both 8, the initial weights $\hat{W}_i(0)=(0)$ and the center values and the widths of Gaussian function zero, and 2, respectively. For the RBFNs, which used to compensate the interconnection nonlinearities, both input vectors are $[\tau_1,\tau_2]^T$, number of hidden layer nodes is 8, the initial weights $\hat{W}_{gi}(0)=(0)$, and the center values and the widths of Gaussian function zero, and $\sqrt{5}$, respectively. The initial condition of controlled plant is $x_1(0)=[0.2,0.2]^T$, $x_2(0)=[0.3,0.2]^T$. The other parameters are chosen as follows: $\Lambda_i=1,k_i=2$, $\gamma_{Wi}=0.001,\gamma_{\phi i}=0.1,\lambda_{\phi i}=0.01,\ \ \alpha_i=10$, $F_i=10I_{Wi}$, $G=2I_{gi}$, with I_{Wi},I_{gi} corresponding identity matrices. Fig.11 and 12 show the results of comparisons of tracking errors and control input of two subsystems, Fig.13 and 14 the comparison of tracking of two subsystems, respectively. Fig.15 and Fig.16 illustrate the norm of the four weights in two subsystems, respectively. From these results, it can be seen that the effectiveness of the proposed scheme is validated, and tracking errors converge to a neighborhood of the zeroes and all signals in system are bounded. Furthermore, the learning rate of neural network controller is rapid, and can track the desired trajectory in less than 3 seconds. From the results of control inputs, after shortly shocking, they tend to be smoother, and this is because neural networks are unknown for objective in initial stages. As desired, though the system is complex, the whole running process is well.

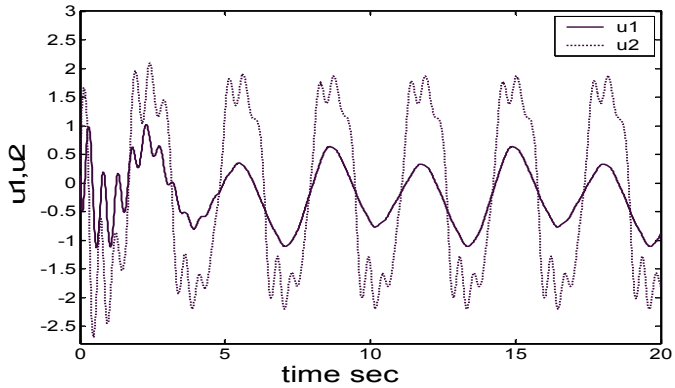

Fig. 12. Control input of subsystem1: u_1 , and subsystem 2: u_2

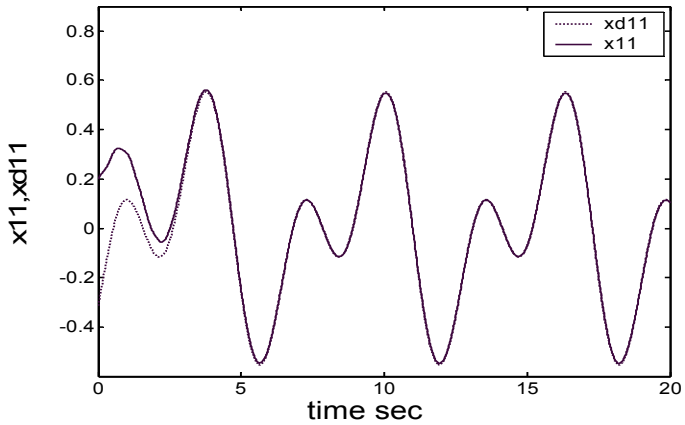

Fig. 13. Comparion of tracking of subsystem 1

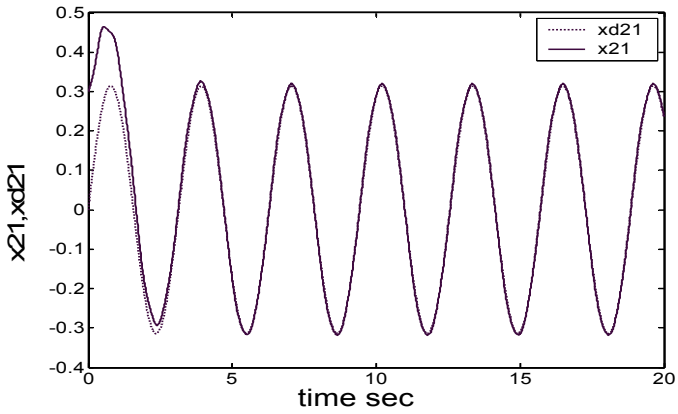

Fig. 14. Comparion of tracking of subsystem 2

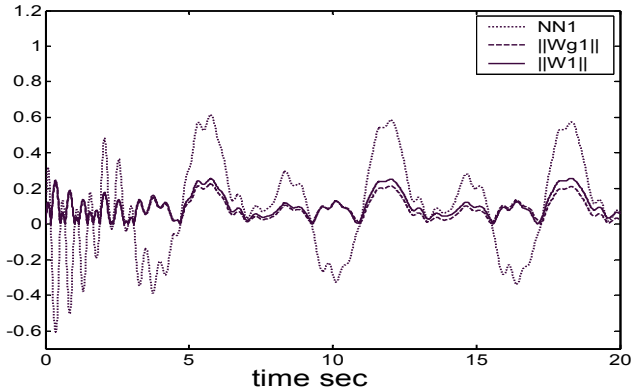

Fig. 15. The norms of weights and output of RBFNof subsystem1

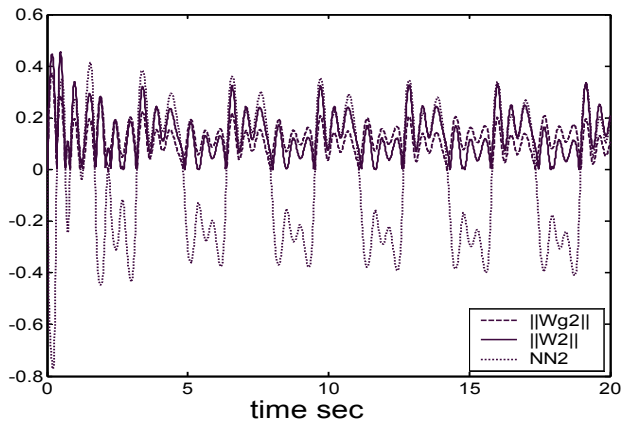

Fig. 16. The norms of weights and output of RBFNof subsystem 2

5. Conclusion

In this chapter, first, a novel design ideal has been developed for a general class of nonlinear systems, which the controlled plants are a class of non-affine nonlinear implicit function and smooth with respect to control input. The control algorithm bases on some mathematical theories and Lyapunov stability theory. In order to satisfy the smooth condition of these theorems, hyperbolic tangent function is adopted, instead of sign function. This makes control signal tend smoother and system running easier. Then, the proposed scheme is extended to a class of large-scale interconnected nonlinear systems, which the subsystems are composed of the above-mentioned class of non-affine nonlinear functions. For two classes of interconnection function, two RBFN-based decentralized adaptive control schemes are proposed, respectively. Using an on-line approximation approach, we have been able to relax the linear in the parameter requirements of traditional nonlinear decentralized adaptive control without considering the dynamic uncertainty as part of the interconnections and disturbances. The theory and simulation results show that the neural network plays an important role in systems. The overall adaptive schemes are proven to

guarantee uniform boundedness in the Lyapunov sense. The effectiveness of the proposed control schemes are illustrated through simulations. As desired, all signals in systems, including control signals, are tend to smooth.

6. Acknowledgments

This research is supported by the research fund granted by the Natural Science Foundation of Shandong (Y2007G06) and the Doctoral Foundation of Qingdao University of Science and Technology.

7. References

Lewis,F.L.; Yesildirek A. & Liu K.(1996). Multilayer neural-net robot controller with guaranteed tracking performance. *IEEE Trans.on Neural Networks,* Vol. 7, No.2, Mar. 1996, pp.388-399, ISSN 1045-9227

Yu, W. & Li, X.(2002). Adaptive control with multiple neural networks. *Proceeding of the American Control Conference,* pp. 1543-1549, ISBN 0-7803-7298-0, May 8-10,2002 Anchorage, AK

Yesidirek, A. and Lewis,F.L.(1995). Feedback linearization using neural networks. *Automatica,* Vol.31, No.11, 1995, pp. 1659-1664, ISSN 0005-1098

Calise,A.J. & Hovakimyan, N. (2001). Adaptive output feedback control of nonlinear system using neural networks. *Automatica,* Vol.37, 2001, pp.1201-1211, ISSN 0005-1098

Ge, S. S. ; Hang, C. C. & Zhang, T.(1997). Direct adaptive neural network control of nonlinear systems. *Proceedings of the American Control Conference*, pp. 1568-1572, ISBN 0-7803-3832-4, 1997, Albuqerque, New Mexico

Ioannou, P.A. (1986). Decentralized adaptive control of interconnected systems, *IEEE Trans. on Automatic Control,* Vol. 31, Apr. 1986, pp. 291-298, ISSN 0018-9286

Siljak, D.D.(1991). Decentralized control of complex systems. Academic, 1991, ISBN-10: 0126434301, Boston

Fu, L.C. (1992). Robust adaptive decentralized control of robot manipulators. *IEEE Trans. on Automatic Control,*Vol.37, 1992, pp.106–110, ISSN 0018-9286

Sheikholeslam, S. & Desor, C.A. (1993). Indirect adaptive control of a class of interconnected nonlinear dynamical systems. Int J Control, Vol. 57, No.3, 1993, pp.742–765, ISSN 0020-7179

Wen, C. (1994). Decentralized adaptive regulation. *IEEE Trans. on Automatic Control,* Vol.39, pp.2163–2166, ISSN 0018-9286

Tang, Y. ; Tomizuka, M. & Guerrero, G. (2000). Decentralized robust control of mechanical systems. *IEEE Trans. on Automatic Control,* Vol.45, No.4, 2000, pp. 2163–2166, ISSN 0018-9286

Spooner, J.T. & Passino, K.M.(1999). Decentralized adaptive control of nonlinear systems using radial basis neural networks, *IEEE Trans. on Automatic Control,* Vol. 44, No.11, 1999, pp.2050-2057, ISSN 0005-1098

Huang, S.; Tan, K.K. & Lee, T.H. (2003). Decentralized control design for large-scale systems with strong interconnections using neural networks, *IEEE Trans. on Automatic Control,* Vol.48, No.5, 2003, pp. 805-810, ISSN 0018-9286

Huang, S.N. & Tan, K.K. (2006). Nonlinear adaptive control of interconnected systems using neural networks. IEEE Trans Neural Networks, Vol.17, No.1, 2006, pp.243–246, ISSN 1045-9227

Nardi, F. & Hovakimyan, N.(2006). Decentralized control of largescale systems using single hidden layer neural networks. *Proceedings of the American control conference*, pp.3123–3127, ISBN 0-7803-6495-3, June 2001,Arilington

Huang, S.N. & Tan, K.K. (2005). Decentralized control of a class of large-scale nonlinear systems using neural networks. *Automatica,* Vol.41, 2005, pp.1645–1649, ISSN 0005-1098

Ge, S. S. ; Hang, C. C. & Zhang, T.(1998). Nonlinear adaptive control using neural networks and its application to CSTR systems. *Journal of Process Control,* Vol.9, 1998, pp.313-323, ISSN 0959-1524

Tsinias, J. & Kalouptsidis,N.(1983). Invertibility of nonlinear analytic single-input systems, *IEEE Trans. on Automatic Control,* Vol.28, No. 9, 1983, pp. 931 – 933, ISSN 0018-9286

Lang, S. (1983). *Real Analysis*, Reading, ISBN-10: 0201141795, MA: Addison-Wesley, Reading

Slotine, J.-J. E. & Li, W.P. (1991). *Applied Nonlinear Control,* Englewood Cliffs, ISBN-10: 0130408905, NJ: Prentice Hall

Polycarpou, M.M.(1996). Stable adaptive neural control scheme for nonlinear system, *IEEE Trans. on Automatic Control,* Vol. 41, No. 3, 1996, pp.447-451, ISSN 0018-9286

Appendix A

As Eq.(19), the approximation error of function can be written as

$$M^T\sigma-\hat{M}^T\hat{\sigma}=M^T\sigma-\hat{M}^T\sigma+\hat{M}^T\sigma-\hat{M}^T\hat{\sigma}=\hat{M}^T(\sigma-\hat{\sigma})+\tilde{M}^T\sigma$$

Substituting (18) into the above equation, we have

$$\begin{aligned}
&\hat{M}^T(\sigma-\hat{\sigma})+\tilde{M}^T\sigma\\
&=\tilde{M}^T[\hat{\sigma}+\hat{\sigma}'\tilde{N}^Tx_{nn}+O(\tilde{N}^Tx_{nn})^2]+\hat{M}^T[\hat{\sigma}'\tilde{N}^Tx_{nn}+O(\tilde{N}^Tx_{nn})^2]\\
&=\tilde{M}^T\hat{\sigma}+\tilde{M}^T\hat{\sigma}'\tilde{N}^Tx_{nn}+\hat{M}^T\hat{\sigma}'\tilde{N}^Tx_{nn}+M^TO(\tilde{N}^Tx_{nn})^2\\
&=\tilde{M}^T\hat{\sigma}+\tilde{M}^T\hat{\sigma}'N^Tx_{nn}-\tilde{M}^T\hat{\sigma}'\hat{N}^Tx_{nn}+\hat{M}^T\hat{\sigma}'\tilde{N}^Tx_{nn}+M^TO(\tilde{N}^Tx_{nn})^2\\
&=\tilde{M}^T(\hat{\sigma}-\hat{\sigma}'\hat{N}^Tx_{nn})+\hat{M}^T\hat{\sigma}'\tilde{N}^Tx_{nn}+\tilde{M}^T\hat{\sigma}'N^Tx_{nn}+M^TO(\tilde{N}^Tx_{nn})^2
\end{aligned}$$

Define that

$$\omega=\tilde{M}^T\hat{\sigma}'N^Tx_{nn}+M^TO(\tilde{N}^Tx_{nn})^2$$

so that

$$M^T\sigma-\hat{M}^T\hat{\sigma}=\tilde{M}^T(\hat{\sigma}-\hat{\sigma}'\hat{N}^Tx_{nn})+\hat{M}^T\hat{\sigma}'\tilde{N}^Tx_{nn}+\omega$$

Thus,

$$\begin{aligned}\omega&=M^T\sigma-\hat{M}^T\hat{\sigma}-\tilde{M}^T(\hat{\sigma}-\hat{\sigma}'\hat{N}^Tx_{nn})-\hat{M}^T\hat{\sigma}'\tilde{N}^Tx_{nn}\\&=M^T\sigma-M^T\hat{\sigma}+\tilde{M}^T\hat{\sigma}'\hat{N}^Tx_{nn}-\hat{M}^T\hat{\sigma}'\tilde{N}^Tx_{nn}\\&=M^T(\sigma-\hat{\sigma})+M^T\hat{\sigma}'\hat{N}^Tx_{nn}-\hat{M}^T\hat{\sigma}'\hat{N}^Tx_{nn}-\hat{M}^T\hat{\sigma}'\tilde{N}^Tx_{nn}\\&=M^T(\sigma-\hat{\sigma})+M^T\hat{\sigma}'\hat{N}^Tx_{nn}-\hat{M}^T\hat{\sigma}'N^Tx_{nn}\end{aligned}$$

Appendix B

Using (46) and (47), the function approximation error can be written as

$$\begin{aligned}&W_i^TS_i-\hat{W}_i^T\hat{S}_i=W_i^TS_i-\hat{W}_i^TS_i+\hat{W}_i^TS_i-\hat{W}_i^T\hat{S}_i=\tilde{W}_i^TS_i+\hat{W}_i^T\tilde{S}_i\\&=\tilde{W}_i^T[\hat{S}_i+\hat{S}'_{\mu i}\tilde{\mu}_i+\hat{S}'_{\sigma i}\tilde{\sigma}_i+O(\tilde{\mu}_i,\tilde{\sigma}_i)^2]+\hat{W}_i^T[\hat{S}_i+\hat{S}'_{\mu i}\tilde{\mu}_i+\hat{S}'_{\sigma i}\tilde{\sigma}_i+O(\tilde{\mu}_i,\tilde{\sigma}_i)^2-\hat{S}_i]\\&=\tilde{W}_i^T\hat{S}_i+\tilde{W}_i^T(\hat{S}'_{\mu i}\tilde{\mu}_i+\hat{S}'_{\sigma i}\tilde{\sigma}_i)+\tilde{W}_i^TO(\tilde{\mu}_i,\tilde{\sigma}_i)^2+\hat{W}_i^T(\hat{S}'_{\mu i}\tilde{\mu}_i+\hat{S}'_{\sigma i}\tilde{\sigma}_i)+\hat{W}_i^TO(\tilde{\mu}_i,\tilde{\sigma}_i)^2\\&=\tilde{W}_i^T\hat{S}_i+\tilde{W}_i^T[\hat{S}'_{\mu i}(\mu_i-\hat{\mu}_i)+\hat{S}'_{\sigma i}(\sigma_i-\hat{\sigma}_i)]+\hat{W}_i^T(\hat{S}'_{\mu i}\tilde{\mu}_i+\hat{S}'_{\sigma i}\tilde{\sigma}_i)+W_i^TO(\tilde{\mu}_i,\tilde{\sigma}_i)^2\\&=\tilde{W}_i^T(\hat{S}_i-\hat{S}'_{\mu i}\hat{\mu}_i-\hat{S}'_{\sigma i}\hat{\sigma}_i)+\tilde{W}_i^T(\hat{S}'_{\mu i}\mu_i+\hat{S}'_{\sigma i}\sigma_i)+\hat{W}_i^T(\hat{S}'_{\mu i}\tilde{\mu}_i+\hat{S}'_{\sigma i}\tilde{\sigma}_i)+W_i^TO(\tilde{\mu}_i,\tilde{\sigma}_i)^2\\&=\tilde{W}_i^T(\hat{S}_i-\hat{S}'_{\mu i}\hat{\mu}_i-\hat{S}'_{\sigma i}\hat{\sigma}_i)+\hat{W}_i^T(\hat{S}'_{\mu i}\tilde{\mu}_i+\hat{S}'_{\sigma i}\tilde{\sigma}_i)+\omega_i(t).\end{aligned}$$

define as

$$\omega_i(t)=\tilde{W}_i^T(\hat{S}'_{\mu i}\mu_i+\hat{S}'_{\sigma i}\sigma_i)+W_i^TO(\tilde{\mu}_i,\tilde{\sigma}_i)^2$$

Thus,

$$\begin{aligned}\omega_i(t) &= \tilde{W}_i^T S_i + \hat{W}_i^T \tilde{S}_i - \tilde{W}_i^T (\hat{S}_i - \hat{S}'_{\mu i}\hat{\mu}_i - \hat{S}'_{\sigma i}\hat{\sigma}_i) - \hat{W}_i^T (\hat{S}'_{\mu i}\tilde{\mu}_i + \hat{S}'_{\sigma i}\tilde{\sigma}_i) \\ &= \tilde{W}_i^T \tilde{S}_i + \hat{W}_i^T \tilde{S}_i + \tilde{W}_i^T (\hat{S}'_{\mu i}\hat{\mu}_i + \hat{S}'_{\sigma i}\hat{\sigma}_i) - \hat{W}_i^T (\hat{S}'_{\mu i}\tilde{\mu}_i + \hat{S}'_{\sigma i}\tilde{\sigma}_i) \\ &= W_i^T \tilde{S}_i + \tilde{W}_i^T (\hat{S}'_{\mu i}\hat{\mu}_i + \hat{S}'_{\sigma i}\hat{\sigma}_i) - \hat{W}_i^T (\hat{S}'_{\mu i}\tilde{\mu}_i + \hat{S}'_{\sigma i}\tilde{\sigma}_i) \\ &= W_i^T \tilde{S}_i + W_i^T (\hat{S}'_{\mu i}\hat{\mu}_i + \hat{S}'_{\sigma i}\hat{\sigma}_i) - \hat{W}_i^T (\hat{S}'_{\mu i}\mu_i + \hat{S}'_{\sigma i}\sigma_i)\end{aligned}$$

Edited by Kwanho You

Adaptive control has been a remarkable field for industrial and academic research since 1950s. Since more and more adaptive algorithms are applied in various control applications, it is becoming very important for practical implementation. As it can be confirmed from the increasing number of conferences and journals on adaptive control topics, it is certain that the adaptive control is a significant guidance for technology development.The authors the chapters in this book are professionals in their areas and their recent research results are presented in this book which will also provide new ideas for improved performance of various control application problems.

ISBN 978-953-51-6405-0

Photo by koya79 / iStock

IntechOpen